

NASA CR- 139457

TDRSS TELECOMMUNICATIONS STUDY PHASE I - FINAL REPORT

(NASA-CR-139157) TDRSS TELECOMMUNICATIONS STUDY. PHASE 1: FINAL REPORT Final Report, Apr. - Aug. 1974 (Magnavox Co., Torrance, Calif.) 537 p HC \$12.50

N75-12177

Unclassified

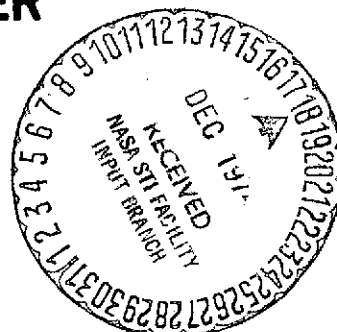
CSCL 17B G3/32 04258

Advanced Products Division
The Magnavox Company
2829 Maricopa Street
Torrance, California 90503

15 September 1974
Final Report for Period April 1974 - August 1974

Prepared for

GODDARD SPACE FLIGHT CENTER
Greenbelt, Maryland 20771



MRL TECHNICAL INFORMATION NOTICE

All entries must be completed prior to printing. If a particular block is not applicable, place N/A (not applicable) in the appropriate block.

DISTRIBUTION DATE Sept 17, 1974

AUTHOR C. R. Cahn R. S. Cnossen	CONTRIBUTORS B. S. Abrams M. M. Goutmann A. E. Zeger	MRL REFERENCE NO. R-4958 DOCUMENT DATE September 15, 1974
TITLE TDRSS TELECOMMUNICATIONS STUDY PHASE I - FINAL REPORT		
SUBJECT/ KEY WORDS Satellite Link Analysis, TDRSS Transponder Design, Modulation Tradeoffs, Phased Arrays.		
GOVERNMENT CLASS, AND MRL CONTROL NO. Unclassified	TYPE OF INFORMATION Waveform Modulation and implementation tradeoffs study for the TDRSS System	NO. OF PAGES 535 NO. OF ILLUST.
MAGNAVOX CLASS None		
ABSTRACT/ CONCLUSIONS The purpose of this study was to perform parametric analysis of the telecommunications support capability of the Tracking and Data Relay Satellite System (TDRSS). Emphasis was placed on maximizing support capability provided to user while minimizing impact on the user spacecraft. This study evaluates the present TDRSS configuration as presented in the TDRSS Definition Phase Study Report, December 1973 to determine potential changes for improving the overall performance. In addition, it provides specifications of the user transponder equipment to be used in the TDRS System.		

BY CUTTING OUT THIS RECTANGLE AND FOLDING ON THE CENTER LINE,
THE ABOVE INFORMATION CAN BE FITTED INTO A STANDARD CARD FILE.

INFORMATION PREPARED FOR: National Aeronautics and Space Administration

APPROVED BY: PROGRAM MANAGER

R. S. Cnossen
R. S. Cnossen

DATE: Sept 16, 1974

DEPARTMENT MANAGER

B. G. Glazer
B. G. Glazer

DATE: Sept 16, 1974

TECHNICAL REPORT STANDARD TITLE PAGE

1. Report No.	2. Government Accession No.	3. Recipient's Catalog No.	
4. Title and Subtitle TDRSS Telecommunications Study Phase I - Final Report		5. Report Date September 15, 1974	6. Performing Organization Code
7. Author(s) C. R. Cahn R. S. Clossen		8. Performing Organization Report No. R-4958	
9. Performing Organization Name and Address The Magnavox Company Advanced Products Division 2829 Maricopa Street Torrance, California 90503		10. Work Unit No.	11. Contract or Grant No. NAS5-20047
12. Sponsoring Agency Name and Address National Aeronautics and Space Admin. Goddard Space Flight Center Greenbelt, Maryland, 20771		13. Type of Report and Period Covered Type III (Final) Apr. 1974 to Aug 1974	
14. Sponsoring Agency Code Code 805			
15. Supplementary Notes			
16. Abstract The purpose of this study was to perform parametric analysis of the telecommunications support capability of the Tracking and Data Relay Satellite System (TDRSS). Emphasis was placed on maximizing support capability provided to user while minimizing impact on the user spacecraft. This study evaluates the present TDRSS configuration as presented in the TDRSS Definition Phase Study Report, December 1973 to determine potential changes for improving the overall performance. In addition, it provides specifications of the user transponder equipment to be used in the TDRSS.			
17. Key Words TDRS Satellite Link Analysis TDRS Transponder Design Modulation Tradeoffs Phased Arrays		18. Distribution Statement /	
19. Security Classif. (of this report) Unclassified	20. Security Classif. (of this page) Unclassified	21. No. of Pages 535	22. Price

PREFACE

Over the past several years, NASA has conducted several studies of a Tracking and Data Relay Satellite System (TDRSS) to augment the current tracking and data network. The results of these studies, which have established that a TDRSS is both feasible and cost effective, led to awards for major definition studies in May 1971. The studies were directed primarily to the relay spacecraft elements of the system. At the same time, several Goddard Space Flight Center (GSFC) in-house studies were directed to the design of the ground elements and overall system operational aspects. The integrated results of all these studies were published in a "TDRSS Definition Phase Study Report", December 1973. Subsequently, the Magnavox Company was awarded a study contract directed toward the telecommunications aspects of the system.

This report, dated September 1974, contains the results of a study to (1) determine the capability of the TDRS System as specified by the TDRSS Definition Phase Study Report, (2) determine potential configuration changes to satisfy all telecommunications performance objectives without major redesign, (3) perform analysis of significant system variables for the purpose of optimizing parameters, and (4) define the TDRSS telecommunications characteristics in greater detail than previously established.

Work on this report, entitled TDRSS Telecommunications Study, was accomplished by the Advanced Products Division of the Magnavox Company and complies with the requirements of Contract Number NAS5-20047. This report is the result of a joint study carried out by Dr. C. R. Cahn and Mr. R. S. Cnossen of the APD/Magnavox Research Laboratories and Dr. M. M. Goutmann and Messrs. B. S. Abrams and A. E. Zeger of the APD/General Atronics Corporation.

Magnavox wishes to acknowledge the help and cooperation received during the course of this contract. In particular, we wish to thank Mr. Leonard F. Deerkoski of NASA/GSFC, Greenbelt, Maryland, for his technical and administrative guidance during the program.

TABLE OF CONTENTS

<u>Section</u>	<u>Title</u>	<u>Page</u>
I	OBJECTIVE AND BACKGROUND DISCUSSION	1-1
	1.1 Spread Spectrum Modulation	1-4
	1.2 Telecommunication System Parameters	1-4
	1.3 Multiple Access System	1-7
	1.4 S-Band Single Access	1-8
	1.5 Ku-Band Single Access	1-9
	1.6 Range and Range Rate Measurement	1-9
	1.7 Summary	1-9
II	MULTIPLE ACCESS SERVICE	2-1
	2.1 Modulation Tradeoffs	2-5
	2.1.1 Spread Spectrum Modulation Techniques	2-5
	2.1.2 Fixed Field of View Forward Link	2-16
	2.1.3 Steered Beam Forward Link	2-29
	2.1.4 Analysis of Range and Range Rate Measurement Accuracy	2-36
	2.1.5 Multiple Access Return Link	2-39
	2.1.6 Recommended Waveform Parameters for Multiple Access System with Steered Transmit Beam	2-58
	2.1.7 Code Generation for PN and FH	2-78
	2.1.8 Further Analysis of Two-Step Acquisition (with FH Preamble) on Forward Link	2-88
	2.2 Implementation Tradeoffs	2-95
	2.2.1 Doppler Resovers vs. Transmitter Frequency Offset	2-95
	2.2.2 Coherent/Noncoherent Transponder Operation	2-97
	2.2.3 Data Clock	2-98
	2.2.4 Clear Mode of Operation	2-98
	2.2.5 Frequency Synthesis	2-99
	2.2.6 Reference Oscillator Stability	2-101
	2.2.7 Digital Tracking	2-108
	2.2.8 Frequency Hopper	2-108
	2.2.9 Integrated Circuit Tradeoffs	2-109

TABLE OF CONTENTS (Cont)

<u>Section</u>	<u>Title</u>	<u>Page</u>
2.3	Recommended M/A Transponder Design	2-113
2.3.1	Waveform Parameters	2-113
2.3.2	Transponder Functional Design	2-115
2.3.3	Size, Weight and Power	2-137
2.3.4	Multiple Access Service Performance Specification	2-140
2.4	Operational Procedures	2-142
2.4.1	Forward Link	2-142
2.4.2	Return Link	2-142
2.4.3	Return Only Link	2-143
2.5	Multiple Access User Transponder Equipment Specifications	2-144
2.5.1	Modes of Operation	2-144
2.5.2	Receiver Precorrelation Channel	2-144
2.5.3	Frequency Hop Preamble	2-144
2.5.4	PN Demodulation	2-145
2.5.5	Carrier Acquisition and Tracking	2-146
2.5.6	Command Data Demodulation	2-146
2.5.7	Transmit Channel	2-147
III	S-BAND SINGLE ACCESS SERVICE	3-1
3.1	Modulation Tradeoffs	3-1
3.1.1	Design of Forward Link Signal	3-2
3.1.2	Acquisition Time on Forward Link	3-3
3.1.3	Design of Return Link Signal	3-4
3.1.4	Functional Description of S-Band Single Access Modulation Equipment	3-6
3.1.5	Range and Range Rate Measurement Accuracy	3-6
3.1.6	Summary	3-7
3.1.7	Two-Way Ranging with Clear Asynchronous Data	3-7
3.1.8	Minimum Power for Two-Way Ranging	3-11
3.1.9	Two-Way Ranging with Separate Non-Spread Data	3-13
3.2	Autotrack Analysis	3-16
3.2.1	System Design for Strong Pulsed RFI	3-17
3.2.2	Choice of Bandwidths in the Autotrack System	3-19
3.2.3	Pointing Error Contributors	3-22
3.2.4	S-Band User Autotrack System Block Diagram	3-27
3.2.5	APC Modification	3-31
3.2.6	Autotrack Scenario	3-32

TABLE OF CONTENTS (Cont)

<u>Section</u>	<u>Title</u>	<u>Page</u>
	3.3 Recommended S-Band Single Access Design	3-32
	3.3.1 S-Band Service Waveform Parameters	3-33
	3.3.2 Transponder Functional Design	3-34
	3.3.3 Size, Weight and Power	3-38
	3.3.4 Performance Specification	3-41
	3.4 Operational Procedure	3-43
	3.4.1 Forward Link Acquisition	3-43
	3.4.2 Return Link Acquisition	3-43
	3.4.3 Return Link Acquisition with Minimum Power Ranging	3-44
	3.5 Transponder Equipment Specifications	3-45
IV	IV Ku-BAND SINGLE ACCESS SERVICE	4-1
	4.1 Modulation Tradeoffs	4-2
	4.1.1 Ku-Band Return Link Performance	4-2
	4.1.2 Soft-Decision Error Correction	4-11
	4.1.3 Tolerable Co-Channel Interference with Quadriphase	4-18
	4.1.4 Two-Way Ranging in Ku-Band System	4-20
	4.2 Autotrack Analysis and Implementation Concept	4-23
	4.2.1 Recommended TDRS Autotrack System	4-23
	4.2.2 Design and Analysis of Recommended TDRS Autotrack	4-25
	4.2.3 TDRS Autotrack Scenario and Requirements on User	4-36
	4.2.4 User Autotrack	4-37
	4.3 Operational Procedures	4-47
V	V TDRS-TO-GROUND LINK	5-1
	5.1 Frequency Plan	5-1
	5.1.1 Out-of-Band Emissions with Hard Limiting of Ku-Band Return Link	5-1
	5.1.2 Out-of-Band Spectrum with Soft Limiting	5-8
	5.1.3 Out-of-Band Spectrum with Biphase Signal	5-14
	5.1.4 Spectral Interference from Ku-Band Forward Link	5-19

TABLE OF CONTENTS (Cont)

<u>Section</u>	<u>Title</u>	<u>Page</u>
5.2	Ku-Band TDRS Polarization Mux	5-23
	5.2.1 Sources of Polarization Crosstalk	5-24
	5.2.2 Statistics of Rain Depolarization at Ku-Band	5-29
	5.2.3 ICS for Polarization Crosstalk Reduction	5-32
	5.2.4 Control System for Crosstalk Cancellation	5-38
	5.2.5 Impact on TDRS	5-48
5.3	RF Combining Techniques	5-49
	5.3.1 System Requirements	5-49
	5.3.2 Combining Techniques	5-50
	5.3.3 Associated Components	5-59
	5.3.4 Amplifier, Preamp Tradeoffs	5-60
	5.3.5 Alternative Combinations	5-64
	5.3.6 Summary and Conclusions	5-71
5.4	Adaptive Ground Implemented Phased Array	5-75
	5.4.1 Backoff Required to Transmit FDM Channels of the Multiple Access Array on TDRS	5-75
	5.4.2 Effect of RFI Upon MA Return Link AGIPA	5-86
5.5	Ground Receiver-Transmitter Design	5-91
	5.5.1 Receiver Transmitter Functional Description	5-91
	5.5.2 Reacquisition of Multiple Access Signal	5-102
	5.5.3 50 MBPS Viterbi Decoding	5-119
	5.5.4 Quadriphase Demodulator for 300 MBPS Data Rate	5-124

APPENDICES

I	PN CORRELATION LOSS DUE TO CHANNEL DISPERSION	I-1
II	CODE PHASE TRACKING WITH COHERENT FREQUENCY HOPPING	II-1
III	DETAILED SYNCHRONIZATION STUDY	III-1
IV	DOPPLER PROCESSOR FOR TDRSS TELECOMMUNICATIONS SYSTEM	IV-1
V	FFT DOPPLER PROCESSOR IMPLEMENTATION	V-1
VI	EIRP MONITORING FOR MULTIPLE ACCESS S-BAND USERS	VI-1
VII	SIMULATION OF MULTIPLE ACCESS WITH COHERENT FH	VII-1
VIII	POSSIBILITY OF UNDESIRED MINOR CORRELATION PEAK WITH SQPN	VIII-1
IX	SOFT-DECISION DECODING FOR BIPHASE MODULATION FOR THE Ku-BAND RETURN LINK	IX-1
X	SOFT-DECISION DECODING FOR QUADRIPHASE MODULATION FOR THE Ku-BAND RETURN LINK	X-1

TABLE OF CONTENTS (Cont)

<u>APPENDICES (Cont)</u>	<u>Title</u>	<u>Page</u>
XI	DYNAMIC SERVO LAG IN THE TDRS AUTOTRACK ANTENNA	XI-1
XII	NOISE ANALYSIS OF AN AUTOTRACK ANTENNA SYSTEM	XII-1
XIII	AN APC LOOP FOR PARAMP PHASE CORRECTION IN TDRSS AUTOTRACK SYSTEMS	XIII-1
XIV	USER EIRP REQUIREMENTS FOR TDRS AUTOTRACK ALTERNATIVES	XIV-1
XV	TDRS AUTOTRACK INITIAL ACQUISITION PROBABILITY	XV-1
XVI	TWO DATA STREAMS ON THE SQPN SIGNAL	XVI-1

LIST OF ILLUSTRATIONS

<u>Figure</u>	<u>Title</u>	<u>Page</u>
1-1	TDRSS Two-satellite System Concept	1-2
1-2	TDRSS Coverage, View Normal to TDRS Plane	1-2
1-3	TDRSS Frequency Plan	1-3
2-1	Adaptive Ground Implemented Phased Array with Fixed FOV MA Command	2-2
2-2	Adaptive Ground Implemented Phased Array with Steered MA Command Beam	2-3
2-3	SQPN Transmitter	2-6
2-4	Plot of Spectral Peaks with Filter BW (Bandpass)/ Chip-Rate = 2.0	2-9
2-5	Plot of Spectral Peaks with Filter BW (Bandwidth)/Chip Rate = 1.5	2-10
2-6	Plot of Spectral Peaks with Filter BW (Bandpass)/Chip Rate = 1.0	2-11
2-7	Correlation Loss with Sharp Cutoff Receive Filter	2-13
2-8	Coherent Frequency Hopping by Rate Multiplier and Quadriphase Modulator	2-14
2-9	Auto- and Cross-Correlation for Coherent FH with 16 Frequencies in Period, 32 Clocks per Dwell ~ Period = 2^9 Clocks	2-16
2-10	Auto Correlation Function of Coherent FH Signal	2-17
2-11	Theoretical Costas Loop Threshold as Function of Maximum Data Rate	2-27
2-12	Illustration of Worst Case Loss	2-32
2-13	Block Diagram of Delay Lock Tracking Loop	2-38
2-14	Processing in FH Receiver for Multiple Access	2-43
2-15	Superposition of High-Rate Interfering Signal on Low-Rate Signal	2-43
2-16	Processing in FH Receiver for Multiple Access	2-49
2-17	Pulse Response	2-50
2-18	Geometry Determining Phase Transient	2-53
2-19	Phase Transient of Switched Antenna	2-55
2-20	Degradation Due to Multiple Access Interference	2-65
2-21	Multiple-access (S-band) Return Link Data Rate vs. User EIRP	2-66
2-22	Distribution of Interference	2-68
2-23	Distribution of Interference	2-70
2-24	Functional Block Diagram of Multiple Access User Receiver	2-73
2-25	Functional Block Diagram of Multiple Access User Transmitter	2-75
2-26	Modular Shift Register Generators Used for Generation of Staggered Quadriphase	2-82
2-27	Frequency Hopping Sequence Generator	2-85
2-28	Autocorrelation Function for Frequency Hopping	2-85
2-29	Frequency Synthesis for the M/A Transponder	2-102

LIST OF ILLUSTRATIONS (Cont)

<u>Figure</u>	<u>Title</u>	<u>Page</u>
2-30	Digital Phase Locked Loop	2-109
2-31	Frequency Hopper, Block Diagram	2-110
2-32	Comparison of Bipolar vs. CMOS Power Dissipation	2-111
2-33	Multiple Access User Transponder	2-116
2-34	Receiver RF and IF Chain	2-119
2-35	Transmitter IF and RF Chain	2-123
2-36	M/A Frequency Synthesis	2-125
2-37	Code Tracking Loop I.P.M.	2-127
2-38	Modular Shift Register Generators Used for Generation of Staggered Quadriphase	2-128
2-39	Local Reference Generator	2-129
2-40	QPSK Modulator for FH and PN	2-131
2-41	SQPN Limits Instantaneous Phase Shifts to 90%	2-133
2-42	Baseband Demodulator for the M/A Transponder	2-134
2-43	Synchronous Demodulator, Simplified Block Diagram	2-135
3-1	Σ -Channel Functional Block Diagram	3-19
3-2	S-Band User Autotrack Pointing Loss vs User Antenna Diameter (99% of the Time)	3-28
3-3	Annotated Block Diagram of S-Band User Autotrack System	3-29
3-4	Access User Transponder	3-36
4-1	Bandwidth-limiting degradation of QPSK and BPSK signals	4-3
4-2	Limiter Input-Output Transfer Function	4-6
4-3	Output Signal-to-Total-Interference Ratio as Function of Average Power Output	4-6
4-4	Two Constant Amplitude Signals in Hard Limiter	4-9
4-5	The Ratio of the Output Signal-to-Signal Power Ratio to the Input Signal-to-Signal Power Ratio as a Function of the Larger Input SNR	4-10
4-6	Degradation in Coding Gain Due to Limiting	4-15
4-7	Average Binary Error Probability for Coherent PSK in the Presence of CW Interference and Gaussian Noise	4-19
4-8	Block Diagram of Ground Station Costas Loop for Measuring Beampointing Accuracy	4-32
4-9	Diagram of Initial Autotrack Search for User Position	4-33
4-10	Block Diagram of TDRS Autotrack System	4-35
4-11	User Autotrack Pointing Loss vs User Antenna Diameter	4-43
4-12	Block Diagram of User Autotrack System	4-45
5-1	TDRS Ku-Band Transmit Frequency Plan	5-2
5-2	Spectral Density After 6-Pole Butterworth Filter (Bandpass = 1.5) and Hard Limiter	5-4
5-3	Frequency Plan for Ku-Band Link, TDRS to Ground	5-6
5-4	Spectrum After Filtering (6-Pole Butterworth, Bandpass = 1.5) and Hard or Soft Limiting	5-10
5-5	Spectrum After Filtering (6-Pole, Bandpass = 1.5 Hz) and Limiting of Biphase Signal Plus Noise	5-16
5-6	Spectrum After Filtering (6-Pole, Bandpass = 1.5 Hz) and Limiting of Biphase Signal	5-17
5-7	Frequency Plan for TDRS Ku-Band Transmit	5-19

LIST OF ILLUSTRATIONS (Cont)

<u>Figure</u>	<u>Title</u>	<u>Page</u>
5-8	Spectral Density of an Angle-Modulated Wave, with Gaussian Frequency Modulation with a Rectangular Spectrum	5-22
5-9	Antenna APX-1293	5-25
5-10	Theoretical Rain Depolarization for Circularly Polarized Waves, After Laur 1	5-27
5-11	Contour of 20 dB Polarization Crosstalk in Rain	5-28
5-12	Geometry of Range in Rain Calculation	5-30
5-13	Number of Hours Per Year that Attenuation and Polarization Crosstalk are Exceeded at Ku-Band for 10° Elevation	5-32
5-14	Data Obtained from PSK Signal-Transmission Experiment with Cochannel Cross-polarization Interference	5-33
5-15	Cumulative Distribution of Rain Attenuation C/N, Cross-polarization Discrimination, and Error Rate	5-33
5-16	Model of TDRS Polarization Crosstalk and Ground Station Depolarization System	5-35
5-17	System for Cancellation of Polarization Crosstalk at IF	5-36
5-18A	Implementation of a Complex Multiplier with a Pair of Bipolar Multipliers	5-38
5-18B	Implementation of a Bipolar Multiplier with Electronically Variable Attenuators	5-39
5-19	ICS Employing the LMS Algorithm	5-44
5-20	LMS System for Cancellation of Polarization Crosstalk	5-46
5-21	Basic Frequency Plan	5-52
5-22	Method 1	5-53
5-23	Method 2	5-53
5-24	Method 3	5-53
5-25	Method 4	5-54
5-26	Method 5	5-54
5-27	Method 6	5-55
5-28	Method 7	5-55
5-29	Method 8	5-56
5-30	Method 9	5-56
5-31	Method 10	5-57
5-32	Method 11	5-57
5-33	Method 12	5-58
5-34	RF Loss Budget	5-59
5-35	Basic Amplifier Costs	5-62
5-36	Cost Chart	5-63
5-37	Low Loss Combining Method	5-64
5-38	Single Feed Combining Method	5-65
5-39	Dual Wideband Ku-Band Combining	5-66
5-40	Combining Before Amplifier Technique	5-67
5-41	Combining in Both Channels with Linear Amplifier	5-68
5-42	Single Wideband Output	5-68
5-43	Combining Techniques a	5-73
5-44	Combining Techniques a and c	5-73
5-45	RF Combiner - Best Solution	5-74
5-46	Equipment Sources	5-75
5-47	Limiter Input-Output Transfer Function	5-78

LIST OF ILLUSTRATIONS (Cont)

<u>Figure</u>	<u>Title</u>	<u>Page</u>
5-48	Reduction of Intermod by Backoff	5-79
5-49	TWT Input-Output Power Transfer Characteristic for Single Carrier	5-80
5-50	Single-Carrier Relative Phase Shift Versus Input Power Transfer Characteristic	5-81
5-51	Carrier to Intermodulation Product Ratio Versus Input Power . . .	5-82
5-52	Characteristics of an Intelsat IV Traveling-wave Tube	5-83
5-53	Results for the Traveling-wave Tube with a Gaussian Input Signal	5-83
5-54	Loss of MA Signal Due to AGIPA Nulling Main Beam RFI	5-90
5-55	Ground Receiver-Transmitter Block Diagram	5-92
5-56	Basic Rate Multiplier	5-94
5-57	Basic Rate Multiplier with Sign	5-95
5-58	IPM Function	5-95
5-59	Rate Multiplier and IPM	5-96
5-60	8-Bit Rate Multiplier	5-98
5-61	128-Step IPM	5-98
5-62	8-Step IPM	5-102
5-63	Cumulative Probability of Acquisition as a Function of Time (Normalized) for Second Order Phase Locked Loop	5-107
5-64	Cumulative Probability of Acquisition as a Function of Time (Normalized) for Second Order Phase Locked Loop	5-108
5-65	Cumulative Probability of Acquisition as a Function of Time (Normalized) for Second Order Phase Locked Loop	5-109
5-66	Second Order Phase Lock Loop Acquisition Time as a Function of Initial Frequency Offset	5-110
5-67	Cumulative Probability of Acquisition as a Function of Time (Normalized) for Third Order Phase Locked Loop	5-111
5-68	Cumulative Probability of Acquisition as a Function of Time (Normalized) for Third Order Phase Locked Loop	5-112
5-69	Acquisition Time as a Function of Frequency Offset for $P_{acq} = .9$ for Third Order Loops	5-113
5-70	Comparison of Acquisition Performance of Second and Third Order Phase Locked Loops	5-114
5-71	Probability of Acquisition Plotted Versus B_L to Illustrate Optimum Acquisition Bandwidth for Second Order Loop	5-115
5-72	Probability of Acquisition Plotted Versus B_L to Illustrate Optimum Acquisition Bandwidth for Third Order Loop	5-116
5-73	Functional Block Diagram of a Viterbi Decoder	5-120
5-74	Critical Path (Typical) Viterbi Metric Computation	5-120
5-75	Soft Decision Maximum Likelihood Decoder Performance	5-121
5-76	Parallel Decoder Operation	5-123
5-77	Encoder for Five Parallel Master/Slave Decoder - $R = 1/2, K = 7$	5-123
5-78	System Functional Diagram	5-125
5-79	Effect of Demodulator Phase Error	5-125

LIST OF TABLES

<u>Table No.</u>	<u>Title</u>	<u>Page</u>
1-1	Space-to-space Forward Links	1-5
1-2	Space-to-space Return Links	1-6
1-3	Minimum Spread Bandwidth	1-7
2-1	Postulated Distribution of User Data Rates	2-67
2-2	Distribution of MA Degradation Due to 100 Kbps Users	2-67
2-3	Summary of Multiple Access System	2-79
2-4	Average Time for FH Acquisition	2-92
2-5	Average Time for PN Acquisition	2-93
2-6	Industry Survey	2-104
2-7	Comparison of 5 MHz Oscillators	2-106
2-8	TCVCXO Characteristics	2-107
2-9	Typical Parameters of the TTL Family	2-112
2-10	Voltage Controlled Oscillator Specification	2-126
2-11	Reference Oscillator Specification	2-127
2-12	M/A Transponder Power, Weight and Size	2-138
2-13	Transponder Comparisons	2-140
3-1	Summary of S-Band Single Access System	3-8
3-2	Calculation of Δ -Channel Noise Temperature	3-21
3-3	S-Band Single Access Transponder Size, Weight, and Power	3-29
4-1	Excess S/N With Hard Limiting	4-14
4-2	Excess S/N With Hard Limiting of QPSK	4-17
4-3	Comparison Summary of Three TDRS Autotrack Alternatives	4-26
4-4	Signal and Noise Power Computations	4-30
5-1	Comparison of Required TDRS to Ground S/N with Floor Due to Ku-Band Hard Limiting Channel	5-7
5-2	S/I in Downlink Channels, Fixed Gain Operation	5-18
5-3	Total Transmit RF Losses Estimate	5-49
5-4	Basic Combiner Specifications	5-49
5-5	Basic Combiners Types - Typical Performance	5-51
5-6	Typical Combiner Isolations	5-52
5-7	Combining Methods Ranking	5-58
5-8	Ku-Band Coax Switch Performance	5-59
5-9	Typical T/R Diplexer Performance	5-60
5-10	RF Amplifier Ku-Band Power Levels	5-61
5-11	Receiver Requirements	5-62
5-12	Typical Vendors	5-70
5-13	Dual Circular Antenna Feeds at 14 GHz	5-71
5-14	Combiner Specifications	5-74
5-15	TCVCXO Characteristics	5-105

SECTION I

OBJECTIVE AND BACKGROUND DISCUSSION

The Tracking and Data Relay Satellite System (TDRSS) is designed to provide a relay capability between a ground station and low altitude user vehicles. Figures 1-1 and 1-2 show the system concept along with the coverage attained⁽¹⁾ via two stationary relay satellites. A forward (command) link to users and a return (telemetry) link from users are the basic communication functions supported. Three different services are available:

- Multiple Access at S-band (20 users)
- S-band Single Access
- Ku-band Single Access

The frequencies for the various links are indicated in Figure 1-3. The multiple access system utilizes a phased array antenna on the TDRS, generating a single electronically steered transmit beam to users* and multiple receive beams (one per user). The single access systems steer directive antennae on the TDRS (two dishes per TDRS).

The multiple access return link functions by transponding the individual signals received at the TDRS on 30 elements, and the multiple receive beams are actually formed in the Adaptive Ground Implemented Phased Array (AGIPA). The basic capability of AGIPA is to derive 15 dB of additional gain by electronically steering a beam to a given user, with the additional benefit of directivity to eliminate unwanted signals from sources outside the main beam. In addition, AGIPA can adapt the array element weightings for each beam to improve the signal-to-interference ratio by reducing side lobes (i.e., null forming) in the direction of unwanted sources.

*Originally, the concept provided a fixed field of view on the multiple access forward link.

1. NASA Goddard Space Flight Center, Tracking and Data Relay Satellite System Definition Phase Study Report, December 1973.

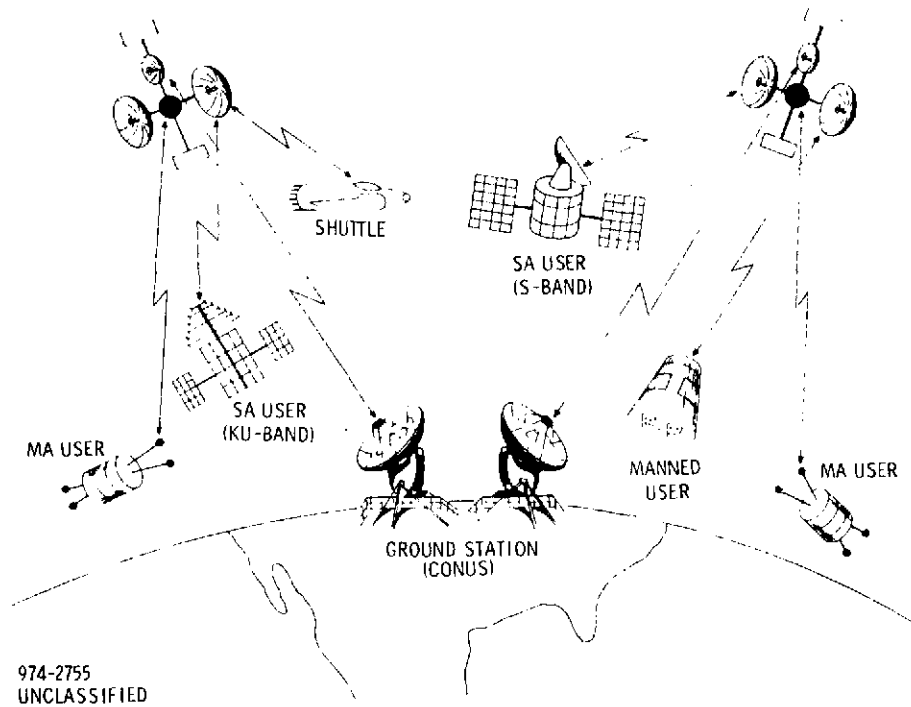


Figure 1-1. TDRSS Two-satellite System Concept

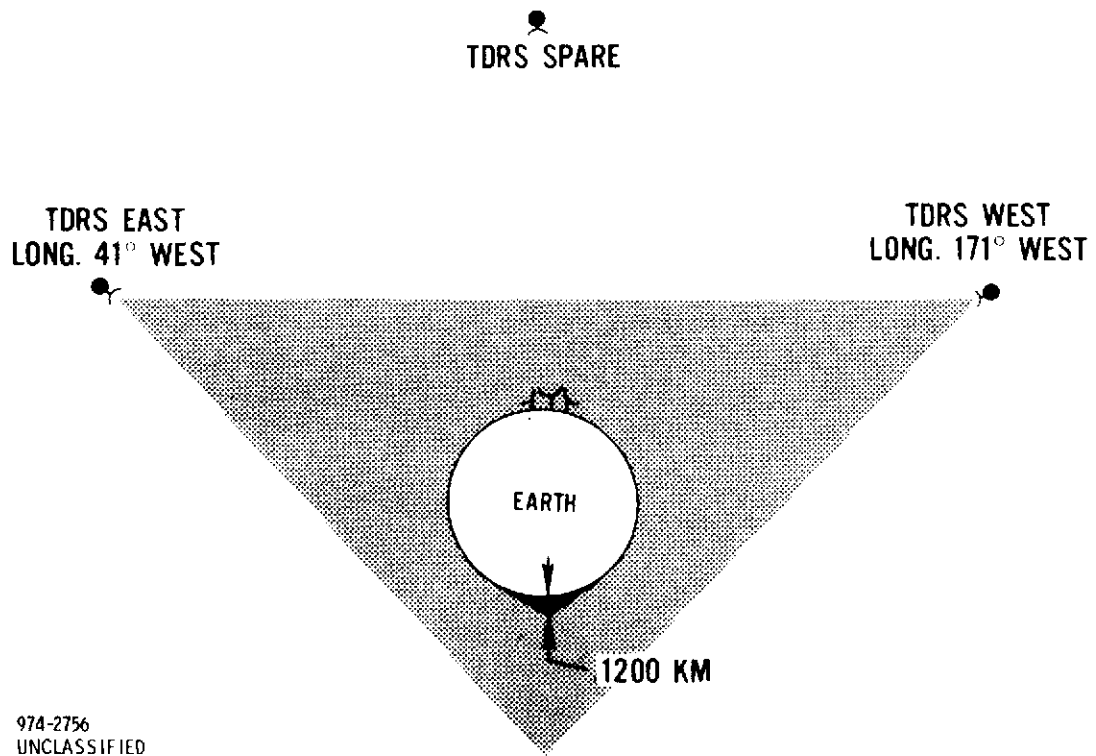
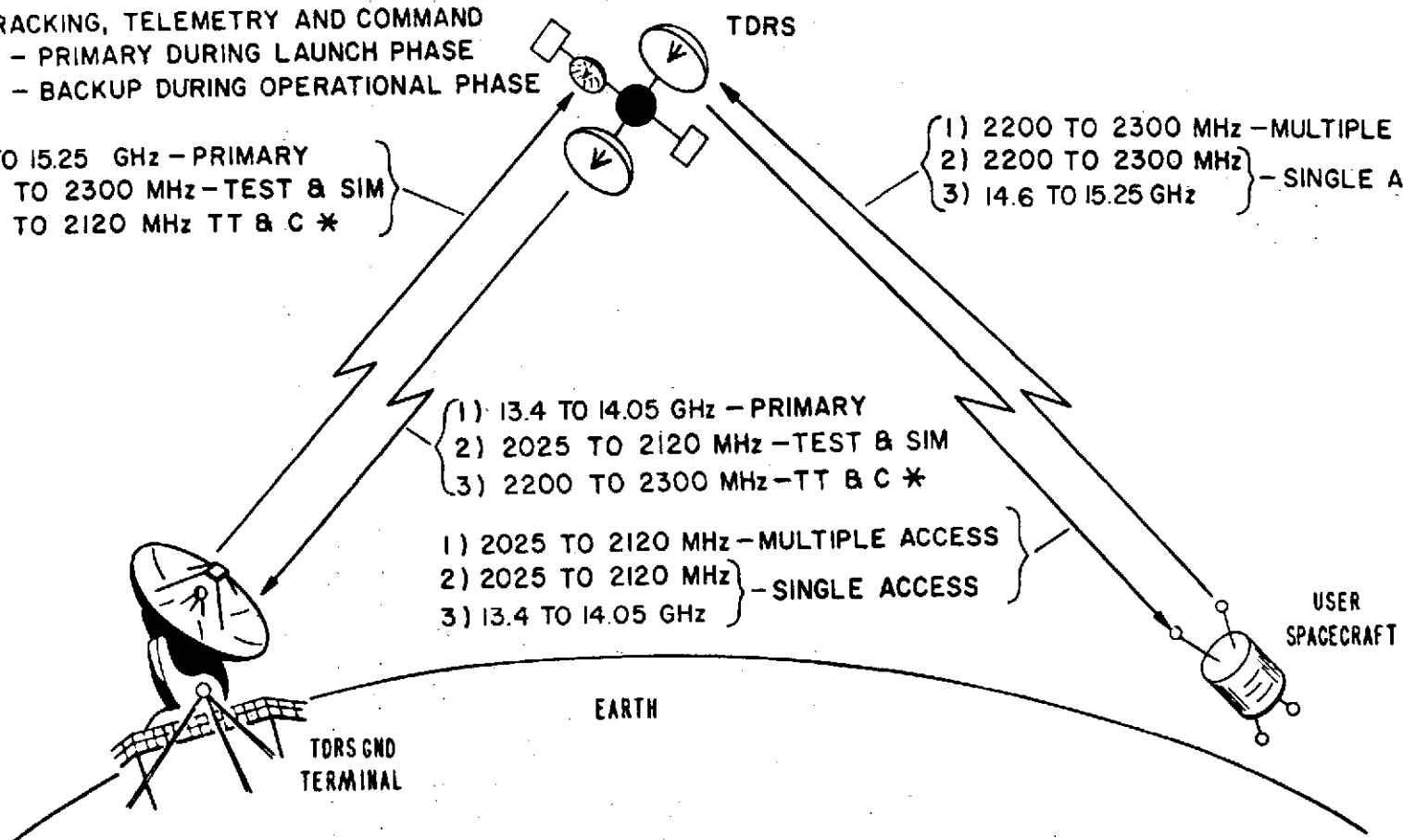


Figure 1-2. TDRSS Coverage, View Normal to TDRS Plane

* TRACKING, TELEMETRY AND COMMAND
- PRIMARY DURING LAUNCH PHASE
- BACKUP DURING OPERATIONAL PHASE

1) 14.6 TO 15.25 GHz - PRIMARY
2) 2200 TO 2300 MHz - TEST & SIM
3) 2025 TO 2120 MHz TT & C *

1) 2200 TO 2300 MHz - MULTIPLE ACCESS
2) 2200 TO 2300 MHz
3) 14.6 TO 15.25 GHz } - SINGLE ACCESS



974-2757
UNCLASSIFIED

Figure 1-3. TDRSS Frequency Plan

1.1 SPREAD SPECTRUM MODULATION

Spread spectrum modulation, generated by a pseudorandom process, is a required technique for TDRS transmissions to users because of limitations imposed on the maximum flux density received on earth in any 4 kHz bandwidth. As an adjunct, spread spectrum enables accurate two-way range and range rate measurement for tracking and orbit determination; this implies spread spectrum on the return link from users as well. Also, spread spectrum discriminates against multipath which can be a problem at S band with users having an omni antenna. Finally, spread spectrum provides processing gain against interfering signals, and this capability is exploited for multiple access operation.

A significant operational "cost" associated with use of spread spectrum is the need for the receiver to acquire synchronization before data can be received. In general, lower received signal-to-noise power density ratios, S/N_o , and higher Doppler offsets produce longer sync acquisition times. Because of the limited duration of time that a user is visible to a TDRS, the objective is to achieve total acquisition times well under one minute. Design of the spread spectrum modulation scheme to be compatible with this acquisition objective has been a primary goal.

1.2 TELECOMMUNICATION SYSTEM PARAMETERS

The purpose of the study has been to perform parametric analyses of the telecommunications support capability of the TDRSS, with the objective of defining the telecommunication system, particularly a user transponder, in greater detail than previously available. The basic system parameters are indicated by the link budgets for the forward and return links. These are, respectively, Tables 1-1 and 1-2.

Table 1-3 lists the minimum spread bandwidths consistent with flux density limitations, for the EIRP values of Table 1-1. For purposes of computing flux density, the signal EIRP is used; this is the EIRP minus the TDRS transponder loss.

Table 1-1. Space-to-space Forward Links

	Multiple-access Link	Single-access Links			
		S-band		Ku-band	
		High	Normal	Normal	High
BER	10^{-5}	10^{-5}	10^{-5}	10^{-5}	10^{-5}
TDRS Antenna Gain (dB)	23.0 (@ $\pm 13^\circ$)	35.4	35.4	52.0	52.0
TDRS T_x Power (dBW)	13.0	14.1	11.5	-3.0	0.5
RF T_x Loss (dB)	-1.0	-2.0	-2.0	-2.0	-2.0
Antenna Pointing Loss (dB)	0	-0.5	-0.5	-0.5	-0.5
EIRP (dBW)	35.0	47.0	44.4	46.5	50.0
Space Loss (dB)	-191.6	-191.6	-191.6	-208.6	-208.6
User Antenna Gain (dB)	G_u	G_u	G_u	G_u	G_u
Polarization Loss (dB)	0	-0.5	-0.5	-0.5	-0.5
P_s Out of User Antenna (dBW)	-156.6	-145.1	-147.7+ G_u	-162.6+ G_u	-159.1+ G_u
T_s (Antenna Output)	824°K	824°K	824°K	710°K	710°K
T_s (dB)	29.2	29.2	29.2	28.5	28.5
KT_s (dBW/Hz)	-199.4	-199.4	-199.4	-200.1	-200.1
P_s/KT_s (dB/Hz)	42.8+ G_u	54.3+ G_u	51.7+ G_u	37.5+ G_u	41.0+ G_u
TDRS Transponder Loss (dB)	-1.0	-1.0	-1.0	-1.0	-1.0
Demod Loss (dB)	-1.5	-1.5	-1.5	-1.5	-1.5
PN Loss (dB)	-1.0	-1.0	-1.0	-1.0	-1.0
Residual Carrier Loss (dB)	0	0	0	-1.0	-1.0
Required E_b/N_0 (Δ PSK)	-9.9	-9.9	-9.9	-9.9	-9.9
System Margin (dB)	-3.0	-3.0	-3.0	-3.0	-3.0
Achievable Data Rate (dB)	26.4+ G_u	37.9+ G_u	35.3+ G_u	20.1+ G_u	23.6+ G_u
FEC Gain, $R = 2, K = 7$	5.2	5.2	5.2	5.2	5.2
Achievable Data Rate (dB)	31.6+ G_u	43.1+ G_u	40.5+ G_u	25.3+ G_u	28.8+ G_u
FEC Gain, $R = 3, K = 7$	5.7	5.7	5.7	5.7	5.7
Achievable Data Rate (dB)	32.1+ G_u	43.6+ G_u	41.0+ G_u	25.8+ G_u	29.3+ G_u
T_s (Ku-band output of antenna)		$ \begin{aligned} &= 253 + 290 (0.6) + T_3 (1.6) + T_{e2} (1.6) (0.03) \\ &= 253 + 193 + 240 + 24 \\ &= 710^\circ \text{ (445° at input to preamp, assumed line loss of 2 dB)} \end{aligned} $			
T_s (S-band output of antenna)		$ \begin{aligned} &= 234 + 290 (0.6) + T_c (1.6) + T_{e2} (1.6) (0.03) \\ &= 234 + 193 + 400 + 16.8 \\ &= 824^\circ \text{ (520° at input of preamplifier, assumed line loss of 2 dB)} \end{aligned} $			

Table 1-2. Space-to-space Return Links

	Multiple-access Link	Single-access Links	
		S-band	Ku-band
BER	10^{-5}	10^{-5}	10^{-5}
User EIRP (dBW)	EIRP	EIRP	EIRP
Space Loss (dB)	-192.2	-192.2	-209.2
Pointing Loss (dB)	-	-0.5	-0.5
Polarization Loss (dB)	-1.0	-0.5	-0.5
TDRS Antenna Gain (dB)	28.0 (@ $\pm 13^\circ$)	36.0	52.6
P_s @ Antenna Output (dBW)	+EIRP	-157.2+EIRP	-157.6+EIRP
T_s (@Antenna Output Term.)	824°K	824°K	710°K
T_i (Other User Interference)	255°K	-	-
$K(T_s + T_i)$ (@Antenna Output Term.) (dB/Hz)	-198.3	-199.4	-200.1
P_s/KT_s (dB/Hz)	33.1+EIRP	42.2+EIRP	42.5+EIRP
TDRS Transponder Loss (dB)	-2.0	-2.0	-2.0
Demod Loss (dB)	-1.5	-1.5	-1.5
PN Loss (dB)	-1.0	0	0
AGIPA Loss (dB)	-0.5	-	-
Residual Carrier Loss (dB)	-	-	-1.0
Required E_b/N_o (dB) (Δ PSK)	-9.9	-9.9	-9.9
System Margin (dB)	-3.0	-3.0	-3.0
Achievable Data Rate (dB)	15.2+EIRP	25.8+EIRP	25.1+EIRP
FEC Gain, $R = 2, K = 7$	5.2	5.2	5.2
Achievable Data Rate (dB)	20.4+EIRP	31.0+EIRP	30.3+EIRP
FEC Gain, $R = 3, K = 7$	5.7	5.7	5.7
Achievable Data Rate (dB)	20.9+EIRP	31.5+EIRP	30.8+EIRP
T_s (Ku-band output of antenna)	= $253 + 290 (0.6 + T_e (1.6) + T_{e2} (1.6) (0.03))$ = $253 + 193 + 240 + 24$ = 710° (445° at input to preamp, assumed line loss of 2 dB)		
T_s (S-band output of antenna)	= $234 + 290 (0.6) + T_e (1.6) + T_{e2} (1.6) (0.03)$ = $234 + 193 + 400 + 16.8$ = 824° (520° at input of preamplifier, assumed line loss of 2 dB)		

Table 1-3. Minimum Spread Bandwidth

	Signal EIRP (DBW)	Flux Density Guide-lines DBW/ $M^2/4\text{ kHz}$	Minimum Spread Bandwidth	Required Chip Rate (1/2 Spread Bandwidth)
MA S-Band	34.0	-154	1.2 MHz	600 K Chips/S
SA S-Band				
Normal Power	43.4	-154	12.0 MHz	6.0 M Chips/S
High Power	46.0	-154	20.0 MHz	10.0 M Chips/S
SA Ku-Band				
Normal Power	45.5	-152	12.0 MHz	6.0 M Chips/S
High Power	49.0	-152	28.0 MHz	14.0 M Chips/S
NOTE				
Minimum Spread Bandwidth (dB = EIRP + 36 - $(4\pi R^2 \text{ in dB})$ - Flux Density).				
Required Chip Rate = 1/2 Minimum Spread Bandwidth.				
$R = \text{Slant Range} = 40,000 \text{ KM}$ ($4\pi R^2 = 163 \text{ dB}$).				

1.3

MULTIPLE ACCESS SYSTEM

Originally, the forward link of the multiple access system had a fixed field of view with coverage as in Figure 1-2 but with 10 dB less EIRP than given in Table 1-1. A user acquired the forward link signal from a TDRS when it became visible, and maintained synchronization until handover to the other TDRS became necessary. Commands were transmitted time sequentially to the users. It is desired to provide service to a user with an omnidirectional antenna, which means a user gain of -3 dB or less. It became apparent that sync

acquisition time would be excessive and the command data could be transmitted too slowly for satisfactory service.

It was decided by NASA Goddard to modify the TDRSS concept to have a steered transmit beam on the multiple access forward link from TDRS. This presumes sufficiently accurate user ephemeris data is available; however, this is already the case for pointing the receive beam on the TDRS towards the user so that AGIPA adaptation could be initiated. The steered beam has EIRP increased by 10 dB, reducing acquisition time and enabling commands to users with poor antennas. A minimum command data rate of approximately 100 bps is now feasible to such users. Two-way coherent range and range rate measurements can be extracted only when the forward link is established.

Data rates on the return spread spectrum signal from a user can range up to 50 Kbps, and rate -1/2 error correction coding sets the maximum symbol rate at 100 Kbps. Higher data rates can be considered as an objective, as compatible with the assumed maximum user EIRP of 35 dBW. Return link performance for a given multiple access user is affected by the interference from other users within the receive beam (and not nulled out by AGIPA adaptation).

It has typically been assumed in the following analyses that the return link of a multiple access user is not initiated except by a command sent over the forward link. However, some users may have a special requirement of being able to transmit return telemetry data without a forward link. A "short code" spread spectrum modulation is suggested to meet this special requirement.

1.4 S-BAND SINGLE ACCESS

Compared with the multiple access system, the S-band single access system is characterized by higher S/N_0 values due to the gain of a dish antenna on the TDRS. Thus, sync acquisition on the forward link is less of a problem than with the multiple access system, although command data rates for single access service are not higher than for multiple access.

The return link may have telemetry data rates in the range from 100 bps up to 5 Mbps. It is assumed that error correction coding is utilized at all data rates with spread spectrum for the lower rates. A user with a dish antenna for high EIRP to support a high telemetry rate may have to autotrack on the forward link spread spectrum signal. However, it is assumed that the TDRS can steer its dish with sufficient accuracy by ground command for S-band operation.

1.5

Ku-BAND SINGLE ACCESS

The Ku-band single access system is intended to handle high return telemetry data rates from 1 Mbps to 300 Mbps without spread spectrum. A forward link Ku-band transmission, which must be spread spectrum to satisfy the flux density limitation, is needed to enable the user to autotrack his directive antenna. Also, the TDRS must autotrack its antenna, since ground commanded pointing is not sufficiently accurate for Ku-band operation.

A special problem of the Ku-band single access service is the limiting which must occur in the TDRS transponding channel because of the high power needed to support the TDRS-to-ground link. It is also desired to be able to reuse the Ku-band frequency allocation by polarization multiplexing two wide bandwidth return channels.

1.6

RANGE AND RANGE RATE MEASUREMENT

Two-way coherent range is obtained by measuring the round-trip propagation delay. With spread spectrum modulation, this is equivalent to comparing the respective instants at which a reference time marker (pseudorandom code phase) is transmitted to the user and received back from the user. An ambiguity in one-way range not less than 10,000 Km is desired by NASA. The required measurement accuracy is 6m systematic error and 2m random error (1σ).

Two-way coherent range rate is obtained by measuring carrier Doppler over a specified averaging interval. This process is independent of the spread spectrum modulation, provided that the receivers can reconstitute carrier phase. The Doppler measurement is the change in carrier phase on the return signal, relative to the transmit signal, accumulated over the averaging interval. The required measurement accuracy is zero systematic error and a random error (1σ) of 0.6 cm/sec for one second averaging and 0.05 cm/sec for 10 seconds averaging.

The uncertainty at the ground station in range is ± 50 Km and in range-rate is ± 100 m/sec, according to NASA Goddard. These uncertainty bounds can be exploited to aid in the process sync acquisition.

1.7

SUMMARY

The following sections provide detailed analyses of the telecommunication services of the various systems, and define the user transponders and critical portions of the TDRS and the ground station equipments. This is in compliance with the Phase I goal of the study:

a. Perform a detailed analysis of the TDRSS as presently defined to verify its compatibility with desired performance objectives.

b. Determine potential changes in system configuration to improve overall performance without major redesign of the TDRS or TDRSS ground terminal equipment.

c. Perform parametric analyses of those system variables that impact telecommunications performance capability and recommend parameter selection as appropriate.

d. Define the TDRS telecommunication system characteristics (including user spacecraft communications terminal) in greater detail than currently established for use as specifications for hardware procurement or such equipment.

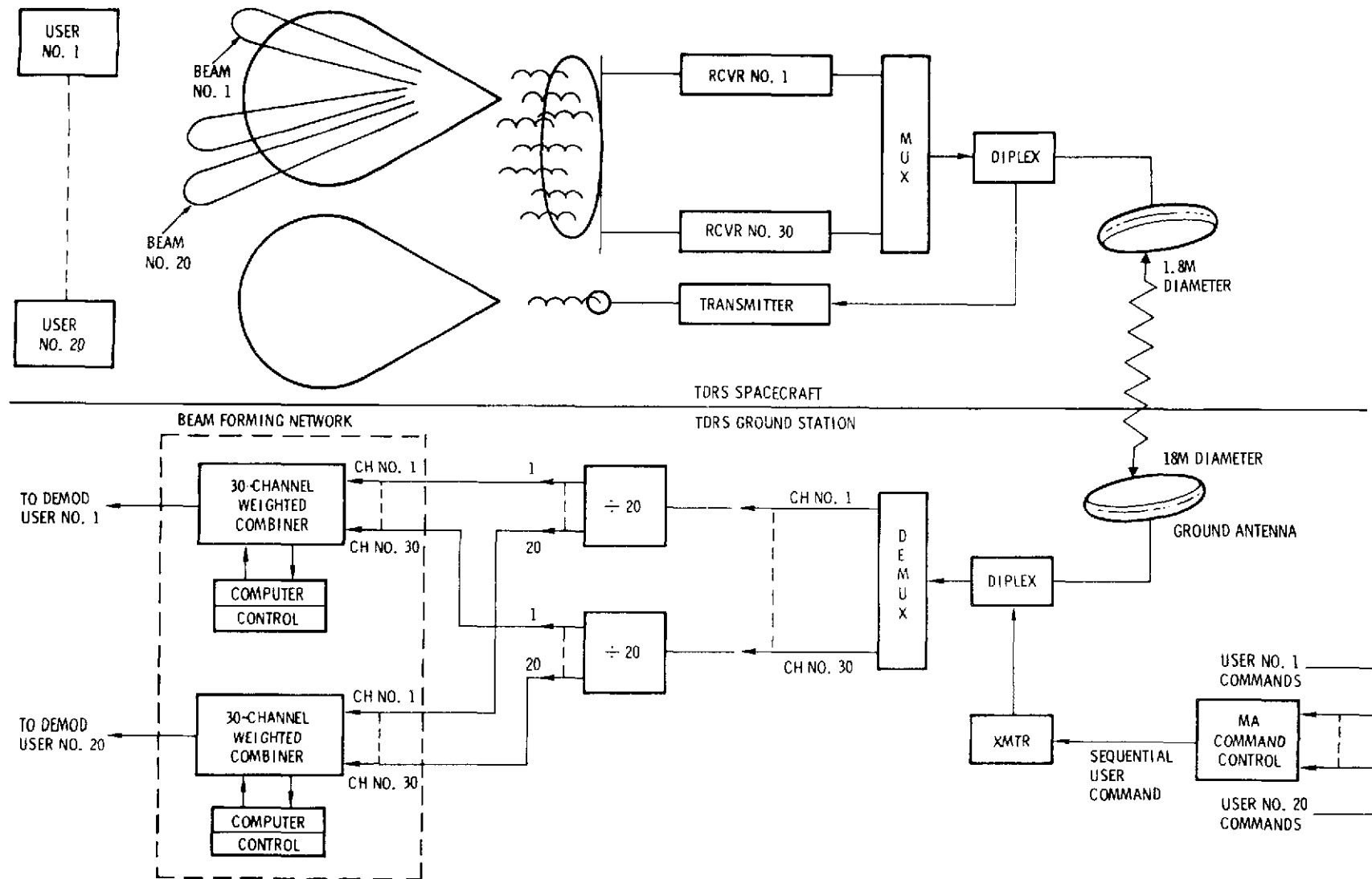
SECTION II MULTIPLE ACCESS SERVICE

The multiple access system provides service to as many as 20 simultaneous users, with time sequential commands on the forward link and multiple access of telemetry in a common return link channel at S-band. Two versions of the multiple access system have been defined by NASA Goddard.

The original system has a fixed field of view (FFOV) on the forward link, as shown in Figure 2-1, but forms multiple directive receive beams via the AGIPA. There are 30 receive antenna elements, and the individual signals are frequency division multiplexed in TDRS for re-transmission to the ground station, where they are combined to produce a directive beam. *A priori* information sufficient to point the beam to the user is assumed available at the ground station. AGIPA attempts to optimize the ratio of signal power (from a selected user) to total interference power (spread spectrum interference from other users plus receiver noise) by adapting the weightings in the beam forming combiner (with a version of a steepest descent algorithm to reduce error in the summed output).

The revised system has a steered transmit beam on the forward link, as indicated in Figure 2-2, controlled by phasing of the transmit antenna elements. The same information used by the ground station for directing the receive beams of AGIPA is needed to steer the transmit beam. Compared with the FFOV system, the steered beam system has a greater command data rate by virtue of 10 dB higher EIRP from the TDRS.

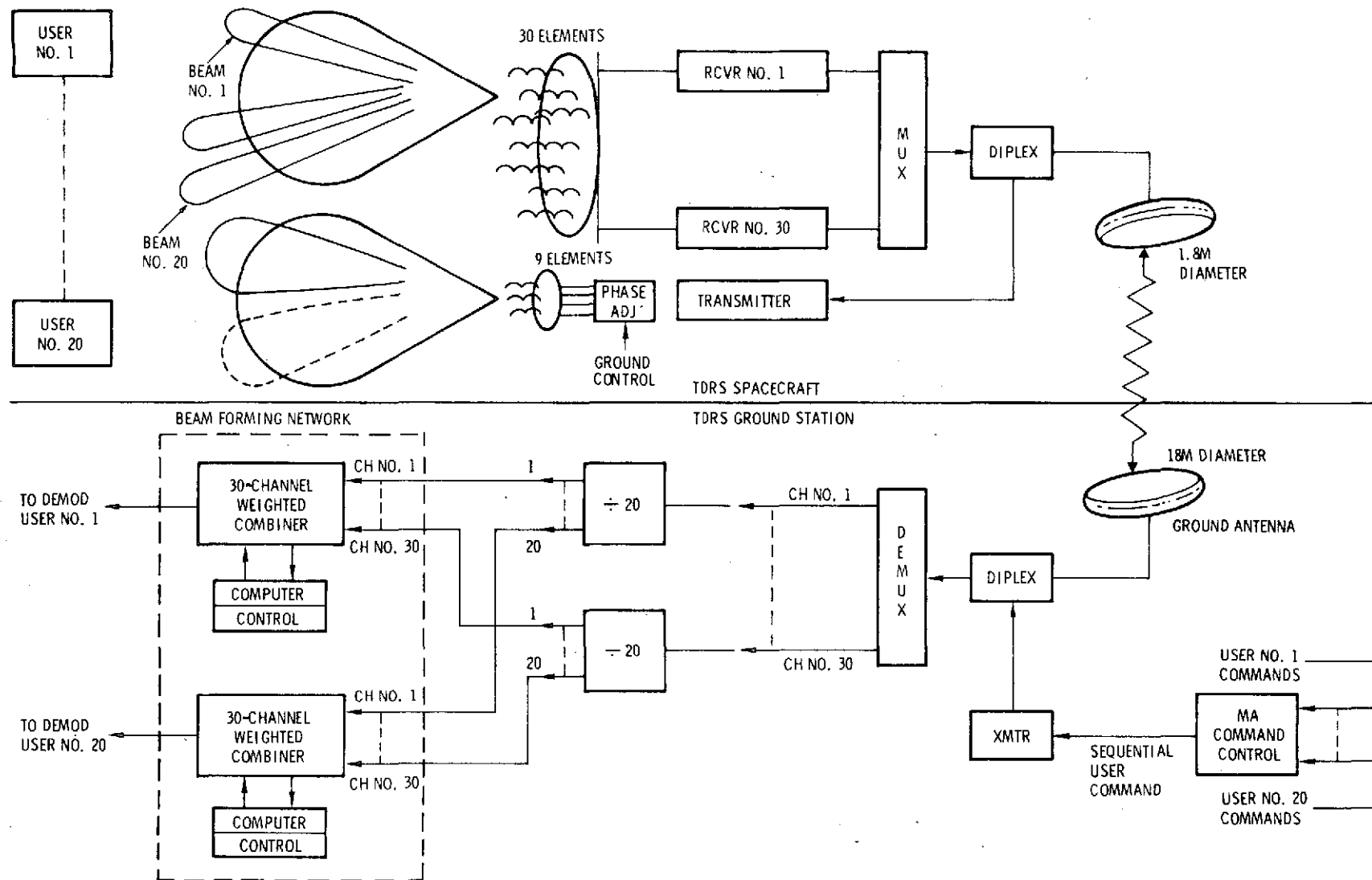
There is a significant operational difference between the two multiple access systems. In the FFOV system, the TDRS transmits a spread spectrum signal which can be acquired by all multiple access users as they come into view of the TDRS. Command data is time sequential, but all users track the forward link signal continually. Thus, two-way range and range rate measurements are continually available for each user. One of the problem areas leading to the abandonment of the FFOV system and introducing the additional complexity on TDRS to form a steered transmit beam is meeting the acquisition requirement when a user can have a poor antenna (-3 dB gain).



974-2758
UNCLASSIFIED

3/22/74-16-LFD
GSFC/TDRSS

Figure 2-1. Adaptive Ground Implemented Phased Array with Fixed FOV MA Command



974-2759
UNCLASSIFIED

3/22/75-17-LFT
GSFC/TDRSS

Figure 2-2. Adaptive Ground Implemented Phased Array with Steered MA Command Beam

The steered transmit beam system yields two-way range and range rate measurements intermittently, only when the forward link is established. Reacquisition is involved whenever a command is to be transmitted to a different user. However, the fact that the signal is to be acquired and tracked only by the designated user allows a spread spectrum signal design which aids acquisition and simplifies the user receiver. In particular, the ground station can take advantage of user orbit information to predict Doppler, and can transmit a special sync preamble.

A possible source of interference to the multiple access system, and also to the S-band single access system, is RFI due to surveillance ground radars located in Eastern Europe. This interference has been studied by ESL⁽¹⁾. It is characterized by pulses from an aggregate of transmitters. The pulses are present about 5 percent of time, and the interval between pulses is random with a mean time of about 75 microseconds. In general, the pulses are received from sidelobes on the transmitting radars. The communications designs have not been necessarily optimized to combat this pulsed interference; however, at low data rates, the interference is ineffective because of its low duty factor. At high data rates (particularly for the return links to TDRS) bursts of errors could be the consequence.

1. J. D. Lyttle, Preliminary Assessment of RFI Impacts on TDRSS in the 2 to 2.3 GHz Band, ESL, Inc., Contract NAS5-20406, 10 May 1974.

2.1

MODULATION TRADEOFFS

We begin with the study of the multiple access system because it presented the most stringent design problems, due to the low S/N_0 values for the communication links. At the outset, we describe spread spectrum modulation in some detail, bringing in desirable alternatives to the familiar pseudorandom biphase structure.

2.1.1

SPREAD SPECTRUM MODULATION TECHNIQUES

The use of pseudonoise (PN) modulation for multiple access in the TDRSS provides interference resistance, multipath discrimination, low emission flux density per unit bandwidth, and a ranging capability as well. Spread spectrum by frequency hopping (FH) can also provide these capabilities and yield essentially the same ranging accuracy. To do this, however, the hopping must be coherent over the spread bandwidth i.e., transmitter and receiver must maintain a constant phase difference as the frequency is switched from channel to channel within the overall spread bandwidth.

The primary advantage of FH compared with PN, and the reason for studying it here, is that the hopping rate is slow compared with the total spread bandwidth. A typical design would hop at a rate equal to the channel spacing, which is the total bandwidth divided by the number of channels. The consequence of this is an inherent advantage of FH with respect to acquisition of synchronization, compared with PN having the same spread. An additional advantage of FH over PN for multiple access is its ability to tolerate larger power ratios between the accessing signals, because frequency selectivity in the receiver eliminates mutual interference unless the frequency channels are close.

As developed in the following paragraphs, FH will be primarily applied as an acquisition aiding scheme for PN. In such an application, coherent hopping is not exploited, and the hopping rate is not forced to be equal to the channel spacing. This enables flexibility in selecting the FH waveform parameters.

2.1.1.1

Staggered Quadriphase PN (SQPN)

It is desirable to employ a hard-limiting transmitter for maximum power efficiency of class-C operation. With biphase PN, and also conventional

quadriphase PN, an attempt to reduce the out-of-band spectrum via sharp cutoff filtering is defeated by the hard limiter, which restores the spectrum due to the sudden 180° phase switches. However, with staggered quadriphase PN (SQPN), the phase is never allowed to change by more than 90° at any switching time. That is, a shift of 180° is done with two 90° switches spaced by a half chip. Consequently, filtering produces smooth phase transitions without the envelope momentarily going to zero as would be the case with sudden 180° phase shifts, and hard limiting no longer restores the original spectrum.

2.1.1.2 Optimization of Bandwidth for SQPN

We desire to optimize the filter bandwidth and the filter skirt steepness (number of poles) so as to reduce the transmitter's out-of-band spectrum level as much as possible. Figure 2-3 shows the idealized model of the hard-limiting transmitter. It may easily be shown that the usual $(\sin x/x)^2$ spectrum is obtained with quadriphase from periodic PN codes if PN code 2 is identical with PN code 1 but displaced by exactly half the period. Since a maximal-length PN code from an n -stage generator has a period = $2^n - 1$, which is odd, staggered quadriphase with exactly the same $(\sin x/x)^2$ spectrum as for biphase is obtained in this way.

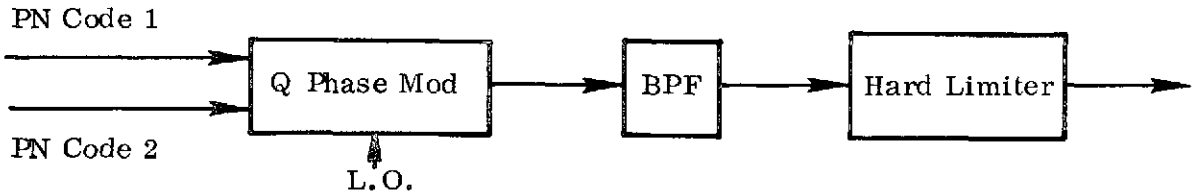


Figure 2-3. SQPN Transmitter

Mathematically, the model of Figure 2-3 is represented for analysis by choosing a sampling rate to yield a time-discrete approximation. Complex samples represent the envelope and phase modulation of the signal, so that the carrier frequency is not a necessary part of the representation. The filter is a low pass version of the desired bandpass transfer function, and a maximally-flat response is obtained via a digital filter which is the z-transform of the Butterworth

transfer function. The ideal bandpass hard limiter is represented simply by normalizing each complex sample to unit amplitude without changing its phase. Then, a Fast Fourier Transform (FFT) is applied to obtain the spectrum of the periodic signal. Start-up transients are allowed to decay initially.

Previous studies have sampled the code period with 2^k samples so as to be compatible with the usual FFT algorithms available in computer subroutine libraries^(2, 3). Since a maximal code has period $2^n - 1$, the location of the sampling times is then slightly different in each chip. This conceivably may affect the spectral values computed. For this reason, a special FFT algorithm applicable to any number of samples in a period was made available. (The transform computation of this FFT algorithm is faster if the number of points to be transformed is highly factorable, with 2^k being the fastest.)

In the analysis, a maximal period $63 = 2^6 - 1$ was employed, with 16 samples per chip so that the FFT algorithm transformed $63 \times 16 = 1008$ points. Note that $1008 = 2^4 \times 3^2 \times 7$, which has many factors. The cases studied included filters with 2, 4, 6, 8, and 10 poles*, and bandpass bandwidths = 1.0, 1.5, and 2.0 times the PN chip rate. With 16 samples per chip, the maximum frequency in the spectrum is 8 times the chip rate before aliasing occurs**. The spectral peaks for each filter bandwidth are plotted in Figures 2-4 to 2-6, for the number of poles yielding the best out-of-band spectrum reduction. With BW/chip rate = 2.0, 10 poles gives a slightly faster cutoff than 8 poles. With narrower bandwidths, an optimum number of poles is observed. For BW/chip rate = 1.5, 4 and 6 poles give the same spectral peaks, while for BW/chip rate = 1.0, 4 poles is optimum. (With 4 poles, results are very similar to those in references 2 and 3.)

* These are the number of poles in the low-pass equivalent.

** Aliasing is noticed near the edge of the frequency range plotted in that the unfiltered spectral level is 3 dB higher than theoretical.

2. DSCS Advanced Modulation System Study - Part II, Vol. IV, Magnavox, Contract No. DAAB-07-69-C-0344, 30 June 1970.
3. S. A. Rhodes, "Effects of Hardlimiting on Bandlimited Transmissions with Conventional and Offset QPSK Modulation", National Telemetering Conference, 1972, p. 20F-1.

The striking conclusion of this study is that the out-of-band spectrum reduction which can be achieved for a hard limited SQPN signal is essentially independent of the filter bandwidth (over the range examined) introduced prior to the limiter. That is, when the skirt steepness of the filter (controlled by the number of poles in a Butterworth transfer function) is optimized, the resulting out-of-band spectrum after hard-limiting is observed to be essentially independent of the 3- dB bandwidth of the filter. Presumably, there is a basic physical principle involved here which lower bounds the out-of-band spectrum level of a hard-limited signal.

The antijam or interference rejection capability is not independent of bandwidth, however. This capability may be measured by the power contained in the highest level spectral line, since the transmitted power is fixed by the hard limiter*. This peak level relative to the unfiltered case is marked in Figures 2-4 to 2-6 as "AJ loss". Thus, a wider filter bandwidth yields a lower AJ loss, and with steeper skirts (more poles) still realizes a low out-of-band spectrum level.

The optimum transmitter filter thus has a bandpass bandwidth (3- dB) approximately equal to 1.5 times the PN chip rate, and can have 4 to 6 poles. The spectral level is down by more than 20 dB outside a bandpass bandwidth equal to twice the PN chip rate.

* Here, we invoke the correlation property that the output noise spectrum is the convolution between signal spectrum and interference spectrum. The latter is narrow band at the peak of the signal spectrum.

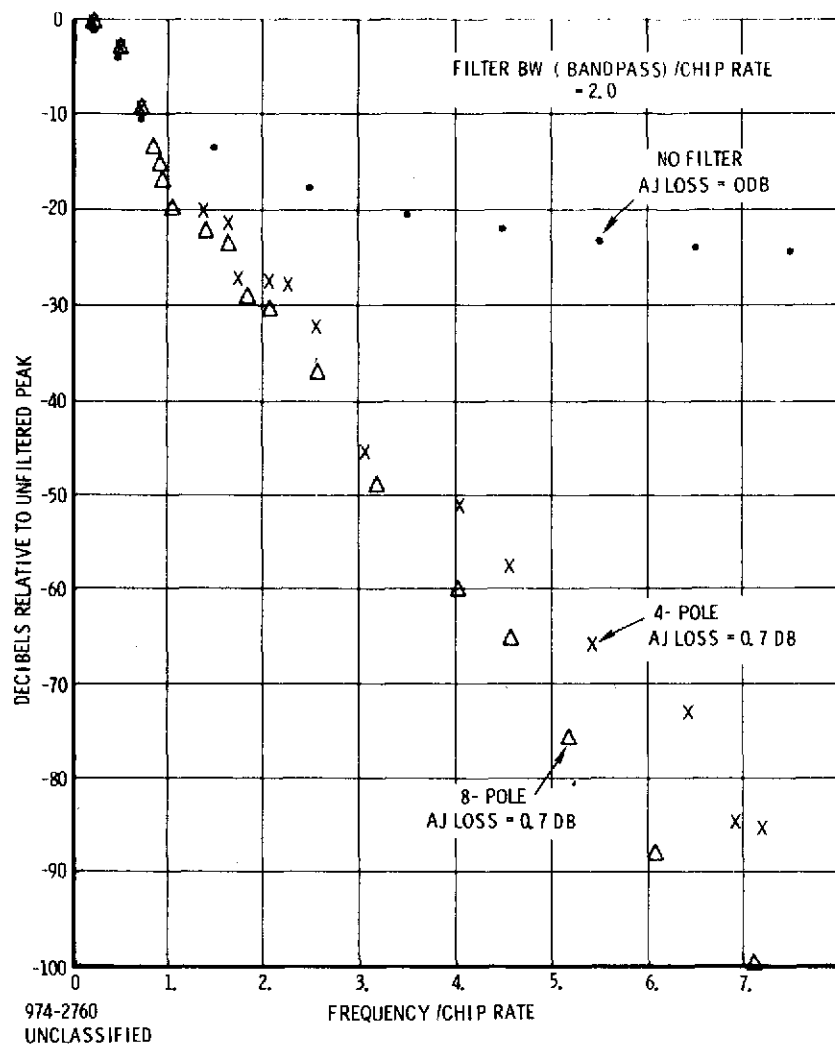


Figure 2-4. Plot of Spectral Peaks with Filter BW (Bandpass)/Chip Rate = 2.0

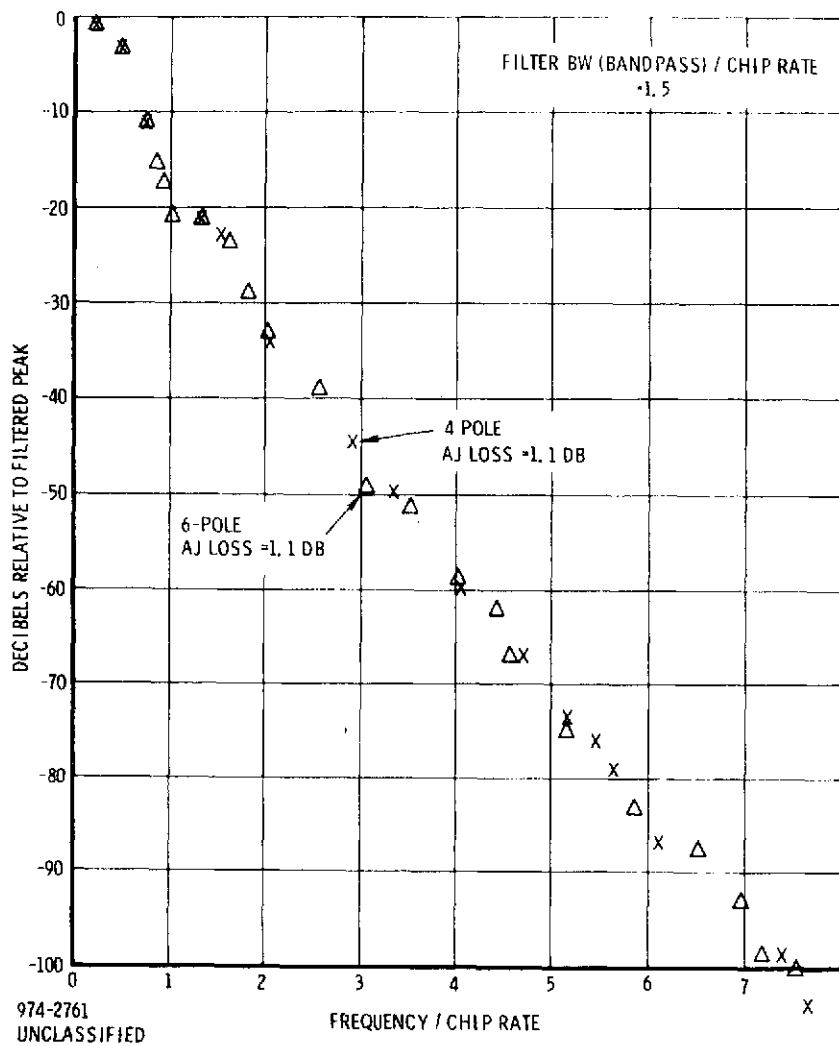


Figure 2-5. Plot of Spectral Peaks with Filter BW(Bandwidth)/Chip Rate = 1.5

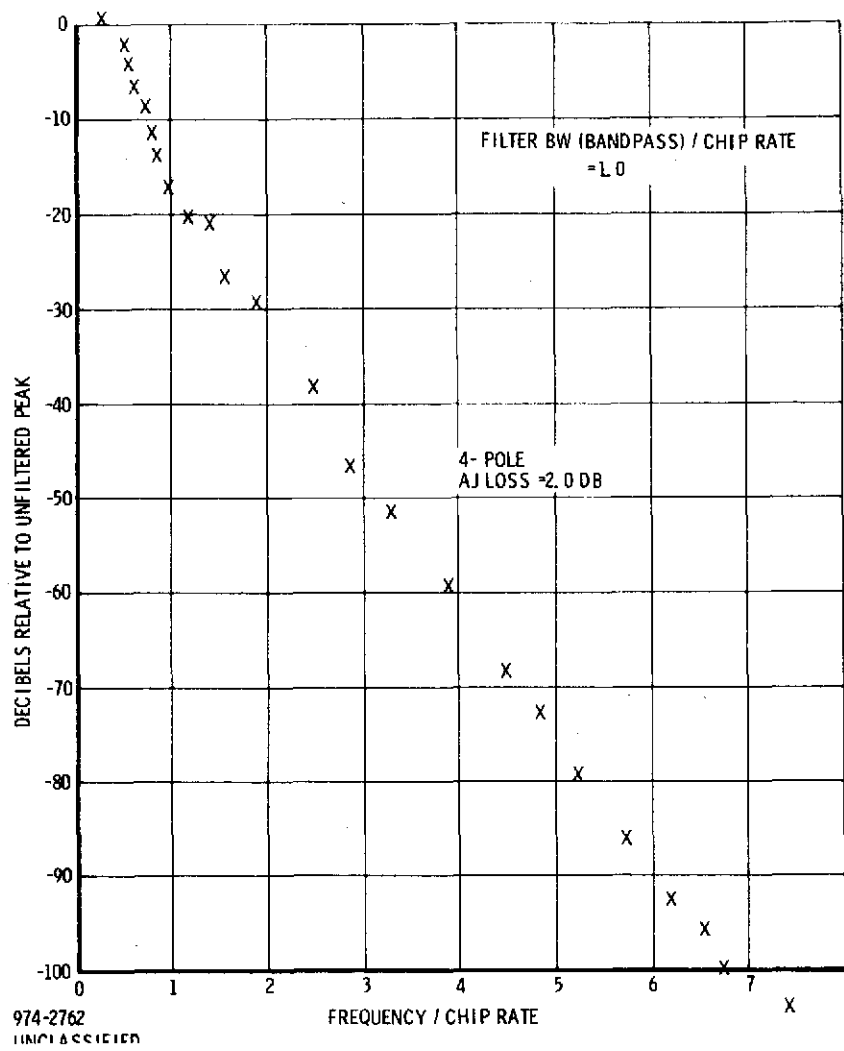


Figure 2-6. Plot of Spectral Peaks with Filter BW (Bandpass)/Chip Rate = 1.0

Now, let us examine the effect of a finite bandwidth filter in the receiver prior to correlation. At this time, we treat the case of an idealized sharp cutoff filter with linear phase, recognizing that phase distortion in a practical filter produces additional degradation as discussed in Appendix I. Cutoff of the received signal spectrum outside a specified bandwidth causes a loss of correlation amplitude, and this can be computed by numerical integration of the power in the spectral lines of the transmitted signal*.

If the interference in the receiver is white noise which is filtered by the receive filter, the output interference power after correlation is computed by summing the power in the spectral lines within the receive bandpass*. Numerically, this is identical with the loss of correlation amplitude. Thus,

$$S/N = \frac{(\text{Correlation Amplitude})^2}{\text{Output Power}} \quad (2-1)$$

with the consequence that for white noise interference

$$S/N \text{ Loss} = \text{Reduction in Correlation Amplitude} \quad (2-2)$$

This is plotted in Figure 2-7 for the recommended transmit filter (Bandpass/chip rate = 1.5).

If the interference in the receiver is CW, there is no change in output interference power due to receiver filtering as long as the CW stays within the receiver bandwidth. Thus, the effect of receiver filtering is to produce an additional AJ loss, according to

$$AJ \text{ Loss} = (\text{Reduction in Correlation Amplitude})^2 \quad (2-3)$$

This is also plotted in Figure 2-7.

* Amplitude in the correlator output is the sum of the line-by-line multiplication of received spectrum with local reference spectrum; hence, one must sum power to compute correlation amplitude. The output interference is also computed as a power sum, but then the result is power rather than amplitude.

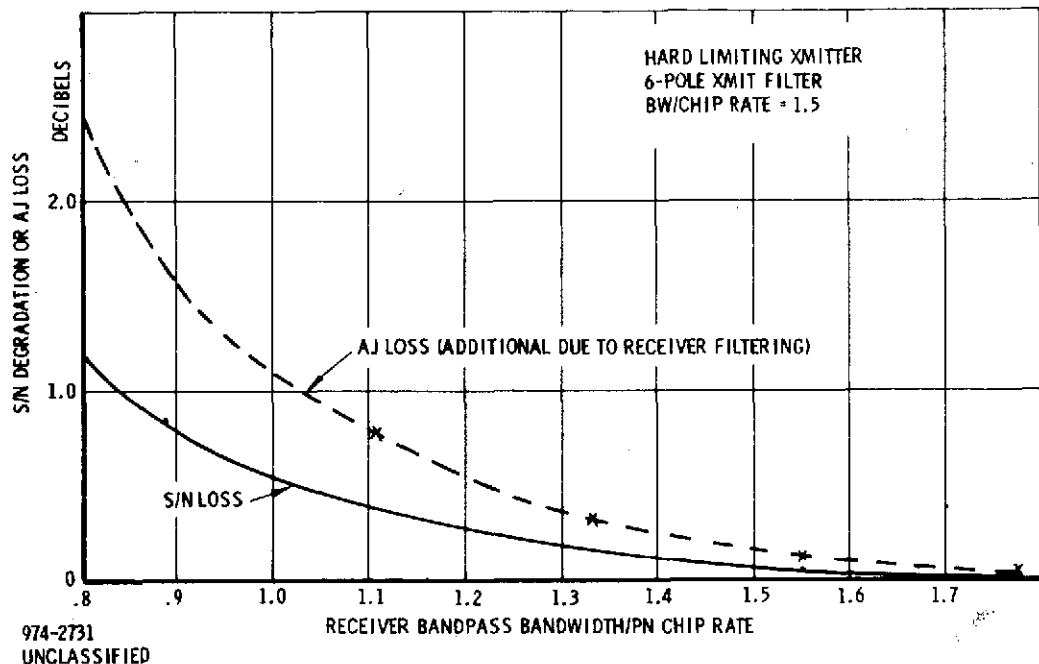


Figure 2-7. Correlation Loss With Sharp Cutoff Receive Filter

It may be concluded that the receiver bandpass can be as narrow as the PN chip rate before significant loss due to receiver filtering is encountered. If the receive bandpass/chip rate = 1.5, the loss is negligible.

2.1.1.3 A Simple Technique for Coherent Frequency Hopping

The practical success of a system incorporating frequency hopping obviously depends on finding a simple implementation of the hopper. One scheme is described here and is based on use of a rate multiplier in combination with discrete

phase modulation. It produces coherent frequency hopping*, and is useful provided that low spurious is not an essential requirement, and indeed, such is the case for the proposed application. The phase coherence is not necessarily exploited.

The basic concept is to generate the desired frequency by approximating it with discrete 90° steps at a prescribed clocking rate. Thus, the modulation overtly is identical with staggered quadriphase PN at half the prescribed clocking rate. The approximation produces spurious due to both the discrete phase steps and the slightly irregular spacing of the instants at which steps occur. Note that 4 steps are required to produce a full cycle of phase change; hence, a spectrum occupancy of B Hz ($\pm B/2$ Hz from the center of the band) requires a clocking rate of $2B$. This is identical to staggered quadriphase at a PN chip rate B .

The conceptual implementation of the coherent hopper based on a rate multiplier driving a quadriphase PN modulator is shown in Figure 2-8. The selected frequency is stored in the n -bit register, and the sign (above or below band center) is selected by the direction of phase rotation. At each clocking instant, the n -bit number in the register is parallel added to the n -bit number in the accumulator. If the sum exceeds $2^n - 1$, overflow occurs, and the overflow bit causes a single 90° phase step. The sum modulo 2^n remains in the accumulator.

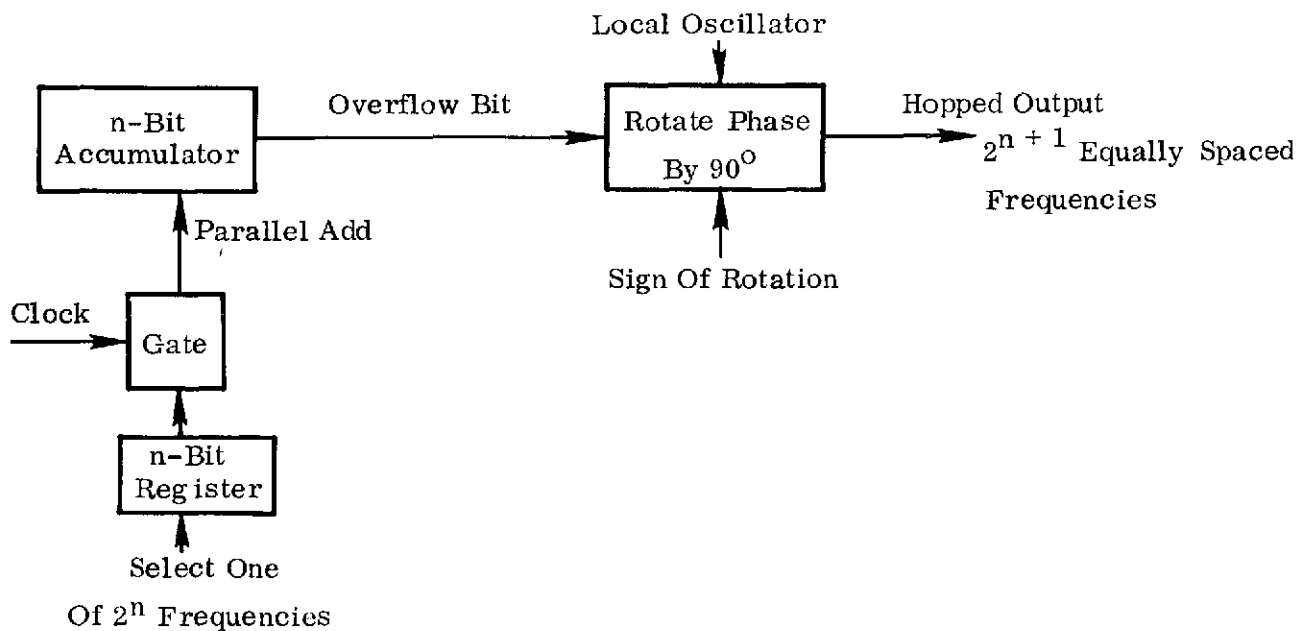


Figure 2-8. Coherent Frequency Hopping by Rate Multiplier and Quadriphase Modulator.

* Coherent frequency hopping is defined to mean that transmitter and receiver maintain a constant phase difference as the hopping takes place.

A computer analysis of this scheme for $n = 10$, thus generating 2048 equally spaced frequencies, showed that the desired frequency component, regardless of frequency selected, is at most 0.9 dB below full output. In other words, the spurious is at most 19 percent of total output, or 23 percent of the desired output frequency component.

It is seen from the generation scheme that transmitter and receiver are coherent exactly as with PN, when the time error is within the clocking interval. When the time error exceeds the clocking interval but is small compared with the dwell on one frequency, the phase difference (correlation) between the received signal and the local replica varies discretely between 0° and 90° , in accordance with the actual switching points. Thus, there is a phase modulated output at zero frequency difference, and at most a loss of 3 dB can occur in the worst case where 0° and 90° occur equally often in the difference output.

An extension of the digital hopping principle is to employ finer quantization of phase. For instance, with an eight-phase modulator, the clock rate would be doubled, but with the benefit of reduced spurious because of the 45° steps, rather than 90° . Implementation is more complex, however.

2.1.1.4 Autocorrelation Function of Coherent FH Signal

A computation of the autocorrelation function of the coherent FH signal generated by the technique of Figure 2-8 with 90° steps was made for periods of 16 and 256 frequencies. A pseudorandom sequence of frequencies was generated* symmetrically placed with respect to center frequency at $\pm .5, 1.5 \dots$, times the hopping rate.

The auto- and cross-correlation functions were computed by use of the Fast Fourier Transform. (The signal is transformed, then an inverse transform is taken on the product in the frequency domain.) For 16 frequencies, the error voltage defined by the in-phase component of the correlation and the magnitude of the autocorrelation is shown in Figure 2-9 for time offsets in the vicinity of $\tau = 0$. (The autocorrelation peak at $\tau = 0$ is unity, of course.) Possible false tracking points in a coherent hopping system, as discussed in more detail in Appendix II, are indicated; however, note that the correlation amplitude at these points is at least 20 dB below the autocorrelation peak.

*The primitive root technique described in Paragraph 2.1.7.2 was used.

974-2764
UNCLASSIFIED

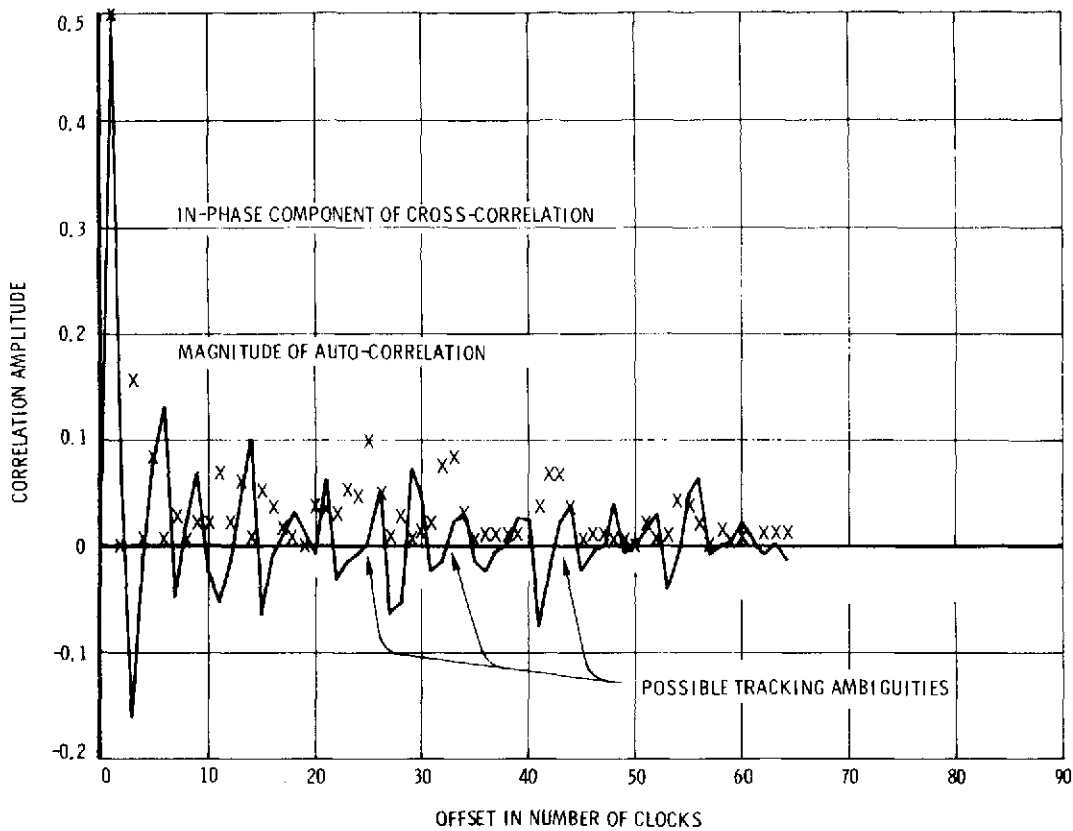


Figure 2-9. Auto- and Cross-Correlation for Coherent FW With 16 Frequencies in Period, 32 Clocks per Dwell - Period = 2^9 Clocks.

With 256 frequencies, only the autocorrelation function was computed, and a plot in the vicinity of $\tau = 0$ is shown in Figure 2-10. The autocorrelation function is well behaved, and if delay-lock tracking is done with an early-late error voltage, a tracking ambiguity exists within a single hop dwell only when the correlation amplitude is very small (roughly 40 dB below the autocorrelation peak). In checking the complete autocorrelation function, a secondary peak only 30 dB down was noted for a shift of 18 frequency hops. This normally would not be detected.

2.1.2 FIXED FIELD OF VIEW FORWARD LINK

We consider first the original multiple access system with a fixed field of view on the forward link. Application of spread spectrum requires a signal

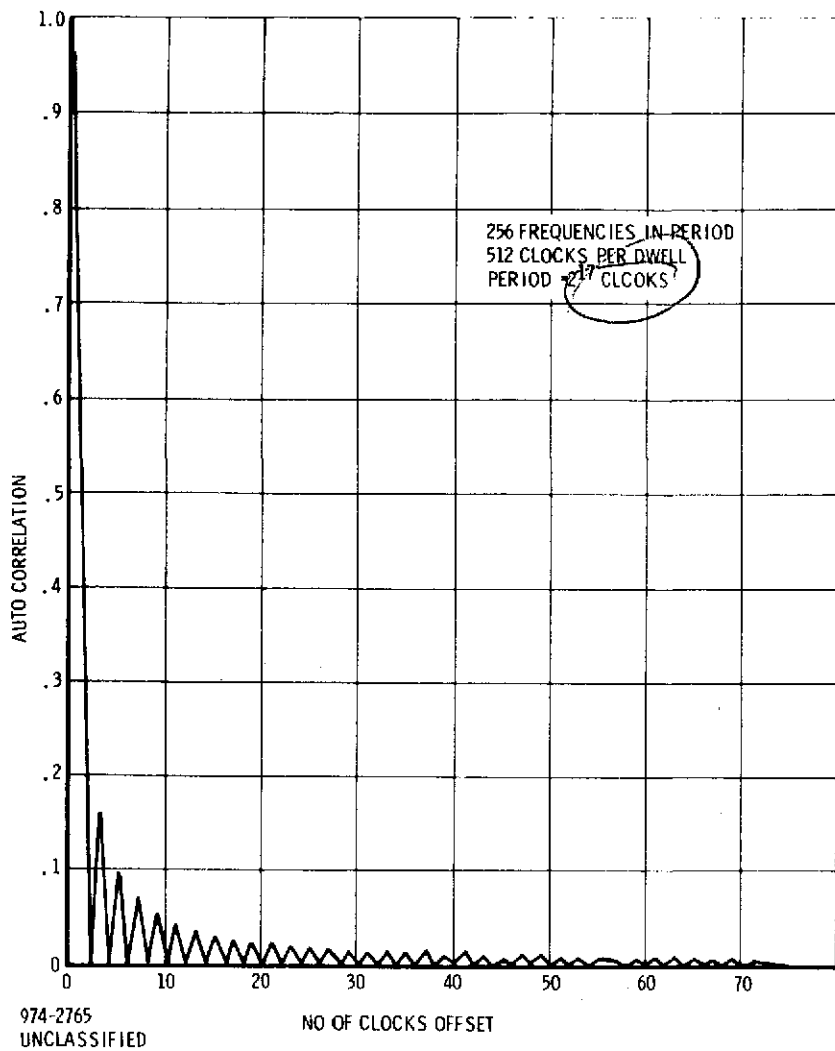


Figure 2-10. Auto Correlation Function of Coherent FH Signal

design which can be acquired rapidly by a user satellite as it comes into view, without preventing other users from continuing to track the signal.

2.1.2.1 Pseudonoise Design

The problem involved with a straight forward application of PN on the forward link is now discussed. Using Table 1-1 (subtracting 10 dB of EIRP) and orbital velocity of a user satellite, the pertinent parameters (not including the demod loss and the PN loss) are:

Forward Link (TDRSS to User)

$$S/N_o = 28.7 \text{ dB} + G_u$$

Doppler = 26 ppm

Carrier Frequency = 2.1064 GHz

A user gain G_u of -3dB, or even lower, might be encountered. Thus, on the forward link, S/N_0 may be as low as 25.7 dB-Hz for a disadvantaged user, corresponding to a data rate of 20 bps for uncoded PSK (after taking into consideration further demodulation losses of 2.5 dB).

As shown in Figure 3 of Appendix III, a maximum search rate of roughly 20 chips/sec is possible at this S/N_0 ; however, note that Doppler causes an offset on the PN chip rate of as much as 78 chips/sec (for a PN chip rate of 3 Mbps) and a carrier offset as high as 55 kHz. It is necessary to break up the total Doppler uncertainty to at least 10 sub-bands in order to make the Doppler on the chip rate significantly lower than the search rate (say 8 chips/sec). This is necessary even if a Doppler processor is incorporated in the user receiver to create a multiple filter bank for sync detection over the total Doppler uncertainty on the carrier.

Using a code period of 1023 chips (340 microsec period at 3 Mbps chip rate) and a search rate of 20 chips/sec, the acquisition time for PN is estimated to be

$$T_s = 10 \times 1023/20 \cong 500 \text{ seconds}$$

with a Doppler processor breaking up each of the ten 5.5 KHz sub-bands into, roughly, a multiple filter bank of 20 Hz filters.

The above PN design is almost at the limit due to rate of change of carrier Doppler. If we assume a worst case acceleration of $1g = 32 \text{ ft/sec}^2$, the velocity changes by 1600 ft/sec^2 in 50 seconds, and the carrier Doppler changes by 3 KHz, almost the width of the sub-band. With a faster rate of change of Doppler, sync detection could be missed even though the sub-bands are tested in sequence.

The above PN design does not satisfy a requirement for protection against multipath, in the sense that the TDRSS geometry on the forward link is such that the multipath replica could have a delay approaching 12 milliseconds (2000 Km user altitude). Increasing the PN code period to eliminate possibility of false lock on multipath would proportionately increase acquisition time, which is already unacceptable, unless this is done by reducing the PN chip rate.

Thus, we seek alternate design approaches. It may be noted that the minimum bandwidth occupancy is determined in Table 1-3 to be 320 kHz. Thus, a PN chip rate of 160 Kbps is about the minimum which can be used on the forward link.

More acceptable acquisition times are obtained if the user has a higher gain. For instance, assume $G_u = +7$ dB so that $S/N_0 = 35.7$ dB-Hz. Now, the search rate can be 200 chips/sec, and the Doppler processor establishes a multiple filter bank of 200 Hz filters. If the Doppler processor can cover the full Doppler uncertainty without sub-bands, the acquisition time for a code period of 1023 chips is

$$T_s = 1023/200 \cong 5 \text{ seconds}$$

The significant impact of decreasing S/N_0 value is evident. However, at 300 Kbps, the PN code period is only 3 millisec, and a period of 12 millisec corresponding to 4095 chips would be preferable to eliminate false acquisition on a multipath-delayed replica. Furthermore, if we find that the Doppler processor with reasonable hardware complexity exploiting high speed logic can only cover about 5 kHz with 200 Hz filters, 10 sub-bands are required. The acquisition time is now computed to be

$$T_s = 10 \times 4095/20 \cong 200 \text{ seconds}$$

which again is unacceptable even at the higher S/N_0 value assumed. Implementation of the Doppler Processor is discussed in Appendix IV and V.

2.1.2.2 A Coherent Frequency Hop Design

Let us now postulate a multiple access system based on coherent frequency hopping. The hopping rate is 2000 per second and there are 256 channels on the forward link for a spread bandwidth of 500 kHz. (Channel spacing is 2 kHz equal to the hopping rate.) A code hopping over all 256 channels in a pseudorandom sequence has a period of 128 milliseconds. Initially, coarse synchronization to the hopping pattern is desired. A subsequent process of fine synchronization ultimately gives time of arrival to an accuracy proportional to reciprocal of total bandwidth. Thus, synchronization is a two-mode process with this modulation concept.

At $S/N_O = 35.7$ dB-Hz on the forward link, assuming $G_u = +7$ dB, the E/N_O per hop is 3.7 dB and coarse synchronization could be detected reliably by noncoherent integration over roughly 20 hops, or 10 milliseconds*. Searching over the code period in steps of half the dwell per hop, the acquisition time is

$$T_S = .01 \times 256 \times 2 \cong 5 \text{ seconds}$$

if the full Doppler uncertainty is covered by the Doppler processor. With a multiple filter bank of 2 kHz spacing, the Doppler coverage is 22 kHz for reasonable hardware complexity; thus, the acquisition time is increased to about 15 seconds to cover the full Doppler uncertainty on the forward link. Note that the code period of 128 milliseconds spans the maximum multipath delay.

At lower values of S/N_O , this approach still leads to rather long, but possibly acceptable acquisition times. If $S/N_O = 25.7$ dB-Hz, for example, the hopping rate could be set at 1000 per second, with 256 channels spaced by 1 kHz. The code period is 0.25 seconds to sequence through all channels. Since $E/N_O = -4.3$ dB per hop, noncoherent integration over about 200 hops is necessary for reliable detection of synchronization, or 0.2 sec. Assuming the Doppler processor can cover approximately 15 kHz with a multiple filter bank spaced by 1000 Hz, the total acquisition time becomes

$$T_S = 4 \times 0.2 \times 256 \times 2 \cong 400 \text{ seconds}$$

where four sub-bands are required to cover the full Doppler uncertainty.

During the initial search for coarse acquisition, coherence of the frequency hopping has deliberately not been exploited. The user receiver can acquire fine synchronization after successfully accomplishing the initial coarse acquisition. For the postulated design of 2000 hops/sec at $S/N_O = 35.7$ dB-Hz, the time error is ± 0.5 millisecond when coarse sync is acquired. The time error after fine synchronization is acquired is then within the chip width of ± 2 microsec, for the

*Appendix III discusses synchronization performance in detail. Here, we base quantitative performance on a detection signal-to-noise rates of approximately 16 dB.

500 kHz bandwidth and the search rate is about 300 chips/sec. Fine sync is detected by the output from a narrow bandwidth filter (say, the Doppler processor scaled to a longer coherent integration). The additional time to achieve fine synchronization is thus

$$T_s]_{\text{fine}} = (500/2)/300 = 0.8 \text{ second}$$

and the total acquisition time at $S/N_0 = 35.7 \text{ dB-Hz}$ then is about 16 seconds. With 2.5 dB of demodulation losses, the data rate (uncoded PSK at 10^{-5} error rate) is 200 bps for this S/N_0 value.

To accommodate data on the forward link, the coherent frequency hopped signal can be biphase modulated at the hopping rate or a sub-multiple thereof (2000 bps or less). This does not degrade the coarse sync mode at all, since phase coherence is not exploited there. For convenience, the number of channels and the code period (number of hops) have been made a power of 2, possibly degrading the correlation properties of the code. The advantage is to maintain a power of 2 relation between hopping rate, data rates, and code repetition rate.

2.1.2.3 Optimization of Frequency Hop Design

In the fixed field of view system, the flux density limitation imposes a minimum spread bandwidth on the TDRS-to-user forward link of approximately 320 kHz. This minimum bandwidth would be selected for the reason that acquisition time is found to be directly proportional to the spread bandwidth at a fixed S/N_0 in the receiver. Of course, a wider spread, up to the nominal maximum of 3 MHz, would be of advantage in improving range measurement accuracy proportionately; however, there is no effect on range-rate accuracy achieved by measuring carrier Doppler.

The coherent FH system requires that the channel spacing equal the hopping rate to eliminate ambiguity in delay lock tracking*. Thus, if the spread bandwidth is B_{RF} and the hopping rate (and channel spacing) equals B_{hop} , we

*See Appendix II.

have the relation

$$\text{Hopping Code Period} = B_{RF}/B_{\text{hop}}^2 \quad (2-4)$$

where the periodic hopping code is assumed to cycle pseudorandomly through all frequency channels (number of channels = B_{RF}/B_{hop}). When the receiver is in perfect time alignment, the signal-to-noise ratio in a channel is ideally $S/N_o B_{\text{hop}}$. To enable a reliable sync decision, post-detection integration over a sequence of channels must be performed, and we denote the number integrated as $n_I(S/N_o B_{\text{hop}})$. Searching in steps of half the dwell time = B_{hop}^{-1} , the initial sync time is computed to be

$$T_{S_1} = 2(B_{RF}/B_{\text{hop}}^2) n_I(S/N_o B_{\text{hop}}) K_{\text{doppler}}(B_{\text{hop}}) \quad (2-5)$$

In (2-5), $K_{\text{doppler}}(B_{\text{hop}})$ denotes the number of sub-bands required in a practical implementation of the Doppler processor to cover the full Doppler uncertainty with a resolution equal to B_{hop} .

We observe the following. If $S/N_o B_{\text{hop}} > 0$ dB, n_I tends to be proportional to B_{hop} ; hence, T_{S_1} is theoretically decreased by increasing B_{hop} . (Also, K_{doppler} tends to decrease with increasing B_{hop} .) For $S/N_o B_{\text{hop}} < 0$ dB, n_I tends to be proportional to B_{hop}^2 , and T_{S_1} is then theoretically independent of B_{hop} . A practical choice is to set $S/N_o B_{\text{hop}} \approx 0$ dB at the minimum design signal level to avoid implementation difficulties associated with detection at low signal-to-noise ratios. For a user with antenna gain $G_u = 0$ dB, $S/N_o = 29$ dB-Hz on the FFOV forward link, and $B_{\text{hop}} \approx 800$ Hz represents the proper value.

The initial noncoherent sync acquisition is followed by a coherent sync acquisition searching over the time uncertainty $\approx B_{\text{hop}}^{-1}$ and the frequency uncertainty $\approx B_{\text{hop}}$ remaining after the initial noncoherent acquisition. This sync time is approximated by*

* Using results from Appendix III.

$$T_{S_2} = \frac{B_{RF}}{B_{hop}} \cdot \frac{16K}{S/N_0} \quad (2-6)$$

where K denotes a factor due to any requisite Doppler search. At worst, K is proportional to B_{hop} ; hence, T_{S_2} tends to decrease or possibly stay constant with increasing B_{hop} .

By virtue of the above rationale, we now select the parameters

$$B_{hop} = 1 \text{ KHz}$$

$$B_{RF} = 256 \text{ KHz (256 channels)}$$

$$\text{Code Period} = 256 \text{ milliseconds}$$

This enables data transmission at 1 Kbps or any submultiple, since the initial sync detection is unaffected by phase modulation impressed at the hopping rate. (However, the subsequent coherent sync decision is degraded by data.)

At $S/N_0 = 29 \text{ dB}$, we have $S/N_0 B_{hop} = -1 \text{ dB}$. For this post-detection integration, performance curves⁽⁴⁾ give $n_I = 80$ to achieve 0.9 probability of detection at a false alarm number of 10^5 . We assume $K_{doppler} = 1$, implying a practical Doppler resolver covering $\pm 55 \text{ kHz}$ in 1 kHz steps. Then (2-5) yields

$$T_{S_1} = 41 \text{ seconds}; G_u = 0 \text{ dB}$$

and if $K = 1$ in (2-6),

$$T_{S_2} = 5 \text{ seconds}; G_u = 0 \text{ dB}$$

4. D. P. Meyer and H. A. Mayer, Radar Target Detection, Academic Press, 1973.

2.1.2.4 Accommodating a Variable Data Rate on the Fixed Field of View

Forward Link

The forward link of the fixed field of view system transmits a single signal which each multiple access user must track to maintain synchronization and enable two-way range and range rate measurements. The forward link conveys data in a time division format, addressing a message to its designated user recipient at a burst data rate accessible to that user. Thus, if a particular user has a high antenna gain, the burst data rate can be proportionately high as dictated by E_b/N_0 for the specified error rate. The problem is posed of enabling a user with a low antenna gain to continue tracking despite the high rate data burst. For this discussion, the burst duration is not operationally restricted and in the worst case can continue indefinitely at some specified maximum rate.

2.1.2.4.1 Bandwidths and Thresholds for Costas or Squaring Loop Tracking

To begin the analysis, we assume biphase suppressed carrier data modulation which is tracked by a Costas loop or squaring loop. (These are equivalent in performance and will not henceforth be distinguished.) The loop signal-to-noise ratio, including effects of squaring⁽⁵⁾, is

$$\alpha_{\text{Costas}} = \frac{S}{4N_0 B_L} \frac{1}{(1 + N_0 W/S)} \quad (2-7)$$

where

S = received power

N_0 = white noise density (one-sided)

B_L = loop noise bandwidth (one-sided)

W = low pass bandwidth to pass data modulation

Note that the loop signal-to-noise ratio for a phase lock loop is defined to be

$$\alpha_{\text{phase lock}} = S/N_0 B_L \quad (2-8)$$

5. C.R. Cahn, "Comparison of Tracking Schemes for PSK", Proc. of Int. Telemetering Conf., September 1971.

The rate of phase slipping is estimated by

$$T_{\text{slip}} = \frac{\pi}{4B_L} \exp(2\alpha) \quad (2-9)$$

applicable to either phase lock or Costas tracking, where

$$T_{\text{slip}} = \text{mean time between phase slips}$$

Comparing (2-7) and (2-8), it is seen that for equal rates of phase slipping, the Costas loop threshold is at least 6 dB degraded compared to a phase lock loop with the same B_L .

The loop signal-to-noise ratio cannot be arbitrarily high in the user receiver because a lower bound is imposed on B_L by dynamics and oscillator phase noise. The steady-state error due to acceleration $\ddot{\omega}$ in a second-order loop or acceleration rate (jerk) $\dot{\ddot{\omega}}$ in a third-order loop is

$$\begin{aligned} \epsilon &= \dot{\ddot{\omega}} / (1.89B_L)^2; \text{ 2nd-order} \\ &= \dot{\ddot{\omega}} / (1.20B_L)^3; \text{ 3rd-order} \end{aligned} \quad (2-10)$$

For a user in a low altitude circular orbit, we find a maximum acceleration of 32 ft/sec^2 and a maximum jerk of $.04 \text{ ft/sec}^3$. Thus, at 2.1 GHz, $\dot{\ddot{\omega}}_{\text{max}} = 422 \text{ rad/sec}^2$ and $\dot{\ddot{\omega}}_{\text{max}} = 0.53 \text{ rad/sec}^3$. Then, for a maximum error of $\epsilon = 0.1$ radian, (2-10) yields $B_L^{\text{min}} = 34 \text{ Hz}$, 2nd-order, and 1.4 Hz , 3rd-order. Clearly, it is advantageous to employ a third-order loop in the receiver of a user in orbit.

Let us now consider the effect of phase noise. Scaling up from typical VHF characteristics ⁽⁶⁾ or down from SHF airborne terminal characteristics ⁽⁷⁾, we obtain a representative flicker noise spectrum at 2 GHz RF

6. C.A. Filippi, Analysis of the Two-Way and One-Way Range Rate TDRS Tracking System, Magnavox Final Report, Contract No. NAS5-21708, March 1973.
7. H.I. Paul, "Phase Noise Measurements and Its Impact on System Performance for the AN/ASC-18 Terminal", Computer Sciences Corp., Interoffice Correspondence, 23 May 1973.

$$S_\phi(f) = .001 f^{-3} \text{ rad}^2/\text{Hz} \quad (2-11)$$

The mean square tracking error in a third-order loop is

$$\begin{aligned} \sigma^2 &= \int_0^\infty S_\phi(f) \frac{f^6}{f^6 + (1.2B_L/2\pi)^6} df \\ &= .016/B_L^2 \text{ rad}^2 \end{aligned} \quad (2-12)$$

where we have substituted (2-11). Thus, if we wish $\sigma \leq .1$ rad, we require $B_L > 1.3$ Hz.

We conclude that $B_L \approx 5$ Hz, 3rd-order will be a practical lower bound to accommodate dynamics of an orbiting vehicle and phase noise of typical oscillators at 2 GHz. From (2-9), we require $\alpha > 5$ (numeric) to achieve a mean time to slip exceeding one hour. Then, from (2-7) we compute the maximum W as a function of S/N_o . For a filter matched to the minimum bit width T_b , $W = 1/2T_b$. For $B_L = 5$ Hz and $\alpha = 5$, the solution is

$$S/N_o \text{ [dB]} = 17 \text{ dB-Hz} + 10 \log_{10} \left\{ 1 + \sqrt{1 + (1/50T_b)} \right\} \quad (2-13)$$

which is plotted in Figure 2-11. It should be noted that this theoretical solution requires the Costas loop to be capable of operating at low E_b/N_o values; for example, if the maximum data rate is 10^4 bits/sec, $E_b/N_o = -11$ dB at the loop threshold, and a practical design is expected to be somewhat degraded from theoretical performance.

2.1.2.4.2 Accommodating High Data Rate

If the burst data rate exceeds the maximum value allowable for the S/N_o received by a particular user, that user will lose track (at least range rate information is lost because the Costas loop slips). The only apparent solution is a power sharing technique such that a portion of the total signal is still amenable to tracking by a disadvantaged user. The remaining portion of the signal conveys the high burst data rate.

One scheme would be to linearly combine two spread spectrum signals with different codes, the second signal intended only to convey high data rates.

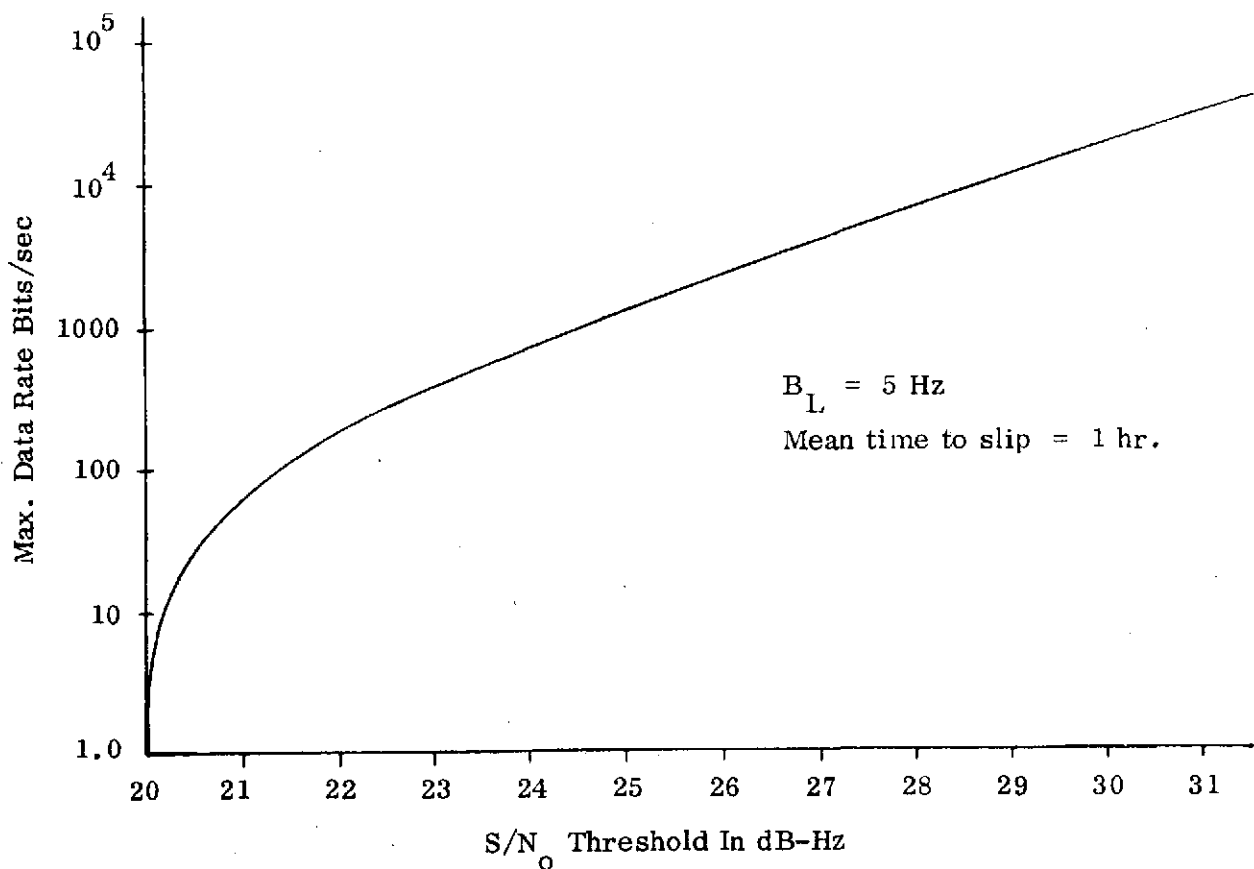


Figure 2-11. Theoretical Costas Loop Threshold as Function of Maximum Data Rate

A second scheme for power sharing would reduce the data modulation index at high data rates (exceeding some maximum low data rate) so as to always leave a carrier component accessible to disadvantaged users. An example would be to employ $\pm 45^\circ$ data modulation, which shares power equally between the high rate data and the carrier component. This scheme would be compatible, with essentially no hardware additions, with a spread spectrum system based on quadrature phase coding. When the high data rate modulation is imposed, the tracking threshold of the disadvantaged user is 3 dB degraded from that determined by the maximum low data rate.

Finally, we observe that it is possible to discard Costas loop tracking in favor of phase lock loop tracking provided that an unmodulated (by data) carrier component is always retained. For this third scheme, we take advantage of the fact, observed above, that a phase lock loop has at least 6 dB better threshold than the Costas loop. Then, a representative design point is to allocate 20 percent of total power to the carrier component, leaving 80 percent to data. Using (2-8) with $B_L = 5$ Hz and still setting $\alpha = 5$ to maintain $T_{\text{slip}} = 1$ hr, and taking into account the fact that the carrier component is 7 dB below total power, the tracking threshold (expressed in terms of total power) is found to be

$$\left. \frac{S}{N}_0 \right]_{\text{dB}} = 21 \text{ dB-Hz} \quad (2-14)$$

independent of data rate. Because the power sharing causes 1 dB loss to the data component, the achievable data rate* for 10^{-5} error rate is computed by adjusting the required E_b/N_0 to $9.6 \text{ dB} + 1.0 = 10.6 \text{ dB}$. (Note that a phase ambiguity does not exist with this scheme.)

The problem is raised for this third scheme of how acquisition is to be accomplished in the user receiver, since the 7 dB reduction of the carrier component would not be tolerable to a disadvantaged user during the process of searching to acquire spread spectrum synchronization. One operational answer is simply to maintain a reference data phase (i.e., transmit 0's) while such a user is attempting to acquire, so that the entire signal is useful for detecting when synchronization occurs in the receiver for that user.

2.1.2.4.3 Conclusions

There is no neat solution for accommodating a variable data rate on the FFOV multiple access forward link when the rate can be over an extremely large range. The basic approach is biphasic suppressed carrier modulation and Costas loop tracking at all data rates. Then, if the minimum data rate were

* At low data rates, the phase error in reconstituting reference phase by phase lock loop tracking must be taken into consideration, and this raises E_b/N_0 further.

100 bps, corresponding to $S/N_o = 30$ dB-Hz, the maximum data rate could be 20 Kbps, provided that 30 dB-Hz is acceptable as the tracking threshold for all users. However, note that designating the maximum low data rate to be 1000 bps and power sharing when necessary to exceed 1000 bps to some user, yields a tracking threshold of 27.5 dB (24.5 dB from Figure 2-11 plus 3 dB for power sharing). The consequence is 3 dB penalty (in achievable data rate) to the high rate user.

2.1.3 STEERED BEAM FORWARD LINK

If the S-band multiple access system is designed with a steered transmit beam on the forward link from TDRS to user, reacquisition is necessary prior to a command transmission to any user. This procedure is compatible with use of a special preamble designed to yield fast acquisition of sync despite a relatively low S/N_o to a disadvantaged user. A basic ground rule is to require any periodic code structure to have a period exceeding 12 milliseconds to insure that a possible specular multipath component can be discriminated unambiguously. (Maximum delay is 12 milliseconds for 2000 Km user altitude.)

2.1.3.1 FH Sync Preamble for Fast Acquisition

A coherent FH waveform for fast acquisition was described previously for the FFOV system. Let us now postulate a waveform with a preamble to enable a two-mode acquisition procedure, with the objective of working with a disadvantaged user having an antenna gain $G_u = -6$ dB so that $S/N_o = 33$ dB-Hz to that user. Coherent tracking is the final mode of the acquisition procedure.

In mode 1, we postulate a preamble with hopping rate of 2 Khps and a periodic frequency hopping code containing 64 frequencies spaced by 32 KHz, for a bandwidth of 2 MHz and a period of 32 milliseconds. In mode 2, we postulate either a coherent frequency hopping waveform with 256 frequencies and a hopping rate of 8 KHz or a PN waveform at a chip rate of 2048 Kbps and a period of 2^{16} chips (maximal length augmented by one chip), so that the period is still 32 milliseconds and the bandwidth is 2 MHz. The preamble is transmitted only long enough for a receiver to acquire sync in mode 1.

The two-mode acquisition procedure is as follows. In mode 1, the receiver searches over the period of 64 frequency hopped pulses to detect occurrence of the preamble, whereupon coarse sync is obtained with an accuracy of ± 250 microseconds. Since E/N_0 per frequency hopped pulse of 500 microsecond duration is +3 dB at $S/N_0 = 36$ dB-Hz, or 0 dB at $S/N_0 = 33$ dB-Hz, reliable detection (.9 probability at a false alarm number of 10^5) is obtained by post-detection integration over 18 pulses or 54 pulses respectively. Thus, the acquisition time to detect occurrence of the preamble signal in mode 1 is

$$T_{s_1} = 2 \times 64 \times .5 \times 10^{-3} \times 18 = 1.2 \text{ seconds at } S/N_0 = 36 \text{ dB-Hz}$$

$$= 2 \times 64 \times .5 \times 10^{-3} \times 54 = 3.5 \text{ seconds at } S/N_0 = 33 \text{ dB-Hz}$$

It is presumed here that a Doppler processor is implemented to cover the frequency uncertainty of ± 64 kHz with a resolution of 2 kHz (matched to the pulse duration of 500 microseconds).

As soon as the receiver detects presence of the preamble signal in mode 1, it switches to mode 2 and searches over the residual time uncertainty of ± 250 microseconds, or 1024 PN chips, with a Doppler frequency uncertainty of ± 1 kHz, resulting from the mode 1 acquisition. A false alarm from mode 1 is ultimately rejected by failure to acquire in mode 2. Reliable serial search can be carried out in mode 2 at a rate such that $E/N_0 = 12$ dB in the time to search one PN chip; thus, the search rate is 250 chips/sec at $S/N_0 = 36$ dB-Hz, or 125 chips/sec at $S/N_0 = 33$ dB-Hz. Consequently, the acquisition time to obtain fine sync in mode 2 is

$$T_{s_2} = 1024/250 = 4 \text{ seconds at } S/N_0 = 36 \text{ dB-Hz}$$

$$= 1024/125 = 8 \text{ seconds at } S/N_0 = 33 \text{ dB-Hz}$$

It is presumed that the residual Doppler uncertainty is acquirable at either search rate. Note that 1 kHz error on the S-band carrier frequency means 1 PN chip/sec at 2 Mbps code rate, and this is negligible compared to the search rate in mode 2 acquisition.

The total acquisition time is

$$T_s = T_{s_1} + T_{s_2} = 5 \text{ seconds at } S/N_o = 36 \text{ dB-Hz}$$

$$= 12 \text{ seconds at } S/N_o = 33 \text{ dB-Hz}$$

At the conclusion of the acquisition process, the receiver is coherently tracking the PN code of 2 MHz bandwidth and 32 milliseconds period.

The question may be raised as to what is the basic advantage gained from use of two acquisition modes. The answer is that a frequency hopping code with a hopping rate of 2 Kbps would require 1024 frequencies spaced by 2 kHz to cover the 2 MHz bandwidth fully (channel spacing equal to hopping rate), and the period would be 0.5 second. Then, the acquisition time would be 55 seconds at $S/N_o = 33 \text{ dB-Hz}$. In mode 1 with only 64 frequencies, the wide spacing of frequencies (32 kHz spacing) does not matter since coherent tracking is not utilized and the ambiguity (peaks spaced by 31 microseconds as shown in Appendix II) of coherent tracking when the spacing exceeds the hopping rate is not of concern for a noncoherent sync detection.

Each user must have a unique code for data transmission after acquisition of sync. In mode 2, the available PN codes (augmented by one chip) give a very large selection (see paragraph 2.1.7.1), and it would be permissible to let all users have the same mode 1 preamble code. If different mode 1 codes are also desired, a family can be generated as described in paragraph 2.1.7.2.

2.1.3.2 Practical Consideration on Discrete Phase Modulation to Approximate Frequency Hopping

In the above, no losses have yet been introduced to take into account the effect of approximating FH with discrete phase steps. In particular, with 90° steps, there can be a loss of 3 dB in the worst-case, as illustrated in Figure 2-12. The phase difference between the received signal and the local reference signal switches by 90° , and if the two values occur equally often (the worst-case), the average amplitude is 0.707.

0°	90°	180°	270°	360°	Received Signal
0°	90°	180°	270°	360°	Reference Signal
0°	90°	0°	90°	0°	Phase Difference

Figure 2-12. Illustration of Worst Case Loss

It is probably desirable to increase the clock rate of phase shifting by two, and utilize 8-phase modulation, implemented by an incremental phase modulator (IPM). Now, the phase switches by 45° , and in the worst-case, the resulting amplitude is

$$|0.5 + 0.5 \angle 45^\circ| = 0.924$$

and the loss is now only 0.7 dB. With, 8-phase modulation, the spurious emissions will be much lower also.

2.1.3.3 PN Sync Preamble

We have in the above designs adhered to the ground rule that a periodic spread spectrum signal should have a code period exceeding the maximum multipath delay. If the multipath has a sufficiently strong specular component, a false acquisition could happen on that component. Then, the code period must exceed twice the multipath delay to enable the receiver to distinguish between the direct signal and a delayed replica. However, at S-band, a specular component is absent or small compared to the diffuse component, and the sense of polarization rotation is reversed⁽⁸⁾. Let us now define a PN system design (either biphase or staggered quadriphase) for the multiple access forward link based on a short code period, with the goal of achieving an acceptable acquisition time rather than insuring protection against specular multipath.

8. J. N. Birch and R. H. French, Definition of Multipath/RFI Experiments for Orbital Testing with a Small Applications Technology Satellite, Final Report, Contract No. NAS9-12705, NASA-MSC, 1 December 1972.

Since we desire to optimize the design with acquisition time as a most important parameter, it is natural to pick the PN chip rate to be the minimum satisfying radiated flux density limits. This rate is approximately 1.6 Mbps for the fixed field of view system. To minimize acquisition time, the period of the code should be short, recognizing that this period ultimately establishes the AJ capability to resist RFI or the other TDRS-to-user forward link signal.

If the PN code period is less than a data bit interval, there is still an ambiguity to be resolved to determine where the data bit edge lies, even though PN code rate and data rate are coherently related. Extending this, there is the goal of resolving the ranging ambiguity, which is many code periods. One way to do this is to add (modulo-2) a "sub-code" which effectively extends the overall period. The sub-code is a short period binary code with a bit rate equal to the repetition rate of the PN code.

To clarify the above by way of numerical illustration, we assume representative system parameters. For a user with $G_u = -6$ dB, $S/N_o = 33$ dB-Hz, and for $G_u = -3$ dB, $S/N_o = 36$ dB-Hz. Thus, we are lead to a PN code repetition rate of approximately 3,000 repetitions/second, when we require that E/N_o per repetition be roughly 0 dB. Let us choose the parameters

PN code rate	=	2.044 Mbps
PN code period	=	511 chips = 250 microseconds
Sub-code period	=	250 bits
Overall period	=	62.5 millisec (ambiguity = 9374 Km)
Data bit interval	=	2.5 millisec

Each successive repetition of the 511 chip PN code is complemented whenever the sub-code bit is 1. The resulting two-way ambiguity of 9374 Km is acceptable for the TDRS tracking and orbit determination computation.

Although a false acquisition to a specular multipath component is not anticipated (for the S-band system), there is the threat of strong diffuse multipath delayed by a multiple of 511 PN bits. The total diffuse multipath could be as strong as 3 dB below the direct signal ⁽⁸⁾. However, the fact that a data bit extends over

10 bits of the pseudorandom sub-code means that there is 10 dB processing gain against such diffuse multipath, in addition to whatever decorrelation results from the PN code itself due to time spread of the multipath. The maximum degradation due to such diffuse multipath, then, is 1.0 dB.

The acquisition search covers the 511 bits of one PN code period. Since the time phase of the sub-code is unknown, a coherent integration of the received signal cannot be extended beyond 250 microsecond. Let us presume a Doppler processor covering ± 55 kHz with 4 kHz windows, and a non-coherent post-detection integration exactly as previously described for frequency hopping.

At $G_u = -6$ dB, we have E/N_o per repetition of the PN code to be -3 dB, and a reliable sync decision requires integration over 170 repetitions, or 42.5 milliseconds. Searching in half-chip steps, the acquisition time is

$$T_s = 2 \times 511 \times 42.5 \times 10^{-3} = 43.4 \text{ seconds}; G_u = -6 \text{ dB}$$

using a Doppler processor covering ± 55 kHz in 4 kHz windows. At $G_u = -3$ dB, E/N_o per repetition = 0 dB, and a reliable sync decision integrates over 54 repetitions, or 13.5 milliseconds, for which

$$T_s = 2 \times 511 \times 13.5 \times 10^{-3} = 13.8 \text{ seconds}$$

The time phase of the sub-code is still unknown; however, this can be resolved in a very short time, certainly less than 1 second. (Note that E/N_o over a 62.5 millisecond sub-code period is 21 dB at $G_u = -6$ dB. The data bit timing is uniquely tied to the sub-code, since one data bit spans 10 bits of the sub-code; in fact, the sub-code period is chosen to have appropriate factors for a count-down to the data rate.

To resolve the time phase of the sub-code, we assume the receiver performs coherent demodulation at the PN code repetition rate of 4000 repetitions/second. Note that the threshold for Costas loop tracking at this maximum data rate is theoretically $S/N_o = 27$ dB-Hz well under the maximum of 33 dB-Hz. A best match with the known sub-code is sought by a digital integration over the 250 bits.

With respect to diffuse multipath, note that the design provides 10 sub-code bits for each data bit at a maximum rate of 400 bps, which is the maximum enabled at $S/N_0 = 36$ dB-Hz (without forward error correction coding). However, since the ambiguity can be resolved in the user transponder before data is impressed on the forward link signal, the maximum data rate could be 4 Kbps, except that protection against diffuse multipath disappears. More generally, since the forward link signal is directed towards a particular user, the design could just as well program a switch to a non-repetitive PN code (very long period), which starts at a marked repetition of the initial 511-bit short code employed for acquisition. The mark would be the starting point of the sub-code, and the receiver starts to search for correlation to the non-repetitive code whenever correlation to the 511-bit short code is lost. Note that at $S/N_0 = 33$ dB-Hz, E/N_0 over the sub-code period is +21 dB, and a reliable detection that the short PN code has ceased can be made unambiguously. Alternatively, the long PN code can be made to have a period of 62.5 milliseconds, exactly equal to that previously formed by the sub-code. Note that the sub-code yields considerable protection against diffuse multipath. Effectively, there is a processing gain equal to the sub-code period, or 24 dB for the numerical illustration given. Since the multipath is weaker than the direct signal, a reliable decision that the short PN code has ceased can be made in the presence of multipath even without the processing gain of the PN.

The above computation for acquisition time calls for a search rate of 11.8 PN chips/sec at $G_u = -6$ dB. However, at a PN chip rate of 2 Mbps, the maximum code Doppler is ± 53 chips/sec, which exceeds the search rate. Hence, the design will not work as described.

One solution is to reduce the coverage of the Doppler processor in the receiver by breaking up the total Doppler uncertainty into sub-bands. The receiver's PN code rate is offset by the Doppler at the center of each sub-band. Setting the maximum code Doppler uncertainty to be 20 percent of the search rate as a reasonable design, this approach calls for 22 sub-bands. The acquisition time for each system is multiplied by the number of sub-bands (neglecting second-order changes as the false alarm rate decreases with the number of windows in the Doppler processor). The consequence is an unacceptable acquisition time.

However, with the steered transmit beam system, only one user at a time is the recipient. Hence, it is feasible to insert a priori knowledge of Doppler on the forward link signal so as to facilitate acquisition of this signal by the user. As given in Section 1-6, the one-way range rate uncertainty is ± 100 m/sec, or ± 0.33 ppm. Then, if the PN code rate is 2.044 Mbps, the maximum code Doppler uncertainty is ± 0.7 PN chips/sec. At the S-band carrier frequency, the maximum carrier Doppler uncertainty is ± 700 Hz. A very desirable advantage of this approach is to simplify the user receiver in the sense of having a much more straightforward Doppler processor design with a modest Doppler coverage. A minor disadvantage is the need to insert a priori knowledge of Doppler into the ground transmitter (on both carrier and code rate).

It may be observed that the design based on frequency hopping does not have a similar difficulty with code Doppler because the hopping rate is much lower than the spread bandwidth.

2.1.4 ANALYSIS OF RANGE AND RANGE RATE MEASUREMENT ACCURACY

The use of spread spectrum for the TDRSS enables precise measurement of range by observation of the round trip propagation delay. The accuracy of this depends on the accuracy associated with the measurement of time-of-arrival of the spread spectrum modulation, relative to a local clock. For PN, this accuracy is typically expressed as the fraction of a code chip. For coherent FH, the equivalent of a chip is the reciprocal of the total spread bandwidth. A delay-lock tracking loop performs the measurement; here, an error voltage controlling the code clock phase is derived by comparing correlation amplitudes for an "early" code replica and for a "late" code replica. The delay-lock loop has a narrow bandwidth so as to reduce the rms error due to noise.

Range rate measurement is made by a Doppler measurement on the carrier frequency. This is the carrier phase change, relative to a local oscillator reference, over the specified averaging time (e.g., 1 second or 10 seconds). In a spread spectrum receiver with carrier reconstitution to enable coherent demodulation of data, such a phase measurement can be performed even though the carrier actually is suppressed by the spread spectrum modulation. The accuracy of the range rate measurement is determined from the phase error in carrier tracking, typically by a Costas loop when the data is binary PSK.

When the chip rate is coherently scaled from the carrier frequency, the delay-lock loop in the receiver can be aided from the carrier tracking loop; that is the Doppler measured in the carrier tracking loop is scaled to the modulation bandwidth (e.g., the PN chip rate) and applied as a tracking aid to cancel out Doppler in the delay-lock loop. As a consequence, the delay-lock loop can be made arbitrarily narrow, since it does not have to track user dynamics as long as the carrier tracking loop stays above threshold and does not slip cycles. It is practical to employ very narrow bandwidths in the delay-lock loop, such as 0.1 Hz or even less.

2.1.4.1 Delay-Lock Loop Measurement Accuracy

With coherent carrier phase tracking, the delay-lock loop has the block diagram shown in Figure 2-13. The resulting measurement accuracy (variance) for a PN receiver with the typical design of $\tau_d = 0.5$ chip, is ⁽⁹⁾

$$\sigma_{\text{bit}}^2 = \frac{N_o B_L^{(\text{code})}}{2S} ; \text{coherent delay lock} \quad (2-15)$$

where $B_L^{(\text{code})}$ is the (one-sided) noise bandwidth of the delay-lock loop.

An alternative delay-lock loop implementation uses noncoherent (envelope) detection of the early and late correlation amplitudes, and does not necessarily depend on maintaining coherent carrier phase tracking. If the IF bandwidth prior to envelope detection is B_{IF} , the measurement accuracy becomes ⁽¹⁰⁾

$$\sigma_{\text{bit}}^2 = \frac{N_o B_L^{(\text{code})}}{2S} \left[1 + \frac{2N_o B_{\text{IF}}}{S} \right] ; \text{noncoherent delay lock} \quad (2-16)$$

where τ_d still is 0.5 chip. Note that the degradation with respect to a coherent demodulator is small provided that $S/N_o B_{\text{IF}} > 0$ dB.

9. C. R. Cahn et al, Timation Modulation Study, Final Report, Contract N00014-71-C-0285, 31 August 1972.

10. C. R. Cahn et al, System 621B Signal Definition Study, Technical Report SAMSO-TR-72-248, Oct 1972.

Finally, we note the hardware simplification of having a single correlation channel time shared between early and late correlation. (This is also called a dither tracking loop.) Effectively, the noise level is doubled by the time sharing, and if τ_d is still 0.5 chip,

$$\sigma_{\text{bit}}^2 = \frac{N_o B_L^{(\text{code})}}{S} [1 + \frac{2N_o B_{\text{IF}}}{S}] ; \text{dither tracking} \quad (2-17)$$

The erosion of theoretical measurement accuracy with dither tracking is offset by implementation convenience, and can be made up by further narrow banding of the delay-lock loop.

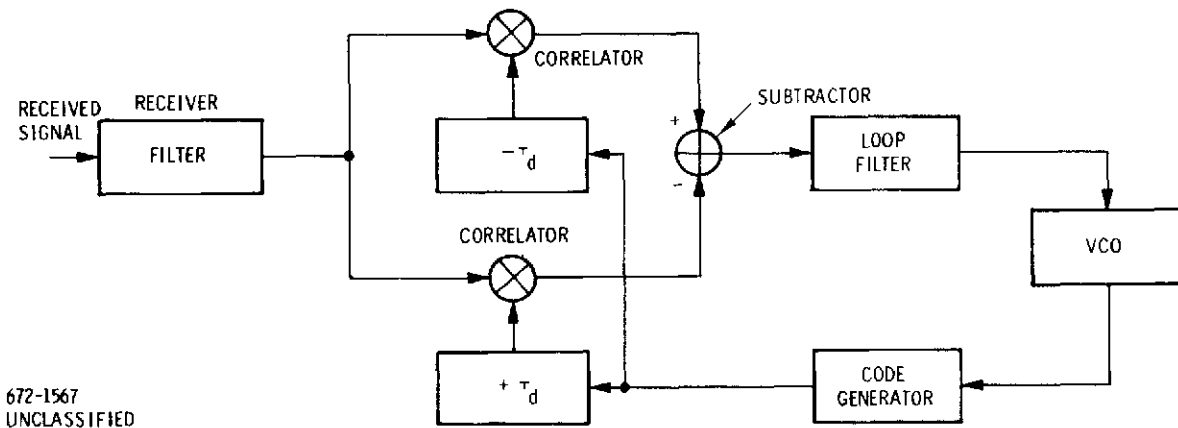


Figure 2-13. Block Diagram of Delay Lock Tracking Loop

2.1.4.2 Carrier Phase Measurement Accuracy

Range rate measurement accuracy is evaluated by assuming independent phase errors at the beginning and the end of the averaging interval, over which the phase difference is accumulated. Paragraph 2.1.2.4 gives the Costas loop signal-to-noise ratio, which is the reciprocal of phase error at the second harmonic of the carrier. Thus, the variance of the phase error at the carrier frequency itself is

$$\sigma_{\text{rad}}^2 = \frac{N_0 B_L^{(\text{carrier})}}{S} \left[1 + \frac{N_0 B_{\text{IF}}}{2S} \right] \quad (2-18)$$

and subtracting the two independent phase measurements doubles the variance. In contrast to the delay-lock loop, the Costas carrier tracking loop cannot be arbitrarily narrow banded because of the requirement to track orbital dynamics. Paragraph 2.1.2.4 indicates expected carrier phase tracking errors due to acceleration in a second-order loop and acceleration rate (jerk) in a third-order loop.

As a general rule, the Costas loop when properly designed should not have a very large tracking error due to dynamics, perhaps at most 0.1 radian, and this error is slowly changing. Consequently, the bias error on range rate caused by orbital dynamics can be considered negligible.

2.1.5 MULTIPLE ACCESS RETURN LINK

The return link is also spread spectrum for purposes of multiple access, range measurement, and multipath discrimination. The first concern, then, is for required acquisition time on the return link, and whether frequency hopping has advantages over pseudonoise in this regard.

With a turnaround transponder, the maximum Doppler is doubled on the return link, and the time uncertainty is determined either by the round trip range uncertainty or by the code period on the return signal (whichever is smaller). The time uncertainty due to range variation is roughly 100 milliseconds; thus, without utilizing available knowledge of user range and range rate, the acquisition time on the return link will be excessive at minimum user EIRP. There is no reason why range and range rate

estimates cannot be inserted into the ground receiver to speed up acquisition on the return link. In that case, use of coherent FH does not offer any advantage with respect to sync acquisition, although it may have a slight advantage in enabling multiple access of signals with unequal data rates and EIRP's.

2.1.5.1 Acquisition

On the return link from user to TDRS, the receiver can take advantage of a priori knowledge of range and range rate. The ground rule is that (one-way) range is known to ± 50 Km and (one-way) range rate to ± 100 m/sec. After the user has acquired the forward link signal, the uncertainties on the return link are twice the one-way uncertainties, since the user operates as a turnaround transponder to enable two-way range and range rate measurements to be made. Thus, for acquisition on the return link, after injecting a priori knowledge, the time uncertainty is ± 330 microseconds and the carrier frequency uncertainty is ± 1.3 kHz.

We presume the user has a minimum EIRP of 7 dBW, for which $S/N_o = 27.6$ dB-Hz + 7 dBw = 34.6 dB-Hz to a directed AGIPA receive beam. (This includes transponder loss of 2 dB, AGIPA loss of 0.5 dB, and leaves 3 dB margin. Demodulation loss of 1.5 dB and PN loss of 1.0 dB is not included.) The search rate can be about 200 PN chips/sec (see Appendix III). For a PN chip rate of 3 Mbps on the return link, the uncertainty is 2000 chips, and the worst-case acquisition time is about 10 seconds (we presume the Doppler uncertainty can be covered). Here, we assume the return signal has a code period equal to that of the forward signal.

2.1.5.2 Multiple Access Capability of Spread Spectrum

The use of coherent frequency hopping as a band-spreading technique has been described previously, emphasizing the advantage with respect to initial sync acquisition. We now wish to examine this waveform for its multiple access performance on the return link at S-band, assuming perfect synchronization of the receiver. For the present discussion, we assume one interfering signal is received, on the average, in any beam of the phased array (AGIPA) on the TDRSS; however, several more occasionally can exist with a respectable probability. The spread bandwidth B_{RF} is nominally 3 MHz, and the data rate R_b can vary from 1 Kbps to 100 Kbps. We assume receiver performance is defined by the minimum required $E_b/N_o = 9.9$ dB + 3 dB = 12.9 dB without error-correction coding, and $E_b/N_o = 4.7$ dB + 3 dB = 7.7 dB

with rate -1/2 coding. The added 3 dB includes the demodulation loss (1.5 dB), PN loss, (1.0 dB) and AGIPA loss (0.5 dB) assumed by NASA Goddard in the space-to-space return link analysis.

Of course, the receiver cannot tolerate any interference whatsoever unless the received power of the desired signal exceeds the minimum defined by the thermal noise level. When the minimum required E_b/N_o is specified, the tolerable interference to signal power ratio, J/S, is computed for conventional PN in a linear channel according to

$$\frac{E_b}{N_o} \leq \frac{S/R_b}{N_r + J/B_{RF}} = \frac{B_{RF}}{R_b} \frac{1}{\frac{N_r B_{RF}}{S} + \frac{J}{S}} \quad (2-19)$$

where B_{RF}/R_b = spread spectrum processing gain and N_r is the receiver thermal noise. As a design point, if S is 3 dB above the minimum requirement imposed by thermal noise,

$$J/S \leq \frac{B_{RF}}{2R_b(E_b/N_o)} \quad (\text{design point}) \quad (2-20)$$

Thus, if $B_{RF} = 3$ MHz, $R_b = 1$ Kbps, $E_b/N_o = 7.7$ dB, (2-20) gives the bound $J/S \leq 24.1$ dB at the postulated design point (3 dB margin for thermal noise alone). If $R = 10$ Kbps, $J/S \leq 14.1$ dB. It should be noted that this 3 dB margin at the design point is not to be confused with a 3 dB allowance for system degradation used in the NASA Goddard Definition Phase Study Report.

Now suppose there is one interfering signal conveying 100 Kbps without coding (a worst-case assumption for any other user). With zero margin with respect to noise alone, the interfering signal must exceed the desired signal conveying 1 Kbps data rate by 20 dB - 3 dB + 12.9 dB - 7.7 dB = 22.2 dB. From this, we reach the conclusion that the conventional PN multiple access system barely succeeds even without bringing in the further problem that the relative signal levels vary inversely as the square of propagation range. In other words, there is very little tolerance to handle a situation where the interfering signal is transmitted with considerable excess margin by the user, because of transmitter overdesign or a momentary geometry where the user's orbit passes relatively close to the TDRSS.

Of course, the problem of multiple access with PN is relieved somewhat if the maximum data rate is reduced, error correction is imposed on all users, and power levels are coordinated more-or-less continuously to prohibit excessive margins and compensate for changes in range (see Appendix VI). A practical design could control EIRP to an accuracy of 3dB, if imposing a gross specification of required user EIRP is not satisfactory for multiple access. Quantitatively, if the maximum data rate for any user is 50 Kbps with rate - 1/2 coding, and we allow that user 3 dB margin with respect to noise alone so as to accommodate interfering signals, the J/S to the receiver for 1 Kbps is 17 dB. A maximum J/S of 24 dB, as computed above, allows the 50 Kbps interfering user to be up to 7 dB stronger than the design point (but then no other interference can be tolerated).

2.1.5.2.1 Multiple Access of Unequal Rate Signals by Coherent Frequency Hopping

Let us now examine a coherent FH system in which hopping occurs at the symbol rate. The idea now is that the receiver for the low-rate signal can ignore occasional hits by the interfering signals. Again, assume the desired signal operates at 1 Kbps with rate - 1/2 coding, while the interfering signal is at 100 K symbols/sec (100 Kbps uncoded, 50 Kbps coded). Thus, the interfering signal hops over 30 frequency slots spaced by 100 kHz in the RF bandwidth of 3 MHz.

The low -rate receiver is presumed to clip in the IF following correlation, where the bandwidth prior to clipping is set equal to the maximum symbol rate of any signal (i. e., 100 kHz). After clipping, the bandwidth is reduced to approximately twice the symbol rate prior to PSK demodulation. The receiver processing is indicated by Figure 2-14. Figure 2-15 shows (in an idealized manner) the low-rate desired signal and the high-rate interfering signal as they impinge on the limiter. The interference falls within the pre-limiting bandwidth with a probability of occurrence ϵ equal to the ratio of filter bandpass to total spread spectrum bandwidth, or $\epsilon = 100 \text{ kHz} / 3 \text{ MHz} = .033$ in the present illustration.

For a very idealized analysis, let us assume hard limiting in the post-correlation IF. When receiving the desired signal in the presence of wideband Gaussian noise only, there is known to be a loss of 1 dB due to the hard limiting. When the strong interfering pulses are present, with probability .033 according to the idealized model, the hard limiter clips them to the level of noise interference. Because the ratio of desired signal power to noise power in the bandpass is low, the nominal value being $7.7 \text{ dB} + 3 \text{ dB} - 20 \text{ dB} = -9.3 \text{ dB}$ in the present example,

the degradation produced by the interfering pulses is due to the "holes" punched in the desired signal. Thus, with one interfering signal, the average amplitude of the desired signal is reduced by the factor $1 - \epsilon = .967$ in the present example, or 0.3 dB. The total degradation is 1.3 dB, including the hard limiter loss of 1.0 dB, regardless of how strong the interfering pulses from the undesired signal may be.

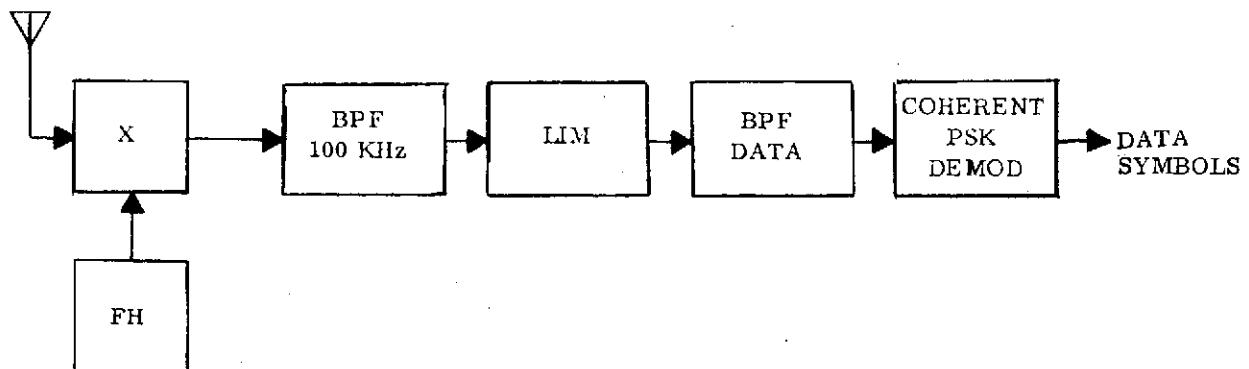


Figure 2-14. Processing in FH Receiver for Multiple Access

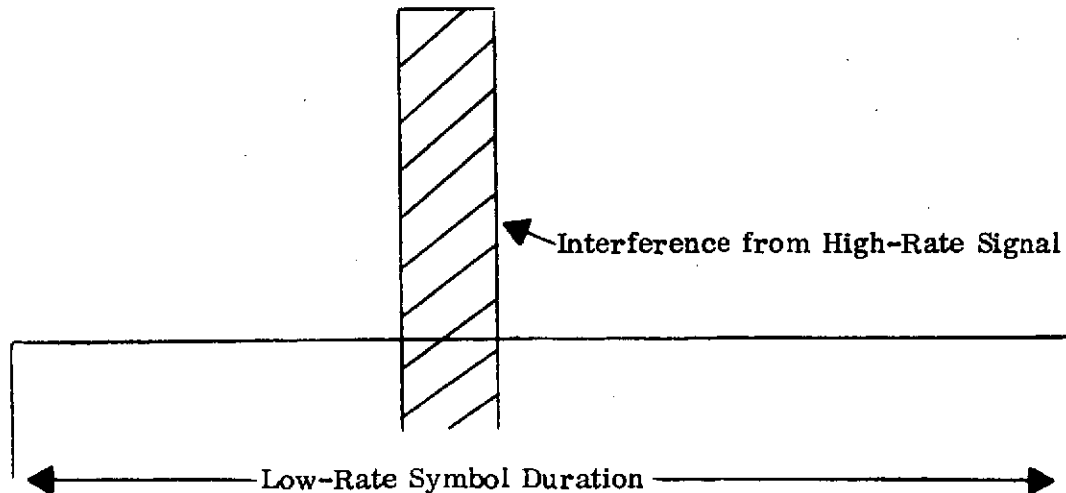


Figure 2-15. Superposition of High-Rate Interfering Signal on Low-Rate Signal

If there are several interfering high rate signals, there is additional degradation due to the greater number of hits. With M interfering signals, the average amplitude of the desired signal becomes $(1 - \epsilon)^M$, and for $\epsilon = .033$ and $M = 7$, this is a reduction of 2 dB. Including the hard limiter loss, the total degradation is 3 dB, which equals the design point postulated above for PN multiple access.

The advantage for multiple access by FH is seen to derive from the receiver's capability to tolerate strong low duty-factor interference. There would be no advantage relative to PN, rather a small loss due to hard limiting, if the power levels could be perfectly coordinated. Of course, in a practical system, the effect of the pulses from the strong interfering signal will become more severe as their level increases because of pulse spreading due to transient ringing in the bandpass filter and spurious emissions from the transmitter. However, the objective here is to provide a reasonable range of power variation.

Interference to the high rate signal from the low rate signal may be ignored because of the difference in power levels. More generally, the high rate signal may encounter strong CW interference in some of the frequency slots, and it is necessary to operate with error-correction coding to combat such interference, which induces an error rate on the received symbols (prior to decoding). The effect of this CW interference is negligible if it is at least 6 dB weaker than the desired signal.

Let us now consider what happens as the interfering signal is reduced in data rate (and therefore hopping rate). Of course, if this were known by prior design, the pre-limiting bandpass filter could be narrowed, and the probability of a hit would go down. We do not assume this here. Thus, the probability of interference remains .033, but the duration of the interfering pulse, when a hit occurs, is longer. The effect is that the degradation due to an interfering signal remains approximately constant until the symbol rate of the interfering signal becomes comparable to that of the desired signal so that the average amplitude is no longer meaningful in establishing receiver performance.

2.1.5.2.2 Multiple Access of Moderate Data Rate Signals

Let us now discuss multiple access of a number of signals with equal symbol rates and equal hopping rates. (Interference from strong but slowly hopping signals is included in this model also.) To quantify the problem, we assume a moderate data rate of either 1 Kbps or 10 Kbps for each signal (2 K symbols/sec or 20 K symbols/sec with rate - 1/2 coding). We also assume, for analysis, that the rate - 1/2 decoding can operate at a symbol error rate of .04, corresponding to $E_b/N_o = 4.9$ dB with PSK hard decisions*.

Since the post-correlation IF bandwidth is 100 KHz, the probability of interference falling within that bandpass is, as previously computed, .033. Assuming the limiting does not significantly change the nature of the interference which tends to persist for the symbol duration, the frequency selectivity of the bandpass filter after limiting rejects the interference provided that it is offset by at least the symbol rate. Thus, for the postulated numerical example of 10 Kbps data rate, the probability of interference is 40 kHz/ 3 MHz = .0133, and the probability of error is less than .0067 for random phasing of the interference. This implies ability to tolerate up to six interfering signals that are strong compared to the desired signal at 10 Kbps.

From the computation of J/S for multiple access by PN, it was found that $J/S \leq 14.1$ dB at the design point, meaning 25 interfering signals at equal power, or 6 interfering signals averaging 6 dB above the desired signal. Thus, it is concluded that coherent FH can outperform PN for multiple access when there is more than 6 dB disparity in signal levels.

A similar calculation for multiple access of users at 1 Kbps data rate leads to a tolerance for 10 times the number of interfering signals as computed for 10 Kbps data rate.

* This means a sequential decoder rather than a Viterbi decoder; however, we do this to simplify the analysis of the effect of interference.

2.1.5.2.3 Multiple Access of High Data Rate Signals

For a signal with a data rate of 25 Kbps, or 50 K symbols/sec with coding, the 100 kHz bandpass in Figure 2-14 suffices to avoid degradation due to intersymbol interference. If there is an interfering signal also at 50 K symbols/sec, the probability of interference falling within the 100 kHz bandwidth is .033, and the probability of symbol error is .017 or less. At most two such interfering signals can be tolerated if they are strong compared with the desired signal.

If the desired signal has a data rate of 50 Kbps, or 100 K symbols/sec with coding, the limiting post-correlation channel of Figure 2-14 would not be needed. A strong interfering signal also at 100 K symbols/sec probably cannot be tolerated; here, we must take into account that the signals are asynchronous and produce significant spectral components over 200 kHz. For small power differentials, the tolerance is similar* to PN, for which (2-20) yields $J/S \leq 7.1$ dB.

2.1.5.2.4 Conclusions

With 20 users served by the S-band multiple access system, there is an average of approximately 1 signal in each of the directed beams from the 30-element phased array. The probability distribution of the number is given by a Poisson distribution.

$$P(k \text{ users in a beam}) = \frac{(\bar{k}) \exp(-\bar{k})}{k!} \quad (2-21)$$

where \bar{k} is the average number. The probability of getting five or more interfering users within a beam serving the desired user is .0036; thus, designing for this number of interfering users in one beam insures a service reliability exceeding 0.996. Of course, interference received at a lower power level (at least 6 dB power) than the desired signal can essentially be ignored, and the problem scenario is that of a low-power, low data rate desired signal received simultaneously with high power, high rate interfering signals up to 100 K symbols/sec. Compared with

* As an illustration, with randomly phased interference 7 dB stronger and hitting the desired signal with .033 probability, and leaving 3 dB margin for noise alone, the symbol error rate during a hit is 0.35, and the average symbol error rate $\cong .02$. This is correctable.

conventional PN, coherent frequency hopping is particularly advantageous for multiple access in this problem scenario. Employing coherent FH, it is found that a user conveying data at 10 Kbps or less is fully compatible with the above interference scenario regardless of data rate distribution or excess margins of the 19 random located interfering signals at least for the idealized analysis employed.

For a user signal above 10 Kbps, the interference scenario is more restricted. As an illustration, a representative mission model for TDRSS indicates five users each transmitting data at approximately 25 Kbps. Two such interfering signals can be tolerated. Since the average number per beam is 0.2, (2-21) shows that the probability of more than two interfering is small (roughly 10^{-3}).

2.1.5.3 Coexistence of Low Rate User and High Rate User on Multiple Access Return Link

The idealized analysis of multiple access has been given above for both PN and coherent FH spread spectrum modulation, the objective being to compare these multiple access schemes. With PN, the effect of various system losses, which effectively degrade E_b/N_0 , was not fully brought in. With FH, practical filter responses were not taken into account. We continue to study the extreme case of a high rate user transmitting 100 Kbps uncoded into the same TDRS antenna beam as a low rate user at 1 Kbps with error correction. According to the user-to-TDRS link budget given by NASA, the high rate user requires an EIRP of 35 dBw, while the low rate user demands an EIRP of 9 dBw. This budget presumed 1 dB increase in receiver noise due to multiple access interference, includes 3 dB of margin, and makes an allowance for various losses in addition.

In the absence of power control on the user's EIRP, the worst interference occurs when the high rate user has minimum range to the TDRS. For 2000 Km altitude, this is 33,862 Km, when directly under the TDRS, and the free space loss is 1.9 dB less than assumed in the link budget. For EIRP = 35 dBw, the power density in the receiver for 3 MHz bandwidth on the return link is - 192.0 dBw/Hz. The link budget assumes a receiver noise density, including multiple access noise, of -198.3 dBw/Hz and 2 dB degradation for TDRS transponder loss. Thus, the total receiver noise, adding TDRS-to-ground noise, is allowed to be -196 dBw/Hz in the link budget.

2.1.5.3.1 Multiple Access by PN

With PN multiple access, the low rate user will encounter a total noise level of -190.5 dBw/Hz when the interference from the high rate user is added to that presumed in the link budget, an increase of 5.5 dB over that planned in the link budget. In other words, the low rate user would need to transmit an EIRP of 14.5 dBw in order to maintain the design margin on the return link during the interval when the high rate user falls in the main beam*. Since the AGIPA beam has a width of 6° , or 2,000 miles near the earth's surface, a user traveling across the beam at 5 mps could stay in the beam for 400 seconds.

It is not the desired operational procedure to force a low rate user to increase his EIRP or decrease data rate to enable coexistence with the 100 Kbps user. The alternative is to impose a restriction on maximum EIRP and, therefore, maximum data rate. For example, if the maximum symbol rate remains at 100 K symbols/sec, but the maximum data rate is 50 Kbps with rate -1/2 coding, the required user EIRP drops to 27 dBw. Then, the power density in the receiver for 3 MHz bandwidth is -200 dBw/Hz at minimum range. The total noise level becomes -194.5 dBw/Hz when the interference from the high rate user is added to that presumed for the link budget. This is an increase of 1.5 dB over that planned in the link budget, and the low rate user requires an EIRP of 10.5 dBw to operate.

Thus, we see that even restricting a user to a maximum data rate of 50 Kbps and requiring forward error correction (with a coding gain of 5.2 dB), the NASA link budget has inadequate allowance (by 1.5 dB) for multiple access interference with PN.

2.1.5.3.2 Multiple Access by Coherent FH

Let us now examine coherent FH as the multiple access technique removing some of the idealizations made in prior analyses**. The objective is still to enable coexistence of a high rate user at 100 Kbps with a low rate user at

* One can view this as requiring an increase in the EIRP of the low rate user so as to not exceed the J/S capability of the spread spectrum receiver to resist the signal from the high rate user.

** Multiple access via PN is more easily analyzed since the interference can be presumed Gaussian and additive to the receiver thermal noise.

1 Kbps. Figure 2-16 shows the postulated receiver processing for the low rate user. If the hopping rate of the interference is 100 Kbps, there is still some response by the filter to pulses considerably offset in frequency due to the frequency hopping. Figure 2-17 gives the envelope of the transient output from the filter when the input pulse is offset in frequency, for a typical filter design (4 pole Butterworth). The input pulse width of 10 microseconds equals the reciprocal of the bandpass (3- dB) bandwidth (100 kHz). The peak pulse response is observed in Figure 2-17 to be about 20 dB down for an offset of ± 200 kHz, even though the CW response at this offset would be down by 48 dB. The typical output pulse width is 20 microseconds.

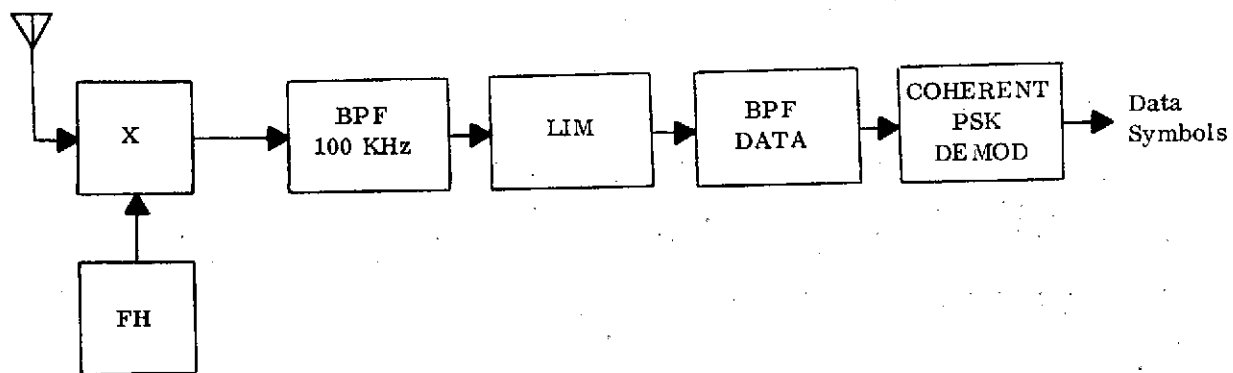
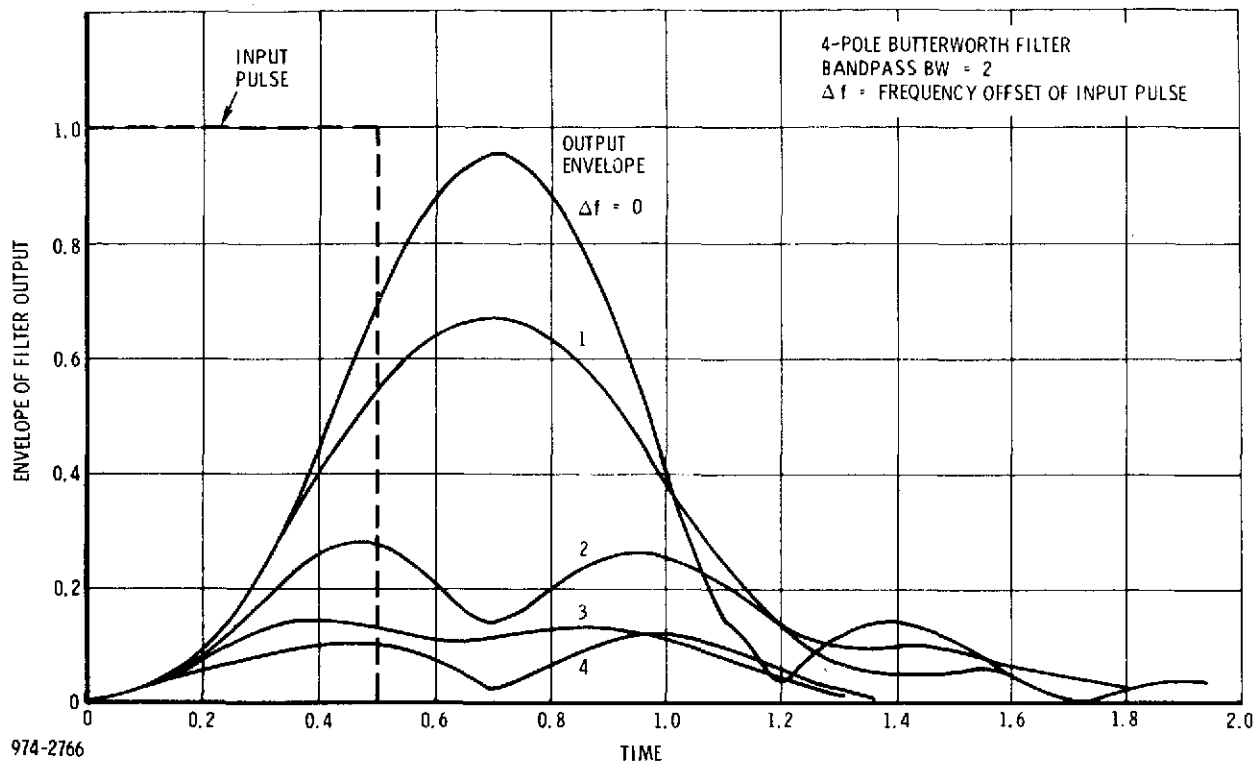


Figure 2-16. Processing in FH Receiver for Multiple Access

For EIRP = 35 dBw at minimum range to TDRS, the interfering pulse power is $35 \text{ dBw} - 190.3 \text{ dB} + 28 \text{ dB} = -127 \text{ dBw}$. The thermal noise (ideally, there is no multiple access noise with FH) in 100 kHz bandwidth, including 2 dB degradation for TDRS transponder loss, is $-199.4 \text{ dBw/Hz} + 2 \text{ dB} + 50 \text{ dB-Hz} = -147.4 \text{ dBw}$. Thus, if the 100 kHz bandpass filter produces an attenuation of at least 20 dB, the output pulse due to the interference at peak EIRP is below the thermal noise power in the filter output. This is the case except when the hopped pulse lies within 400 kHz bandwidth about the receiver's channel, or 13 percent of the total 3 MHz band. Assuming limiting of the filter output at the thermal noise level (a peak clipper), we conclude that the worst effect of interference from the high rate, high EIRP user is to suppress a portion of each symbol of the low rate user. Since the pulse interference is broadened by a factor of 2 and is negligible on 87 percent of the channels, the symbol is not suppressed at least $100 - 2 \times 13 = 74$ percent of the time, and the loss is less than 2.6 dB.



974-2766
UNCLASSIFIED

Figure 2-17. Pulse Response

A further possibility for interference is due to spurious frequencies produced by the implementation of frequency hopping as an approximation with discrete phase steps. To estimate this, let us evaluate the spectrum when the phase step is $\Delta\theta = 2\pi/L$, and there is no jitter due to clocking. A Fourier coefficient at the n th harmonic is given by

$$C_n = \frac{1}{2\pi} \int_0^{2\pi} f(\theta) e^{-jn\theta} d\theta \quad (2-22)$$

where $f(\theta)$ denotes the staircase approximation to a linear change of 2π over one cycle of the frequency offset. Thus,

$$\begin{aligned}
 |C_n| &= \frac{1}{2\pi} \left| \sum_{\ell=0}^{L-1} e^{j\ell 2\pi/L} \int_{\ell 2\pi/L}^{(\ell+1)2\pi/L} e^{-jn\theta} d\theta \right| \\
 &\approx \frac{\sin \pi n/L}{\pi n/L} \quad ; \quad n = 1 + kL \\
 &= 0 \quad ; \quad n \neq 1 + kL \tag{2-23}
 \end{aligned}$$

where k is an integer (positive, negative, or zero). For $L = 8$, corresponding to phase steps of 45° , the largest spurious output occurs at $n = -7$, and is 17 dB down. Thus, we may conclude that the spurious frequencies are typically at the output thermal noise level in the 100 kHz filter, for interference at the strongest EIRP, and do not further degrade performance of a low rate user.

Let us now consider what happens if the maximum EIRP is reduced to 27 dBw on the basis of restricting the maximum data rate to 50 Kbps and requiring rate $-1/2$ forward error correction. Now, the filter output is at the noise level if the filter produces an attenuation of at least 12 dB. This is the case except within 200 kHz bandwidth, or 6.7 percent of the total 3 MHz band. Since the pulse is now broadened by the factor 1.5, the symbol from the low rate user is not suppressed for at least $200 - 1.5 \times 6.7 = 90$ percent of the time, and the loss is less than 1.0 dB.

It should be remembered that the introduction of a peak clipper causes a small additional degradation. Theoretically, bandpass hard limiting in Gaussian noise causes a loss of 1 dB, and the loss is less with peak clipping (i. e., soft limiting). This additional loss for coherent FH is about the same as the NASA link budget of allowance of about 1 dB for multiple access loss with PN.

2.1.5.3.3 Conclusions

For a maximum EIRP of 35 dBw, required to convey 100 Kbps uncoded, multiple access by PN causes 5.5 dB degradation to a low rate user, compared with the NASA link budget. However, if the maximum data rate is restricted to 50 Kbps with forward error correction, maximum EIRP is reduced by 8 dB (3 dB for rate reduction plus 5 dB coding gain) to 27 dBw. Now, there is 1.5 dB degradation compared with the NASA link budget.

The analysis of multiple access by coherent FH with practical filters leads to degradation of the low rate user by about 2.6 dB for a maximum EIRP of 35 dBw to support 100 Kbps uncoded, and 1.0 dB for a maximum EIRP of 27 dBw to support 50 Kbps, coded. Appendix VII presents simulation results in agreement with the analysis.

Thus, it is concluded that while coherent FH does offer some advantage over PN in enabling coexistence of a high rate user and a low rate user, the degradation is still excessive when the maximum data rate is 100 Kbps, uncoded. However, if a requirement for forward error correction coding providing a coding gain of 5 dB is imposed on all users, reducing the maximum data rate to 50 Kbps and the maximum EIRP to 27 dBw, there is almost no advantage for coherent FH over PN. Furthermore, PN offers the advantage that the multiple access noise is Gaussian so that error correction decoders perform as expected.

It is concluded that it is adequate for multiple access to design the return link on the basis of PN, imposing a restriction on maximum EIRP to 27 dBw as required to convey 50 Kbps with rate - 1/2 coding providing a coding gain of 5 dB. This means a revision of the NASA link budget so as to increase required EIRP for low rate users by 1.5 dB. Then, a total data rate of 50 Kbps for all interfering users in one beam can be tolerated. There appears to be no significant benefit from controlling user EIRP unless a high rate user can possibly orbit to a point closer than 33, 862 Km to the TDRS (this is the closest approach for 2000 Km altitude).

2.1.5.4 Considerations on Effects of Phase Transient with an Electronically Despun Antenna

If an S-band multiple access user is spin-stabilized, gain may be maintained towards the TDRS by switching antenna elements synchronously with the vehicle rotation. The Synchronous Meteorological Satellite (SMS) is a representative design example. The S-band antenna consists of 32 elements spaced uniformly on a cylinder of radius 26 inches. The spin rate is 100 rpm; hence, the phase transient due to switching is periodic with a repetition frequency of $32 \times 100/60 = 53.3$ Hz. The phase variation is due to the motion of the antenna's phase center as the vehicle rotates, changing the distance to the receiver. Also, there is a phase jump when antenna switching occurs. Figure 2-18 shows the geometry. This is the worst case where the spin axis is perpendicular to the direction towards the TDRS. More generally, the sine of this angle multiplies the distance variations.

For purposes of this discussion, we assume a typical antenna gain to be 8 dB and the EIRP to be 18 dBw for a multiple access user⁽¹¹⁾. Then, the return link can support a data rate, with error correction coding, of about 5 Kbps.

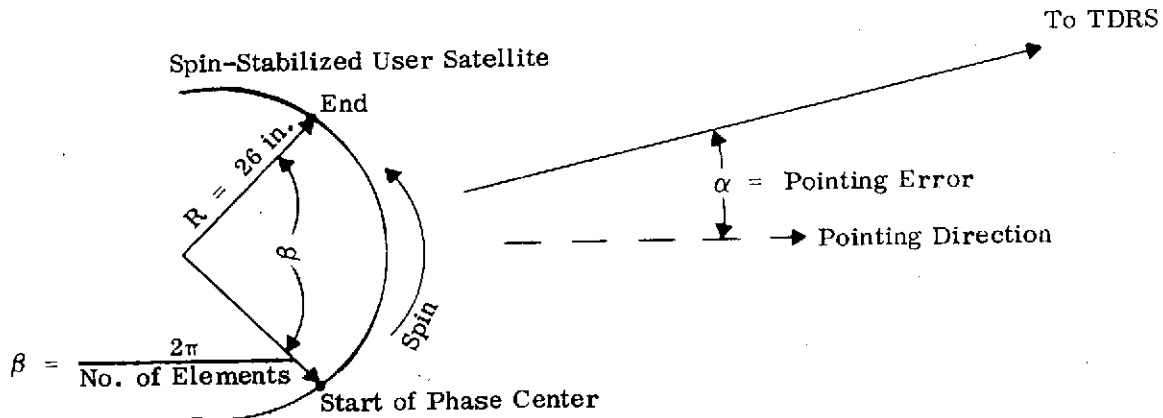


Figure 2-18. Geometry Determining Phase Transient

2.1.5.4.1 Calculation of Phase Transient

The approach to evaluation of the phase transient is to compute the variation in distance from antenna phase center to the TDRS⁽¹²⁾. From Figure 2-18, this variation with time is

$$\varphi(t) = \frac{2\pi R}{\lambda} \cos(\omega_0 t - \alpha); -\beta/2 < \omega_0 t < \beta/2 \quad (2-24)$$

where ω_0 denotes the angular frequency of spin and β is the angular spacing of the antenna elements. For a 32 element antenna, $\beta = 11.25^\circ$, and an instantaneous switch causes the phase center to move suddenly from $\beta/2$ to $-\beta/2$. The return link carrier frequency is 2.2875 GHz; hence, for $R = 26$ inches

$$\frac{2\pi R}{\lambda} = 1812^\circ \quad (2-25)$$

11. NASA Goddard Definition Phase Study Report, Section 6.

12. Philco-Ford, Synchronous Meteorological Satellite, Phase C Design Report, NASA-Goddard, Contract NAS6-21575, 30 June 1971, Analysis No. 16

Two measures of significance are the peak-to-peak variation $\Delta\phi$ and the phase jump φ_{jump} when the switch occurs. We find

$$\begin{aligned}\Delta\phi &= \frac{2\pi R}{\lambda} \left[1 - \cos \left(\frac{\beta}{2} + |\alpha| \right) \right] \\ &= \frac{4\pi R}{\lambda} \sin^2 \left(\frac{\beta}{4} + \frac{|\alpha|}{2} \right)\end{aligned}\quad (2-26)$$

$$\begin{aligned}\varphi_{\text{jump}} &= \frac{2\pi R}{\lambda} \left[\cos \left(-\frac{\beta}{2} + \alpha \right) - \cos \left(\frac{\beta}{2} + \alpha \right) \right] \\ &= \frac{4\pi R}{\lambda} \sin \alpha \sin(\beta/2)\end{aligned}\quad (2-27)$$

For the given parameters, (2-26) and (2-27) are plotted in Figure 2-19. The striking feature of these plots is the relatively small phase variation when the pointing error is close to zero.

2.1.5.4.2 Effect of Phase Transient on the Receiver

The phase transient due to antenna motion and particularly the instantaneous phase jump due to switching cause a degradation in performance of a biphase modulated data transmission system. Presuming Costas loop tracking to reconstitute carrier phase, one source of degradation is the tracking error φ_e which exists at any instant due to the phase transient. This degradation is measured by $\cos \varphi_e$ in a biphase data modulation system. Note that φ_e is less than ϕ because of the loop tracking, which improves as the loop bandwidth is widened.

A second source of degradation is the greater tendency for the Costas loop to slip when the tracking error starts to become large.

A third potential problem arises because the periodic phase transient creates sidebands separated from the carrier by multiples of the repetition frequency (53.3 Hz). The Costas loop possibly could acquire one of these sidebands, if it were sufficiently strong.

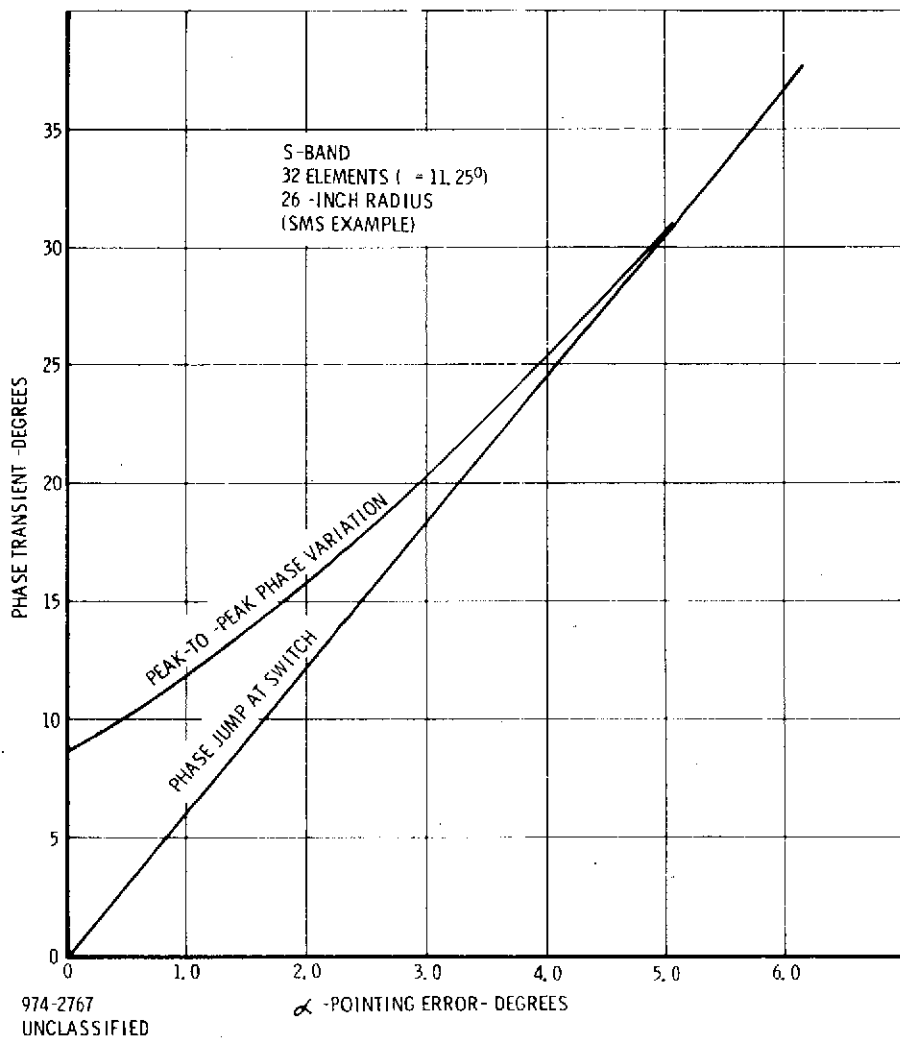


Figure 2-19. Phase Transient of Switched Antenna

Let us now consider typical Costas loop design parameters. For operation at $E_b/N_0 \cong 5$ dB with rate $-1/2$ error correction coding, simulation studies demonstrate that the loop tracking bandwidth (one-sided noise bandwidth) B_L should not exceed about 3 percent of the symbol rate⁽¹³⁾. For a typical data rate of 5 Kbps, this means $B_L \leq 300$ Hz, and the first few harmonics of the periodic phase transient are tracked with negligible phase error. (Also, Doppler due to

13. C. R. Cahn, G. K. Huth and C. R. Moore, "Simulation of Sequential Decoding with Phase-Locked Demodulation", IEEE Trans. on Comm., Vol. COM-21, February 1973, pp. 89-97.

orbital dynamics is tracked with negligible error.) Mainly, the instantaneous phase jump when the antenna is switched remains until the loop recovers in accordance with its closed-loop response. Thus, as a pessimistic approximation, we have

$$\text{Degradation Due to Tracking Error} \cong 20 \log_{10} \cos \varphi_{\text{jump}} \quad (2-28)$$

A degradation of 0.5 dB results for a phase jump of 19° , and this represents a reasonable design criterion. From Figure 2-19, this corresponds to a pointing error of not more than $\pm 3^\circ$.

When the switch occurs, the Costas loop momentarily has the phase error φ_{jump} , and could possibly be forced into a cycle slip. In the absence of noise, a slip will not occur until the phase jump approaches 90° , beyond which point the loop will track at a phase error of 180° . When noise is present, a slip can occur for a smaller phase jump because the phase jump can be additive to a momentarily large tracking error due to noise. Analytical characterization of the statistics of this nonlinear tracking problem is difficult.

A simple analysis based on a linearized loop is now presented. The loop signal-to-noise ratio for a Costas loop is

$$S/N = \frac{S}{N_0 B_L} \left[\frac{1}{1 + N_0/2ST_s} \right] \quad (2-29)$$

where a matched filter to the symbol duration T_s is presumed. The variance of the phase error due to noise is $(S/N)^{-1}$. For the typical design parameters with rate $-1/2$ coding postulated above, $S/N = 36$ (15.6 dB), and the rms tracking error due to noise is $1/6$ radian = 9.5° . As a pessimistic estimate of the maximum tolerable phase jump for which a cycle slip is unlikely, let us require

$$5 \times 9.5^\circ + \varphi_{\text{jump}} < 90^\circ \quad (2-30)$$

where we take the 5σ point as the peak phase error due to noise. Then, we require

$$\varphi_{\text{jump}} < 42^\circ \quad (2-31)$$

to insure a low probability of a slip when the phase jump occurs. This is less stringent than previously imposed by data demodulation performance.

To test this rough analysis, a computer simulation was performed where a phase jump is applied to a second-order Costas loop with the typical parameters described above for rate $-1/2$ error correction coding. The jump was applied after the loop had been driven by noise for an interval $2B_L^{-1}$. A cycle slip was declared if the phase error reached 90° within $8B_L^{-1}$ after the jump occurred. Ten trials were taken for each value of phase jump. A slip was not observed until the phase jump = 46° . This is in good agreement with the rough analysis above. As a further test, a periodically occurring phase jump was applied to a second-order Costas loop, and the mean time to a phase slip T_{slip} was measured as a function of the magnitude of the phase jump. The repetition rate of the phase jumps was set at $B_L/6.4$, as a typical design. The loop signal-to-noise ratio was set so that $B_L T_{\text{slip}} \approx 100$ without the phase jumps. It was found that T_{slip} was not significantly reduced until $\omega_{\text{jump}} = 40$, again in good agreement with the rough analysis.

Let us now consider the magnitude of the sidebands due to the phase variation. A sinusoidal variation with a peak-to-peak magnitude $\Delta\phi$ produces first-order sidebands with amplitude $J_1(\Delta\phi/2)$. For a pointing error of 3° , $\Delta\phi = 20^\circ$, and the first-order sidebands are 21 dB down. For the postulated design parameters, the Costas loop is perhaps 6 dB above its tracking threshold*; hence, there is no possibility of falsely acquiring a sideband of this magnitude. There would be a problem if the Costas loop were made to have a bandwidth considerably smaller than 53 Hz.

2.1.5.4.3 CONCLUSIONS

Taking the SMS antenna is a representative design for an S-band multiple-access user, the effect of sudden antenna switching to electronically de-spin the antenna pattern appears to be of minor concern unless there is a large pointing error. A pointing error of $\pm 3^\circ$ is tolerable without significant performance penalty (degradation less than 0.5 dB) to a biphase modulated data transmission system with Costas loop phase tracking.

* Note, a Costas loop has a 6 dB poorer tracking threshold than a conventional phase lock loop, for the same B_L . Thus, a threshold of $S/N = 3$ dB for a conventional loop corresponds to $S/N = 9$ dB in a Costas loop.

2.1.6 RECOMMENDED WAVEFORM PARAMETERS FOR MULTIPLE ACCESS SYSTEM WITH STEERED TRANSMIT BEAM

The current TDRSS design concept calls for a transmit beam to be steered from the TDRS to the user on the forward link of the multiple access system. Thus, only one user can be commanded at a time, and reacquisition of the user receiver is necessary prior to each command. During the time that the forward link is established to a user along with the return link, two-way range and range rate measurements may be taken. One-way range rate measurements can be made when only the return link is established. The operational value of one-way range rate for tracking and orbit determination is dependent on the accuracy (particularly short term) of the user's reference oscillator.

The main advantage of the steered transmit beam is to increase EIRP so as to enable a higher data rate to a user with a poor receiving antenna. The objective is to be able to work with a user antenna gain as low as $G_u = -6$ dB. The obvious disadvantage of this concept is the greater TDRS complexity, since multiple transmitting antenna elements and a method of phase shifting to steer the beam must be provided. Also, there is time lost in reacquisition of the forward link prior to transmission of a command to the user.

Since the multiple access users do not continuously track the forward link signal with this steered transmit beam concept (in contrast to the fixed field of view concept), the possibility is brought in of aiding the sync acquisition process by taking advantage of a priori knowledge of range and range rate to the user. In particular, the range rate uncertainty after a priori information is introduced is small enough to simplify the user transponder by eliminating necessity for a Doppler processor in the spread spectrum receiver to cover the full Doppler uncertainty of an orbiting vehicle.

The basic ground rule is assumed that multipath should be discriminated for any possible delay relative to the direct signal. For a user altitude of 2,000 Km, this maximum delay is 13 milliseconds. Although the multipath at S-band is predominately diffuse, it would appear as narrowband noise without discrimination by the correlation detection process in the spread spectrum receiver if the delay exactly equals a period of a repetitive signal. The multipath can

approach the strength of the direct signal, and conceivably may be received by the user even stronger than the direct signal if the user antenna pattern happens to favor the multipath direction of arrival.

A goal for two-way ranging is to have an ambiguity not less than 10,000 Km. This implies a repetition period of at least 66.7 milliseconds in the spread spectrum modulation utilized to make the range measurement, or, alternatively, a scheme for resolving the ambiguity by means of the data modulation.

2.1.6.1 Design of Forward Link Signal

On the forward link, the multiple access requirement is to accommodate at most two signals, one from each TDRS. The power ratio will be close to 0 dB. Also, the power variation at the user receiver will be relatively small, primarily due to variation of the receive antenna gain with vehicle orientation. We wish to discriminate against multipath by having the signal period exceed the maximum multipath delay. At the same time, we desire to use the maximum available bandwidth, the objective being to optimize the range measurement accuracy if this does not conflict with other requirements.

Suppose that we employ a periodic PN code with the chip rate set at 3 Mbps, where a channel bandwidth of 4.5 MHz is suggested to essentially eliminate PN loss* when staggered quadriphase (SQPN) is used. The PN code period must then be at least 39,000 chips to meet the objective of discriminating against multipath up to the maximum delay. An acceptable acquisition time cannot be realized for this relatively long code period.

A solution to this problem lies in the use of a sync preamble which is easily acquired while still providing multipath discrimination. The steered transmit beam concept, moreover, is compatible with such a preamble, since only the intended user receiver needs the signal. One preamble approach is described in para. 2.1.3.1. Here, the preamble has a frequency hopping structure with a period exceeding the

* The SQPN waveform at 3 Mbps is filtered to 4.5 MHz bandwidth and hard-limited. If the receiver has 4.5 MHz bandwidth and negligible phase distortion, the PN loss is 0.1 dB, according to Figure 2-7 of Section 2.1.1.2.

multipath delay and also satisfying the ranging ambiguity goal. A second preamble approach is based on a short PN code as described in paragraph 2.1.3.3, where a sub-code (a form of data modulation) is introduced to achieve an overall long period for resolving the ranging ambiguity. With either preamble approach, the transmitter switches to a nonrepetitive PN code (or one with a period exceeding 66.7 milliseconds as set by the ranging ambiguity goal) after the preamble has been transmitted for a sufficiently long interval that the user receiver will have acquired.

The frequency hopping preamble approach with an implementation based on staggered quadriphase appears to be simple and straightforward, while guaranteeing protection against long multipath delays. It is therefore recommended for the forward link design. Somewhat modifying the parameters previously described we suggest for the preamble

Hopping rate	= 3 kHz
Frequency spacing	= 12 kHz
Code period	= 256 hops = 85.3 milliseconds
Bandwidth	= 3.072 MHz (equals chip rate* of SQPN)

The code period exceeds twice the maximum multipath delay. The range ambiguity is 12,800 Km, which exceeds the goal of 10,000 Km.

After the preamble has been transmitted, the forward link signal is switched to SQPN with a code period of 85.3 milliseconds and a PN chip rate of 3.072 Mbps. The code period is $2^{18} = 262144$ chips, which is a maximal length extended by one chip.

The acquisition procedure on the forward link is as follows:

1. Direct a transmit beam from TDRS to user.
2. Insert user address, selecting the preamble hopping code and the subsequent PN code to be transmitted.

* The precise chip rate is still to be selected, and will be dependent on a detailed design study of frequency synthesis and intermodulation considerations, but is suggested to be nominally 3 Mbps. The ground system reference standard is 5 MHz.

3. Insert a priori range rate information (see discussion subsequently) into the transmitter.
4. Wait a sufficient time for acquisition of the preamble to be completed by the user receiver.
5. Switch to long period PN code and wait for receiver acquisition again. (Possibly, indication of PN acquisition is transmitted back on the return link.)
6. Define data bit timing.

2.1.6.2 Acquisition Time on Forward Link

We now estimate the acquisition time on the forward link. To begin, assume $G_u = -3$ dB. Then, the received S/N_o including 1 dB transponder loss, is approximately 36 dB-Hz, for a TDRS EIRP of 34.9 dBw (this includes 10 dB additional gain from the directed transmit beam). If the receiver covers the full Doppler of ± 55 kHz with a coherent processing by a Doppler processor extended over one frequency hop interval of 333 microseconds, Figure 10 of Appendix III shows that the search rate for probability of detection = .8 is approximately 63 chips/sec, based on $E/N_o = 18$ dB. Since the preamble has 256 chips (chip is here a frequency hopped pulse), this acquisition step takes 4 seconds. Note that $E_b/N_o = E/N_o - 16.7$ dB = 1.3 dB, which is realized with the 3 Khps hopping rate and $S/N_o = 36$ dB-Hz.

If $G_u = -6$ dB, the acquisition time for this step would be, at most, quadrupled to about 16 seconds. Also, note that Doppler on the chip rate of 3 Khps is not a problem, since the worst Doppler causes an offset of only .08 chip/sec, far less than the search rate. In contrast, if the preamble were PN at a chip rate of 3 Mbps, the Doppler on the chip rate could be 78 chips/sec, exceeding the search rate, and such a preamble would not be satisfactory.

We can improve the acquisition performance by taking advantage of a priori information of range rate to reduce the Doppler uncertainty. A ground rule is that the range rate uncertainty is ± 100 m/sec, corresponding to ± 700 Hz Doppler uncertainty at S-band. Still letting the coherent integration extend over 333 microseconds, the degradation at 700 Hz offset is 0.8 dB according to (2) of Appendix III. For probability of detection = .8, Figure 5 of Appendix III shows that with $G_u = -4$ dB, or $S/N_o = 35$ dB-Hz, the search rate is 160 chips/sec, based on $E/N_o = 12.2$ dB + 0.8 dB. With a period of 256 chips, this acquisition step takes 1.5 seconds. Note from

the referenced figure that $E_b/N_0 = 0$ dB at this design point, and this is approximately the case for the present parameters (E_b/N_0 in 333 microseconds = 0.3 dB at $S/N_0 = 35$ dB-Hz). For $G_u = -6$ dB, or $S/N_0 = 33$ dB-Hz, the acquisition time for this step is increased, at most, to approximately 4 seconds. Thus, very acceptable acquisition performance is achieved when a priori range rate information is inserted in the ground transmitter. Also, a short PN code preamble now could be used, since the code Doppler uncertainty is 1 chip/sec. Note that a correction to the two-way range rate measurement will be necessary as a consequence of the offset transmit frequency.

The above computation does not take into consideration any loss in E/N_0 associated with the digital implementation of frequency hopping as an approximation by phase stepping. The maximum loss is 3 dB for 90° steps and 0.7 dB with 45° steps. Implementation is somewhat more complex with 45° steps, requiring an 8 step IPM which can offset frequency by ± 1.5 MHz.

When acquisition is detected with the frequency hop preamble, the time uncertainty is then approximately the width of the hopping pulse, or 333 microseconds. This corresponds to 1,000 PN chips of uncertainty in the PN code following the preamble. At $G_u = -4$ dB, the search rate is still 160 chips/sec, so that acquisition of the PN code requires 6 seconds additional time, and this becomes, at most, 15 seconds at $G_u = -6$ dB. The total acquisition time is thus about 8 seconds at $G_u = -4$ dB, and would be, at most, 13 seconds at $G_u = -6$ dB.

The last step of acquisition is to define the data bit timing. If the data is synchronous with the PN code, the data clock can be derived as a countdown from the PN code rate. Data modulation is applied as NRZ differential biphase, and the receiver has a Costas loop for carrier tracking. This approach would allow asynchronous data to be accepted by the ground transmitter by reclocking the asynchronous bits in a first in, first out (FIFO) buffer. The typical situation is that the data clock is nominally correct, which implies a maximum offset of 2.6×10^{-5} when the transmitter inserts the estimate of Doppler. At a data rate of 1,000 bps, there could develop a shift of one bit after 38 seconds. Thus, the FIFO buffer for reclocking asynchronous command data need not have a very large capability. It may be pointed out that this approach has been successfully implemented in the AN/USC-28 satellite communications modem to accept asynchronous teletype and relock it into synchronous data at 75 bps.

An alternative is to transmit asynchronous data without maintaining any coherence with the PN code rate. This is feasible when the processing gain is not too small (say at least 20 dB) and entails in the transmitter simply reclocking the data bit edges to coincide with possible PN code transitions. In the receiver, however, there now is additional complexity of a data bit synchronizer. Also, there is a requirement for the data to be sufficiently random that the bit timing can be established uniquely*.

2.1.6.3 Design of Multiple Access Return Link Signal

Although a frequency hopping modulation scheme potentially would facilitate coexistence of a high data rate user with a low data rate user on the multiple access return link, the advantage in practice over PN was shown in paragraph 2.1.5.3 to be rather small. Furthermore, use of PN guarantees that error correction coding will produce the anticipated coding gain computed for a coherent PSK channel with Gaussian noise interference. Thus, for the return link, we recommend a SQPN modulation with a PN chip rate = 3.072 Mbps and a code period of 2^{18} chips, or 85.3 milliseconds, identical with that on the forward link.

After the forward link is established, the user is commanded to interrupt the one-way mode and start transmitting on the return link in a turnaround transponding mode. Now, a priori range and range rate information is inserted into the ground receiver, where the uncertainties are ± 50 Km and ± 100 m/sec, respectively. Thus, the range uncertainty at the ground receiver, after coherent turnaround in the transponder, is 2050 PN chips, and the Doppler uncertainty is ± 1400 Hz. If the minimum user EIRP is 7 dBw (10 watts with antenna gain of -3 dB), the received S/N_0 into a directed receive beam is 34.6 dBw with typical multiple access interference. For a probability of detection of 0.8, the search rate (based on $E/N_0 = 13$ dB) is 140 PN chips/sec, and the acquisition time to search the range uncertainty is about 15 seconds at the minimum user EIRP.

After acquisition in the ground receiver has been accomplished, the user can be commanded transmit data asynchronously to the PN code clock, although it would appear feasible in many user satellites to supply clock from the transponder to the data source so that data is returned synchronously. Of course,

* There may not be enough transitions with NRZ data. Manchester is a technique to insure one transition per data bit; however, then an ambiguity could exist.

accommodating data asynchronously provides maximum system flexibility, and imposing a need for a bit synchronizer in the ground receiver is not of much concern, except that bit tracking with error correction coding and low E_b/N_0 is more difficult. It should be noted that the coherent FH scheme would demand the data be synchronous with the hopping rate.

With PN multiple access, the interference due to other users within the same beam is additive to the receiver thermal noise. Although the interference effect varies somewhat with relative chip phasing, we simply take the good approximation here for performance computations that the interference power is spread uniformly to a 3 MHz bandwidth. To estimate the tolerable interference within the beam, we assume the typical range to the interfering users is about 23,000 miles, for which the free space loss is 191 dB. Taking the gain of the receive beam as 28 dB, the power density in the receiver for 3 MHz bandwidth is

$$\begin{aligned} \text{Interference power density} &= \text{EIRP}_{\text{Int}} - 191 \text{ dB} + 28 \text{ dB} - 10 \log_{10} (3 \times 10^6) \\ &= \text{EIRP}_{\text{Int}} - 228 \text{ dBw/Hz} \end{aligned} \quad (2-32)$$

The NASA link budget allows for a multiple access degradation by 1.2 dB and a TDRS transponder loss of 2 dB (which is presumed to be an increase in noise level due to a finite signal-to-noise ratio on the TDRS to ground link). Since the receiver noise temperature is 824°K , the total noise in the ground receiver is found by combining the three contributions:

$$\begin{aligned} \text{Receiver thermal noise} &= -199.4 \text{ dBw/Hz } (T_s = 824^{\circ}\text{K}) \\ \text{TDRS-to-ground noise} &= -200.6 \text{ dBw/Hz} \\ \text{MA interference noise} &= \text{EIRP}_{\text{Int}} - 228 \text{ dBw/Hz} \end{aligned} \quad (2-33)$$

The multiple access degradation is the increase in total noise level when interfering users are present, and this is plotted in Figure 2-20. The total data rate on the interfering users falling within the beam is shown in Figure 2-21 (taken from NASA Goddard Definition Phase Study Report) as a function of total interfering EIRP.

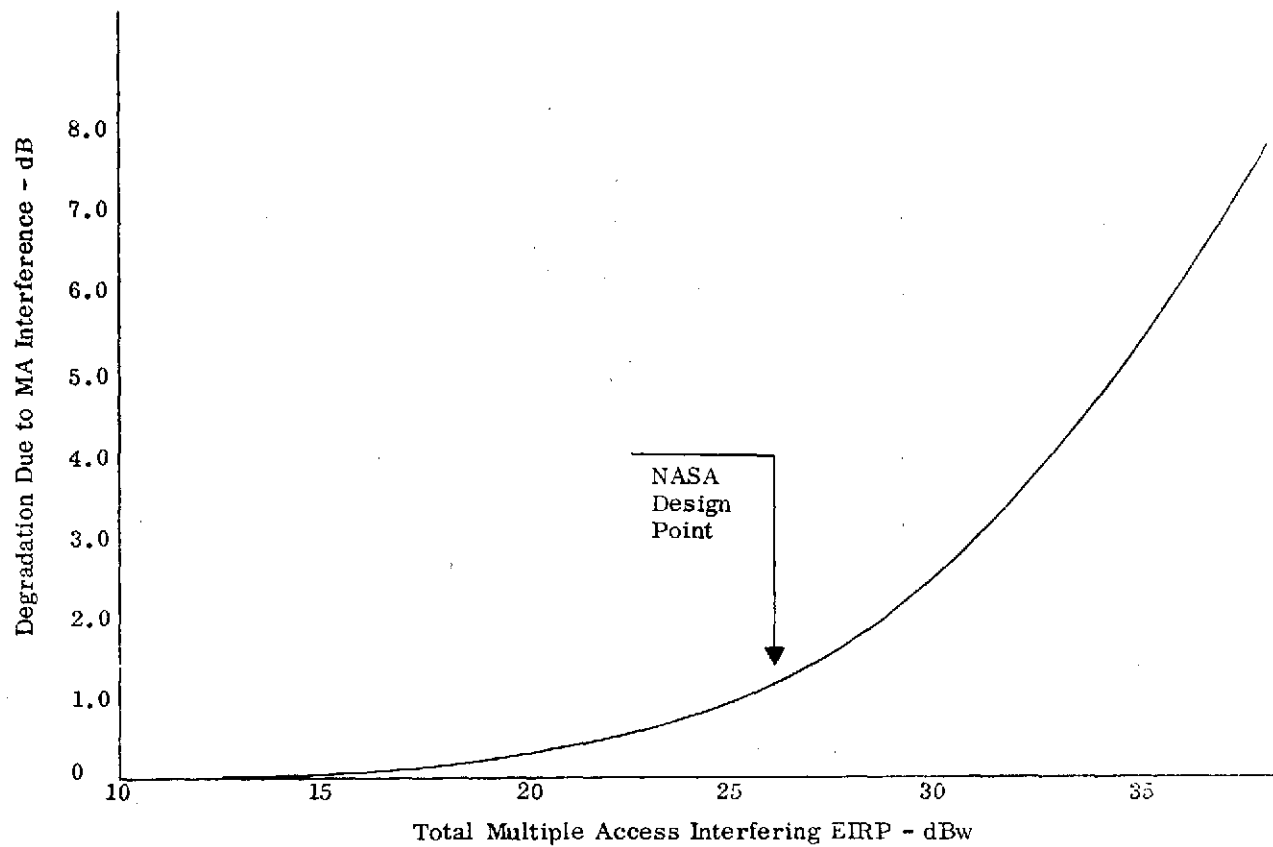


Figure 2-20. Degradation Due to Multiple Access Interference

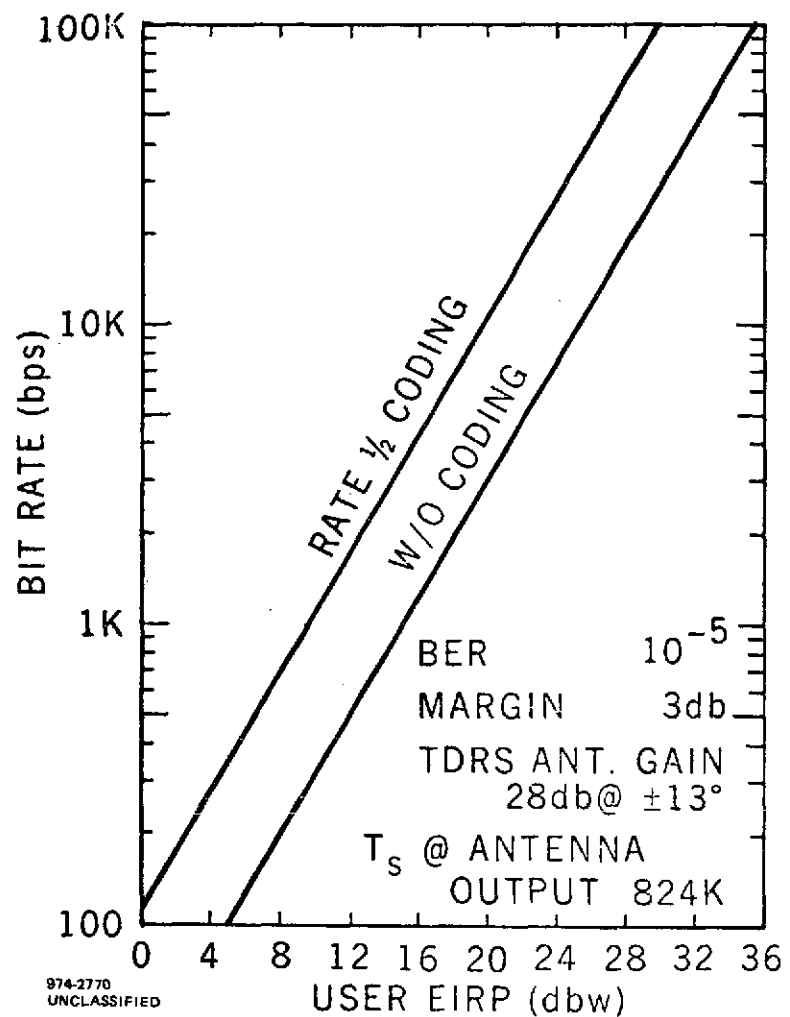


Figure 2-21. Multiple-access (S-band) Return Link Data Rate vs. User EIRP

2.1.6.4 Distribution of Multiple Access Interference

To obtain a feel for the likelihood that a multiple access user will experience excessive interference from other users within the same beam, we postulate a distribution of user data rates*. This distribution is given in Table 2-1.

Table 2-1. Postulated Distribution of User Data Rates

Data Rate (Kbps)	0-5	5-10	10-15	15-20	20-25	25-30	30-35	100
No. of Users	4	2	2	2	2	3	2	2
EIRP/User (dBw)	13.6	18.5	20.6	22.0	23.1	24.0	24.7	34.8

The table supposes each user has the EIRP specified by Figure 2-21 for the data rate at the midpoint of its range, and all users except the 100 Kbps users employ rate -1/2 error correction coding. We assume that a user causes no interference unless it falls within the beam directed toward the desired user so that the AGIPA system cannot form a null. The probability of this is assumed to be .032. (This presumes a gain of 15 dB for the directed beam over that for a single antenna element covering the same total field of view, and ignores orbital distributions and eclipse effects.)

As a simple calculation to begin with (and also a lower bound), we take only the 100 Kbps users. Then, the probability distribution of interference power and corresponding multiple access degradation from Figure 2-20 is shown in Table 2-2.

Table 2-2. Distribution of MA Degradation Due to 100 Kbps Users

Cumulative Probability Distribution	Two interfering users at 100 Kbps	
	EIRP	MA Degradation
.001	37.8 dBw	8 dB
.063	34.8	5.3
.937	Negligible	0

*Verbal information from NASA Goddard.

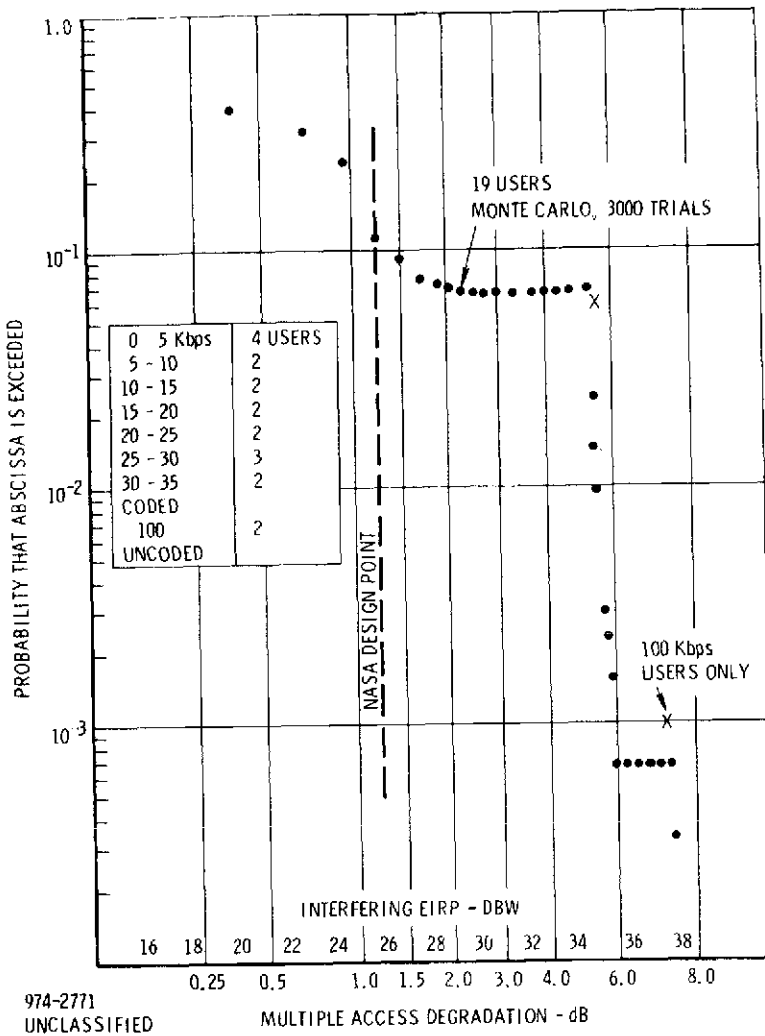


Figure 2-22. Distribution of Interference

Next, considering all users listed in Table 2-1, we obtain * the distribution of total power and multiple access degradation given in Figure 2-22. Note that the tail of the distribution is due almost entirely to the existence of two high-EIRP users.

* This distribution was obtained by a Monte Carlo simulation to approximately measure the distribution of total interference power, quantized into increments, for the postulated statistical model.

For a comparison, let us now assume the two highest data rate users are at 50 Kbps data rate with error correction so that their EIRP is 26.6 dBw, while the lower rate users are as in Table 2-1. The resulting distribution of power and MA degradation is shown in Figure 2-23.

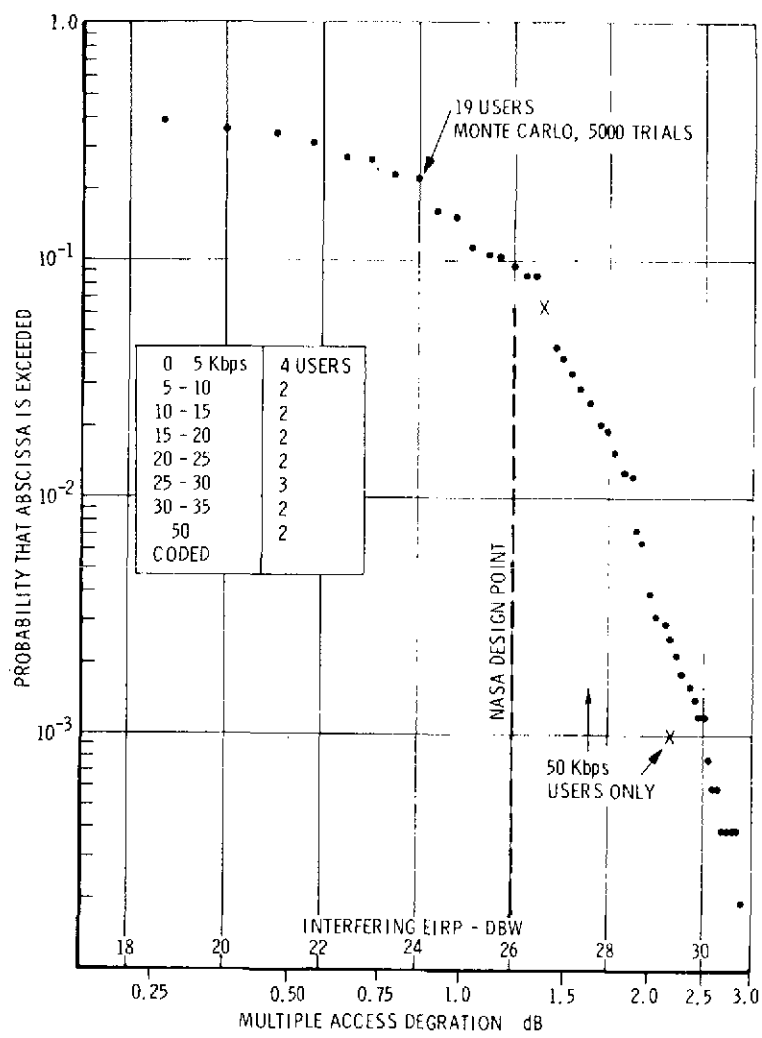
2.1.6.5 An Alternative to Interrupting the Return Link to Switch to Coherent Turnaround Transponding

With the system concept described above, the return link must be interrupted whenever two-way range and range rate measurements are to be made. The reason for this is to enable the user transponder to switch into a coherent turnaround mode while the forward link is established to that user. Then, the two-way range and range rate measurements are made on the ground by comparing receive and transmit phase (PN code phase for range, carrier phase for counting Doppler cycles). This interruption may not pose any operational difficulty to a typical user with a memory to store the return data during the short interruption while the return link resynchronizes.

A user who cannot tolerate interruption of the return link has an alternative, which is now described. Basically, the measurements are made in the user and transmitted as data to the ground. If range is measured with a resolution of 1/128 chip, a total of 25 bits suffices for the full code period. Similarly, if Doppler is measured to a resolution of 1/128 cycle over one second averaging, 24 bits suffices for Doppler of ± 65 kHz. Therefore, a data rate of one per second.

With this alternate scheme, the user continually transmits on the return link with a fixed frequency from its internal oscillator, and the ground receiver continually makes a one-way measurement of range rate. The ground equipment also operates as a coherent turnaround transponder to transmit on the forward link to the user. The user tracks code and carrier phase of the forward link signal. Thus the user can make its own two-way range measurement by comparing receive and transmit code phases, and a range rate measurement by comparing receive and transmit carrier phases to count Doppler cycles.

The data describing these measurements simply are the contents of counters which store the phase differences and are read out periodically (say once per second). This implementation is particularly straightforward if the user receiver tracks by digital phase shifting (see Section 2.1.1.6).



974-2772
UNCLASSIFIED

Figure 2-23. Distribution of Interference

The range and range rate measurement data can be time division multiplexed with the user's telemetry data by a technique which has previously been implemented in spread spectrum modems to multiplex an order wire capability with a data channel. Essentially, a fraction of the PN code bits are designated to convey the order-wire data, and the receiver has an extra correlation channel to demodulate this order-wire data. It should be noted that this concept has the disadvantage that the accuracy of the measurements is dependent on the stability of the user's oscillator, and this is poor compared with the ground station standard. Also, the data rate becomes rather high (500 bps) for the multiple access system if measurements are required at a rate as high as ten per second.

Based on the comments from potential NASA users of TDRS, there appears to be no inherent objection to interrupting the return link so as to switch into two-way coherent transponding on the multiple access system. Thus, the concept of a user satellite making its own range and range rate measurements is not further recommended for application to the multiple access system. Use of an order wire for status data is still plausible; however, in general, the user's telemetry system can make status bits available (e.g., to indicate forward link acquisition).

2.1.6.6 Functional Description of Multiple Access Modulation Equipment

This section presents functional block diagrams of the modulation equipment for the multiple access system. In Figure 2-24, we start with the receiver portion of the user transponder since it contains all the basic implementation elements. All frequencies are synthesized from a fixed reference oscillator so as to implement coherent turnaround in the two-way mode of operation. The receiver does not have a VCO; instead, there is digital tracking via IPMs. Thus, the switch from one-way operation to two-way operation is entirely digital.

When synchronized, the receiver correlates with a replica of the PN code of period 2^{18} chips at 3.07 Mbps, and tracks carrier phase by a Costas loop configuration. The error signal is filtered to give a third-order transfer function with a loop noise bandwidth (one-sided) around 5 Hz, and the carrier phase tracking is done by controlling (or stepping) the carrier IPM. The IPM resolution is set by the requisite tracking accuracy; for example, a 64-step IPM produces a lower bound

on rms phase error of .0045 cycle (1.6°) due to quantization. The receiver tracks code phase by a "dither" early-late delay-lock loop, which compares (by alternately switching back and forth) correlation for early and late versions of the PN code.

The error signal is filtered to give the desired transfer function (typically second order), and the code phase tracking is done by controlling the code IPM. The code IPM has the requisite quantization; e.g., 64 steps yields a lower bound in rms error of .0045 chip. Note that the clock is corrected for Doppler by scaling from the carrier IPM. This removes Doppler from the code tracking loop, which then can be made quite narrow band (say 0.1 Hz) to enable accurate range measurement.

For initial FH synchronization (mode 1), the PN code is removed and a frequency hopping sequence with a period of 2^8 hops is generated at 3 Khps. The rate multiplier scheme described in Section 2.1.1.3 is utilized to synthesize the frequencies by approximating them with 90° phase steps via the SQPN modulator. (An 8 step IPM can also be implemented easily to obtain the improved performance with 45° phase steps.) The hopping clock is derived by counting down from the PN clock, and the search is done in half chip steps (167 microsecond steps) by inhibiting the countdown. Correlation is detected by a sequential detection process which recognizes a build-up of amplitude at the output of a 3 kHz bandpass filter (integrate-and-dump filter was described in Appendix III). The receiver then switches to PN synchronization (mode 2). The PN code generator is set to the phase indicated by the FH sequence position at which sync was detected in mode 1, and a fine search is now implemented by controlling the clock IPM. Again, a build-up of amplitude is to be detected in the bandpass filter. At this point, the code and carrier tracking loops are operative*. Final sync detection is recognized by the action of carrier acquisition, which is indicated when $I^2 - Q^2$ exceeds a threshold. AGC action sets all thresholds. Then, data can be demodulated with the synchronous timing derived from the PN clock by countdown. Some error correction coding could be used on the forward link if desired, although none as shown in Figure 2-24.

* The frequency error presented to the Costas carrier tracking loop is large relative to the loop bandwidth. It may be reduced by a frequency discriminator (a digital implementation counts phase crossings) to estimate frequency, or alternatively, a frequency sweep may be implemented in the loop for frequency acquisition.

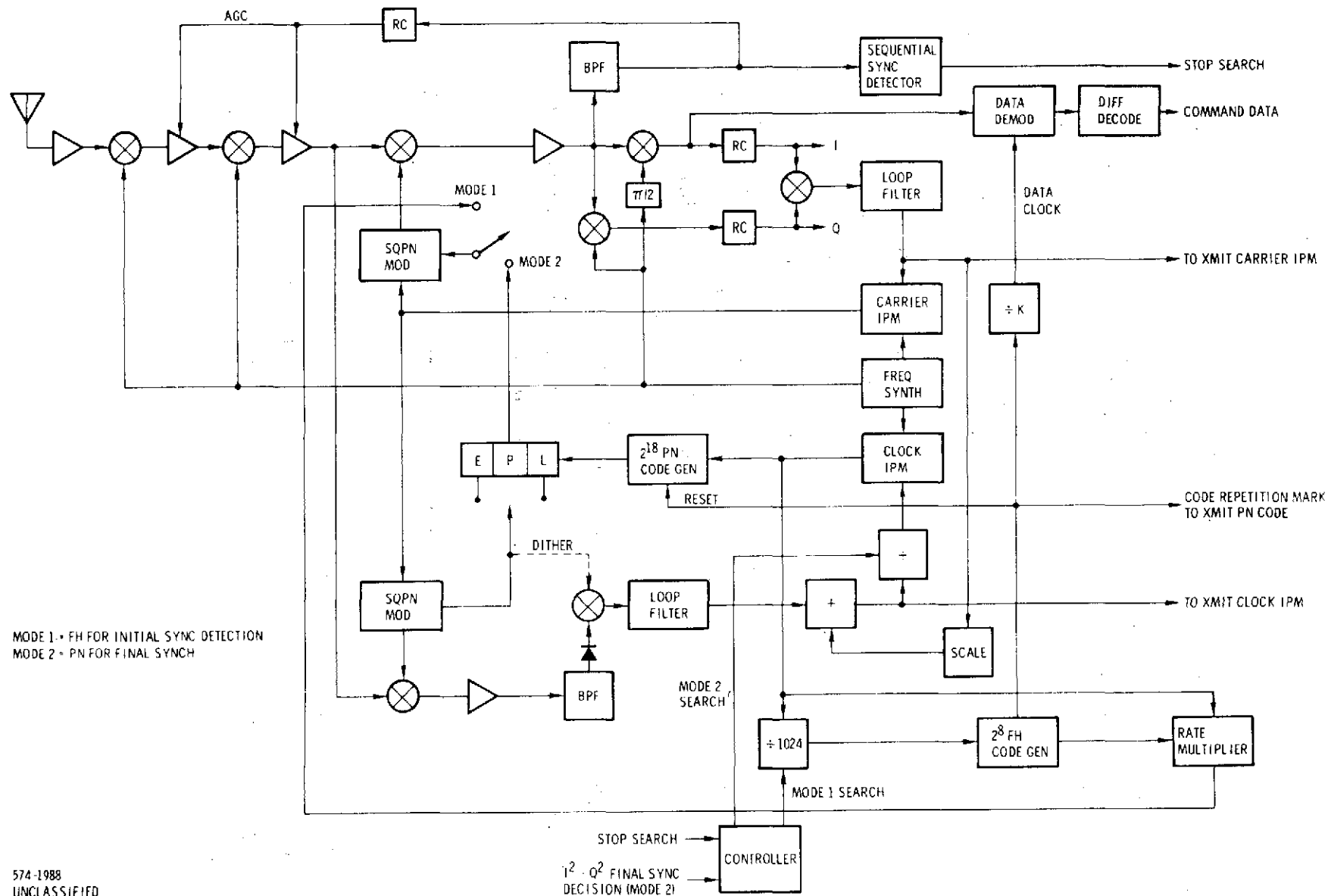


Figure 2-24. Functional Block Diagram of Multiple Access User Receiver

Figure 2-25 shows the transmitter portion of the user transponder. The frequency synthesizer is, of course, shared with the receiver portion, and the requirement for coherent transponding is that all frequencies be generated from a single oscillator. Since carrier tracking is done digitally in the receiver, the transmitter is offset by the receive Doppler also digitally with scaling by 240/221. The transmit PN code is generated in phase with the receiver code; here, there is no scaling required to turnaround the receive code Doppler.

The data is differentially encoded and then error correction encoded. The data clock can be asynchronous to the PN clock, in which case the data transitions are simply reclocked to coincide with the closest possible PN code transition.

Because of the essential similarities to the user equipment, we do not show separate block diagrams of the ground transmitter and receiver. Both require Doppler offsetting of carrier and code to facilitate acquisition, as discussed previously. The digital number commanding the offset is input to a rate multiplier, the output of which drives the carrier IPM to produce the Doppler on the carrier. The code IPM is similarly driven with a scaled version to produce the Doppler offset on the code. The command is updated as required while a search for acquisition is being conducted*.

2.1.6.7 Range and Range Rate Measurement Accuracy

As given in paragraph 2.1.4, the range measurement accuracy for a dither-type, noncoherent delay-lock loop tracking a PN signal is described by its variance

$$\sigma_{\text{chips}}^2 = \frac{N_o B_L^{(\text{code})}}{S} \left[1 + \frac{2N_o B_{\text{IF}}}{S} \right] \quad (2-34)$$

where B_{IF} is the bandwidth prior to envelope detection. With biphase data, a matched integrate-and-dump filter sets $B_{\text{IF}} = T_b^{-1}$. On the forward link, $S/N_o = 33 \text{ dB-Hz}$ for a user antenna gain $G_u = -6 \text{ dB}$; hence, for a data rate of 100 bps, $B_L^{(\text{code})} = 0.1 \text{ Hz}$, and 3.07 Mbps chip rate,

$$\left. \sigma_{\text{range}} \right]_{\substack{\text{forward} \\ \text{link}}} = 0.72 \text{ meters}$$

*The range rate of an orbiting user cannot change by more than 10 m/sec; hence, the range rate estimate need be changed only every few seconds, since the uncertainty is $\pm 100 \text{ m/sec}$.

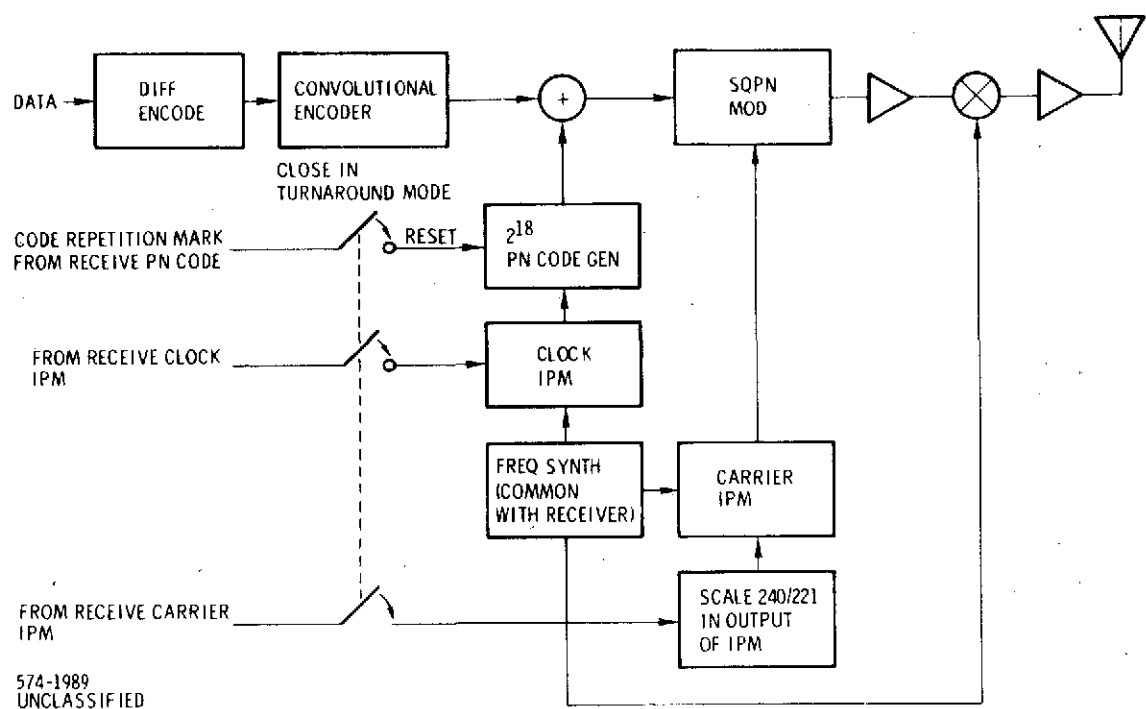


Figure 2-25. Functional Block Diagram of Multiple Access User Transmitter

The minimum S/N_0 on the return link is about the same; however, with coding, the data rate can be 300 bps, or 600 symbols/sec, and $B_{IF} = 600$ Hz. For $B_L^{(code)} = 0.1$ Hz and chip rate = 3.07 MHz,

$$\sigma_{range} \left[\begin{array}{l} \text{return} \\ \text{link} \end{array} \right] = 0.87 \text{ meters}$$

Since the errors on the two links are independent, the resulting two-way range measurement error is obtained by combining the one-way errors rms and dividing by two; thus,

$$\sigma_{range} \left[\text{two-way} \right] = 0.57 \text{ meters}$$

This applies at minimum power levels, and implies a tracking accuracy better than .01 chip, which has been realized in prior practical implementations, such as the MX-450 satellite navigation receiver.

Also as given in paragraph 2.1.4, the Costas tracking loop in the receiver can measure carrier phase with a variance

$$\sigma_{rad}^2 = \frac{N_0 B_L^{(carrier)}}{S} [1 + N_0 B_{IF}^2 / 2S] \quad (2-35)$$

At minimum $S/N_0 = 33$ dB-Hz on the forward link with $B_L^{(carrier)} = 5$ Hz and $B_{IF} = 100$ Hz matched to the data rate, we obtain

$$\sigma_{phase} \left[\begin{array}{l} \text{forward} \\ \text{link} \end{array} \right] = .008 \text{ cycle}$$

On the return link with $S/N_0 = 33$ dB-Hz, a data rate of 300 bps with coding so that $B_{IF} = 600$ Hz, and $B_L^{(carrier)} = 20$ Hz,

$$\sigma_{phase} \left[\begin{array}{l} \text{return} \\ \text{link} \end{array} \right] = .017 \text{ cycle}$$

Since the phase tracking errors are independent and a Doppler measurement is made by taking the increment of carrier phase over the specified averaging time, the resultant two-way Doppler measurement accuracy is

$$\sigma_{\text{range rate}} \Big|_{\text{two-way}} = 0.17 \text{ cm/sec; } 1 \text{ second averaging}$$
$$= 0.017 \text{ cm/sec; } 10 \text{ second averaging}$$

Similar calculations can be made for a one-way measurement; however, now there is a bias due to user frequency error. Phase measurements made one second or more apart are presumed statistically independent. This accuracy is dependent on having a tracking error increment not exceeding 0.1 radian (6^0), which is within practical implementation feasibility. Although the accuracy theoretically improves with higher S/N_0 values, the above values are felt to represent practically achievable performance.

2.1.6.8 Code Generation

The 18-stage PN code generator can generate 7776 different maximals, and a different maximal would be assigned to each user. Further computer study is necessary to demonstrate that the cross-correlation properties are adequate even when the maximal period is augmented by one chip*. The concern is the possible existence of a cross-correlation value which could cause a false acquisition or interfere with data transmission after a correct acquisition. In this regard, use of a 17-stage generator would be preferable, since $2^{17} - 1$ is prime and therefore the cross-correlation peaks tend not to be as large. There are 7710 maximals from a 17-stage generator.

The frequency hopping preamble of 256 chips is needed only on the forward link where only one user is addressed from each TDRS at a time. Again, further computer study is needed to demonstrate the existence of a sufficient number of different FH codes. Techniques for generating a code family are described in paragraph 2.1.7. One such is to employ an 8-stage maximal generator with period augmented by one chip, letting the 8-bit number in the register after each clock define the frequency. Different codes are obtained by adding a fixed 8-bit number, the code address, bit by bit modulo-2.

*Adding an extra zero to the string of $n - 1$ zeros is suggested for an n -stage maximal code generator.

2.1.6.9 Conclusions

A design concept has been established for the multiple access system concept with a steered transmit beam from TDRS to user and multiple receive beams from user to TDRS. A summary is given in Table 2-3. Performance objectives for the system can be met. The spread spectrum modulation is SQPN with a period long enough to discriminate against multipath and satisfy the ranging ambiguity goal. To aid sync acquisition on the forward link, a frequency hopped preamble is employed, with implementation as digital phase stepping by 90° steps similar to SQPN or, better, with 45° steps by an IPM. A Doppler processor can be provided in the user receiver to cover the total Doppler uncertainty, or, alternatively, the ground transmitter can be offset by the Doppler corresponding to the estimate of range rate. Both Doppler and range estimates are inserted into the ground receiver to aid acquisition.

Operationally, an indication that forward link acquisition has been accomplished is desired on the return link, when that is already established in a one-way mode. If the user already incorporates a data multiplexer, one channel can be reserved for this purpose. Alternatively, an order-wire implementation by TDM at the PN chip rate can provide this independent low data rate channel on the return link. Then, the ground transmitter could send the FH preamble until the user indicates acquisition of the preamble in mode 1 and switches to the PN code in mode 2. The ground transmitter then also switches to PN and waits for acquisition of the PN to be indicated on the return link. Commands to the user, such as to switch to coherent turnaround transponding, can then be transmitted. Since the round trip propagation delay is 0.5 second, waiting for an indication of acquisition does not materially affect acquisition times.

2.1.7 CODE GENERATION FOR PN AND FH

This section discusses methods of generating a family of pseudorandom codes suitable for PN or FH applications.

2.1.7.1 PN Code Generator for Code Division Multiple Access

At any one instant of time there will be no more than 20 simultaneous multiple access (MA) users. However, since missions may extend to 5 years, it becomes desirable to have the capability to communicate with as many as 100 different users but no more than 20 at any one time. Code division multiplexing

Table 2-3. Summary of Multiple Access System

Forward Link - Steered Transmit Beam, EIRP = 34.9 dBw

PN chip rate \cong 3.0 Mbps (exact value dependent on hardware tradeoffs)

SQPN Modulation

Code period = 2^{18} chips

Frequency hop preamble (implemented via digital phase shifting) = 2^8 chips

Preamble hopping rate \cong 3 Kbps

Data rate = 3000/K bps (synchronous biphase differential data) down to 100 bps

Acquisition time ($G_u = -6$ dB); probability \cong 0.8

with Doppler estimate inserted into transmitter \cong 19 seconds

with Doppler processor in user receiver \cong 31 seconds

Return Link - Directed Receive Beam, Gain = 28 dB

PN chip rate \cong 3.0 Mbps (same as forward link)

SQPN Modulation

Code period = 2^{18} chips

Two-way range ambiguity = 12,800 Km

Data rate, asynchronous, 100 bps to 50 Kbps, rate -1/2, constraint length 7, nonsystematic, transparent, convolutional error correction coding

Acquisition time (user EIRP=7 dBw); probability \cong 0.8 with range and Doppler estimates inserted into ground receiver \cong 15 seconds

Two-way range error (1σ) = 0.6 m

Two-way range rate error (1σ) = 0.2 cm/sec, 1 second average
= 0.02 cm/sec, 10 second average

One-way range rate error (1σ) = 0.3 cm/sec, 1 second average
= 0.03 cm/sec, 10 second average

One-way range rate bias dependent on user frequency accuracy
(10^{-9} error causes 30 cm/sec bias)

has been selected for multiple access. Hence, a large family of orthogonal PN sequences must be selected. This memorandum describes the PN code generator which is recommended to provide the required orthogonal PN sequences.

2.1.7.1.1 PN Code Selection

Large families of PN sequences having acceptably low cross-correlation properties are the Gold sequences. These sequences are generated by the modulo two addition of "preferred" maximal linear sequences. Since a staggered quadri-phase PN (SQPN) waveform is being proposed, two maximal code generators are required to generate the SQPN waveform, because of the correlation properties as discussed in Appendix VIII. Since, an 18-stage PN code generator is being recommended for the multiple access system, there are 7776 different maximal linear sequences which can be generated. In order to accommodate 100 different users, 200 different sequences are required. Two sequences are needed per user, one each being used for each of the two biphase modulated signals to be combined in phase quadrature to generate SQPN.

Two possible design approaches are acceptable. The first approach is the simplest, and selects a unique pair of maximal codes for each user. The number of available maximal sequences is much greater than required; however, there is no control of the peak cross-correlation between the sequences. A complete listing⁽¹⁴⁾ of maximal sequences up to 19th degree and a partial listing⁽¹⁵⁾ to 34th degree are available.

A second approach generates the codes as a Gold code family which is generated by a pair of maximals selected to have low cross-correlation. Such a pair is designated by the roots α^1 and α^{2k+1} , provide that the latter is a maximal. The roots are given in the listing of reference 15; for example, polynomials with the roots α^1 and α^5 form a Gold pair for degree 18. These are (first listed in octal form, which is converted into a binary number to give the polynomial coefficients).

$$1000201 = x^{18} + x^7 + 1$$
$$1002241 = x^{18} + x^{10} + x^7 + x^5 + 1$$

14. R. W. Marsh, Table of Irreducible Polynomials over GF(2) Through Degree 19, BP 161693, Oct 24, 1957, US Dept of Commerce.

15. Peterson and Weldon, Error-Correcting Codes, MIT Press, 2nd Edition, 1972, Appendix C.

The exponents define the feedback taps of the code generator. There are 2^{18} members of a Gold code family produced by 18th degree generators. The period is $2^{18} - 1$; however, we recommend augmenting the period to 2^{18} by adding one extra chip to each code. (The low cross-correlation property is then degraded to some extent).

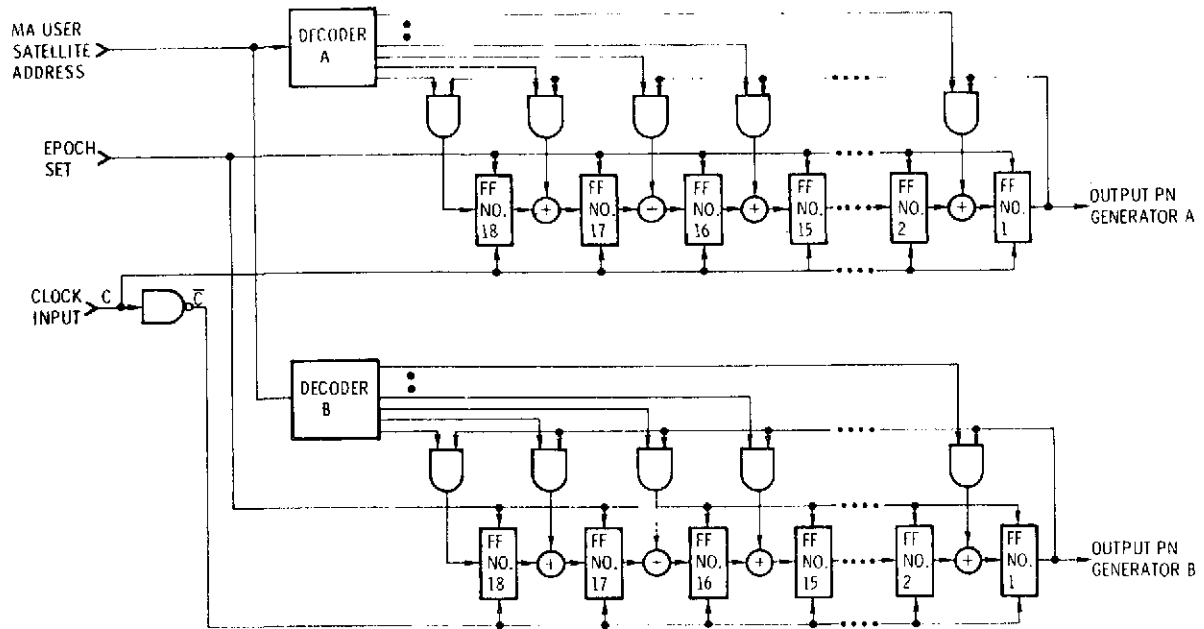
A listing of some maximal polynomials of 18th degree (in octal form) taken from reference 15 follows:

1000047	1000333	1000621	1001023
1000077	1000347	1000743	1001141
1000115	1000355	1000751	1001165
1000173	1000407	1000757	1001253
1000201	1000517	1001013	1001361

2.1.7.1.2 PN Code Generator

Figure 2-26 illustrates the preferred PN code generator. Each PN code generator consists of an 18 stage shift register generator (SRG). Each SR is constructed as a modular SRG or MSRG. This is as opposed to a simple shift register generator SSRG. In the SSRG the feedback taps are modulo two added with the sum being fed back to the last flip flop. This can result in many levels of modulo two logic whereby feedback delays cascade. In the MSRG, a transformation of the SSRG, there can only be at most one logic level of delay due to modulo two addition.

The configuration as shown in Figure 2-26 is programmable. The decoder A and B select the feedback taps corresponding to the selected MA user satellite address. The complexity associated with the ability to be programmed is present only at ground station facilities. Code generator implementation for transponders need not be programmable and hence feedback connections are hard wired.



974-2773
UNCLASSIFIED

Figure 2-26. Modular Shift Register Generators
Used for Generation of Staggered
Quadriphase

The epoch set initializes the SR's an all ones vector state to start the PN sequence generation. On the uplink, it occurs in synchronism with the end of the frequency hopping sequence. The master clock drives one SR and its inverse drives the other SR. The SR outputs are thus phase shifted by 180° with respect to one another to produce staggered quadriphase PN.

2.1.7.2

Pseudorandom Code for Frequency Hopping

A repetitive short code for frequency hopping has similar requirements as one for PN. Specifically, the correlation function, appropriately defined, must be essentially zero except at the desired peak. For multiple access, a set of codes with cross-correlation functions that are essentially zero is needed.

The basic auto- or cross-correlation function for frequency hopping may be defined as the number of matching frequencies over the period of the code. That is, the product correlation process subtracts frequency values, and the sync detector looks for the number of zeros differences which occur. However, because of Doppler shift on the received frequency, we must extend the definition to look also for multiple occurrences of non-zero frequency differences within a code period, up to the maximum possible Doppler offset.

2.1.7.2.1 Use of Maximal Generator

One method of generating a frequency hopping code is by a maximal linear binary sequence generator of n stages. This produces a sequence of $N = 2^n - 1$ distinct n -bit numbers. For instance, $n = 3$ yields Figure 2-27 and the sequence of period $N = 7$

1 4 2 5 6 7 3

where 0 cannot occur. Figure 2-28a presents the autocorrelation function of this code, defined as the number of occurrences of each possible frequency difference. In the absence of Doppler shift, the code would be ideal; however, allowing Doppler, the peak to maximum side lobe ratio is seen to be $7/3$, a relatively poor ratio.

For $n = 7$ yielding a period of 127, a computer analysis of the auto-correlation function for the sequence produced by the maximal polynomial $x^7 + x^3 + 1$ showed the ratio to be $127/8$, so that longer period codes tend to be reasonably satisfactory. It may be noted that 2^n different sequences of period $2^n - 1$ are obtained by modulo 2 adding, bit by bit, any fixed n -bit number to the contents of the n -stage maximal generator. In fact, the result is a Reed-Solomon code of period N on an alphabet of size $N + 1 = 2^n$. The code has distance $N - 1$, which unfortunately tells nothing about the effect of Doppler shift.

2.1.7.2.2 Generation by Primitive Root

There is a simple technique for generating a single code with the desired autocorrelation function for frequency hopping even after a Doppler shift. This can be done for any period $N = p-1$, where p is a prime number. The technique is based on the existence of a primitive root g such that the sequence g^i forms N distinct numbers modulo p . (This technique is similar to that used to generate random number sequences on a digital computer.) The sequence of frequencies is

$$f_i = g^i \text{ modulo } p \quad (2-36)$$

with period $N = p - 1$. The desired autocorrelation property follows by taking the frequency difference for a shift τ ,

$$\begin{aligned} f_{i+\tau} - f_i &= g^{i+\tau} - g^i \text{ modulo } p \\ &= g^i (g^\tau - 1) \text{ modulo } p \end{aligned} \quad (2-37)$$

Thus, the sequence of frequency differences consists of distinct values unless $\tau = 0$, corresponding to the autocorrelation peak.

As an example, let $p = 7$ to generate a sequence of period 6. A primitive root is 3; hence, the sequence is

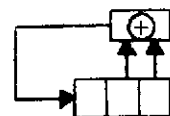
1 3 2 6 4 5

Figure 2-28b gives the autocorrelation for frequency hopping, and this is the best possible.

As one special case, $257 = 2^8 + 1$ is prime, so that the primitive root technique generates a frequency hopping sequence of period $256 = 2^8$. Similarly, $17 = 2^4 + 1$ is prime.

A small set of frequency hopping codes for multiple access can be generated by setting

$$f_i^{(m)} = g^i + m^\Delta \text{ modulo } p \quad (2-38)$$



$$0 \ 0 \ 1 = 1$$

$$1 \ 0 \ 0 = 4$$

$$0 \ 1 \ 0 = 2$$

$$1 \ 0 \ 1 = 5$$

$$1 \ 1 \ 0 = 6$$

$$1 \ 1 \ 1 = 7$$

$$0 \ 1 \ 1 = 3$$

Maximal Polynomial is $x^3 + x + 1$
Period = 7

Figure 2-27. Frequency Hopping Sequence Generator

	-6	-5	-4	-3	-2	-1	0	1	2	3	4	5	6
0	0	0	0	0	0	0	7	0	0	0	0	0	0
1	0	0	0	2	0	2	0	0	2	0	1	0	0
2	0	0	1	0	1	3	0	0	0	1	0	0	1
3	0	1	1	0	1	0	0	1	1	1	0	1	0
4	0	1	0	1	1	1	0	0	1	0	1	1	0
5	1	0	0	1	0	0	0	3	1	0	1	0	0
6	0	0	1	0	2	0	0	2	0	2	0	0	0

(a)

Sequence = 1 4 2 5 6 7 3

Table lists number of occurrences of each frequency difference

	-5	-4	-3	-2	-1	0	1	2	3	4	5
0	0	0	0	0	0	6	0	0	0	0	0
1	0	1	0	1	1	0	1	1	0	1	0
2	0	0	1	1	1	0	1	1	1	0	0
3	1	0	1	0	1	0	1	0	1	0	1
4	0	0	1	1	1	0	1	1	1	0	0
5	0	1	1	0	1	0	1	1	0	1	0

(b)

Sequence = 1 3 2 6 4 5

Table lists number of occurrences of each frequency difference

Figure 2-28. Autocorrelation Function for Frequency Hopping

where Δ exceeds the Doppler uncertainty expressed as number of frequency channels and $0 \leq m\Delta < p$. Now

$$f_{i+\tau}^{(r)} - f_i^{(s)} = g^i (g^\tau - 1) + (r - s)\Delta \text{ modulo } p \quad (2-39)$$

and if $\tau \neq 0$, the sequence of differences are all different values. If $\tau = 0$, the differences are all equivalent to $(r - s)\Delta$; hence, exceed the maximum Doppler offset.

2.1.7.2.3 FH Code Family Based on Primitive Roots

As described above an FH code of period 256 can be generated by a primitive root g for the prime number 257. The sequence is

$$f_i = g^i, \text{ mod } 257 \quad (2-40)$$

and all numbers from 1 to 256 are included in the period. All primitive roots are of the form 3^k , where k is relatively prime to 256.

Now suppose we generate two different sequences using different primitive roots, as

$$\begin{aligned} a_i &= g_a^i, \text{ mod } 257 \\ b_i &= g_b^i, \text{ mod } 257 \end{aligned} \quad (2-41)$$

and define a code family by

$$f_i^{(n)} = a_i - b_{i+n}, \text{ mod } 256 \quad (2-42)$$

The mod 256 means to add 256 if the difference is less than 1; hence, the result lies in the range 1 to 256 and has period 256. There are 256 distinct codes in the family.

The cross-correlation of two members of the family is obtained from the frequency difference

$$f_i^{(n)} - f_{i+\tau}^{(m)} = a_i - b_{i+n} - a_{i+\tau} + b_{i+\tau+m} \quad (2-43)$$

understanding that 256 may have to be added or subtracted from (2-43).

Substituting (2-41) and rearranging

$$\begin{aligned}
 f_i^{(n)} - f_{i+\tau}^{(m)} &= g_a^i - g_b^{i+n} - g_a^{i+\tau} + g_b^{i+\tau+m} \\
 &= g_a^i (1 - g_a^\tau) - g_b^{i+n} (1 - g_b^{\tau+m-n}) \\
 &= g_a^{i+\alpha} - g_b^{i+\beta} \\
 &= a_{i+\alpha} - b_{i+\beta}; \tau + m - n \neq 0, \text{ mod } 256 \quad (2-44)
 \end{aligned}$$

where α and β are integers and mod 257 is implicit in the powers. This result is obtained because multiplying g^i by an integer is equivalent to shifting i . If $\tau + m - n = 0, \text{ mod } 256$, we have

$$f_i^{(n)} - f_{i+n-m}^{(m)} = g_a^{i+\alpha} \quad (2-45)$$

If $\tau = 0, \text{ mod } 256$, we have

$$f_i^{(n)} - f_i^{(m)} = -g_b^{i+\beta} \quad (2-46)$$

The value of τ leading to (2-45) or (2-46) are seen to yield a correlation value of unity, since there are 256 different frequency differences in the period, according to the property of a primitive root. All other values of τ lead to the general form of (2-44), regardless of the particular pair of codes being correlated. Note that (2-44) actually represents the code sequences of the family.

The peak auto- or cross-correlation was computed numerically for the code family of period 256 generated by $g_a = 3$ and $g_b = 27$. The two sequences a_i and b_i , defined in (2-41), were generated, and each member of the code family was generated in succession according to (2-42). For each member, the maximum number of occurrences of any one frequency was noted, and the maximum over the code family was read out. The result was

$$\text{peak correlation value} = 6 \quad (2-47)$$

Next, only the frequencies corresponding to differences close to zero were counted (the values 1 to 9 and 246 to 256). Now, the result was

$$\left. \begin{array}{l} \text{peak correlation value} \\ \text{within Doppler} \\ \text{uncertainty} \\ \text{of } \pm 9 \text{ frequencies} \end{array} \right\} = 4 \quad (2-48)$$

It should be remembered that (2-47) and (2-48) actually are upper bounds for the reason that the frequency differences have been taken modulo 256.

2.1.7.7.4 Conclusions

For the period 256, the primitive root technique enables a code family of 256 codes to be generated such that the peak auto- or cross-correlation value is at most 6. (This is the number of occurrences of any one frequency difference.) For frequency differences within the Doppler uncertainty (± 9 lines means ± 108 kHz for a spacing of 12 kHz as described in paragraph 2.1.5, the peak correlation value is 4. This appears to be a very satisfactory design with respect to TDRSS user addressing by a unique code.

It is interesting to note the similarity between the technique (2-42) for generating the FH code family and that for generating a Gold PN code family.

Unfortunately, the primitive root technique can be applied only to periods of the form $p - 1$, where p is a prime.

2.1.8 FURTHER ANALYSIS OF TWO-STEP ACQUISITION (WITH FH PREAMBLE) ON FORWARD LINK

The recommended design for the multiple access forward link, and also for the S-band single access forward link, utilizes a frequency hop preamble to enable fast acquisition of a pseudonoise signal. The FH preamble is transmitted only for the duration necessary for the first step of receiver acquisition; a second step is then needed to acquire the PN signal which immediately follows the preamble. The time uncertainty remaining after FH acquisition determines the search aperture for PN acquisition. Since this time uncertainty equals the width of a frequency hopped pulse, the number of PN chips to be searched in the second step equals the ratio of the spread bandwidth to the hopping rate. In the recommended design, the FH signal and the PN signal have the same period in milliseconds, so that the number of PN chips to be searched in the second step of acquisition can also be expressed as the ratio of the periods in chips.

The acquisition performance calculations made in paragraph 2.1.6.2 set the probability of detection equal to .9 for both acquisition steps; hence, the overall probability is 0.81 at the designated signal-to-noise ratio. A further discussion of the operational consequences is appropriate, and procedures to improve acquisition reliability are described.

2.1.8.1 Forward Link Acquisition Procedure With Preamble

Operationally, a user would like to transmit the FH preamble on the forward link only until the transponder receiver acquires the signal on the first step of serial search for synchronization. If the return link of the multiple access system is already established, receiver acquisition can be sent back as a status word, and the switch to PN transmission is then made. For initial acquisition (also, for single access acquisition), the return link does not exist, and the user has no way of knowing when receiver acquisition of the preamble occurs. Then, he must transmit the preamble for a predetermined interval which suffices for a high probability of first step acquisition to the FH preamble.

With a serial search, each complete pass through the code period gives an independent chance for sync detection. Thus, if P_d is the probability of detection on a single pass, the probability after M passes is

$$P_d^{(M)} = 1 - (1 - P_d)^M \quad (2-49)$$

Therefore, if a search rate yields a probability of detection of 0.9 in a given time, the probability becomes 0.99 in twice the time, 0.999 in three times the time, etc*. The conclusion is reached that a design philosophy which allows for several passes through the FH code period can reach a probability of detection very close to unity on the preamble (first step of acquisition).

On the second step, or PN acquisition, a different design philosophy can prevail. Here, the user starts transmitting PN immediately after terminating the FH preamble. Assuming FH acquisition was successful, the transponder receiver keeps searching through the remaining time uncertainty until PN acquisition

* Obviously, a user prefers to have a probability of detection of unity, but in practice, a design value in the range 0.9 to 0.99 is effectively unity.

is completed. This happens sooner or later*, and the average acquisition time is probably the most meaningful measure for this acquisition step. Presumably the transponder would be programmed to start transmitting on the return link as soon as forward link PN acquisition is completed**.

2.1.8.2 Design Tradeoffs on Multiple Access Forward Link

We study the forward link of the multiple access system in some further detail, to investigate the effects of parameter changes from the design in paragraph 2.1.6.1. That design called for a hopping rate of 3 Khps, a FH code of 256 chips (85.3 milliseconds), and a spread bandwidth of 3.07 MHz. The code period is set by the minimum acceptable range measurement ambiguity, currently stated by NASA to be 10,000 Km. Acquisition time for the FH preamble is directly proportional to the code period; however, this has no affect on acquisition time for the second step.

The maximum multipath delay dictates a lower bound on code period, and to provide protection against false acquisition to a specular multipath, the code period should be at least twice the delay. For a user satellite at 2000 Km altitude, this maximum delay is 13.3 milliseconds. The delay is 33.3 milliseconds for 5000 Km altitude. It is concluded that a significant reduction in acquisition time is not attainable by reducing the preamble code period, even if the reduced range ambiguity were accepted.

The spread bandwidth of 3 MHz is dictated by radiated flux density requirements, and a reduction of this parameter is not tolerable.

The hopping rate of 3kHz is flexible over a modest range. We investigate this tradeoff by its effect on the average time to detect sync on the FH preamble. If the average time to search through the code period once is T_s , the average time to detect sync is

$$T_s^{(av)} = T_s M^{(av)} = T_s (-.5 + 1/P_d) \quad (2-50)$$

*Because of code Doppler, the uncertainty region grows with time. For example, with a range rate error of 100 m/sec, the code Doppler at 3 Mbps (for the multiple access system) is one chip/sec. Even after 100 seconds, the original 1000 chips (see TSA-CRC-19) of uncertainty has grown to at most 1200 chips.

**In the multiple access system with the return link previously established, PN acquisition presumably would be indicated by a status word.

where $M^{(av)}$ is the average number of passes through the code period prior to detecting sync*. Figure 5 of Appendix III relates P_d to signal-to-noise ratio (we use the curve for lower bias).

Let us continue to assume a range rate error of 100 m/sec, or ± 700 Hz Doppler error at S-band. With FH implementation by digital phase shifting in 45° increments, the maximum loss (see Section 2.1.3.2) due to the quantized phase is 0.7 dB. The loss due to Doppler is given by (2) of Appendix III, presuming integrate-and-dump at the hopping rate, or

$$\text{dB loss due to offset } \Delta f = 20 \log_{10} \frac{\sin(\pi \Delta f T_{\text{hop}})}{\pi \Delta f T_{\text{hop}}} \quad (2-51)$$

where T_{hop} is the dwell on one frequency (reciprocal of hopping rate). Assume a fixed code period of 85.3 milliseconds as the hopping rate is varied. Then, the average time to search one period is (Figure 5 of Appendix III states an average search rate of .041 chips/hop)

$$T_s = \frac{85.3 \text{ millisec}}{T_{\text{hop}}} \times \frac{T_{\text{hop}}}{.041 \text{ chips/hop}} = 2.08 \text{ sec} \quad (2-52)$$

which is independent of the hopping rate (because the number of FH chips in the period is proportional to the hopping rate).

* The average number of independent trials to obtain success is $1/P_d$, where P_d is the probability of success per trial. On the average, acquisition is detected half-way through the final pass.

Carrying through the calculations yields the results in Table 2-4. It can be seen* that the optimum hopping rate for FH acquisition is in the range of 1.5 Khps to 3 Khps. However, a faster hopping rate decreases the uncertainty remaining for PN acquisition and, therefore, decreases the total time for acquisition. It is concluded that the original choice of 3 Khps for the FH preamble is essentially optimum for the multiple access forward link.

Table 2-4. Average Time for FH Acquisition

	Hopping Rate		
	6 Khps	3 Khps	1.5 Khps
S/N _o to omni	39.0 dB-hz	39.0 dB-Hz	39.0 dB-Hz
Discrete Phase Loss	- .7 dB	- .7 dB	- .7 dB
Doppler Offset Loss	- .2 dB	- .8 dB	- 3.4 dB
User Antenna Gain	- 6.0 dB	- 6.0 dB	- 6.0 dB
Net S/N _o	32.1 dB-Hz	31.5 dB-Hz	28.9 dB-Hz
E _{hop} /N _o	- 5.7 dB	- 3.3 dB	- 2.9 dB
P _d	.1	.5	.6
M ^(av)	9.5	1.5	1.2
T ^(av) _s	19.8 sec	3.1 sec	2.5 sec

Since Table 2-4 indicates $P_d = .5$ for $G_u = -6$ dB at 3 Khps, five passes through the code period will produce $P_d^{(5)} = .97$ for FH acquisition. The search time** for five passes is 10.4 seconds.

*If the hopping rate were further decreased below 1.5 Khps, a search in frequency would be required to accommodate Doppler, and the acquisition time would tend to increase. Alternatively, we could implement a Doppler processor (multiple filter band).

**This actually is the average search time for five passes through the period. The simulation in Appendix III found the standard deviation of the dismissal time to be 15.8 chips when the average is 12.2. Since there are 512 dismissals per code period (half chip search steps), the 1σ fluctuation in search time for five passes is 2.6 percent.

When FH acquisition is accomplished, the time uncertainty is 1000 PN chips for 3 Khps (assuming the time error after FH acquisition is less than half a chip). Still coherently integrating over 333 microseconds during the search for PN acquisition, $E_{coh}/N_o = -2.6$ dB, since the loss for discrete phase increments in FH does not apply, and $P_d = .65$. A practical implementation would utilize the same sync detector for both acquisition steps; however, let us investigate the effect of varying the coherent integration interval. Now, the average time to search through the 1000 PN chips of uncertainty is

$$T_s = 1000 \frac{T_{coh}}{.041 \text{ chips/interval}} \quad (2-53)$$

Table 2-5 displays the computed results. Here, a coherent integration interval of 333 microseconds minimizes the average time for PN acquisition.

Table 2-5. Average Time for PN Acquisition

	Coherent Integration Interval		
	167 μ sec	333 μ sec	667 μ sec
S/N _o to omni	39.0 dB-Hz	39.0 dB-Hz	39.0 dB-Hz
Doppler Offset Loss	-.2 dB	-.8 dB	-.3.4 dB
User Antenna Gain	-.6.0 dB	-.6.0 dB	-.6.0 dB
Net S/N _o	32.8 dB-Hz	32.2 dB-Hz	29.6 dB-Hz
E_{coh}/N_o	-.5.0 dB	-.2.6 dB	-.2.2 dB
P_d	.2	.65	.72
$M^{(av)}$	4.5	1.04	.89
T_s	4.1 sec	8.1 sec	16.2 sec
$T_s^{(av)}$	18.5 sec	8.4 sec	14.4 sec

2.1.8.3

Conclusions

A more detailed examination of the parameters of the forward link of the multiple access system supports the parameter values selected in paragraph 2.1.6.1. The acquisition strategy is to allow several passes through the FH preamble period, so as to achieve a probability of FH acquisition which is essentially unity. For a user receiver antenna gain of -6 dB, the design calls for a FH preamble duration of about 11 seconds to give a probability of detection of 0.97. The average PN acquisition time is about 8 seconds. Thus, we can claim a total acquisition time for the user receiver of approximately 19 seconds at $G_u = -6$ dB.

By reducing the code period by a factor of two (range measurement ambiguity is now 5000 Km), acquisition time for the FH preamble is reduced to about 6 seconds, and the total acquisition time is approximately 14 seconds at $G_u = -6$ dB.

With the above procedure, there is the possible disadvantage that a relatively strong specular multipath signal could be acquired (although with low probability) instead of the direct signal. Protection against specular multipath is provided with time discrimination; i. e., the direct signal always precedes the multipath. To avoid possible acquisition to the multipath, the receiver must have essentially unity probability of acquiring the direct signal on a single pass. This means a design which searches at a slower rate and achieves a higher probability of detection on a single pass, than seen in Tables 2-4 and 2-5. This should not affect the optimization of parameters (e.g., hopping rate) found above.

Having recommended waveform parameters for a multiple access service using TDRS steered transmit beam (a result of the modulation tradeoff studies presented in paragraph 2.1), we now consider the implementation tradeoffs involved in selecting user transponder hardware design which will best meet the operational and performance potential available to multiple access users.

2.2.1 DOPPLER RESOLVERS VS. TRANSMITTER FREQUENCY OFFSET

For the multiple access user, there is a ± 55 kHz Doppler uncertainty which must be resolved during the acquisition process before a tracking and data retrieval mode can be established. Two different approaches for resolving this uncertainty were studied:

- Doppler Processor implementation to resolve Doppler frequency offsets at the user receiver.
- Frequency offset of the ground transmitter to compensate for Doppler offsets at the user receiver.

2.2.1.1 Doppler Processor

To assess the hardware impact of a Doppler processor designed to meet the system requirements for the current multiple access user transponder, three candidate implementations were evaluated. The first configuration was the serial search/MOS memory type implementation which is similar to the present Doppler Processor configuration implemented in the Multimode Transponder. This configuration involves searching the complete Doppler frequency range (± 64 kHz) in a serial fashion such that the full Doppler range is searched in one, two, or even four frequency sweeps. The second configuration was the parallel search/MOS memory configuration which involves parallel searching the full Doppler uncertainty range in two or four segments in a parallel configuration. The third and last configuration analyzed was the parallel search/RAM memory-type implementation which involves parallel searching the full Doppler uncertainty range in four segments by utilizing a parallel processing technique which incorporates random access memories (RAMs) and read-only memories (ROMs). A report on these configurations is included in Appendix IV.

In conclusion, the parallel search/RAM memory configuration uses the least amount of hardware and offers the best overall performance characteristics at almost no risk. In addition, there are no potential problems associated with

interfacing this configuration with the carrier or clock tracking loops since the Doppler offset can be located in one frequency sweep. For this configuration, 195 ICs are required for implementation. Conservatively, this approach would require three 4" x 5" PC boards and consume 10 watts of power, which is an undesirable feature for most user satellite applications.

2.2.1.2 Fast Fourier Transform Doppler Resolver

A FFT approach to a Doppler resolver was investigated and the results are presented in Appendix V. In summary, the FFT approach can be implemented with lower speed logic than the discrete Fourier transform method described earlier. It is comparable in performance and clearly becomes the implementation choice when a region of frequency uncertainty must be divided into several hundred frequency slots.

It is estimated that this approach would require three 4" x 5" PC boards and consume 6 watts of power. The reduction in power consumption with respect to the discrete Fourier transform is clearly an advantage; however, there would be more risk in its development.

2.2.1.3 Transmit Frequency Offset

Rapid acquisition (less than 20 seconds) could be realized without a loss of performance and without a Doppler resolver, if the arriving signal at a user transponder could be corrected for Doppler frequency offsets. One way user Satellite range and range rate of change in an established orbit can be estimated to within

$$\begin{aligned}\Delta \text{ range} &= \pm 50 \text{ km} \\ \Delta \text{ range rate} &= \pm 100 \text{ m/sec}\end{aligned}$$

This range rate corresponds to $\pm .33$ ppm or ± 700 Hz of uncertainty. In other words, if a forward link ground transmitter is offset to the estimated user satellite Doppler, the received signal at the satellite user transponder will be within ± 700 Hz of center frequency.

As an acquisition aid in the return link, the ground receiver could be offset by the Doppler estimate in a noncoherent transpond mode or by two times the Doppler estimate in a coherent return link mode. The offset frequencies would also include compensation for predictable long term VCO instability (on the order of ± 5 kHz in 3 years).

In the user transponder, it is recommended that a sync detection circuit be implemented at baseband with a bank of five band pass filters to cover a frequency

uncertainty of ± 3 kHz. This amount of coverage makes allowances for tolerance buildup. It is estimated that this approach would require one-half of a 4" x 5" PC board to implement with active filter devices and would consume approximately 0.5 w watt of power.

2.2.1.4 Conclusions

Doppler resolver implementations were considered for use in a user satellite receiver to resolve the ± 55 kHz of frequency uncertainty during acquisition. It was concluded that power consumption is excessive with this approach. The ground transmit frequency offset approach substantially relieves user transponder hardware and power consumption requirements, provides the desired performance and is satisfactory from an operations standpoint.

2.2.2 COHERENT/NONCOHERENT TRANSPONDER OPERATION

Coherent transponder operation is required to provide two-way range and range rate measurement capability. However, since the multiple access service will use a pointed beam in the forward link which will be time shared among all participating users, a continuous coherent mode of operation is not practical. The logical solution for this situation is to design the M/A link so that a transponder can be commanded to operate in either a coherent or a noncoherent mode of operation.

There are some hardware tradeoffs to consider for a coherent/noncoherent capability. A minimum hardware approach would be to build a coherent transponder using a single VCO for the tracking loop in the receiver which would also serve as a frequency reference in the transmitter. In this configuration, a return link mode could be continued after forward link loss of lock by slowly grounding the VCO input. The problem with this approach is that the forward link could not be reestablished until the telemetry data dump in the return link was complete. However, at the cost of some additional hardware, independent forward and return operations could be implemented in the transponder. The impact would be the addition of a reference oscillator and an RF synthesis chain for the transmitter along with RF and logic switches to select the coherent or noncoherent modes.

The proposed M/A transponder provides for independent forward and return operation as well as coherent operation. Acquisition of the forward link for user satellite command messages will not disrupt an established return link during a data dump. Upon command, the transponder will operate in a coherent mode for range and range rate measurement. The hardware impact for this approach is

estimated at one 4" x 3" PC board to provide a reference oscillator for the user transmitter, RF switching and synthesis of the transmitter PN code. (The first and second L.O.s are common to both the receiver and transmitter and are synthesized from the reference oscillator during a noncoherent mode and from the receiver VCO during a coherent mode.) Carrier tracking in the receiver is accomplished in a short loop (3rd and 4th L.O.s) for a noncoherent mode and in a long loop (1st, 2nd, 3rd, 4th L.O.s) for a coherent transpond mode.

2.2.3 DATA CLOCK

2.2.3.1 Telemetry Data Clock

For the return link, data clock will not be synthesized from the PN code clock for several reasons: (1) operationally it is desirable to have data clocks independent of the transponder frequency reference. (2) The data/PN clock ratio is not low enough to result in any appreciable quantization loss. (3) The data clock acquisition and tracking loop would be located in ground equipment and would not burden the user satellite equipment. (4) A data clock loop with a bandwidth sufficient to track the Doppler rate (approximately 30 Hz max) would have a good signal/noise ratio even at low data rates and performance loss due to clock jitter would be negligible.

2.2.3.2 Command Data Clock

On the other hand, data will be synchronized to the PN code epic for the forward link because: (1) Code repetition rate is lower than the lowest data rate so that no clock ambiguity results. (2) Data clock can be derived from a countdown of the code epic which represents a minimum hardware configuration in the user transponder. (3) Since command messages are finite, (on the order of 1000 bits or less) they can be buffered and reclocked at the ground station. (4) Coherent data clock without ambiguity would be available for data processing in the transponder at the instant of PN correlation.

2.2.4 CLEAR MODE OF OPERATION

Potential users have identified a requirement to operate in a clear mode (non-spread spectrum mode). Under special circumstances (i.e., ground-user-ground links) this would be accomplished in the user PN transponder with a command instruction and would be implemented with minor hardware impact by removing the PN sequence from the modulator and the receiver local reference on command. The Costas demodulator would then be used to demodulate the biphase PSK signal. For waveforms with a pilot carrier, the Costas loop would be converted to a carrier

tracking loop by removing the I channel from the 3rd multiplier. For higher data rates, the received signal would be routed through a wideband 4th IF amplifier and demodulated via a second inphase (I) data channel.

Data modulation in the transmitter, would be accomplished at the first IF of the upconversion chain. For modulation waveforms other than biphasic PSK, a special modulator would have to be implemented. It should be pointed out that, even in a clear mode of operation, the transponder would still function in a noncoherent or coherent carrier mode.

2.2.5 FREQUENCY SYNTHESIS

This section describes the development of a frequency synthesis scheme for the multiple access user transponder. It lists the basic system constraints which apply to frequency synthesis, outlines some of the self-imposed good design practice rules used for the design and mentions several techniques which were not used. A number of frequency synthesis approaches which were first considered are described and finally, a recommended synthesis approach is then presented.

2.2.5.1 System Constraints

Basic system constraints placed on the M/A user transponder frequency synthesis design include:

- Receive Frequency - 2106.40625 MHz
- Transmit Frequency - 2287.5 MHz
- Coherent translation from Rx to Tx frequencies to accommodate a two-way doppler measurement capability.
- Rx/Tx = 221/240
- Minimize power consumption and hardware complexity consistent with performance requirements.

2.2.5.2 Design Ground Rules

Some of the most important ground rules for the synthesizer design include:

- No appreciable n^{th} order synthesis products from any L.O. into any IF.
- Use common synthesis chains for both Rx and Tx whenever practical to minimize hardware and minimize multiplier noise differences.

- LO/RF ratio ≤ 0.95 so that filter Q is less than 20.
- Correlation LO and PN modulator LO should be >40 MHz and <150 MHz.
- Last IF should be ≤ 2 MHz.
- 1 RF section, 3 IF sections.
- Gain should be distributed between RF and IF with approximately 35 dB/frequency.

2.2.5.3 Frequency Synthesis Approaches

Four different frequency synthesis approaches were considered for use in the M/A transponder:

- One fixed frequency reference with separate VCO's for carrier and code tracking.
- Separate VCO's for carrier and code tracking.
- One VCO for carrier and code tracking with an IPM for phase corrections in the PN code loop.
- One VCO, one Fixed Reference for coherent/noncoherent operation.

The first approach used a fixed frequency oscillator at 10 MHz mixed with a 0.46875 MHz VCO to synthesize the required LO frequencies. The advantage of this approach is that the major component of the frequency reference is derived from a very stable and clean fixed frequency oscillator while tracking is accomplished with a lower frequency VCO with less stable characteristics. Also, a separate VCO for code tracking eliminates the need for an IPM. The problem with this approach is that 3 oscillators are required.

The second approach used two VCO's, one for carrier tracking and one for code tracking. For this technique the VCO must be pulled ± 30 ppm to cover the Doppler uncertainty. This pull range can be obtained with a temperature compensated crystal stabilized voltage controlled oscillator with good stability characteristics.

The third approach used a single VCO for both carrier and code tracking. The PN code frequency and frequency dynamics are scaled from the carrier tracking VCO with only small and slowly varying errors due to ionospheric variations. These small errors along with initial code phase errors are nulled with an incremental phase modulator (I. P. M.) in $1/96^{\text{th}}$ of a code chip increments.

The fourth approach shown in Figure 2-29 is the selected approach. It uses a single VCO for both carrier and code tracking in the coherent transpond mode (i.e., all L.O.'s are synthesized from the carrier VCO). In the noncoherent mode, the receiver tracks the incoming signal with a carrier VCO via the 3rd and 4th L.O.'s, while the transmitter upconversion and 1st and 2nd L.O.'s of the receiver are synthesized from a fixed reference oscillator.

2.2.6 REFERENCE OSCILLATOR STABILITY

The following section discusses the degradation of VCO (Voltage Controlled Oscillator) frequency stability due to various environmental factors such as temperature, vibration, g-force loading and electrical variations. These environmental conditions cause the VCO frequency stability to degrade in an RSS (Root, Sum, Square) fashion. The effects on the clock stability due to the different environmental conditions will also be considered for various fixed frequency standards. Physical parameters and cost are included for a comparison to aid in the selection of a VCO and reference oscillator with the desired characteristics.

2.2.6.1 Analysis

The long term stability or aging rate of an oscillator is the predominate factor in maintaining a reasonable time ambiguity region. The aging rate describes the average rate of the oscillators' (clock) output frequency assuming the environmental parameters are constant. The defining relationship that relates accumulated clock error and time between synchronizations is given by equation 1.

$$E = E_0 + \left(-\frac{\Delta F}{F} \right) t + \frac{a}{2} t^2 \quad (2-54)$$

E_0 - the initial time error

$\Delta F/F$ - Overall fractional frequency deviation due to environmental effects.

a - long term stability or aging rate

t - elapsed time

The perturbations due to the environmental conditions, i.e., vibration, temperature, etc., are independently caused and randomly distributed. Thus, the rms perturbations of the overall frequency deviation is the root mean square of the sum of the individual frequency deviations. The overall frequency deviation is given by equation 2-55 below:

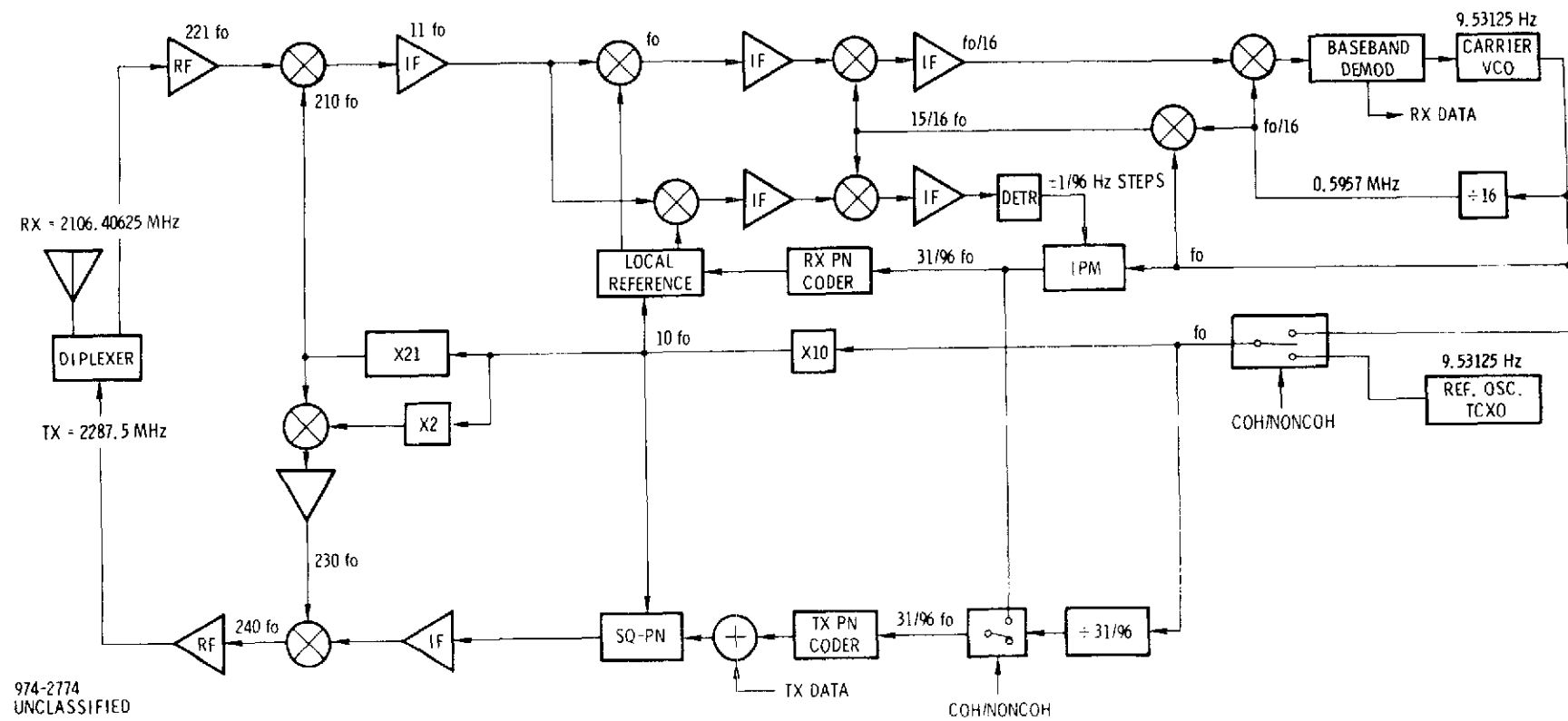


Figure 2-29. Frequency Synthesis for the M/A Transponder

$$\Delta F/F = \sqrt{\left(\frac{\Delta F}{F}\right)_{\text{Temp}}^2 + \left(\frac{\Delta F}{F}\right)_{\text{Vib}}^2 + \left(\frac{\Delta F}{F}\right)_{\text{G-Force}}^2 + \left(\frac{\Delta F}{F}\right)_{\text{Load Change}}^2 + \left(\frac{\Delta F}{F}\right)_{\text{Volt Change}}^2} \quad (2-55)$$

2.2.6.2 Space Qualifiable Fixed Frequency Standards

A frequency standard is a critical item in achieving the low carrier phase noise required for achieving near theoretical range and range rate measurement and data demodulation performance at S and Ku-band RF frequencies. In addition to space rating requirements, stringent standard long-term stability requirements must be imposed. Several viable candidates for this application are shown in Table 2-6. Crystal oscillators have space experience and will meet the short-term stability requirements according to published data. The cesium standards can easily meet the long-term requirements but not short-term stabilities without special crystal/cesium slave designs. The smallest units which could potentially be used for space is the Efratom rubidium standard. Some criteria for selection consideration include the following:

FEI CRYSTAL OSCILLATOR

- Long-term drift difficult to model.
- Space-rated unit available.
- Five year life cycle should be no problem.
- Not atomic in nature.
- Basically qualified.
- FLEET SATCOM flights planned late in 70's.
- Smallest.

CESIUM STANDARD

- Requires crystal/CS combination for good short-term stability.
- Long-term stability is excellent.
- No modeling required.
- No prototype space-rated unit tested.
- Five year life cycle is questionable.
- Properties of Cs operation consume source.
- Qualification time is approximately 3-5 years.
- Power requirement approximately 25 watts.

Table 2-6. Industry Survey*

Manufacturer	Model No.	Stability	Size (in.)	Weight (lb)	Input Power (Wdc)	Notes
Rubidium Standards						
Efratom	FRK	1×10^{-10} /MO 5×10^{-11} ($\tau = 1$ sec)	4 x 4 x 4	3	13	Commercial available**
HP	5065A	1×10^{-11} /MO 5×10^{-12} ($\tau = 1$ sec)	16-3/4 x 18-3/8 x 5-7/32	34	35	Commercial available
Tracor	308A	3×10^{-11} /MO 2×10^{-11} ($\tau = 1$ sec)	12 x 5-1/4 x 17-1/3	20	50	Commercial available
Collins Radio		2×10^{-11} /MO 5×10^{-11} ($\tau = 10$ sec)	19 x 5-1/2 x 9	44	35	Not presently in production
Cesium Standards						
HP	5061A	3×10^{-12} /MO 5.6×10^{-12} ($\tau = 1$ sec)	16-3/4 x 18-3/8 x 8-3/4	67	27	16-in. tube unit, commercial available
HP	5062C	1×10^{-11} /MO 7×10^{-11} ($\tau = 1$ sec)	16-3/4 x 19 x 5-7/32	45	30	Not available till mid-74, 6-in. tube
Freq & Time Sys			7-5/8 x 4-7/8 x 19	30	20	Not available till late 74
Hydrogen Maser						
Smithsonian JPL Goddard		1×10^{-14} /MO	30 x 30 x 30	75+	50	Custom design for NASA, experimental unit
Crystal Oscillators						
FEI	FEI 800D FEI 800DS	2×10^{-11} /day 8×10^{-13} ($\tau = 1$ sec)	3.5 in. x 4.5 in. x 9.25 in.	6.5	1.8	For FLEETSATCOM, space-rated

* Supplied by North American Rockwell

** Space Qualification expected to begin by mid '74.

EFRATOM RUBIDIUM STANDARD

- Good short-term stability.
- Good long-term stability.
- Can be accurately modeled for excellent long-term requirements.
- Low risk to space qualify.
- Five year life cycle no problem.
- Properties of Rb operation do not consume source.
- Qualification time approximately one year.

2.2.6.3 Crystal Oscillators

Table 2-7 is a comparison of 5 MHz oscillators under various environmental conditions. The vibration and acceleration are shown for the worst case g's encountered. Listed also is the size, weight and cost of the particular type of oscillator to meet the specifications that are listed. It will be noted that the difference between what has been termed a second grade ovenized and a first grade ovenized oscillator is that the former has a single oven whereas the latter has a thermally insulated proportional control double oven to achieve the higher order stability.

2.2.6.4 Rubidium Standard

With modeling, the long-term stability for the Rb frequency standard can achieve a few parts in 10^{13} , for sampling times from 1 hour to 1 day. Digital tuning of output frequency over a range of

$$\frac{\Delta f}{f} = 4 \times 10^{-9}$$

could be accomplished by means of an externally supplied direct current, which provides a controlled magnetic field (C-field) around the rubidium optical resonator cell. A digital command word would be converted by the D/A converter to a direct current for use in the C-field of the frequency standard. The total range required in the command word to cover the entire frequency range is then:

$$\frac{4 \times 10^{-9}}{4 \times 10^{-2}} = 1000$$

A 10 bit data word will then suffice to cover the entire tuning range.

The quartz oscillator in the rubidium frequency standard has an aging rate of $5 \text{ pp } 10^8$ per month for the first month and $5 \text{ pp } 10^9$ per month thereafter. In

Table 2-7. Comparison of 5 MHz Oscillators

Parameter	TCXO	Second Grade Ovenized	First Grade Ovenized
Temp: -54°C to 71°C	$\pm 1 \times 10^{-6}$	$\pm 3 \times 10^{-9}$ to 60°C	$\pm 2 \times 10^{-9}$ to 60°C
Vib: 5 g max.	$\pm 3 \times 10^{-8}$	$\pm 6 \times 10^{-9}$	$\pm 6 \times 10^{-10}$
Accel: 2g max.	$\pm 2 \times 10^{-9}$	$\pm 2 \times 10^{-9}$	$\pm 2 \times 10^{-9}$
$\pm 5\%$ volt change	$\pm 1 \times 10^{-7}$	13.5V, $\pm 2 \times 10^{-11}$	13.5V, 1×10^{-11}
$\pm 10\%$ load change	$\pm 1 \times 10^{-7}$	$\pm 5 \times 10^{-11}$	$\pm 1 \times 10^{-11}$
Short Term Stability (one sec ave)	$\pm 1 \times 10^{-9}$	$\pm 5 \times 10^{-12}$	$\pm 2 \times 10^{-12}$
Long Term Stability	$\pm 2 \times 10^{-8}$ /day	$\pm 5 \times 10^{-10}$ /day	$\pm 5 \times 10^{-11}$ /day
Warm up time to reach long term stability	Zero	3 days	7 days
Early aging from initial turn on	-	$\pm 2 \times 10^{-8}$ in 1 hr. $\pm 2 \times 10^{-9}$ in 24 hrs.	$\pm 2 \times 10^{-8}$ in 1 hr. $\pm 2 \times 10^{-9}$ in 24 hrs.
Warm up power	Zero	8W (for 1 hr)	8W (for 1 hr)
Continuous power	.2W	2W	1.8W
Size (in) ³	3.2	39	47
Weight (lbs)	.2	2	1.8
Cost (\$) per 100 units/1975	1000	1100	4200

addition, radiation testing demonstrated a 6-v change in the VCXO control voltage for the equivalent of 5 years natural environment. The capture range of the loop is 5 pp 10^7 . To bring the quartz oscillator within a capture range, an 8-bit D to A converter could be used.

2.2.6.5 Temperature Compensated Voltage Controlled Crystal Oscillator

Characteristics for a candidate user transponder VCO are shown in Table 2-8. These specifications are for a temperature compensated voltage controlled crystal oscillator available from Frequency Electronics, Inc., and are typical of the performance which could be expected from any one of a number of TCVCXO suppliers. Space qualification of this VCO is not considered a risk because crystal oscillators have previously been space qualified.

Table 2-8. TCVCXO Characteristics

Frequency Range	2-33 MHz
Frequency Stability	
1 second	$\pm 2 \text{ pp } 10^9$
1 hour	$\pm 1 \text{ pp } 10^7$
24 hours	$\pm 1 \text{ pp } 10^6$
1 year	$\pm 6 \text{ pp } 10^6$
Modulation Range	$+50 \text{ pp } 10^6$
Modulation Rate	DC to 20 kHz
Modulation Sensitivity	-10 ppm/v
Modulation Linearity	$\pm 5\%$
Output Power	0 to +3 dBm
Temperature Range	-20°C to +70°C
Temp. Frequency Stability	$\pm 3 \text{ ppm}$
Stabilization Time	5 seconds
Input Voltage	+12 VDC $\pm 1\%$
Input Power	120 mW
Size	2" x 2" x .8"
Weight	4 oz.

Long term stability is a problem for VCO's which must be pulled over a frequency range of ± 50 pp 10^6 . The problem is that the effective Q of an oscillator must be spoiled to allow tuning over the pull range and as a result, long term drifts are not just a function of crystal aging but are a function of the aging of all components in an oscillator tuning circuit. The value of \pm pp 10^6 /year reported in the specification could be reduced to ± 2 pp 10^6 /year if the oscillator was subjected to an accelerated aging process.

2.2.6.6 Conclusions

A temperature compensated crystal oscillator similar to the TCXO oscillator described in Table 2-7 should be selected as a reference oscillator for the user transponder. In addition, a TCVCXO with the characteristics described in Table 2-8 should be used for the transponder VCO. Atomic standards represent some risk and the long term stability offered by such devices is not required since long term drift in crystal oscillators can be accurately modeled and this drift can be compensated by offsetting ground station transmit frequency.

2.2.7 DIGITAL TRACKING

One technique which was considered for phase locked loops tracking in the M/A transponder was the use of a digital tracker as described in Figure 2-30. In this scheme an analog tracking error signal in the baseband demodulator is A/D converted and filtered digitally. The resulting error signal is converted into a series of pulses in a rate multiplier (the number of pulses is proportional to the magnitude of the filtered error signal). These pulses in turn step an incremental phase modulator. A fixed stepping rate results in a fixed offset frequency at one of the down conversion mixers of the receiver.

After careful consideration, a digital tracking technique for carrier tracking (i.e., IPM, rate multiplier and digital filter) was ruled out for two reasons; (1) analog techniques require less power and, (2) phase step (3°) granularity decreases frequency multiplication which is required in generating L.O.'s for S-band frequencies.

2.2.8 FREQUENCY HOPPER

Two different approaches were considered for implementation of the frequency hop generator in the M/A transponder. The first and more conventional approach was an analog mechanization using a PLL in combination with a programmable divider to synthesize a pseudorandom sequence of 512 discrete frequencies.

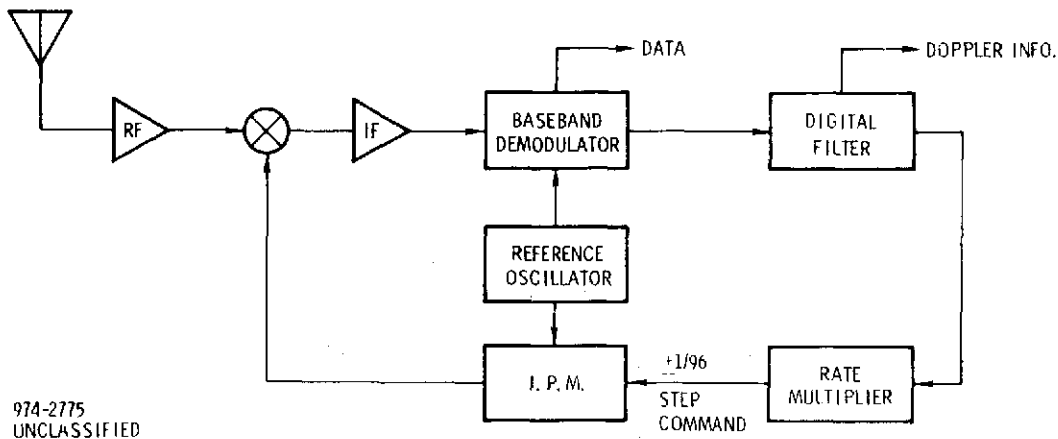


Figure 2-30. Digital Phase Locked Loop

The second approach was a digital implementation using a rate multiplier in conjunction with an up/down counter to drive a quadriphase modulator. In this case discrete frequencies are generated by stepping a carrier in 45° steps at the desired rate. Block diagrams of these two approaches are shown in Figure 2-31.

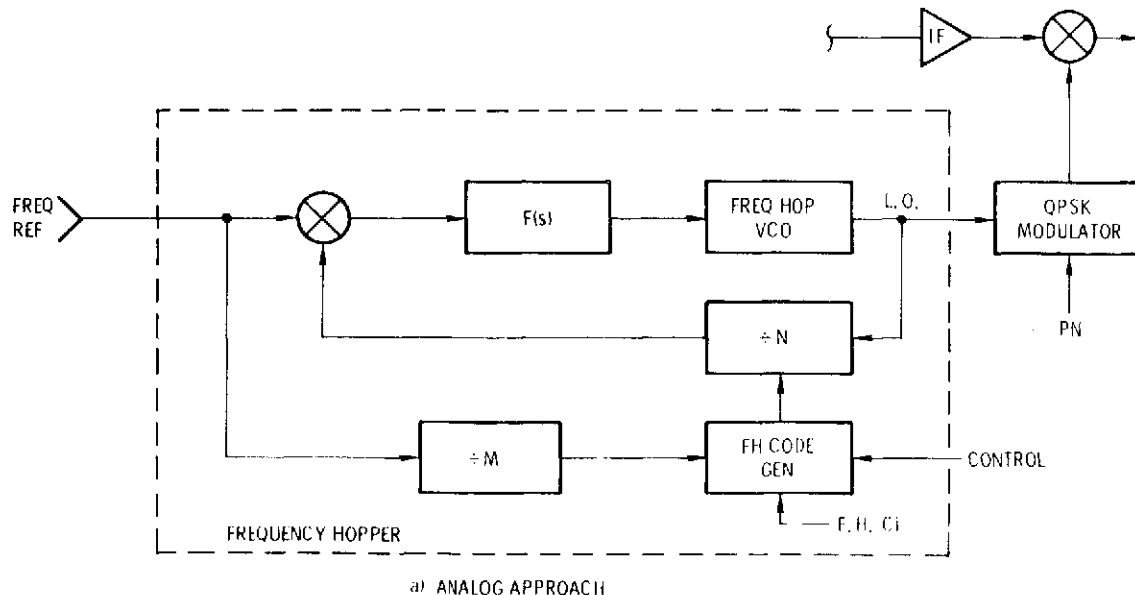
The digital approach was selected over the analog approach for the following reasons: (1) reliability of an all IC implementation; (2) no loss in performance due to PLL acquisition time for each hop; (3) minimum hardware, since hopper is integral to the SQPN modulator. The digital frequency hopper can be implemented on a single 4" x 5" PC card and will consume 1.5 watts of power at 5 VDC. Details of the design are presented in paragraph 2.3.1.6.

2.2.9 INTEGRATED CIRCUIT TRADEOFFS

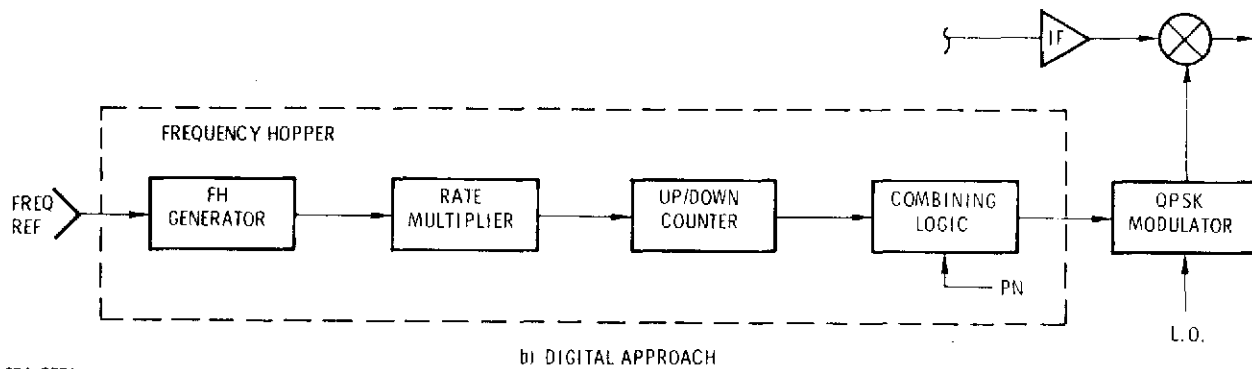
There are a number of critical tradeoffs which must be evaluated in selecting integrated circuits for a user transponder. Some of the most important tradeoffs are:

- Power dissipation
- Speed requirements
- Multiple source availability
- Reliability
- Availability of LSI and MSI functions
- Interface compatibility

Figure 2-32 is a comparison between bipolar and CMOS power dissipation. CMOS power dissipation is negligible at dc and increases linearly with frequency, whereas bipolar dissipation tends to be constant. Thus at low to intermediate frequencies,



a) ANALOG APPROACH



b) DIGITAL APPROACH

974-2776
UNCLASSIFIED

Figure 2-31. Frequency Hopper, Block Diagram

CMOS can represent a dramatic reduction in dissipation. It is recommended that CMOS be used for low speed counters and control functions where clock speeds are below 100 kHz. For the PN coder, FH generator, IPM and other high speed logic circuits which require logic speeds on the order of 1-10 MHz, bipolar families should be selected.

As illustrated by Table 2-9, the TTL family includes the following members in order of speed:

- 54S/74S Schottky
- 54H/74H High Speed

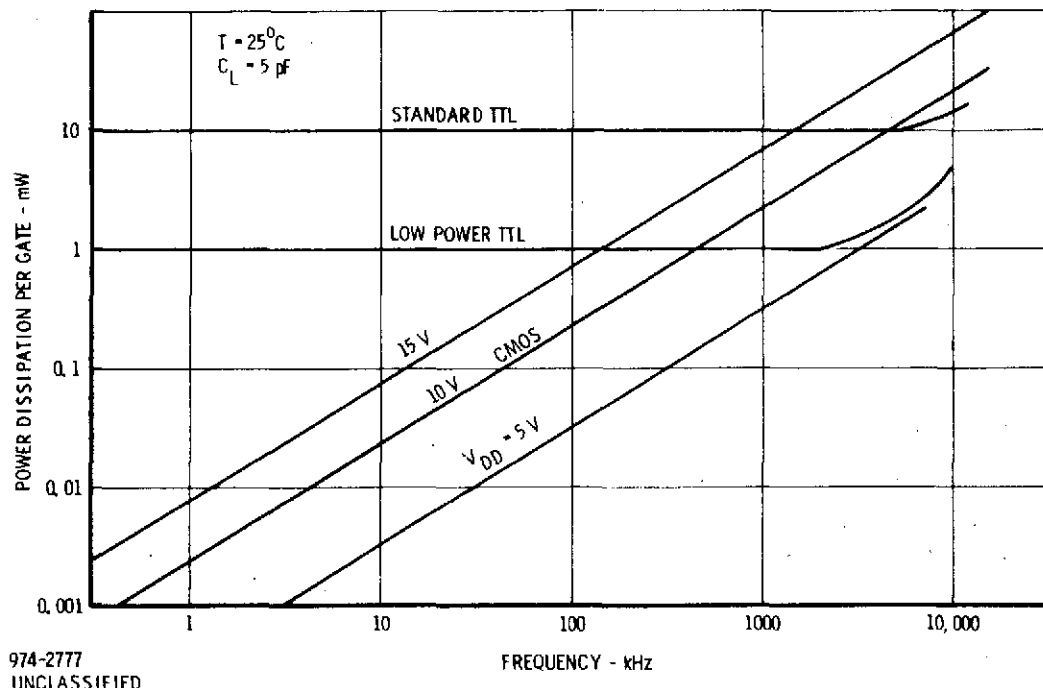


Figure 2-32. Comparison of Bipolar vs. CMOS Power Dissipation

- 54/74 Standard
- 54L/74L Low Power
- 54LS/74LS Low Power Schottky

For logic speeds of 10 MHz and less it appears that Low Power TTL most nearly meets the requirements for a user transponder. However, it should be noted that if a general class of devices is selected for all logic circuits, Low Power Schottky device has the lowest speed-power product. The only problem associated with this device are (1) limited number of currently available LSI functions and (2) multi-source availability. These problems should disappear by 1976. Therefore, the low power Schottky logic family represents the best choice for future user transponder equipment and is used for estimating purposes in this report.

Table 2-9. Typical Parameters of the TTL Family

Typical dc Characteristics	54S/ 74S	54H/ 74H	54/ 74	54L/ 74L	54LS/ 74LS
Supply Voltage V	5	5	5	5	5
High Level Input Voltage Min. V	2	2	2	2	2
Low Level Input Voltage Max. V	0.8	0.8	0.8	0.7	0.7
High Level Output Voltage Min. V	2.7	2.4	2.4	2.4	2.5
Low Level Output Voltage Max. V	0.5	0.4	0.4	0.3	0.4
High Level Noise Margin Min. mV	700	400	400	400	500
Low Level Noise Margin Min. mV	300	400	400	400	300
Fan Out	10	10	10	10	10
Av. Power Dissipation/Gate* mW	20	23	10	1	2

*Duty Cycle 50% $V_{cc} = 5V$ $T_A = 25^\circ C$

Typical ac Characteristics	54S/ 74S	54H/ 74H	54/ 74	54L/ 74L	54LS/ 74LS
Delay Time High to Low Level nsec	3	6	8	31	10
Delay Time Low to High Level nsec	3	6	12	36	9
Speedpower Product pJ	6C	138	100	33	19

2.3

RECOMMENDED M/A TRANSPONDER DESIGN

This section presents a multiple access transponder design which is a result of the waveform and implementation tradeoffs presented in paragraphs 2.1 and 2.2. First the major waveform parameters are summarized, then the functional design of the transponder which is compatible with these waveform parameters is presented. Next, size, weight and power estimates for this transponder are presented and finally, performance specifications are listed.

2.3.1 WAVEFORM PARAMETERS

FORWARD LINK

Preamble:

Type	Pseudorandom Frequency Hop
Code Generation	Primitive Root
Code Period	256
Hop Rate	3.006 kHz
Spacing	12.023 kHz
Repetition Interval	85.172 mS
Preamble Duration	11 seconds

PN Modulation:

Type	SQPN - Staggered Quadriphase Pseudonoise
Code Family	Maximal Code Pairs augmented by one chip
Code Period	2^{18}
PN Chip Rate	3.078 MHz
Repetition Interval	85.172 mS

Command Data:

Modulation	Synchronous biphasic differential, NRZ-M
Rates (select 1)	94 bps
	188 bps
	376 bps
	752 bps
Word Length	User defined
Coding	User defined

RF Signal:

Frequency	2106.40625 MHz
Doppler	± 56 kHz
Range Rate Uncertainty	± 100 m/sec $\approx \pm .65$ kHz

RETURN LINK

PN Modulation:

Type	SQPN - Staggered Quadriphase Pseudonoise
Code Family	Maximal code pairs augmented by one chip
Code Period	2^{18}
PN Chip Rate	3.078 MHz
Repetition Interval	85.172 mS

Telemetry Data:

Modulation	Asynchronous biphase differential, NRZ-M
Rate	1000 - 50,000 bps
Word Length	User defined

Data Encoding:

Type	Convolutional, nonsystematic, transparent
Constraint Length	7
Code Rate	1/2
Code Gain	5 dB at BER = 10^{-5}
Symbol Rate	100 kbs max
Data Type	Delta mod, PCM, NRZ-M

RF Signal:

Frequency	2287.5 MHz
Doppler	± 112 kHz
Range Uncertainty	± 100 Km
Range Rate Uncertainty	± 200 m/sec

2.3.2 TRANSPOUNDER FUNCTIONAL DESIGN

2.3.2.1 General Description

The M/A user transponder consists of fourteen modules:

- RF Down Converter
- IF Chain
- RF Synthesizer No. 1
- RF Synthesizer No. 2
- Demodulator
- Sync Monitor
- Incremental Phase Modulator
- PN Coder
- Local PN/FH Reference Generator
- Controller
- Modulator
- Transmitter
- Power Supply Post Regulator
- Chassis

Major functions of these modules and their interconnections are shown in a block diagram of the transponder in Figure 2-33.

A forward link signal is amplified and down converted in the RF Down Converter module. The signal is dehopped during the FH preamble and its PN modulation is stripped off during a track mode in the correlator (second mixer) of the IF Chain leaving a PSK modulated carrier at its output. Bandwidth reduction and AGC action occurs in the second IF amplifier and, after passing through a third IF stage, the signal is delivered to the Demodulator. A sync detector senses the presence of a signal and, after sync verification is made, a Costas demodulator extracts the data. This command data is subsequently processed, differentially decoded and delivered to a satellite command decoder.

Major modules involved with demodulating the frequency hop during acquisition and subsequently acquiring and tracking the pseudonoise portion of the signal are:

- Modulator
- Local Reference
- PN Coder
- IPM

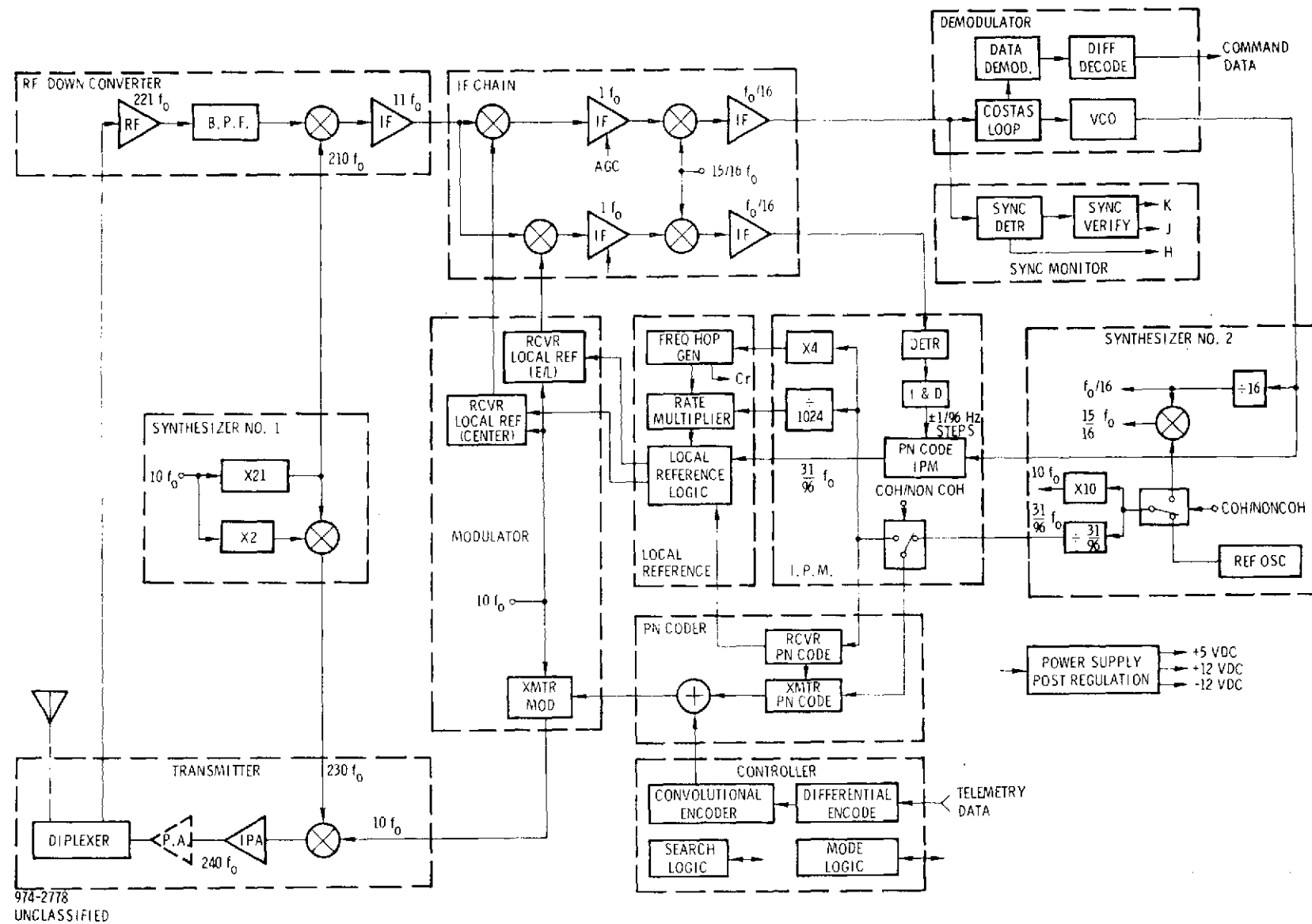


Figure 2-33. Multiple Access User Transponder

Basically, the Modulator consists of three QPSK modulators which (1) provide the local references for the carrier channel (center phase or bogey), (2) provide the local references for the code tracking channel (early-late phases) and (3) provide the SQPN modulated signal to the transmitter module. The Local Reference provides the required staggered PN sequence to the Modulator for both the receiver and the transmitter functions and it also generates the appropriate frequency hop sequence for the receiver local reference. The PN Coder generates two pairs of orthogonal PN codes for use in the Local Reference module. Finally, the IPM module retards the PN code phase in quarter chip steps during a PN acquisition mode and it advances and retards the PN code phase in approximately 3° steps during a code tracking mode.

The Transmit module contains a single up conversion stage, a power amplifier to provide the desired EIRP (different for each application) and a diplexer for separating the receive and transmit signals.

Synthesizer No. 1 provides the first L.O. for both the receiver and the transmitter. Synthesizer No. 2 provides all of the additional L.O. signals. The Controller provides all programming functions including mode control and FH/PN search sequences. Differential and convolutional encoding (if used) is also contained in this module. All power supply potentials for all portions of the transponder are post regulated to insure uninterrupted performance due to power transmits, buss switching, etc.

The transponder provides the capability to operate in the following modes on command:

- Clear Mode
- Coherent Transpond
- Noncoherent Transmit/Receive
- Short Code Return Only

Optional features of the M/A transponder include:

- Retrace for Multipath
- VCO Drift Monitor

More complete detail on these modes as well as many other implementation topics will be presented in the preceding sections.

Although there is little likelihood that multipath will be a problem at S-band for PN during acquisition, both frequency hop and pseudonoise retrace capability will be provided for resolving possible false lock to multipath on command. This involves a minor controller routine modification. The only disadvantages to this mode is approximately a 2 to 1 increase in acquisition time.

Since the transponder will use a temperature compensated voltage controlled oscillator for tracking in the forward link to minimize power consumption, and the long term drift on this oscillator may exceed the initial acquisition bandwidth of the receiver, the voltage offset of the VCO during a track mode will be recorded via an A/D converter and periodically sent back to the ground station as a status word via the telemetry link. This information will be used to compute new transmit frequency offsets for future forward link acquisitions of the user satellite.

2.3.2.2 RF/IF Design

Major parameters for each of the RF and IF Amplifier stages of the multiple access user transponder are described below including the requirements of the diplexer and the receiver RF amplifier along with the gain and bandwidth requirements for the three IF amplifiers. The resultant S + N budget for the receiver is also included. For the transmitter chain, gain distributions, signal levels and bandwidth requirements are presented.

2.3.2.2.1 Receiver Chain

The RF and three IF amplifier chains for the M/A User Transponder are shown in Figure 2-34. A maximum signal of ~ 115 dBm is assumed and a tracking threshold of ~ 145 dBm is assumed for the user requiring a 100 bps command data rate. Since signals must be linearly amplified prior to demodulation in the Costas loop, all amplifiers must have sufficient apertures to accommodate S + N without any clipping prior to the 2σ level.

The diplexer will provide the needed isolation between the Tx and Rx signals. Recommended specifications for this device follow:

Mechanical Requirements

The Diplexer should be approximately 2.5" x 1.5" x 5".

2-119

SIGNAL MIN

<u>SIGNAL (dBm)</u>	-115
<u>NOISE (dBm)</u>	-174/Hz

-65

-95

-99

-80

-36

-51

-10

-174/Hz

-79

-65

-34

-66

-25

SIGNAL MIN

<u>SIGNAL (dBm)</u>	-145
<u>NOISE (dBm)</u>	-174/Hz

-65

-125

-129

-80

-36

-51

-10

-174/Hz

-79

-35

-4

-36

+5

GAIN (dB)

-0.3

-0.7

+21

-1

-3

-7

+59

-3

-6

+50

-6

-3

-6

+41

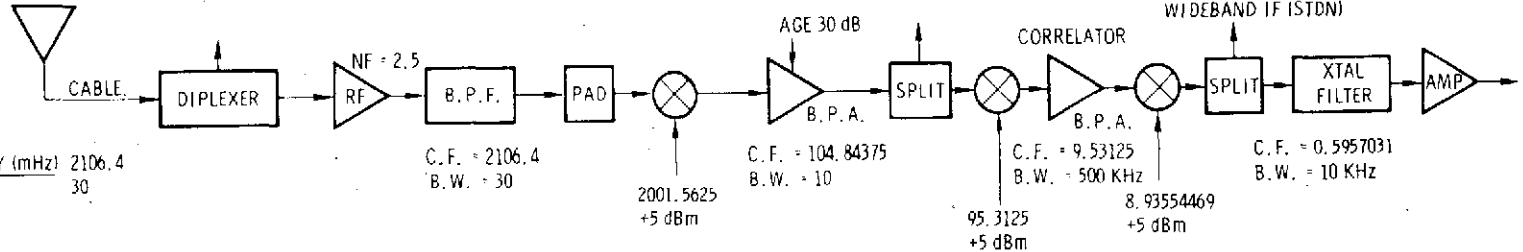


Figure 2-34. Receiver RF and IF Chain.

Electrical Requirements

The Diplexer shall have two ports at the following center frequencies:

Port 1	2287.5 MHz
Port 2	2106.4 MHz

The two ports shall be combined onto one common port for connection to an antenna. The diplexer is used at the RF input to a receiver and RF output of a transmitter.

Impedance

The impedance looking into any one of the three ports at its respective center frequency shall be 50 ohms nominal.

VSWR

The midband VSWR of any port shall be 1.25 or less for ± 5 MHz about f_o .

Insertion Loss

The insertion loss, in both directions, between the common port and each of the isolated ports at their respective midband frequencies shall be 0.6 dB maximum.

Passband Ripple

Passband ripple shall be ± 0.1 dB maximum.

Matched Bandwidth

The matched bandwidth of each port shall be 10 MHz minimum, 30 MHz maximum.

Input Power

The unit shall be capable of handling one watt incident average power at any one of the two frequencies with no degradation of performance.

Phase Linearity

In a ± 4 MHz band centered about each center frequency, the phase shift at any one frequency shall not deviate more than $\pm 5^\circ$ from the best straight line approximation of the phase response.

Bandwidths

BW ₁	±11 MHz Min.
BW ₃	±15-23 MHz Min-Max.
BW ₆₀	±137 MHz Max.

Group Delay

10 ns maximum for F_o ±5 MHz

Port-to-Port Isolation

The minimum isolation required between any two ports is 65 dB.

The RF section has 21 dB of gain to reduce the first mixer noisy losses to ≤ 0.1 dBm with respect to the receiver input. Since the RF amplifier is a wideband device, a bandpass filter is placed before the first mixer to insure that both sum and difference noise will not be translated to the first IF frequency. Recommended specifications for the RF amplifier follow:

Frequency Range	2.0 - 2.2 GHz
Gain	21 dB nominal
Flatness	±1 dB
Noise	2.5 dB max.
VSWR	1.35 Max.
Compression Point (1 dB)	+3 dBm
Size	3" x 2" x 3/4" nominal

After the first conversion, the signal is amplified in an AGC amplifier. The AGC signal is generated from noise prior to signal acquisition and is generated by signal only after acquisition. As a result of this AGC action, the signal remains at a constant level into the correlator over the dynamic range of the input signal.

Prior to the PN correlator (second conversion) the wideband signal (5 MHz) is split to drive separate carrier and PN code tracking loops. After correlation (second IF) the signal bandwidth should only be wide enough to accommodate the data sidebands to minimize S + N aperture problems with additional gain in the third IF. A three section crystal filter was selected for this purpose with the following specifications:

Center Frequency	9.53125 MHz
Bandwidth	10 \pm 2 kHz
Type	3 pole Butterworth
Insertion Loss	6 \pm 1 dB
Impedance	50 ohm nominal

In the third IF the output signal level is set to -10 dB to keep from clipping on peak noise. To reduce the power requirements for linear amplification the impedance level of the output stage is converted from 50 ohms to 1000 ohms nominal, which is adequate to feed the FET choppers in the Costas loop. The bandwidth requirements for this stage are set at a nominal 50 kHz to remove the mixing products.

2.3.2.2.2 Transmit Chain

IF and RF amplifier chains for the transmit section are shown in Figure 2-35. SQPN modulation of the transmit signal occurs at an IF frequency of 95.3125 MHz (same frequency as the correlator local reference in the receiver). After reducing the spectrum to 5 MHz in a three-section bandpass filter, the modulating signal is translated to RF with a 2192.1875 MHz LO. Unwanted mixing products are stripped from the RF signal with a bandpass filter with a 3 dB bandwidth of 30 MHz.

A Class A intermediate power amplifier (IPA) is used to level convert the signal to +11 dBm. Specifications for this IPA follow:

Center Frequency	2287.5 MHz
Bandwidth	400 MHz nominal
Gain	30 dB
Output Level	+11 dBm \pm 2 dB
Output Compression Point	+16 dBm nominal
Output Intercept Point	+28 dBm nominal
Intermods	-34 dB down from +11 dBm output
Size	1.5" x 1" x .7" max.
Power	15 V @ 50 ma
Noise Figure	4 dB nominal

For some applications, depending on antenna gain and data rate, this level may meet the requirements for the minimum EIRP. For a low gain antenna (-6 dB) and high data rates up to 100 KBS, 0 to 30 dB of additional RF gain will be required.

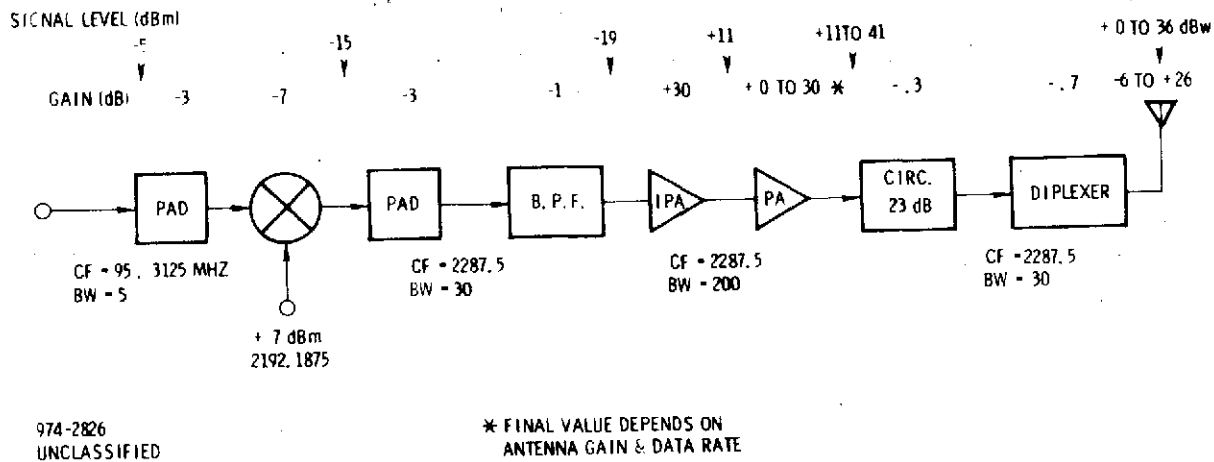


Figure 2-35. Transmitter IF and RF Chain

This is furnished by an additional power amplifier stage. Specifications for a typical PA are shown below:

Center Frequency	2287.5 MHz
Bandwidth	400 MHz nominal
Type	Class C
Output Level	11 watts
Output Power Saturated Gain	12-13 watts
Input VSWR	2:1 max
Load VSWR, $P_o = 12$ W	∞ :1, all phase angles
Power	22 V @ 1.4 amps
Efficiency	35%

Isolation is provided between the PA stages and the diplexer to provide resistive loading for the amplifier and good termination for the diplexer to insure its performance characteristics which were specified in the receiver section.

2.3.2.3 Frequency Synthesis

Figure 2-36 shows the details of frequency synthesis for the multiple access transponder. This scheme coherently synthesizes all L.O.'s to provide a Receiver/Transmitter ratio of 221/240 at 2106.40625 MHz and 2287.5 MHz, respectively, from a 9.53125 MHz source. In addition, PN and FH clocks are provided using a 31/96 x 9.53125 MHz reference to keep nth order products from mapping into the IF amplifier bands.

During a noncoherent mode of operation, all clocks and L.O.'s are generated from the receiver VCO. However, during a noncoherent mode, the transmit signal is generated from a fixed frequency oscillator along with the transmitter PN code, and the 1st and 2nd L.O.'s of the receiver while the 3rd and 4th L.O.'s of the receiver are synthesized from the VCO for tracking purposes. Refer to Tables 2-10 and 2-11 for oscillator specifications.

2.3.2.4 Incremental Phase Modulator for the Code Loop

In the code tracking loop an IPM is used to advance or retard the phase of the coder clock in discrete increments of either 1/96 or 1/4 chips. This circuit is shown with detail in Figure 2-37. Fractional cycle movement is implemented with three dividers:

$$\div 8, \div 3, \div 4 \longrightarrow \div 96$$

Each time a countdown sequence in the $\div 8$ circuit is lengthened or shortened by one count, the IPM output is respectively retarded or advanced.

The IPM incorporates commonly used mix and divide techniques for synthesizing its output. Double balanced mixers are used for conversion and bandpass amplifiers are used to filter unwanted mixer components.

2.3.2.5 PN Coder

Figure 2-38 illustrates the PN code generator. Each PN code generator consists of an 18 stage shift register generator (SRG). Each SR is constructed as a modular SRG or MSRG. This is as opposed to a simple shift register generator SSRG. In the SSRG the feedback taps are modulo two added with the sum being fed back to the last flip flop. This can result in many levels of modulo two logic. In the MSRG, a transformation of the SSRG, there can only be at most one logic level of delay due to modulo two addition and thus slower speed logic families can be employed with lower power dissipations.

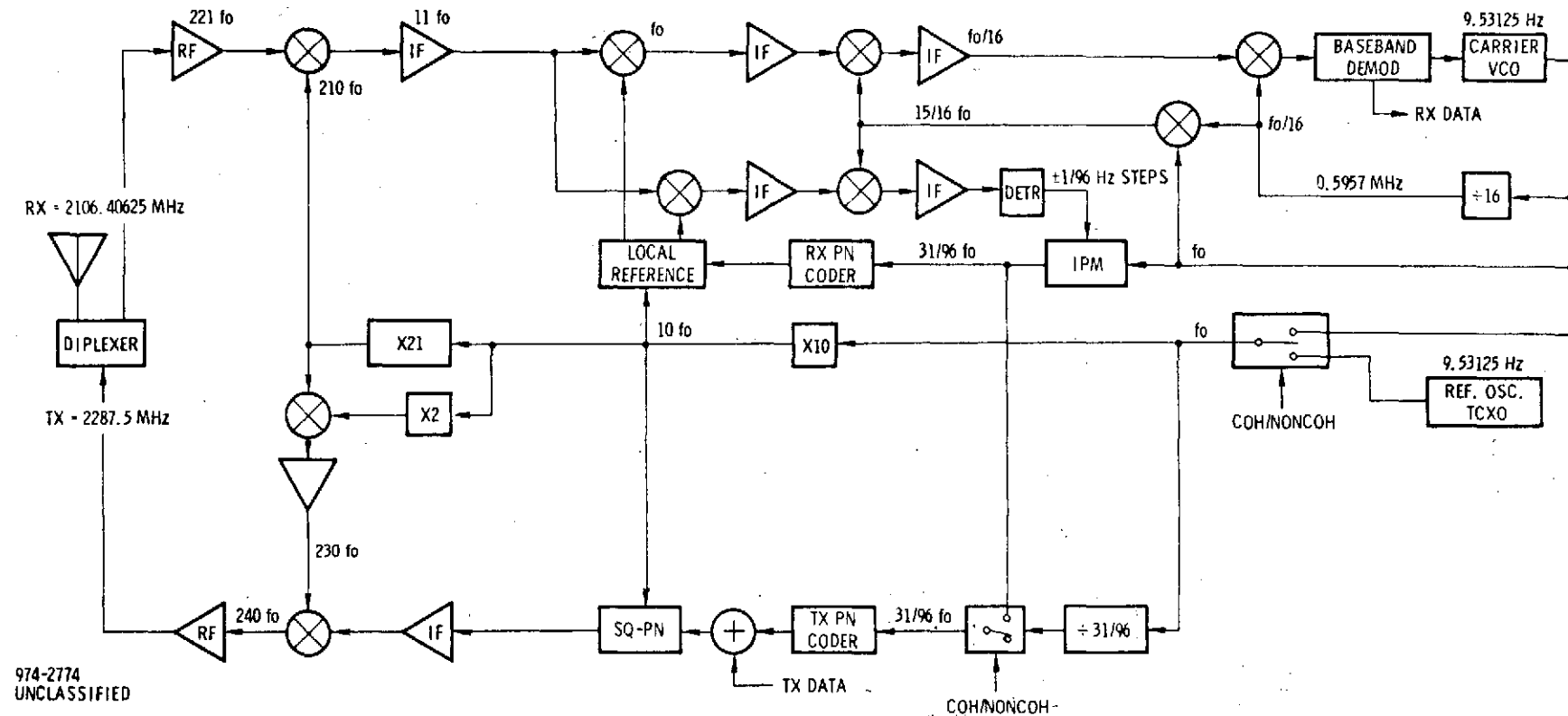


Figure 2-36. M/A Frequency Synthesis

Table 2-10. Voltage Controlled Oscillator Specification

Frequency	9.53125 MHz
Frequency Stability	
1 second	$\pm 2 \text{ pp } 10^9$
1 hour	$\pm 1 \text{ pp } 10^7$
24 hours	$\pm 1 \text{ pp } 10^6$
1 year	$\pm 2 \text{ pp } 10^6$
Modulation Range	$\pm 30 \text{ pp } 10^6$
Modulation Rate	DC to 20 kHz
Modulation Sensitivity	-10 pp M/V
Modulation Linearity	$\pm 5\%$
Output Power	TTL compatible
Temperature Range	-20° C to +70° C
Temp. Frequency Stability	$\pm 1 \text{ ppm}$
Stabilization Time	1 second
Input Voltage	+12 VDC $\pm 1\%$
Input Power	120 mW
Size	2" x 2" x .8"
Weight	4 oz.

Although the configuration shown in Figure 2-38 is programmable, the code generator implementation for transponders will use hard wired feedback connections. This mechanization conserves power and besides with 7776 codes being available, there will always be more than a sufficient number of PN codes to prevent overlap use of codes.

The epoch set initializes the SR's to an all ones vector state to start the PN sequence generation. On the uplink, it occurs in synchronism with the end of the frequency hopping sequence. The master clock drives one SR and its inverse drives the other SR. The SR outputs are thus phase shifted by 180° with respect to one another. This then prevents the phase of the carrier from changing by 180°. Carrier phase changes are restricted to 90° jumps.

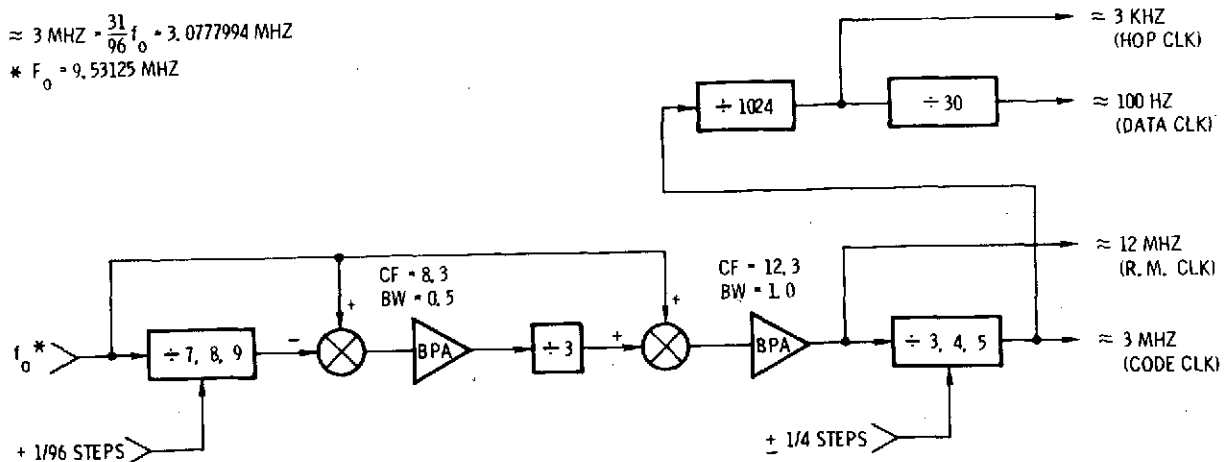
For the return only mode the PN code of the transmitter will be shortened to provide return link acquisition without the aid of a forward link within 10 seconds. The code length selected for this mode is as follows:

Table 2-11. Reference Oscillator Specification

Frequency	9.53125 MHz
Frequency Stability	
1 second	$\pm 1 \text{ pp } 10^9$
1 hour	$\pm 1 \text{ pp } 10^8$
24 hours	$\pm 2 \text{ pp } 10^8$
1 year	$\pm 2 \text{ pp } 10^6$
Output Power	TTL compatible
Temperature Range	-20°C to +70°C
Temp. Frequency Stability	$\pm 1 \text{ ppm}$
Stabilization Time	1 second
Input Voltage	+12 VDC $\pm 1\%$
Input Power	120 mW
Size	2" x 2" x .8"
Weight	4 oz.

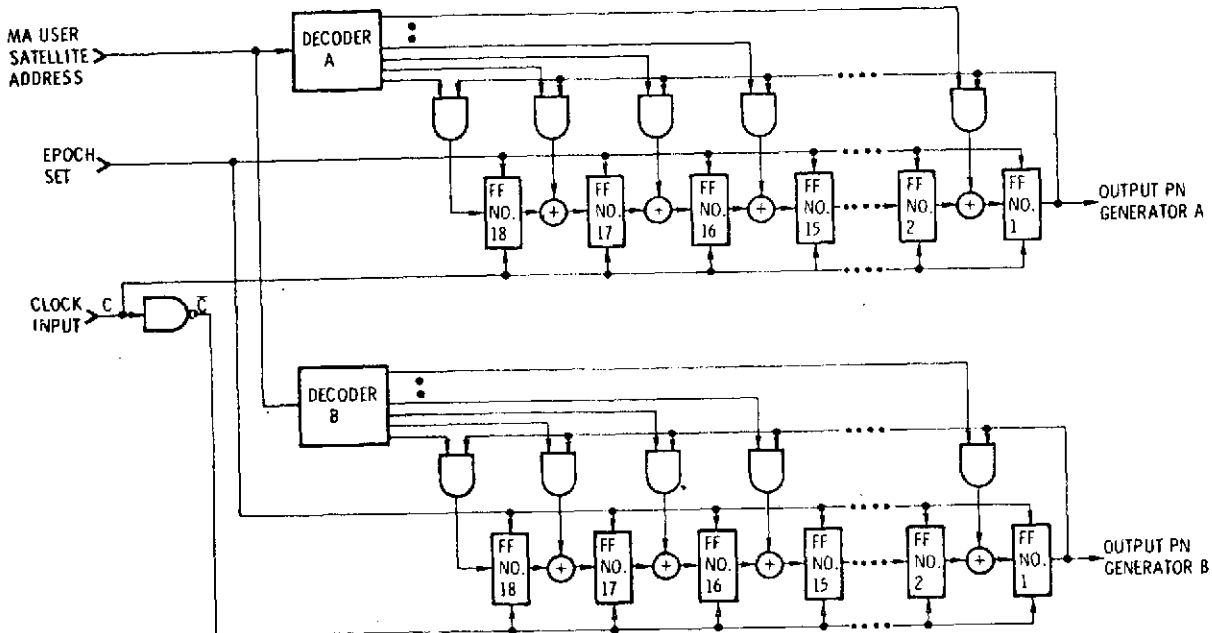
$$\approx 3 \text{ MHZ} \cdot \frac{31}{96} f_0 \approx 3.0777994 \text{ MHZ}$$

* $f_0 = 9.53125 \text{ MHZ}$



974-2780
UNCLASSIFIED

Figure 2-37. Code Tracking Loop I. P. M.



974-2773
UNCLASSIFIED

Figure 2-38. Modular Shift Register Generators
Used for Generation of Staggered Quadriphase

<u>Data Rate</u>	<u>Code Length</u>
1 - 10 kbs	2^{11}
10 - 25 kbs	2^{15}
>25 kbs	2^{13}

2.3.2.6 Local Reference Generator

In the M/A transponder, the local reference generator is required to generate two types of reference signals for proper operation of the transponder. The reference signals are: (1) frequency hop preamble which is used in the first step of the forward link synchronization procedure, and (2) SQPN reference which is used for final PN code acquisition and tracking after frequency hop. The following frequency hop parameters apply.

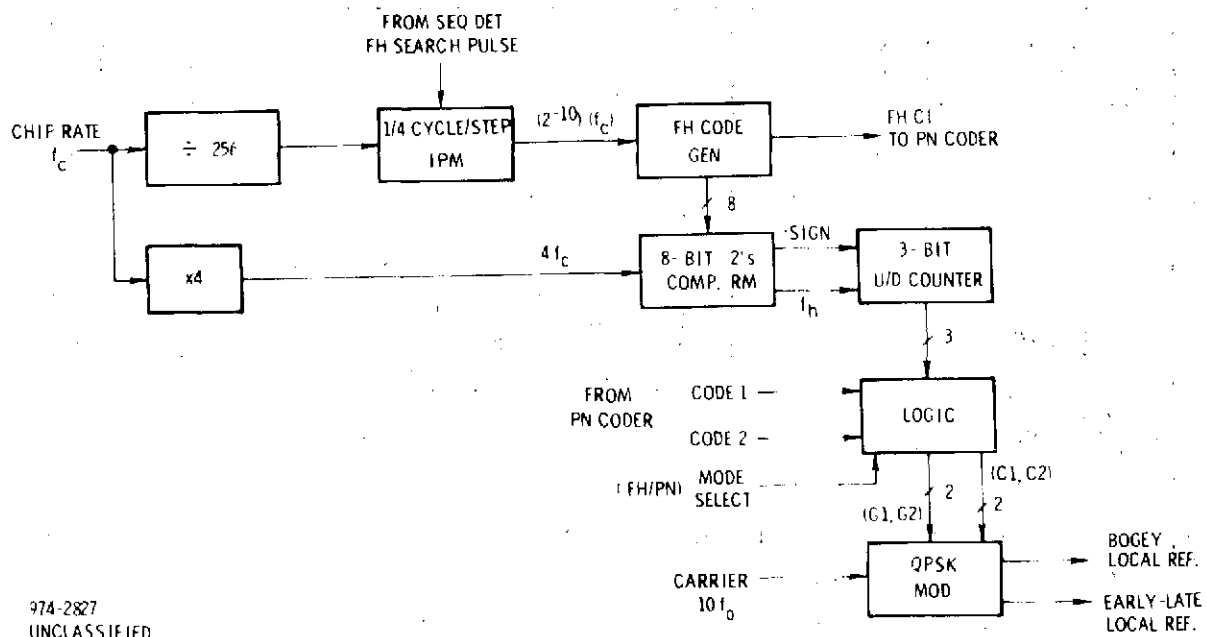
Hopping rate	= 3 kHz
Frequency spacing	= 12 kHz
Code period	= 256 hops = PN code period
Bandwidth	= 3.072 MHz

These parameters suggest the implementation of the local reference generator shown in Figure 2-39.

2.3.2.6.1 Frequency Hop Mode

The chip rate clock at f_c Hz is first divided by 256 and then by a 1/4 cycle per step IPM, yielding a final clock at $f_c/1024$ to the FH code generator under normal condition (i.e., no FH search pulses). The FH clock is roughly 3.1 kHz.

The FH code is generated by equations 2-41 and 2-42 in paragraph 2.1.7 and is stored in ROM's. There are 256 binary-words, each of 8-bit long and corresponding to the 256 hops, in the FH code. At each FH clock time (i.e., 3.1 kHz rate), a code word is read from memory and presented to a rate multiplier circuit. The RM treats each word as an 8-bit, binary number in 2's complement notation and converts it to pulse rate. Along with a sign signal which is the MSB of the code word the pulses are applied to a 3-bit U/D counter whose content is logically decoded to drive a QPSK modulator to effect frequency hopping.



974-2827
UNCLASSIFIED

Figure 2-39. Local Reference Generator

The RM circuit uses $4 f_c$ (roughly 12 MHz) as its reference clock. Thus, for an 8-bit number, the pulse rate, f_H , with sign is:

$$f_H = \left(\frac{4 f_c}{128} \right) (N)$$

where $N = -128, -127, \dots, 0, \dots, 127$. (The sequence is pseudorandom, of course.) At $N = -128$, the frequency deviation is roughly -1.5 MHz.

To obtain FH synchronization, a sequential sync detector is used to search for the received FH code. The search step is 1/2 chip per trial and is effected via the 1/4 cycle per step IPM. Since there are 256 hops in the FH code and since the hop rate is $f_c/1024$, the FH period is $2^{18}/f_c$, which is exactly that of the PN code. Thus, when FH sync is achieved, a FHCI can be used to reset the PN coder to start the next synchronization process.

To implement frequency hopping using 45 degree step IPM, we employ vector addition method rather than the "divide-and-translate" or the "single side band" schemes previously described. This is because, to effect ± 1.5 MHz frequency offset, the vector addition technique uses slower frequency and therefore lower power, logic elements. The new method is illustrated in the following diagram:

STEPS	1	2	3	4	5	6	7	8	1
I	→	→	•	→	→	→	•	→	→
Q	•	↑	↑	↑	•	↓	↓	↓	•
I + 2	→	↗	↑	↖	→	↘	↓	↖	→

974-2781
UNCLASSIFIED

The I and Q are quadrature carriers whose amplitude are either 1 or 0 and whose phase are either 0° or 180° , depending on the desired phase shift of $I + Q$. To phase modulate the output carrier by 360° , we simply carry out the addition steps 1 to 8 as indicated. For -360° modulation, we reverse the order of steps (i. e., 8 to 1). In any case, the stepping rate determines the amount of frequency offset from an unmodulated carrier. Because I and Q are constant-amplitude sinusoids, $I + Q$ will have a 3-dB amplitude variation. However, this is of no consequence to the frequency hopping process and is readily eliminated by passing it through a hard limiter.

To carry out the vector addition of I and Q, we use the circuit shown in Figure 2-40. The balance modulators generate the 2 phases, 0° and 180° , of the quadrature carriers which are gated to the summer in accordance with the vector diagram. In frequency hop mode, C1, C2, G1, and G2 are logical functions of a 3-bit U/D counter's content which represents the 8 addition steps. That is,

$$\begin{aligned} C1 &= \begin{cases} 1 & \text{for steps 1, 2, 8} \\ 0 & \text{otherwise} \end{cases} \\ C2 &= \begin{cases} 1 & \text{for steps 2, 3, 4} \\ 0 & \text{otherwise} \end{cases} \\ G1 &= \begin{cases} 1 & \text{(open switch) for steps 3, 7} \\ 0 & \text{(close switch) otherwise} \end{cases} \\ G2 &= \begin{cases} 1 & \text{(open switch) for steps 1, 5} \\ 0 & \text{(close switch) otherwise} \end{cases} \end{aligned}$$

2.3.2.6.2 PN Mode

After FH synchronization has been achieved, the transponder enters PN mode.

In PN mode, G1 and G2 are set to "0" (i.e., switches in the QPSK modulator are closed continually), and C1 and C2 are simply the two PN codes from the coder. The circuit in Figure 2-40 then operates as a conventional QPSK modulator.

For the bogey reference signal, the C1 and C2 codes are the on-time codes. To generate the early-late reference for code tracking, the basic circuit is still the same QPSK modulator of Figure 2-40. However, the C1 and C2 logic are the early-late codes of code 1 and code 2, respectively.

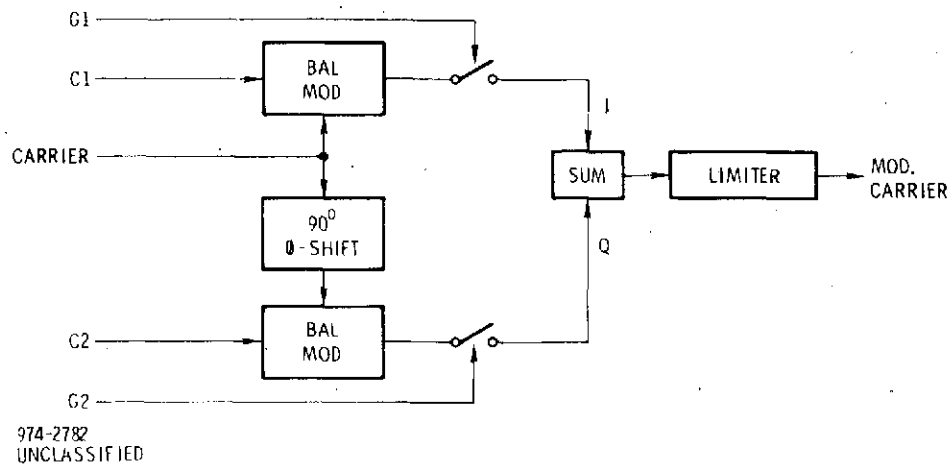


Figure 2-40. QPSK Modulator for FH and PN

For staggered quadriphase, code 1 and code 2 are phase shifted by 1/2 chip, relative to each other. The C1 and C2 logic remain unchanged. Figure 2-41 shows that SQPN is generated by summing two biphase modulated carriers. The carrier phases are in quadrature, and the two modulating PN sequences are displaced by 1/2 chip with respect to each other. Also shown in the same figure are pertinent waveforms illustrating the phase shift characteristics of SQPSK, i.e., the resultant phase rotation can only be 0 or $\pi/2$ during any code chip transition.

2.3.2.7 Baseband Demodulator

A detailed description of the baseband demodulator for the multiple access user transponder is described in this report. The major functions of the baseband demodulator include:

- Costas Loop
- Sequential Sync Detector
- Sync Verification and AGC
- Data Processor
- Convolutional Decoder (Optional)

Interconnections between these major functions are illustrated by a block diagram of the baseband processor shown in Figure 2-42. Values for the major parameters are presented including bandwidths, time constants and center frequencies.

2.3.2.7.1 Costas Demodulator

Biphase shift keyed data is demodulated from the third IF at 0.5957 MHz with a Costas loop. This loop operates in conjunction with a 9.53125 MHz VCO. The divide-by 16 chain provides the carrier in-phase and quadrature references for the loop. The side integrators are simple RC lowpass filters which have their corner frequency set to the data rate. The loop has a second order response with a two-sided noise bandwidth of 33 Hz.

When PN sync is detected the VCO is swept over the frequency uncertainty range of 700 Hz at the rate of:

$$\text{Sweep rate} = 2\pi f_n^2 \cong 600 \text{ Hz}$$

until phase lock is obtained. After acquisition the Costas loop is designed to track over the full ± 55 kHz doppler uncertainty region.

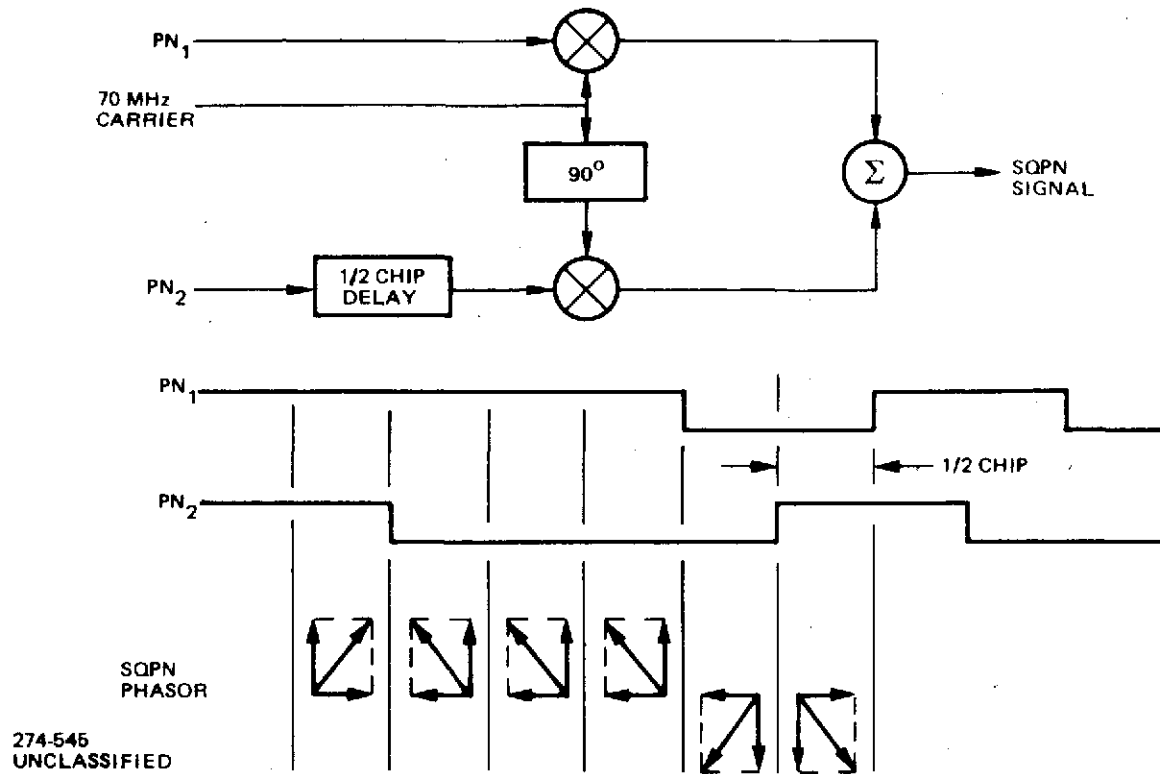


Figure 2-41. SQPN Limits Instantaneous Phase Shifts to 90%

If operation with STDN is desired, the Costas loop can be commanded to function as a phase locked loop (PLL) by disabling the I channel input to the third multiplier. Once phase lock to a pilot carrier is achieved, the STDN tones can be demodulated from the wideband I channel.

The theory of operation for a Costas demodulator is presented as follows and its associated block diagram is shown in Figure 2-43. The input signal to the demodulator is a biphasic modulated signal whose analytical expression is:

$$\text{Demodulator Input} = \cos(\omega_c t + \Theta);$$

where ω_c is the IF carrier frequency and Θ is the biphasic data modulation where Θ is either 0° or 180° . The output of the carrier voltage-controlled oscillator is:

$$\text{Carrier VCO} = \cos(\omega_c t + \alpha) \text{ or } -\cos(\omega_c t + \alpha);$$

where α is a small assumed phase error in the tracking loop. One property of this type of tracking loop is that it can lock up in either of two stable states: One inphase and the other 180° out-of-phase with the incoming suppressed carrier. Thus, the

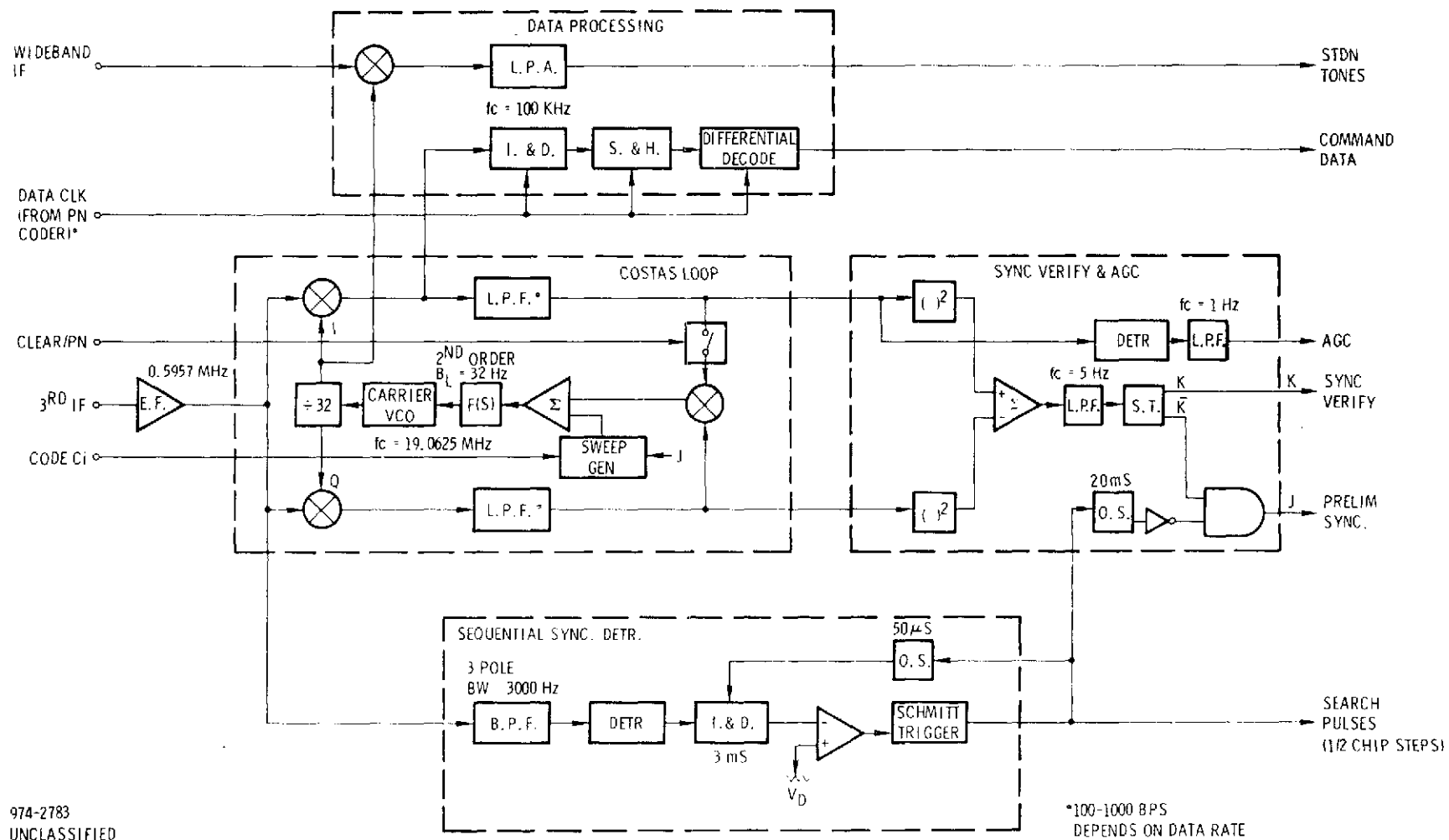


Figure 2-42. Baseband Demodulator for the M/A Transponder

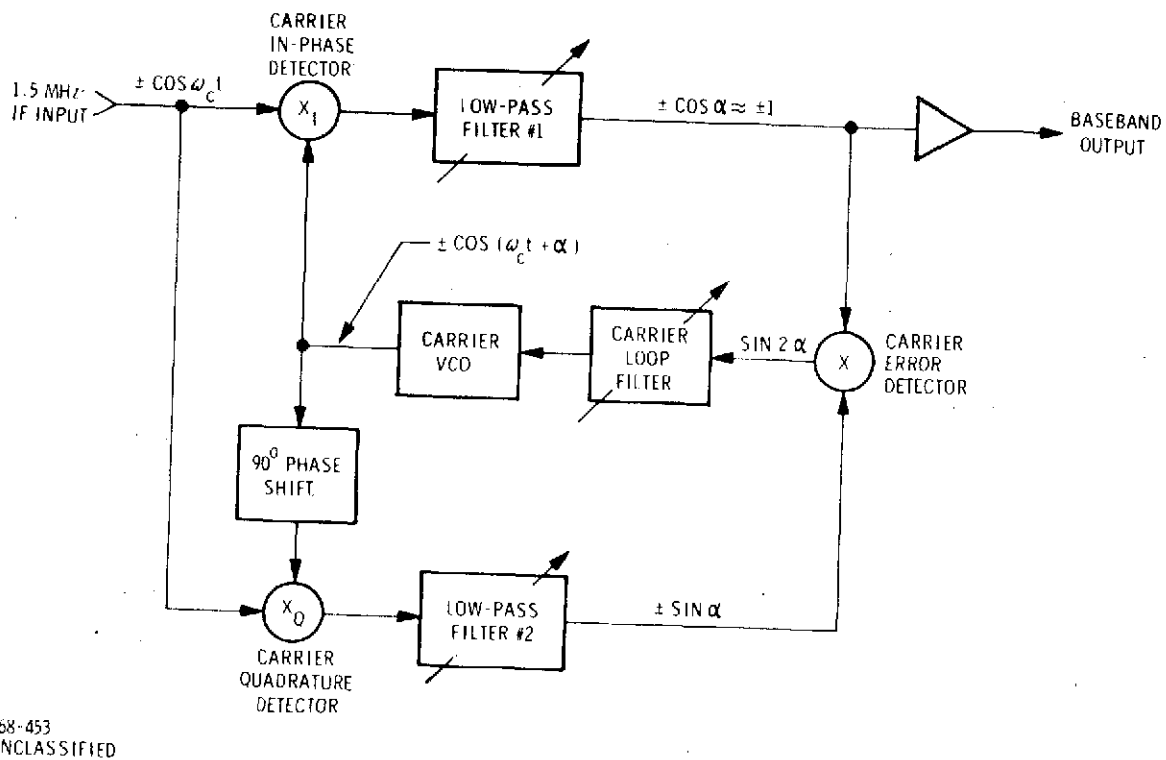


Figure 2-43. Synchronous Demodulator, Simplified Block Diagram

expression for the carrier VCO may either be $\cos(\omega_c t + \alpha)$ or $-\cos(\omega_c t + \alpha)$. The output of the carrier in-phase detector (X_I) after appropriate filtering by lowpass filter No. 1 is:

$$\cos(\alpha + \Theta) = \pm \cos \alpha.$$

Similarly, the output of the carrier quadrature detector (X_Q) becomes:

$$\sin(\alpha + \Theta) = \pm \sin \alpha.$$

The outputs of the two detectors are then multiplied in the carrier error detector as shown with a resultant output of:

$$\sin 2 \alpha \text{ which for small phase errors} = 2$$

This represents a DC error signal and is applied to the carrier VCO via the carrier loop filter. For small phase errors: $\cos \alpha \approx 1$, this expression simplifies to ± 1 . The output of the carrier inphase detector, after filtering, is thus seen to be the baseband information (or its complement if the VCO is at $-\cos(\omega_c t + \alpha)$).

2.3.2.7.2 Sequential Sync Detector

A functional element of major importance which was incorporated as part of the baseband demodulator design is the sequential sync detector. The major functional elements of this detector were shown in Figure 2-42.

A predetection filter with a bandwidth of 3000 Hz at baseband (5 parallel 700 Hz filters) conditions the signal. Next, the full-wave rectifier and low-pass filter develop a measure of the total power (noise or signal plus noise) in the 700 Hz bandwidth of the filter. Before code synchronization is achieved the output voltage from the low-pass filter is proportional to the measured noise power and its magnitude is less than the bias voltage $-V_b$. This causes the output of the integrator to ramp downward in the negative direction from zero until its magnitude exceeds that of the threshold voltage $+V_D$. The threshold detector output voltage which is normally at zero volts, now changes to +5 volts indicating a dismissal of PN code or hop sync. The positive change in the detector's output-voltage level initiates a sequence of search pulses with an average rate of 240 - 1/2 chip or hop steps per second.

When code correlation is finally achieved, a signal appears in the intermediate-frequency increasing the total power to the full-wave rectifier by 6 dB. The magnitude of the voltage becomes larger than the bias voltage so that the integrator output now grows positive. As a result, the threshold detector remains dormant and search pulses are no longer generated.

2.3.2.7.3 Sync Verification and AGC

Preliminary sync (J) is indicated when no search pulses occur for an interval of six 1/2 chip search pulse intervals (≈ 20 mS) and phase lock has not occurred. During acquisition, when the first time J occurs, frequency hop stops and a PN search is initiated. The second time J occurs, 3000 Hz frequency sweep is initiated until the Costas loop locks.

Phase lock or sync verification (K) is obtained from:

$$K = I^2 - Q^2$$

This signal is filtered by a 5 Hz low pass filter and drives a Schmitt trigger. When the PLL acquires, a DC level is generated by $I^2 - Q^2$ which in turn triggers the ST.

An AGC signal is obtained by integrating the rectified I channel. Prior to phase lock, an AGC voltage is developed from rectified noise. After lock, an AGC signal is developed from the I channel signal (data is removed by rectification) which

is proportional to the signal level. This AGC signal is applied to the second IF amplifier. The AGC loop holds the signal into the Costas to within 1 dB over the 30 dB dynamic range of the RF signal. The AGC loop has a gain of 30 dB/1 dB and a time constant of approximately 0.5 seconds.

2.3.2.7.4 Data Processing

Command data is extracted from the I channel of the Costas demodulator. Analog data from the synchronous demodulator is processed through a matched filter. Since the data clock is derived from the "all ones" vector of the PN coder during PN synchronization, it is phase coherent and is used to clock an integrate and discharge filter, which implements this matched filter. The data from the synchronous demodulator drives a linear integrator. The integrator is dumped by a very narrow pulse (< 1 μ s) at the end of each bit time by the local data clock.

Just prior to the dump, a zero level comparator, which translates the integrator voltage into standard logic levels, monitors the integrated data signal. The comparator output is clocked into a flip-flop and drives an exclusive OR gate, which differentially decodes the data. At the beginning of the dump pulse, the output of the exclusive OR indicates whether two adjacent received bits are alike or different; a logical "0" is decoded if they are alike and a logical "1" is decoded if they are different.

STDN tones may be extracted from the wideband output (500 kHz) of the third IF by mixing with I channel of the Costas loop modified to function as a PLL. Subsequently, a low pass amplifier filters and level converts these tones for application to the phase modulator in the transmitter section of the transponder.

2.3.3 SIZE, WEIGHT AND POWER

Major functions of the Multiple Access User Transponder have been apportioned into 14 major assemblies. The basis for these groupings is: (1) commonality of component type (i.e., RF, analog or digital), (2) construction techniques (i.e., shielded assemblies for RF functions, isolation of high impedance analog circuits and multilayer PC boards with ground and voltages planes for digital circuits), (3) minimum interassembly wiring, and (4) circuit area requirements.

Anticipated power, weight and size requirements for the major assemblies of the M/A transponder are presented in Table 2-12. All assemblies have been categorized as conventional narrowband assemblies or PN assemblies for purposes of

Table 2-12. M/A Transponder Power, Weight and Size

Modules	Power (watts)	Weight (oz.)	Size (in. ³)
<u>Narrowband Transponder</u>			
RF Down Converter	1	16	24
IF Chain	1.5	12	24
Synthesizer No. 1	2.0	10	24
Synthesizer No. 2	1.5	10	24
Demodulator	2	10	24
Sync Monitor	.5	6	12
Controller	1.5	6	12
Transmitter (100 mW)	2	24	36
Post Regulator	3	24	36
Chassis	<u>—</u>	<u>72</u>	<u>72</u>
Subtotal	15	190	288
<u>Pseudonoise Assemblies</u>			
IPM	2	10	24
PN Coder	1.5	6	12
Local Reference	1.5	6	12
Modulator	<u>1</u>	<u>12</u>	<u>24</u>
Subtotal	6	34	72
TOTAL	21	224	360

comparison with existing transponders. In providing these estimates, 1977 technology was assumed and low power logic, standard LSI circuits and second source components were used to the maximum extent.

In summary, the M/A Transponder will require approximately 21 watts of power (assuming a 100 mW transmitter), weigh on the order of 14 lbs., and occupy 360 cubic inches in a 5" x 6" x 12" configuration.

2.3.3.1 Size

The length and width dimensions of each assembly are 4.5" x 6" with a useful circuit area of 24 square inches. The height dimension varies from 0.5" for logic boards to 1" for analog and RF assemblies to 1.5" for transmitter and power supply assemblies.

The physical configuration of the transponder is envisioned as a tray of fixed-mount assemblies supported by a pair of rigid walls. Estimated dimensions for the transponder are 5" x 6" x 12" with 288 in.³ of the 360 in.³ apportioned to the narrowband functions and 72 in.³ to the PN functions.

2.3.3.2 Weight

The estimated weight for the various assemblies is itemized in Table 2-12. In general, logic assemblies are lighter than analog assemblies and much lighter than "canned" RF assemblies. The heaviest item in the transponder is the chassis at 4.5 lbs. The second heaviest items are the power supply and transmitter modules at 1.5 lbs. each. In summary, the transponder weight is estimated at 14 lbs. with 20% of this total appropriated for PN functions.

2.3.3.3 Power

Power estimates for the receiver, transmitter, and PN functions are 14, 2, and 7 watts, respectively. The largest variation in these values for potential users lies in the transmitter, since the EIRP requirements vary over a range of 30 dB. For purposes of an estimate, a 100 mW watt transmitter requirement was assumed.

Variation in power supply requirements from satellite to satellite also poses somewhat of a problem in estimating power requirements for the transponder. For this estimate, power supply regulation was assumed for all receiver and PN functions with an average operating efficiency of 80%.

Low power Schottky logic was assumed for digital circuits, since the highest clock rate is 12 MHz (rate multiplier). Use of a TCVCO eliminates the need for an ovenized oscillator, thereby reducing power.

2.3.3.4 Transponder Comparisons

Table 2-13 compares the critical parameters of three satellite transponders: 1) the Apollo Type Transponder, 2) TDRSS Transponder, and 3) Motorola "M" series. The TDRSS transponder lies between the other two transponders with respect to power, weight and size. Size/Power and Size/Weight ratios for all three models are close. Keep in mind that the TDRSS transponder contains the additional functions for a pseudonoise mode of operation and has a tracking threshold of -145 dBm requiring additional IF gain.

Table 2-13. Transponder Comparisons

Transponder	Power	Weight	Size	Size/ Power	Size/ Weight	Notes
Apollo Type Transponder	25 watts	24 lbs.	624 in. ³	25	26	Includes Redundancy PA = 100 mW
TDRSS Transponder						Includes PN Functions PA = 100 mW -145 dBm threshold
- NB Functions	15 watts	11 lbs.	270 in. ³			
- PN Functions	<u>8</u>	<u>3</u>	<u>90 in.³</u>			
Total	23 watts	14 lbs.	360 in. ³	16	25	
Motorola "M" Series Transponder	6.5 watts	6 lbs.	120 in. ³	18	20	PA = 10 mW

2.3.4 MULTIPLE ACCESS SERVICE PERFORMANCE SPECIFICATION

FORWARD LINK

FH Acquisition:

G_u	-6 dB
P_d	.97 (five passes)
Acq. Time	12 seconds

PN Acquisition:

G_u	-6 dBW
Acq. Time	8 seconds (average)

Data Demodulation:

E_b/N_o	12.5 dB
BER	10^{-5}

RETURN LINK

PN Acquisition:

EIRP	7 dBW
Acq. Time	15 seconds (average)

Data Demodulation:

BER	10^{-5} at $E_b/N_o = 12.5$ dB
BER (with encoding)	10^{-5} at $E_b/N_o = 7.5$ dB

RETURN ONLY LINK

PN Acquisition:

Data Rate	≥ 16 kbs
Acq. Time	≤ 10 seconds, average
Data Rate	16-4 kbs
Acq. Time	2.5-10 seconds, average
Data Rate	4-1 kbs
Acq. Time	2.5-10 seconds, average

TWO-WAY RANGE

Return Link EIRP	7 dBW
Forward Link G_u	-6 dB
Data Rate	100 bps (forward) 300 bps (return)
Error (1 σ)	.8 meters

TWO-WAY RANGE RATE

Return Link EIRP	7 dBW
Forward Link G_u	-6 dB
Error (1 σ)	.2 cm/sec (sec ave) .02 cm/sec (10 sec ave)

2.4 OPERATIONAL PROCEDURES

2.4.1 FORWARD LINK

The acquisition sequence on a forward link of the multiple access service is as follows:

1. Ground station directs a transmit beam from TDRS to user.
2. Inserts user address which selects preamble hopping code and the subsequent PN code to be transmitted.
3. Inserts a priori range rate information (doppler estimate plus estimate of satellite VCO offset due to long term drift).
4. Transmits FH preamble for 12 seconds, synchronously switches to PN mode and then informs ground user that user satellite will, on the average, be ready to receive command data within 8 seconds. (Ground user has option to begin sending repetitive command data immediately. Also, if return link has been previously established, indication of PN acquisition at user could be relayed back on the return link.)
5. Meanwhile, satellite receiver, upon acquiring FH signal, synchronously switches to PN mode and begins a PN search, acquires and subsequently establishes a PN track mode.
6. Ground station transmits command data.

2.4.2 RETURN LINK

The acquisition sequence on a return link of a multiple access service is as follows:

1. User receives a command message: (a) If command message does not request a return link response, no return mode occurs. (A return link may already be established.) (b) If the command message requests a coherent transpond mode, all transmit frequencies are synthesized from the receiver VCO. (c) If the command message requests a noncoherent return mode, all transmit frequencies are synthesized from a fixed frequency reference oscillator.
2. The return link transmit PN coder is synchronized to the receiver PN code and, if applicable, the return link antenna is pointed and a PN transmission begins.

3. AGIPA is supplied with pointing information for initial acquisition. Meanwhile, the ground receiver gets a range and range rate estimate and begins a PN search (range-rate values for a noncoherent return link are approximately one-half coherent return link estimates).

4. When PN acquisition is accomplished, a two way range and range rate measurement is made in a coherent transpond mode.

5. When the R&R measurement is complete or in a noncoherent return mode, a command word is sent to the user to begin a telemetry data dump.

6. Upon loss of lock, the receiver performs a 50 second auto search about the point of loss of lock. If reacquisition fails, it reverts back to a standby mode.

2.4.3 RETURN ONLY LINK

1. Upon satellite request, a shortened PN sequence is transmitted for a sufficient time to acquire the return link receiver.

2. Ground receiver is instructed to use short PN sequence and gets a range rate estimate for arriving signal.

3. Receiver does a continuous search until it acquires the PN signal.

4. Receiver acquires data bit sync and demodulates data.

5. User performs a telemetry data dump via the return link.

6. Upon loss of lock, the receiver reverts back to a PN search mode.

2.5

MULTIPLE ACCESS USER TRANSPONDER EQUIPMENT SPECIFICATIONS

This section presents a summary of the major M/A user transponder equipment specifications. Major categories include:

- Modes of Operation
- Receiver Precorrelation Channel
- Frequency Hop Preamble
- PN Demodulation
- Carrier Acquisition and Tracking
- Command Data Demodulation
- Transmit Channel

2.5.1 MODES OF OPERATION

- Coherent Transpond
- Forward Link Only
- Return Link Only
- Clear Mode (Optional)
- Acquisition Retrace (Optional)

2.5.2 RECEIVER PRECORRELATION CHANNEL

Center Frequency	2106.40625 MHz
Noise Figure	2.5 dB max
Bandwidth (3 dB)	5 MHz min (at 2nd IF)
VSWR	1.5:1 over to ± 2.25 MHz
Phase Response	Linear to within $\pm 5^\circ$ over to ± 1.75 MHz
Amplitude Response	Flat to within 1/2 dB over to ± 1.74 MHz
Dynamic Signal Range	40 dB
Maximum Signal and Noise	-130 dBW
Minimum Signal	-180 dBW

2.5.3 FREQUENCY HOP PREAMBLE

FH Code:

Type	Pseudorandom, coherent frequency hop
Code Generation	Primitive root
Code Period	256

Hop Rate	3.006 kHz
Spacing	12.023 kHz
Repetition Interval	85.172 mS

Local Reference:

Bandwidth (3 dB)	5 MHz
Phase Response	Linear to within $\pm 5^\circ$ over to ± 1.75 MHz
Amplitude Response	Flat to within 1/2 dB over to ± 1.75 MHz
Implementation Technique	Discrete 45° phase stepping
Spurious Responses	20 dB down outside to ± 3 MHz

Acquisition:

Signal Bandwidth	3.078 MHz
Signal Detector	Sequential Detector
Detection Bandwidth	3 kHz
Signal Integration Interval	6 mS
Search Rate	120 hops/sec average
Frequency Uncertainty	700 Hz nominal, 3000 Hz maximum

FH Losses:

Discrete Phase Loss	0.7 dB
Doppler Offset	0.8 dB (700 Hz)
Other	0.5 dB

2.5.4 PN DEMODULATION

PN Code:

Type	SQPN - Staggered Quadriphase Pseudonoise
Code Family	Maximal code pairs augmented by one chip
Code Period	2^{18}
PN Chip Rate	3.078 MHz
Repetition Interval	85.172 mS

Local Reference:

Bandwidth (3 dB)	5 MHz
Phase Response	Linear to within $\pm 5^\circ$ over to ± 1.75 MHz
Amplitude Response	Flat two within 1/2 dB over to ± 1.75 MHz
Carrier Suppression	50 dB or greater

Code Loop:

Dither	$\tau_d = .5$ chip
Track Resolution	1/96 chip
Order	1st
Bandwidth (B_L)	0.1 Hz
Dynamics Aiding	From carrier loop

Acquisition:

Search Steps	1/2 chip
Search Rate	120 chips/sec (average)
Signal Detector	Sequential Detector
Detector Bandwidth	3 kHz
Frequency Uncertainty	700 Hz nominal, 3000 Hz maximum
Time Uncertainty	1000 PN chips

PN Losses:

Bandwidth	Negligible
Channel Distortion	.7 dB
Imperfect Tracking	.3 dB

2.5.5 CARRIER ACQUISITION AND TRACKING

Type of Loop	Costas/PLL
Loop Order	2nd
Loop Bandwidth (B_L)	32 Hz
Damping Factor	.707
Frequency Offset	
Acquisition	± 3 kHz
Tracking	± 60 kHz
Incidental FM	6° RMS in 10 Hz with good S/N, maximum

Carrier Tracking Losses:

Incidental FM	.2 dB
Non-linearities	.5 dB at threshold
AGC Noise	.3 dB at threshold

2.5.6 COMMAND DATA DEMODULATION

Demodulator	Costas Loop
Fixed Data Rate	94, 188, 376 or 752 bps (user selected)
Data Processing	Integrate and dump

Data Decoding	Differential
Data Clock	Derived from PN code
Data Interface	TTL

Implementation Losses:

Carrier Reference at threshold	1 dB at 100 bps
Non-linearity	.3 dB
Bandlimiting	.2 dB

2.5.7 TRANSMIT CHANNEL

Transmitter:

Type	Solid State Class C
Center Frequency	2287.5 MHz
Bandwidth (3 dB)	30 MHz nominal
Amplitude Response	Flat to within 1/2 dB over 70% of 3 dB bandwidth
Phase Response	Linear to within $\pm 5^\circ$ over 70% of 3 dB bandwidth

Modulator:

Modulation	SQPN
Code Family	Maximal code pairs augmented by one chip
PN Chip Rate	3.078 MHz
Code Length	
Transpond Mode	2^{18}
Return Only Mode	2^{11} for bit rate of 1-4 kbs 2^{13} for bit rate of 4-16 kbs 2^{15} for bit rates ≥ 16 kbs
Bandwidth	5 MHz
Filter Type	Butterworth, 4-pole
Carrier Suppression	30 dB or greater
Spurious Responses	20 dB down outside of ± 3 MHz

Telemetry Data:

Modulation	Biphase data modulo-two added to both codes of the maximal pair. Alternate of two data streams modulo-two added to individual codes (see Appendix XVI).
Rate	1 kbs-50 kbs
Clock	Asynchronous, user supplied
External Interface	TTL compatible
Encoding	
Type	Convolutional
Constraint Length	7
Rate	1/2
Encoding	
Type	Differential

SECTION 3

S-BAND SINGLE ACCESS SERVICE

The S-band single access system has much in common with the multiple access system, but it represents an easier design problem because of the greater EIRP transmitted by TDRS. Also, there is a single signal on the return link. The multiple access system design has been adapted by modifying parameters to fit the S-band single access system.

The most significant difference is that the return link can convey telemetry data up to 5 Mbps, which is non spread. However, at lower data rates, spread spectrum is necessary for purposes of ranging and multipath discrimination (if the user transmits on the return link from an omni antenna). A method of spread spectrum ranging when a high data rate is transmitted must be available also.

Since the digital rates are reasonable, the design for the return link assumes serial data on a single carrier. Because the TDRS transponding channel for the S-band single access is not hard limiting, the alternative of transmitting data on parallel carriers could be employed instead. This is discussed later in Section 4.1.1.2 as a possibility for Ku-band single access, and the problem of computing requisite backoff from hard limiting is similar for S-band.

3.1 MODULATION TRADEOFFS

The design of the S band single access system is based on requirements very similar to the multiple access system, except that multiple access on the return link is not a consideration. Thus, the design for single access is basically a deviation from the multiple access design approach described in Section 2.

The S-band single access system requires the user to operate in a coherent turnaround transponding mode. Because of the high EIRP from the TDRS, a wider bandwidth spread spectrum is required to meet the flux density limitation compared to the multiple access system. The frequency plan calls for 10 MHz bandwidth on the return link. SQPN with a chip rate up to 6.7 Mbps would

then have a negligible loss due to the finite bandwidth of the channel. A chip rate of approximately 6 Mbps is assumed to satisfy flux density limitations; which calls for spreading over 13 MHz for EIRP = 44.4 dBw from the TDRS.

Not including 2.5 dB for demodulation loss and PN loss, the NASA link budget yields a received S/N_o in the user of 41.7 dB-Hz for a user antenna gain $G_u = -6$ dB on the forward link. Following the ground rule that the code period should exceed the maximum multipath delay which could be 33 milliseconds for a maximum user altitude of 5,000 Km, a PN code must have a period of at least 200,000 bits to insure multipath discrimination. Based on $E/N_o = 13$ dB (see Appendix III), the search rate would be 700 chips/sec, and the acquisition time on the forward link would be 300 seconds. This is unacceptable.

3.1.1 DESIGN OF FORWARD LINK SIGNAL

The frequency hop preamble approach introduced to aid acquisition in the multiple access system is a good solution here also. The parameters of the S-band single access link suggest:

Hopping rate = 6 kHz

Frequency spacing = 12 kHz

Code period = 512 hops = 85.3 milliseconds

Bandwidth = 6.144 MHz (equals chip rate* of SQPN)

The code period exceeds twice the maximum multipath delay, and the range ambiguity is 12,800 Km.

After the preamble has been transmitted for a long enough interval to insure acquisition, the forward link signal is switched to SQPN with a code period of 85.3 milliseconds and a PN chip rate of 6.144 MHz. The code period is $2^{19} = 524288$ chips. The acquisition procedure on the forward link is as follows:

1. Point TDRS antenna towards user.

*The precise chip rate is selected later, and will be dependent on a detailed design study of frequency synthesis and intermodulation considerations. The nominal value is 6 Mbps.

2. Insert user address, selecting the preamble hopping code and the subsequent PN code to be transmitted.
3. Insert a priori range rate information (see discussion subsequently) into the transmitter.
4. Wait a sufficient time for acquisition of the preamble to be completed by the user receiver (at which point the user switches to the long period PN code and again searches for acquisition).
5. Switch to long period PN code in the ground transmitter and wait a sufficient time for user receiver acquisition again.
6. Define data bit timing and send a command to start transmitting on the return link. This return transmission is the final confirmation of user receiver acquisition.

3.1.2 ACQUISITION TIME ON FORWARD LINK

We now estimate the acquisition time on the forward link. A loss* of approximately 3 dB will be attributed to the digital implementation of frequency hopping as 90° phase steps. The received S/N_o is 41.7 dB-Hz for $G_u = -6$ dB. Thus, with the FH preamble, implementation reduces the effective S/N_o to about 39 dB-Hz. If the receiver covers the full Doppler of ± 55 kHz with coherent processing by a Doppler processor extended over one frequency hop interval of 167 microseconds, Figure 10 of Appendix III shows that the search rate for probability of detection = .8 is approximately 125 chips/sec based on $E/N_o = 18$ dB. Since the preamble has 512 chips, this acquisition step takes 4 seconds. Note that $E_b/N_o = E/N_o - 16.7$ dB = 1.3 dB, which is realized with 6 khps hopping rate and $S/N_o = 39$ dB-Hz.

As noted for the multiple access system also, observe that a preamble approach based on a short PN code of 6 Mbps chip rate would be unsatisfactory.

*In the multiple access system, the lower chip rate enables implementation of an 8-step IPM which has a very small loss due to the smaller phase steps. Here, we will use the SQPN modulator as equivalent to a 4-step IPM. The rate multiplier described in Section 2.1.1.3 to generate FH by discrete 90° phase steps is required to operate at a clock of 12 Mbps, for 6 MHz spread.

since the code Doppler could be as high as 156 chips/sec, which exceeds the attainable search rate.

If a priori range rate information is inserted into the ground transmitter, we improve the acquisition performance and simplify the user receiver by eliminating the Doppler processor. The Doppler uncertainty is ± 700 Hz for a range rate uncertainty of ± 100 m/sec. Now, the search rate can be 400 chips/sec, based on $E/N_0 = 13$ dB (see Figure 5 of Appendix III), and this acquisition step takes 1.3 seconds. (Also, a short PN code preamble could now be used as an alternative to FH, since the code Doppler uncertainty is 2 chips/sec.) Note that a correction to the two-way range rate measurement will be necessary as a consequence of the offset transmit frequency.

When acquisition is detected with the FH preamble, the time uncertainty is one FH chip, which is 167 microseconds, or 1000 PN chips. Since $S/N_0 = 41.7$ dB-Hz for PN acquisition, the search rate is 740 chips/sec, based on $E/N_0 = 13$ dB, and this acquisition step takes 1.3 seconds. The total acquisition time is 5.3 seconds without range rate insertion into the ground transmitter and 2.6 seconds with range rate insertion.

3.1.3 DESIGN OF RETURN LINK SIGNAL

The return link of the S-band single access system handles data rates from about 1 kbps up to about 5 Mbps. Spread spectrum is to be used for enabling a two-way range measurement at low data rates; however, accurate range information in principle, can be obtained with a conventional PSK demodulator from the bit synchronizer tracking the data clock at high data rates. In practice, there remains the problem of implementing a frame synchronizer to meet the range ambiguity goal if range is to be obtained via the data clock.

At low data rates on the return link, we recommend SQPN at 6.144 Mbps chip rate with a code period 2^{19} chips, identical with the forward link and giving a range ambiguity of 12,800 Km. If the minimum user EIRP is 7 dBw (10 watts with $G_u = -3$ dB), the received S/N_0 (not including 1.5 dB demodulation loss) is $S/N_0 = 44.2$ dB-Hz. The a priori range uncertainty is ± 50 Km, and after

coherent turnaround the range uncertainty is 4,000 PN chips and the Doppler uncertainty is ± 1400 Hz. Based on $E/N_0 = 13$ dB, the search rate is 1300 chips/sec, and this acquisition requires 3 seconds.

At low data rates, the data can be supplied asynchronously to the user transmitter, which imposes need for a bit synchronizer in the spread spectrum receiver. This has no impact on the range measurement, which is taken from the PN delay lock tracking loop.

If PN is not used on the return link at high data rates, the data must be supplied synchronously to the user transmitter if a two-way range measurement is to be performed entirely on the ground. To receive and demodulate the data, the ground receiver uses a conventional PSK demodulator. The problem still remains of establishing frame synchronization over a span exceeding the range ambiguity goal. A solution to this problem is to acquire PN synchronization prior to data transmission and then track the data clock, which is coherent to the PN clock, thereafter. At high data rates, the bit synchronizer will have a negligible probability of slipping, so that the range ambiguity resolution initially done by PN stays valid during subsequent data transmission.

The question is raised as to the demarkation between "low data rate" and "high data rate". The answer is dependent on detailed hardware implementation studies, but the upper limit of "low data rate" is believed to be about 10 percent of the PN chip rate. The implication is that the ground receiver is implemented as a spread spectrum demodulator when the data rate is low, and as a PSK demodulator for a high data rate.

An alternate concept is to have a separate PN signal added to the high data rate PSK signal for the purpose of two-way ranging. The advantage is to allow two-way ranging even when data is supplied asynchronously on the return link.

Because of the coding gain realized thereby, rate -1/2 forward error correction coding is to be used at all data rates. At 6 Mbps, this raises the problem that the binary transmission rate is doubled to 12 Mbps, which is excessive for the 10 MHz channel bandwidth on the return link. An answer to this problem is

to require staggered quadriphase (SQPSK) data modulation at all coded data rates exceeding 3 Mbps. Note that the SQPN modulation at a chip rate of 6 Mbps is identical in structure with SQPSK at 12 Mbps; hence, the SQPN modulator in the user transmitter can handle all data rates, either biphase or quadriphase, without modification.

3.1.4 FUNCTIONAL DESCRIPTION OF S-BAND SINGLE ACCESS MODULATION EQUIPMENT

The user transponder equipment for PN operation is almost identical with that described in Section 2.1.6 for the multiple access system. The FH code period is now 2^9 and the PN code period is 2^{19} . Also, the chip rate has been doubled to 6 Mbps for SQPN and 6 Kbps for the FH preamble. Hence, the functional block diagrams are not repeated here.

3.1.5 RANGE AND RANGE RATE MEASUREMENT ACCURACY

With higher S/N_0 values and a higher PN chip rate, the range and range rate measurement accuracies will be theoretically better than computed for the multiple access system. The range error variance is

$$\sigma_{\text{chips}}^2 = \frac{N_0 B_L^{(\text{code})}}{S} \left[1 + \frac{2N_0 B_{\text{IF}}}{S} \right] \quad (3-1)$$

for dither tracking of the delay lock loop. On the forward link, minimum $S/N_0 = 41.7$ dB-Hz. For a chip rate of 6 Mbps, a data rate of 1 kbps, $B_{\text{IF}} = 1$ kHz, and with $B_L^{(\text{code})} = 0.1$ Hz (presumes aiding from the carrier tracking loop),

$$\sigma_{\text{range}} \left. \right|_{\substack{\text{forward} \\ \text{link}}} = .0028 \text{ chip} = 0.14 \text{ meter}$$

On the return link for a chip rate of 6 Mbps, a minimum S/N_0 of 44.2 dB-Hz, a data rate of 5 kbps with coding, $B_{\text{IF}} = 10$ kHz, and $B_L^{(\text{code})} = 0.1$ Hz, we obtain

$$\sigma_{\text{range}} \left. \right|_{\substack{\text{return} \\ \text{link}}} = .0026 \text{ chip} = 0.13 \text{ meter}$$

Thus,

$$\sigma_{\text{range}} \left. \right|_{\substack{\text{two-way}}} = 0.1 \text{ meter}$$

This theoretical computation is probably better than can be achieved in practice.

The phase error variance for Costas loop tracking is

$$\sigma_{\text{rad}}^2 = \frac{N_o B_L^{(\text{carrier})}}{S} [1 + N_o B_{\text{IF}}/S] \quad (3-2)$$

On the uplink with $B_L^{(\text{carrier})} = 30 \text{ Hz}$ at minimum S/N_o ,

$$\sigma_{\text{phase}} \begin{bmatrix} \text{forward} \\ \text{link} \end{bmatrix} = .007 \text{ cycle}$$

On the return link with $B_L^{(\text{carrier})} = 300 \text{ Hz}$ at minimum S/N_o

$$\sigma_{\text{phase}} \begin{bmatrix} \text{return} \\ \text{link} \end{bmatrix} = .019 \text{ cycle}$$

Presuming independent errors at the ends of the averaging interval, we obtain

$$\begin{aligned} \sigma_{\text{range rate}} \begin{bmatrix} \text{two-way} \end{bmatrix} &= 0.14 \text{ cm/sec; 1 second averaging} \\ &= 0.014 \text{ cm/sec; 10 second averaging} \end{aligned}$$

This accuracy probably does not improve in practice as the S/N_o increases over the minimums.

3.1.6 SUMMARY

The modulation design for the S-band single access system is very similar to the multiple access system, and meets the requirements. A summary is given in Table 3-1.

3.1.7 TWO-WAY RANGING WITH CLEAR ASYNCHRONOUS DATA

The user satellite preferably transmits data asynchronously with respect to the receive PN clock. For low data rates with spread spectrum, this causes no difficulty in two-way ranging because the transmit PN can be forced to be synchronous with the receive PN in the user transponder, and ranging is performed via the PN. At high data rates (say greater than ten percent of the PN chip rate), data should not be asynchronous to the PN clock, because there would be excessive performance degradation due to jitter of the data bit edges when they are reclocked to a PN transition.

Table 3-1. Summary of S-Band Single Access System

Forward Link - EIRP = 44.4 dBw

PN chip rate \cong 6 Mbps (exact value dependent on hardware tradeoffs)

SQPN modulation

Code period = 2^{19} chips

Frequency hop preamble (implemented via digital phase shifting) = 2^9 chips

Preamble hopping rate = 6 Kbps

Data rate = 6000/K bps (synchronous biphase differential data) down to 100 bps

Acquisition time ($G_u = -6$ dB); probability \cong 0.8

with Doppler estimate inserted into transmitter \cong 3 seconds

with Doppler processor in user receiver \cong 5 seconds

Return Link

PN chip rate \cong 6 Mbps

SQPN modulation

Code period = 2^{19} chips

Two-way range ambiguity = 12,800 Km

Data rate, asynchronous, 1000 bps to 100 kbps; synchronous, 100 kbps to 6 Mbps (if two-way ranging is done)

Error correction coding, rate -1/2, constraint length 7, nonsystematic, transparent, convolutional

Max data rate (6 Mbps) requires quadriphase data if rate -1/2 coded

Acquisition time (user EIRP = 7 dBw); probability \cong 0.8 with range and Doppler estimate inserted into ground receiver \cong 3 seconds

Two-way range error (1σ) = 0.1 m

Two-way range rate error (1σ) = 0.14 cm/sec; 1 second averaging = 0.014 cm/sec; 10 second averaging

We now discuss one plausible scheme for accommodating asynchronous user telemetry data. This scheme for two-way ranging calls for slaving the clock on the return link to the user's data clock, which is allowed to be asynchronous to the PN clock tracking the forward link command signal. Presuming IPM (digital) code tracking in the user receiver, as described in Section 2.1.6.6, the user transponder continuously has a count of the variable displacement between the received clock and the transmit clock. This displacement is sent to the ground via the order wire, requiring about 25 bits per transmission. Thus, even at a transmission rate of ten measurements per second, the order wire data rate is only 250 bps, which is negligible compared with a telemetry data rate exceeding 100 kbps. The ground station measures apparent two-way range in the usual manner (e.g., counting the interval from transmission to reception of the "all-ones"). The user transponder measures the interval from reception to transmission of the "all-ones", and sends this measurement down on the order wire to enable the ground station to correct the apparent range.

3.1.7.1 Error Due to User Clock Drift

The question is raised as to the error introduced by clock error in the user transponder. The simplest conceptual implementation of the measurement causes the user transponder to count the time displacement from receive to transmit with its internal clock. The maximum displacement for the S-band single access design is one PN code period, or 85 milliseconds. Thus, as an illustration, a clock offset of one part in 10^6 in the user transponder would introduce a maximum measurement error of 85 nanoseconds, or 13 meters in one-way range.

Since the user transponder for the S-band single access system is coherently turning around Doppler, the possibility exists of correcting the displacement count made over the measurement interval into units at the receive frequency, which is not affected by user clock drift (since it is locked to the ground transmitter with a known Doppler offset). All that has to be done is to add the change of the receive PN code phase which accumulates during the measurement interval (implemented by counting IPM pulses during the interval). On the ground, the count must then be corrected for the known Doppler offset at that measurement time. (Note, maximum change in Doppler over 85 milliseconds is 0.85 m/sec , or 3×10^{-9} ; hence, the instant at which Doppler is measured is not critical.) Even simpler, the ground can calibrate the user clock by correcting the receive frequency for the known Doppler offset.

3.1.7.2 Order Wire Implementations

One possible order wire implementation based on TDM at the PN chip rate is described in Section 2.1.6. At high return data rates for the single access system, however, this implementation would not be applicable. An alternate and simple order wire implementation impresses a low-index phase modulation on the carrier. This phase modulation is a subcarrier which is biphase modulated with the order wire data. The subcarrier can be extracted from the error signal derived as part of the standard process of reconstituting a reference phase for coherent PSK demodulation of the telemetry data (e.g., Costas loop tracking). We presume the order wire data to be synchronous with the return PN clock.

3.1.7.3 Elimination of Range Ambiguity Due to Bit Slips With Clear Data

If the return link conveys clear data, there is no sure way of detecting a slip in the bit synchronizer of the ground receiver, after which occurrence erroneous two-way range measurements are given. As described above, by initially transmitting a PN code on the return link, an unambiguous range measurement can be obtained prior to data transmission, and the range ambiguity resolution remains valid during subsequent clear data transmission unless a bit slip occurs.

On the S-band single access system, error correction coding is presumed at all data rates. If a PN code is always used on the return link (the PN clock is synchronized to the user's data clock), a bit slip can be detected by examination of the metrics in the Viterbi decoder*. A bit slip causes mismatch of the PN, and this creates an error rate of 0.5. The metrics in the Viterbi decoder will indicate when such a condition of operation exists.

3.1.7.4 Conclusions

Two-way range measurement is conceptually possible even with high rate asynchronous data on the return link. This may be done by measuring the instantaneous displacement between receive code phase and transmit code phase in the user transponder, and conveying this measurement to the ground via an "order wire". The ground station then corrects the apparent two-way range (displacement of transmit and receive code phase at the ground) by this displacement.

*The metrics are examined also to find node synchronization in a Viterbi decoder.

Note that coherent two-way range rate measurements are made by the carrier tracking process using a coherent Doppler turnaround which scales by the ratio of forward and return link frequencies (240/221 for S-band), and this is independent of whether return data is synchronous or asynchronous.

3.1.8 MINIMUM POWER FOR TWO-WAY RANGING

3.1.8.1 Introduction

In the current system operational concept, it is planned to command Ku band users via an S-band transponder, and make two-way range and range rate measurements on the S-band single access system. The user would not have a Ku band transponder, but only a Ku band transmitter to transmit data on the Ku band return link. The user would need a Ku band receive capability only for autotrack to point the antenna towards the TDRS.

In this mode, the user would want to minimize his S-band EIRP, since no data needs to be transmitted on the S-band return link. In the description of the S-band single access system in Section 3.1.3, an EIRP of 7 dBW was assumed on the return link. Now, we wish to assess the consequences of reducing this EIRP.

3.1.8.2 Lower Bound on User EIRP at S-Band For Acquisition

The lower bound on required user EIRP at S-band is set either by the measurement accuracy requirements or by acquisition time on the return link. To ascertain which dominates, let us postulate a reduced EIRP, compared with Section 3.1.3. Specifically, assume -3 dBW, corresponding to 2 watts and a user antenna gain of -6 dB (for an omni). This is 10 dB below the assumption in Section 3.1.3, and $S/N_o = 34.2$ dB-Hz for this EIRP value.

The time uncertainty on the return link due to a one-way range estimation error of ± 50 km is 4000 PN chips at a chip rate of 6 Mbps. (The one-way uncertainty is multiplied by 2 due to coherent transponding.) Similarly, the Doppler uncertainty due to a range rate estimation error of 100 m/sec is ± 1400 Hz. Applying Figure 5 of Appendix III, we see that with a single filter of bandwidth equal to about 3 kHz, (i.e., $E_b/N_o = -0.6$ dB at the available S/N), an acquisition reliability of about 0.9 is achieved with $E/N_o = 13.2$ dB in the time to search one PN chip. For $S/N_o = 34.2$ dB-Hz, this means a search rate of 125 chips/sec, or a total acquisition time (to search 4000 chips) of 32 seconds. Furthermore, with 1400 Hz frequency offset, there is a degradation of about 3 dB in the response of the 3 kHz filter. Thus, a

search over the frequency uncertainty will also be necessary (either in parallel with a Doppler processor covering a few kHz or by serial search in frequency as well as time).

Since the goal is to achieve an acquisition time under 30 seconds, the conclusion is reached that the minimum EIRP for acquisition should be 0 dBW. Then, the filter can be widened to 6 KHz, comfortably enclosing the Doppler uncertainty, and the search rate is doubled to 250 chips/sec. The acquisition time is then computed to be 16 seconds.

3.1.8.3 Lower Bound on User EIRP For Ranging

Instead of the ground receiver parameters assumed in Section 3.1.5 we can utilize a carrier phase lock tracking loop with $B_L^{(\text{carrier})} = 5 \text{ Hz}$, limited by dynamics and phase noise (see Section 3.1.1.4). Assume no data is to be transmitted on the S-band return link. The phase error variance for phase lock loop tracking is

$$\sigma_{\text{rad}}^2 = \frac{N_0 B_L^{(\text{carrier})}}{S} \quad (3-3)$$

To meet an rms measurement accuracy requirement of 0.6 cm/sec in one-way range rate for 1 second averaging, or 0.05 cm/sec for 10 second averaging, with the error introduced almost entirely on the return link at 2.2 GHz, we need $\sigma_{\text{rad}} = 0.3 \text{ rad}$. Then, (3-3) yields

$$\left. \frac{S}{N_0} \right|_{\substack{\text{minimum for} \\ \text{range rate}}} = 16.8 \text{ dB-Hz}; \quad B_L^{(\text{carrier})} = 5 \text{ Hz}$$

which corresponds to a user EIRP = -20.4 dBW.

To meet an rms measurement accuracy requirement of 2 m in one-way range, with the error introduced almost entirely on the return link with a chip rate of 6 Mbps, we need $\sigma_{\text{chips}} = .08 \text{ chip}$. The range error variance (for coherent dither tracking without data modulation) is

$$\sigma_{\text{chips}}^2 = \frac{N_0 B_L^{(\text{code})}}{S} \quad (3-4)$$

Again taking $B_L^{(\text{code})} = 0.1 \text{ Hz}$ as a practical design (presuming aiding from the carrier tracking loop), (3-4) yields

$$S/N_o \left[\begin{array}{l} \text{minimum} \\ \text{for range} \end{array} \right] = 11.9 \text{ dB-Hz}; B_L^{(\text{code})} = 0.1 \text{ Hz}$$

which corresponds to EIRP = -25.3 dBW.

It is found that the S/N_o threshold for tracking is dominated by the range rate measurement accuracy requirement.

3.1.8.4 Conclusions

If the S-band single access return link is to be used only for two-way range and range rate measurements through the S-band coherent transponder, with data returned at Ku band, it is found that the minimum user EIRP ≥ 0 dBW to enable an acceptable acquisition on the return link (~ 16 seconds).

After acquisition, the user transponder could be commanded to reduce EIRP to as low as -20 dBW, which is the minimum needed to maintain tracking and meet the range and range rate measurement accuracies required for two-way measurements.

3.1.9 TWO-WAY RANGING WITH SEPARATE NON-SPREAD DATA

In addition to data transmission, the S-band single access system is intended to provide two-way coherent range and range rate information, using spread spectrum on both the forward (necessary to meet flux density limits) and, if necessary, on the return link. The return link is to be capable of transmitting data up to about 5 Mbps, and it is operationally preferred that the user supply the data asynchronously to the PN clock. One approach for accommodating asynchronous high rate data is described in Section 3.1.7; however, this has the disadvantage of complicating the user transponder*.

An alternate solution to this problem is now described**. It is based on separate spread spectrum and data signals (data bits and PN chips are not synchronous) transmitted by the user in a common band. This is in contrast to the more familiar approach used with low data rates of modulating the data on the PN code so that there is a single signal.

*The forward link PN is asynchronous to the return link PN and the displacement between the two codes is returned as "order wire" data.

**This solution was suggested by L. Deerkoski of NASA Goddard. It has a similarity to the Unified S-band System.

3.1.9.1 Mutual Interference Between Data and PN Ranging

The application of the suggested approach is for a return data rate exceeding approximately 300 kbps (based on a maximum allowed asynchronous data rate after rate -1/2 coding equal to roughly ten percent of the PN chip rate when the data is modulated on the PN signal). From the NASA Goddard Definition Phase Study Report, the user EIRP must exceed 23 dBW at 300 kbps data rate (coded).

If there is a PN return signal used only for ranging, Section 3.1.8 shows that a user EIRP of 0 dBW suffices to enable a reasonable acquisition time on the return link (about 16 seconds based on a range error of 50 Km and a range rate error of 100 m/sec), and there is 20 dB margin to the point at which the specified rms range and range rate measurement accuracy is met (2 m and .05 cm/sec for 10 second averaging).

The suggested approach, then, provides a PN signal at low EIRP simultaneously with the data signal at a minimum of 23 dBW EIRP (for 300 kbps). These are in an overlapping spectrum and can be combined at IF and hard limited for transmission through a class-C power amplifier.

Let us now examine the mutual interference effect for these two signals, which occupy the same band. Maximum EIRP for the data signal is 35 dBW (at a data rate of about 5 Mbps, coded), for which the S/N at the TDRS is +6.9 dB in 10 MHz bandwidth. The data signal at maximum EIRP thus raises the total noise level seen by the PN ground receiver by at most 7.7 dB. At the minimum data signal EIRP of 23 dBW, the received S/N at the TDRS is -5.1 dB, which raises the noise level by at most 1.2 dB. As a consequence of operation with overlapping spectra, the EIRP of the PN signal should be +1.2 dBW for 23 dBW data signal and +7.7 dBW for 35 dBW data signal. (This is 0 dBW plus the increase in noise level due to the data signal.) It may be concluded that the PN signal will be at least 22 dB below the data signal over the range of data rates, 300 kbps to 5 Mbps.

If the weak PN signal and the strong data signal are hard limited after combining at IF, there is a 3rd order intermodulation product at the same level as the PN*. This intermodulation product, of the form $2f_{\text{data}} - f_{\text{PN}}$, is the only

*Hard limiting suppresses the PN by 6 dB, but this can be compensated by adjusting the relative levels prior to limiting so as to produce the desired ratio after limiting.

significant product, and it has a reversed PN spectrum. Thus, if the PN is quadriphase as has been recommended, no correlation exists between the desired PN and the intermodulation product. The total interference presented to the data signal is at least 19 dB down. Since the TDRS to ground link is designed for $S/N = 14$ dB, according to the NASA Goddard Definition Phase Study Report, the separate PN ranging signal causes negligible degradation to the data.

3.1.9.2 Conclusions

The operational concept of having a PN ranging signal separate from the data signal on the return link turns out to give acceptable system performance in all cases of interest. Applied to the S-band single access link, this scheme would be employed for data rates exceeding 300 kbps* so as to accommodate asynchronous user data without affecting the capability to obtain accurate two-way range and range rate measurements. The ground has separate and independent receivers, one for the PN ranging signal, the other for the PSK data signal.

The data signal and the PN signal can have overlapping spectra without excessive degradation to the data. (The EIRP of the PN signal is increased so as to compensate for the jamming by the data signal, but this EIRP is still much smaller than that of the data signal.) The user transmitter can simply hard limit after combining the two signals at IF.

*For lower data rates, the asynchronous data can be modulated on the PN signal, which has 6 Mbps chip rate.

3.2

AUTOTRACK ANALYSIS

S-band single access service may impose an autotrack requirement on the user. Such a requirement arises if the user has no other means of aiming his S-band antenna to keep the pointing loss below -0.5 dB. Such means would include on-board navigation computation or autotrack for Ku-band service.

The TDRS, on the other hand, will be able to point its single access S-band antenna accurately enough by ground station command. No TDRS autotrack is required for S-band single access service.

This section presents the design and analysis of an autotrack system for an S-band single access user who has no Ku-band communication capability. It is assumed that the user has sufficient *a priori* knowledge to steer his S-band beam within its 3 dB points toward the TDRS. This places the pointing error within the autotrack range, whence the autotrack system must adjust the pointing angle to reduce the pointing loss to less than 0.5 dB.

The S-band transmission from the TDRS is assumed to emanate with an EIRP of 44.4 dBW. It is assumed to be spread over a 13.2 MHz bandwidth to meet the flux density requirements.

The range of user antenna diameters to be considered is one foot to 5.8 feet. As will be seen, an user antenna diameter of 5.8 feet (corresponding to an half-power beamwidth of 5.25°) allows reception of rate one-third coded data that occupies a bandwidth of 13.2 MHz with no further spreading.

The receiver structure uses the Σ -channel for autotrack and for data demodulation. For hardware economy, the azimuth and elevation Δ -beams are quadrature multiplexed to share a common Δ -channel receiver which has a high noise temperature compared to that in the Σ -channel.

The S-band system may be subjected to strong pulsed RFI which must be protected against to maintain proper autotrack operation. That problem and its solution is examined first, and then autotrack error components will be quantified to show that the desired pointing loss is less than 0.5 dB.

3.2.1 SYSTEM DESIGN FOR STRONG PULSED RFI

The S-band RFI problem as viewed from the TDRS was outlined in a verbal communication from Mr. Jim Lyttle of ESL to Dr. Charles Cahn of Magnavox. The RFI is caused by radar pulses that are three to four microseconds in duration with an average period of 75 microseconds. Its power spectral density level is expected to be -141 dBW/MHz re a 0 dB antenna, with an additional 40 dB peak factor for the case where a radar antenna is pointed directly at the TDRS. The level received on the user is expected to be possibly 20 dB stronger, because of reduced range. Compared to the user received level of -153.7 dBW [1, Table 3-1] re a 0 dB antenna spread over 13.2 MHz, it is a severe problem. Even if received on a side-lobe of the user antenna, it could be stronger than the desired signal.

Since the RFI is pulsed it may be rejected by the combination of limiting in the receiver and spread spectrum demodulation of the transmitted signal. Proper operation of the autotrack system is then dependent on the operation of the data demodulator.

The RFI effect on autotrack may be determined by reference to the functional block diagram of the Σ -channel given in Figure 3-1. The Δ -channel would have a similar structure. AGC detection and control is presumed to be part of the Σ -channel spread spectrum processor. For the Δ -channel, the bandwidth W_1 must be chosen so that receiver noise captures the limiter, even at the edge of the autotrack range, thereby keeping the strength of the signal component at the limiter output linear with that at its input. For matching purposes, W_1 in the Σ -channel will be made the same as in the Δ -channel. W_1 also will equal or exceed the spread spectrum bandwidth.

Assuming that noise captures the limiter, the signal is reduced by a factor of $4/\pi$ relative to noise [2], so that the output signal power from the Σ -channel in Figure 3-1 is

$$P_S = \left(\frac{P_A}{1.59}\right) G \left(\frac{N_R}{N_{R_1}}\right) \left(\frac{\pi}{4}\right) \quad (3-5)$$

[1] NASA Goddard, TDRSS Definition Phase Study Report, December 1973.

[2] Jain, Pravin C., "Limiting of Signals in Random Noise," IEEE Trans on Information Theory, vol. IT-18, no. 3, May 1972, p. 332.

where P_A is the Σ -beam signal power at the receive antenna output. The output noise power is given by

$$P_N = kT_R W_2 G \left(\frac{N_R}{N_{R_1}} \right) \quad (3-6)$$

where k is Boltzmann's constant, and T_R is the receiver noise temperature at the front end of the amplifier. Thus, we have as the Σ -channel carrier-to-noise ratio

$$CNR_{\Sigma} = \frac{P_S}{P_N} = \frac{0.494 P_A}{kT_R W_2} \quad (3-7)$$

The power level out of the limiter is N_R , so the pulsed RFI power level at the Σ -channel output is

$$P_{RFI} = N_R (\tau/T) (W_2 / 1.32 \times 10^7), \text{ for } W_2 \leq 1.32 \times 10^7 \text{ Hz} \quad (3-8)$$

where τ is the pulse duration, T is the pulsed period, and $1.32 \times 10^7 / W_2$ is approximately the spread spectrum processing gain. With

$$\begin{aligned} \tau &= 4 \mu\text{s} \\ T &= 75 \mu\text{s} \end{aligned}$$

we have

$$P_{RFI} = 4.04 \times 10^{-9} W_2 N_R \text{ for } W_2 \leq 1.32 \times 10^7 \text{ Hz} \quad (3-9)$$

From (3-5) and (3-9) we have

$$\frac{P_S}{P_{RFI}} = \frac{1.223 \times 10^8 G P_A}{W_2 N_{R_1}} \text{ for } W_2 \leq 1.32 \times 10^7 \text{ Hz} \quad (3-10)$$

But from Figure 3-1

$$N_{R_1} = kW_1 T_R G \quad (3-11)$$

giving

$$\frac{P_S}{P_{RFI}} = \frac{1.223 \times 10^8 P_A}{kT_R W_1 W_2}, \text{ for } W_2 \leq 1.32 \times 10^7 \text{ Hz} \quad (3-12)$$

3.2.2 CHOICE OF BANDWIDTHS IN THE AUTOTRACK SYSTEM

It is conceivable that the spread spectrum processor in Figure 3-1 could strip data as well as the spread spectrum code. For the sake of this analysis, however, code stripping only is presumed. W_2 , then, is made equal to the maximum data bandwidth which could be supported by the link. The data bandwidth is assumed to be 1.5 times the bit rate: from [1, Figure 3.3], the maximum data rate is related to the user's antenna gain G_A by

$$R = 3 \times 10^3 G_A \text{ bits/sec} \quad (3-13)$$

for uncoded data using biphase PSK. For data coded with a rate 1/3 code, the bit rate is

$$R_B = 3R \text{ bits/sec}$$

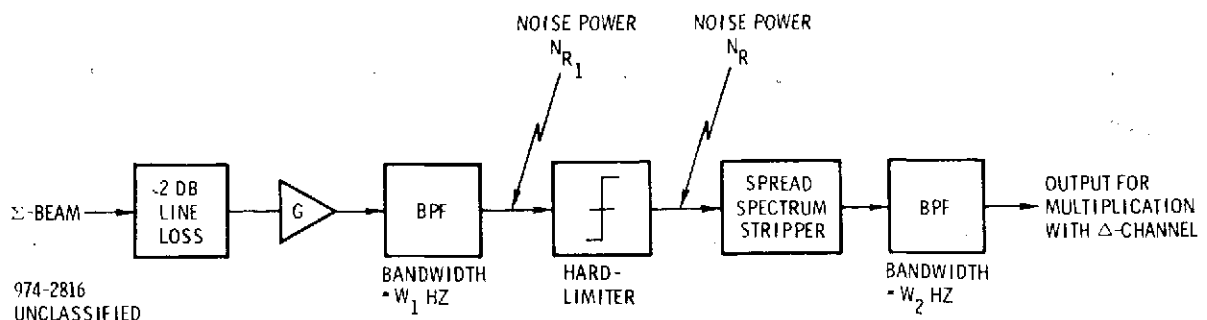


Figure 3-1. Σ -Channel Functional Block Diagram

so that the bandwidth W_2 is given by

$$\begin{aligned} W_2 &= 1.5R_B \\ &= 1.35 \times 10^4 G_A \end{aligned} \quad (3-14)$$

Using [3]

$$G_A = 27,000/\theta_B^2 \quad (3-15)$$

we have

$$W_2 = 3.64 \times 10^8 / \theta_B^2 \text{ in Hz} \quad (3-16)$$

where θ_B is the two-sided 3 dB beamwidth in degrees. When $\theta_B = 5.25^\circ$, then $W_2 = 13.2$ MHz, the full spread bandwidth.

We will choose W_1 as narrow as possible within two constraints: it must be at least as wide as the spread bandwidth and it must be wide enough to let receiver noise capture the limiter in the Δ -channel when operating at the edge of the autotrack range. Assuming that the Δ -beam antenna output after quadrature multiplexing has signal power of $P_A/2$ at the edge of autotrack range, W_1 is chosen so that the signal-to-noise ratio into the Δ -channel limiter is -6 dB

$$\frac{P_A}{2(1.59)kW_1 T_{RA}} = 0.25 \quad (3-17)$$

The spread bandwidth of 1.32×10^7 Hz may cause W_1 to be larger than the value resulting from (3-17). Now from [1, Table 3-1],

$$P_A = 4.27 \times 10^{-16} G_A \quad (3-18)$$

³ H. Jasik, Antenna Engineering Handbook, Mc Graw-Hill, 1961, p. 12-12.

The noise temperatures assumed in Table 3-2, combined with Equations (3-15), (3-17) and (3-18) and spread bandwidth considerations give

$$W_1 = \begin{cases} 9.28 \times 10^8 / \theta_B^2 \text{ Hz for } \theta_B \leq 8.38^\circ \\ 1.32 \times 10^7 \text{ Hz for } \theta_B > 8.38^\circ \end{cases}$$

Assuming that the antenna structural resonance frequency is 1 Hz or greater, the servo loop noise bandwidth is chosen to be

$$b_n = 0.5 \text{ Hz}$$

Table 3-2. Calculation of Δ -Channel Noise Temperature

Paramp Σ -Receiver Noise Temperature at Preamp Front End (From [1, Table 3-1])	520° K
Paramp Preamp Noise Temperature	250° K
Antenna Output Noise Temperature at Σ -Receiver Preamp Front End, T_A (520° K - 250° K)	270° K
Antenna Output Noise Temperature at Δ -Receiver Preamp Front End with 3 dB combiner loss (270° K / 2)	135° K
Assumed TDA or Transistor Δ -Receiver Preamp Noise Temperature	1000° K
TDA or Transistor Δ -Receiver Noise Temperature at Preamp Front End, $T_{R\Delta}$ (1000° K + 135° K)	TOTAL
	1135° K

3.2.3 POINTING ERROR CONTRIBUTORS

The following sources of pointing error must be considered: dynamic servo lag, noise bias error due to the autotrack comparator gain imbalance, RFI bias error, noise variance, and offset errors with signal only. These error components will be quantified and combined to determine the worst-case pointing loss as a function of antenna diameter.

3.2.3.1 Dynamic Servo Lag

The angular velocity which the user antenna must track has two components: the angular velocity due to user positional motion relative to the TDRS 0.0127 deg/sec maximum from Appendix XI and the angular velocity due to user spin relative to the TDRS. The user orientation is assumed fixed relative to the earth's center, so that relative to the TDRS, the maximum value of the second component is 360°/orbit period. For the users tabulated in [4, Table 4.4-2-1], the shortest period is 90 minutes for HEAO, so that the maximum value of the second angular velocity component is 0.0667 degrees/second. The two components combined produce a maximum angular velocity of 0.0794 degrees/second. For a type "1," critically damped autotrack servo system of noise bandwidth b_n , the dynamic servo lag error is determined from Appendix XI to be

$$\theta_L = 1.985 \times 10^{-2} / b_n \text{ degrees} \quad (3-19)$$

For $b_n = 0.5$ Hz, we have

$$\theta_L = 3.97 \times 10^{-2} \text{ degrees}$$

3.2.3.2 Noise Bias Error

In Appendix XII the bias error $\bar{\theta}_I$ caused by isotropic received noise with a gain imbalance factor "a" in the autotrack comparator is found to be

$$\frac{|\bar{\theta}_I|}{\theta_B} = \frac{(1+a)^2 (N_{IA} - a^2 N_{IB})}{11.1(1+a^2)P_S} (\theta_B / \theta_q) \quad (3-20)$$

[4] Pullara, J. C., et al, "Dual S- and Ku-Band Tracking Feed for a TDRS Reflector Antenna," Final Report[Phase I], submitted by Martin-Marietta Aerospace Corp. to GSFC, July 1974.

where

θ_B is the full 3 dB beamwidth of each of the squinted beams (A and B)

θ_q is the squint angle

N_{IA} is the output noise power of the Σ -receiver resulting from isotropic noise received in the A beam

N_{IB} is the output noise power of the Σ -receiver resulting from isotropic noise received in the B beam.

We assume an amplitude imbalance of 0.4 dB so that

$$a = 0.955$$

and we assume

$$N_{IA} = N_{IB} \quad (3-21)$$

N_{IA} is related to the antenna noise temperature T_A as seen at the Σ -receiver front end by

$$N_{IA} = kW_2^{-T_A} G(N_R / N_{R_1}) \quad (3-22)$$

Similar to (3-7), we obtain

$$\frac{P_S}{N_{IA}} = \frac{0.494 P_A}{kT_A W_2} \quad (3-23)$$

Applying (3-15), (3-16), and (3-18) to (3-23) with

$$T_A = 270^\circ K$$

from Table 3-2 gives

$$\frac{P_S}{N_{IA}} = 4.20 \quad (3-24)$$

Applying $a = 0.955$, (3-21) and (3-24) to (3-20) with

$$\theta_B/\theta_q = 2 \quad (3-25)$$

gives

$$|\bar{\theta}_I| = 7.54 \times 10^{-3} \theta_B \quad (3-26)$$

3.2.3.3 RFI Bias Error

The bias error resulting from RFI, $\bar{\theta}_{RFI}$, may also be determined from (3-20) under the worst-case assumption that

$$N_{IA} = P_{RFI} \quad (3-27)$$

and

$$N_{IB} = 0$$

i.e., all the RFI is received in one squinted beam and not in the other. From (3-20), (3-25), (3-27) and $a = 0.955$ we have

$$|\bar{\theta}_{RFI}|/\theta_B = 0.360 \frac{P_{RFI}}{P_S} \quad (3-28)$$

Applying (3-12) to (3-28) gives

$$|\bar{\theta}_{RFI}|/\theta_B = 2.94 \times 10^{-9} k T_R W_1 W_2 / P_A \quad (3-29)$$

for

$$W_2 \leq 1.32 \times 10^7 \text{ Hz}$$

As a worst case we will use the Δ -channel value of T_R from Table 3-2, namely,

$$T_R = T_{R\Delta} = 1135^\circ\text{K} \quad (3-30)$$

and the Δ -channel equivalent of P_A , which, due to the quadrature combiner is 1/2 that given in (3-15). Applying these equations along with (3-15), (3-16) and (3-29) gives

$$|\bar{\theta}_{RFI}| = \begin{cases} 2.70/\theta_B & \text{for } 5.25^\circ \leq \theta_B \leq 8.38^\circ \\ 3.84 \times 10^{-2} \theta_B & \text{for } \theta_B > 8.38^\circ \end{cases} \quad (3-31)$$

3.2.3.4 Noise Variance

The noise variance is given by

$$\sigma_\theta^2 = \frac{0.52}{\text{CNR}_\Sigma} (b_n/W_2) \left(1 + \frac{1}{\text{CNR}_\Sigma}\right) \theta_B^2 \quad (3-32)$$

Inserting (3-15), (3-16) and (3-30) in (3-7) with P_A equal to 1/2 that given in (3-18) gives as a worst case for evaluation of (3-32)

$$\text{CNR}_\Sigma = 0.499 \quad (3-33)$$

Then using (3-16), (3-20) and (3-33) we have

$$\sigma_\theta^2 = 6.56 \times 10^{-5} \theta_B^2 \quad (3-34)$$

3.2.3.5 Offset Error

With the autotrack sum channel used for data reception as well, there are no significant feed offset errors. The only significant offset error contributors are precomparator amplitude and phase imbalance, and post-comparator phase imbalance between the sum and difference receivers [4, p. 4-51]. The resulting offset error is determined by

$$\frac{\Delta\theta}{\theta_B} = 0.183 \left(\frac{\theta_B}{\theta_q} \right) \ln \left\{ \left| \frac{A_2}{A_1} \right| \left[-\sin\alpha \tan\beta + \sqrt{1 + \sin^2\alpha \tan^2\beta} \right] \right\} \quad (3-35)$$

where $|A_2/A_1|$ is the ratio of precomparator amplitude

α is the precomparator phase difference

β is the post-comparator phase difference

$\Delta\theta$ is maximized when $|A_2/A_1| < 1$ and $\beta > 0$. Thus, as a worst case, we have from [3, p. 4-51],

$$\begin{aligned} |A_2/A_1| &= 0.955 \text{ (0.4 dB imbalance)} \\ \alpha &= 5^\circ \\ \beta &= 20^\circ \end{aligned} \tag{3-36}$$

Using (3-36) in (3-35) with $\theta_B/\theta_q = 2$ gives

$$|\Delta\theta| = 0.0288\theta_B \tag{3-37}$$

3.2.3.6 Total Pointing Loss

The total pointing error θ_e is determined by combining the components in (3-26), (3-31), (3-34) and (3-37). The combination will use $3\sigma_\theta$ so that with Gaussian jitter, the required pointing accuracy is maintained at least 99.6% of the time. Thus, we have

$$\theta_e = \theta_L + |\bar{\theta}_I| + |\bar{\theta}_{RFI}| + 3\sigma_\theta + |\Delta\theta| \tag{3-38}$$

or

$$\begin{aligned} \theta_e \text{ (degrees)} &= 3.97 \times 10^{-2} + 1.968 \times 10^{-4} \theta_B^2 + 3.63 \times 10^{-2} \theta_B \\ &+ \begin{cases} 2.70/\theta_B & \text{for } 5.25^\circ \leq \theta_B \leq 8.38^\circ \\ 3.84 \times 10^{-2} \theta_B & \text{for } \theta_B > 8.38^\circ \end{cases} \end{aligned} \tag{3-39}$$

The pointing loss resulting from the pointing error θ_e given in (3-39) is, assuming a Gaussian-shaped beam,

$$L_p = -10 \log_{10} [e^{-2.773(\theta_e/\theta_B)^2}] \quad (3-40)$$

The antenna diameter D is assumed to be related to the beamwidth by [3]

$$\begin{aligned} D &= 65\lambda/\theta_B \\ &= 30.4/\theta_B \text{ feet} \end{aligned} \quad (3-41)$$

Using (3-39), (3-40) and (3-41), a curve of autotrack pointing loss vs antenna diameter is given in Figure 3-2.

3.2.4 S-BAND USER AUTOTRACK SYSTEM BLOCK DIAGRAM

The analysis of Section 3.2.3 was performed for user antenna diameters between 1 and 5.8 feet. This section will present an autotrack system design with antenna diameter D as a parameter, for $1 \text{ foot} \leq D \leq 5.8 \text{ feet}$.

The power received at the input to the Σ -channel preamp following 2 dB of line losses is determined from (3-15), (3-18) and (3-41) to be

$$\begin{aligned} \frac{P_A}{1.59} &= 7.85 \times 10^{-15} D^2 \text{ watts} \\ &= \begin{cases} -111 \text{ dBm, } D = 1 \text{ ft} \\ -96 \text{ dBm, } D = 5.8 \text{ ft} \end{cases} \end{aligned} \quad (3-42)$$

Using the range of received levels given in (3-42), a block diagram of the user autotrack system is given in Figure 3-3.

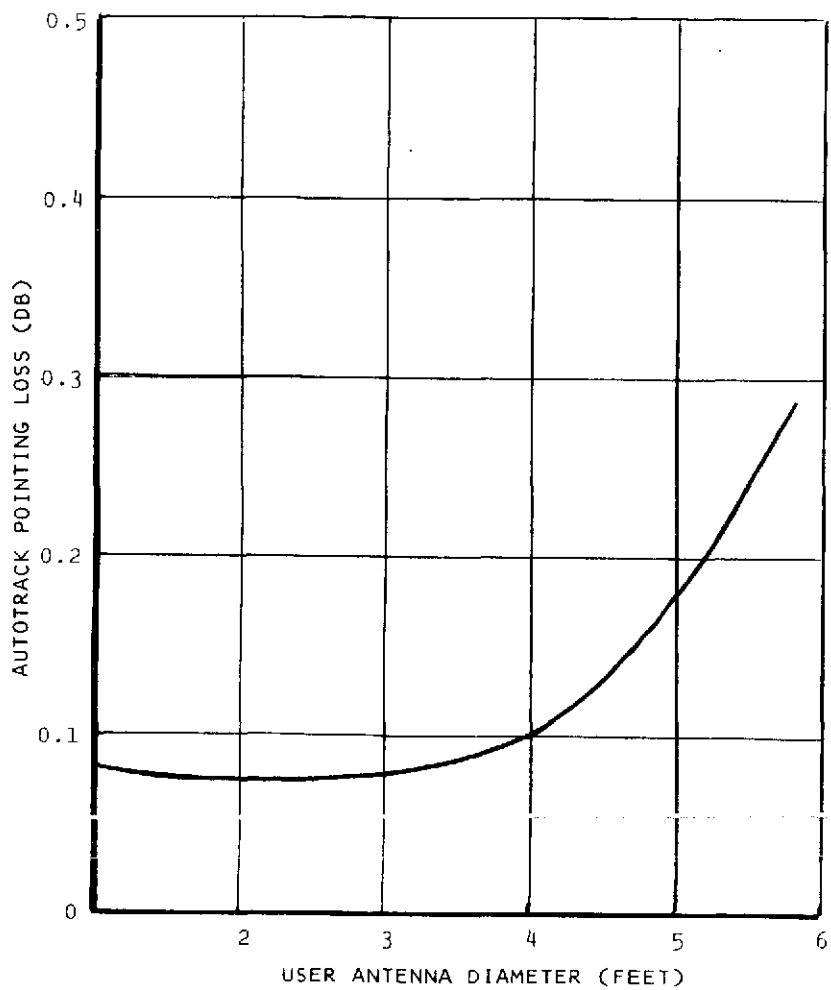


Figure 3-2. S-Band User Autotrack Pointing Loss vs User Antenna Diameter (99% of the Time)

The block diagram shows two channels, one for the Σ -beam, and one for the quadrature multiplexed Δ -beams. Quadrature multiplexing of the two Δ -channels can be used since the Σ -channel signal is fully coherent with both Δ -channel signals. It may later be used as a coherent reference to demultiplex the two quadrature channels.

Two IF's are used in the design, 300 MHz and 70 MHz, allowing reasonable Q values of the bandpass filters shown. Down-conversion to the first IF is accomplished with a fixed 1.807 GHz local oscillator. Down-conversion to the second IF is accomplished with a local oscillator provided by the spread spectrum processor, nominally at 230 MHz, which is modulated by the correctly synchronized spectrum code and is shifted for doppler correction (± 55 kHz max). The Σ - and Δ -channels must be phase matched across both the W_1 and W_2 bandwidths.

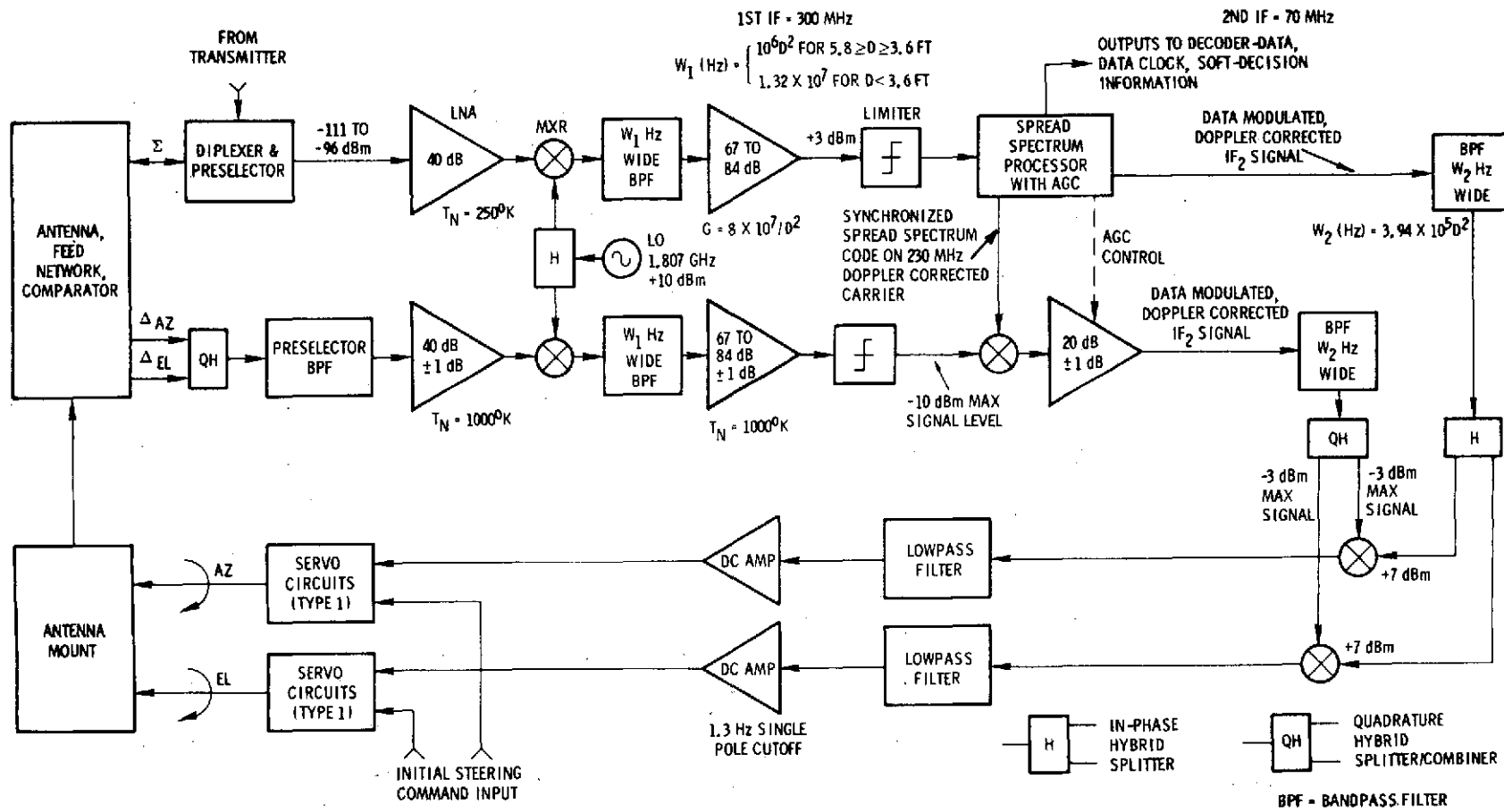


Figure 3-3. Annotated Block Diagram of S-Band User Autotrack System

The Σ -channel receiver input is obtained from the Σ -channel antenna output through a diplexer at a level of -111 to -96 dBm, depending on the dish size. A low noise (250°K) S-band parametric amplifier is used to provide 40 dB of gain. Following S-band gain, the Σ -channel signal is down-converted to 300 MHz. At 300 MHz the signal is amplified to a level of +3 dBm to drive the limiter with a power gain related to the antenna diameter (in feet) by

$$G = 8 \times 10^7 / D^2 \quad (3-43)$$

It is also filtered before limiting by a bandpass filter of bandwidth W_1 determined from (3-20) and (3-41) to be

$$W_1 (\text{Hz}) = \begin{cases} 10^6 D^2 & \text{for } 5.8 \text{ ft} \geq D \geq 3.6 \text{ ft} \\ 1.32 \times 10^7 & \text{for } D < 3.6 \text{ ft} \end{cases} \quad (3-44)$$

The limiter is used prior to spread spectrum processing as pulsed RFI protection. A strong RFI pulse will have its amplitude limited at this point as well as in preceding circuitry. Since the pulse duration is 3-4 microseconds, all circuitry should be designed to have a pulse recovery time of the order of 0.1 microsecond.

The spread spectrum processor following the limiter is required for data demodulation, but its signal processing capabilities are needed for autotrack operation as well. For autotrack purposes it is sufficient for it to strip the spread spectrum code and correct for doppler in the Σ -channel, producing a data modulated signal at 70 MHz. It must also provide an AGC control signal for the Δ -channel, and a doppler shifted LO signal at nominally 230 MHz that carries the spread spectrum code for Δ -channel processing. For data purposes it also provides outputs need by the decoder; coded data, data clock, and soft-decision information, if required.

The Σ -channel output of the spread spectrum processor is assumed to be a +10 dBm level, so that the drive level to each of the two phase detector mixers is +7 dBm. It is bandpass filtered by W_2 , the coded data bandwidth, determined from (3-16) and (3-41) to be

$$W_2 = 3.94 \times 10^5 D^2 \quad (3-45)$$

The Δ -channel receiver chain has frequency conversions and filtering identical to those in the Σ -channel receiver chain. The same RF and IF_1 amplifier gains are used as well, providing sufficient receiver gain for noise to operate the limiter. Because of expected high levels of pulsed RFI, the Δ -channel S-band amplifier should be a transistor type rather than a tunnel diode amplifier. With noise capturing the limiter, the Δ -channel is linear with respect to the signal provided by the Δ -beam. AGC control of Δ -channel gain for maintaining constant autotrack loop gain is provided at the 70 MHz IF, with the spread spectrum processor providing the control signal. Since Δ -channel gain variations are not detected or corrected by the AGC, the three Δ -channel amplifiers are allowed to vary ± 1 dB each, contributing ± 3 dB variation to the autotrack loop gain.

The maximum Δ -channel input level to the phase detector mixers is -3 dBm (at the edge of the autotrack range). This insures linear operation of the mixers for the Δ -input, while giving a maximum DC output of about 140 mV. This level is over 40 dB above good DC amplifier offset levels, so that a 40 dB Δ -beam null may be achieved.

The Δ -channel is split in a quadrature hybrid to regain the Δ_{AZ} and Δ_{EL} signals, which are then separately synchronously detected against the Σ -channel reference. The resulting DC voltages are amplified with a single-pole lowpass cutoff of $f_0 = 1.3$ Hz, determined from Equation (27) of Appendix XI,

$$f_0 = \frac{\omega_0}{2\pi} = \frac{1.61n}{2\pi} = 1.3 \text{ Hz} \quad (3-46)$$

The DC amplifier outputs are then used to control the azimuth and elevation servos, which each have a single pole at the origin (type 1 system).

3.2.5 APC MODIFICATION

The analysis of Section 3.2.3 used an assumption for the maximum phase imbalance between the Σ -receiver and Δ -receiver of 20° . This assumption was obtained from [4, p. 4-51]. Subsequent communication with L. Deerkoski and P. Dalle-Mura of NASA-GSFC has indicated that NASA's experience does not support this assumption when a paramp receiver is used.

An automatic phase control (APC) loop is described in Appendix XIII for the problem of phase drift in the Σ -channel paramp. With this type of modification to the system, the performance calculations remain valid.

3.2.6 AUTOTRACK SCENARIO

The following scenario is described for establishing and maintaining the communications link between the TDRS and an S-band single-access user.

a. The ground station commands the TDRS to point its antenna at the user.

b. The TDRS steers its antenna to within an uncertainty region of 0.45 degrees in radius, which corresponds to an S-band pointing loss of 0.4 dB.

c. Either (a) the user continually maintains its antenna pointed at the TDRS, or (b) the ground station commands the user via TDRS S-band relay to point at the TDRS. (This requires an S-band omnidirectional antenna on the user.) The initial pointing accuracy is within the 3 dB user beamwidth.

d. On command from the ground station, the TDRS transmits an S-band signal to the user for user autotrack to reduce the 3 dB pointing loss to less than 0.5 dB.

e. During the user autotrack acquisition process the ground station determines when link performance is acceptable and notifies the user to start data transmission. A data transmission begins.

f. The TDRS maintains S-band transmission as long as autotrack is to be maintained. The TDRS transmits with an EIRP of +44.4 dBW spread over 13.2 MHz. TDRS tracking of the user is maintained by ground station command.

3.3 RECOMMENDED S-BAND SINGLE ACCESS DESIGN

This section presents a recommended S-band single access design which is based on the modulation trade studies in paragraph 3.1 and autotrack analysis presented in paragraph 3.2. The design includes a (1) listing of critical waveform parameters, (2) a functional description of the transponder (3) a size, weight and power estimate and (4) expected S-band single access service performance specifications.

3.3.1 S-BAND SERVICE WAVEFORM PARAMETERS

FORWARD LINK

FH Preamble:

Type	Pseudorandom frequency hop
Code Generation	Maximal augmented by one chip
Code Period	512
Hop Rate	6.012 kHz
Spacing	12.023 kHz
Repetition Interval	85.172 mS
Preamble Duration	6 seconds
Bandwidth	6.012 MHz

PN Modulation:

Type	SQPN - Staggered quadriphase pseudonoise
Code Family	Maximal pairs augmented by one chip
Code Period	2^{19}
PN Chip Rate	6.156 MHz
Repetition Interval	85.172 mS

Command Data:

Modulation	Synchronous biphasic differential, NRZ-M
Rates (any one of the following)	94 bps
	188 bps
	376 bps
	752 bps
	1504 bps
	3008 bps
	6016 bps
Word Length	User defined
Coding	User defined

RF Signal:

Frequency	2025 - 2120 MHz
Doppler	+60 kHz
Range Rate Uncertainty	$\pm 100 \text{ m/sec} = \pm 700 \text{ Hz}$

RETURN LINK

PN Modulation:

Type	SQPN - Staggered quadriphase pseudonoise
Code Family	Maximal pairs augmented by one chip
Code Period	2^{19}
PN Chip Rate	6.156 MHz
Repetition Interval	85.172 mS

Telemetry Data (PN Mode):

Data Modulation	Asynchronous differential biphasic, NRZ-M
Data Rate	1-300 kbs, encoded 1-600 kbs, not encoded

Telemetry Data (Clear Mode):

Data Modulation	Asynchronous differential PSK
Data Rate	
Biphase	300 - 3000 kbs, encoded, rate 1/2
Quadriphase	3000 - 6000 kbs, encoded rate 1/2

Data Encoding:

Type	Convolutional, nonsystematic, transparent
Constraint Length	7
Code Rate	1/2
Code Gain	5 dB at BER = 10^{-5}
Symbol Rate	6 Mbps max
Data Type	Delta mod, PCM, NRZ-M

RF Signal:

Frequency	240/221 x receive frequency
Doppler	± 120 KHz
Range Uncertainty	± 100 Km
Range Rate Uncertainty	± 200 m/sec = ± 700 Hz

3.3.2 TRANSPONDER FUNCTIONAL DESIGN

3.3.2.1 General Description

The S-band single access transponder consists of fifteen modules

- a. RF Down Converter
- b. IF Chain
- c. RF Synthesizer #1
- d. RF Synthesizer #2
- e. Demodulator
- f. Sync Monitor
- g. Incremental Phase Modulator
- h. PN Coder
- i. Local PN/FH Reference Generator
- j. Local Reference Modulator
- k. Controller

- 1. Modulator
- m. Transmitter
- n. Power Supply Post Regulator
- o. Chassis

Major functions of these modules and their interconnections are shown in a block diagram of the transponder in Figure 3-4.

This transponder is very similar to the multiple access transponder. One difference is that a second modulator board has been added to provide both a minimum power ranging signal and a PSK data signal in the return link. Another minor difference is that higher speed logic is used to accommodate the higher PN chip rate and a higher frequency hop generator rate. Also, bandwidth and center frequencies are scaled to operate at different S-band frequencies and data rates. Finally, a separate reference oscillator is not needed for non-coherent mode of operation in the single access transponder since the forward link will not be time shared and require reacquisition during a telemetry data dump.

Because of the similarity of these two transponders, the implementation tradeoff studies presented in Section II for the M/A transponder apply directly to the design of the single access transponder. Also the detailed designs are so similar to the M/A detailed design that it will not be repeated in this section.

A forward link signal is amplified and down converted in the RF Down Converter module. The signal is dehopped during the FH preamble and its PN modulation is stripped off during a track mode in the correlator (second mixer) of the IF Chain leaving a PSK modulated carrier at its output. Bandwidth reduction and AGC action occurs in the second IF amplifier and, after passing through a third IF stage, the signal is delivered to the Demodulator. A sync detector senses the presence of a signal and, after sync verification is made, a Costas demodulator extracts the data. This command data is subsequently processed, differentially decoded and delivered to a satellite command decoder.

Major modules involved with demodulating the frequency hop during acquisition and subsequently acquiring and tracking the pseudonoise portion of the signal are:

- Modulator
- Local Reference

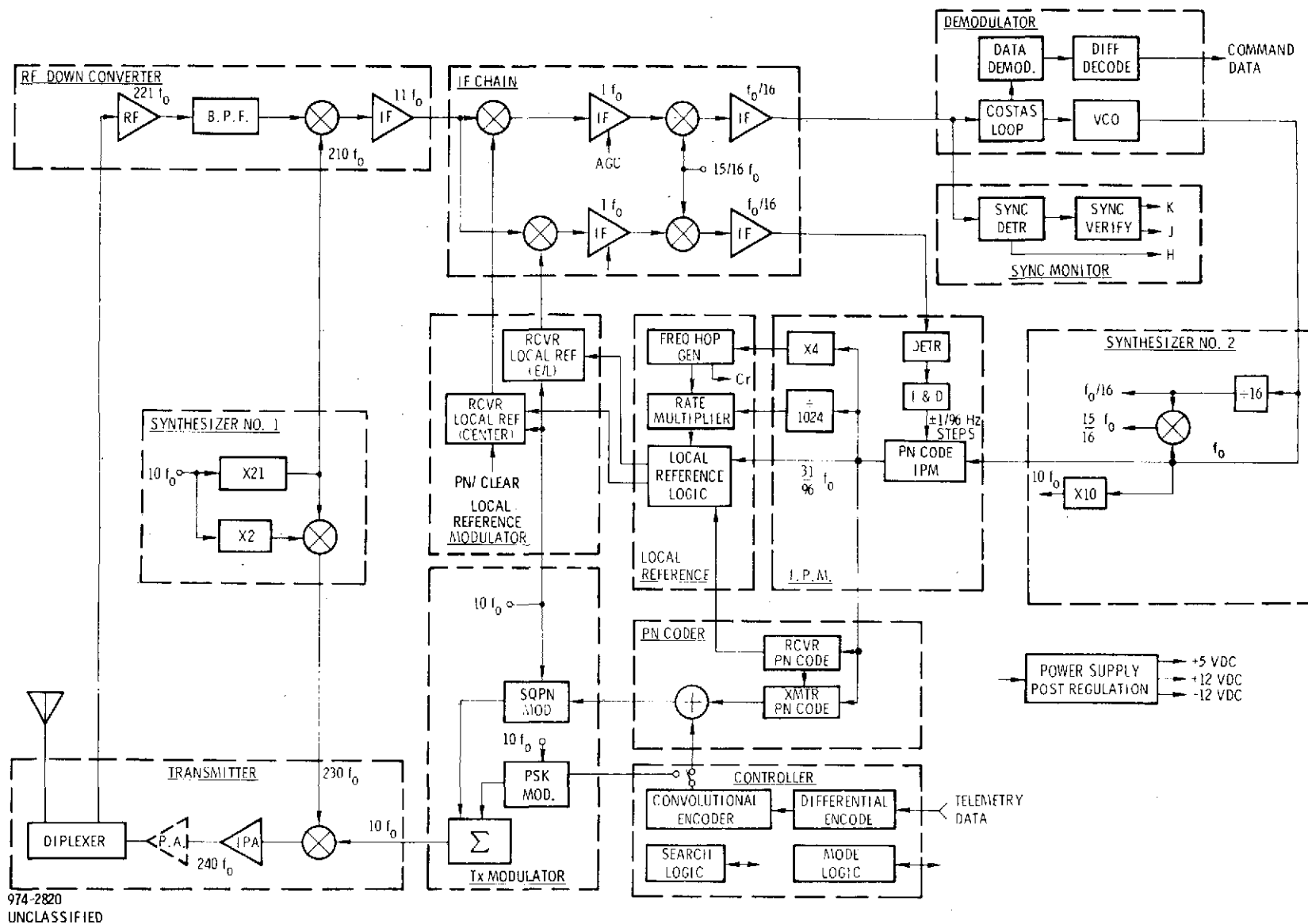


Figure 3-4. Access User Transponder

- PN Coder
- IPM

The Local Reference Modulators consists of two QPSK modulators whose outputs provide (1) a FH reference to the carrier channel during FH signal acquisition (2) a SQPN reference to the carrier channel (center or bogey) and a (3) SQPN reference to the code channel (early-late phases) during a PN acquisition and track mode. The Local Reference provides the required staggered PN sequence to the Modulator for both the receiver and the transmitter functions and it also generates the appropriate frequency hop sequence for the receiver local reference. The PN Coder generates two pairs of orthogonal PN codes for use in the Local Reference module. Finally, the IPM module retards the PN code phase in quarter chip steps during a PN acquisition mode and it advances and retards the PN code phase in approximately 3° steps during a code tracking mode.

The Tx Modulator contains a SQPN modulator for minimum power ranging and a PSK modulator for data transmissions. The Transmit module contains a single up conversion stage, a power amplifier to provide the desired EIRP (different for each application) and a diplexer for separating the receive and transmit signals.

Synthesizer #1 provides the first L. O. for both the receiver and the transmitter. Synthesizer #2 provides all of the additional L. O. signals. The Controller provides all programming functions including mode control and FH/PN search sequences. Differential and convolutional encoding (if used) is also contained in this module. All power supply potentials for all portions of the transponder are post regulated to insure uninterrupted performance due to power transmits, buss switching, etc.

3.3.2.2 Modes of Operation

The transponder provides the capability to operate in one of the two following modes of operation.

- Coherent Transpond
- PSK Telemetry with Minimum Power Ranging

Optional Features of the single access transponder include:

- Retrace for Multipath
- VCO Drift Monitor

3.3.2.3 Low Power Ranging

This transponder will offer a low power two-way ranging mode which operates in conjunction with a PSK telemetry return link. To minimize the hardware impact, both the low power PN signal and the PSK signal with asynchronous data will utilize a single RF carrier. The PN code will be synchronized to the forward link PN code to provide a two-way range capability. Both signals will be resistively summed together and band limited in the Tx modulator to provide a constant envelope transmit signal.

3.3.2.4 Retrace for Multipath

Although there is little likelihood that multipath will be a problem at S-band for PN during acquisition, both frequency hop and pseudonoise retrace capability will be provided for resolving possible false lock to multipath on command. This involves a minor controller routine modification. The only disadvantages to this mode is a 2 to 1 increase in acquisition time.

3.3.2.5 VCO Drift Monitor

Since the transponder will use a temperature compensated voltage controlled oscillator for tracking in the forward link to minimize power consumption, and the long term drift of this oscillator exceeds the initial acquisition bandwidth of the receiver, the voltage offset of the VCO during a track mode will be recorded via an A/D converter and periodically sent back to the ground station as a status word via telemetry link. This information will be used to compute new transmit frequency offsets for future forward link acquisitions of the user satellite.

3.3.3 SIZE WEIGHT AND POWER

Major functions of the single access S-band transponder are similar to the Multiple Access transponder. The major exception is the addition of a modulator assembly to provide a PSK data signal summed with a separate PN ranging signal on the return link. Another difference between the two transponders is the extra power required by the Single Access transponder to generate faster PN and data clocks.

Anticipated power, weight and size requirements for the major assemblies of the Single Access S-band transponder are presented in Table 3-3. All assemblies

Table 3-3. S-Band Single Access Transponder Size, Weight, and Power

Modules	Power (watts)	Weight (oz.)	Size (in. ³)
<u>Narrowband Transponder</u>			
RF Down Converter	1	16	24
IF Chain	1.5	12	24
Synthesizer #1	2	10	24
Synthesizer #2	1.5	10	24
Demodulator	2	10	24
Sync Monitor	.5	6	12
Controller	1.5	6	12
Modulator	1	16	24
Transmitter (100 mW)	2	24	36
Post Regulator	3	24	36
Chassis	-	72	78
Subtotal	<u>16</u>	<u>206</u>	<u>318</u>
<u>Pseudonoise Assemblies</u>			
IPM	2	10	24
PN Coder	2	6	12
Local Reference	1.5	6	12
Local Reference Modulator	<u>1.5</u>	<u>12</u>	<u>24</u>
Subtotal	<u>7</u>	<u>34</u>	<u>72</u>
TOTAL	23	240	390

have been categorized as conventional narrowband assemblies or PN assemblies for purposes of comparison with existing transponders. In providing these estimates, 1977 technology was assumed and low power logic, standard LSI circuits and second source components were used to the maximum extent.

In summary, the Single Access S-band Transponder will require approximately 23 watts of power (assuming a 100 mW transmitter), weigh on the order of 15 lbs., and occupy 390 cubic inches in a 5" x 6" x 13" configuration.

3.3.3.1 Size

The length and width dimensions of each assembly are 4.5" x 6" with a useful circuit area of 24 square inches. The height dimension varies from 0.5" for logic boards to 1" for analog and RF assemblies to 1.5" for the transmitter and power supply assemblies.

The physical configuration of the transponder is envisioned as a tray of fixed-mount assemblies supported by a pair of rigid walls. Estimated dimensions for the transponder are 5" x 6" x 13" with 318 in.³ of the 390 in.³ apportioned to the narrowband functions and 72 in.³ to the PN functions.

3.3.3.2 Weight

The estimated weight for the various assemblies is itemized in Table 3-3. In general, logic assemblies are lighter than analog assemblies and much lighter than "canned" RF assemblies. The heaviest item in the transponder is the chassis at 4.5 lbs. The second heaviest items are the power supply and transmitter modules at 1.5 lbs. each. In summary, the transponder weight is estimated at 15 lbs. with 14% of this total appropriated for PN functions.

3.3.3.3 Power

Power estimates for the receiver, transmitter, and PN functions are 14, 2, and 7 watts, respectively. The largest variation in these values for potential users lies in the transmitter, since the EIRP requirements vary over a range of 30 dB. For purposes of an estimate, a 100 mW watt transmitter requirement was assumed.

Variation in power supply requirements from satellite to satellite also poses somewhat of a problem in estimating power requirements for the transponder. For this estimate, power supply regulation was assumed for all receiver and PN functions with an average operating efficiency of 80%.

Low power Schottky logic was assumed for digital circuits, except for the rate multiplier circuits in the local reference assembly and portions of the PN coder assembly, where the highest clock rate is 24 MHz. For these cases TTI Logic was employed. Use of a TCVCO eliminates the need for an ovenized oscillator, thereby reducing power.

3.3.4 PERFORMANCE SPECIFICATION

FORWARD LINK

FH Acquisition:

G_u	-6 dB
P_D	.97 (five passes)
Acquisition Time	6 seconds

PN Acquisition:

G_u	-6 dB
Acquisition Time	2 seconds (average)

Data Demodulation:

E_b/N_o	12.5 dB
BER	10^{-5}

RETURN LINK

PN Acquisition:

EIRP	7 dBW
Acquisition Time	4 seconds (average)

PN Acquisition - Low Power Ranging Mode:

EIRP	0 dBW
Acquisition Time	16 seconds

Data Demodulation:

BER	10^{-5} at $E_b/N_o = 12.5$ dB
BER (with coding)	10^{-5} at $E_b/N_o = 7.5$ dB

TWO-WAY RANGE

Forward Link:

G_u	-6 dB
Data Rate	1 kbs

Return Link:

EIRP	7 dBW
Data Rate	5 kbs
Measurement Error (1σ)	0.2 meter

TWO-WAY RANGE (LOW POWER RANGING MODE)

Forward Link:

G_u	-6 dB
Data Rate	1 kbs

Return Link:

EIRP	-18 dBW
Data Rate	0 bps
Measurement Error (1σ)	2 meters

TWO-WAY RANGE RATE

Forward Link:

G_u	-6 dB
Data Rate	1 kbs

Return Link:

EIRP	7 dBW
Data Rate	5 kbs
Measurement Error (1σ)	.2 cm/sec (1 sec ave) .02 cm/sec (10 sec ave)

TWO-WAY RANGE RATE (LOW POWER RANGING MODE)

Forward Link:

G_u	-6 dB
Data Rate	1 kbs

Return Link:

EIRP	-18 dBW
Data Rate	5 kbs
Measurement Error (1σ)	.5 cm/sec (1 sec ave) .05 cm/sec (10 sec ave)

3.4 OPERATIONAL PROCEDURE

3.4.1 FORWARD LINK ACQUISITION

The acquisition procedure on the forward link of an S-band Single Access service is as follows:

1. Ground station commands the TDRS to point its antenna at the user.
2. TDRS steers its antenna toward the user.
3. Ground station inserts appropriate user address into transmitter to select the preamble hopping code and the subsequent PN code to be transmitted.
4. Ground station inserts a priori range rate information into the transmitter.
5. Ground transmitter sends FH preamble for 6 seconds, synchronously, switches to PN code and continues transmission for two seconds or more before sending command data.
6. User acquires FH preamble, switches to PN code and auto searches until the forward link is acquired. If the forward link PN signal is not acquired within 10 seconds after detection of the FH signal, the user returns to a FH search.
7. Ground station sends command data via established forward link.

3.4.2 RETURN LINK ACQUISITION

The acquisition procedure on the return link of an S-band Single Access service is as follows:

1. Ground station sends a beam pointing instructions to user. (Only required for high data rate applications where beam pointing is required to meet EIRP requirements commanded pointing is assumed.)
2. Ground station inserts range and range rate information into ground receiver.
3. Ground station sends a command for user to start PN transmission on the return link.
4. User begins PN transmission.

5. TDRS acquires user.
6. Ground receiver acquires user signal in approximately 4 seconds.
7. Ground station sends instruction for user to begin telemetry data dump.
8. Ground station acquires data bit timing and demodulates telemetry data.
9. Ground station performs two-way range and range rate measurements on user.

3.4.3 RETURN LINK ACQUISITION WITH MINIMUM POWER RANGING

The acquisition procedure for an S-band Single Access user employing a minimum power PN ranging mode in conjunction with a high data rate PSK mode is as follows:

1. Ground station sends a beam pointing instruction to user.
2. Ground station inserts range and range rate information into Ground receiver.
3. Ground station sends a command for user to start PN transmission on the return link at an EIRP of 0 dBW.
4. User begins a PN transmission.
5. TDRS acquires user.
6. Ground station acquires user PN signal in approximately 16 seconds.
7. Ground sends instruction for user to reduce PN signal power to not less than -18 dBW and begin PSK transmission.
8. Ground station acquires data bit timing and demodulates telemetry data.
9. Ground station performs two-way range and range rate measurement on user.

This section presents a summary of the major Single Access transponder equipment specifications.

MODES OF OPERATION

Coherent Transpond
PSK Telemetry with Low Power Ranging

RECEIVER PRECORRELATION CHANNEL

Center Frequency	2025-2120 MHz
Noise Figure	2.5 dB max
Bandwidth (3 dB)	10 MHz min (at 2nd IF)
VSWR	1.5:1 over to ± 4.5 MHz
Phase Response	Linear to within $\pm 5^\circ$ over to ± 3.5 MHz
Amplitude Response	Flat to within 1/2 dB over to ± 3.5 MHz
Dynamic Signal Range	40 dB
Maximum Signal and Noise	-130 dBW
Minimum Signal	-180 dBW

FREQUENCY HOP PREAMBLE

FH Code:

Type	Pseudorandom, coherent frequency hop
Code Generation	Maximal augmented by one chip
Code Period	512
Hop Rate	6,012 KHz
Spacing	12,023 KHz
Repetition Interval	85.172 mS

Local Reference:

Bandwidth (3 dB)	10 MHz
Phase Response	Linear to within $\pm 5^\circ$ over to ± 3.5 MHz
Amplitude Response	Flat to within 1/2 dB over to ± 3.5 MHz
Implementation Technique	Discrete 45° phase stepping
Spurious Responses	20 dB down outside to ± 6 MHz

Acquisition:

Signal Bandwidth	10 MHz
Signal Detector	Sequential Detector
Detection Bandwidth	3 KHz (5-700 Hz filters in parallel)
Signal Integration Interval	2 mS
Search Rate	400 hops/sec average
Frequency Uncertainty	700 Hz nominal, 3000 Hz maximum

FH Losses:

Discrete Phase Loss	0.7 dB
Doppler Offset	0.8 dB (700 Hz)
Other	0.5 dB

PN DEMODULATION

PN Code:	
Type	SQPN - Staggered Quadriphase Pseudonoise
Code Family	Maximal code pairs augmented by one chip
Code Period	2^{19}
PN Chip Rate	6.156 MHz
Repetition Interval	85.172 mS
Local Reference:	
Bandwidth (3 dB)	10 MHz
Phase Response	Linear to within $\pm 5^\circ$ over to ± 3.5 MHz
Amplitude Response	Flat to within 1/2 dB over to ± 3.5 MHz
Carrier Suppression	50 dB or greater
Code Loop:	
Dither	$\tau_d = .5$ chip
Track Resolution	1/96 chip
Order	1st
Bandwidth (B_L)	0.1 Hz
Dynamics Aiding	From carrier loop
Acquisition:	
Search Steps	1/2 chip
Search Rate	740 chips/sec (average)
Signal Detector	Sequential Detector
Detector Bandwidth	3 kHz (S-700 Hz filters in parallel)
Frequency Uncertainty	700 Hz nominal, 3000 Hz maximum
Time Uncertainty	1000 PN chips
PN Losses:	
Bandwidth	Negligible
Channel Distortion	.7 dB
Imperfect Tracking	.3 dB

CARRIER ACQUISITION AND TRACKING

Type of Loop	Costas
Loop Order	2nd
Loop Bandwidth (B_L)	32 Hz
Damping Factor	.707
Frequency Offset	
Acquisition	± 3 kHz
Tracking	± 60 kHz
Incidental FM	6° RMS in 10 Hz with good S/N, maximum
Carrier Tracking Losses:	
Incidental FM	.2 dB
Non-linearities	.5 dB at threshold
AGC Noise	.3 dB at threshold

COMMAND DATA DEMODULATION

Demodulator	Costas Loop
Fixed Data Rate	94, 188, 376, 752, 1504, 3008, 6016 bps (user selected)
Data Processing	Integrate and dump
Data Decoding	Differential
Data Clock	Derived from PN code
Data Interface	TTL
Implementation Losses:	
Carrier Reference at threshold	1 dB at a data rate at 96 bps
Non-linearity	.3 dB
Bandlimiting	.2 dB
Modulation:	
Data Rate = 1-300 kbs	Biphase data modulo - two added to PN code
Data Rate = 300 kbs-3 mbs	Biphase data
Data Rate = 3 mbs-6 mbs	Quadriphase data

TRANSMIT CHANNEL

Transmitter:	
Type	Solid State Class C
Center Frequency	240/221 x receive frequency
Bandwidth (3 dB)	30 MHz nominal
Amplitude Response	Flat to within 1/2 dB over 70% of 3 dB bandwidth
Phase Response	Linear to within $\pm 5^\circ$ over 70% of 3 dB bandwidth
PN Modulator:	
Modulation	SQ PN (1-300 kbs)
Code Family	Maximal code pairs augmented by one chip
PN Chip Rate	6.156 MHz
Code Length	2^{19}
Bandwidth	10 MHz
Filter Type	Butterworth, 4-pole
Carrier Suppression	30 dB or greater
Spurious Responses	20 dB down outside of ± 6 MHz
Data Modulation	Biphase data modulo - two added to PN code
PSK Modulator	
Modulation:	
Data Rate = 300 kbs-3 mbs	Biphase PSK
Data Rate = 3 mbs-6 mbs	SQ PSK
Bandwidth	10 MHz
Carrier Suppression	30 dB
Spurious Responses	30 dB down outside of ± 6 MHz

Telemetry Data:

Rate	1 kbs~6 mbs
Clock	Asynchronous x 2 clock, user supplied
External Interface	TTL compatible
Encoding	
Type	Convolutional
Constraint Length	7
Rate	1/2
Encoding	
Type	Differential

SECTION 4

Ku-BAND SINGLE ACCESS SERVICE

The Ku-band single access service is primarily intended to provide a high data rate return link capability, up to a maximum of 300 Mbps in 225 MHz channel bandwidth. Forward link commands will be transmitted over the S-band single access system, in the current operational concept. Hence, attention is directed mainly at Ku-band return link performance.

It should be noted that a forward link Ku-band transmission still will be necessary for user antenna autotrack, and this transmission must be spread spectrum for meeting flux density limitations. Forward link transmission of data or video may be a special requirement of some users, such as Shuttle; however, these potential requirements are not discussed in regard to impact on the user transponder. Another potential requirement is to utilize the Ku-band single access system for two-way ranging, and a technique for this is described.

A special problem associated with the Ku-band return link is that the TDRS channel saturates because of the high EIRP needed to support the TDRS-to ground link. Effect of hard and soft limiting in the TDRS channel is discussed in detail.

Another special problem of the Ku-band return link is the objective of being able to reuse the 225 MHz spectrum allocation so as to support two independent return links from different users (individually autotracked with the two available TDRS antennas). Polarization multiplexing enables such reuse. On the user-to-TDRS link, multiplexing by sense of circular polarization (RHC vs. LHC) is straightforward, and protects against interference between channels due to antenna sidelobes. Since there are no atmospheric effects to create coupling between orthogonal polarization modes, sufficient decoupling would exist even when the beams overlap. Polarization multiplexing on the TDRS-to-ground link is a more complex question, studied further in Section 5.

4.1 MODULATION TRADEOFFS

This section presents results of analyses for various problems of the Ku-band return link, with the point of view of illustrating how the return link channel can be used.

4.1.1 Ku BAND RETURN LINK PERFORMANCE

The return link at Ku band passes through a finite bandwidth repeater channel in the TDRS, and this bandwidth sets the limitation on maximum achievable data rate. The noise is primarily introduced on the user-to-TDRS link (which is the opposite of the typical ground-satellite-ground communication system). With serial uncoded data transmission, hard or soft limiting in the repeater channel will not affect performance except to the extent that the relative noise contribution from the TDRS-to-ground link increases with backoff of the repeater from saturation.

Use of serial data has the practical disadvantage of forcing the user satellite to employ very high speed logic and to format the data into a high speed time division multiplex structure. An alternative is to have multiple carriers, with lower rate parallel data streams in subchannels. Now, limiting in the repeater channel is significant because of the intermodulation produced, and soft limiting is essential to control the intermodulation between subchannels. In the user satellite transponder, the impact is to increase the peak required EIRP because of the multiple carriers, and possibly, to somewhat increase average EIRP to overcome the intermodulation due to soft limiting in the repeater channel.

4.1.1.1 Serial Data Transmission

The increase in required E_b/N_o with serial data because of the finite channel bandwidth, which causes intersymbol interference, can be estimated from [1]. Figure 4-1 shows degradation for $P_e = 10^{-6}$ as a function of channel bandwidth with number of poles as a parameter (Chebyshev filter with 0.1 dB ripple is little different than Butterworth). This figure applies for white noise added after the channel filter but before the data filter (which could be either integrate-and-dump or 2-pole Butterworth as indicated). The modulation can be biphase, quadriphase or staggered quadriphase.

1. J. J. Jones, "Filter Distortion and Intersymbol Interference Effects on PSK Signals", IEEE Trans. on Comm. Tech., Vol COM-19, April 1971, pp. 120-132.

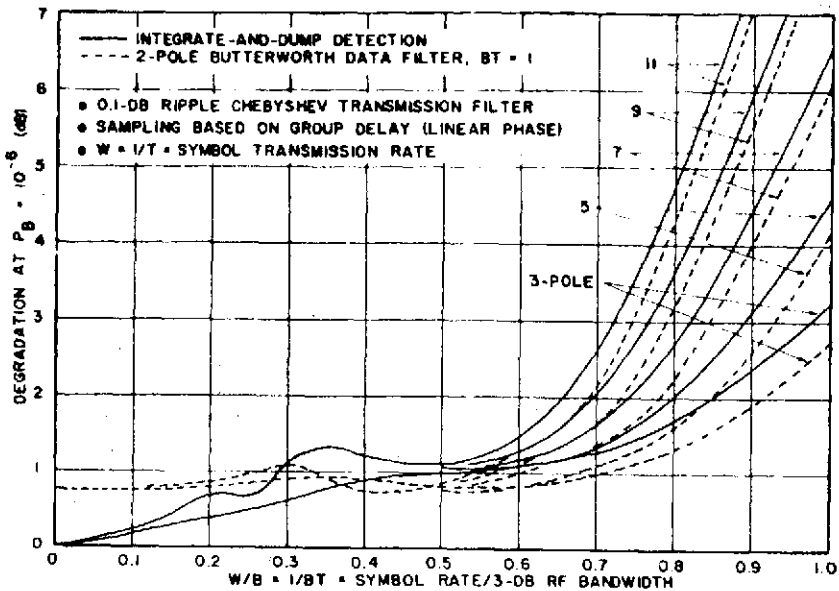


Figure 4-1. Bandwidth-limiting degradation of QPSK and BPSK signals

To apply Figure 4-1 to the present case, we must correct for the fact that the primary noise contribution is before the channel filter; thus, the noise power is reduced somewhat. The 2-pole Butterworth data filter has bandwidth (at bandpass) equal to the symbol rate. Then, when white noise is introduced after the channel filter, as in Figure 4-1, the noise power is proportional to

$$\int_0^{\infty} \frac{df}{1 + f^4} = 1.11 \quad (4-1)$$

Now assume a 6-pole Butterworth (or Chebyshev with 0.1 dB ripple) channel filter with bandwidth (at bandpass) equal to 1.5 times the symbol rate. Figure 4-1 shows a degradation of 1.2 dB when the noise is introduced after the channel filter. When the white noise is introduced before the channel filter, the resulting noise power is proportional to

$$\int_0^{\infty} \frac{df}{[1 + (f/1.5)^{12}] (1 + f^4)} = 1.00 \quad (4-2)$$

evaluated by numerical integration. Thus, the noise power is reduced by 0.4 dB when introduced before the channel filter.

Thus, for a channel filter providing a 6-pole Butterworth transfer function with a 3- dB bandpass bandwidth of 225 MHz, the estimated degradation in E_b/N_o due to the restricted bandwidth is 0.8 dB when the noise is introduced before the channel filter, at a bit rate of 150 Mbps for biphase and 300 Mbps for quadriphase.

The above calculation is an estimate because the effect of hard or soft limiting has not been brought in. The limiting occurs after the channel filter but before the data filter. A study has been made of the case where the noise is introduced after hard limiting^[2], with degradation results similar to Figure 4-1. Consequently, the existence of limiting in the repeater channel should have little effect on the estimated degradation for transmitting serial uncoded data.

4. 1. 1. 2 Parallel Data Transmission

High bandwidth efficiency with multiple carriers (i.e., subchannels) is possible by spacing adjacent carriers by the symbol rate to achieve orthogonality. Then, an integrate-and-dump detection over the symbol duration has a response only from the desired carrier, assuming the Doppler offset has been removed. The multiple carriers can be each quadriphase modulated* with parallel data streams, all synchronous to a common clock. To transmit 300 Mbps with quadriphase, the bandwidth is 150 MHz plus guard space (proportional to the bandwidth of the individual subchannels); thus, using parallel subchannels instead of a single serial data stream does not degrade the bandwidth utilization of the repeater channel.

There is a cost involved in providing a suitably linear channel. First, there is the impact to the user of transmitting multiple carriers. Two alternatives are (1) to have individual amplifiers for each subchannel combined at IF or RF, and (2) to have an amplifier with a peak power high enough to avoid excessive intermodulation. The required peak factor allowance is computed similarly to the discussion below for the repeater channel.

The impact to the TDRS is a requirement for operating the repeater channel backed off into soft limiting to reduce intermodulation to an acceptable

*Staggered quadriphase is not allowed since the orthogonality between the parallel carriers is maintained only with synchronized symbols.

2. C. R. Cahn and C. R. Moore, "Bandwidth Efficiency for Digital Communications via a Hard Limiting Channel", Proc. Int. Telem. Conf., 1972.

level. Assuming a reasonably large number of channels, the composite signal has the statistics of Gaussian noise, and the intermodulation due to soft limiting can be computed analytically^[3]. Furthermore, with a tandem link, the best compromise between excessive intermodulation and excessive backoff can be evaluated, as a function of the desired signal-to-noise ratio in a subchannel.

The analysis in reference 3 assumes a soft limiter with the input-output characteristic plotted in Figure 4-2, given by the formula (where x is input envelope and y is output envelope)

$$\begin{aligned}
 y &= x ; 0 < x < \frac{\pi}{4} \\
 &= .5[\sqrt{1 - (\pi/4x)^2} + \frac{4x}{\pi} \sin^{-1}(\pi/4x)] ; x > \pi/4
 \end{aligned} \tag{4-3}$$

Equation 4-3 evaluates the fundamental (first zone) output for symmetrical peak clipping at a finite limiting level. Note that the onset of clipping for a single carrier input occurs when the output power is 2.1 dB below the saturation output.

Figure 4-3 presents the output signal-to-noise-plus-intermodulation when the limiting channel, with the characteristic of Figure 4-2, is backed off from saturation. (Here, the curve is plotted with saturation output defined as +2.1 dB; i. e., the onset of clipping occurs at 0 dB.) The application of this curve is now described.

The NASA Goddard Definition Phase Report calls for a signal-to-noise ratio of 25 dB on the TDRS-to-ground link of the Ku band single access return link, so as to yield a tandem link loss of 1 dB at maximum data rate. Assuming this requirement applies to the sum of intermodulation and noise on the TDRS-to-ground link, Figure 4-3 shows that the optimum operating point to yield an output signal-to-noise-plus-intermodulation ratio of 25 dB backs off the repeater about 7.5 dB from saturation. However, if we allow a tandem link loss of 2 dB, the required signal-to-noise-plus-intermodulation ratio on the TDRS-to-ground link is reduced to 21.3 dB, and the required backoff from saturation is reduced to about 6.5 dB. Allowing an additional 1 dB of tandem link loss corresponds to the degradation estimated in Section 4.1.1.1 for serial data in a finite bandwidth.

3. C. R. Cahn, "Crosstalk due to Finite Limiting of Frequency-Multiplexed Signals", Proc. IRE, Vol. 48, January 1960, pp. 53-59.

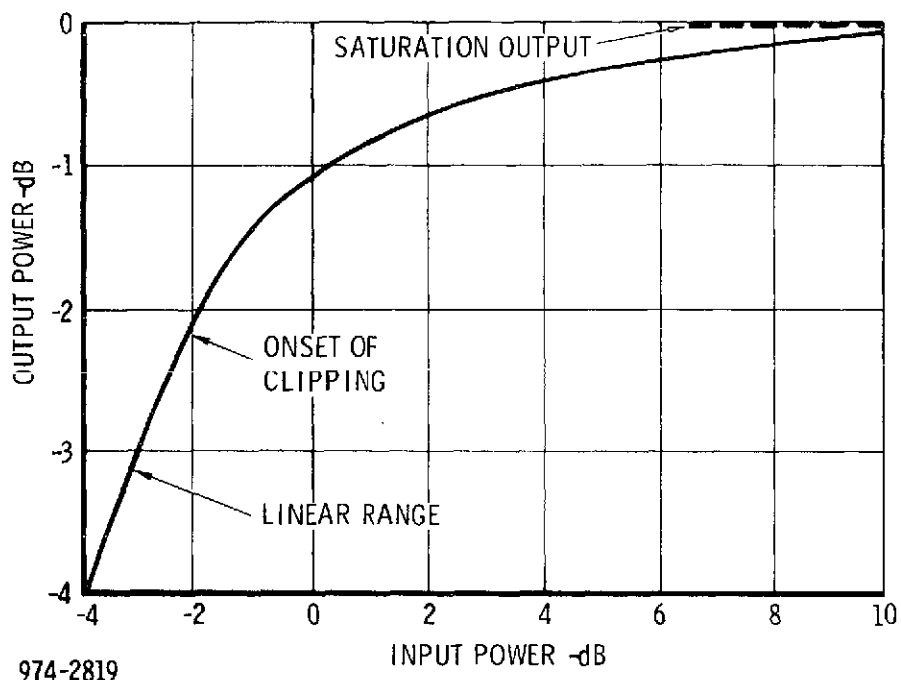


Figure 4-2. Limiter Input-Output Transfer Function

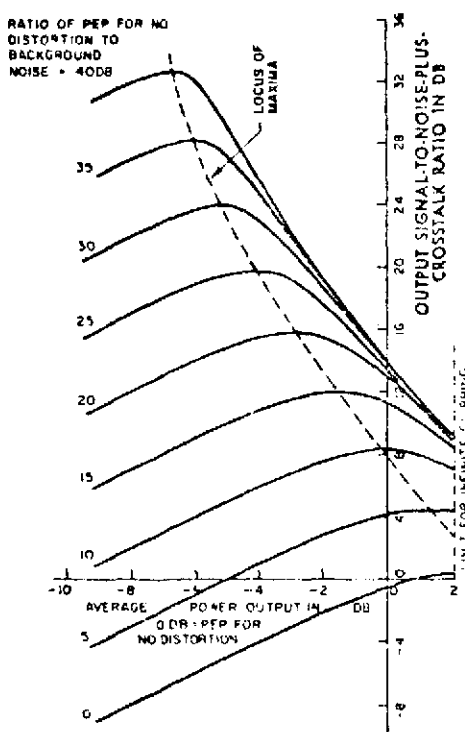


Figure 4-3. Output signal-to-total-interference ratio as function of average power output

If the TDRS-to-ground link is designed for 1 dB tandem link loss at optimum backoff, note from Figure 4-3 that the loss remains within 2 dB for backoffs ranging between 4 dB and 11 dB. Thus, the precise backoff to accommodate multiple carriers is not critical.

4.1.1.3 Accommodating Two Independent Data Signals in Limiting Channel

A Ku band user, such as the Space Shuttle, may wish to transmit two independent data signals on the return link, one conveying high data rate scientific data, the second carrying low data rate engineering data. One approach is to modulate these data streams on separate carriers. This raises the question as to the effect of a hard or soft limiting repeater channel. However, a basic consideration of intermodulation products with two carriers leads to the conclusion that they do not fall directly on the carriers.

To show the behavior analytically, we assume the signals to be considerably narrower than the channel bandwidth, so that channel filtering effects need not be brought in. As an illustration, suppose the high data rate signal is 25 Mbps and the low data rate is 200 Kbps, both within the repeater channel bandwidth of 225 MHz. Let us also assume the frequency separation of the carriers equals the bit rate on the high data rate signal, the objective being to place the narrow signal in a spectral null of the wideband signal.

Over the duration of one bit on the low rate signal, the input signal to the limiter is

$$s(t) = A \cos(\omega t + 2\pi t/T + \theta) + a \cos \omega t \quad (4-4)$$

where T is the high data rate bit duration and θ denotes the phase modulation on the high data rate signal. Without considering noise, hard limiting in the repeater channel yields an instantaneous output of

$$w(t) = \frac{s(t)}{[A^2 + a^2 + 2Aa \cos(2\pi t/T + \theta)]^{0.5}} \quad (4-5)$$

Then, coherent demodulation at the frequency ω integrating over the duration T gives

$$\begin{aligned} w &= \frac{2}{T} \int_0^T w(t) \cos \omega t dt \\ &= \frac{1}{2\pi} \int_0^{2\pi} \frac{A \cos(x + \theta) + a}{[A^2 + a^2 + 2Aa \cos(x + \theta)]^{1/2}} dx \end{aligned} \quad (4-6)$$

where $x = 2\pi t/T$.

By inspection of (4-6), we see that the integral is independent of phase modulation which holds constant over the duration T . The integral can be expressed in terms of complete elliptic integrals, as follows:

$$w = \frac{1}{\pi a} \left\{ (a - A) K \left(\frac{2\sqrt{aA}}{a + A} \right) + (a + A) E \left(\frac{2\sqrt{aA}}{a + A} \right) \right\} \quad (4-7)$$

Figure 4-4 plots (4-7) in terms of the input ratio a/A . One curve is the suppression relative to total output power of the hard limiter. The other curve is relative to output from a linear amplifier with same total output power. For $a \ll A$, the asymptotic result is

$$w = a/2A \quad (4-8)$$

which is the usual 6 dB suppression for hard limiting of a weak signal in the presence of stronger constant envelope interference. Extending the coherent demodulation over the bit duration of the low data rate signal, assumed to be a multiple of T , the result is seen to be independent of the phase modulation on the high data rate signal, despite the hard limiting in the repeater. The effect of limiting is to suppress the weaker signal by 6 dB.

Now, let us introduce noise into the limiting repeater channel. If the strong signal exceeds the noise power, the suppression of the weaker signal still occurs. Figure 4-5 presents analytical results^[4] for relative suppression of two carriers with noise present, and by the reasoning leading to (4-6), phase modulation on the carriers does not change these results. Figure 4-5 indicates that the 6 dB suppression of the weaker signal substantially occurs when the input signal-to-noise ratio in the repeater channel of the stronger signal is as low as, roughly, 4 dB. With soft limiting in the repeater channel, of course, the suppression of the weaker signal relative to the stronger is reduced.

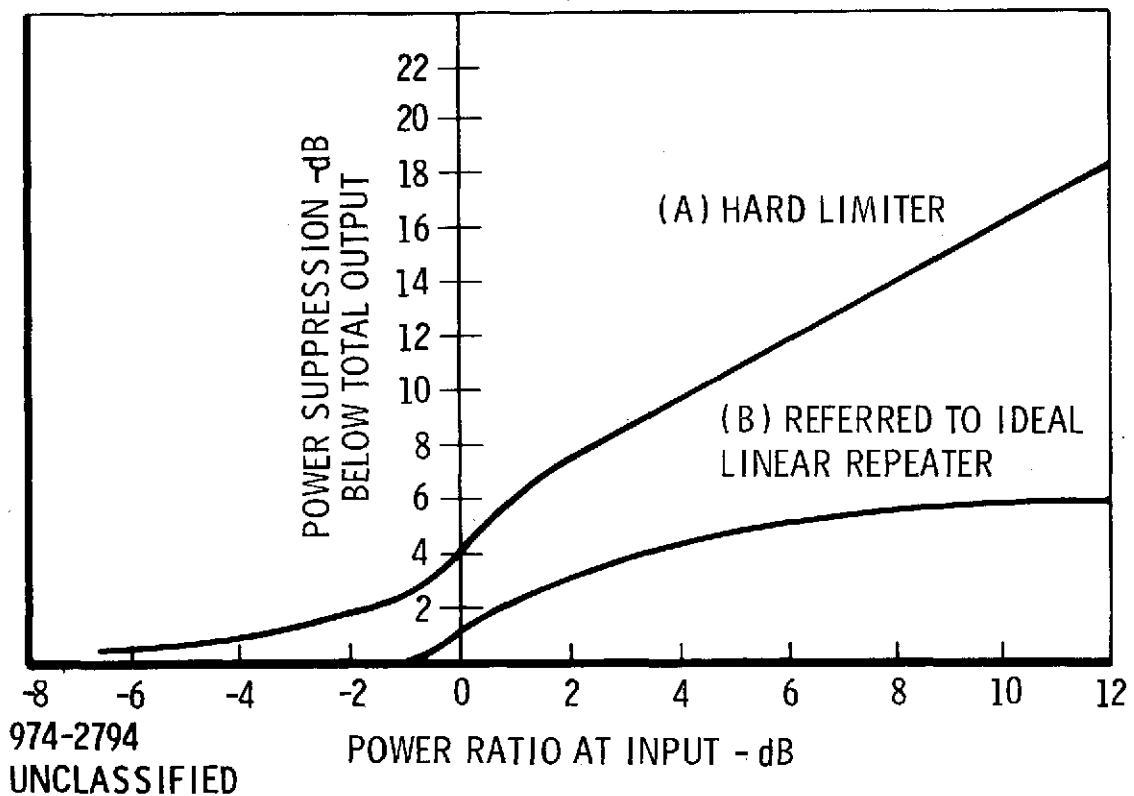


Figure 4-4. Two Constant Amplitude Signals in Hard Limiter

4.1.1.4 Conclusions

Serial data with staggered quadriphase modulation is the most efficient technique to transmit a high data rate with good bandwidth utilization through a limiting repeater channel (300Mbps in 225 MHz channel) and small EIRP penalty to the

4. J. J. Jones, "Hard-Limiting of Two Signals in Random Noise", IEEE Trans. on Info. Theory, Vol. IT-9, January 1963, pp. 34-42.

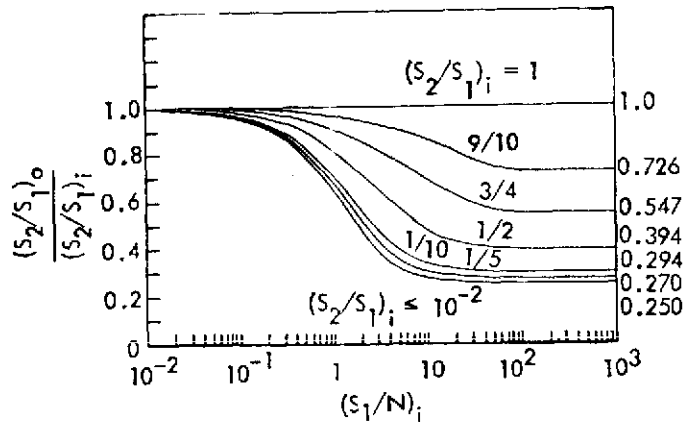


Figure 4-5. The ratio of the output signal-to-signal power ratio to the input signal-to-signal power ratio as a function of the larger input SNR

user satellite (theoretically, 0.8 dB increase in E_b/N_0 from ideal biphase or quadrature due to the intersymbol interference).

An alternate modulation approach would employ multiple carriers to transmit parallel data streams on subchannels. The main advantage of this is to eliminate the need for high speed logic to format data into a serial stream on board the user satellite. The disadvantage is the requirement to handle high peak EIRP in the user transponder transmitter (or alternatively to have multiple transmitters), and more important, a need to operate the TDRS repeater channel significantly backed off from saturation. At a maximum data rate of 300 Mbps, the repeater channel must then have a saturation output about 7 dB above the power level given in the NASA Goddard Definition Phase Report. The precise backoff is not critical, and can be controlled by an AGC circuit in the TDRS which holds a fixed average output power from the repeater channel.

As the data rate and user EIRP are decreased from the design maximum (300 Mbps and 60 dBW), a proportional backoff from the design output of the repeater channel is allowable. Furthermore, backoff is shown later in Section 5 to be desirable to reduce interference in other channels of the TDRS-to-ground link when a signal is absent from the channel. Thus, a reasonable design approach for the repeater is to set a fixed gain (possibly controllable by ground command) such that saturation output is reached for the maximum EIRP signal (corresponding to 19 dB signal-to-noise ratio in 225 MHz bandwidth).

Even with a hard limiting repeater channel, the special case of two independent data streams on separate carriers can be accommodated. Separating the two carriers by the chip rate of the high rate data stream places the low rate data signal in a spectral null (in fact, there would be complete orthogonality if the data streams were synchronous). The limiting suppresses the weaker signal by up to 6 dB but does not cause intermodulation to fall on the signal.

4.1.2 SOFT-DECISION ERROR CORRECTION

It is expected that the TDRS channel for the Ku-band return will operate at or near hard limiting for high data rates. Then, the gain associated with use of soft decisions for Viterbi error correction will be reduced from the value (2 dB over use of hard decisions) applicable to a linear channel. The problem is that the limiting occurs after the largest noise contribution on the user-to-TDRS link. Of course, the worst possibility is loss of the full 2 dB; in which case, the value of error correction becomes marginal.

4.1.2.1 Biphase Data Modulation

On the coherent Gaussian channel with symbol energy/noise γ , the probability of error for the Viterbi decoder with soft decisions and biphase modulation is approximated by

$$P_e = \frac{M}{\sqrt{2\pi}} \int_{\sqrt{2d\gamma}}^{\infty} \exp(-x^2/2) dx \approx \frac{M}{\sqrt{2\pi(2d\gamma)}} \exp(-d\gamma) \quad (4-9)$$

where M is a constant depending on the error paths and d is the minimum Hamming distance to an error path through the "trellis" describing the short constraint length convolutional error correcting code. The exponential behavior as d grows is described by

$$-\frac{1}{d} \ln P_e \approx \gamma \quad (4-10)$$

and this has been derived directly from the asymptotic approximation to the tail of the Gaussian distribution.

For other channels with the same error correcting code, we desire to find an exponential behavior for probability of error of the form

$$P_e = M \exp(-d\zeta) \quad (4-11)$$

where ζ is a function of γ . By comparing ζ with γ , the degradation with respect to the coherent Gaussian channel is obtained. Note that

$$-\frac{1}{d} \ln P_e + \zeta \quad (4-12)$$

shows how to obtain the exponent.

With bandpass hard limiting which retains phase information only, the exponential behavior is obtained by considering the sum

$$t = \sum_{i=1}^d \cos \theta_i \quad (4-13)$$

where the quantity $t_i = \cos \theta_i$ is available for each symbol. The sum in (4-13) is taken over the d symbols by which the closest error path differs from the correct path for the error correcting code. The Viterbi algorithm makes an error if $t < 0$ on an error path, where the true phase in the absence of noise is presumed to be 0 for each symbol.

The Chernoff bound^[5] is an exponential bound of the form

$$\text{Prob}\{t < 0\} \leq [E\{\exp(-\lambda_0 \cos \theta)\}]^d \quad (4-14)$$

for any $\lambda_0 > 0$, and the tightest bound is found by varying λ_0 to minimize the expectation. Then, in accordance with (4-12), the exponential behavior as d increases is given by

$$-\frac{1}{d} \ln[\text{Prob}\{t < 0\}] \geq -\ln[E\{\exp(-\lambda_0 \cos \theta)\}]_{\min} \quad (4-15)$$

5. Wozencraft and Jacobs, Principles of Communication Engineering, John Wiley, 1965, pp. 97-106.

Since the probability distribution of the random variable $\cos \theta$ depends on γ , we implicitly have the exponential behavior as a function of γ .

At a low signal-to-noise ratio, the probability density of phase is approximated by the first terms of a Fourier series, according to

$$p(\theta) \approx \frac{1}{2\pi} [1 + \sqrt{\pi\gamma} \cos \theta] \quad -\pi < \theta < \pi \quad (4-16)$$

Then,

$$\begin{aligned} E\{\exp(-\lambda_0 \cos \theta)\} &\approx \frac{1}{2\pi} \int_{-\pi}^{\pi} [1 + \sqrt{\pi\gamma} \cos \theta] \exp(-\lambda_0 \cos \theta) d\theta \\ &= I_0(\lambda_0) - \sqrt{\pi\gamma} I_1(\lambda_0) \end{aligned} \quad (4-17)$$

For $\gamma \rightarrow 0$, the λ_0 minimizing the expectation also $\rightarrow 0$, and we have the approximation to quadratic terms

$$I_0(\lambda_0) - \sqrt{\pi\gamma} I_1(\lambda_0) \approx 1 + \frac{\lambda_0^2}{4} - \sqrt{\pi\gamma} \frac{\lambda_0}{2} \quad (4-18)$$

This is minimized at $\lambda_0 = \sqrt{\pi\gamma}$, and

$$E\{\exp(-\lambda_0 \cos \theta)\}_{\min} \approx 1 - \frac{\pi}{4}\gamma \quad (4-19)$$

The tightest exponent upper bounding the probability of error then is

$$-\ln[E\{\exp(-\lambda_0 \cos \theta)\}_{\min}] \approx \frac{\pi}{4}\gamma \quad (4-20)$$

which shows a degradation of $\pi/4$ or 1.0 dB with respect to (4-10). This was the expected result at low γ .

For an arbitrary γ , the probability density of the decision variable $t = \cos \theta$ is

$$p(t) = \frac{e^{-\gamma}}{\pi \sqrt{(1-t^2)}} \left\{ 1 + \sqrt{\pi\gamma} t e^{\gamma t^2} [1 + \operatorname{erf}(\sqrt{\gamma}t)] \right\} \quad (4-21)$$

We wish to evaluate

$$E\{\exp(-\lambda_o t)\} = \int_{-1}^1 \exp(-\lambda_o t) p(t) dt \quad (4-22)$$

Numerically [6], we have the approximation

$$\int_{-1}^1 \frac{f(x)}{\sqrt{1-x^2}} dx \approx \sum_{i=1}^n \frac{\pi}{n} f(\cos((2i-1)\pi/2n)) \quad (4-23)$$

which avoids the singularities at $t = \pm 1$ in (4-21).

A numerical evaluation with $n = 256$ was carried out to find λ_o minimizing (4-21) as a function of γ . Results are given in Table 4-1, which compares the hard limiting case with the ideal coherent channel, and the degradation is plotted as a function of γ in Figure 4-6.

Table 4-1. Excess S/N With Hard Limiting

γ	Optimizing λ_o	Exponent	Degradation
2 dB	2.1	1.21	1.17 dB
4 dB	3.1	1.88	1.26 dB
6 dB	4.1	2.90	1.38 dB
8 dB	5.5	4.40	1.57 dB

The tightness of the Chernoff bound for small d may be tested by directly computing probability or error by convolution of (4-21) to give the distribution of t and the probability that $t < 0$. Numerical results are plotted in Figure 4-6 and show excellent agreement with the degradation found via the Chernoff bound. Consequently, the degradation should apply accurately to a short constraint length convolutional code, a linear metric is employed in the decoder.

6. R. W. Hamming, Numerical Methods for Scientists and Engineers, McGraw-Hill, 1962, p. 160

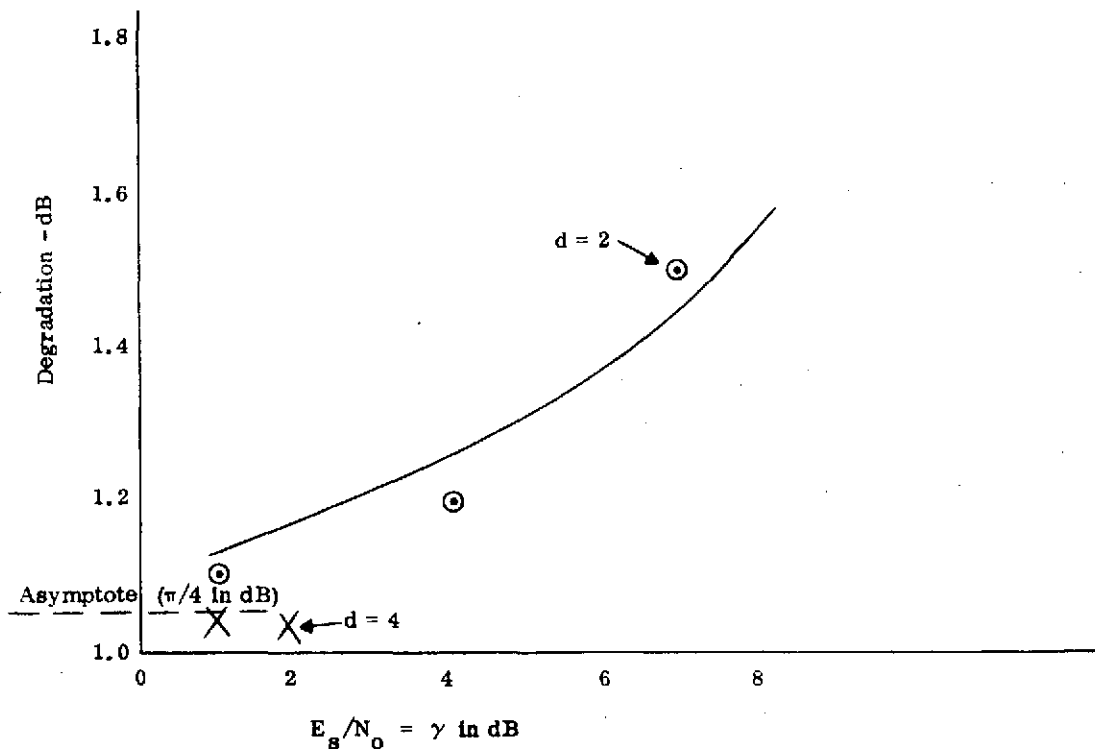


Figure 4-6. Degradation in Coding Gain Due to Limiting

4.1.2.2 Quadriphase Data Modulation

We now extend the Chernoff bound approach to quadriphase data modulation. A linear, unquantized metric is presumed, again, for decoding.

The analysis postulates two independent data streams on the respective in-phase and quadrature (I and Q) carriers, in which case the distance d of the closest code word sets the asymptotic performance. If the code word is sent alternately on I and Q, there will be some dependence of errors and the results to be obtained do not apply precisely.

After hard limiting and product demodulation say to I, the decision is made on the polarity of the sum

$$t = \sum_{i=1}^d \cos(\theta_i \pm \pi/4) \quad (4-24)$$

where the quantity $t_i = \cos(\theta_i \pm \pi/4)$ is available for each symbol and θ_i is the phase error. The choice of sign of $\pi/4$ depends on the bit in Q. The Chernoff bound on probability of error gives

$$\text{Prob}\{t < 0\} \leq [E\{\exp(-\lambda_o \cos(\theta \pm \pi/4))\}]^d ; \lambda_o > 0 \quad (4-25)$$

and the tightest bound as a function of λ_o is given by

$$-\frac{1}{d} \ln[\text{Prob}\{t < 0\}] \geq -\ln[E\{\exp(-\lambda_o \cos(\theta \pm \pi/4))\}]_{\min} \quad (4-26)$$

Because $p(\theta)$ is symmetrical, the expectation does not depend on the sign of $\pi/4$; also, staggered quadriphase (SQPSK) is affected the same as QPSK by the limiting.

At a low signal-to-noise ratio,

$$p(\theta) \approx \frac{1}{2\pi} [1 + \sqrt{2\pi\gamma} \cos \theta] \quad (4-27)$$

where γ is the symbol energy/noise ratio. (With quadriphase, the distribution of phase is specified by 2γ .) The expectation in (4-25) is

$$E\{\exp(-\lambda_o \cos(\theta + \pi/4))\} = I_o(\lambda_o) - \sqrt{\pi\gamma} I_1(\lambda_o) \quad (4-28)$$

which is the same as for the BPSK case, and the degradation is $\pi/4$ or 1.0 dB.

Note that (4-27) leads to the conclusion that a linear metric is optimum at low S/N for both BPSK and QPSK.

For an arbitrary S/N, the expectation in (4-25) is

$$\begin{aligned} E\{\exp(-\lambda_o \cos(\theta + \pi/4))\} &= \frac{1}{2\pi} \int_{-\pi}^{\pi} p(\theta) \exp\left(-\frac{\lambda_o}{\sqrt{2}} \cos \theta\right) \exp\left(\frac{\lambda_o}{\sqrt{2}} \sin \theta\right) d\theta \\ &= \frac{1}{\pi} \int_0^{\pi} p(\theta) \exp\left(-\frac{\lambda_o}{\sqrt{2}} \cos \theta\right) \cosh\left(\frac{\lambda_o}{\sqrt{2}} \sin \theta\right) d\theta \\ &= \int_{-1}^1 p(u) \exp(-\lambda'_o u) \cosh(\lambda'_o \sqrt{1-u^2}) du \end{aligned} \quad (4-29)$$

where $u = \cos \theta$ and $\lambda'_0 = \lambda_0 / \sqrt{2}$. The probability density $p(u)$ is

$$p(u) = \frac{e^{-2\gamma}}{\pi \sqrt{1-u^2}} [1 + \sqrt{2\pi\gamma} e^{2\gamma u^2} [1 + \operatorname{erf}(\sqrt{2\gamma} u)]] \quad (4-30)$$

noting again that the distribution of phase is set by 2γ with quadriphase.

A numerical evaluation with 256 points was carried out to minimize (4-29) as a function of λ'_0 , with results listed in Table 4-2. The degradation is the loss due to hard limiting, compared with soft decisions on the ideal coherent channel.

Table 4-2. Excess S/N With Hard Limiting of QPSK

γ	Optimizing λ'_0	Exponent	Degradation
2 dB	2.3	1.26	1.0 dB
4	3.3	2.02	.95
6	4.9	3.25	.88
8	7.3	5.21	.83

4.1.2.3 Computer Simulation Results

Appendix IX and X present a more detailed analysis of the hard limiting channel with biphasic or quadriphase modulations, and for the latter considers use of a nonlinear metric for the decoder. Also simulation results for Viterbi decoding are presented. Agreement with theory is obtained in that the loss due to hard limiting is less for quadriphase than for biphasic modulation. The loss is roughly 1.2 dB for biphasic and 0.8 dB for quadriphase with a linear decoder metric. With a nonlinear decoder metric, the loss for quadriphase is roughly 0.5 dB.

4.1.3 TOLERABLE CO-CHANNEL INTERFERENCE WITH QUADRIphASE

Suppose that antenna polarization multiplexing is utilized to transmit two Ku-band single access return links in a common spectrum assignment; in particular, from TDRS to ground. If the isolation between the two polarization modes is not perfect, there will be co-channel interference of one quadriphase data signal due to the residual presence of the second signal. The interference has the worst effect if it happens to be unmodulated; i.e., is CW. More generally, the interfering signal has an arbitrary time phase with respect to data bit transitions, and its interference effect is somewhat less severe.

Since the two signals originate from two separate users, it is reasonable to assume a random carrier phase relation even though the nominal carrier frequencies may be equal. The probability of error due to randomly phased CW interference has been derived ^[7] for coherent demodulation of a biphase data signal received in presence of Gaussian noise, and is shown in Figure 4-7. The parameter K_D = interference amplitude relative to desired signal. The abscissa indicates the energy per bit/noise density ratio not including the CW interference.

Figure 4-7 may also be applied to quadriphase since the receiver effectively performs two orthogonal demodulations to extract a pair of binary data signals. (In other words, quadriphase is the sum of two biphase modulated carriers, combined in phase quadrature and each having half the total power.) However, K_D now equals the interference/desired amplitude ratio multiplies by $\sqrt{2}$.

For uncoded data at $P_e = 10^{-5}$, Figure 4-7 shows that the increase in E_b/N_o due to the CW interference is negligible for $K_D = 0.1$; this corresponds to the interference being 23 dB below the desired quadriphase signal. At $K_D = 0.2$, or interference 17 dB down, the increase in E_b/N_o is about 1 dB. (This is for the worst case of no data modulation on the interfering signal.)

It is concluded that 17 dB of isolation between the two polarization modes is barely adequate provided that the quadriphase uncoded data signals are multiplexed with equal amplitudes. With error correction coding, poorer isolation could be tolerated.

7. J.N. Birch and R.H. French, Definition of Multipath/RFI Experiments for Orbital Testing with a Small Applications Technology Satellite, Final Report, Contract No. NAS9-12705, NASA-MSC, 1 December 1972.

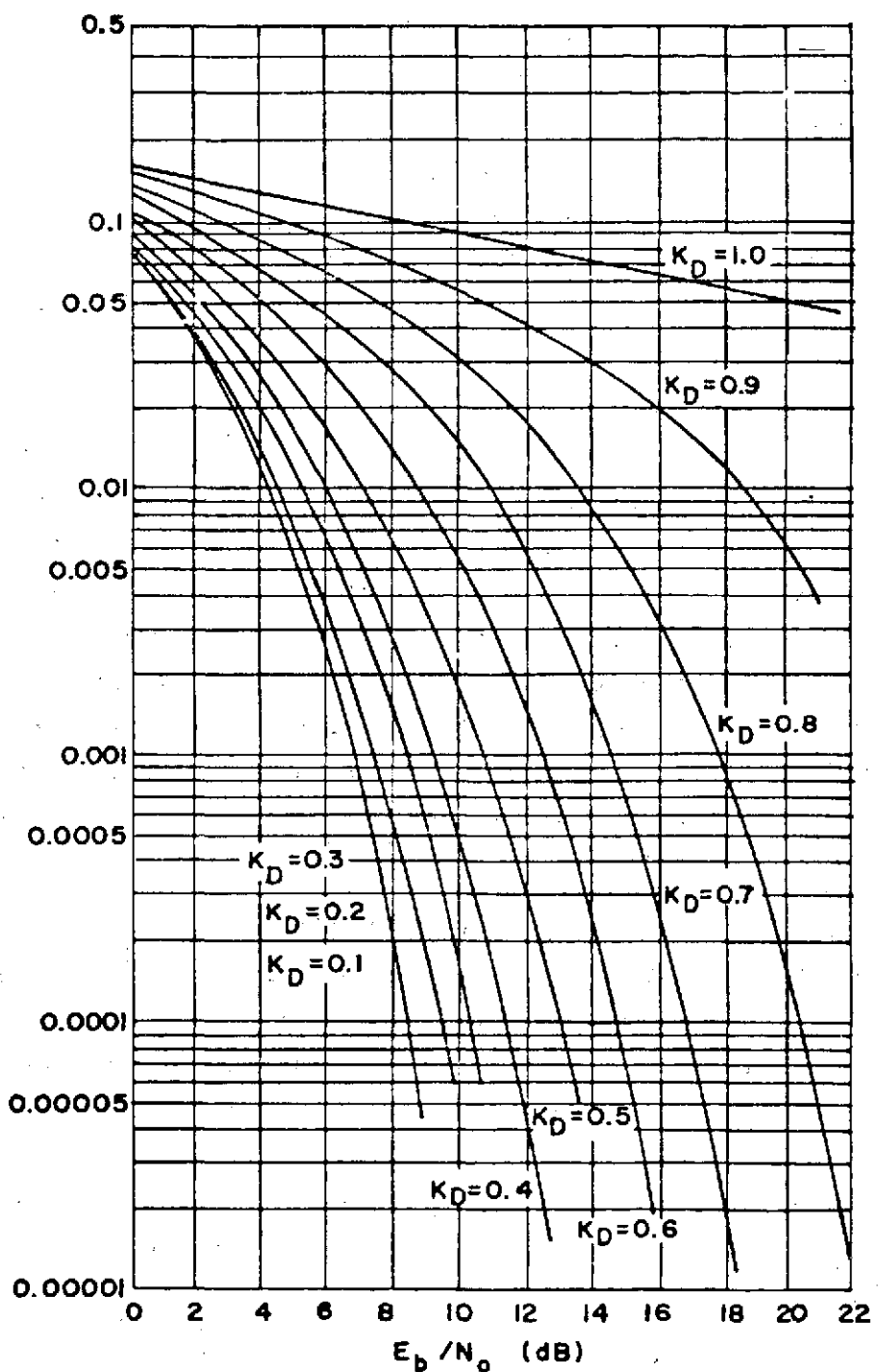


Figure 4-7. Average Binary Error Probability for Coherent PSK in the Presence of CW Interference and Gaussian Noise

4.1.4 TWO-WAY RANGING IN Ku-BAND SYSTEM

Although the current operational system concept does not require coherent transponding at Ku-band, two-way range and range rate measurement at Ku-band is likely to be a future need. Then, the problem of handling asynchronous high rate data on the return link is the same as for S-band. In addition, the problem is raised that the TDRS autotrack design, described below in Section 4.2, is predicated on a non-spread Ku-band return link signal (minimum data rate is 1 Mbps).

As suggested for S-band single access, a separate PN signal can be transmitted over the Ku-band return link. The first question to be answered is the minimum required PN signal EIRP for ranging. As at S-band, this minimum power is dictated by the requirement for an acceptable acquisition time. To compute EIRP, it is convenient to note that the user-to-TDRS links at S-band and Ku-band are almost exactly the same* with respect to signal-to-noise ratio. However, at Ku-band, the two-way Doppler uncertainty for 100 m/sec range rate error is 10 kHz. Also, we presume a spread bandwidth corresponding to 12 Mbps chip rate, so that the search aperture corresponding to a range error of 50 Km is 8000 PN chips. With EIRP = 8 dBW, the detection filter bandwidth can be about 40 kHz (scaling from Section 3.1.8.2), which comfortably encompasses the 10 kHz Doppler uncertainty. The search rate is about 1500 chips/sec (again scaling for the increased EIRP), and the acquisition time is about 5 seconds.

The minimum EIRP for a data signal is 30 dBW, corresponding to 1 Mbps (coded), according to the NASA Goddard Definition Phase Study Report. The received S/N at TDRS in 18 MHz (1.5 x PN chip rate) is 0 dB for this EIRP. Thus, the interference from the data signal in an overlapping spectrum with the PN effectively raises the noise level by 3 dB. To tolerate this increase in noise level, the required EIRP for the PN signal is thus increased to 11 dBW, which is still 19 dB below the data signal. Higher data rates on the data signal will necessitate further increases in EIRP of the PN ranging signal, but less than the increase in EIRP of the data signal.

The effect of hard limiting, as before, is to create an intermodulation product at the same level as the PN; hence, the total PN interference is 16 dB below

*Antenna gain increase compensates for free space loss increase, and the noise temperatures are nearly the same.

the data signal. Since the S/N in 18 MHz for the 1 Mbps data signal is 0 dB at the TDRS (see above), the PN is 16 dB below the noise and therefore introduces a degradation of 0.1 dB on the data performance at this 1 Mbps (coded) data rate.

Next, let us assume a data signal with EIRP = 40 dBW corresponding to 10 Mbps (coded). Now*, the S/N received at TDRS in 19 MHz is +10 dB, which requires the EIRP of the PN signal in the same 18 MHz band to be raised to 18.4 dBW. Thus, the EIRP of the PN is 21.6 dB below the data signal. After hard limiting, which creates a 3rd order intermod, the total PN interference is 18.6 dB below the data signal, or 8.6 dB below the noise in 18 MHz bandwidth. The degradation to the data signal is 0.6 dB, based on a computation which assumes the PN ranging signal lies in the same spectrum and adds to the total noise power level.

This assumption is not valid when the PN chip rate is comparable to or less than the data rate on the data signal. With hard limiting of the combined signals in the user transmitter, a better way to describe the interference by PN to the data signal is that a phase perturbation is produced on the latter. If the PN is 21.6 dB below the data signal after hard limiting, the ratio is 15.6 dB prior to limiting. The maximum phase perturbation (randomly positive or negative) is 9.6° . With a bi-phase data signal, the maximum degradation is given simply by $\cos(9.6^\circ)$, or 0.12 dB. With quadriphase, the degradation asymptotically approaches $\sin(45^\circ - 9.6^\circ) / \sin(45^\circ)$, or 1.7 dB, for low error rate (uncoded). With coding, however, it is more accurate to compute degradation at a moderate error rate. For instance, using tables of the probability distribution of phase of a carrier in Gaussian noise, we find the more representative degradation to quadriphase at 10^{-2} error rate is about 0.7 dB due to a 10° phase perturbation**.

Fixing the PN code rate at 12 Mbps, we see that further increasing the data rate (with coding) does not change the S/N received at TDRS in 18 MHz bandwidth, since the signal bandwidth broadens directly proportional to data rate, on the assumption of random data. The EIRP in the PN signal does not have to be raised above 18.4 dBW computed for 10 Mbps data, even though the EIRP in the data signal increases above 40 dBW directly proportional to data rate. It is seen, therefore,

*We assume here a quadriphase data signal with bandwidth approximately equal to the PN bandwidth.

**The computation evaluates the probability of noise shifting phase outside the correct decision sector from -35° to $+55^\circ$, and assumes one bit error in this event.

that the degradation caused by the PN ranging signal to the data signal decreases as the data rate increases above approximately 10 Mbps (coded), for the reason that the PN becomes relatively weaker as the data rate increases.

Now let us consider a maximum data rate of 120 Mbps without coding in 88 MHz bandwidth, for which the data signal has an EIRP of 56 dBW and the S/N in the 88 MHz bandwidth, or any narrower bandwidth, is 19 dB. Now, the EIRP of the PN ranging signal has to be $8 \text{ dBW} + 19 \text{ dB} = 27 \text{ dBW}$, which is 29 dB below the data signal. Assuming hard limiting in the user transmitter, the maximum phase perturbation is 4° . Taking 10^{-5} error rate as representative without coding, the degradation to quadriphase is 0.3 dB due to the 4° phase perturbation. For a maximum data rate of 300 Mbps without coding in 225 MHz bandwidth, the required EIRP of the PN ranging signal remains 27 dBW, since the S/N of the data signal is still 19 dB, but the EIRP of the data signal is 60 dBW. Now, the maximum phase perturbation is 2.5° , and the degradation to the data signal caused by the PN ranging signal is about 0.1 dB.

4.2

AUTOTRACK ANALYSIS AND IMPLEMENTATION CONCEPT

Ku-Band single access serve requires an autotrack system both on the TDRS and on the user. Both autotrack systems are analyzed in this section, and their implementations are discussed.

4.2.1 RECOMMENDED TDRS AUTOTRACK SYSTEM

Three different TDRS autotrack systems are compared in Appendix XIV on the basis of user EIRP requirements for steering the Ku-band antenna. All three are compared on the basis of pointing the Ku-band beam with a pointing loss of less than 0.5 dB. The required user EIRP for each system is found to be less than that required for user data transmission of the same bandwidth. In addition to user EIRP, the other important design considerations are size and weight of the auto-track hardware on the TDRS. All these factors are considered in this discussion to arrive at a recommended system.

4.2.1.1 Autotrack Baseline System Ku-Band, Unspoiled Beam

The autotrack system considered to be the "baseline" is the unspoiled beam Ku-band system, in which the TDRS data receive beam to be pointed is also the sum beam of the autotrack system. This system was found to have the lowest EIRP requirements of the three considered. The user EIRP required for data transmission is 20 dB greater than that required for autotrack. Some of this margin can be used to minimize the TDRS equipment, e.g., by omitting RF front end amplifiers from the autotrack difference channel receivers.

The initial pointing uncertainty of $\pm 0.45^\circ$ is not within the autotrack antenna's capture range, but a search of only one circle scan around the initial pointing direction would suffice for initial acquisition. The search can be commanded and evaluated from the ground station, causing no impact on the hardware required on the TDRS.

4.2.1.2 Ku-Band - Spoiled Beam Autotrack

Beamspoiling at Ku-band for autotrack acquisition purposes is accomplished by adding a separate Ku-band spoiled-beam feed system to the TDRS antenna. Slight offset of the autotrack feed system with respect to the data beam feed contributes an additional component of pointing error estimated to be 0.029 degrees. The

autotrack sum beam now needs a dedicated receiver, separate from the one used for the unspoiled Ku-band beam. Furthermore, the EIRP requirement computed in Appendix XIV shows only a few dB of margin compared to that required for transmission of coded data. It is felt that the additional antenna feed system, the extra Ku-band receiver, the additional offset pointing error, and the reduced power margin combined make the spoiled beam Ku-band system less attractive than the baseline unspoiled beam Ku-band autotrack system described above.

4.2.1.3 S-Band Autotrack

Since the TDRS has both S-band and Ku-band feeds, the S-band system may be used to steer the Ku-band beam. As in the above case, slight offset of the autotrack feed system with respect to the data beam feed contributes an additional component of pointing error, estimated to be 0.048 degrees. [8, Section 4.4.1.2]

Ku-band users also have S-band transmitters which, in some cases, may not need to operate at high EIRP (above +8 dBW). In order to allow the autotrack system to operate on low power S-band transmissions, the autotrack receiver bandwidth W must be made small (see Appendix XIV). As W is reduced, the autotrack system then must be modified to accommodate doppler shifts as large as ± 26 PPM, or ± 60 kHz. Thus, the S-band autotrack system forces a choice to be made of building doppler tracking receivers on the TDRS or requiring the user EIRP to be above +8 dBW at S-band.

S-band also has a peculiar RFI problem, resulting from pulsed radar transmission in Europe. Verbal communication from Mr. Jim Lytle of ESL to Dr. Charles Cahn of Magnavox has indicated that the composite effect of these radars is to cause in-band pulses received at the TDRS that are 3 to 4 microseconds in duration with an average period of 75 microseconds. The received power spectral density level is usually -141 dBW/MHz re a 0 dB gain TDRS antenna when the pulse is present, with an additional 40 dB in the case where the radar antenna happens to be pointed directly at the TDRS. The $\pm 1\sigma$ bandwidth is 10 MHz for the interference.

The TDRS S-band beamwidth is 2.33° between its 3 dB points and can illuminate a circle on the earth approximately 800 miles in diameter. If all the radars are located within the circle, then the full 36 dB antenna gain is applied, making the received level -105 dBW/MHz, with an additional 40 dB peak factor. Normal user data transmission, on the other hand, is received at about -130 dBW/MHz.

8. J. C. Pullara, et al, "Dual S- and Ku-Band Tracking Feed for a TDRS Reflector Antenna Tradeoff Study, "Martin-Marietta Aerospace Corp. Final Report (Phase I) to NASA-GSFC, July 1974.

Since the RFI is pulsed, its presence can be detected and used to open gating circuits in the sum and difference receivers to remove the RFI. This is an additional complicating subsystem for the TDRS equipment. It is felt that the combination of S-band RFI protection, doppler tracking receivers, and the additional offset pointing error makes the S-band autotrack system less attractive than the baseline unspoiled beam Ku-band autotrack system.

4.2.1.4 Summary and Conclusions for TDRS Autotrack Recommendation

The Ku-band unspoiled beam autotrack system is recommended as the system of choice for the TDRS antenna to track Ku-band users. Users with only S-band transmitters may be tracked by command from the ground station. A comparison summary of the recommended system with the S-band autotrack and spoiled beam Ku-band autotrack systems is given in Table 4-3.

4.2.2 DESIGN AND ANALYSIS OF RECOMMENDED TDRS AUTOTRACK

Section 4.2.1 recommended a Ku-band unspoiled beam autotrack system for the TDRS. This section will detail the design of the system for tracking and acquisition, and will analyze its performance.

As pointed out above, 20 dB less user EIRP is required for autotrack than is required for data. It is assumed for this design and analysis that, for the duration of user tracking, the user always transmits a signal of spectral density +30 dBW/MHz (the level required for data transmission) with a minimum bandwidth of W Hz, where W is the bandwidth of the autotrack receivers.* Some of this margin will be used to simplify the autotrack receivers by combining the azimuth and elevation difference beams in phase quadrature to share a single Δ channel receiver, and also by deleting the Δ -channel low noise RF amplifier.

4.2.2.1 Choice of Autotrack Parameters

4.2.2.1.1 Choice of Receiver Bandwidth W

The minimum Ku-band user data rate is assumed to be 10^6 bits per second, so that an autotrack receiver bandwidth of $W = 1.5 \times 10^6$ Hz will receive almost all its power. It is assumed that higher data rate users will maintain the same ratio of EIRP to data rate, so that the signal power received in $W = 1.5 \times 10^6$ Hz will be constant.

*This means quadriphase data modulator, when rate 1/2 error correction coding is being employed.

Table 4-3. Comparison Summary of Three TDRS Autotrack Alternatives

Ku-Band - Unspoiled Beam

- EIRP Margin >20 dB, which may be used to omit the low noise RF front end amplifiers from the difference channel receivers and to multiplex the difference channels into a single receiver.
- Simple initial search procedure for acquisition using ground station command and evaluation.

Ku-Band - Spoiled Beam

- Additional antenna feed system required.
- Additional low noise Ku-band receiver required for sum channel.
- Low EIRP margin; requires RF low noise amplifiers in two separate difference channels.
- Additional pointing error due to autotrack feed offset.

S-Band

- Requires doppler tracking receiver or user EIRP of more than +8 dBW.
- Pulsed RFI protection required.
- Additional pointing error due to autotrack feed offset.

The effect of doppler is most pronounced for the 1 Mbps user. The maximum doppler shift is $\pm 26 \times 10^{-6}$ of the carrier frequency, or ± 390 kHz. The worst case doppler loss is

$$L = 10 \log_{10} \left(\frac{1.5 - 0.39}{1.5} \right) = -1.3 \text{ dB}$$

A higher value of W would reduce the doppler loss, but would also allow more noise power into the autotrack receiver without additional signal power for the 1 Mbps user. Thus,

$$W = 1.5 \times 10^6 \text{ Hz} \quad (4-31)$$

is selected as the bandwidth for the autotrack receivers. The user EIRP requirement is +30 dBW in the 1.5 MHz autotrack receiver band.

4.2.2.1.2 Choice of Servo Loop Noise Bandwidth

The analysis of Appendix XIV indicates that with a TDA front end and $W = 1.5 \times 10^6$, the optimum noise bandwidth is $b_n = 0.75$ Hz. Extrapolating from those results, a higher noise figure receiver as suggested here would result in a smaller optimum noise bandwidth. Furthermore, with an antenna structure that resonates at 1 Hz, a safe choice for servo loop noise bandwidth would be

$$b_n = 0.5 \text{ Hz} \quad (4-32)$$

4.2.2.2 Loss Due to Beampointing Error

The most important sources of pointing error are:

- a. offset errors due to slight misalignment of the autotrack feed system from the data beam feed system, and due to precomparator and post-comparator amplitude and phase imbalance,
- b. dynamic servo tracking error,
- c. received noise bias error due to precomparator amplitude imbalance, and
- d. variance in the pointing angle due to receiver noise.

The total beampointing error will be determined by adding these four components. The sum will use three times the noise variance, so that with Gaussian jitter the resulting pointing accuracy is obtained 99.9% of the time.

4.2.2.2.1 Offset Error

A recent report [8] has delineated and quantified the sources of offset error. Using the autotrack sum channel for the data signal as well means that there are no significant feed system offset errors. The only offset error contributors are precomparator amplitude and phase imbalance and post-comparator phase imbalance between the sum and different receivers.

The effect of these contributors gives an offset error $\Delta\theta$ determined by the formula [8, p.A-21]

$$\frac{\Delta\theta}{\theta_B} = 0.183 \left(\frac{\theta_B}{\theta_q} \right) \ln \left\{ \left| \frac{A_2}{A_1} \right| \left[-\sin\alpha \tan\beta + \sqrt{1 + \sin^2\alpha \tan^2\beta} \right] \right\} \quad (4-33)$$

where $|A_2/A_1|$ is the ratio of precomparator amplitudes

α is the precomparator phase difference

β is the post-comparator phase difference

θ_B is the 3 dB beamwidth of each of the squinted autotrack beams

θ_q is the squint angle.

$\Delta\theta$ is maximized when $|A_2/A_1| < 1$ and $\alpha\beta > 0$. Thus, as a worst case we have from

$$|A_2/A_1| = 0.954 \text{ (0.4 dB imbalance)} \quad (4-34)$$

$$\alpha = 15^\circ$$

$$\beta = 20^\circ$$

Using (4-34) in (4-33) with $\theta_B/\theta_q = 2$ gives

$$\Delta\theta/\theta_B = 0.0521 \quad (4-35)$$

$$\text{with } \theta_B = 0.35^\circ$$

$$\Delta\theta = 0.0182^\circ$$

4.2.2.2.2 Dynamic Servo Lag Error

From Appendix XIV, the worst-case dynamic servo lag is

$$\theta_L = K_{2\max}/4b_n \quad (4-37)$$

where $K_{2\max} = 0.0127$ deg/sec is the maximum angular velocity to be tracked, and b_n is the servo loop noise bandwidth in Hz. From (4-32) and (4-37)

$$\theta_L = 0.00635 \text{ degrees} \quad (4-38)$$

4.2.2.2.3 Noise Bias Error

The control signal bias error caused by noise received at the antenna and a precomparator amplitude imbalance of 0.4 dB is found in Appendix XIV to be

$$\overline{\theta} = 3.17 \times 10^{-2} \theta_B \frac{kWT_A}{P_S} \quad (4-39)$$

where $\theta_B = 0.35^\circ$ is the 3 dB beamwidth of each of the squinted beams
 $k = 1.38 \times 10^{-23}$ watts/Hz/°K

T_A = antenna noise temperature in °K

P_S = effective sum beam signal power in watts

Table 4-4 shows the computation of P_S/kWT_A for the Δ -channel to be

$$P_S/kWT_A = 5.62 \quad (4-40)$$

As a worst case, we assume the same value to hold for the Σ -channel, whence

$$\overline{\theta} = 0.0020 \text{ degrees} \quad (4-41)$$

4.2.2.2.4 Noise Variance

The noise variance is given in Appendix XIV as

$$\sigma_\theta = \theta_B \sqrt{\frac{0.52kT_R b_n}{P_S} \left(1 + \frac{kWT_R}{P_S}\right)} \quad (4-42)$$

where T_R is the total receiver noise temperature in °K. In Table 4-4, P_S/kWT_R is determined for the Δ -channel to be

$$P_S/kWT_R = 0.19 \quad (4-43)$$

As a worst case, we assume the same value to hold for the Σ -channel whence

$$\sigma_\theta = 0.00083 \quad (4-44)$$

Table 4-4. Signal and Noise Power Computations

SIGNAL

User EIRP in W = 1.5 MHz	+30 dBw
Doppler loss	-1.3 dB
Space loss*	-209.2 dB
Pointing loss*	-0.5 dB
Polarization loss*	-0.5 dB
Line losses*	-2.0 dB
Antenna gain*	+52.6 dB
Quadrature Δ -channel combiner loss	-3.0 dB
RF-IF conversion loss in Δ -channel	-10 dB
Effective autotrack sum channel power, $10 \log_{10} P_S$ (worst case with inclusion of Δ -channel losses)	-143.9 dBw

NOISE

Paramp Receiver noise temperature at receiver front end*	450° K
Paramp noise temperature	100° K
Antenna noise temperature at receiver front end less 10 dB converter loss, T_A	35° K
IF front end noise temperature	1000° K
Total receiver noise temperature, T_R	1035° K
$10 \log_{10} kWT_A$	-151.4 dBW
$10 \log_{10} kWT_R$	-136.6 dBW

SIGNAL-TO-NOISE RATIOS

$$10 \log_{10} P_S - 10 \log_{10} kWT_A = -143.9 + 151.4 = 7.5 \text{ dB} \rightarrow P_S/kWT_A = 5.62$$

$$10 \log_{10} P_S - 10 \log_{10} kWT_R = -143.9 + 136.6 = -7.3 \text{ dB} \rightarrow P_S/kWT_R = 0.19$$

*Refer to GSFC Definition Phase Study Report of the TDRSS, Table 3-2.

4.2.2.2.5 Total Pointing Error

The total pointing error is determined from (4-36), (4-38), (4-41) and (4-44) to be

$$\begin{aligned}\theta_e &= \Delta\theta + \theta_L + \theta + 3\sigma_\theta \\ &= 0.029 \text{ degrees}\end{aligned}\quad (4-45)$$

Assuming a Gaussian shaped beam, this pointing error corresponds to a pointing loss of

$$\begin{aligned}L_p &= 10 \log_{10} [e^{-2.773(\theta_e/\theta_B)^2}] \\ &< 0.1 \text{ dB}\end{aligned}\quad (4-46)$$

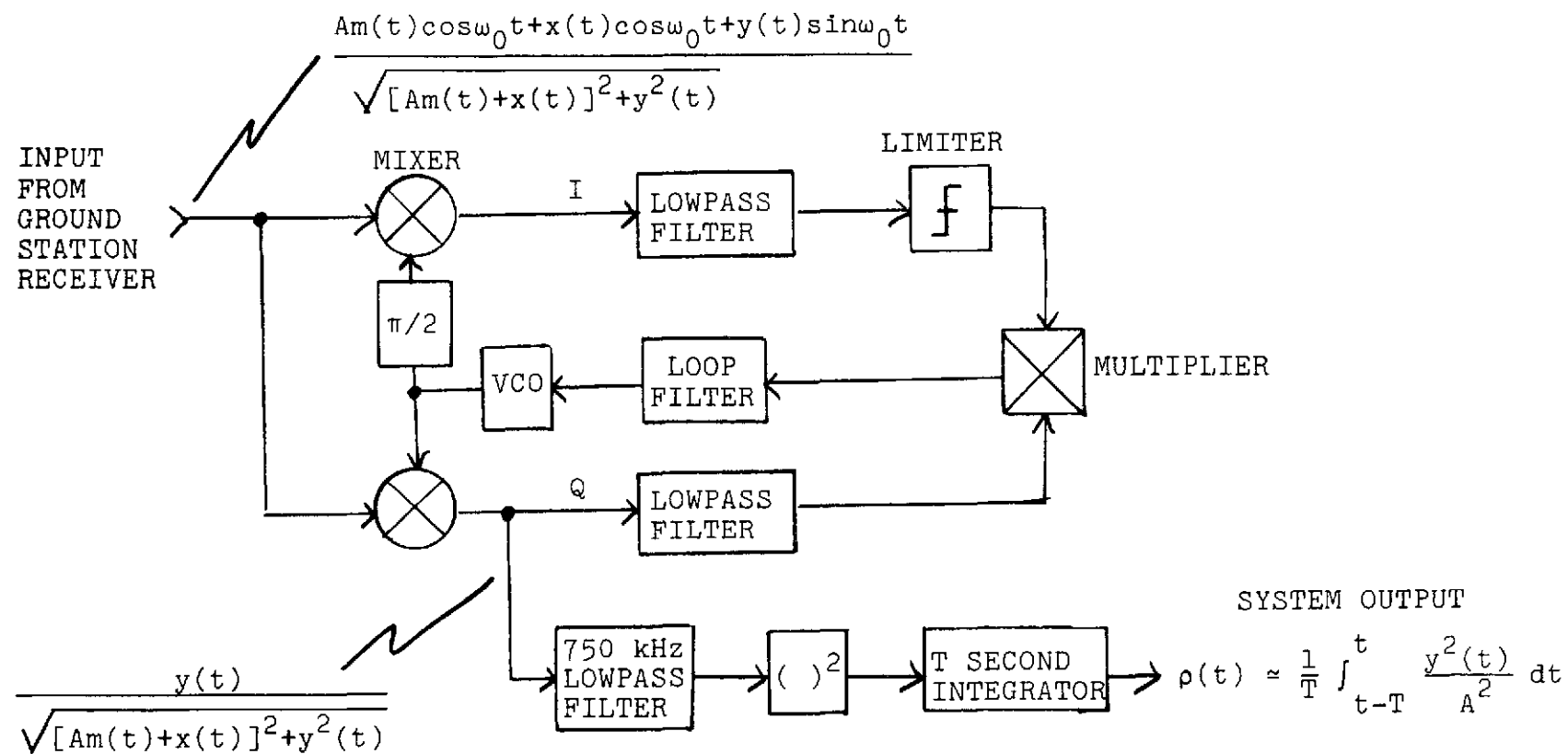
4.2.2.3 Autotrack Acquisition

Initial acquisition is begun by a ground station command to the TDRS antenna to steer in the direction of the user. The autotrack range is conservatively $\pm\theta_B$, which is not sufficient to encompass the initial uncertainty of $\pm 0.45^\circ$. Thus, a short search procedure is used to reduce the pointing error to within the autotrack range.

The beampointing error during the search could be determined by measuring received user power at the TDRS. Instead, a ground station measurement is recommended to minimize the TDRS equipment. Since the user signal is hard-limited when relayed by the TDRS, a power measurement at the ground station serves no purpose. Instead, measurement of the phase noise (and hence noise-to-signal ratio) in a Costas loop demodulator is recommended, as shown in Figure 4-8.

Figure 4-8 is diagrammed with a 750 kHz wide filter preceding a square law device and integrator for noise power measurement. The 750 kHz bandwidth is commensurate with the minimum user bandwidth of 1.5 MHz. The system output ρ is monitored as a function of search position, and the correct location is determined to be that for which ρ is minimum. After the search, the beam is commanded to return to that position and autotrack is begun.

One possible search pattern commanded by the ground station is shown in Figure 4-9. The TDRS beam center is steered in a circle around its initial commanded position in the center of the figure, with the beam center following the path



$Am(t)\cos\omega_0 t$ = biphasic PSK signal

$m(t)$ = sequence of ± 1 's

$x(t)\cos\omega_0 t + y(t)\sin\omega_0 t$ = bandpass Gaussian noise process

Figure 4-8. Block Diagram of Ground Station Costas Loop for Measuring Beampointing Accuracy

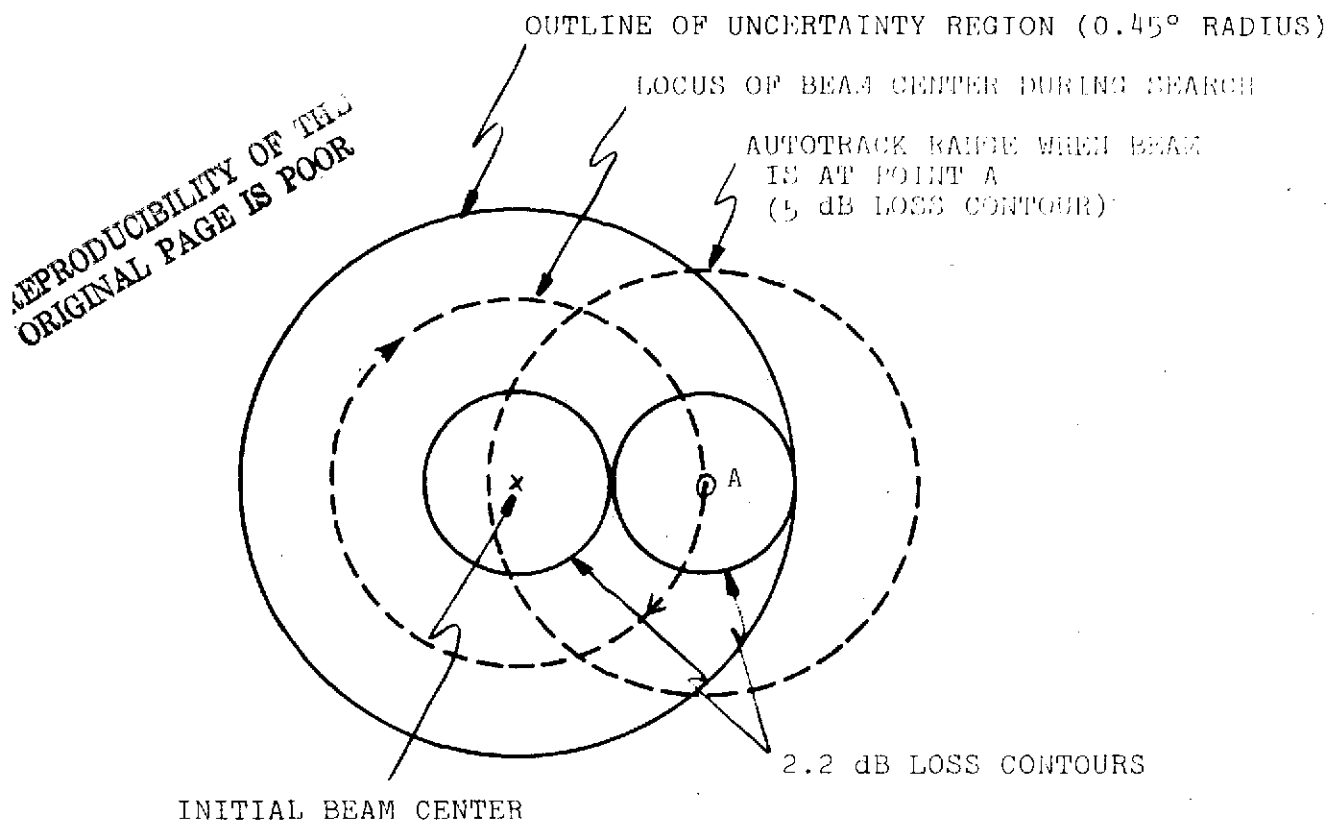


Figure 4-9. Diagram of Initial Autotrack Search for User Position

as shown. The beam covers the uncertainty region so that every point is examined within 2.2 dB of the beam peak. The total path length used for the search is

$$\theta_S = \frac{2}{3} (0.45^\circ) (2\pi) \quad (4-47)$$

$$= 0.19^\circ$$

Assuming an antenna velocity of 1 degree/sec, the total search time is

$$T_S \approx 2 \text{ seconds}$$

The pointing time is at most an additional 1 second after the search is completed. In addition, there is 0.15 second propagation delay on the search command and on the search readout and on the final pointing command. Thus, the total acquisition time is 3.45 sec. This seems to be a small addition to the initial command response time which could be as large as 30 seconds.

An analysis of the acquisition probability is done in Appendix XV. It is shown there that the acquisition probability exceeds 0.99999.

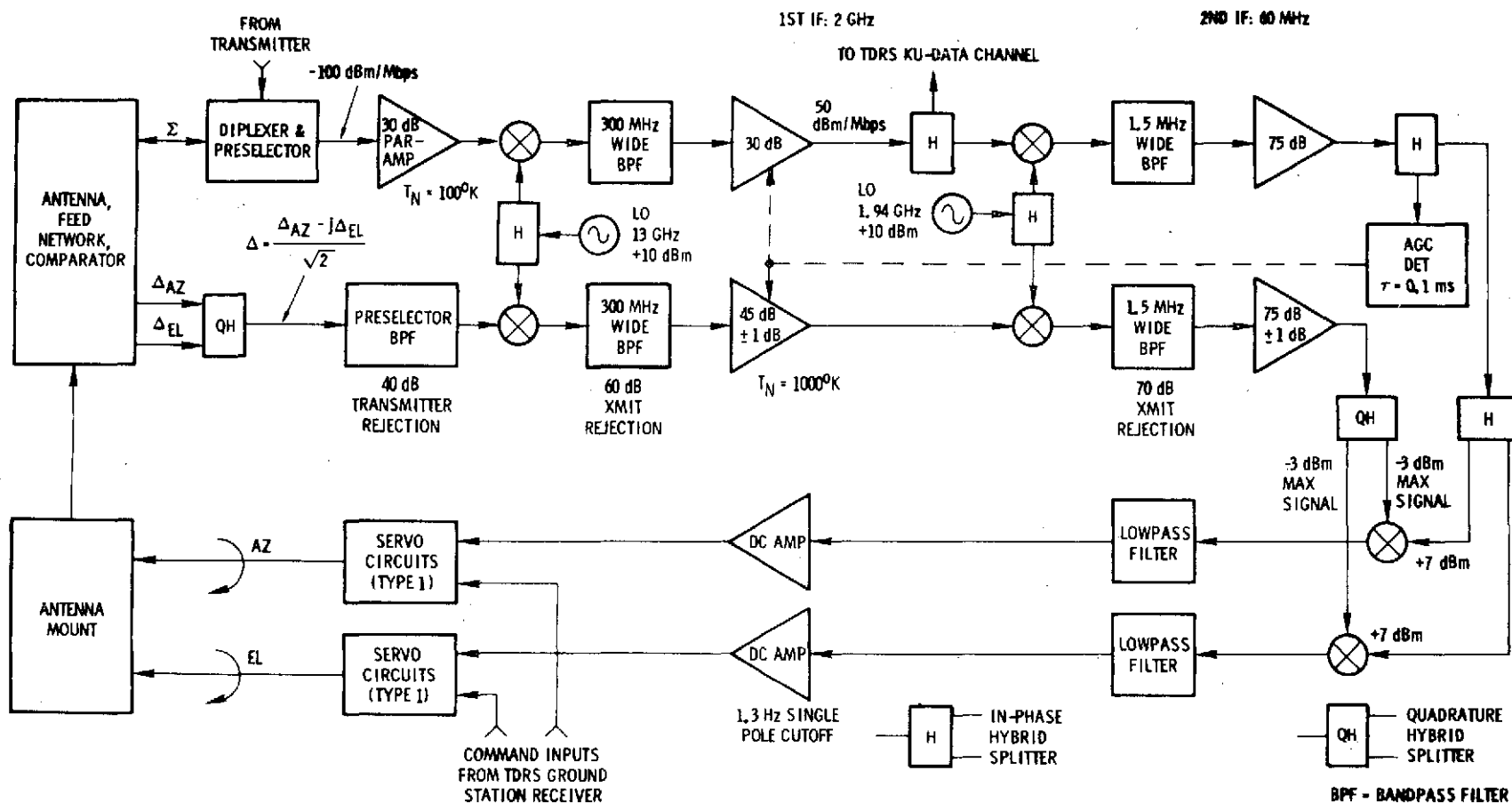
4.2.2.4 TDRS Autotrack System Block Diagram

An annotated block diagram of the recommended TDRS autotrack system is given in Figure 4-10. It shows two channels, one for the Σ -beam, which is also the Ku-band data beam, and one for the quadrature-multiplexed Δ -beams. Quadrature multiplexing of the two Δ -channels can be used since the Σ -channel signal is fully coherent with both Δ -channel signals. It may later be used as a coherent reference to demultiplex the two quadrature channels.

Two IF's are used in the design, 2 GHz and then 60 MHz, to allow gains to be distributed, circumventing oscillation problems. The IF's were chosen to allow reasonable Q values of the bandpass filters shown. The data channel is separated from the autotrack Σ -channel after 2 GHz amplification. The Σ - and Δ -channels must, of course, be phase matched across the 1.5 MHz second IF band.

The Σ -channel is received from the Σ -comparator output through a diplexer at a level of -100 dBm/Mbps. A low noise (100° K) 30 dB gain parametric amplifier is used followed by an RF-IF₁ down-conversion to 2 GHz. At this point the signal is filtered with a 300 MHz wide bandpass filter to reject transmitter leakage, spurious signals, and broadband noise, while passing data signals as wide as 225 MHz. After 30 dB of IF amplification, the signal level is up to -50 dBm, at which point the data signal is separated. A second downconversion to 60 MHz allows 1.5 MHz wide bandpass filtering, followed by 75 dB of gain, giving a +7 dBm drive level to the autotrack phase detector mixers. The 75 dB amplifier also feeds an AGC detector to keep constant the Σ and Δ signal levels. The AGC detector time constant is chosen to be 0.1 ms, much faster than system time constants in search (1.3 ms) or tracking (\approx 2 sec), yet many times the reciprocal of the 1.5 MHz predetection bandwidth.

The Δ -channel receiver chain has similar frequency conversions and filtering as the Σ -channel receiver chain. However, its gain distributions are different. First, in the interest of economy, there is no Ku-band amplifier. The 75 dB amplifier at 60 MHz is the same as in the Σ -channel and the total Δ -channel gain is chosen to make the maximum Δ -level into the phase detector mixers -3 dBm (at the edge of the autotrack range). This ensures linear operation of the mixers for the Δ -input, while giving a maximum DC output of about 140 mV. This level is



974-2795

UNCLASSIFIED

Figure 4-10. Block Diagram of TDRS Autotrack System

over 40 dB above good DC amplifier offset levels, so that a 40 dB Δ -beam null may be achieved. The 45 dB second IF amplifier achieves this desired Δ -channel gain level. Since Δ -channel gain variations are not corrected by the AGC, the two Δ -channel amplifiers are allowed to vary ± 1 dB each, contributing ± 2 dB variation to the autotrack loop gain.

An important function of the filters in both the Σ - and Δ -channels is rejection of the 1 watt Ku-band transmitter. The minimum required rejection levels are noted on the diagram to keep the transmitter signal from saturating mixers and amplifiers and from interfering with the autotrack control.

The Δ -channel is split in a quadrature hybrid to regain the Δ_{AZ} and Δ_{EL} signals, which are then separately phase detected against the Σ -channel reference. The resulting DC voltages are amplified with a single pole lowpass cutoff of $f_0 = 1.3$ Hz, determined from Equation (27) of Appendix XI.

$$f_0 = \frac{\omega_0}{2\pi} = \frac{16b_n}{2\pi} = 1.3 \text{ Hz} \quad (4-48)$$

The DC amplifier outputs are then used to control the azimuth and elevation servos, which each have a single pole at the origin (type 1 system).

4.2.2.5 APC Modification

The analysis of Section 4.2.2.2 uses an assumption [8, p 4-51] for the maximum phase imbalance between the Σ -receiver and the Δ -receiver of 20° . Subsequent communication with L. Deerkoski and P. Dalle-Mura of NASA-GFSC has indicated that NASA's experience does not support this assumption when a paramp receiver is used.

An automatic phase control (APC) loop is described in Appendix XIII to compensate for the problem of phase drift in the Σ -channel paramp. With this type of modification to the system, the performance calculations remain valid.

4.2.3 TDRS AUTOTRACK SCENARIO AND REQUIREMENTS ON USER

The following scenario is described for establishing and maintaining the communications link between the TDRS and a Ku-band single-access user.

a. The ground station commands the TDRS to point its antenna at the user.

b. The TDRS steers its antenna to within an uncertainty region of 0.45 degrees in radius.

c. Either (a) the user continually maintains its antenna pointed at the TDRS, or (b) the ground station commands the user via TDRS S-band relay to point at the TDRS and turn on its Ku-band transmitter. (This requires an S-band omnidirectional antenna on the user.)

d. The user transmits a Ku-band signal to the TDRS (EIRP = +32 dBW in the 1.5 MHz TDRS autotrack band) for the TDRS autotrack search procedure. The search is controlled and evaluated by the ground station.

e. After the TDRS antenna alignment toward the user to 0.5 dB pointing loss, then on command from the ground station, the TDRS transmits a Ku-band signal to the user for user autotrack.

f. After the user autotrack acquisition is complete, the ground station determines if link performance is acceptable and notifies the user to start data transmission. Data transmission begins.

g. Both the TDRS and the user maintain Ku-band transmission as long as autotrack is to be maintained. The user transmission must be a signal (data or otherwise) with +32 dBW of EIRP within the 1.5 MHz TDRS autotrack band. The TDRS must transmit a signal of +43.5 dBW in the 7.5 MHz user autotrack band.

4.2.4 USER AUTOTRACK

4.2.4.1 S-Band Autotrack for Ku-Band Beamsteering

There are a number of contributors to the Ku-band beampointing error in an S-band autotrack system: dynamic servo lag, antenna noise bias error with comparator gain imbalance and/or nonisotropic noise, noise variations on the control signal, autotrack feed offset relative to the Ku-band feed, and offset due to precomparator amplitude and phase imbalance and post-comparator phase imbalance. It will be shown that the imbalances assumed make the pointing error due to the last contributor listed so large, that it disqualifies an S-band autotrack system for pointing a Ku-band beam.

The imbalance offset error is given by (4-49)

$$\frac{\Delta\theta}{\theta_B} = 0.183 (\theta_B/\theta_q) \ln \left\{ \left| A_2/A_1 \right| \left[-\sin\alpha \tan\beta + \sqrt{1+\sin^2\alpha \tan^2\beta} \right] \right\} \quad (4-49)$$

where $|A_2/A_1|$ is the ratio of precomparator amplitudes

α is the precomparator phase difference

β is the post-comparator phase difference

θ_B is the 3 dB beamwidth of each of the squinted autotrack beams

θ_q is the squint angle.

is maximized when $|A_2/A_1| < 1$ and $\alpha\beta > 0$. Thus, as a worst case we have

$$\begin{aligned} |A_2/A_1| &= 0.954 \text{ (0.4 dB imbalance)} \\ \alpha &= 5^\circ \\ \beta &= 20^\circ \end{aligned} \tag{4-50}$$

Using (4-50) in (4-49) with $\theta_B/\theta_q = 2$ gives

$$\Delta\theta/\theta_B = 0.0295 \tag{4-51}$$

With a pointing error θ_e , the Ku-Band pointing loss, assuming a Gaussian-shaped beam, is

$$L_P = -10 \log_{10} [e^{-2.773 (\theta_e/\theta_b)^2}] \text{ in dB} \tag{4-52}$$

where

$$\theta_b = \left(\frac{2106.4 \text{ MHz}}{13,775 \text{ MHz}} \right) \theta_B \tag{4-53}$$

is the Ku-band half-power beamwidth. Using (4-53) in (4-52) gives

$$L_P = -10 \log_{10} [e^{-118.6 (\theta_e/\theta_B)^2}] \text{ in dB} \tag{4-54}$$

Using $\theta_e = \Delta\theta$, as given in (4-51) results in a pointing loss of

$$L_P = 0.45 \text{ dB} \tag{4-55}$$

If a total pointing loss of 0.5 dB is required, there remains only 0.05 dB of allowable pointing loss due to all the other sources. Thus, S-band autotrack for steering the Ku-Band beam is not considered a feasible approach.

Further efforts on the user autotrack design will concentrate on the unspoiled Ku-band approach.

4.2.4.2 Analysis and Design of Ku-Band User Autotrack

TDRSS Ku-band users are required to point their Ku-band transmit beams at the TDRS with an accuracy that maintains the autotrack beampointing loss below 0.5 dB. This requirement implies, for a Gaussian-shaped beam, that the pointing error can be no more than 20% of the half-power two-sided beamwidth. No data are received by the user at Ku-band, so that a low noise Σ -channel receiver is not required.

It is assumed that the user can initially point his antenna to be within its 3 dB beamwidth, which is within the autotrack range. From that point, the autotrack system will reduce the pointing error so that the pointing loss is less than 0.5 dB.

In the interest of hardware simplicity, no Ku-band amplifiers will be used in the autotrack receivers. Furthermore, quadrature multiplexing of the azimuth and elevation Δ -signals will be employed so that a single Δ -channel receiver can be used.

4.2.4.2.1 Tracking Error Analysis

The following tracking error components must be considered:

a. **Dynamic Servo Lag.** The angular velocity which the user antenna must track has two components: the angular velocity due to user positional motion relative to TDRS (0.0127 deg/sec max) and the angular velocity due to user spin relative to TDRS. The user orientation is assumed fixed relative to earth center, so that relative to TDRS, the maximum value of the second component is 360°/orbit period. The shortest period is 90 minutes for HEAO, so the maximum value of the second angular velocity component is 0.0667 degrees/second. The two components combined produce a maximum angular velocity of 0.0794 degrees/second. For a type "1", critically damped autotrack servo system of noise bandwidth b_n , the dynamic servo lag error from Appendix XI is

$$\theta_L = \frac{0.0794}{4b_n} = 1.985 \times 10^{-2} / b_n \text{ degrees} \quad (4-56)$$

b. **Noise bias error.** For isotropic received noise, the noise bias due to a 0.4 dB gain imbalance in the autotrack comparator is determined in Appendix XIV to be

$$\overline{\theta}_I = 3.14 \times 10^{-2} \theta_B \frac{kWT_A}{P_S} \text{ degrees} \quad (4-57)$$

where θ_B is the full 3 dB beam width of each of the Ku-band squinted beams,

k is Boltzmann's constant (1.38×10^{-23} watts/ $^{\circ}$ K/Hz)

W is the bandwidth of the autotrack receivers in Hz

T_A is the antenna noise temperature in $^{\circ}$ K

P_S is the received signal power in the sum channel in watts

c. Noise variance. From Appendix XIV,

$$\sigma_{\theta} = \theta_B \sqrt{\frac{0.52kT_R b_n}{P_S} \left(+ \frac{kWT_R}{P_S} \right)} \text{ degrees} \quad (4-58)$$

d. Offset Error. With the autotrack sum channel used for the Ku-band data transmission as well, there are no significant feed offset errors. The only significant offset error contributors are precomparator amplitude and phase imbalance, and postcomparator phase imbalance between the sum and difference receivers. The resulting offset error $\Delta\theta$ is determined by

$$\frac{\Delta\theta}{\theta_B} = 0.183 \left(\frac{\theta_B}{\theta_q} \right) \ln \left| \frac{A_2}{A_1} \right| \left[-\sin\alpha \tan\beta + \sqrt{1 + \sin^2\alpha \tan^2\beta} \right] \quad (4-59)$$

where $|A_2/A_1|$ is the ratio of precomparator amplitudes

α is the precomparator phase difference

β is the post-comparator phase difference

θ_q is the autotrack beam squint angle.

$|\Delta\theta|$ is maximized when $|A_2/A_1| < 1$ and $\alpha\beta > 0$. Thus, as a worst case, we have [8, p 4-51]

$$|A_2/A_1| = 0.954 \text{ (0.4 dB imbalance)} \quad (4-60)$$

$$\alpha = 15^{\circ}$$

$$\beta = 20^{\circ}$$

Using (4-60) in (4-59) with $\theta_B/\theta_q = 2$ gives

$$|\Delta\theta/\theta_B| = 0.052 \text{ degrees} \quad (4-61)$$

The total tracking error θ_e is determined by combining the four components in (4-56), (4-57), (4-60) and (4-61). The combination will use $3\sigma_\theta$ so that with Gaussian jitter, the required pointing accuracy is maintained at least 99.6% of the time. Thus, we have

$$\theta_e = \theta_L + \theta_I + 3\sigma_\theta + \Delta\theta$$

or

$$\theta_e = \frac{1.985 \times 10^{-2}}{b_n} + 3.14 \times 10^{-2} \theta_B \frac{kWT_A}{P_S} + 3\theta_B \sqrt{\frac{0.52kT_R b_n}{P_S} (1 + \frac{kWT_R}{P_S})} + 0.052\theta_B \quad (4-62)$$

The pointing error in (4-62) will be determined as a function of user antenna diameter for the low TDRS EIRP level (+43.5 dBW). For meeting the flux density requirements, it is assumed that the TDRS transmission is spread over a 7.5 MHz bandwidth. The autotrack receiver bandwidth W will be made equal to the spread bandwidth,

$$W = 7.5 \times 10^6 \text{ Hz} \quad (4-63)$$

The effects of doppler (± 390 kHz maximum) may be neglected for this wide a bandwidth.

The received signal power as the user antenna output is one-fourth that of the high TDRS EIRP level. From the TDRSS Definition Phase Study Report, the received signal power is related to the user antenna gain by:

$$\begin{aligned} P_A &= 1.09 \times 10^{-16} G_A / 4 \\ &= 2.74 \times 10^{-17} G_A \text{ watts} \end{aligned} \quad (4-64)$$

Allowing 3 dB for multiplexing the Δ -channels and 10 dB for mixer conversion and other losses before the first IF amplifier, we have

$$\begin{aligned} P_S &= P_A / 20 \\ &= 1.37 \times 10^{-18} G_A \text{ watts} \end{aligned} \quad (4-65)$$

The user antenna gain is assumed to be related to its beamwidth by [9]

$$G_A = 27,000/\theta_B^2 \quad (4-66)$$

so that

$$P_S = 3.70 \times 10^{-14} / \theta_B^2 \text{ watts} \quad (4-67)$$

Using the same noise temperatures as in Section 4.2.2, we have

$$\begin{aligned} T_A &= 35^\circ \text{ K} \\ T_R &= 1035^\circ \text{ K} \end{aligned} \quad (4-68)$$

We then have from (4-63), (4-67) and (4-68)

$$\begin{aligned} kWT_A/P_S &= 9.79 \times 10^{-2} \theta_B^2 \\ kWT_R/P_S &= 2.89 \theta_B^2 \end{aligned} \quad (4-69)$$

Using (4-69) in (4-62) with $b_n = 0.5$ Hz gives

$$\theta_e = 0.0398 + 3.07 \times 10^{-3} \theta_B^3 + 9.50 \times 10^{-4} \theta_B^2 \sqrt{1 + 2.89 \theta_B^2} + 0.052 \theta_B \quad (4-70)$$

The Ku-band beampointing loss resulting from the pointing error θ_e in (4-70) is, assuming a Gaussian-shaped beam,

$$L_P = -10 \log_{10} [e^{-2.773 (\theta_e/\theta_B)^2}] \quad (4-71)$$

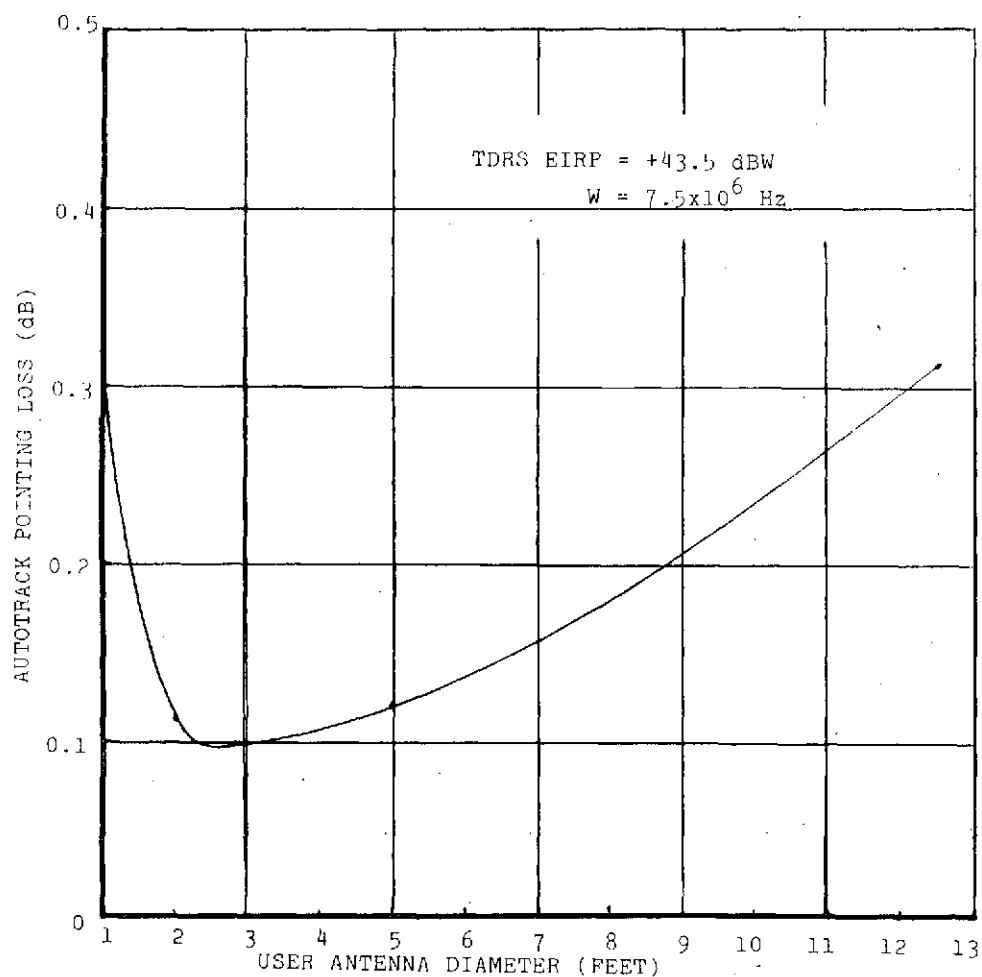
The antenna diameter D is assumed to be related to the beamwidth by [9]

$$\begin{aligned} D &= 65\lambda/\theta_B \\ &= 4.64/\theta_B \text{ feet} \end{aligned} \quad (4-72)$$

Using (4-70), (4-71) and (4-72), a curve of autotrack pointing loss vs antenna diameter is given in Figure 4-11.

⁹• Jasik, H. (ed.), Antenna Engineering Handbook, McGraw-Hill Book Co, New York, 1961, p. 12-12.

REPRODUCIBILITY OF THE
ORIGINAL PAGE IS POOR



974-2796
UNCLASSIFIED

Figure 4-11. User Autotrack Pointing Loss vs User Antenna Diameter

4.2.4.2.2 User Autotrack System Block Diagram

The power level received at the Σ -beam antenna output is determined from (4-64), (4-66) and (4-72) to be

$$P_A = 3.44 \times 10^{-14} D^2 \text{ watts}$$

$$10 \log_{10} P_A = \begin{cases} -105 \text{ dBm, } D = 1 \text{ ft} \\ -83 \text{ dBm, } D = 12.5 \text{ ft} \end{cases} \quad (4-73)$$

Using the range of received levels given in (4-73), a block diagram of the user autotrack system is given in Figure 4-12.

The block diagram shows two channels, one for the Σ -beam, and one for the quadrature multiplexed Δ -beams. Quadrature multiplexing of the two Δ -channels can be used since the Σ -channel signal is fully coherent with both Δ -channel signals. It may later be used as a coherent reference to demultiplex the two quadrature channels.

Two IF's are used in the design, 2 GHz and then 60 MHz, to allow gains to be distributed, circumventing oscillation problems. The IF's were chosen to allow reasonable Q values of the bandpass filters shown. The Σ - and Δ -channels must, of course, be phase matched across the 7.5 MHz second IF band.

The Σ -channel receiver input is obtained from the Σ -channel antenna output through a diplexer at a level of -105 to -83 dBm, depending on the dish size. In the interest of hardware simplification, no Ku-band amplifier is used. The input signal is immediately processed by an RF-IF₁ down-conversion to 2 GHz. At this point the signal is filtered with a 300 MHz wide bandpass filter to reject transmitter leakage, spurious signals, and broadband noise. After 50 dB of IF amplification, the signal level is up to a range of -65 to -43 dBm. A second down-conversion to 60 MHz allows 7.5 MHz wide bandpass filtering, followed by 64 to 86 dB of gain, giving a +7 dBm drive level to the autotrack phase detector mixers. The gain G of the 60 MHz amplifier is determined by the antenna diameter:

$$G = 4 \times 10^8 / D^2 \quad (4-74)$$

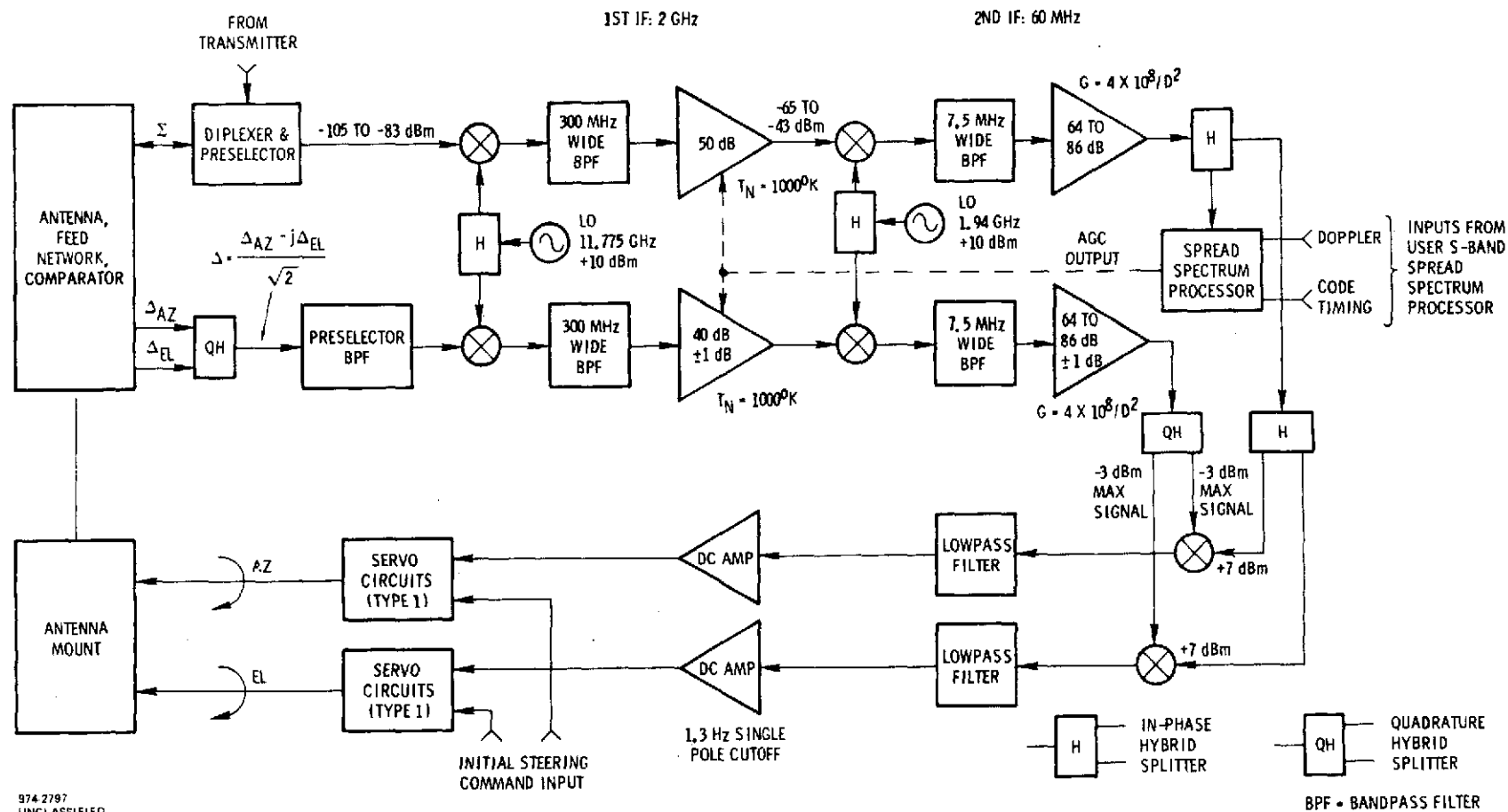


Figure 4-12. Block Diagram of User Autotrack System

The range of sum beam signal-to-noise ratio in the W Hz receiver bandwidth is determined from (4-69) and (4-72)

$$\text{SNR} = \begin{cases} -18 \text{ dB for 1 ft dish} \\ +4 \text{ dB for 12.5 ft dish} \end{cases} \quad (4-75)$$

The sum beam signal-to-noise ratio in the range given in (4-75) is not sufficient to provide reliable AGC on the signal level if a noncoherent detector is used. Coherent detection is provided by locking a spread spectrum processor to the Ku-band PN code. This processor is similar to that in the user S-band transponder. Its initial doppler acquisition and code timing information may be supplied from the user's S-band spread spectrum processor, thereby reducing the complexity and time required for initial acquisition.

The Δ -channel receiver chain has similar frequency conversions and filtering as the Σ -channel receiver chain. However, its gain distributions are different. The 60 MHz amplifier is the same as in the Σ -channel and the total Δ -channel gain is chosen to make the maximum Δ -level into the phase detector mixers ~ 3 dBm (at the edge of the autotrack range). This ensures linear operation of the mixers for the Δ -input, while giving a maximum DC output to about 140 mV. This level is over 40 dB above good DC amplifier offset levels, so that a 40 dB Δ -beam null may be achieved. The 40 dB first IF amplifier achieves this desired Δ -channel gain level. Since Δ -channel gain variations are not corrected by the AGC, the two Δ -channel amplifiers are allowed to vary ± 1 dB each, contributing ± 2 dB variation to the autotrack loop gain.

The Δ -channel is split in a quadrature hybrid to regain the Δ_{AZ} and Δ_{EL} signals, which are then separately synchronously detected against the Σ -channel reference. The resulting DC voltages are amplified with a single pole lowpass cutoff of $f_0 = 1.3$ Hz, determined from Equation (27) of Appendix XI,

$$f_0 = \frac{\omega_0}{2\pi} = \frac{16b}{2\pi} = 1.3 \text{ Hz} \quad (4-76)$$

The DC amplifier outputs are then used to control the azimuth and elevation servos, which each have a single pole at the origin (type 1 system).

OPERATIONAL PROCEDURES

The following operational procedures for establishing a two-way link are proposed for a Ku-band single access system:

1. Point TDRS S-band antenna towards user.
2. Insert user address, selecting the preamble hopping code and the subsequent PN code to be transmitted at S-band.
3. Insert a priori range rate information for a forward link transmission and both a priori range and range rate for a return link reception at S-band.
4. Ground station transmits a FH preamble at S-band for a sufficient time to acquire the user receiver with an omni S-band antenna (at which point the user receiver switches to PN).
5. Ground station switches to PN and transmits for a sufficient time to acquire the S-band user receiver again.
6. Command the user to point its S-band autotrack antenna and begin a forward link autotrack mode, if applicable.
7. Command the user to start a return link PN (or PSK) transmission at S-band.
8. TDRS acquires the user S-band signal.
9. Ground station PN receiver acquires and tracks the user signal, and makes a range and range rate measurement, if applicable. (Suitable tracking performance is the final confirmation of a satisfactory two-way S-band link.)
10. Instruct the user to begin Ku-band autotrack on forward link, with command pointing instructions, if applicable.
11. Ground station transmits a PN signal at Ku-band for a sufficient interval for the user to (1) autosearch (approximately ± 10 PN chips) and reacquire the PN signal and (2) autotrack the forward Ku-band signal.
12. Command the user to begin (1) PN, (2) PSK, or (3) PSK with a separate low power PN signal transmission at Ku-band.

13. TDRS institutes acquisition search, and autotracks the return link Ku-band signal.

14. Ground station PN receiver acquires and tracks the Ku-band user signal. (Suitable tracking performance is the final confirmation of a satisfactory Ku-band link.)

15. Command the user to send telemetry data.

16. Measure range and range rate at Ku-band, if applicable.

SECTION 5

TDRS-TO-GROUND LINK

This section covers the design tradeoffs associated with the TDRS-to-ground link. These include techniques for RF combining and feasibility of FDM operation on the downlink. The feasibility of polarization multiplexing of two Ku-band return channels, both 225 MHz bandwidth, is discussed in detail, with an implementation for improving the isolation between the two polarization modes. Also covered are problems associated with AGIPA operation.

5.1 FREQUENCY PLAN

The frequency plan for the TDRS-to-ground transmissions is shown in Figure 5-1, which also indicates the assignment for TDRS-to-user Ku-band transmissions. Link budget computations from the NASA Goddard Definition Study Report lead to the requirements:

Multiple Access FDM Signal	-	52 mW (total)
S-band Single Access Return	-	44 mW (each)
Ku-band Return	-	3.2W (each)

which are the normal power levels (at TWT) for use when rain attenuation in the atmosphere is not a problem. (See new values in Section 5.3.1.)

Because of the high power assigned to the Ku-band return link channel, excessive interference with the other return channels is possible due to the out-of-band spectral emissions which can arise from channel limiting. Behavior both with and without a signal in the Ku-band return channel must be studied.

5.1.1 OUT-OF-BAND EMISSIONS WITH HARD LIMITING OF Ku-BAND RETURN LINK

Use of staggered quadriphase has previously been shown in Section 2.1.1.2 to have the desirable feature that the out-of-band spectrum can be made very low by sharp cutoff filtering despite subsequent limiting (non-linear amplification). The Ku-band return link channel of the TDRS will approach hard limiting, and thus, SQPN or

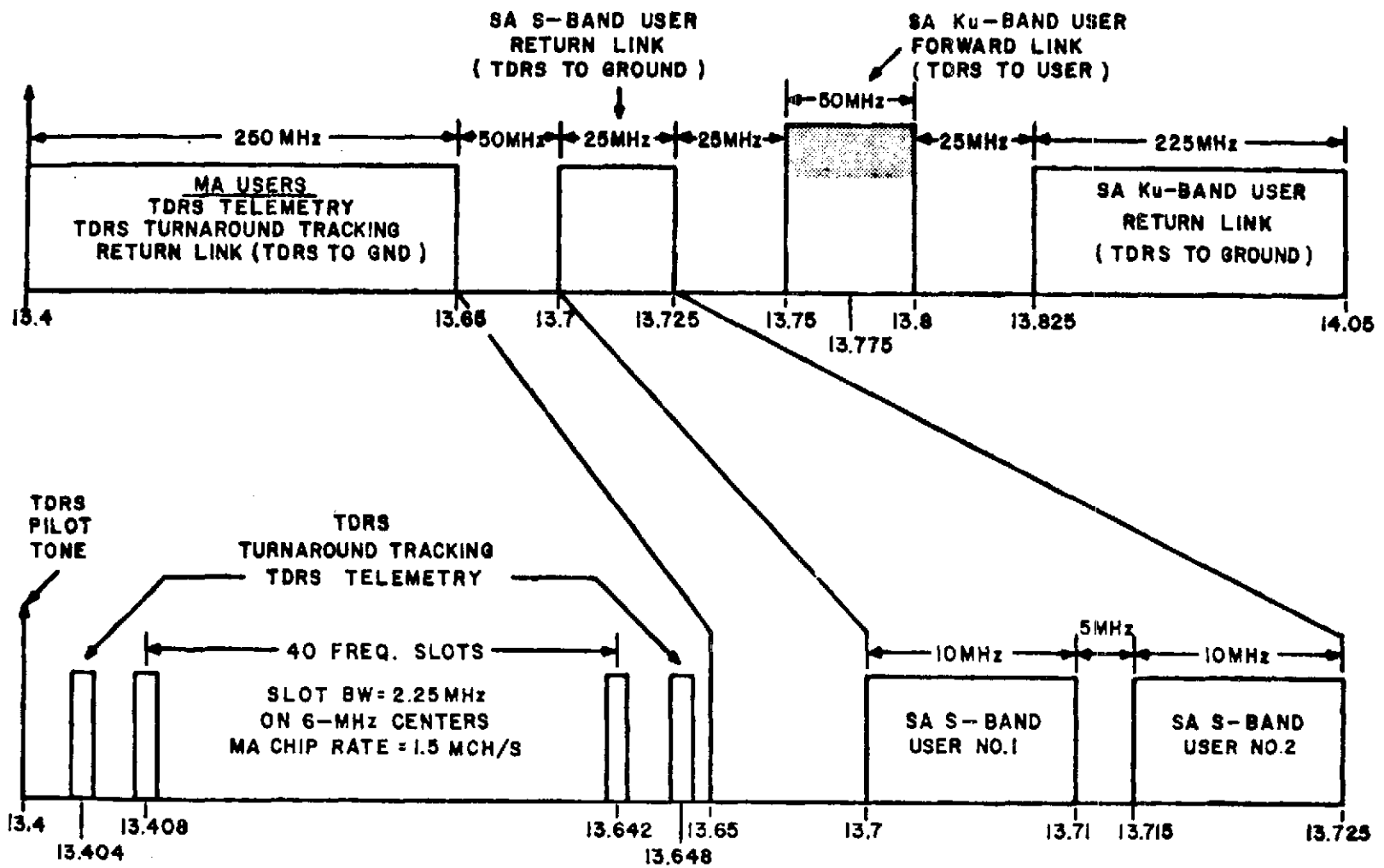


Figure 5-1. TDRS Ku-band Transmit Frequency Plan

SQPSK is recommended to reduce interference with the other return links multiplexed into the TDRS to ground signal.

If the SQPSK signal is not present, the Ku band return channel could be allowed to hard limit on receiver thermal noise. Now, there is a different out-of-band spectrum than when the SQPSK signal is present. Theoretical computations have been made for hard limiting of Gaussian noise with an idealized rectangular passband^[1,2], and an asymptotic approximation has been given^[2] for the out-of-band spectrum when the bandpass $S(f)$ is symmetrical. This out-of-band approximation (normalized to have unit power in the first zone) is

$$S_h(f) = \beta^2 / 2 |f - f_o|^3 \quad (5-1)$$

where f_o is the center frequency and β is the rms bandwidth^[3] defined by

$$\beta = \left[\frac{\int_{f_o}^{\infty} (f - f_o)^2 S(f) df}{\int_{f_o}^{\infty} S(f) df} \right]^{0.5} \quad (5-2)$$

If $S(f)$ is a 6-pole Butterworth with cutoff at ± 0.75 Hz from center*, (5-2) yields $\beta = .454$. Figure 5-2 plots the asymptotic spectrum according to (5-1). Note that the filter cutoff has no effect on the out-of-band spectrum after limiting, except as it affects the rms bandwidth. In particular, a steeper filter cutoff would not reduce the out-of-band spectrum.

1. Lawson and Uhlenback, *Threshold Signals*, McGraw-Hill, 1950, p. 58.
2. R. Price, "A Note on the Envelope and Phase-Modulated Components of Narrow-Band Gaussian Noise," *IRE Trans. on Info. Theory*, Vol. IT-1, September 1955, pp. 9-13.
3. P. M. Woodward, *Probability and Information Theory with Applications to Radar*, Second Edition, Pergamon Press, 1964, p. 102.

* A frequency of 1 Hz is a normalization for convenience to the chip rate of SQPN.

REPRODUCIBILITY OF THE
ORIGINAL PAGE IS POOR

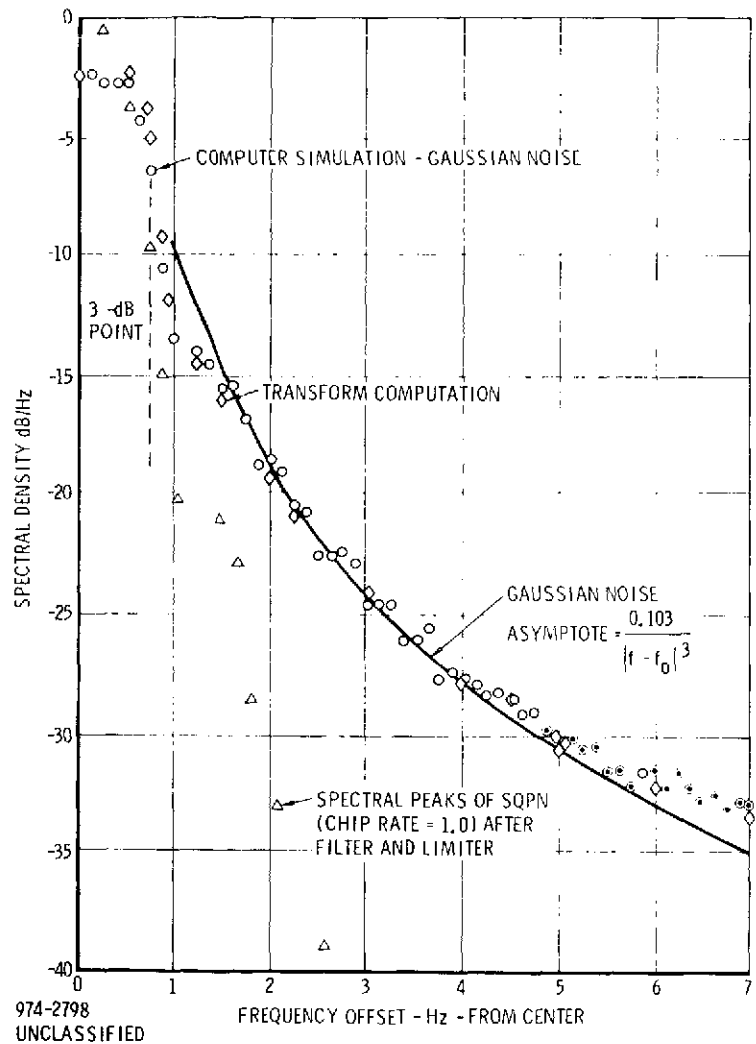


Figure 5-2. Spectral Density After 6-Pole Butterworth Filter (Bandpass = 1.5) and Hard Limiter

5.1.1.1 Computations of Spectrum

A computer simulation* was performed to measure the spectral density for hard limiting of Gaussian noise with a Butterworth spectrum. The result is plotted in Figure 5-2 and shows excellent agreement with the asymptote. (At $f = 8$, a 3 dB error results due to aliasing, since the sampling rate of the simulation is 16.) Also plotted in Figure 5-2 are the spectral peaks of SQPN, as found in Section 2.1.1.2.

An analytical computation of the spectrum for Gaussian noise after hard limiting proceeds as follows for the case of a symmetrical input spectrum. Let

$$o(\tau) = \rho_o(\tau) \cos \omega_o \tau \quad (5-3)$$

denote the normalized input autocorrelation ($\rho(0) = \frac{1}{2}$). Then, after hard limiting ($\pm \pi/4$ clipping level yields unit amplitude in the first zone), the autocorrelation function is^{1}

$$\rho_h(\tau) = \frac{\pi}{8} \sin^{-1} [\rho_o(\tau) \cos \omega_o \tau] \quad (5-4)$$

and the output spectrum is

$$\begin{aligned} S_h(f) &= 4 \int_0^\infty \rho_h(\tau) \cos 2\pi(f + f_o)\tau \, d\tau \\ &= \frac{\pi}{2} \int_0^\infty g(\rho_o(\tau)) \cos 2\pi f\tau \, d\tau \end{aligned} \quad (5-5)$$

* Gaussian noise samples were generated at 16 samples/sec, filtered, and hard limited. A duration of 8192 samples was transformed by an FFT, and the power in 64 adjacent lines was averaged. Thus, points spaced by 0.125 Hz are obtained and plotted. This measurement technique is in accordance with one procedure suggested by Blackman and Tukey[4].

4. Blackman and Tukey, *The Measurement of Power Spectra*, Dover Publications, 1959, pp. 115-116.

where f_0 is assumed arbitrarily large (no overlap from higher zones into the first zone around f_0). The function $g(y)$ is a generalized complete elliptic integral

$$\begin{aligned}
 g(y) &\stackrel{\Delta}{=} \frac{1}{2\pi} \int_0^{2\pi} \sin^{-1}(y \cos x) \cos x \, dx \\
 &= \frac{2}{\pi} y \int_0^{\pi/2} \frac{1 - \sin^2 x}{\sqrt{1 - y^2 \sin^2 x}} \, dx \\
 &= \frac{2}{\pi} y [\text{cel2}(y; 1, 0)]
 \end{aligned}
 \tag{5-6}$$

The function $\text{cel2}(y; A, B)$ is a subroutine in the IBM-360 Scientific Subroutine Package.

The computational procedure is to approximate the Fourier transform by a discrete transform, and apply the FFT algorithm. Thus, we compute ρ_0 as the transform of the assumed low pass spectrum $S(f)$. Then, $g(\rho_0)$ is computed calling the cel2 routine, and the inverse transform (5-5) is computed. Results are plotted in Figure 5-2, with evaluation by 256-point FFT computations. Agreement with the simulation results is excellent at all frequencies, and the asymptote is seen to be correct. This gives confidence in the simulation approach when a theoretical analysis is not feasible.

5.1.1.2 Application to TDRS to Ground Link

It is concluded that the out-of-band spectrum from a hard limiting channel is considerably higher when the input is Gaussian noise than when it is SQPN. We now consider the Ku-band link from TDRS to ground. The applicable frequency plan is shown in Figure 5-3. The Ku-band single access channel operates as a saturating amplifier

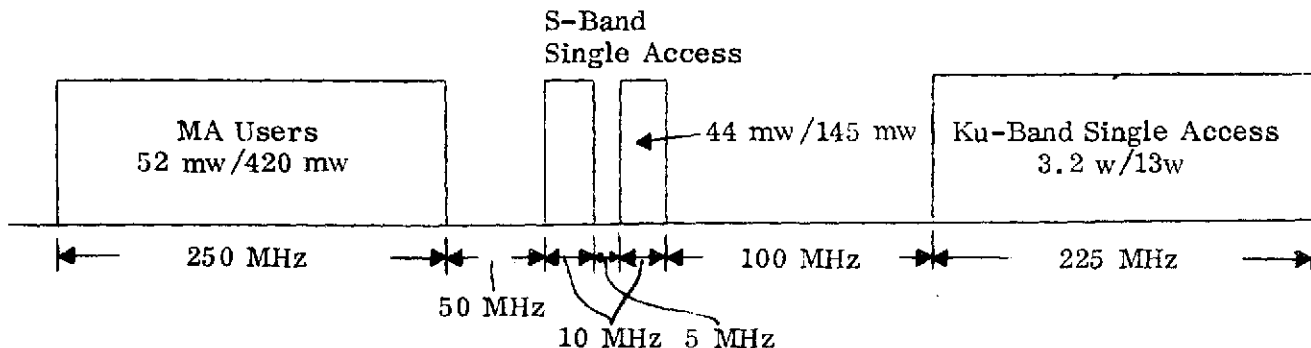


Figure 5-3. Frequency Plan for Ku-Band Link, TDRS to Ground

and therefore causes interference with the S-band single access channels and the MA channel. It is assumed for the moment that no selectivity is available from the combiner for the four signals. We take the normal power levels indicated in Figure 5-3.

If SQPN at a chip rate of 150 Mbps (with SOPSX, the total data rate = 300 Mbps) is received in the Ku-band single access channel at a high S/N, the spectrum after filtering and hard limiting is as indicated in Figure 5-2 (6-pole Butterworth filter), where $1.0 \text{ Hz} = 150 \text{ MHz}$ here. The spectral peaks are 21 dB down in the closer S-band single access channel, and 33 dB down at the edge of the MA channel. Then, the floor on TDRS to ground signal-to-noise ratio due to the interference from the Ku-band single access channel is 13 dB for the MA channel and 14 dB for the S-band single access channel*.

If there is just Gaussian noise in the Ku-band single access channel, Figure 5-2 shows the spectrum to be 15 dB down in the closer S-band single access channel, and 18 dB down at the edge of the MA channel. Then, the floor on TDRS to ground signal-to-noise ratio due to the interference from the Ku-band single access channel is 12 dB for the MA channel and 22 dB for the S-band single access channel.

The above results are summarized in Table 5-1 for the TDRS to ground link, except that a minimum of 14 dB of isolation is presumed from RF combining,

Table 5-1. Comparison of Required TDRS to Ground S/N with Floor Due to Ku-Band Hard Limiting Channel

	S/N Due to Ku-Band Channel		S/N Required
	With Signal	Without Signal	
SSA Channel	28 dB	22 dB	14.0 dB
MA Channel	27 dB	12 dB	6.5 dB
14 dB isolation in combiner			

* The out-of-band spectrum value is adjusted for the ratio of powers and also for the ratio of bandwidths. Note that the spectral values in Figure 5-2 are normalized to 150 MHz chip rate.

as discussed in Section 5.3. Acceptable operation results with SQPN or SQPSK in the Ku-band single access return channel; however, operation is marginal when the signal is absent, unless additional selectivity can be realized in the RF combiner or unless backoff from hard limiting is allowed in the absence of a signal.

Note that interference from only one Ku-band single access return signal is included, since the second signal is presumed to be on an orthogonal polarization. That is, the TDRS to ground link carries two wideband Ku-band single access return signals multiplexed on orthogonal circular polarization modes. (This is discussed in detail in Section 5.2.)

5.1.2 OUT-OF-BAND SPECTRUM WITH SOFT LIMITING

This section considers the possible use of soft limiting in the Ku-band channel rather than hard limiting with the objective of controlling interference into the adjacent channels.

A typical input-output transfer function for soft limiting is the error function

$$v_{\text{out}} = \sqrt{2} \operatorname{erf}(\lambda v) = \sqrt{8/\pi} \int_0^{\lambda v} \exp(-x^2) dx \quad (5-7)$$

where v is the input envelope and v_{out} is the output envelope. The soft limiter is presumed to create no phase distortion (i.e., there is no AM to PM conversion). Note that when λ is small, the limiter becomes linear with gain $\sqrt{8/\pi}\lambda = 1.6\lambda$, while $\lambda \rightarrow \infty$ produces a hard limiter with output amplitude equal to $\sqrt{2}$ (so that saturation output power is normalized to unity).

If v is the envelope of Gaussian noise of unit power, we can compute the mean output amplitude to be

$$\begin{aligned} E\{v_{\text{out}}\} &= \sqrt{8/\pi} \int_0^{\infty} v \exp(-v^2/2) dv \int_0^{\lambda v} \exp(-x^2) dx \\ &= 2[\lambda^2/(1+2\lambda^2)]^{0.5} \end{aligned} \quad (5-8)$$

Reduction of mean amplitude below the saturation value of $\sqrt{2}$ is one possible definition of the backoff from hard limiting.

Another definition of backoff from hard limiting is the reduction in average output power. A simple closed form result as a function of λ does not seem available.

5.1.2.1 Spectrum Computation for Soft Limiting

The Monte Carlo simulation described in Section 5.1.1 was modified to measure the spectrum of Gaussian noise after soft limiting*. The only change to the program was to introduce the soft limiter defined by (5-7). The simulation has already been validated by its demonstrated accuracy for the hard limiting case. The output average power was also measured in the simulation to give the backoff (by one definition).

Simulation results are presented in Figure 5-4 for various degrees of backoff, with a 6-pole Butterworth input spectrum of bandpass ≈ 1.5 .

5.1.2.2 Effect on Tandem Link Performance for Weak Desired Signal in Channel

We now evaluate the tandem link performance (measured by E_b/N_o in the ground receiver) for a weak signal at the input to the soft limiting channel defined by (5-7). If the desired signal amplitude is a and the instantaneous amplitude of the noise is v , the instantaneous envelope at the input to the soft limiter is

$$r = (a^2 + v^2 + 2av \cos \phi)^{0.5} \quad (5-9)$$

where ϕ is the instantaneous phase difference. The instantaneous output amplitude of the desired signal then is

$$a_{\text{out}} = \frac{1}{2\pi} \int_0^{2\pi} (a + v \cos \omega) \frac{\sqrt{2} \operatorname{erf}(\lambda r)}{r} d\omega \quad (5-10)$$

*Analytical computation of the spectrum of Gaussian noise after soft limiting could be carried out via a series expansion, but the simulation approach has the advantage of flexibility and adaptability to non-Gaussian inputs.

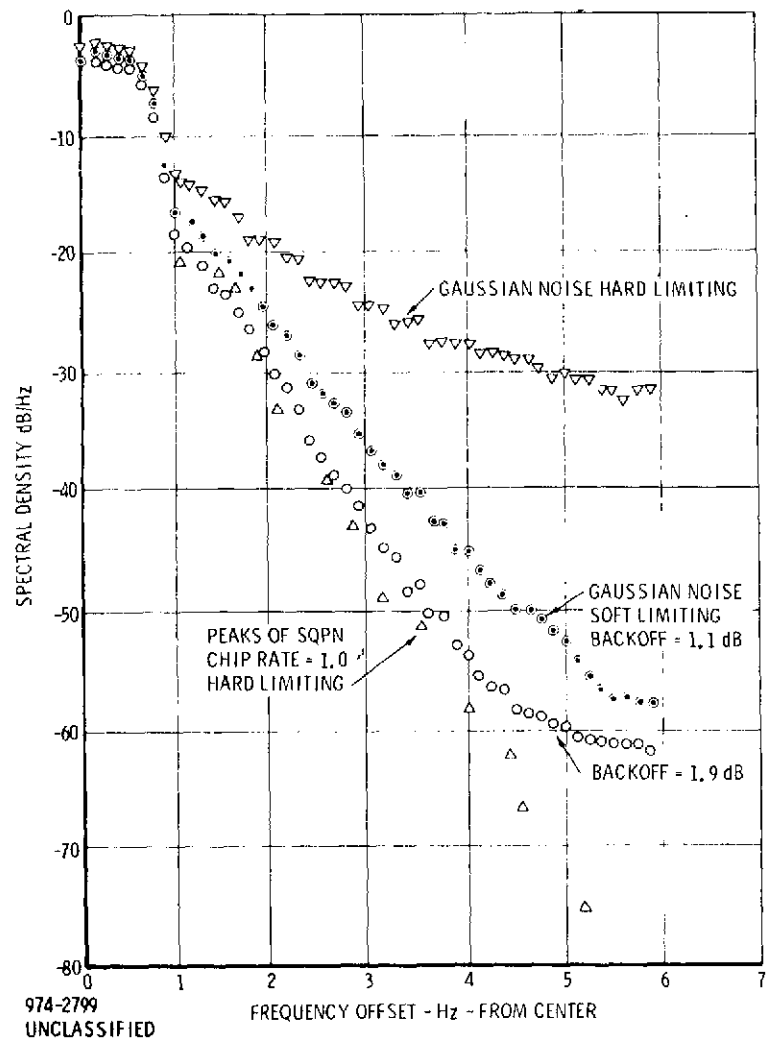


Figure 5-4. Spectrum After Filtering (6-Pole Butterworth, Bandpass = 1.5) and Hard or Soft Limiting

introducing (5-7) and averaging over a uniform distribution of phase φ . Then, averaging over the distribution of noise amplitude v , the output amplitude of the desired signal is

$$E\{a_{out}\} = \int_0^\infty a_{out} v \exp(-v^2/2) dv \quad (5-11)$$

using the Rayleigh distribution for the noise envelope v .

We can evaluate the derivative of (5-10) with respect to the parameter λ ; thus,

$$\begin{aligned} \frac{da_{out}}{d\lambda} &= \frac{1}{2\pi} \int_0^{2\pi} (a + v \cos \varphi) \sqrt{\frac{8}{\pi}} \exp(-\lambda^2 r^2) d\varphi \\ &= \sqrt{\frac{8}{\pi}} \exp(-\lambda^2 (v^2 + a^2)) [a I_0(2av\lambda^2) - v I_1(2av\lambda^2)] \\ &\cong \sqrt{\frac{8}{\pi}} a (1 - v^2 \lambda^2) \exp(-\lambda^2 v^2) \end{aligned} \quad (5-12)$$

for $a \rightarrow 0$. The mean of this is

$$\begin{aligned} E\{da_{out}/d\lambda\} &= \sqrt{\frac{8}{\pi}} a \int_0^\infty (1 - v^2 \lambda^2) \exp(-\lambda^2 v^2) v \exp(-v^2/2) dv \\ &= \sqrt{\frac{8}{\pi}} a (1 + 2\lambda^2)^{-2} \end{aligned} \quad (13)$$

Finally, by integrating with respect to λ

$$\begin{aligned} E\{a_{out}\} &= \sqrt{\frac{8}{\pi}} a \int_0^\lambda \frac{dx}{(1 + 2x^2)^2} \\ &= \sqrt{\frac{2}{\pi}} a \left\{ \frac{\lambda}{1 + 2\lambda^2} + \frac{1}{\sqrt{2}} \tan^{-1}(\sqrt{2} \lambda) \right\} \end{aligned} \quad (14)$$

As a check,

$$\begin{aligned} E\{a_{\text{out}}\} &\rightarrow \sqrt{\frac{8}{\pi}} \lambda a ; \quad \lambda \rightarrow 0 \\ &\rightarrow \sqrt{\frac{\pi}{2}} a ; \quad \lambda \rightarrow \infty \end{aligned} \quad (5-15)$$

which are the correct limits (linear and hard limiting cases, respectively).

For $\lambda = \sqrt{.75}$, yielding the 1.9 dB backoff curve of Figure 5-4, (5-14) gives a reduction in average output amplitude of 1.2 dB, compared with hard limiting ($\lambda = \infty$). Consequently, if noise dominates on the user to TDRS link, rather than on the TDRS to ground link, there is an improvement by going to soft limiting; however, this improvement is offset by the reduced signal-to-noise ratio on the TDRS to ground link. There is an optimum λ ; however, the choice is not critical.

Analytically, the ground receiver performance is characterized by $(E_b/N_o)_{\text{ground}}$, which is given by

$$(E_b/N_o)_{\text{ground}} = \frac{T_b [E\{a_{\text{out}}\}]^2 / 2}{(N_o)_{\text{limiter}} + (N_o/S)_{\text{ground}}} \quad (5-16)$$

where $(N_o)_{\text{limiter}}$ is the spectral density at band center normalized to saturation output as given in Figure 5-4, and $(S/N_o)_{\text{ground}}$ is the parameter for the TDRS to ground link. The signal-to-noise ratio in the bandpass prior to limiting is

$$\frac{1}{B_{\text{IF}}} (S/N_o)_{\text{TDRS}} = a^2 / 2 \quad (5-17)$$

where $(S/N_o)_{\text{TDRS}}$ is the parameter for the user to TDRS link. Substituting (5-14) and (5-17) into (5-16), we have

$$(E_b/N_o)_{\text{ground}} = (E_b/N_o)_{\text{TDRS}} (2/\pi) \frac{\left[\frac{\lambda}{1+2\lambda^2} + \frac{1}{\sqrt{2}} \tan^{-1}(\sqrt{2}\lambda) \right]^2}{[(N_o)_{\text{limiter}} + (N_o/S)_{\text{ground}}] B_{\text{IF}}} \quad (5-18)$$

The NASA Goddard Definition Phase Report calls for $(S/N_o B_{\text{IF}})_{\text{ground}} = 25.1$ dB.

For λ small, we have, using the linear gain,

$$(N_o)_{\text{limiter}} B_{\text{IF}} = \frac{8}{\pi} \lambda^2 \quad (5-19)$$

Then, (12) becomes for $\lambda \rightarrow 0$

$$\frac{(E_b/N_o)_{\text{ground}}}{(E_b/N_o)_{\text{TDRS}}} = \frac{1}{1 + \frac{1}{\lambda^2} (N_o/S)_{\text{ground}} B_{\text{IF}}} \quad (5-20)$$

We obtain a tandem link loss of 1 dB for transponding a weak signal when $\lambda = 0.11$, corresponding to backoff by about 15 dB.

To show that backoff from hard limiting improves the performance, we compute $(E_b/N_o)_{\text{ground}}$ from (5-18) for the values $\lambda = \infty$ (hard limiting), $\lambda = \sqrt{1.5}$ (1.1 dB backoff), and $\lambda = \sqrt{.75}$ (1.9 dB backoff). From Figure 5-4, $(N_o)_{\text{limiter}} = -2.2$ dB, -3.1 dB, and -3.9 dB, respectively, with $B_{\text{IF}} = 1.5$ (normalized value of bandwidth). The result is

$$\begin{aligned} \frac{(E_b/N_o)_{\text{ground}}}{(E_b/N_o)_{\text{TDRS}}} &= -0.62 \text{ dB; hard limiting} \\ &= -0.24 \text{ dB; 1.1 dB backoff} \\ &= -0.08 \text{ dB; 1.9 dB backoff} \end{aligned}$$

The improvement with backoff is due to the reduction in limiter suppression, while the noise contributed by the TDRS to ground link remains negligible for a small backoff.

5.1.2.3 Conclusions

The spectrum of Gaussian noise after soft limiting approaches that of SQPN with only a relatively small backoff (approximately 2 dB) of the channel output power from the saturation value. Table 5-1 in Section 5.1.1 then would show the same S/N floor both with and without a signal being present in the Ku-band channel. Furthermore, operation of the Ku-band channel with backoff is consistent with the fact that the TDRS to ground link has need for a high power only to handle the high data rate case (300 Mbps in 225 MHz bandwidth). At lower data rates, but with the same power on the TDRS to ground link, the tandem link loss becomes negligible, and backoff improves performance by reducing the degradation in S/N due to limiter suppression effects. The degree of backoff when the channel soft limits on receiver noise only is not critical. It is desired to approach full saturation output from the channel when a 300 Mbps data signal is received from the user at the EIRP necessary to support such a data rate.

5.1.3 OUT-OF-BAND SPECTRUM WITH BIPHASE SIGNAL

Staggered quadriphase has been shown to have a low out-of-band spectrum after filtering and hard or soft limiting in the Ku-band return channel. Section 5.1.2 showed that limiting on Gaussian noise alone produces a similar out-of-band spectrum when there is a modest backoff from hard limiting. (An error function limiter transfer function is presumed.) The problem is now brought up to evaluate the out-of-band spectrum with a biphasic signal in the channel. The objective is to specify the maximum allowable biphasic chip rate which does not create unacceptable out-of-band emissions.

5.1.3.1 Monte Carlo Simulation Approach

We utilize the Monte Carlo simulation approach described in Section 5.1.2 for a soft limiting bandpass channel with Gaussian noise input. Now, a biphasic PN signal centered in the channel is added to the Gaussian noise. The PN code period is equal to the FFT period; hence, the chip rate is selected by choosing the number of stages of the maximal linear PN generator*.

In the absence of signal, soft limiting is desirable to control the out-of-band spectrum due to Gaussian noise alone, and Section 5.1.2 suggests a backoff in the range 1.1 dB to 1.9 dB. With signal present, one operational concept is to maintain a fixed gain prior to limiting in the TDRS Ku-band return link channel; thus, as the signal power increases, the channel approaches hard limiting. However, since backoff on the downlink from TDRS to ground is acceptable in proportion to the reduction in data rate from the maximum to be accommodated in the channel (300 Mbps for 225 MHz bandwidth), the alternative concept can be advanced to control gain (AGC or from ground) with changes in the signal level.

5.1.3.2 Simulation Results

We assume a received S/N in the channel TDRS corresponding to uncoded data at a specified data rate. From the NASA Goddard Definition Phase Study Report, S/N is 19 dB for 300 Mbps data rate, and there is a proportionate reduction in S/N at

* Gaussian noise samples are generated at 16 samples/sec and added to the PN signal with a period of 8192 samples. The sum is filtered and soft limited. After allowing for decay of the initial transient, a period is transformed by a FFT algorithm, and the power in 64 adjacent lines is averaged. Thus, points spaced by $64 \times 16/8192 = 0.125$ Hz are computed and plotted. The PN chip rate is $16N/8192$, where N is the code period in chips.

reduced data rates. Figure 5-5 presents simulation results (1 Hz is the normalization which corresponds to 150 MHz) on the spectrum for several biphasic data rates, with fixed gain operation such that the backoff would be 1.1 dB on input noise alone. Thus, with signal present, the TDRS channel is operating essentially in hard limiting.

Figure 5-5 should be compared with Figure 5-4 of Section 5.1.2. It is observed that with a biphasic signal at a low chip rate, the spectral density is lower near the band edge but tends to be higher out-of-band than was previously found for SQPSK at the maximum bit rate or Gaussian noise with soft limiting. For a biphasic chip rate of 0.248, a crossover occurs at 2 Hz (compared to a backoff of 1.1 dB on Gaussian noise alone). For a biphasic chip rate of 0.498, the spectrum is higher beyond 1 Hz.

Figure 5-6 presents results for the maximum biphasic data rate of unity (i.e., 150 Mbps). Observe that the spectrum with essentially hard limiting (limiter is set for 1.1 dB backoff on noise alone) is very close to the theoretical $(\sin x/x)^2$ of unfiltered biphasic. However, a modest backoff into soft limiting significantly reduces the out-of-band spectrum. With 1.8 dB of backoff, the spectral peaks for biphasic lie at or below the peaks of SQPSK with hard limiting (compare with Figure 5-4 of Section 5.1.2).

5.1.3.3 Interference Caused by Ku-Band Downlink Channel

We may now apply the simulation results to compute the signal-to-interference ratios caused by the Ku-band return link channel on the TDRS-to-ground downlink. The approach is the same as followed in Section 5.1.1. Table 5-2 gives the computed ratios*, assuming a minimum of 14 dB of isolation is provided by the combiner (see Section 5.3).

*These ratios are computed by taking the ratio of transmitted power levels, adding the dB by which the peak interfering spectral density is below 0 dB/Hz, and correcting for the bandwidth ratio.

REPRODUCIBILITY OF THE
ORIGINAL PAGE IS POOR

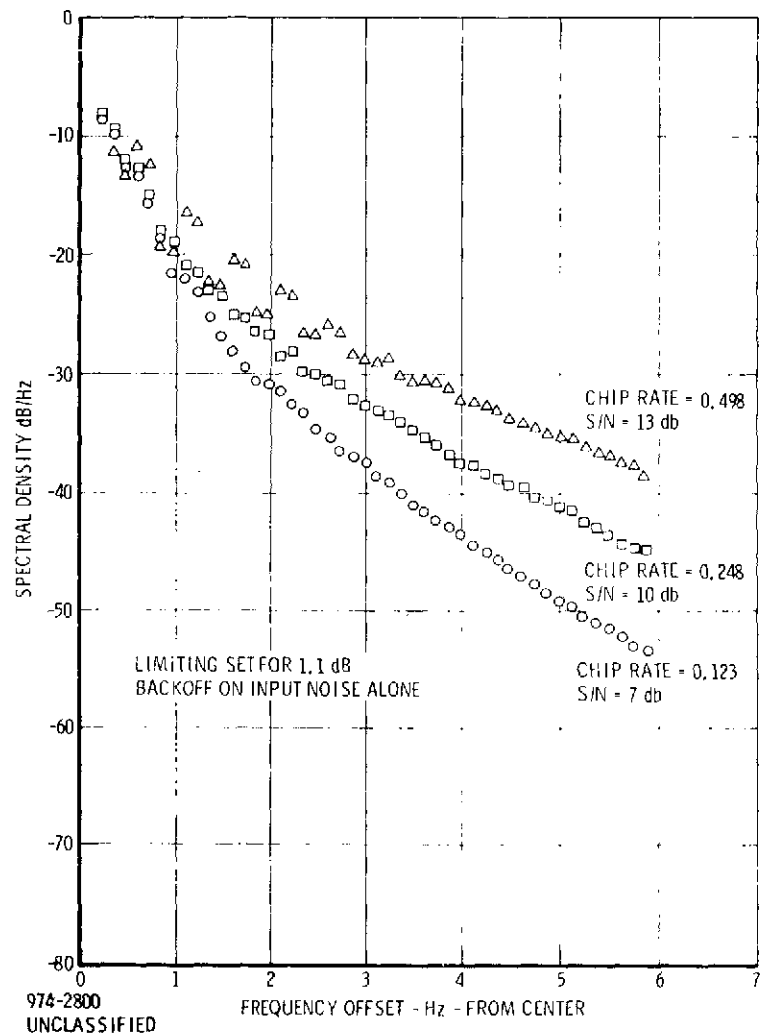


Figure 5-5. Spectrum After Filtering (6-Pole, Bandpass = 1.5 Hz) and Limiting of Biphase Signal Plus Noise

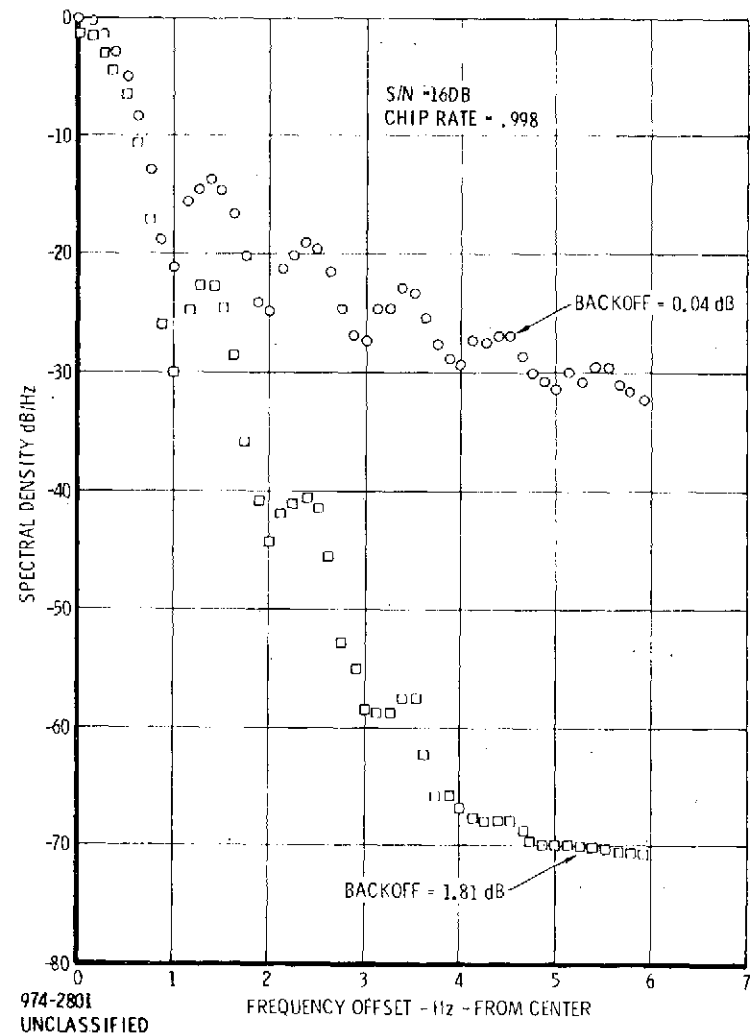


Figure 5-6. Spectrum After Filtering (6-Pole, Bandpass = 1.5 Hz) and Limiting of Biphase Signal (S/N = 16 dB; Chip Rate = .998)

Table 5-2. S/I in Downlink Channels, Fixed Gain Operation
(1.1 dB Backoff on Noise Alone)

Ku-Band Saturation Output = 3.2 W					Required S/I
300 Mbps SQPSK	No. Signal 1.1 dB Backoff	75 Mbps BPSK	150 Mbps BPSK		
SSA Channel 44 mW	28 dB	27 dB	26 dB	20 dB	14 dB
MA Channel 52 mW	27 dB	23 dB	17 dB	13 dB	6.5 dB
Includes combiner isolation of 14 dB					

5.1.3.4 Conclusions

With a minimum of 14 dB of combiner isolation between the Ku-band return link channel and the S-band single access or the multiple access channel on the TDRS-to-ground downlink, there are adequate signal-to-interference ratios for biphase data in the Ku-band channel up to about 75 Mbps. Operation at 150 Mbps biphase produces marginal S/I ratios.

The above results are based on fixed gain operation of the TDRS Ku-band return link channel such that the backoff is 1.1 dB on noise alone. The channel is essentially hard limiting for the bit rates studied. If the TDRS channel has gain control (AGC or ground command) producing a modest backoff, the S/I ratios improve considerably. For example, at 150 Mbps biphase, with 1.8 dB of backoff*, Figure 5-6 shows an improvement in S/I of 8 dB for the S-band single access channel, and an improvement of 21 dB for the multiple access channel, compared with Table 5-2 at 150 Mbps. (These are the reductions in the spectral peaks from Ku-band falling into these channels.)

* Note that 3 dB of backoff can be tolerated at a bit rate of 150 Mbps, since the saturation power is sized for 300 Mbps data rate.

5.1.4 SPECTRAL INTERFERENCE FROM Ku BAND FORWARD LINK

Although the TDRS to user Ku-band forward link is transmitted on a different antenna than the TDRS to ground link, there would be mutual interference whenever the user satellite passes through the beam directed to the ground. We wish to assess the interference caused to the S-band single access system and the multiple access system on the TDRS to ground link. We assume no reduction of interference has been realized from possible different polarization modes.

The EIRP for high power operation of the Ku-band forward link transmitter (without pointing loss) is 50 dBW, according to the NASA Goddard Definition Report. The TDRS to ground EIRP is $42.8 \text{ dB} + P$, where in the normal mode, $P = -13.6 \text{ dBW}$ (44 mW) for the single access signal and -12.8 dBW (52 mW) for the multiple access signal.

The Ku-band forward link can be spread spectrum, in which case a PN chip rate of 15 Mbps suffices to meet IRAC flux density limitations. Alternatively, the Ku-band forward link can convey FM video, with the parameters 4.2 MHz video baseband and ± 10 MHz peak deviation. We wish to compute the S/N in the S-band single access channels and the multiple access channels due to interference from the Ku-band forward link. The applicable frequency plan is shown in Figure 5-7.

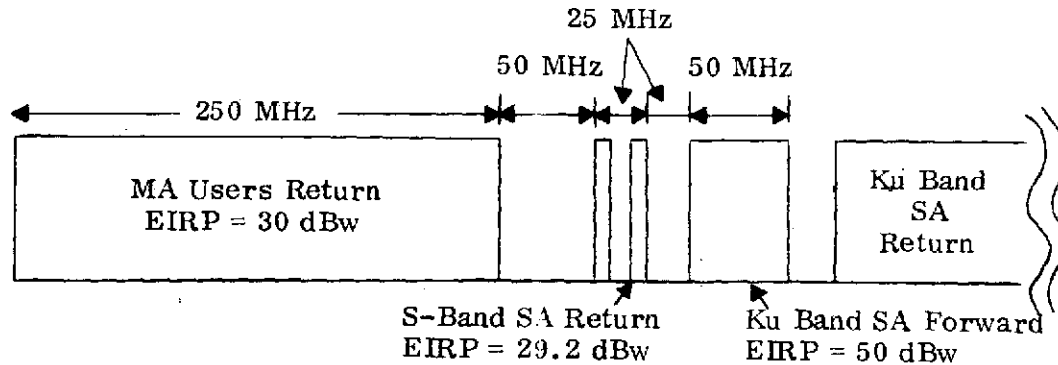


Figure 5-7. Frequency Plan for TDRS Ku-Band Transmit

5.1.4.1 Spectrum for SQPN Modulation

The spectrum of a SQPN modulated Ku-band single access forward link is shown in Section 2.1.1.2 for a hard limiting transmitter. For a chip rate of 15 Mbps, the interference to the S-band single access channel is 50 dB down at the band edge (normalized frequency separation of $50 \text{ MHz}/15 \text{ MHz} = 3.3$). The interference at the band edge of the multiple access channel (normalized frequency separation of $125 \text{ MHz}/15 \text{ MHz} = 8.3$) is, theoretically, more than 100 dB down. These numbers refer to spectral density measured in a bandwidth equal to the PN chip rate.

5.1.4.2 Spectrum for Video Test-Tone Modulation

With video FM on the Ku-band forward link, the spectrum must be estimated for some typical cases. Hard limiting has no effect, since FM is constant envelope. To begin, assume a test-tone at $f_m = 4 \text{ MHz}$ producing a $\pm 10 \text{ MHz}$ deviation, a deviation ratio of 2.5. The resulting spectrum of the FM signal is discrete with a line spacing of 4 MHz. The power in the discrete line at kf_m from the center is given by $[J_k(2.5)]^2$, relative to total power^[5], where $J_k(x)$ is the Bessel function of order k .

For $k \gg x$, we have the approximation

$$J_k(x) = x^k / (2^k k!) \quad (5-21)$$

Thus, at the edge of the S-band single access, $k = 50 \text{ MHz}/4 \text{ MHz} = 12$, and the interference power is 150 dB down. (Since the line spacing is 4 MHz, this power level may be interpreted as spectral density in 4 MHz bandwidth.) It is even further down, theoretically, at the edge of the multiple access band ($k = 125 \text{ MHz}/4 \text{ MHz} \approx 31$).

[5] S. Goldman, Frequency Analysis, Modulation and Noise, McGraw-Hill, 1948, p. 150.

5.1.4.3 Spectrum for Random Video Modulation

As a second calculation, let us assume the video can be described as a Gaussian random modulation. The video spectrum after pre-emphasis is assumed here to be flat out to 4 MHz, at which point it cuts off sharply. We assume an rms frequency deviation of 8 MHz or an rms deviation ratio $\sigma = 2$, to fit an available computation. This yields a peak deviation exceeding ± 10 MHz; however, a lower rms deviation will produce still lower out-of-band emissions.

Figure 5-8 presents the spectral density of the FM carrier for this case^[6]. The quasi-static approximation is given by

$$S(f) = \frac{1}{\sqrt{2\pi\sigma W}} \exp\left(-\frac{1}{2\sigma^2} \left(\frac{f}{W}\right)^2\right) \quad (5-22)$$

where W is the baseband cutoff. The quasi-static approximation is derived on the basis that the spectral density at f is proportional to the probability density of having that deviation.

At the edge of the S-band single access system, $f/W = 50$ MHz/4 MHz = 12.5. Figure 5-8 yields a spectral density approximately 80 dB down, referenced to the 4 MHz cutoff bandwidth. The spectral density at the edge of the multiple access band will be much smaller yet.

5.1.4.4 Conclusions

Considering the situation where the Ku-band user passes through the TDRS to ground beam, SQPN modulation at a chip rate of 15 Mbps on the Ku-band forward link produces more interference in adjacent channels than does video FM with ± 10 MHz deviation. The resulting S/N in 10 MHz bandwidth of the S-band single access system is 31 dB, when the difference in EIRP levels is introduced*. Since

*Interference is down by 50 dB + $10 \log_{10} (15/10) = 51.8$ dB for equal EIRP, but the EIRP levels differ by 20.8 dB.

[6] V. K. Prabhu, "Spectral Density Bounds on FM Wave," IEEE Trans on Comm., Vol. COM-20, October 1972, pp. 980-984.

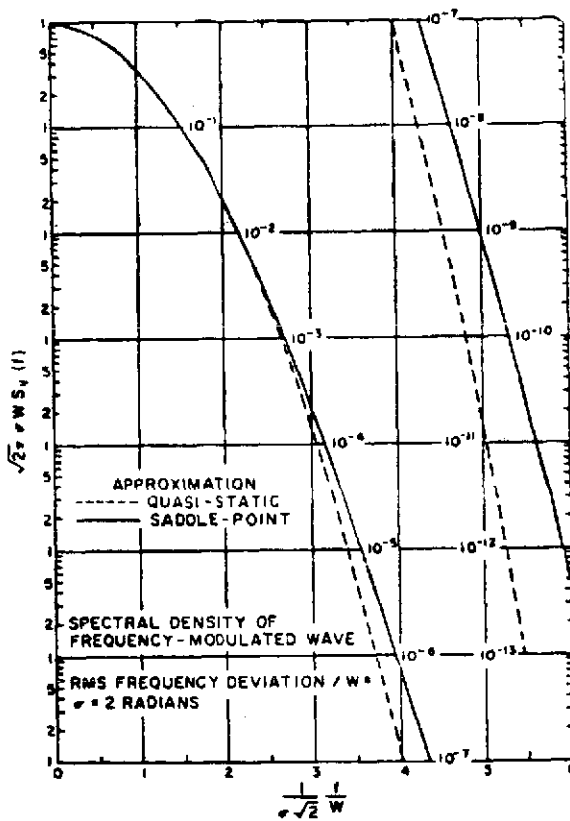


Figure 5-8. Spectral Density of an Angle-Modulated Wave, with Gaussian Frequency Modulation with a Rectangular Spectrum. $\sigma = 2$ rad. Vertical scale has been indicated along curves.

the required S/N is 14 dB, this interference is negligible. Interference to the multiple access system is even more negligible. This applies even without polarization mode discrimination.

Presented below is an analysis of the technique of using orthogonal RF wave polarization to multiplex two Ku-band signals from SA users for TDRS to ground station transmission in a common frequency band. Polarization crosstalk is caused by rain^[7, 8] and by antenna tolerance limitations and can limit error rate performance.

The effect of cochannel interference on error rates in PSK systems has previously been analyzed and reported on in the open literature, e.g.,^[9]. In Section 4.1.3, it was pointed out that for uncoded data at $P_e = 10^{-4}$ there is a negligible effect when a CW interference is 23 dB below a desired quadriphase signal. When the CW interference is only 17 dB below, one must increase E_b/N_0 by about 1 dB (to 9.4 dB) to restore $P_e = 10^{-4}$. We define the minimal acceptable level of polarization crosstalk to be 20 dB below the desired signal level.

The polarization crosstalk is proportional to EIRP on the TDRS. Thus increasing the EIRP of the dual polarized KSA signals on the TDRS will not improve the S/I ratio at the ground station. The pair of dual polarized KSA signals received by the ground station contains additive polarization crosstalk and can be processed to greatly reduce the mutual interference. A coherent interference cancellation system (ICS) for polarization crosstalk reduction at the TDRSS ground station will be described.

It should be noted that we have assumed that the EIRP on the TDRS for each KSA user is the same for each component of polarization. If the EIRP provided for, say, vertical polarization is greater, then the depolarization crosstalk would be a more severe problem in the horizontal channel at the ground station.

7. Laur, R. R., "Rain Depolarization: Theory and Experiment," COMSAT Technical Review, Spring 1974, pp. 187-190.
8. Morrison, J. A. and M. J. Cross, "Scattering of a Plane Electromagnetic Wave by Axisymmetric Raindrops," BSTJ, July-August, 1974, pp. 955-1019.
9. Shimbo, O., and R. Fang, "Effects of Cochannel Interference and Gaussian Noise in M-ary PSK Systems," COMSAT Technical Review, Spring 1973, pp. 183-206.

5.2.1 SOURCES OF POLARIZATION CROSSTALK

5.2.1.1 Antenna Tolerances

Consider a pair of ideal orthogonal linearly polarized transmitting antennas and a similar pair of receiving antennas. If there is a relative rotation angle ϵ between the Tx and Rx antennas, there will be a crosstalk electric field vector proportional to $\sin\epsilon$ and a desired signal electric field proportional to $\cos\epsilon$. The polarization (isolation) crosstalk ratio XP will be given by

$$XP \text{ (dB)} = -20 \log_{10} (\tan\epsilon) \quad (5-23)$$

In order to satisfy the 20 dB crosstalk ratio specified above we require that

$$|\epsilon| \leq \tan^{-1} (10^{-1}) = 5.7^\circ$$

Note that the loss (LP) due to depolarization is:

$$LP \text{ (dB)} = -20 \log_{10} (\cos\epsilon) \quad (5-24)$$

A polarization loss of 0.5 dB has been predicted [10] for the SA Ku-Band links. This could result from $\epsilon = \cos^{-1} [10^{-0.025}] = 19^\circ$ and by Equation (5-23) a corresponding polarization isolation of only 9.1 dB.

Now let us relax the assumption that the dual polarization transmit (and receive) antenna provides perfect isolation between its orthogonal modes. We present here technical data on a readily available antenna with high isolation between polarizations. The antenna is manufactured by American Electronic Laboratories, Inc., Colmar, Pa., and is designated APX-1293. It is a crossed planar log periodic antenna, capable of receiving orthogonal linearly polarized waves. Its specifications are included as Figure 5-9. This broadband antenna maintains greater than 26 dB

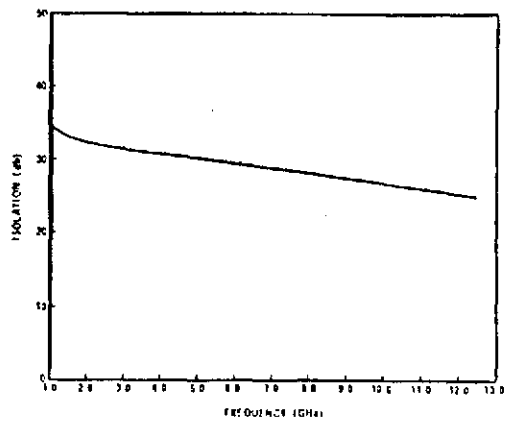
10. "Definition Phase Study Report on the TDRSS," Section 3, Telecommunications NASA/GSFC.

TYPICAL ELECTRICAL PERFORMANCE

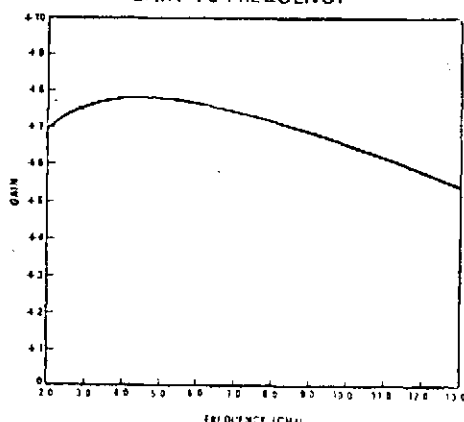
<i>Frequency</i>	1.0-12.4 GHz
<i>VSWR</i>	< 2.5:1
<i>Beamwidth E plane</i> (3 db)	55°
<i>H plane</i>	70°
<i>Gain (db)*</i>	7
<i>Isolation (db)</i>	25
<i>Connectors (2)</i>	OSM Female

* referred to a linear isotropic source

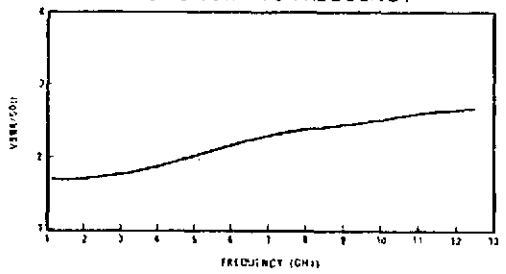
ISOLATION VS FREQUENCY



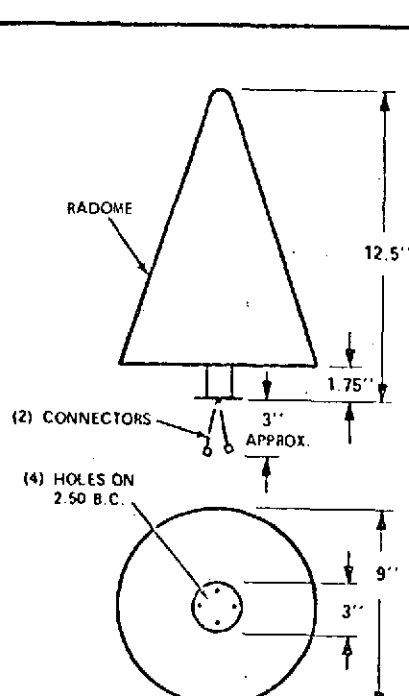
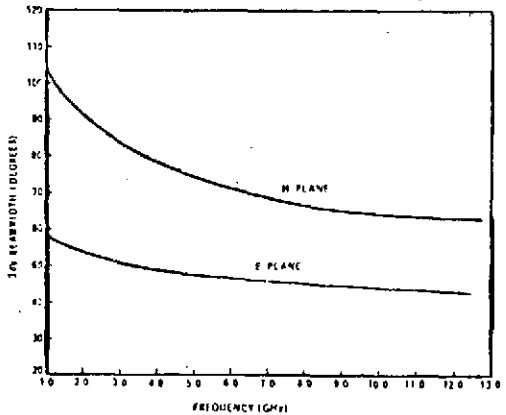
GAIN VS FREQUENCY



TYPICAL VSWR VS FREQUENCY



3 db BEAMWIDTH VS FREQUENCY



974-2804
UNCLASSIFIED

Figure 5-9. Antenna APX-1293

polarization isolation from 1.0 GHz to 12.5 GHz. Conversations with the manufacturer have confirmed that at least 26 dB of isolation can be expected across a 225 MHz wide band at 14 GHz by modifying the APX-1293 antenna.

5.2.1.2 Rain Depolarization

The oblateness of raindrops imposes differential phase shifts upon orthogonal polarizations of microwaves propagating through the drops. Spherical raindrops would not cause this differential phase shift which results in depolarization. The degree of polarization crosstalk depends upon the radio frequency (f), the rate of rainfall (R), and the path length (r) through the rain. Theoretical and experimental results for circularly polarized (CP) waves are presented in a Note by Laur^[7]. It is shown in this Note that experimental results (at 4 GHz) support the theoretical model. Figure 5-10 presents the theoretical rain depolarization for CP waves at 14 GHz as a function of rain rate R with r = 2.5, 5.0, and 10 km as a parameter.

The theoretical results can be summarized by the following expression for the polarization crosstalk ratio.

$$XP \text{ (dB)} = 80 - 20 \log_{10} (Rrf) \quad (5-25)$$

where R = rain rate in mm/hr

r = rain range (or path length) in km

f = frequency in GHz

The TDRSS Ku-band frequency plan^[11] reserves the 225 MHz wide band from 13.825 to 14.05 GHz for the SA user TDRS to ground return link. Setting f = 14 and XP = 20 dB in Equation (5-25) and solving for Rr yields the rainfall condition for minimal acceptable performance.

$$Rr = 500/7 = 71.43 \text{ square meters/hour}$$

This hyperbola is plotted in Figure 5-11 and provides the rainfall conditions for 20 dB polarization crosstalk. Above the curve polarization isolation is less than 20 dB and

11. "TDRSS Frequency Plan", October 1973, DOC 16151/1-2.3.6/4.9.2, NASA/GSFC, Greenbelt, Md.

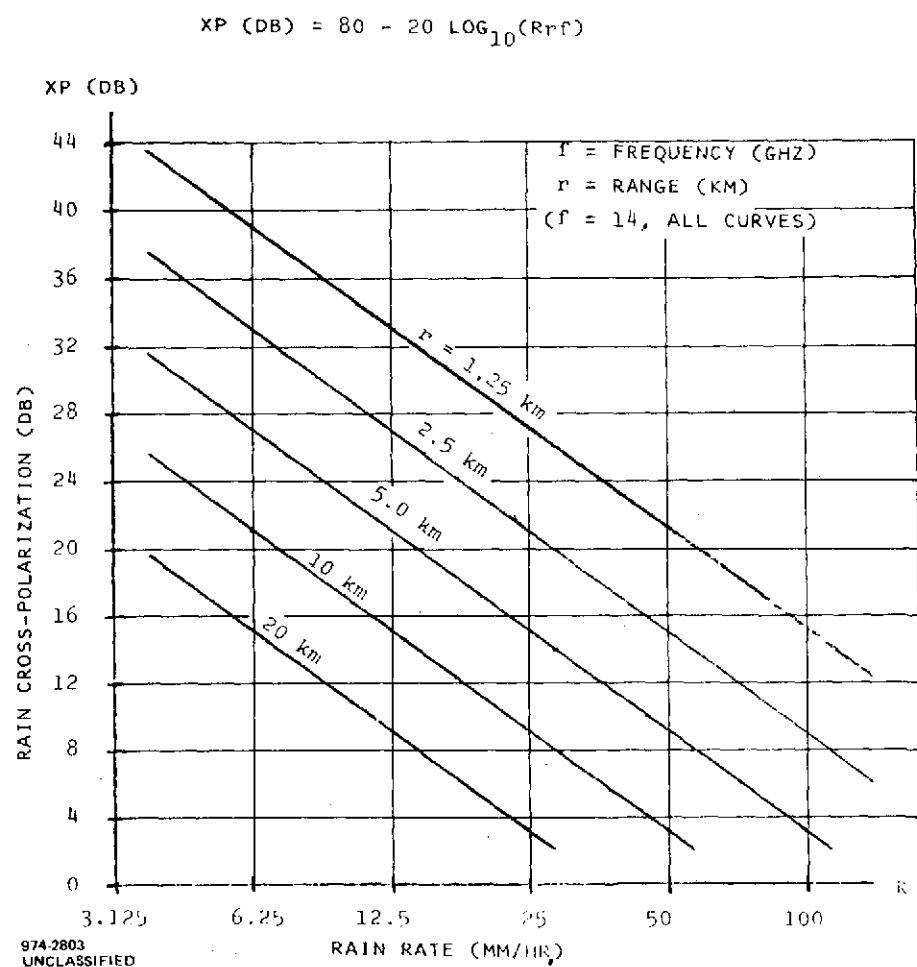


Figure 5-10. Theoretical Rain Depolarization for Circularly Polarized Waves, After Laur 1

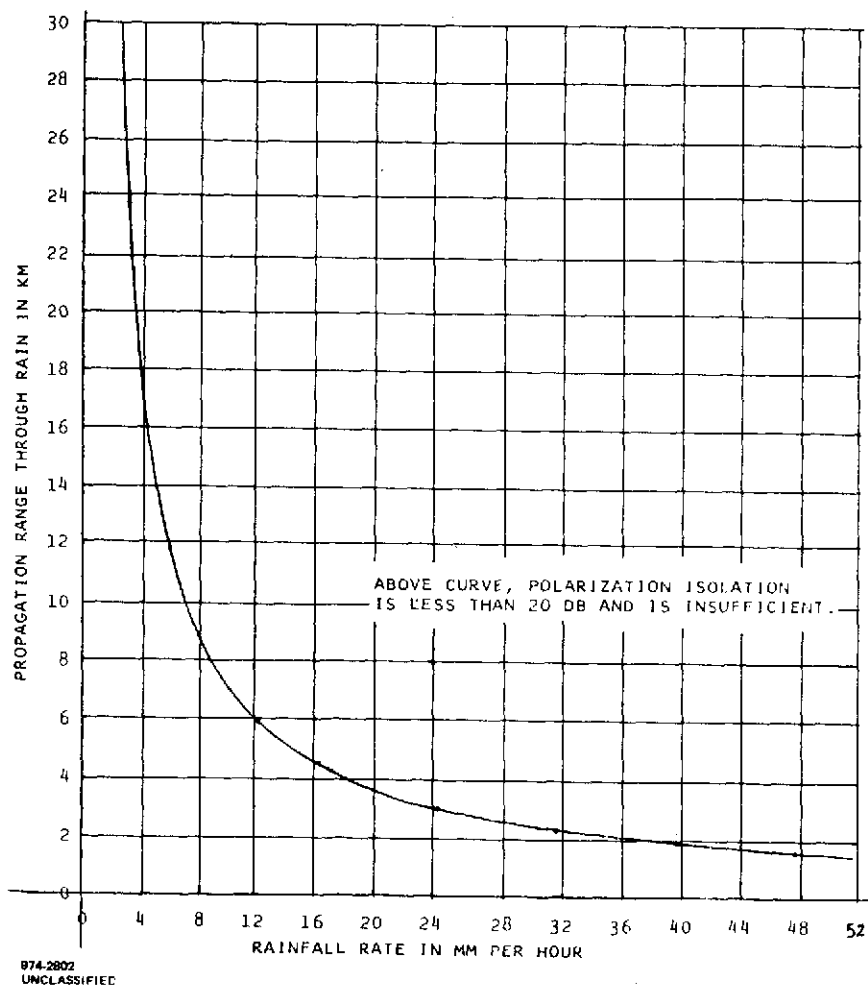


Figure 5-11. Contour of 20 dB Polarization Crosstalk in Rain

is insufficient for adequate P_e performance. It is in this region that an interference cancellation system (ICS) [12, 13, 14] could be used to restore adequate polarization isolation by reducing the rain-induced crosstalk.

5.2.2 STATISTICS OF RAIN DEPOLARIZATION AT Ku-BAND

In this section we will compute the cumulative probability distribution function for rain-induced polarization crosstalk. The cumulative distribution function for rain attenuation at Ku-band for White Sands Test Facility has been given in Figure 3-16 of reference [10] for a TDRS at 10° elevation. The dual abscissas on Figure 3-17 of [10] relate the rain rate to the attenuation level. Combining these two abscissas on Figure 3-16 of [10] allows one to reconstruct the number of hours per year that a particular rain rate R is exceeded.

Our computation will be completed by associating a polarization cross-talk isolation XP with rain rate using either Figure 5-10 or Equation (5-25) above. In order to use Equation (5-25) we must calculate the range r that the radio wave spends in rain. The geometry of this situation is illustrated in Figure 5-12. Using the law of sines we have

$$\frac{r}{\sin(\text{PCG})} = \frac{h+R_e}{\sin(\text{PGC})} = \frac{R_e}{\sin(\text{CPG})} \quad (5-26)$$

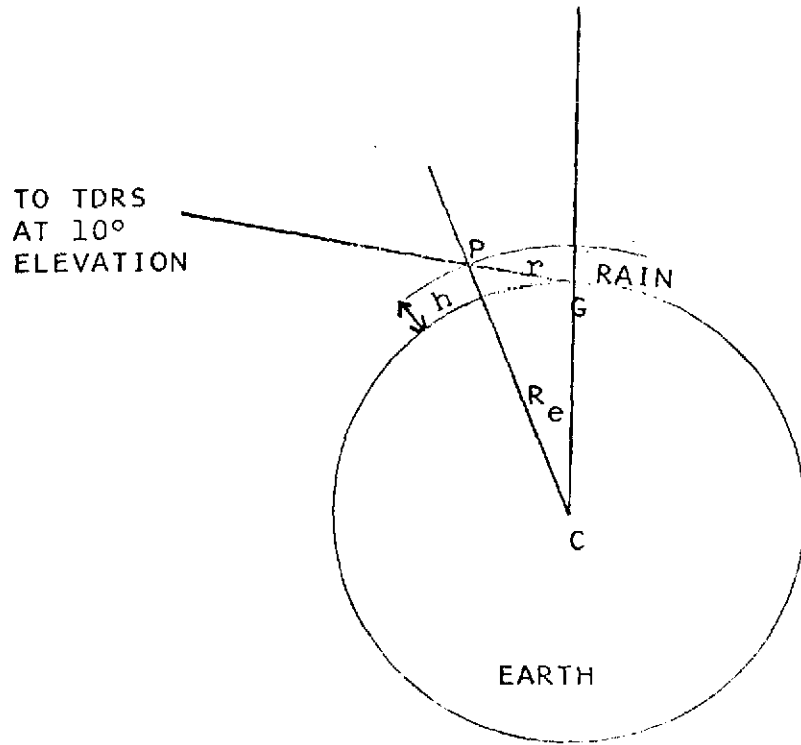
Using the right-hand equality of Equation (5-26) we obtain:

$$\text{CPG} = \sin^{-1} \frac{R_e \sin 100^\circ}{h+R_e} \quad (5-27)$$

But $\text{PCG} = 180^\circ - 100^\circ - \text{CPG}$. Again using Equation (5-26), we solve for the rain range:

$$r = \frac{h_e \sin (80^\circ - \text{CPG})}{\sin(\text{CPG})} \quad (5-28)$$

- 12. Abajian, A., et al, "Wideband Spectrum Notcher," Tri-Service Radar Symposium, Session 6, July 16-18, 1974, West Point, N.Y.
- 13. Request for Proposal IS-662, "Adaptive Interference Reduction Networks," INTELSAT, Washington, D.C. 20024, Statement of Work, dated 19 June 1974.
- 14. Zeger, A.E. and B.S. Abrams, "Interference Cancellation System for Sensors," presented at the Adaptive Antenna Systems Workshop, U.S. Naval Research Laboratory, Washington, D.C., 11-13 March 1974.



G = TDRSS GROUND STATION

C = CENTER OF EARTH

P = POINT AT WHICH RADIO RAY EXITS RAIN

r = PG = RANGE IN RAIN

R_e = GC = RADIUS OF EARTH

$h + R_e$ = PC

$\angle PGC = 90^\circ + \text{ELEVATION } X = 100^\circ$

h = HEIGHT OF RAIN CLOUDS

Figure 5-12. Geometry of Range in Rain Calculation

Taking the earth's radius $R_e = 6400$ km and a rain cloud height $h = 2$ km, Equations (5-27) and (5-28) yield the rain range $r = 11.46$ km.

This rain range (and $f = 14$ GHz) is inserted into Equation (5-25) to obtain the cross polarization isolation (XP) as a function of rain rate R :

$$\begin{aligned} \text{XP (dB)} &= 80 - 20 \log_{10} (160.4R) \\ &= 35.89 - 20 \log_{10} R \end{aligned} \quad (5-29)$$

Using Equation (5-29) and the previously obtained statistics for R , we plot in Figure 5-13 the number of hours per year that rainfall causes Ku-band attenuation and polarization crosstalk to exceed given levels for a TDRS at 10° elevation. For example, rain will cause 7.5 dB attenuation about 8 hours per year. During these same 8 hours per year, polarization isolation will not exceed 18 dB. Note that polarization crosstalk will exceed 20 dB about 9.5 hours per year, during which rain will cause an attenuation of at least 6.5 dB.

The maximum rain margin is 7.5 dB^[10] in the wideband KSA return link. Therefore, there will be an average of only 1.5 hours per year when the polarization isolation drops below 20 dB due to rain, while the attenuation level is still acceptable. This does not appear to be a serious penalty to pay for dual Ku-band return links.

At higher TDRS elevation angles, the rain range is reduced and so is the attenuation and the polarization crosstalk. When rain limits polarization isolation to 20 dB at an elevation angle of 10° ($r = 11.46$ km), the expected isolation at zenith ($r = h = 2$ km) is

$$\text{XP} = 20 \text{ dB} + 20 \log_{10} (11.46/2) = 35.2 \text{ dB}$$

Polarization crosstalk at elevation angles between 10° and 90° will decrease monotonically from 20 dB to 35.2 dB.

The polarization crosstalk analysis reported here is basically confirmed by some recently published experimental results^[15] at 20 GHz over a 2.8 km path

15. Yoshikawa, T. and M. Kuramoto, "20 GHz High-Speed Digital Radio Transmission Experiment During Heavy Rainfall," Proc IEEE (Letters), July 1974, pp. 1036-1037.

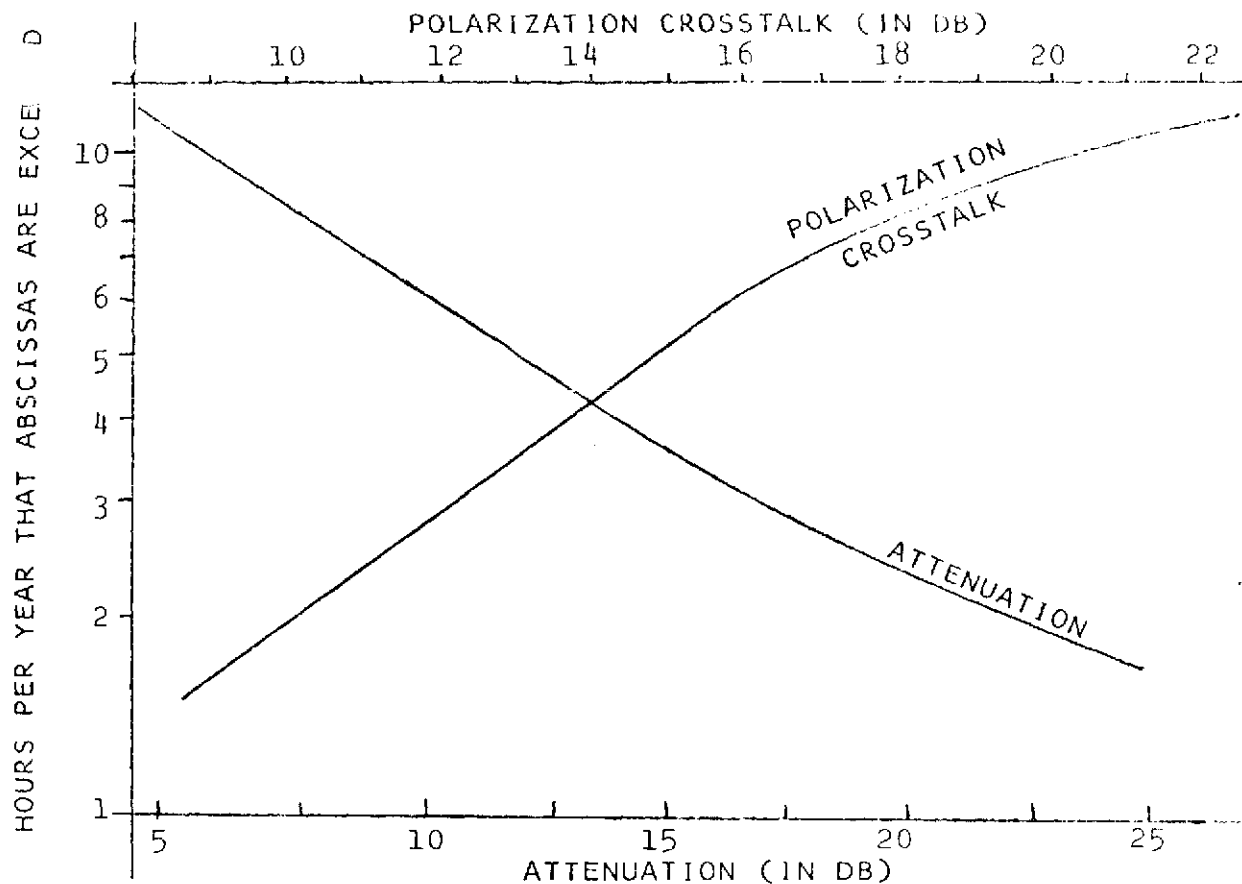


Figure 5-13. Number of Hours Per Year that Attenuation and Polarization Crosstalk are Exceeded at Ku-Band for 10° Elevation

in heavy rainfall. Reproduced below in Figures 5-14 and 5-15 (without permission) are the experimental results [15, Figures 2 and 3] of rain attenuation and cross-polarization plotted vs time and vs percentage of time.

5.2.3 ICS FOR POLARIZATION CROSSTALK REDUCTION

The depolarization processes (rain, etc.) described above are linear. The depolarization interference is additive and the crosstalk level is proportional to the signal levels transmitted by the TDRS. At the ground station, the waveforms received with vertically (R_v) and horizontally (R_h) polarized antennas are a linear

REPRODUCIBILITY OF THE
ORIGINAL PAGE IS POOR

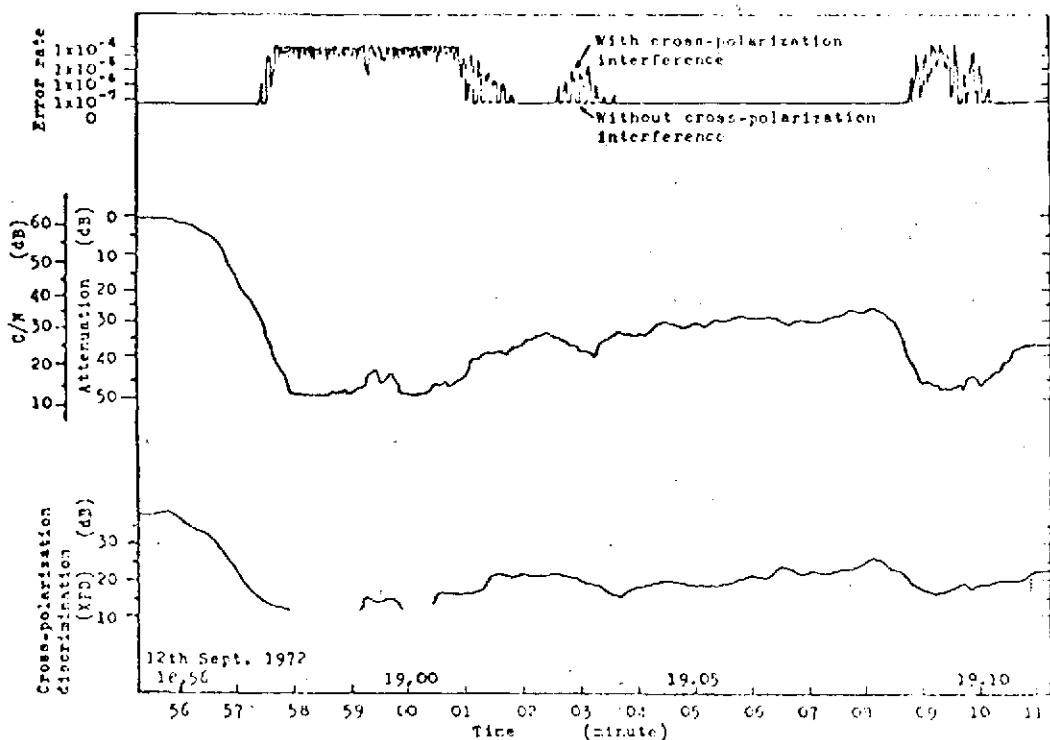


Figure 5-14. Data Obtained from PSK Signal-Transmission Experiment with Cochannel Cross-polarization Interference

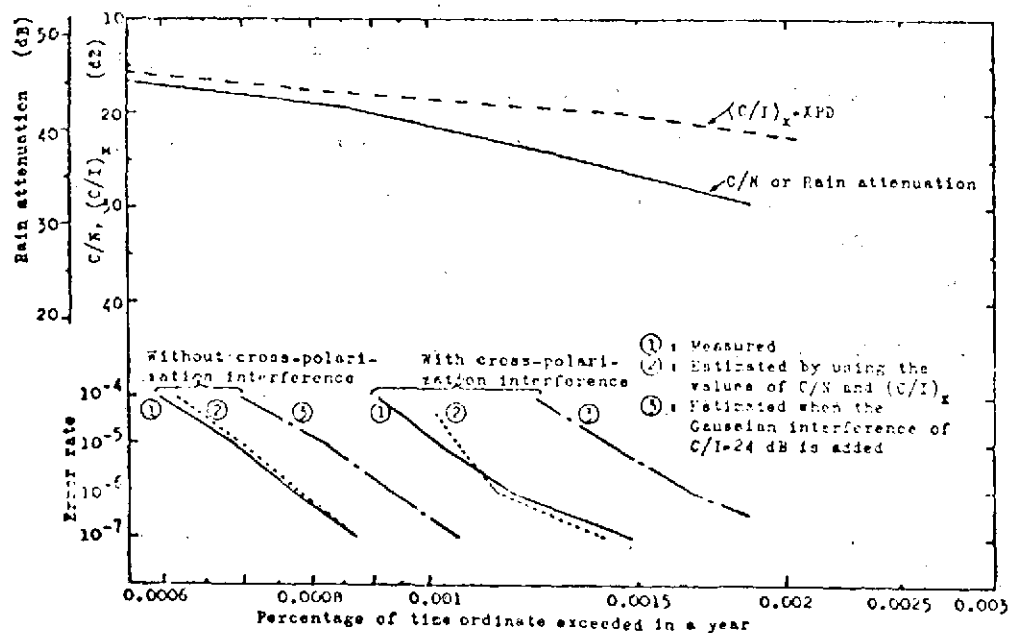


Figure 5-15. Cumulative Distribution of Rain Attenuation C/N, Cross-polarization Discrimination, and Error Rate

sum of the signals transmitted by the TDRS with vertical (T_v) and horizontal (T_h) polarization. In Matrix notation this depolarization coupling is represented [16] as:

$$\begin{pmatrix} R_v \\ R_h \end{pmatrix} = \begin{bmatrix} C_v & C_{hv} \\ C_{vh} & C_h \end{bmatrix} \begin{pmatrix} T_v \\ T_h \end{pmatrix} \quad (5-30)$$

When the off-diagonal phasor coupling coefficients C_{vh} and C_{hv} are zero, then there is no polarization crosstalk. The vertical and horizontal path losses are given by $|C_v|^2$ and $|C_h|^2$, respectively. The isolation of the vertical SA channel from polarization crosstalk due to the horizontal SA channel is given by the ratio $|C_{hv}/C_v|^2$, and vice versa for the horizontal channel isolation. Aside from additive noise, one could perfectly recover T_v and T_h by a linear processing of the received signals R_v and R_h which contain crosstalk terms. Inverting the matrix in Equation (5-30) leads to:

$$\begin{pmatrix} T_v \\ T_h \end{pmatrix} = \begin{bmatrix} C_v & C_{hv} \\ C_{vh} & C_h \end{bmatrix}^{-1} \begin{pmatrix} R_v \\ R_h \end{pmatrix} = \begin{bmatrix} C_h/C & -C_{hv}/C \\ -C_{vh}/C & C_v/C \end{bmatrix} \begin{pmatrix} R_v \\ R_h \end{pmatrix} \quad (5-31)$$

This removal of polarization crosstalk is diagrammed in Figure 5-16 where we denote the determinant of the coupling matrix by $C = C_v C_h - C_{hv} C_{vh}$. The outputs \hat{T}_v and \hat{T}_h of the matrix inversion system are only estimates of the transmitted signals T_v and T_h because of additive noise, imperfect knowledge of the polarization coupling matrix, and other factors. Four wideband multipliers are shown in Figure 5-16 in order to scale the 225 MHz wide received signals by the complex weights C_h/C , C_{vh}/C , C_{hv}/C and C_v/C . Actually, only two such wideband multipliers are required. A simplified block diagram of such a polarization demultiplexer is shown implemented at IF in Figure 5-17.

The received signals in Figure 5-17 are again given by Equation (5-30) and the vertical signal R_v contains the horizontal crosstalk term $C_{hv} T_h$. A portion

16. Cox, D. C., "Design of the Bell Laboratories 19 and 28 GHz Satellite Beacon Propagation Experiment," IEEE 1974 International Communications Conference Record, 17-19 June 1974, Minneapolis, Minn.

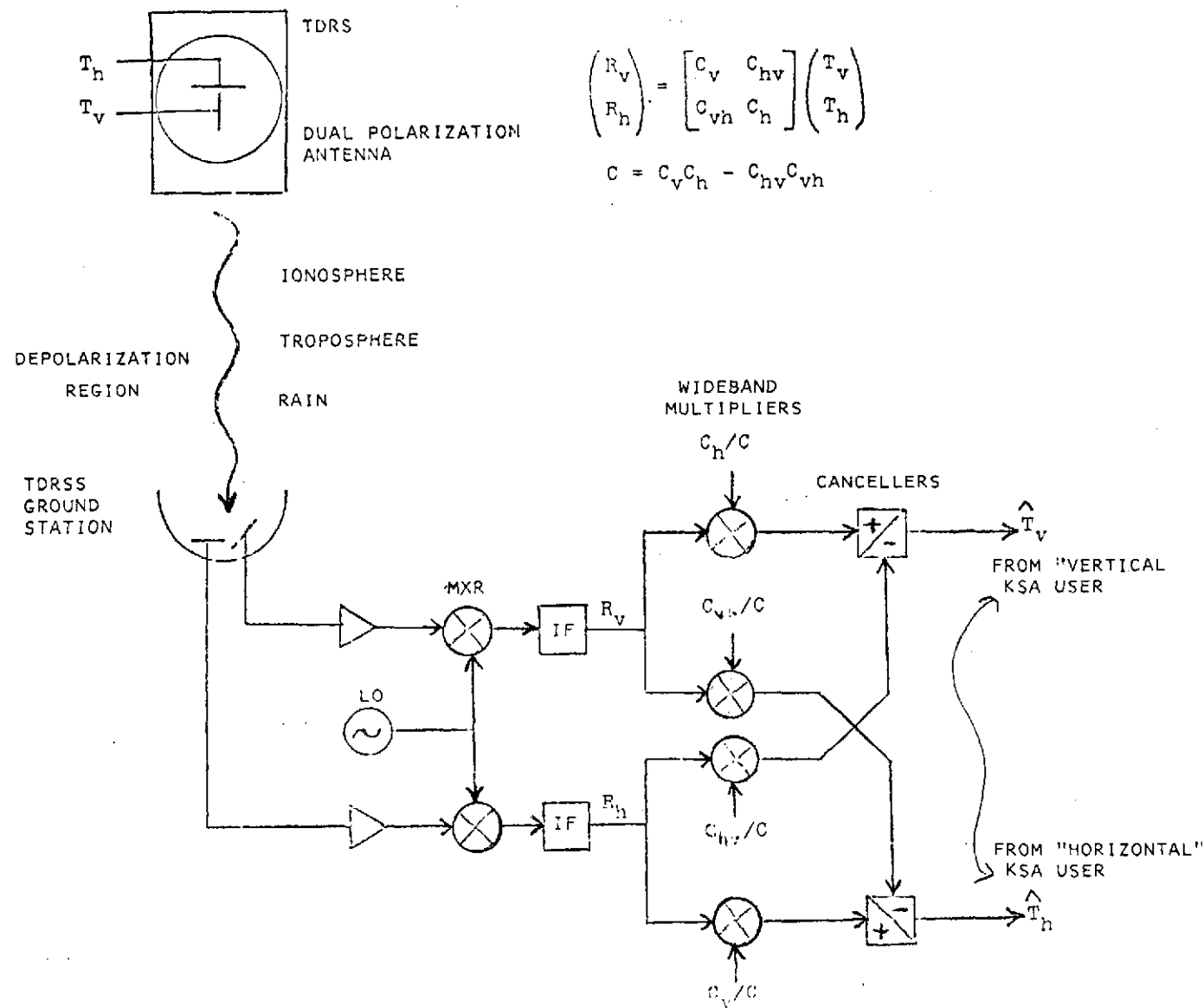


Figure 5-16. Model of TDRS Polarization Crosstalk and Ground Station Depolarization System

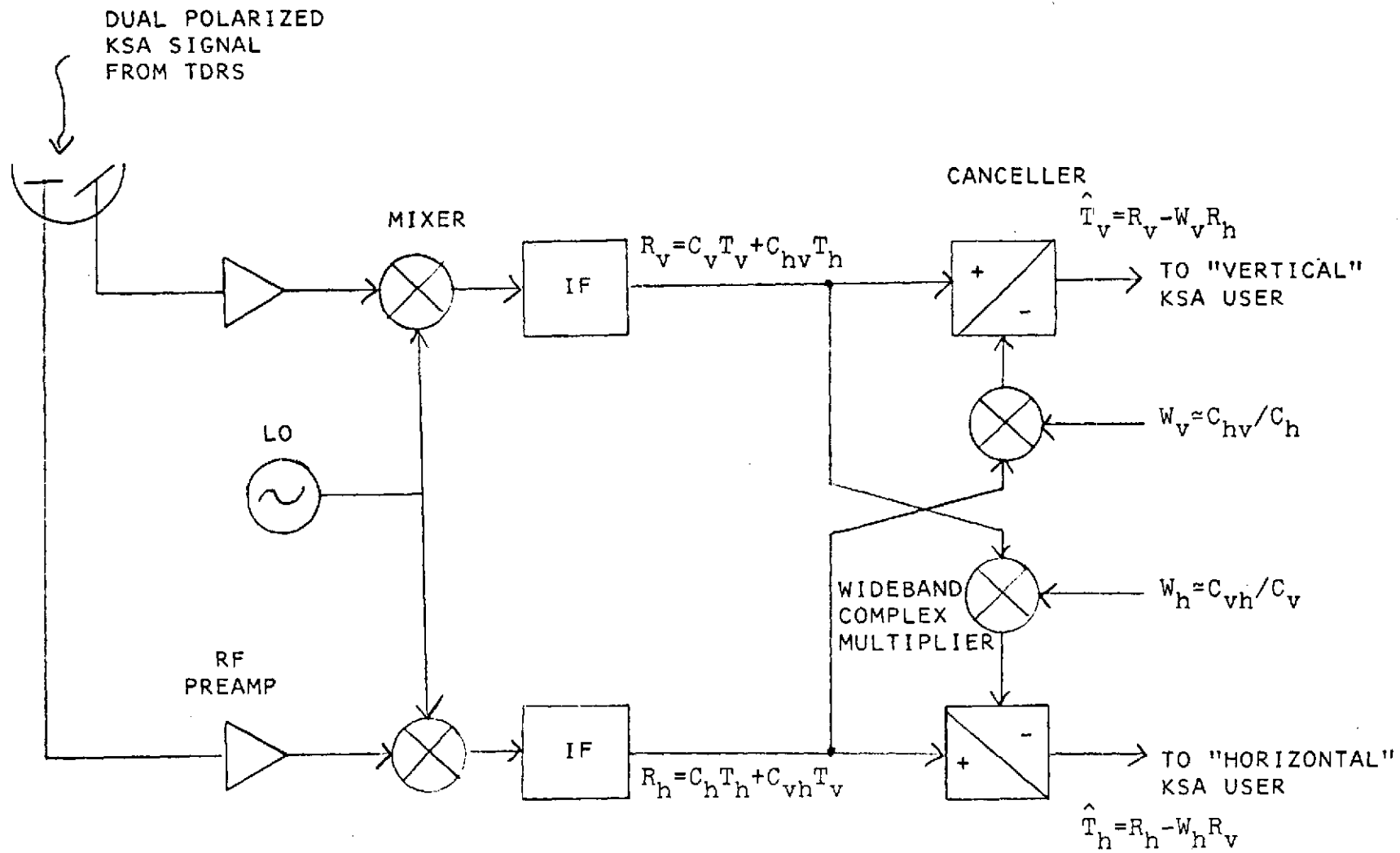


Figure 5-17. System for Cancellation of Polarization Crosstalk at IF

of the received horizontal signal is weighted by the complex scalar W_v and is subtracted from R_v . The resulting estimate \hat{T}_v of the SA user's signal T_v is given by:

$$\begin{aligned}\hat{T}_v &= R_v - W_v R_h \\ &= (C_v - W_v C_{vh}) T_v + (C_{hv} - W_v C_h) T_h\end{aligned}\quad (5-32)$$

The unwanted horizontal crosstalk term in Equation (5-32) is removed by setting W_v equal to its optimal value

$$(W_v)_{\text{opt}} = C_{hv}/C_h \quad (5-33)$$

Inserting Equation (5-33) into Equation (5-32) yields the vertical user's signal isolated from horizontal user crosstalk:

$$\hat{T}_v = (C_v - C_{hv} C_{vh}/C_h) T_v \quad (5-34)$$

Similarly, by setting the horizontal weight to its optimal value

$$(W_h)_{\text{opt}} = C_{vh}/C_v \quad (5-35)$$

we obtain the horizontal user's signal isolated from the vertical user's crosstalk

$$\hat{T}_h = (C_h - C_{hv} C_{vh}/C_v) T_h \quad (5-36)$$

It still remains to be shown how the optimal weights W_v and W_h given in Equations (5-33) and (5-35) can be determined since the polarization coupling coefficients C_v , C_h , C_{vh} and C_{hv} are unknown a priori and are time varying.

One approach to implementing the complex multipliers (weights) used in the cancellation systems of Figures 5-16 and 5-17 is indicated in the simplified diagrams shown in Figure 5-18. In Figure 5-18A, the wideband input waveform is split by a 90° hybrid into inphase (I) and quadrature (Q) components. These I and Q components pass through a pair of bipolar multipliers where they are weighted by the real and imaginary parts of the complex weight value W .

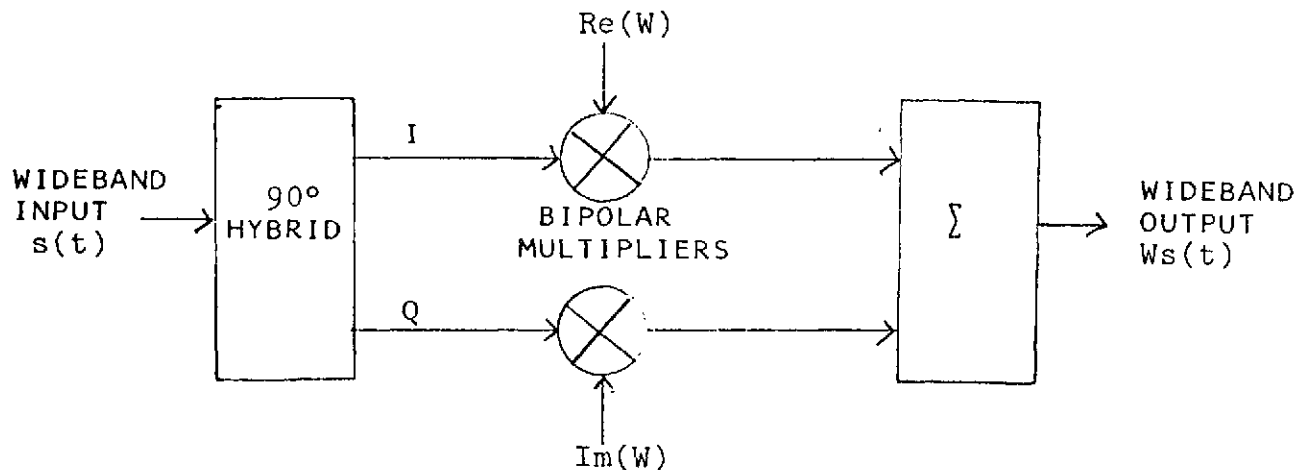


Figure 5-18A. Implementation of a Complex Multiplier with a Pair of Bipolar Multipliers

In Figure 5-18B we illustrate an implementation of a bipolar multiplier. The variable attenuators R_1 and R_2 are controlled by $Re(W)$ or $Im(W)$ and are operated push-pull. When $R_1 = R_2$, the output is zero and the zero multiplication factor has been applied to the input waveform. When $R_1 < R_2$, the output is in phase with the weight input and when $R_1 > R_2$, the output is 180° inverted. The variable attenuators have been implemented [17] using biased PIN diodes.

5.2.4 CONTROL SYSTEM FOR CROSSTALK CANCELLATION

5.2.4.1 Measurement/Program Technique

In this approach the complex values of the four polarization coupling coefficients are measured directly at the ground station. From these measured quantities, the optimum W_v and W_h are computed according to Equations (5-33) and (5-35) and these weight values are programmed into the appropriate ports in Figure 5-17.

17. Sauter, W. A., "RF Signal Controller," U.S. Patent 3,550,041
22 December 1970.

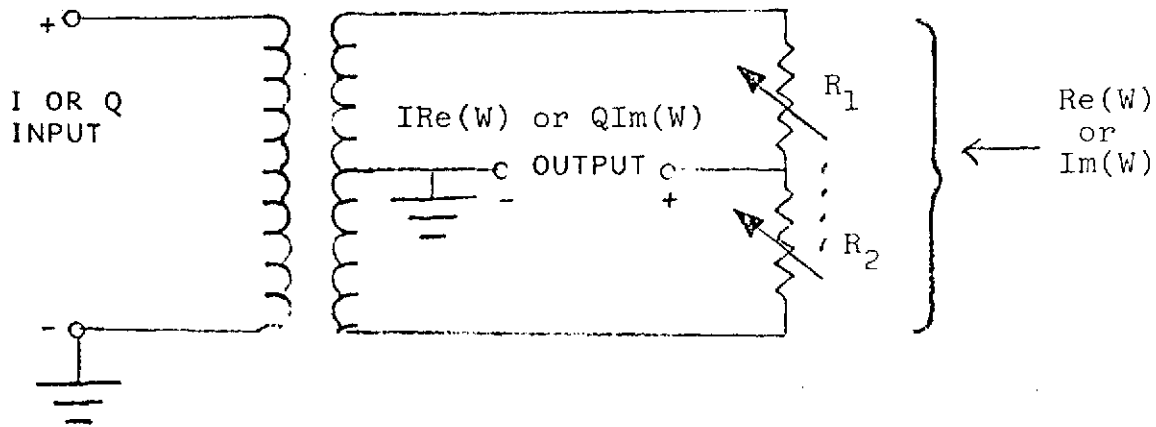


Figure 5-18B. Implementation of a Bipolar Multiplier with Electronically Variable Attenuators

If the TDRS briefly turns off its "horizontal" transmitter, then C_v and C_{vh} can be measured from signals received at the ground station on the vertical and horizontal channels, respectively. Similarly, by turning off the "vertical" transmitter on the TDRS the values of C_{hv} and C_h can be measured from the vertical and horizontal channels, respectively, at the ground station. An alternative procedure to measure the four coupling coefficients would be to transmit orthogonal vertical and horizontal pilot signals from the TDRS. Then vertical and horizontal pilot receivers on both vertical and horizontal ground station channels would permit direct measurement of C_v , C_h , C_{vh} and C_{hv} without interrupting the signals transmitted by the TDRS. This "open loop" system is subject to measurement, computation and weight programming errors and heavily involves the TDRS and is, therefore, not as reliable a solution as the closed loop LMS control system described below.

5.2.4.2 Adaptive Search Algorithm Control

We have seen that polarization crosstalk can be cancelled by the system shown in Figure 5-17 when the complex weights W_v and W_h assume the optimal values

given in Equations (5-33) and (5-35). The uncancelled crosstalk component in the vertical channel is obtained from Equation (5-32):

$$\begin{aligned}(C_{hv} - W_v C_h) T_h &= [(C_{hv}/C_h) - W_v] C_h T_h \\ &= [(W_v)_{opt} - W_v] C_h T_h\end{aligned}\quad (5-37)$$

From Equation (5-37) we obtain the unwanted crosstalk power P_{xv} in the vertical channel.

$$\begin{aligned}P_{xv} &= |[(W_v)_{opt} - W_v] C_h T_h|^2 = |(W_v)_{opt} - W_v|^2 |C_h T_h|^2 \\ &= \{\text{Re}^2[(W_v)_{opt} - W_v] + \text{Im}^2[(W_v)_{opt} - W_v]\} |C_h T_h|^2 \\ &= \{\text{Re}^2(\Delta W_v) + \text{Im}^2(\Delta W_v)\} |C_h T_h|^2\end{aligned}\quad (5-38)$$

From (5-38) we see that P_{xv} is a quadratic function of the real and imaginary parts of the error, ΔW_v , in the vertical weight setting. In order to minimize P_{xv} it is thus necessary to simultaneously determine the correct settings for $\text{Re}(W_v)$ and $\text{Im}(W_v)$.

Suppose we can demodulate the output vertical channel signal (\hat{T}_v in Figure 5-17) and determine its short-term probability of error Pe by using information from an error-detecting decoder. Then the proper choices of $\text{Re}(W_v)$ and $\text{Im}(W_v)$ can be found by noting the change δPe in error rate produced by small trial changes in δW_v . This search for the best point in control parameter space W_v , corresponding to minimum Pe , could be conducted by a hardware or software implementation of one of the efficient adaptive search algorithms described by Barron [18]. For high data rates on the KSA return link, it may not be practical to add parity code bits for Pe performance monitoring. In this case some other measure of polarization isolation must be employed to guide W_v optimization. This can be accomplished by "tagging" the unwanted cross-polarization components in some fashion.

Suppose that vertical and horizontal pilot signals were added to the vertical and horizontal KSA information signals transmitted by the TDRS via orthogonal polarizations to the ground station. Further assume that these two pilot

18. Barron, R. L., "Theory and Application of Cybernetic Systems: An Overview," Proc IEEE National Aerospace and Electronics Conference, 13-15 May 1974, Dayton, Ohio, pp. 107-118.

signals are known a priori and can be separated at the ground station from the KSA signals and from each other by correlation/filtering techniques. The vertical output \hat{T}_v can thus be processed to isolate and measure its content of h-pilot. The weight W_v can then be adjusted by a search algorithm to drive the level of h-pilot in \hat{T}_v to zero and thereby reduce the crosstalk in the vertical channel of Figure 5-17. Additive pilot signals impose a hardware burden on the TDRS and are therefore not as attractive a means for increasing polarization isolation as is the LMS system described below.

5.2.4.3 Bandwidth of Polarization Crosstalk Coupling

We describe in a later section a polarization crosstalk cancellation system which does not require the addition of vertical (v) and horizontal (h) pilot signals nor the addition or parity code bits to the return link KSA waveforms. It does, however, require a slight offset in center frequency between the v-KSA and h-KSA signals and a demodulation of these signals at the ground station. The frequency offset $|f_v - f_h|$ must be about an order of magnitude greater than the largest expected bandwidth B_c of the depolarization coupling coefficients in Equation (5-30). This will permit timely adjustment of the complex weights W_v and W_h in Figure 5-17 as rain conditions (R, etc.) fluctuate. We thus require

$$|f_v - f_h| > 10 B_c$$

A crude, but conservative, estimate of the bandwidth B_c of the rain depolarization coupling coefficients can be made by determining how often the ground station antenna looks at the TDRS through a new set of raindrops. The gain of an antenna of area A operating at wavelength λ with an efficiency η is given by the equation:

$$G = 4\pi\eta A/\lambda^2 \quad (5-39)$$

Setting $G = 1$ we can solve for the effective area A_{iso} of an isotropic radiator:

$$A_{iso} = \lambda^2 / (4\pi\eta) \quad (5-40)$$

We thus view the dish antenna as a coherent array of G isotropic elements, each of linear dimension $\sqrt{A_{iso}} = \lambda / \sqrt{4\pi\eta}$. The antenna response can change whenever each of these G elements looks at a new rain situation. The time Δt it takes rain to fall or

be blown by wind past one of these isotropic elements is given by the expression

$$\Delta t = \sqrt{A_{iso}}/v \quad (5-41)$$

where v = velocity of rain across the antenna. The bandwidth of this process is approximately

$$B_c = 1/\Delta t = v/\sqrt{A_{iso}} = 2v\sqrt{\pi\eta}/\lambda \quad (5-42)$$

The maximum velocity of falling raindrops [19] is 10 meters/sec (22.4 miles/hour); hence, we assume that $v_{max} = 50$ m/sec under severe wind and rain conditions. In order to evaluate B_c we further assume $\eta = 70\%$ and $\lambda = 0.02$ meters. Then by Equation (5-42)

$$B_c = 2(50\text{m/sec})\sqrt{0.7\pi}/(0.02\text{m}) = 7,415 \text{ Hz}$$

In order to satisfy Equation (5-38) we will require that the vertical and horizontal center frequency offsets will exceed 100 kHz, i.e.,

$$|f_v - f_h| \geq 100 \text{ kHz}$$

This 100 kHz offset represents one part out of 140,000 of the Ku-band center frequency and only one part out of 2,250 of the 225 MHz bandwidth and should not be difficult to implement.

5.2.4.4 LMS Control Algorithm for Crosstalk Cancellation

The least mean square (LMS) adaptive control algorithm combines a steepest (gradient) descent procedure with time-derivative control to effect real time optimization. This technique has been applied to adaptive nulling antenna arrays [20] and has been found convenient to implement in analog circuitry [14] for the control of an interference cancellation system.

19. Berry, Bollay, and Beers (eds.), Handbook of Meteorology, McGraw-Hill Book Co., New York, 1945, p. 115.

20. Widrow, B., et al., "Adaptive Antenna Systems," Proc IEEE, December 1967, pp. 2143-2159.

The LMS control algorithm is defined by the following equation:

$$\frac{dW}{dt} = -g \overline{\frac{\partial \epsilon^2}{\partial W}} \quad (5-43)$$

where the overbar denotes a lowpass correlation operation and

ϵ = the error signal to be minimized

W = the control parameter (weight) to be adjusted to
minimize ϵ

g = feedback loop gain factor ($g > 0$)

A simplified block diagram of an ICS incorporating LMS control is illustrated in Figure 5-19. The reference $r(t)$ is a replica of the interference $i(t)$ and is related by the complex scale α :

$$\alpha r(t) = i(t) \quad (5-44)$$

It is assumed that $i(t)$ and the signal $s(t)$ and noise $n(t)$ are uncorrelated. The "error signal" in Figure 5-19 is therefore found to be:

$$\epsilon(t) = s(t) + (\alpha - W) r(t) + n(t) \quad (5-45)$$

Integrating both sides of Equation (5-43) yields

$$W = -g \int \overline{\frac{\partial \epsilon^2}{\partial W}} dt = -2g \int \overline{\epsilon \frac{\partial \epsilon}{\partial W}} dt \quad (5-46)$$

From Equation (5-45) we note that

$$\frac{\partial \epsilon}{\partial W} = -r(t) \quad (5-47)$$

Hence Equation (5-46) leads to the control law illustrated in the ICS of Figure 5-19.

$$W = 2g \int \overline{\epsilon r(t)} dt \quad (5-48)$$

Inserting Equation (5-45) into Equation (5-48) yields:

$$W = 2g \int \overline{(\alpha - W)r^2(t)} dt \quad (5-49)$$

For a constant average power reference $\overline{r^2(t)} = P_r$, Equation (5-49) can be rewritten as an ordinary differential equation:

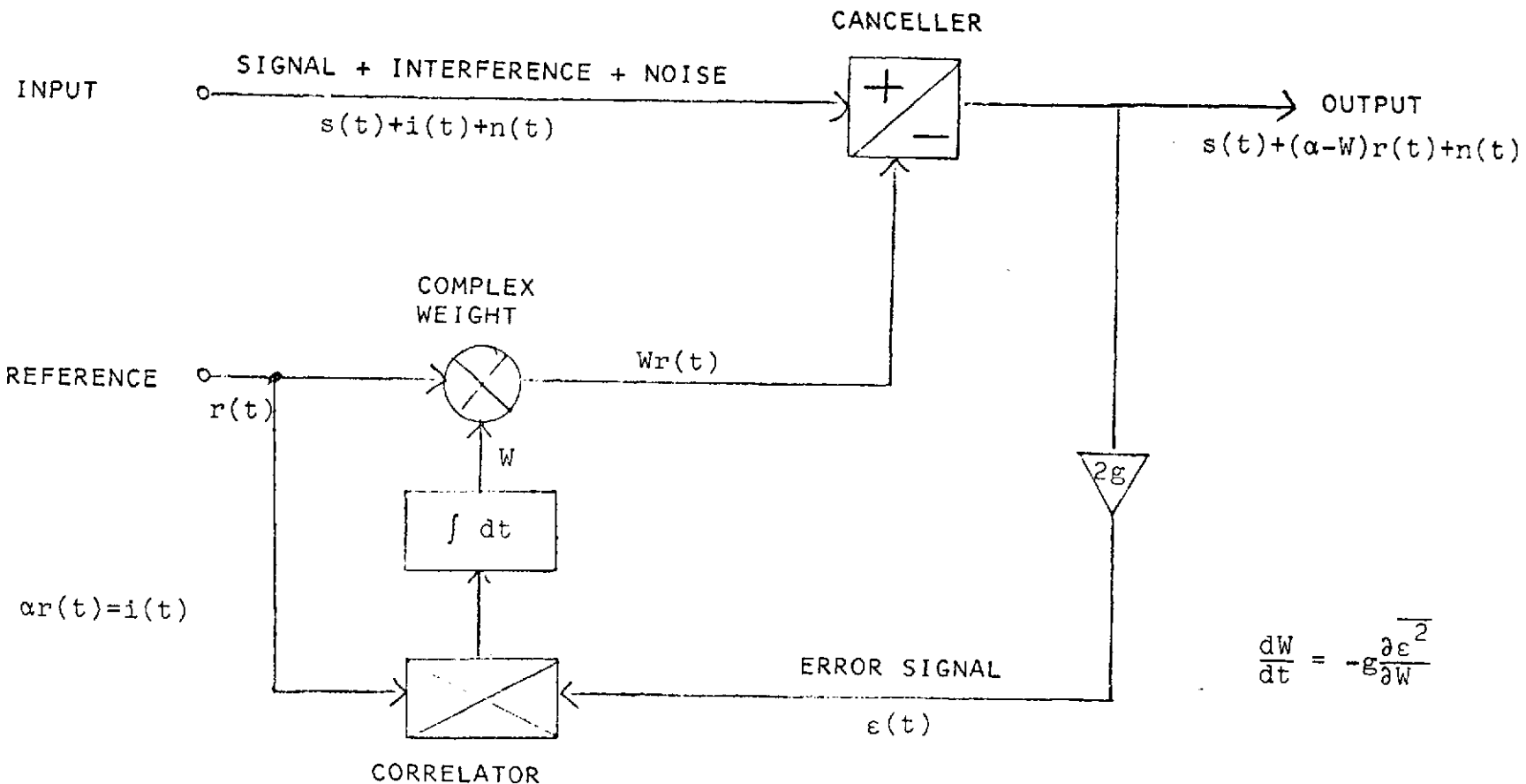


Figure 5-19. ICS Employing the LMS Algorithm

$$W + 2gP_r W = 2g\alpha P_r \quad (5-50)$$

Choosing $W = 0$ at $t = 0$, the solution of Equation (5-50) is

$$W = \alpha(1 - e^{-2gP_r t}) \quad (5-51)$$

As $t \rightarrow \infty$ the desired steady state weight $W = \alpha$ is obtained. Thus perfect interference cancellation is theoretically achieved since the ICS output given by Equation (5-45) becomes $\epsilon(t) = s(t) + n(t)$.

In order to cancel the polarization crosstalk in the vertical channel, the horizontal channel becomes the reference for the ICS. However, this reference contains vertical signal as seen by reviewing Equation (5-30) and means must be taken to assure cancellation of the crosstalk and not the desired signal. Use of the frequency separation $|f_v - f_h| \geq 100$ kHz described above will be made to effect proper cancellation.

The LMS system for cancellation of polarization crosstalk is illustrated in Figure 5-20. There are actually a pair of ICS's employed, one for the v-KSA channel and one for the h-KSA channel. The operation of the v-channel ICS in Figure 5-20 is dependent upon obtaining the proper weight W_v in order to cancel unwanted horizontal KSA signals in the v-channel at the top of Figure 5-20. The control law given in Equation (5-48) is modified by replacing the ideal integrator with a more realizable lowpass filter (LPF). Since we want W_v to respond only to correlation of unwanted (horizontal) components in R_v , we must remove the vertical signal components from the reference (R_h) and error (ϵ_v) waveforms.

The h-KSA modem's data are brought over (via dashed lines in Figure 5-20) to strip the horizontal data from R_h and ϵ_v . Narrowband filters (NBF) tuned to f_h then pass only h-waveform components to the v-correlator to yield the weight control W_v . Because of the $f_v - f_h$ frequency offset, W_v responds only to h-crosstalk and not to v-signal even when identical data appear on both v and h KSA channels. A pair of delay lines corresponding to one h-data bit (T_b) is provided at points prior to each data stripping operation to permit the modems to generate reliable data. For 100 Mbps data, $T_b = 10$ ns and the delay lines can be short lengths of coaxial cable.

This bootstrap system of Figure 5-20 can get started providing the initial signal-to-crosstalk ratio is greater than about 6 dB, at which point the data

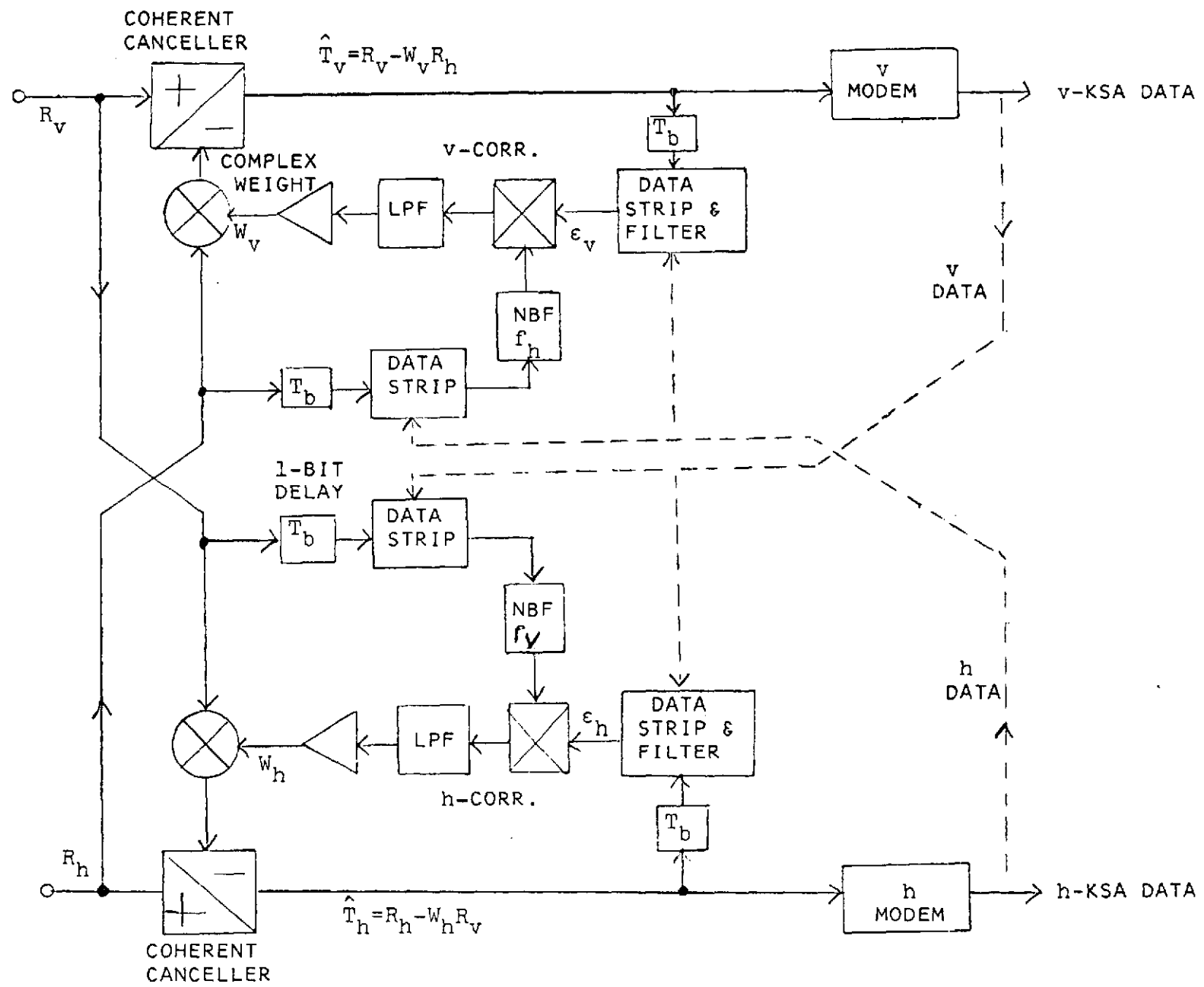


Figure 5-20. LMS System for Cancellation of Polarization Crosstalk

from the modem will be reliable enough to initiate data stripping. Once data stripping starts, crosstalk cancellation begins and the signal-to-crosstalk ratio improves, then the data gets better and the improvement process continues until additive thermal noise, rather than crosstalk, limits the error rate.

5.2.4.5 Crosstalk Cancellation Implementation

The most critical component of the ICS shown in Figure 5-20 is the pair of complex weights. Weight implementation will limit the bandwidth over which cancellation can be achieved. The author does not know of any ICS that has demonstrated cancellation across a 225 MHz band. Cancellation has been demonstrated over a 50 MHz band [12] and INTELSAT has recently issued an RFP [13] for an ICS to cover the entire 3.7 to 4.2 GHz band. It is likely that the development of an ICS capable of cancelling a 225 MHz wide waveform will follow from existing designs using PIN diode weights. Since the cancellation required for equal strength v- and h-KSA signals ($T_v = T_h$) will not exceed 20 dB, the component tolerances on the crosstalk ICS of Figure 5-20 are relatively easy to meet. Cancellation of UHF interference by up to 80 dB using an LMS controlled ICS has been experimentally demonstrated [21].

An additional limitation to cancellation of dual broadband KSA signals is differential time delay in the vertical and horizontal transmission lines prior to the coherent cancellers in Figure 5-20. It has been shown [14] that the best possible cancellation ratio (CR) that can be obtained upon a noise-like interference of bandwidth B when there is a differential time delay τ of the reference waveform is given by

$$CR = 2 \left[1 - \frac{\sin(\pi B \tau)}{\pi B \tau} \right] \quad (5-52)$$

In order to determine the delay tolerances for 20 dB cancellation we set $CR = 0.01$ and $B = 2.25 \times 10^8$ in Equation (5-52) to obtain:

$$|\tau| \leq 0.25 \text{ ns}$$

Therefore cable lengths must be kept to an overall agreement of about 3" from the v and h antennas to the canceller.

21. Sauter, W. and Ghose, R., "Active Interference Cancellation Systems," Rome Air Development Center, Final Technical Report RADC-TR-69-41, April 1969, Griffiss AFB, New York 13441.

The ICS described above for removal of polarization crosstalk could provide increased yearround KSA user isolation in addition to restoring a minimal acceptable isolation during an expected nine hours per year that rain depolarization will exceed 20 dB (see Section 5.2.2).

In order to assure the availability of a broadband (225 MHz wide) ICS on a timely basis, it is recommended that an effort be sponsored in the near future to develop a complex PIN diode weight, suitable for TDRS ground station use at Ku-band.

5.2.5 IMPACT ON TDRS

The implementation of the dual polarization RF distribution system for KSA frequency reuse is discussed in Section 5.3.

5.3 RF COMBINING TECHNIQUES

5.3.1 SYSTEM REQUIREMENTS

The main purpose of this paper is to determine the requirements, implementation, expected performance, and tradeoffs for the Ku-Band transmit combiner. The Ku-Band combiner required in Figure 3.10 of the NASA TDRSS Definition Phase report can be implemented in various ways. The first question is what are the specific requirements? There are no specific values, thus they must be assigned. The system gain budget allows for a total rf loss of 2 dB between the amplifier output and the antenna. This low loss is definitely near the state-of-the-art, and will require the best components and methods to achieve this low value. The gain budget of Table 5-3 was made to properly proportion losses. Obviously waveguide techniques must be employed to meet the desired budget. Based on this budget, and other known requirements for rf components, the basic specifications for the combiner as shown in Table 5-4 were made.

Table 5-3. Total Transmit RF Losses Estimate

	<u>Waveguide</u>	<u>Coax</u>
Combiner	0.5 dB	1.0 dB
T/R Diplexer	0.4 dB	1.0 dB
2 ea Switch	0.7 dB (coax)	0.7 dB
Interconnects + Mismatch	0.5 dB	1.0 dB
Total Loss	2.1 dB	3.7 dB

Table 5-4. Basic Combiner Specifications

Ins. Loss	0.7 dB max.
Interchannel Isol.	15 dB min.
RF Power	20W min.
VSWR	1.22:1 max.
δLIN	5% max.

The total losses must be kept low due to the impact on rf power out and thus dc power, and on system noise temperature. These tradeoffs will be discussed later.

5.3.2 COMBINING TECHNIQUES

There are various basic means to combine the Ku-Band signals. These are the resistive combiner, hybrid combiner, multiplexer, polarization diversity, and with dual signals through a linear amplifier. The performance of each is listed in Table 5-5. Due to their inherent high insertion losses, the resistive combiner and hybrid combiner techniques are not acceptable. The approach using multiple signals through a single amplifier is not desirable, due to strong intermodulation products, excess amplifier rf power requirements and resulting extra dc drain. This latter approach may be feasible for the weaker signals. The type 1, 2 and 4 techniques in addition require bandpass filters to clean-up the transmitted signal. Thus, the basic non-contiguous type multiplexer is selected as the combiner. The multiplexers are basically just a bank of filters combined together. Thus, the multiplexer not only allows low loss combining of two non-coherent signals, but also provides a band-pass filter at each input frequency.

A significant specification on the combiner is the worst case band edge interchannel isolation. It is true multiplexers can be built with isolations of only 5-10 dB, with apparent low insertion losses, but in reality this allows an extra 1 dB of power loss through the adjacent channel. Therefore a minimum of 15 dB isolation is desired to reduce the extra losses due to interchannel losses to less than 0.2 dB. The multiplexers are designed so the matched bandwidth is generally slightly greater than the full passband. This allows uniform performance across the entire desired passbands. The band edges losses are usually only 0.2 dB above the band center losses.

Various combining methods using multiplexers have been analyzed for use at Ku-Band. In general, waveguide types will give half the loss of coax types. The achievable unloaded Q^S for each are 6000 and 2000 respectively. In addition, waveguide types are double the volume, but half the weight of coax types. All of the techniques listed will have volumes less than 40 in³ and weights less than 1 lb.

The basic frequency plan for combining is shown in Figure 5-21. The loss for the 13 watt channels is especially important, whereas channels 1 and 2 can stand higher losses than 0.5 dB. Twelve different solutions are shown in Figures 5-22 through 5-33. Band 3 is not used. Band 1 contains 30 IF combined signals with a total average power of 52/420 mW. Band 2 contains two signals with a total overage power of 44/350 mW.

Table 5-5. Basic Combiners Types - Typical Performance

1)	N-WAY RESISTIVE COMBINER	
	VSWR	1.1
	ϕ_{LIN}	1%
	Loss	6 dB (2-way)
	Isolation	6 dB (2-way)
	Power	5W
2)	N-WAY HYBRID COMBINER, 90°, 180° or IN-PHASE	
	VSWR	1.3
	ϕ_{LIN}	2%
	Loss	4 dB (2-way)
	Isolation	15-20 dB
	Power	50W
3)	N-WAY MULTIPLEXER	
	VSWR	1.2
	ϕ_{LIN}	5%
	Loss	0.5 dB
	Isolation	15 dB
	Power	100W
4)	POLARIZATION DIVERSITY AND/OR MULTIPLE SIGNAL WITH LINEAR AMPS	
	VSWR	1.2
	ϕ_{LIN}	<5%
	Loss	0
	Isolation	20 dB
	Power	20W peak
	IMD	-10 dB SS amps -20 dB TWT ^S

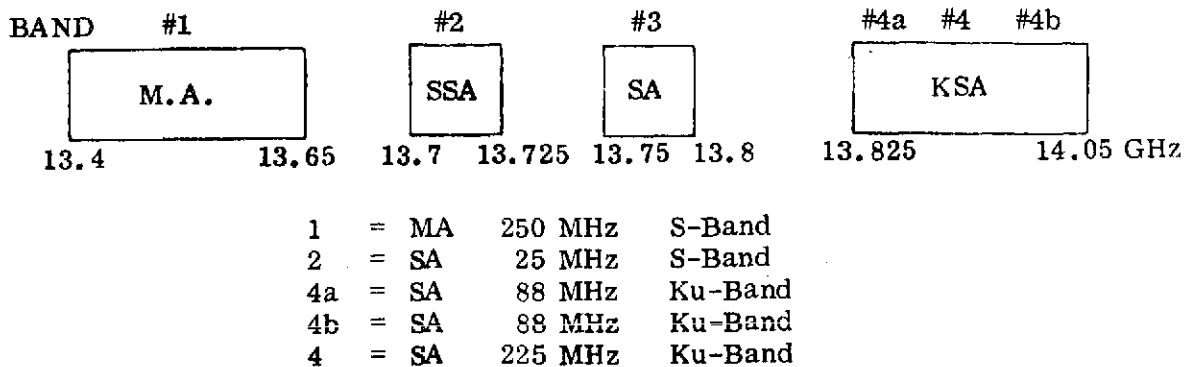


Figure 5-21. Basic Frequency Plan

Bands 4a, 4b and 4 are either 3.2 or 13 watts, but not simultaneously. The losses are due to the combiner only.

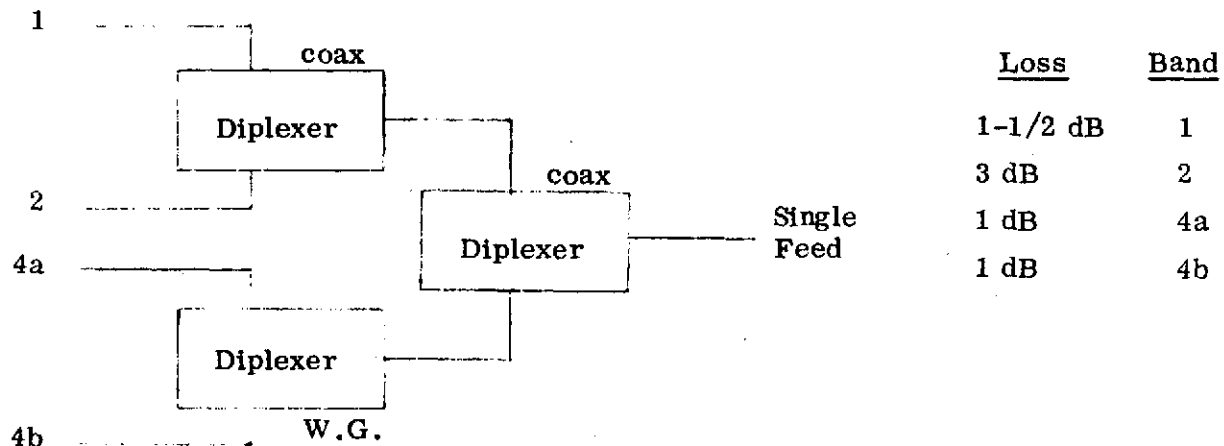
All of the methods are designed with a minimum isolation of 14 dB.

Typical interchannel isolations are shown in Table 5-6. Where a signal goes direct to another antenna feed, the antenna polarization isolation determines the inter-channel isolation. This is typically 15-30 dB. All amplifiers are before the combiners unless otherwise shown.

The combiner methods are ranked in Table 6-7. Method 6 provides the best overall answer for low loss, good isolation, and minimum performance impact on the rest of the system. Methods 4, 5, 7, 9, and 11 are unique in that they allow for the TWT 13W signal to be connected directly to the antenna without any losses due to a combiner or T/R diplexer. Thus, either extra antenna power out is achieved or the 13W TWT can be reduced to about 9 watts. The band 4 KSA channel connected directly to the antenna can be defined to always be the high power KSA signal with say horizontal polarization. Since only one polarization is received, only one T/R diplexer is required. This could be placed in the combined signal output path.

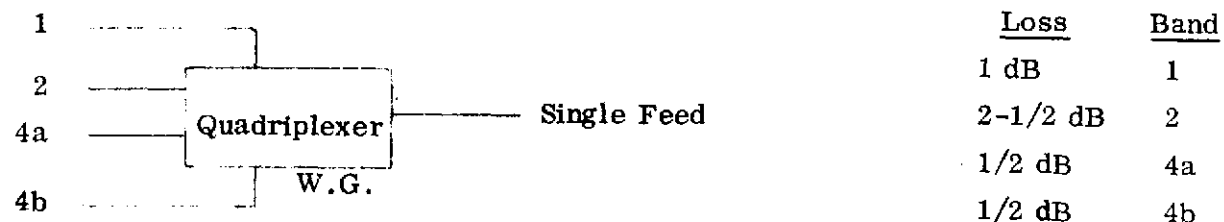
Table 5-6. Typical Combiner Isolations

<u>Channel</u>	<u>Typ. Isolation</u>
1 → 2	14 dB
2 → 1	20 dB
1, 2 → 4a	30 dB
2 → 4	15 dB
4a → 4b	14 dB



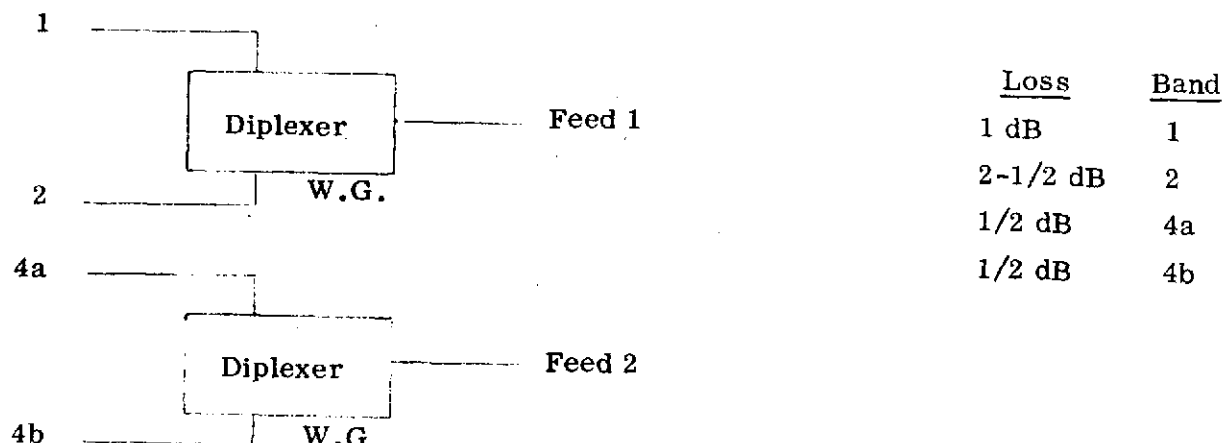
Comments: relatively easy to build, medium loss on band 4 channels

Figure 5-22 . Method 1



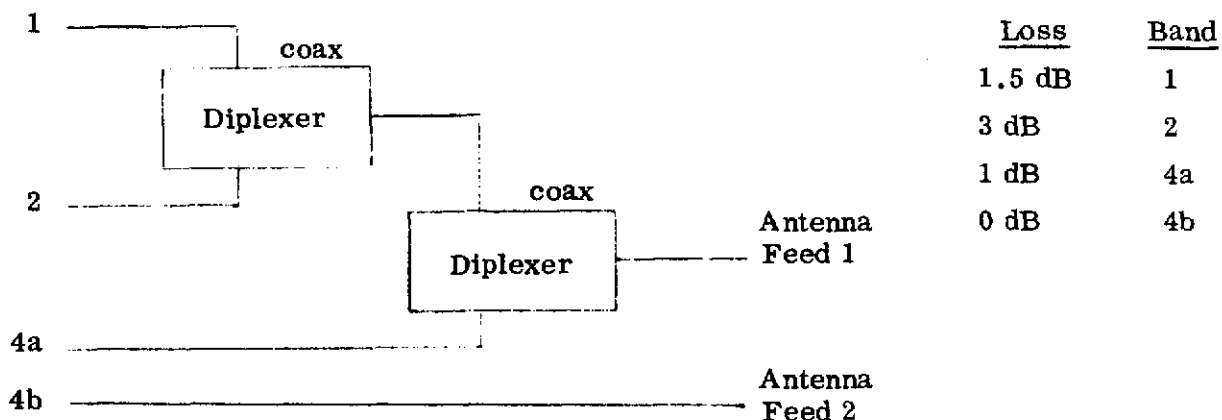
Comments: Very hard to build in W.G.; too lossy in coax

Figure 5-23. Method 2



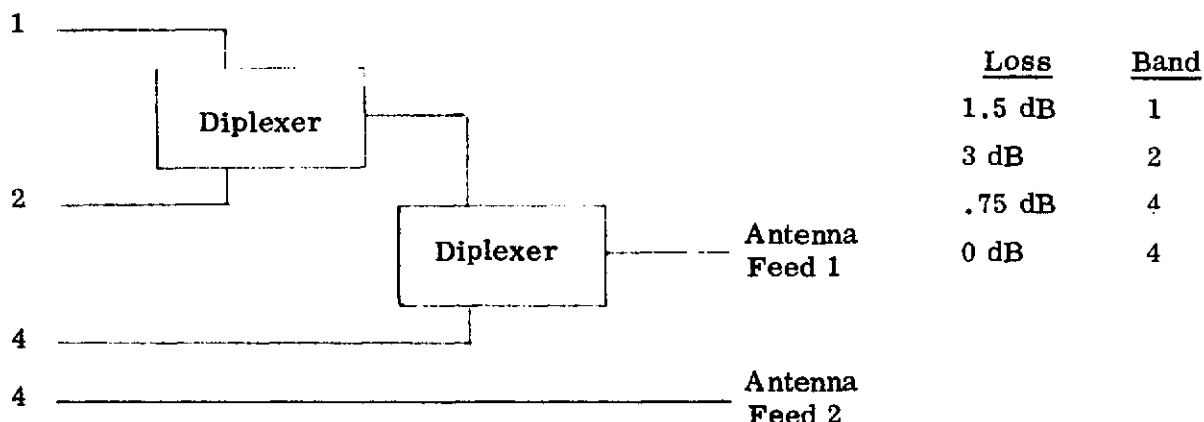
Comments: use dual feed orthogonal antenna, saves 1/2 dB loss. Easy to build, saves space.

Figure 5-24. Method 3



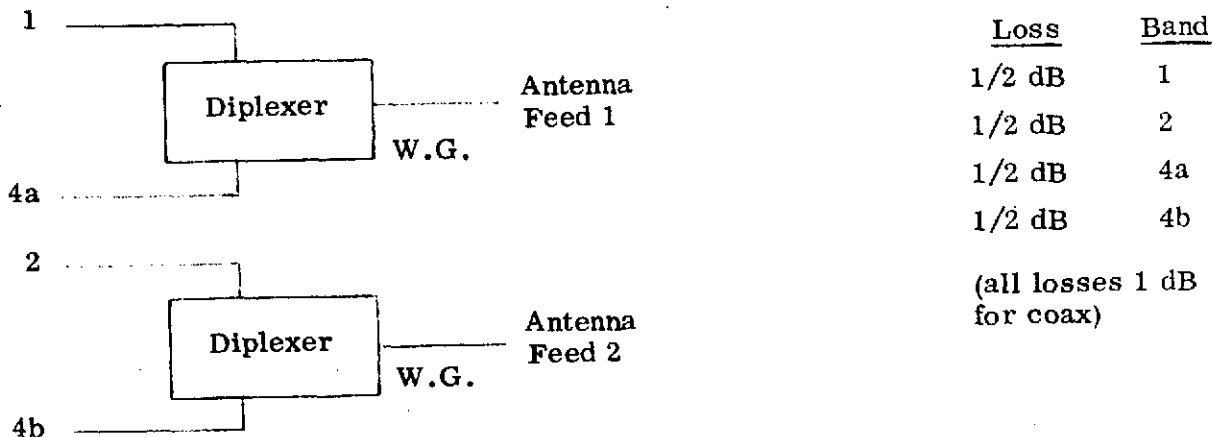
Comments: use dual feed orthogonal antenna, no loss to channel 4b. Could make this the "13W" channel and reduce TWT power.

Figure 5-25. Method 4



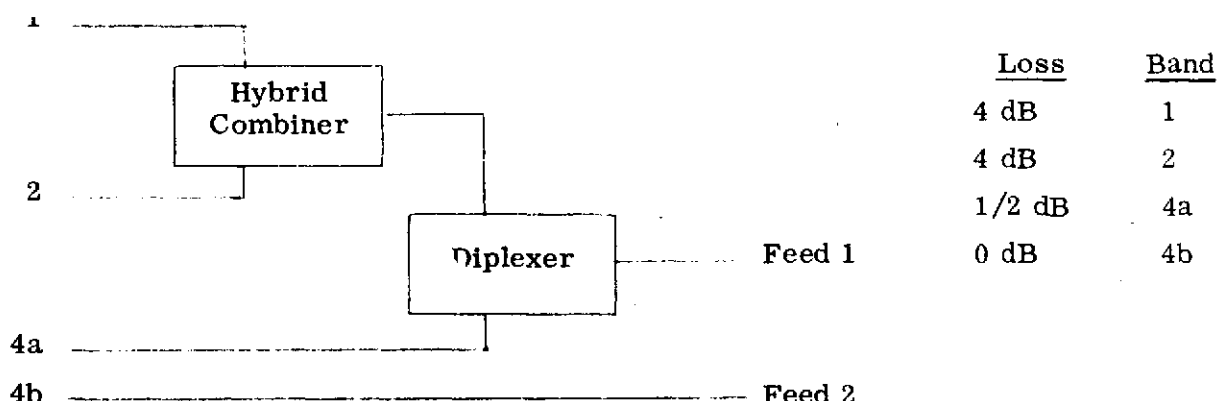
Comments: use dual feed orthogonal antenna, full power wideband

Figure 5-26. Method 5



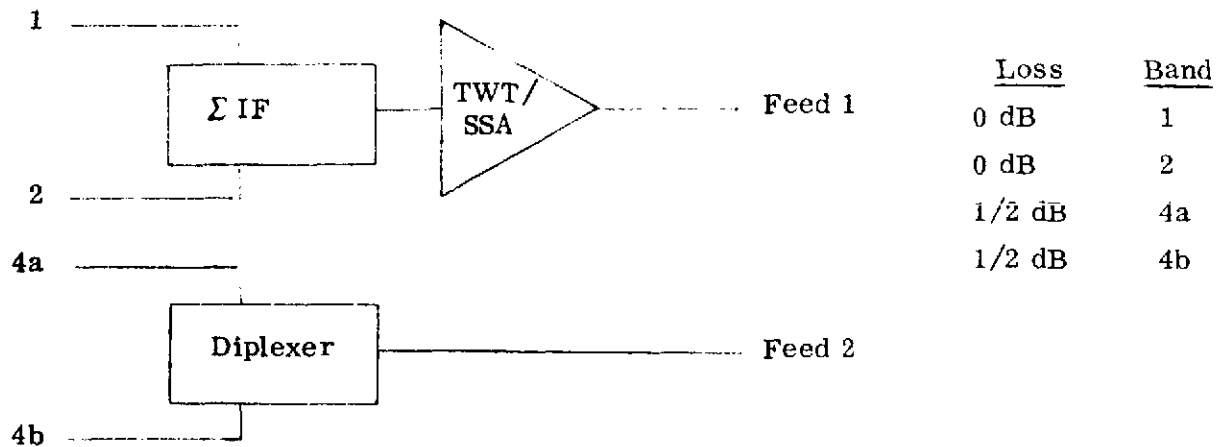
Comments: use dual feed orthogonal feed. Lowest avg. loss to all channels.
Minimum hardware.

Figure 5-27. Method 6



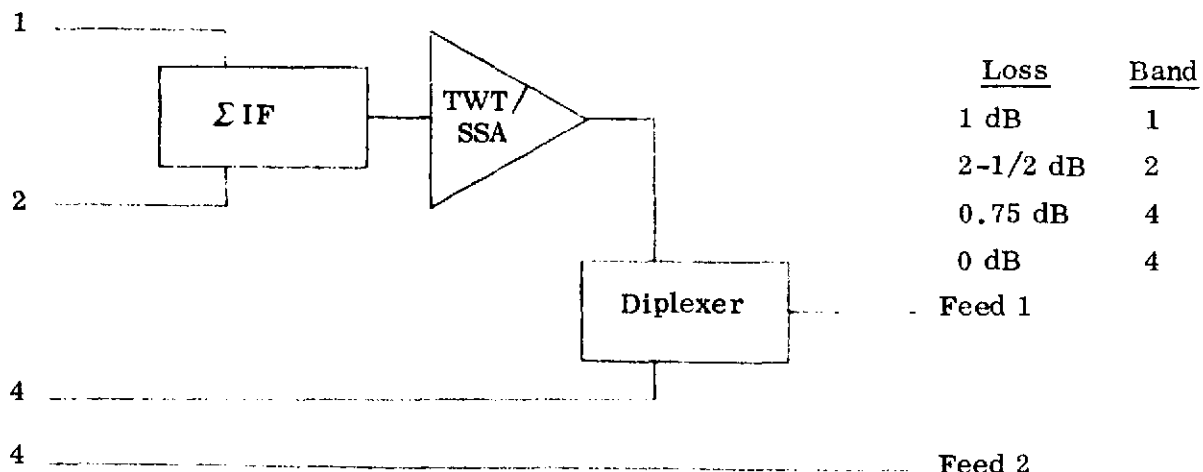
Comments: used hybrid combiner for 1, 2, providing high isolation, but loss too high

Figure 5-28. Method 7



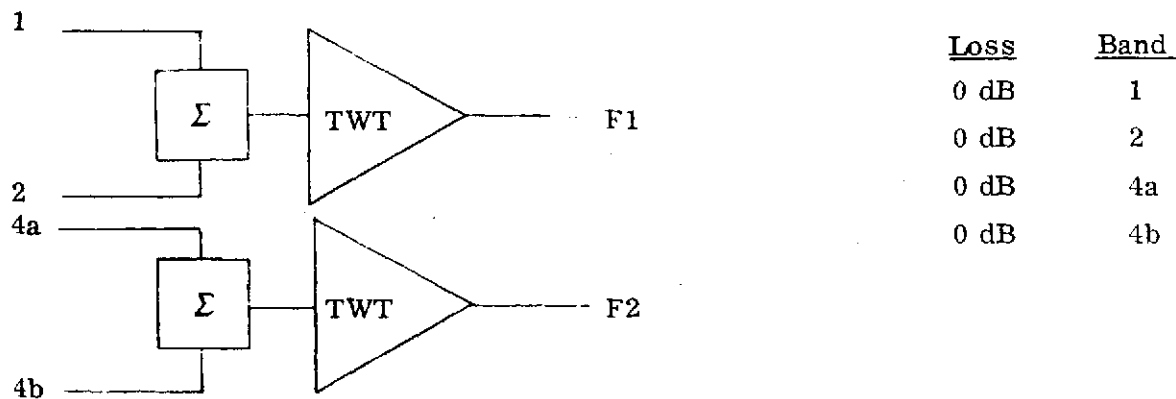
Comments: intermods in 1-2 ampl down typ. 20 dB, not worth it, rel. to Method 5

Figure 5-29. Method 8



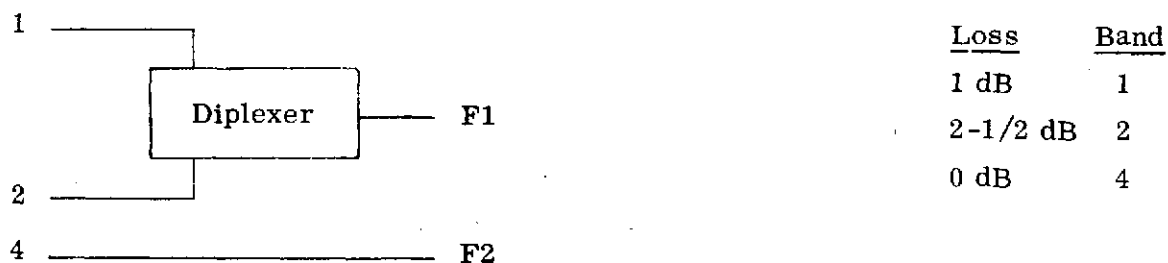
Comments: intermods in 1-2 amp down typ. 20 dB, not worth it, rel. to Method 4

Figure 5-30. Method 9



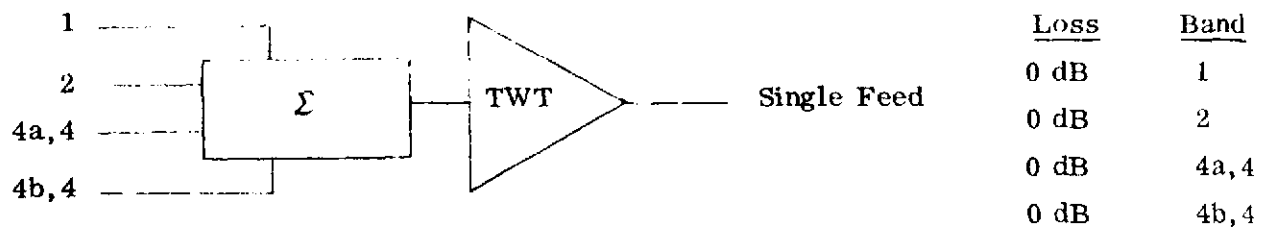
Comments: intermod problems in each TWT.

Figure 5-31. Method 10



Comments: single wideband channel

Figure 5-32. Method 11



Comments: intermod problems would need about a 35W TWT for reasonable IM^S . Average power drain about same. Peak power would be higher. Assur only one 13W band 4 or 4a/4b on at a time.

Figure 5-33. Method 12

Table 5-7. Combining Methods Ranking

	<u>Single Feed</u>	<u>Dual Feed</u>	<u>Dual Signal Linear Amp.</u>
BEST		6	
↑		11	
		5	9
1	3		8
2	4		10
	7		12

If a single feed system is required, method 1 is the only real answer. This would cause the TWT power outputs to be increased about 0.5 dB to 3.6 and 14.5 watts respectively to meet the original expected powers at the antenna. The power out of the MA band 1 would be required to increase 2-1/2 dB to about 1.25 watts average. This is the maximum present output power capability of Impatt solid-state amplifiers. No margin for peaking is allowed. Thus, a TWT would be required here for safety and IM^S . Methods 8, 9, 10 and 12 are questionable due to the intermods produced and the larger TWT^S required. Methods 4 and 5 are nearly identical and would allow switching from wideband KSA service to narrowband with little change. Method 11 can be used for a single low loss wideband KSA channel.

5.3.3 ASSOCIATED COMPONENTS

The typical individual losses for each of the components that make up the allowed 2 dB rf losses are shown in Figure 5-34.

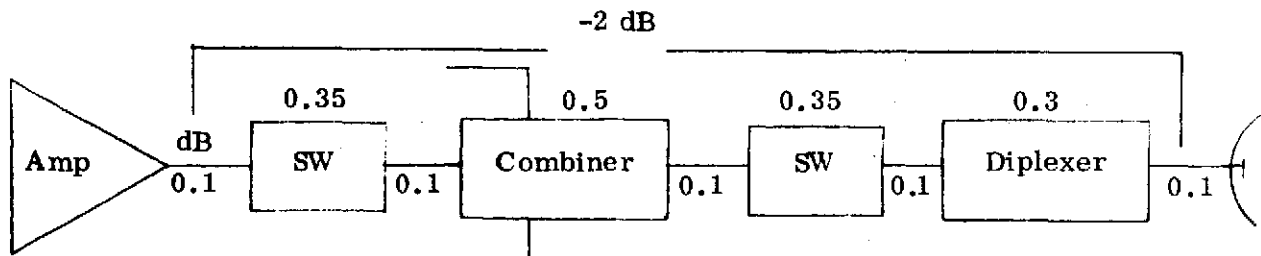


Figure 5-34. RF Loss Budget

The switches in the output are coax type SP2T, 3T or 4T as needed and each have the typical performance shown in Table 5-8.

Table 5-8. Ku-Band Coax Switch Performance

VSWR	1.4 dB
Isolation	60 dB
Loss	0.35 dB
RF Power	30W

The Ku-Band T/R diplexer must pass the entire transmit band while isolating the transmitter signal and noise from the receiver passband. The diplexer must provide 90 dB of Tx to Rx isolation to prevent Tx noise from overriding thermal noise of the receivers. In addition, 80 dB of Rx to Tx isolation is required to prevent transmitter overload and intermods in the receiver. This will provide intermods down 40 dB for TDA or parametric amplifier front ends or down 80 dB for mixer or MESFET amplifier front ends. The latter are highly desired. An 8 section waveguide diplexer is required to achieve the performance required. Typical overall performance is shown in Table 5-9.

The interconnecting cable or waveguide losses must be minimized. Since these are a function of distance, very short runs must be made to the antenna by mounting all rf hardware as close to the antenna as possible. Five feet of WG-62 waveguide has near 0.5 dB of loss.

Table 5-9. Typical T/R Diplexer Performance

Tx F₁	13.4 - 14.05 GHz
Rx F₂	14.6 - 15.25 GHz
Isolation	90 dB
RF Power	25 watts
Loss	0.3 dB (waveguide) 0.7 dB (coax)
BW_{matched}	800 MHz maximum

5.3.4 AMPLIFIER, PREAMP TRADEOFFS

The various power outputs required for Ku-Band are summarized in Table 5-10. The instantaneous peak powers developed during cresting is of particular interest for the MA signals. The power amplifier linearity and power output capabilities determine the output intermods. The amplifier for this channel should be at least 10 dB above the maximum total average power and ideally 15 dB to keep the amplifier distortions down. A solid-state Impatt amplifier falls short of this. The Impatt solid-state amplifier does not work good for multiple signals. When the peak power is at the amplifier rated power, the IMD is -8 dB, for -20 dB backoff, it is -40 dB. The recommended type for each service and power level is shown in Table 5-11. These values are for an assumed total rf loss of 2 dB. A typical cost study is shown in Figure 5-35 along with typical efficiencies. The solid-state amplifiers can not be used for either the band 1 or band 2 cases if IMD^S of -8 dB are not acceptable: this is very poor and the right answer is to go to a 20 watt TWT. Linear Impatt amplifiers are being developed, but are not available now. Available Impatt power levels are typically 1 watt with very poor 1-1/2% efficiencies. Solid-State amplifiers are not recommended by manufacturers for use with multiple signals.

Table 5-10. RF Amplifier Ku-Band Power Levels

<u>Service</u>	<u>Band</u>	<u>Power</u>	<u>No. of Channels</u>	<u>P_{avg.} ea.</u>	<u>P_{avg.} TOT</u>	<u>P_{pk} TOT</u>	<u>Frequency GHz</u>	<u>P_{sat} Min</u>	<u>Amp. Type</u>	<u>IMD</u>
MA	1	Normal +6 dB	30	1.73 mw	52 mw	1.56W	13.4-13.65	.5W	S.S./TWT Impatt	-8/-20
		High +15 dB	30	14 mw	420 mw	12.6W	13.4-13.65	4W	TWT	-15
SSA	2	Normal +6 dB	2	44 mw	88 mw	176 mw	13.7-13.725	.1W	S.S./TWT Impatt	-16/-20
		High +15 dB	2	350 mw	700 mw	1.4W	13.7-13.725	1.2W	S.S./TWT Impatt	-8/-20
KSA	4,4a,4b	Normal +0 dB	1	3.2W	3.2W	3.2W	13.825-14.05	13W	TWT	-
		High +6 dB	1	13W	13W	13W	13.825-14.05	13W	TWT	-

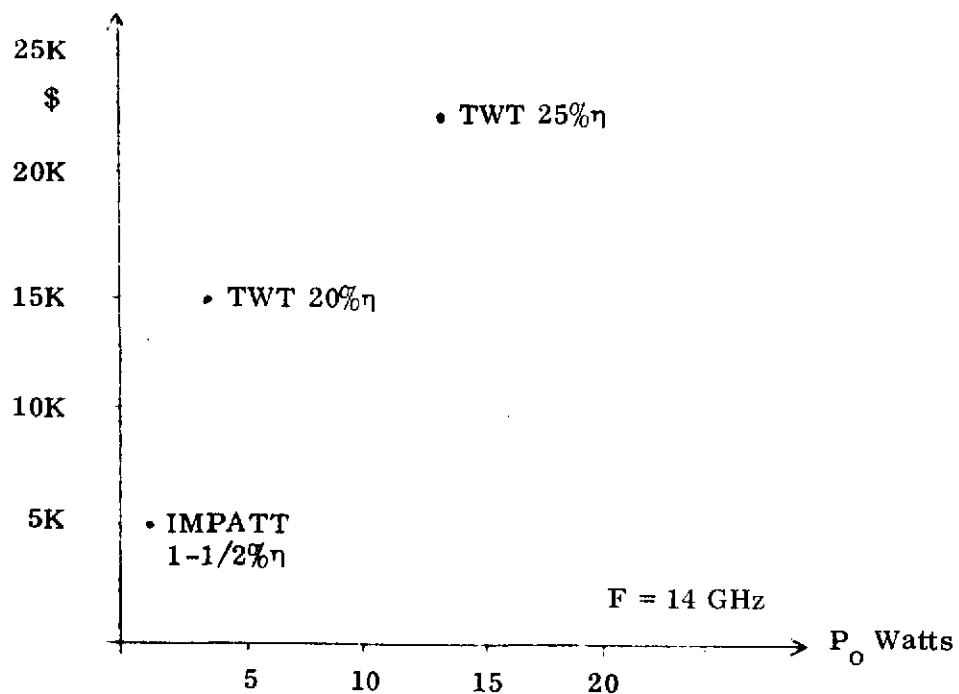


Figure 5-35. Basic Amplifier Costs

A listing of desired preamp noise figures is shown in Table 5-11, with recommended types. A typical cost chart for each type is shown in Figure 5-36. This shows the need to minimize losses, to prevent requiring higher cost, lower noise preamp.

Table 5-11. Receiver Requirements

Band	Service	T_R Spec.	Frequency	Type	Avail.	Vendors
1	MA S-B	250° K	2-2.3	Trans.	220°	Amplica
2	SA S-B	250° K	2.0-2.3	Trans.	220°	Amplica
3	TT&C S-B	250-750° K	2.0-2.3	Trans.	220°	Amplica
4	SA Ku-B	150° K	14.5-15.05	P.A.*	330° K 77° K	Micromega AIL
5	GND-TDRS Ku-B	1000° K	14.5-15.05	Mesfet TR Quietmixer TDA*	900 1050 1050	Watkins- Johnson Hughes Aertech

*Poor Dyn. Range

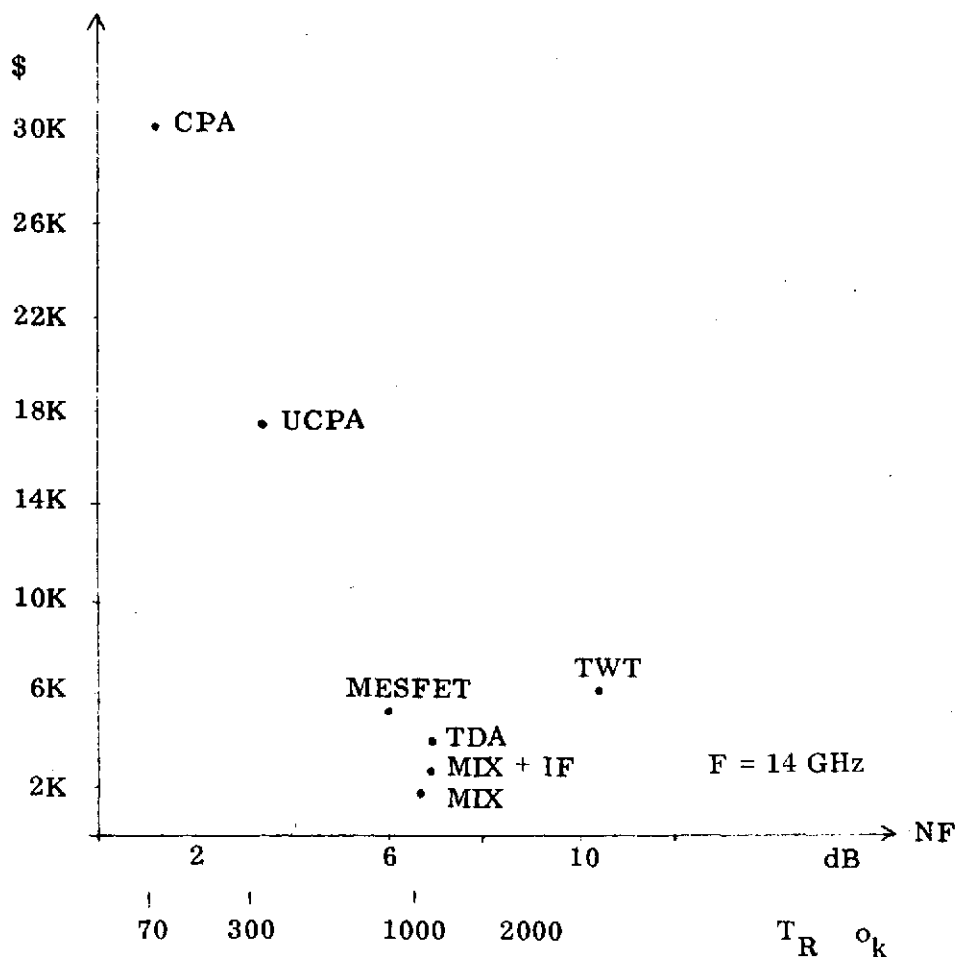


Figure 5-36. Cost Chart

5.3.5 ALTERNATIVE COMBINATIONS.

The diagrams of Figures 5-37, 38, 39, 40, and 41 show the most promising methods for the TDRSS Ku-Band rf system. All provide more than 14 dB isolation. Required amplifier average powers shown are for constant antenna power. Method 6 in Figure 5-37 represents the best overall answer. This meets all the performance goals of the NASA Report. Method 1 in Figure 5-38 is used if only one antenna feed is allowed, even though 4a and 4b have more loss. The extra loss of band 1-2 will require a TWT amplifier. Figure 5-39 is the best for maximum antenna power for the wideband KSA service at a minimum dc drain. But bank 1 and possibly 2 will have to go to TWT^S to handle the cresting.

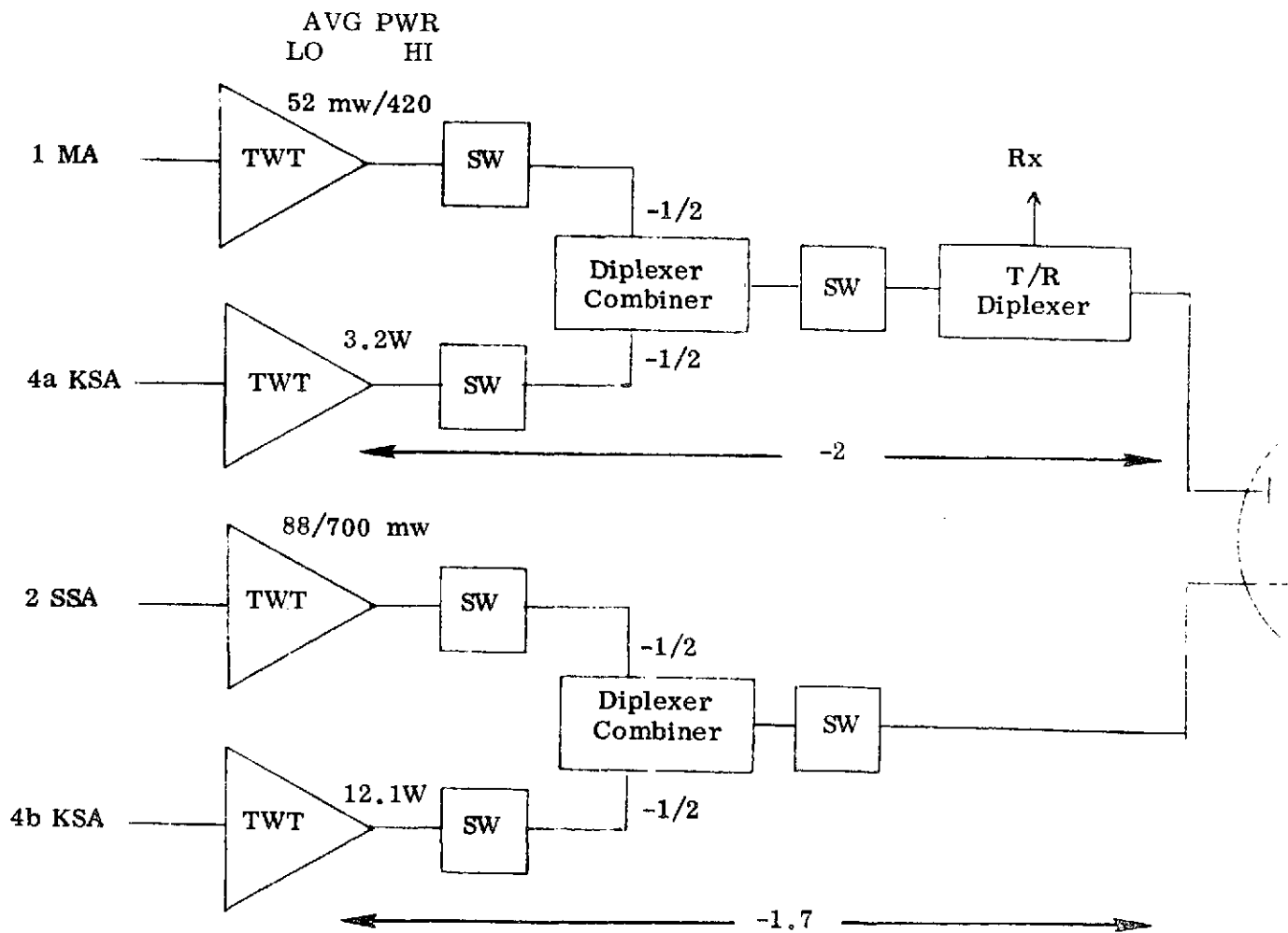


Figure 5-37. Low Loss Combining Method

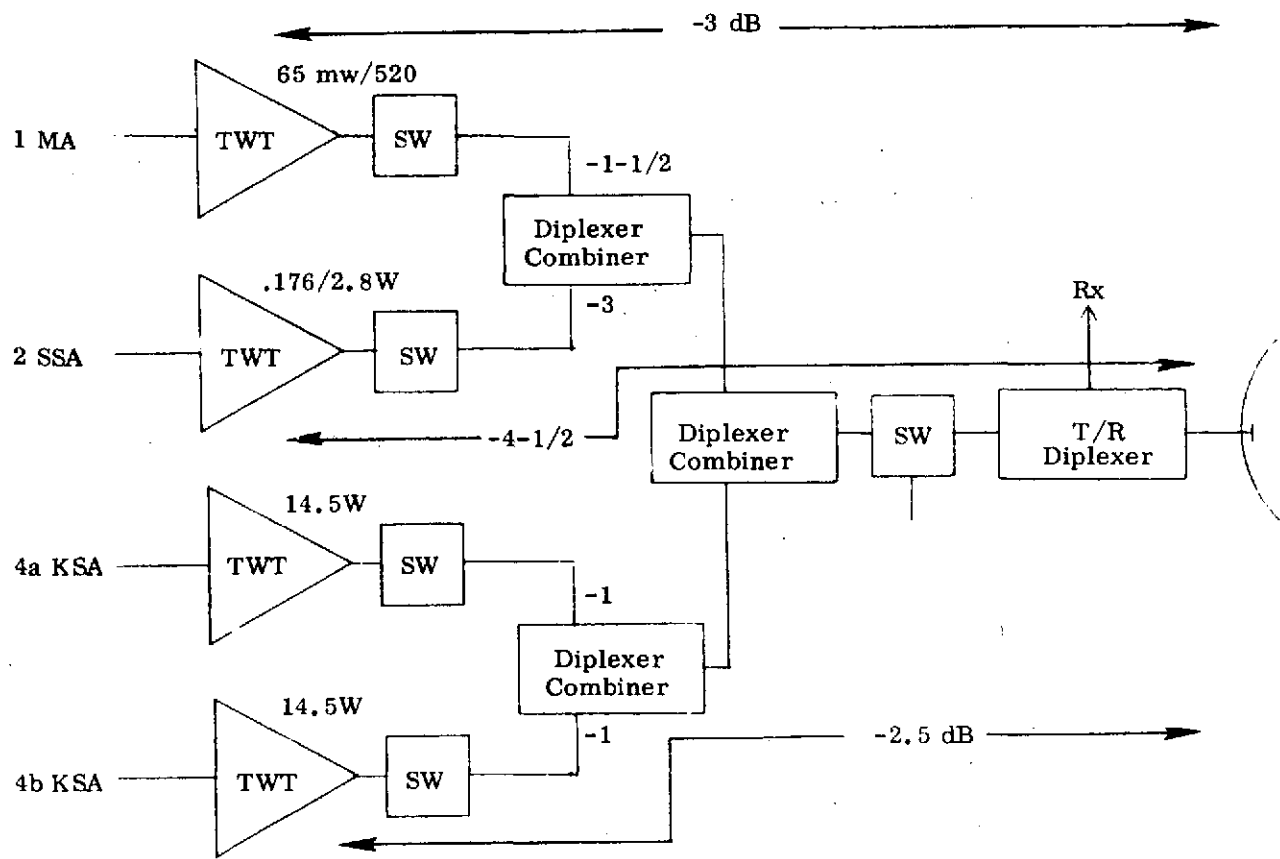


Figure 5-38. Single Feed Combining Method

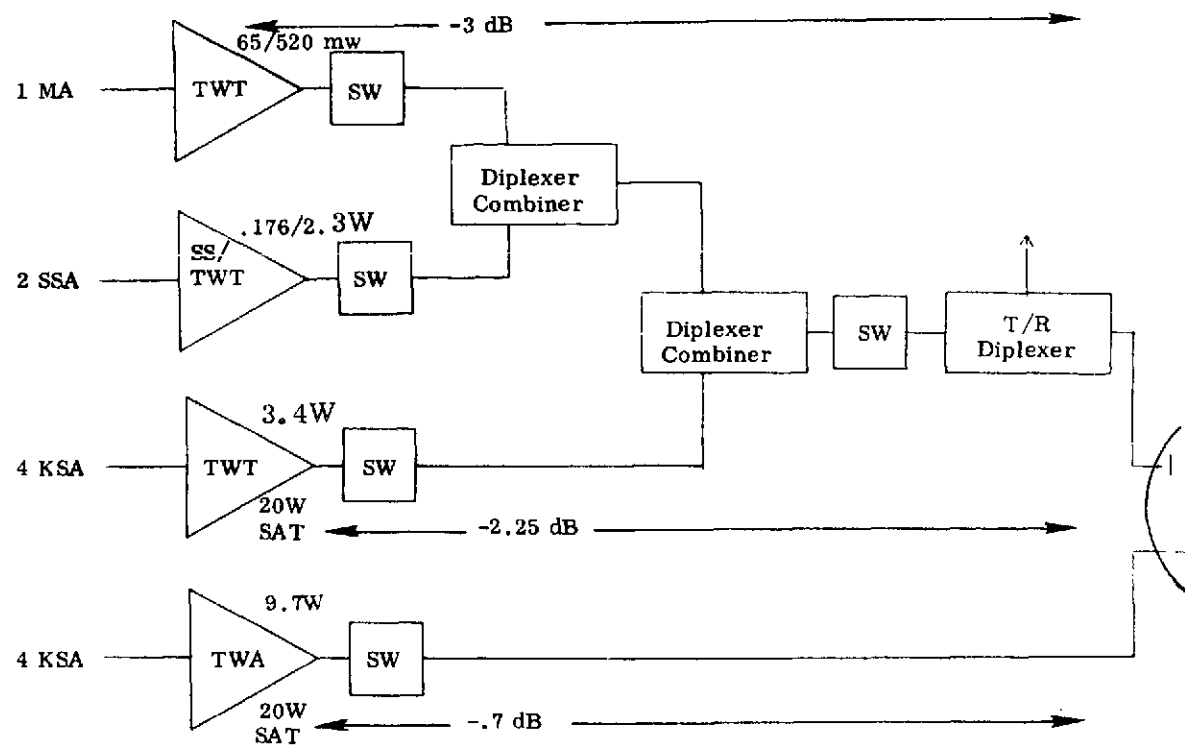


Figure 5-39. Dual Wideband Ku-Band Combining

Method 8 shown in Figure 5-40 uses the IF summing before the amplifier. The peak cresting will require going to a TWT for band 1 and 2. The band 4a and 4b TWT^s only need to run at 11.6W for full antenna power. This saves dc power. The intermods through 1-2 will typically be down only 15 to 20 dB.

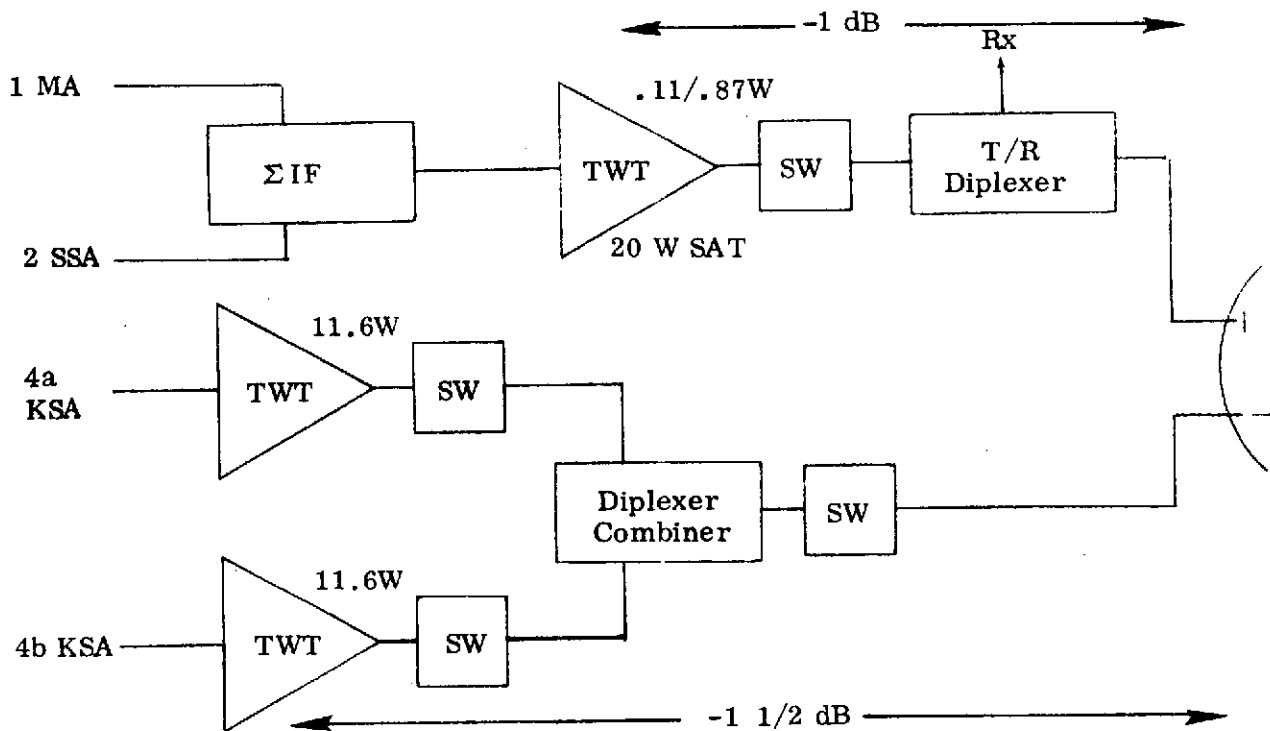


Figure 5-40. Combining Before Amplifier Technique

Method 8 in Figure 5-40 provides for both narrowband KSA channels with less power required from both TWT^s than the nominal 13 watts. Bands 1 and 2 still have the IM problems.

Method 10 of Figure 5-41 use IF combining for all channels with two TWT^s. The intermod and dc power problems with the KSA channels will be higher than desired.

Method 11 of Figure 5-42 provides for a single wideband KSA channel, with low loss.

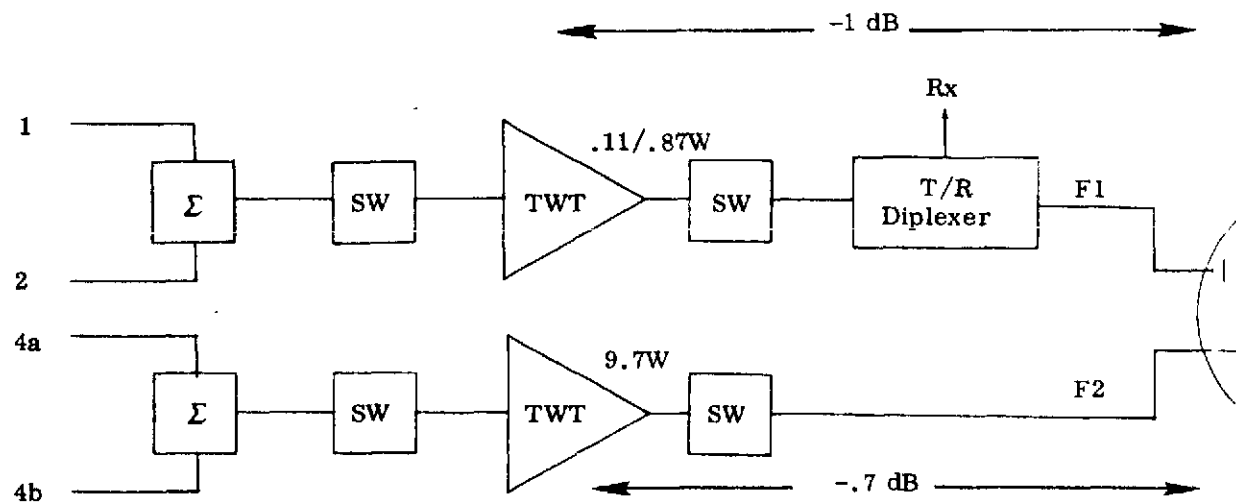


Figure 5-41. Combining in Both Channels with Linear Amplifier

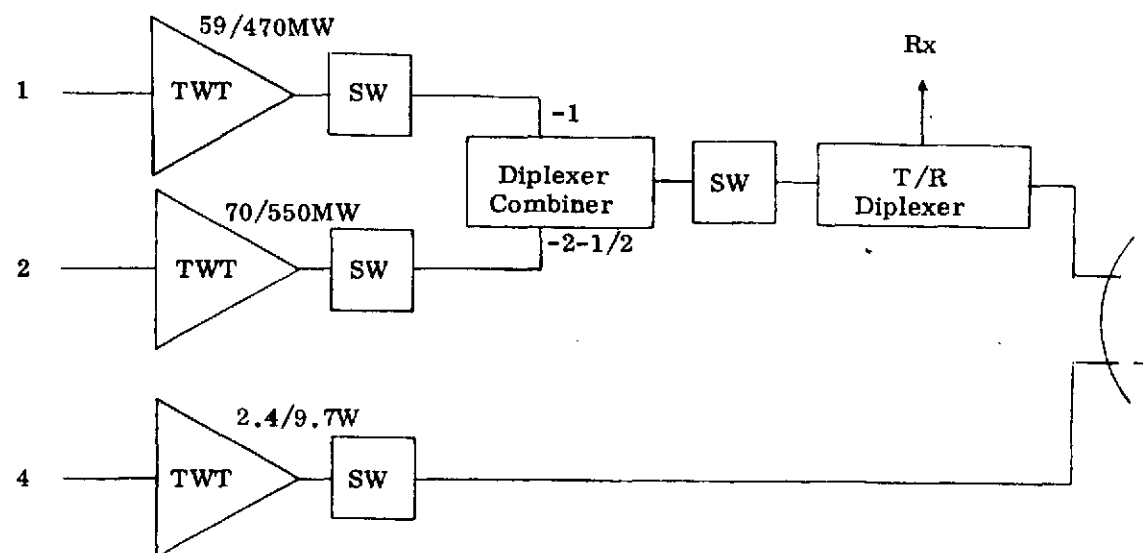


Figure 5-42. Single Wideband Output

In summary, Figures 5-37 and 5-40 are the only techniques that satisfy the original goals of maximum 2 dB rf losses with a given dc drain. Figure 5-40 will have a lower dc power requirement than Figure 5-37 for the same antenna powers. The only question is the use of an extra TWT and the resulting intermods. Typical intermods values for a 20W Sat power TWT used for bands 1 and 2 would be -20 dB. That remains to be determined acceptable.

No final choice can be made between Figures 5-37 to 5-42 without knowing the relative importance between dc power drain, rf power out, intermods and wideband channels versus narrowband channels. At this time, Figure 5-37 looks the most attractive for meeting most constraints. A further study will compare methods based on these questions, as well as show the best technique for providing both wideband and narrowband KSA outputs with a given single setup.

Typical vendors listed in Table 5-12 look qualified to supply the appropriate Ku-Band pieces.

Table 5-12. Typical Vendors

<u>Mixers</u>	<u>LNA Paramp</u>	<u>LNA TDA</u>	<u>LNA Transistor</u>	<u>Coax Switch</u>	<u>Ku-Band TWT</u>	<u>S.S. Impatt</u>	<u>BPF, Diplexer, Combiner</u>
W-J	Micromega	Aertech	Amplica	Transco	Hughes	Hughes	Delta Micro
RHG Space Kom	AIL	Int. Microwave	Watkins-Johnson	Teledyne	W-J	Varian	MDL
Aertech	Aertech				Teledyne		

5.3.6 SUMMARY AND CONCLUSIONS

The tradeoffs between combining techniques is greatly influenced by the choices of all the individual rf components between the IF stages and the antenna feeds. This section summarizes the choices at this time based on all known system goals and constraints. Such considerations as efficiency, heat, size, space qualified production, dc power drain and intermodulation were carefully considered. The initial NASA goal of 2 dB total rf loss provided a stimulus to achieve a unique design and components at the state of the art. The final design allows these goals to be met, with some additional features and benefits.

The combiner solution provides for minimum loss of the Ku wideband band signals between the rf inputs and the dual circular polarized antenna. This ultimately saves dc power.

Since the dual circular antenna feed is part of the rf loss, its performance must be known. Five different dual feeds are proposed by Watkins-Johnson are listed in Table 5-13, with preference in order of listing. The orthogonal mode transducer is a square wave guide to circular waveguide transition. This dual feed is electrically the best, but some questions remain as to the mechanical rigidity

Table 5-13. Dual Circular Antenna Feeds at 14 GHz

1)	Orthogonal mode transducer and polarizer
	n \approx 55 - 60%
	isol = 30 dB min
	feed = waveguide mechanically poor
2)	Circular symmetrical scalar horn and polarizer
	7 = 55%
	isol = 20 dB Good Phase Center
	feed = W. G.
3)	Quadrifigured horn and polarizer
	n = 50 - 55%
	isol = 30 dB
	feed = coax Lossy Feed
4)	RHC, LHC helixes
	n = 50%
	isol = 17dB
	feed = coax Poor Phase Center
5)	Orthogonal dipoles and quadriture hybrid
	n = 55%
	isol = 15 dB
	feed = W. G. Too Narrowband, Poor Phase Response

Three combiner solutions relating to Figure 5-25, Figure 5-30, and Figure 5-39 are shown in Figures 5-43 and 5-44. Peak power is shown at each point. These come from Table 5-10, which shows the amplifier output peak power based on a total rf loss of 2 dB. The peak power is important in determining intermodulations. TWT's are required for all amplifiers in order to keep intermods to less than -20 dB. Class C solid state amplifiers are not useable above 1 watt average or 1/4 watt peak powers due to intermod problems. The total peak power through the amplifier must be less than the 1 dB compression point for this to occur even though the average power may be milliwatts. In most cases shown, a 13 w TWT will satisfy this.

The best solutions to the combiner and associated components are shown in Figure 5-45. Average low and high power levels are shown. This combiner is characterized by the performance shown in Table 5-14. In addition, this system will also work with minor performance degradation for the narrowband KSA service by simply changing the input signals from wideband to narrowband. Maximum use of combining at low power levels before the TWT's is done to improve system efficiency. Therefore the combiner losses are relatively unimportant since they represent only gain loss instead of high power loss.

This system allows the "13" watt wideband KSA to always go directly to one antenna feed (say LHC), while the combined 1, 2 and 4 signals go through the T/R diplexer to the other feed (RHC). Therefore reception must be only on the combined signal feed (in this example - RHC). This method minimizes lossy and troublesome relays and greatly minimizes rf power outputs and therefore dc power drains. The exact details of redundant failsafe switching must be worked out, but no problems exist here. Figure 5-46 shows recommended vendors and related part numbers for the rf hardware.

It was decided that combining before the TWTs would provide many advantages, as long as the interchannel intermods were greater than 20 dB below the respective signals. The intermod for bands 1 and 2 are acceptable. Thus, the combining techniques of Figure 5-44b is a safe acceptable method. The method of Figure 5-44c could cause intermods from bands 1 and 2 to 4 and vice versa, but the advantages are numerous. The main advantages are two TWTs instead of three, less dc power drain, less parts (a much simplified non-high performance combiner), lower rf power ratings of components, and the possibility of providing a high power

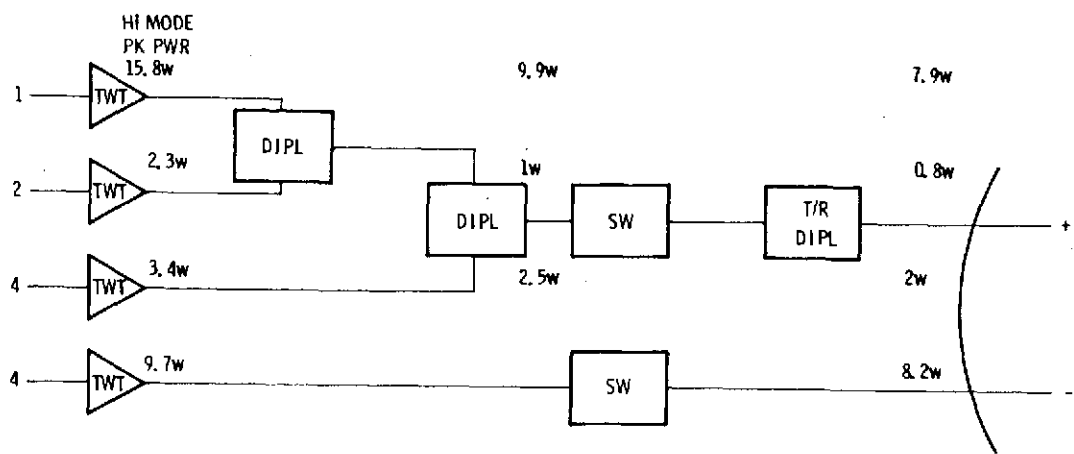
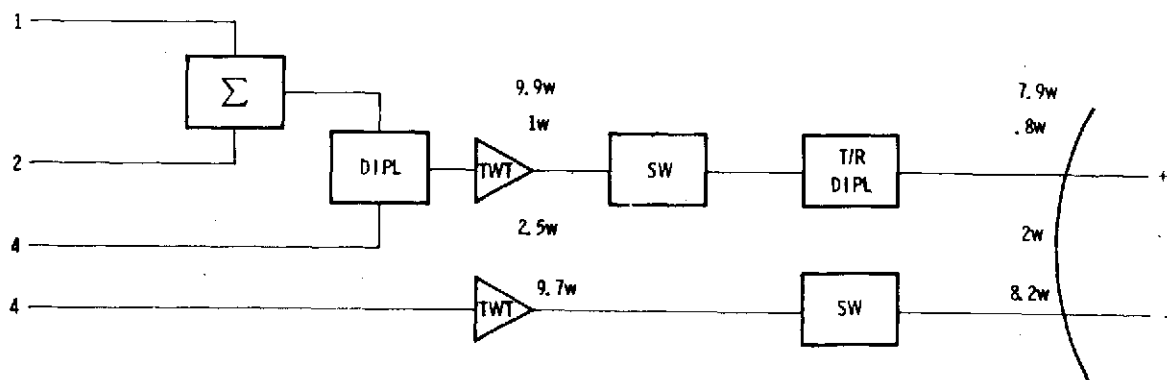
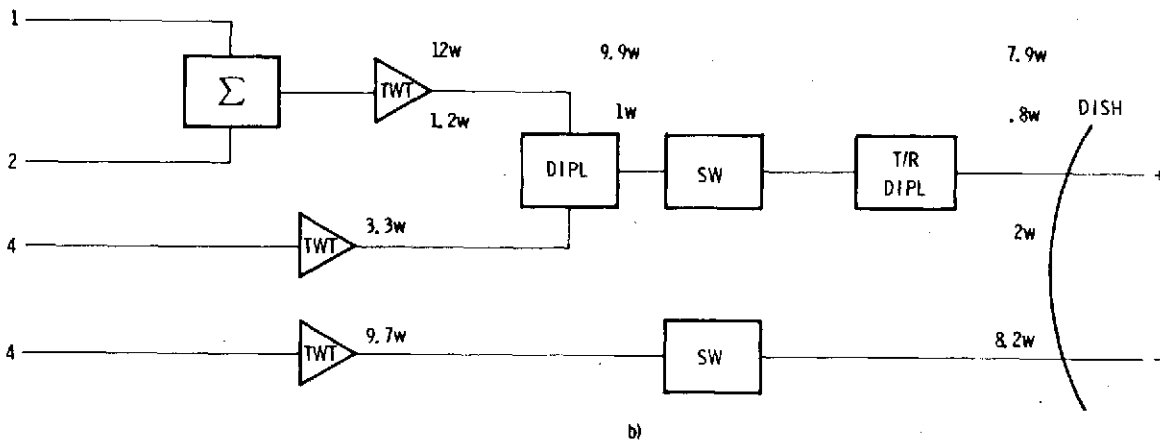


Figure 5-43. Combining Techniques a



974-2824
UNCLASSIFIED

Figure 5-44. Combining Techniques a and c

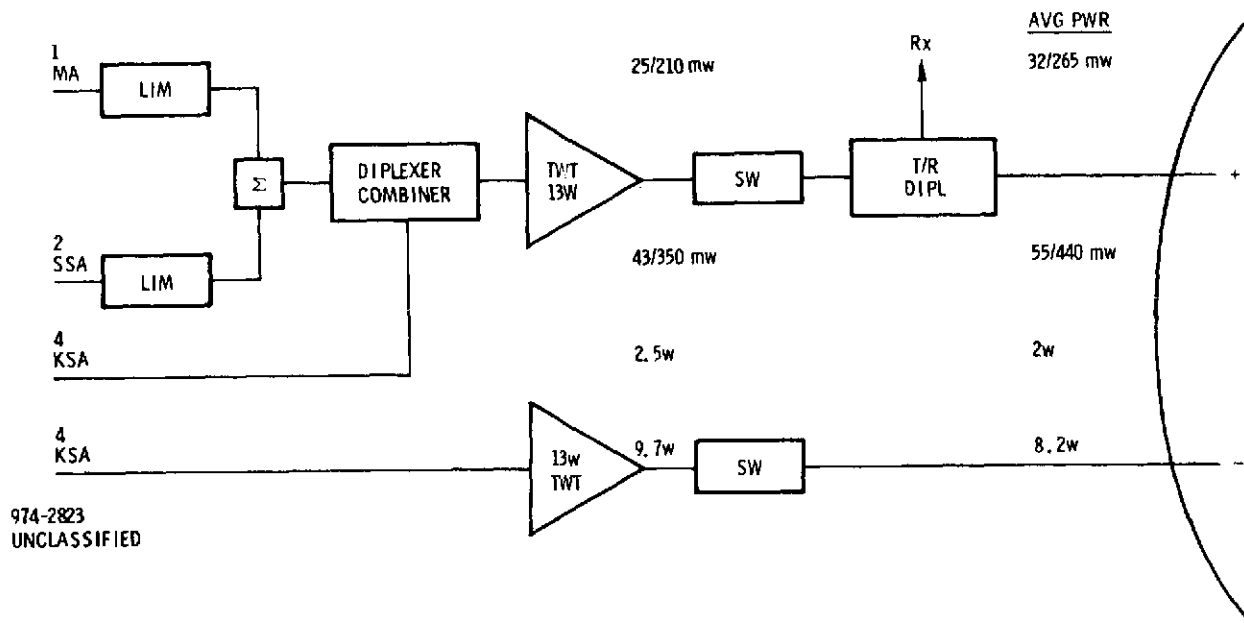
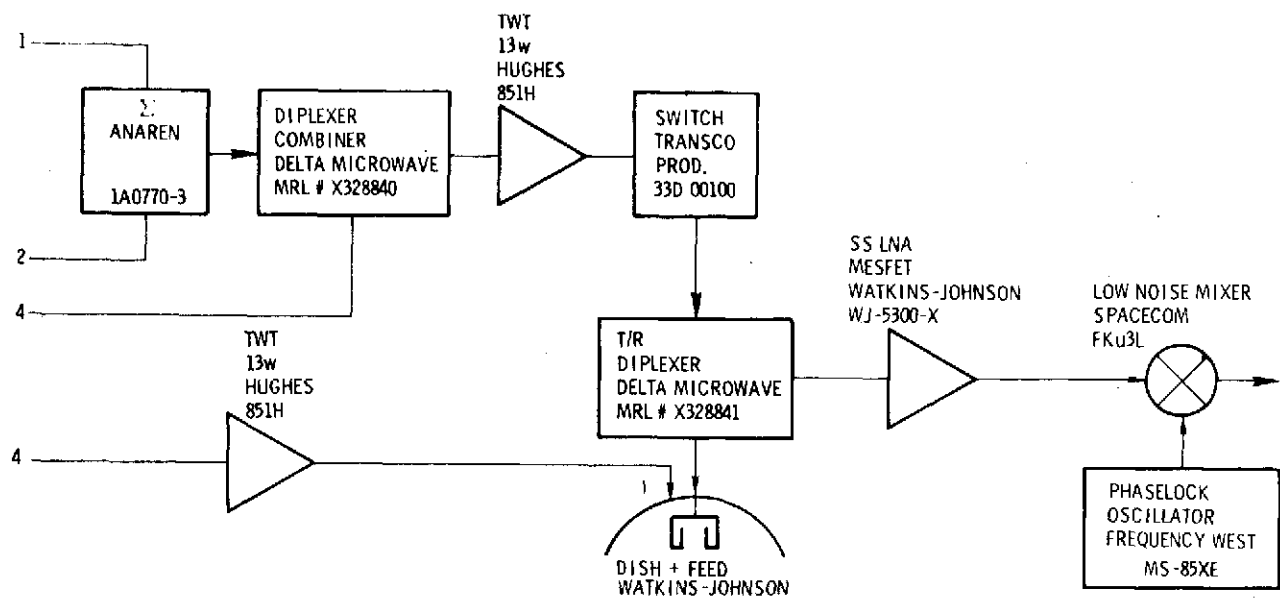


Figure 5-45. RF Combiner - Best Solution

Table 5-14. Combiner Specifications

Parameter	Ch 1	Ch 2	Ch 4
1. Loss (dB)	2	2	2
2. Frequency (GHz)	13.4-13.65	13.7-13.725	13.825-14.05
3. Interchannel Isolation (dB)	15	15	15
4. RF Power (watts)	1	1	1
5. VSWR	1.5	1.5	1.5
6. ϕ Linearity (degrees)	5	5	5

mode (13W) independently for bands 1, 2 or 4 if needed. The intermods between channel 1 and 2 will not cause performance degradation, thus a limiter was placed before the TWT input. This removes the high peak power crests, and thus reduces any intermods of channel 4 into the 1-2 composite signal. This is the only point of possible concern for intermods. An analysis here yields an average signal power of 2.5 watts from channel 4 mixing with a composite 1-2 signal which has an average power of 1 watt. If a 13 watt TWT was used, the IMD would be down 2 ($43 - 33 + 10$) dB = 40 dB below the respective band 1-2 or band 4 signals. Since the 1-2 signal is about



974-2825
UNCLASSIFIED

Figure 5-46. Equipment Sources

4 dB less than the band 4 signal, the IMD would be down 36 dB below the 1-2 signal. In addition, the individual signals (up to 30) in band 1 are down as much as $10 \log 30 = 15$ dB below the total average power of band 1. Thus, the intermods of band 4 into band 1 composite will be $36-15 = 21$ dB below the individual signals in band 1, which appears to be satisfactory.

For the strictly narrowband KSA case, the methods 4 and 6 shown in Figure 5-25 and 5-27 are recommended.

5.4 ADAPTIVE GROUND IMPLEMENTED PHASED ARRAY

This section discusses some aspects of AGIPA performance.

5.4.1 BACKOFF REQUIRED TO TRANSMIT FDM CHANNELS OF THE MULTIPLE ACCESS ARRAY ON TDRS

5.4.1.1 Introduction

The frequency division multiplexing scheme on the TDRS for relaying the individual signals from the 30-element multiple access receiving array needs to be analyzed for the requisite dynamic range of the transmitter. A detailed study is conducted here, with a consideration of AM to PM conversion effects as well as saturation.

5.4.1.2 FDM Model

As described by AIL [18], the received signal from each array element (desired signal plus interfering signals plus receiver noise) is translated in frequency to its assigned FDM frequency channel, with 6 MHz spacing, and 32 such channels are linearly combined for power amplification at Ku band. After transmission from the TDRS to ground, the channels are demultiplexed, translated back to a common frequency, and made available as parallel outputs to AGIPA. By appropriately weighting the respective channel outputs (I, Q control) and summing, a receive beam can be pointed in a desired direction. In addition, AGIPA has an algorithm to adapt the weights to reduce undesired interfering signals.

The effect of saturation and AM to PM conversion in the TDRS power amplifier is to create intermodulation between the equally spaced FDM channels. Considering an interfering signal arriving at the array, there is a signal with equal amplitude in each channel. The intermod products are sum and difference terms, hence have frequencies falling directly on the channel signals. Thus, with an interfering signal received by the array, intermodulation in the FDM system has an effect equivalent to cross-coupling between the array elements themselves. Such cross-coupling tends to raise the side lobe level on the directed receive beam and, in addition, may affect the adaption process of AGIPA.

5.4.1.3 Effect of Cross-Coupling on Side Lobe Level

We are concerned primarily with the ability to direct a receive beam toward a desired multiple access user and, at the same time, reject an undesired side lobe level of the pattern. We interpret cross-coupling between the array elements as equivalent to a weighting error. The maximum allowable rms error to prevent a significant increase in the side lobe level is to be determined.

We can directly derive an expression for the average side lobe level with a small random phase shift error ϵ in the weighting of each element. Let the errors be unbiased and statistically independent. In a designated direction, the antenna power pattern with the random phase errors is

18. AIL, Design Analysis, Tracking and Data Relay Satellite Simulation System, Contract No. N00017-72-C-4401, January 1974.

$$\begin{aligned}
 |G_\epsilon|^2 &= \left| \sum_m A_m e^{j(\theta_m + \epsilon_m)} \right|^2 \\
 &= \sum_m \sum_n A_m A_n^* e^{j(\theta_m - \theta_n)} e^{j(\epsilon_m - \epsilon_n)} \quad (5-53)
 \end{aligned}$$

where A_m is the weighting of the m th element and θ_m is the phase shift due to the element location. Now the expectation

$$\begin{aligned}
 E\left\{e^{j(\epsilon_m - \epsilon_n)}\right\} &= 1 \quad ; \quad m = n \\
 &\cong 1 - \sigma^2 \quad ; \quad m \neq n \quad (5-54)
 \end{aligned}$$

where σ is the standard deviation of the phase error in radians. Then, the expectation of the power pattern is

$$\begin{aligned}
 E\{G_\epsilon\}^2 &= (1 - \sigma^2) \sum_m \sum_n A_m A_n^* e^{j(\theta_m - \theta_n)} + \sigma^2 \sum_m |A_m|^2 \\
 &= (1 - \sigma^2) |G_0|^2 + \sigma^2 \sum_m |A_m|^2 \quad (5-55)
 \end{aligned}$$

where G_0 is the design gain in the designated direction.

Equation (5-55) is interpreted by noting the first term corresponds to a gain reduction on the pattern for zero phase errors, while the second term is the mean side lobe level due to the random phase errors.

If there are N elements and equal weighting,

$$\begin{aligned}
 |G_0| &\cong \left| \sum_m A_m \right| = N \\
 \sum_m |A_m|^2 &= N \quad (5-56)
 \end{aligned}$$

and (5-55) yields

$$\frac{\text{Mean side lobe level due to phase errors}}{\text{Main beam gain}} \cong \frac{\sigma^2}{N} \quad (5-57)$$

Applying the Schwarz inequality shows that (5-57) is a lower bound on the mean side lobe level. For $\sigma = 0.1$ radian and $N = 25$, (5-57) predicts a mean side lobe level of -34 dB or higher.

5.4.1.4 Cross-Coupling Due to Intermod of Saturating Amplifier

To produce an rms weighting error of 0.1, the intermod products must be 20 dB down. We can estimate the requisite backoff of a saturating amplifier (i.e., limiting but no AM/PM conversion) so as to achieve this intermod level, when driven by the summation of multiple carriers. The multiple carriers are treated as summing to Gaussian noise in the analytical model [19], and the presumed input/output power transfer function for the amplifier is shown in Figure 5-47. The resultant signal-to-intermod ratio is given in Figure 5-48, obtained by combining Figures 4 and 5 of reference [19].

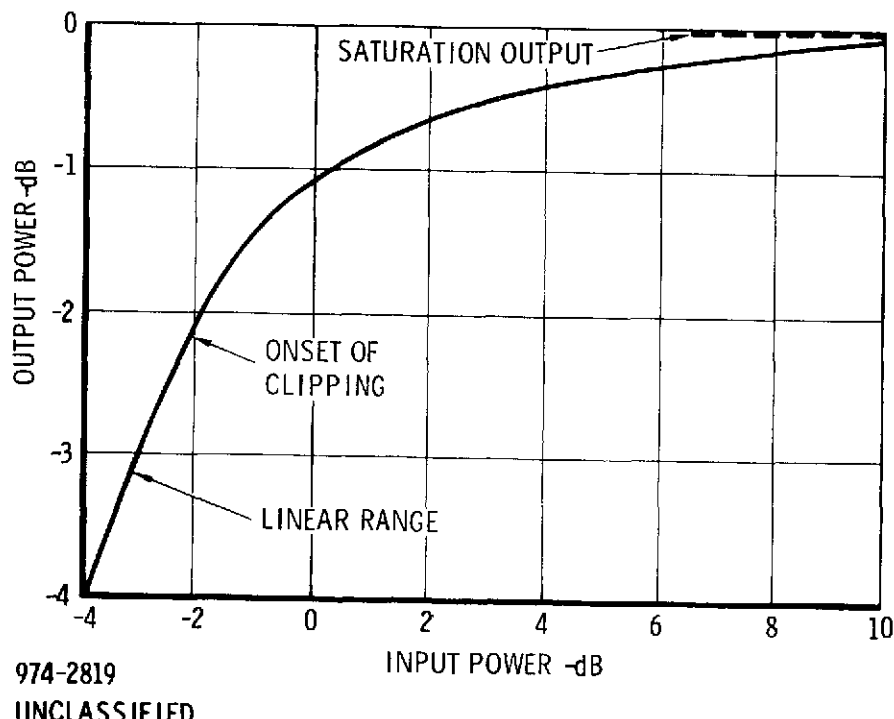


Figure 5-47. Limiter Input-Output Transfer Function

19. C. R. Cahn, "Crosstalk Due to Finite Limiting of Frequency-Multiplexed Signals", Proc. IRE, Vol. 48, January 1960, pp. 53-59.

If a signal-to-intermod ratio of 20 dB is tolerable, Figure 5-48 predicts an output backoff of 5 dB from saturation will suffice. An output backoff of 7 dB gives a ratio of 30 dB.

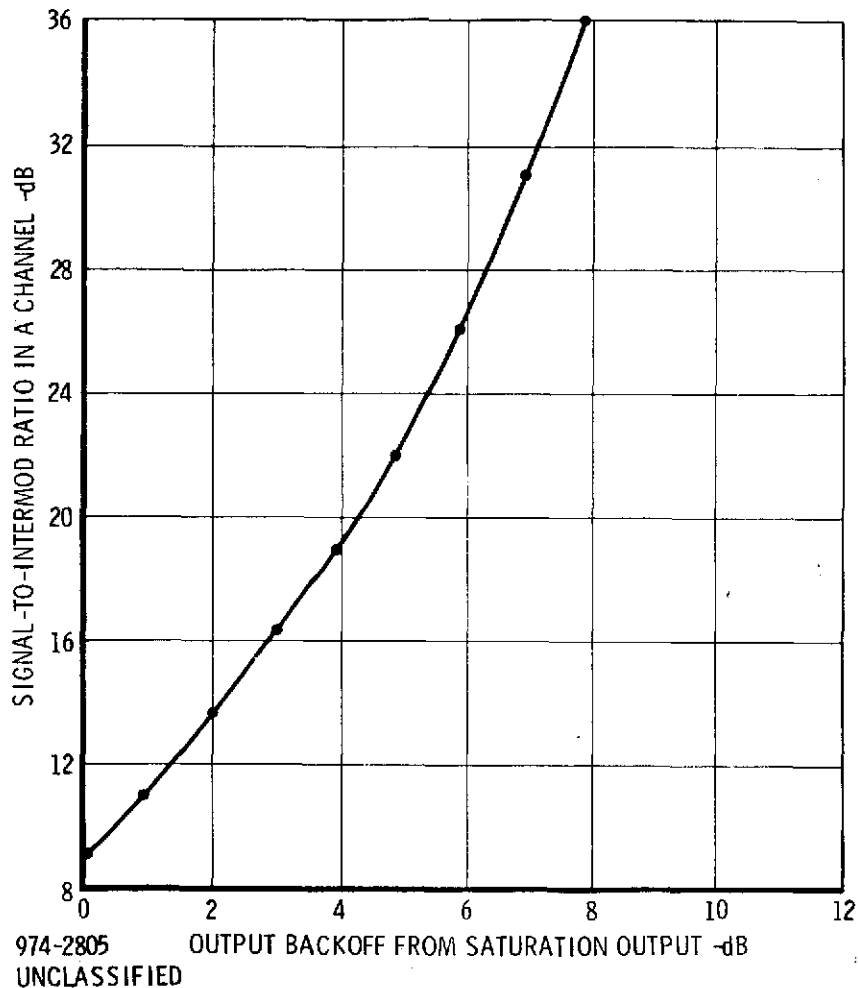


Figure 5-48. Reduction of Intermod by Backoff

5.4.1.5 Intermod Due to AM to PM Conversion

A nonlinear amplifier such as a TWT also displays AM to PM conversion, and this creates intermod products. Physically, the amplifier is characterized by a

phase shift which is a function of input power level. Figures 5-49 and 5-50 present the input/output power transfer function and phase shift for a typical TWT [20], and may be used to compute intermodulation products.

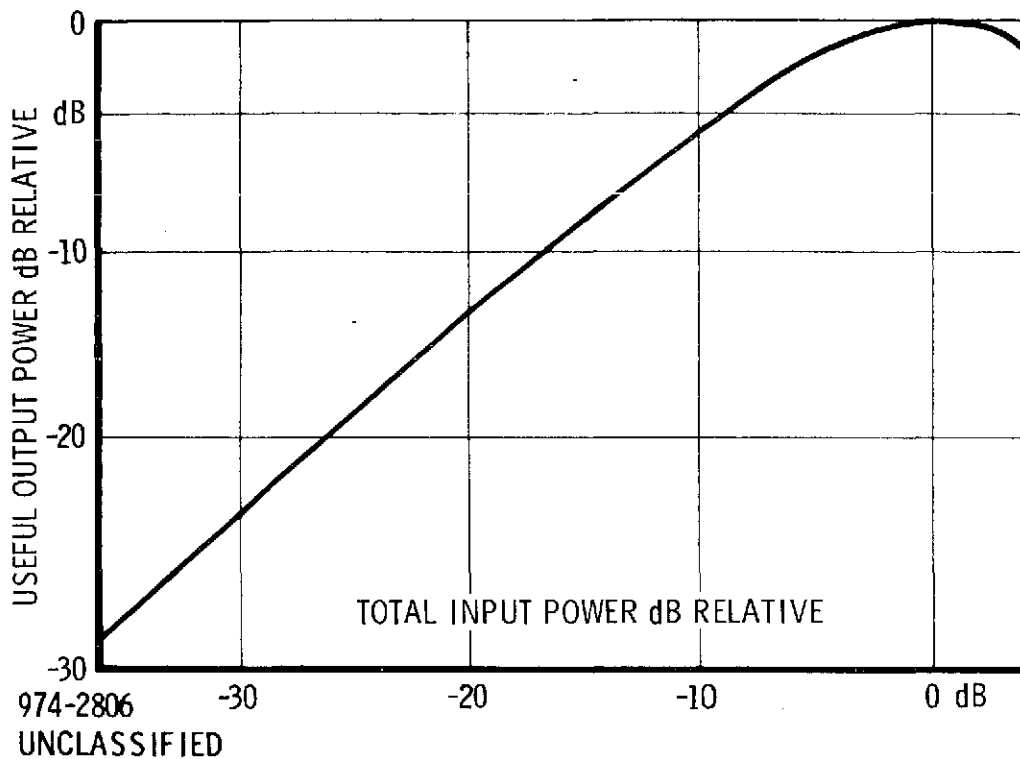
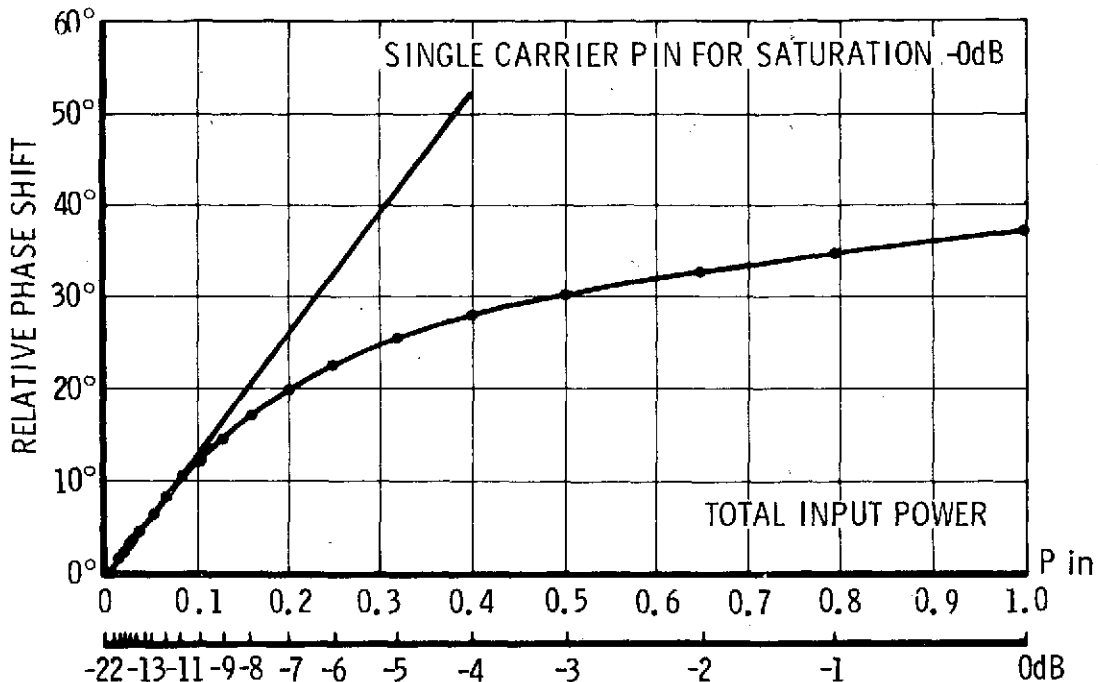


Figure 5-49. TWT Input-Output Power Transfer Characteristic for Single Carrier

The third-order intermod product ("sideband") resulting from two equal input carriers for the TWT of Figures 5-49 and 5-50 is given in Figure 5-51 as a function of input power. Note that the computed effect of saturation (producing AM)

20. A. L. Berman and C. E. Mahle, "Nonlinear Phase Shift in Traveling-Wave Tubes as Applied to Multiple Access Communication Satellites", IEEE Trans. on Comm. Tech., Vol. COM-18, February 1970, pp. 37-48.



974-2807
UNCLASSIFIED

Figure 5-50. Single-Carrier Relative Phase Shift
Versus Input Power Transfer Characteristic

is comparable to that of AM to PM conversion (producing PM) at all input levels, but the effect of AM to PM conversion tends to be dominant (by about 3 dB) at low power levels. The computed total intermodulation product is in reasonable good agreement with the measurement over a large range of input power levels.

The output backoff necessary to give a carrier-to-intermodulation ratio exceeding 20 dB is evaluated from Figure 5-51 in conjunction with Figure 5-49. Note from Figure 5-51 that the input power must not exceed -13.4 dB relative to single carrier saturation; this yields an output backoff of about 8 dB, using Figure 5-49. Similarly, to obtain a carrier-to-intermodulation ratio exceeding 30 dB, the output backoff is 11.5 dB.

Another example [21] of intermodulation computation is for a TWT having the input/output characteristics of Figure 5-52, similar to Figures 5-49 and 5-50. A quadrature carrier model with different nonlinear characteristics in the two

21. A. R. Kaye, D. A. George, and M. J. Eric, "Analysis and Compensation of Bandpass Nonlinearities for Communications", IEEE Trans. on Comm., Vol. COM-20, October 1972, pp. 965-972.

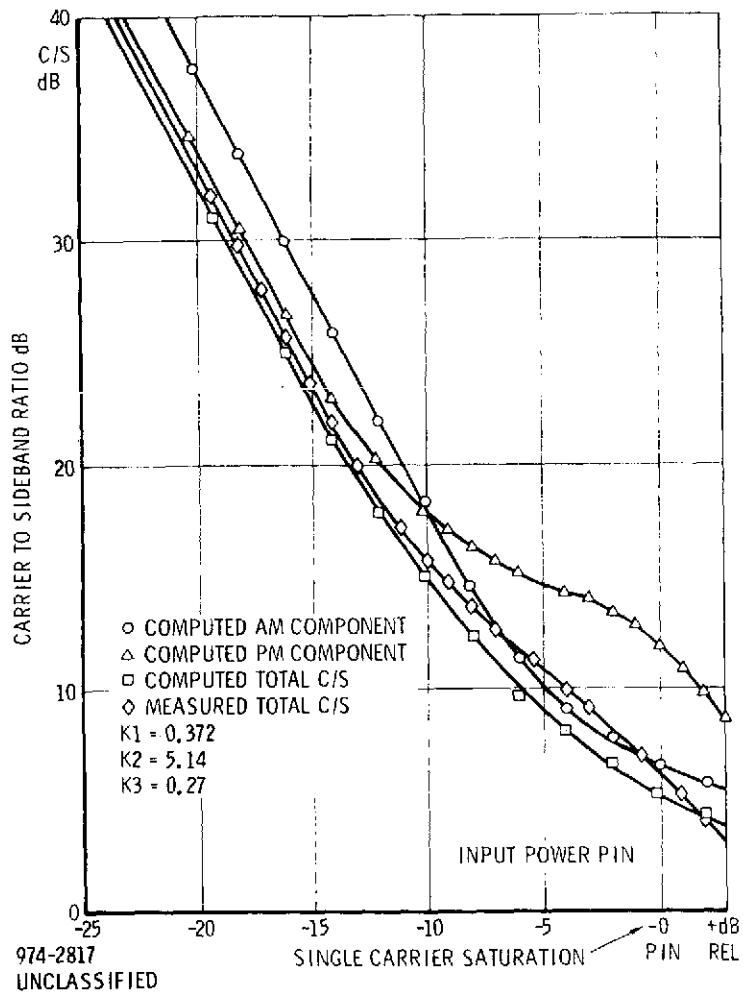


Figure 5-51. Carrier to Intermodulation Product Ratio Versus Input Power

channels represents both input/output saturation and AM to PM conversion. Figure 5-53 presents the computed signal-to-intermodulation ratio for a Gaussian noise input, representing the summation of multiple carriers. A ratio of 20 dB is seen to correspond to an output backoff of about 6 dB.

5.4.1.6 Saturation With Noisy Signals

The above discussion of intermodulation due to saturation has not taken into account the fact that the individual elements of the array operate at a low signal-to-noise ratio. According to the NASA Goddard Definition Study Report, the maximum signal-to-noise ratio in any element is about -10 dB (for EIRP of 36 dBW and receiver

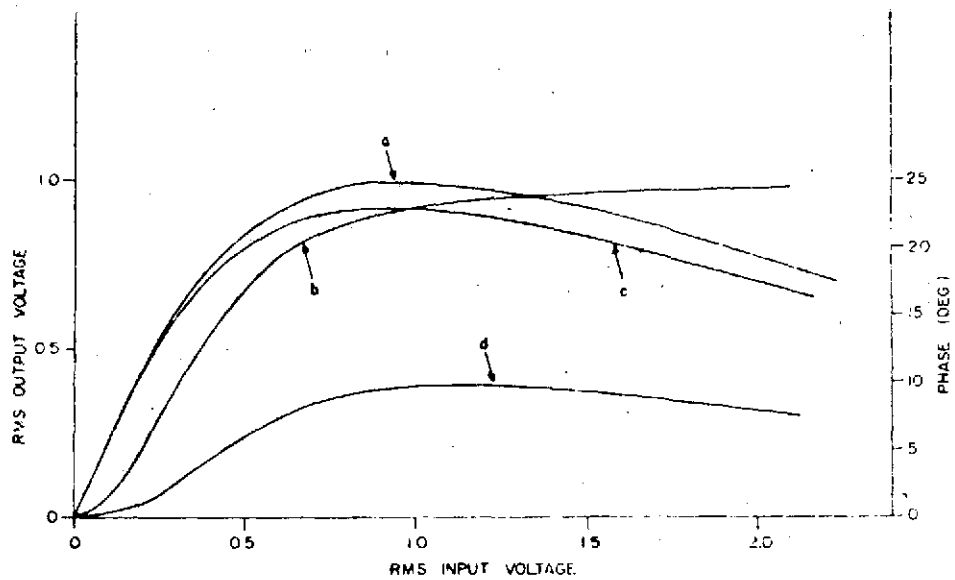


Figure 5-52. Characteristics of an Intelsat IV Traveling-wave Tube. (Voltages are Normalized to Unity at Saturation.) Curve a-Envelope Voltage Transfer Function. Curve b-Phase Shift Versus Input Envelope Voltage. Curve c-Inphase Nonlinearity of Quadrature Model (Envelope Transfer Function). Curve d-Quadrature Nonlinearity of Quadrature Model (Envelope Transfer Function).

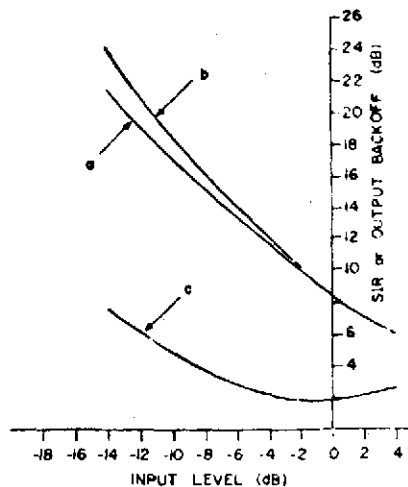


Figure 5-53. Results for the Traveling-wave Tube with a Gaussian Input Signal. Curve a-SIR. Curve b-SIR Generated by Amplitude Distortion Alone. Curve c-Output Backoff.

bandwidth of 5 MHz). The consequence is that a saturating amplifier tends to be linearized by this additive Gaussian noise. To discuss this effect analytically, it is convenient to assume a saturating amplifier with a memoryless nonlinearity described by the error function, or

$$y = \operatorname{erf}(x/\sqrt{2}\gamma) \quad (5-58)$$

where x is the instantaneous input and y is the output*. An alternate expression equivalent to (5-58) is

$$y = \frac{2}{\pi} \int_0^{\infty} \sin(ux) e^{-u^2\gamma^2/2} \frac{du}{u} \quad (5-59)$$

which is more useful in the following. Hard limiting is reached when $\gamma \rightarrow 0$.

Let the input be

$$x(t) = s(t) + n(t) \quad (5-60)$$

where s is the FDM of the sinusoidal signals in the respective array elements and $n(t)$ is Gaussian noise of variance σ^2 resulting from FDM of the receiver noises in the respective elements. The expectation of the output, averaging over the Gaussian noise, is

$$\begin{aligned} E\{y(t)\} &= \frac{2}{\pi} \int_0^{\infty} E\{\sin(us(t) + un)\} e^{-u^2\gamma^2/2} \frac{du}{u} \\ &= \frac{2}{\pi} \int_0^{\infty} \sin(us) E\{\cos(un)\} e^{-u^2\gamma^2/2} \frac{du}{u} \\ &= \frac{2}{\pi} \int_0^{\infty} \sin(us) e^{-u^2(\gamma^2+\sigma^2)/2} \frac{du}{u} \end{aligned} \quad (5-61)$$

*Note, the input/output power transfer function is somewhat different than an error function, since the bandpass filter retains only the first zone.

The significance of (5-61) when compared to (5-59) in the absence of noise is that the noise effectively linearizes the amplifier nonlinearity by increasing γ to

$$\gamma_{\text{eff}} = \sqrt{\gamma^2 + \sigma^2} \quad (5-62)$$

in the error function characteristic of (5-58).

Suppose that $s(t)$ is the FDM of the array signals for a received signal at maximum EIRP, so that

$$s(t) = \sqrt{\frac{2}{N}} \sum_{i=1}^N \cos(\omega_i t + \theta_i) \quad (5-63)$$

normalized to a total power of unity. If $\gamma \rightarrow 0$, we have the extreme of hard limiting, and the output power is -0.9 dB*. Large γ gives a linear amplifier with gain $\sqrt{2/\pi}/\gamma$. On this approximation, an output backoff of 7 dB is achieved with $\gamma \approx 2.0$, if there were no additive noise. As a check, we find that $\gamma = 2$ in the error function limiter yields a signal-to-intermodulation ratio of 25 dB, which suffices for proper array operation.

Since $\sigma^2 = 10$ or greater, we find from (5-62) that $\gamma_{\text{eff}} \geq 3.2$ even if the amplifier is operated in hard limiting, and reference [22] predicts a signal-to-intermodulation ratio of 33 dB for the error function limiter with $\gamma = 3.2$.

5.4.1.7 Conclusions

The effect of intermodulation causing crosstalk between the FDM channels from TDRS to ground is to degrade the side lobe level of a directed receive beam of the multiple access array on the TDRS. A signal-to-intermodulation ratio of 20 dB is about the lowest for which the increase in side lobe level can be accepted. (The resulting mean side lobe level due to the cross-coupling of intermodulation is roughly 30 dB down.) An output backoff of 5 to 8 dB, depending on the specific computational approach, suffices in a typical TWT even without consideration of receiver noise.

*The output of the hard limiter is a square wave, with 0.189 of the total power falling into the third, fifth, etc., harmonics, which are outside the first zone.

22. J. S. Lee, "Signal-to-Crosstalk Power Ratio in Smoothly Limited Multichannel FDM Signals", IEEE Trans. on Comm. Tech., Vol. COM-16, February 1968 pp. 63-67

According to the NASA Goddard Definition Phase Study Report, the strongest received signal (36 dBW EIRP) is about 10 dB below the single element noise level in 5 MHz bandwidth. Then, it is found that the amplifier for the FDM signal could be hard limiting and still achieve a signal-to-intermodulation ratio exceeding 30 dB.

It should be remembered that noise falling into an adjacent FDM channel as a consequence of the out-of band spectrum of PN does not have the same deleterious effect as intermodulation. This out-of-band spectrum simply adds to the receiver noise level for the individual elements. Thus, the out-of-band spectrum can contribute only a negligible amount of additional noise, and the design of filters to be associated with multiplexing and demultiplexing has little effect on multiple access system performance.

5.4.2 EFFECT OF RFI UPON MA RETURN LINK AGIPA

The AGIPA has approximately 42,000 km of TEM transmission line (free space) between each element of its aperture on the TDRS and its beamformer on the earth. The RFI due to ground-based S-band radars incident on the TDRS must be accurately transmitted to earth if it is to be nulled out by the ground-based array processor [23, 24]. In this section we examine the power level of this RFI at several critical points of the MA return link.

5.4.2.1 RFI Model (f = 2,287.5 MHz, $\lambda = 13.1$ cm)

The RFI from S-band radars on the earth consists of in-band (f = 2,287.5 MHz) pulses of 3 to 4 microsecond duration with an average interpulse period of 75 microseconds. The incident power spectral density of these pulses at the TDRS is -141 dBW/MHz (when the pulse is present) as received in a 0 dBI (omnidirectional) gain antenna. The $\pm 1\sigma$ bandwidth is 10 MHz for the interference. When the radar is pointed at the TDRS, the radar pulses are 40 dB stronger.

23. "Adaptive Ground Implemented Phased Array," AIL Final Report, February 1973 for NASA/GSFC under Contract NAS5-21653.

24. "Design Analysis Tracking and Data Relay Satellite Simulation System," AIL Report, January 1974, for the Johns Hopkins Univ., Applied Physics Lab, under Contract N00017-2-C-4401.

5.4.2.1.1 EIRP of RFI Radars

The MA space loss at $\lambda = 13.1$ cm from user to TDRS is given as -192.2 dB. Assuming the same space loss for the radars between the earth and the TDRS we deduce the following EIRP's for the cumulative offending S-band radars (when the pulse is present):

$$\begin{aligned} \text{EIRP (main beam)} &= -141 \text{ dBW/MHz} + 192.2 + 40 \\ &= +91.2 \text{ dBW/MHz} \end{aligned} \quad (5-64)$$

$$\begin{aligned} \text{EIRP (average sidelobe)} &= -141 \text{ dBW/MHz} + 192.2 \\ &= 51.2 \text{ dBW/MHz} \end{aligned} \quad (5-65)$$

By way of comparison, a 100 kbps user without coding [25, Figure 3-2] only requires an EIRP of 35 dBW for 2.25 MHz or 31.5 dBW/MHz.

5.4.2.1.2 RFI Peak Level Frequency and Duration

In order to obtain an estimate of how long and how often the radar's main beam illuminates the TDRS we will assume that the RFI is from a mechanically scanning search type radar. We assume that the RFI search radar has a parabolic dish antenna with the following characteristics:

$$\begin{aligned} \text{diameter} &= 13\lambda = 1.7 \text{ meters} \\ \text{gain} &= 30 \text{ dB} \\ 3 \text{ dB beamwidth} &= 1/13 \text{ rad} = 4.4^\circ \\ \text{efficiency} &= 60\% \\ \text{main beam solid angle} &= (\pi/4)/(13)^2 = 4.6 \times 10^{-3} \text{ steradians} \\ \text{no. of hemispherical search cells} &= 2\pi/4.6 \times 10^{-3} = 1352 \\ \text{azimuthal scan period} &= 2 \text{ seconds} \\ \text{azimuthal scan rate} &= \pi \text{ radians/second} \end{aligned} \quad (5-66)$$

Hence the probability of the TDRS being in the main beam is approximately 1/1352. The typical dwell time of the radar on the TDRS = $(13\pi)^{-1} = 24.5 \text{ ms}$.

25. NASA/GSFC, "Definition Phase Study Report of the TDRSS," Section 3: Telecommunications.

5.4.2.2 RFI at Each MA Array Element on TDRS

The gain of each MA array element on the TDRS is deduced to be [25] 13 dB. Hence at the TDRS the received power levels when a pulse is present are:

$$\text{RFI (radar sidelobe)} = -141 \text{ dBW/MHz} + 13 \text{ dB} = -128 \text{ dBW/MHz} \quad (5-67)$$

$$\text{RFI (radar main beam)} = -141 \text{ dBW/Hz} + 40 \text{ Hz} = -88 \text{ dBW/MHz} \quad (5-68)$$

5.4.2.3 RFI at the AGIPA Output

5.4.2.3.1 RFI Outside User Beam

When the RFI radar is located outside the 28 dB gain TDRS MA main beam (of the desired user), the AGIPA will maximize the ratio $S/(N+1)$. This ratio will be maximized by directing a spatial null toward the RFI source to drive I to zero at the AGIPA output. The desired user code will permit identification [23] of each desired signal to avoid nulling the desired user.

5.4.2.3.2 RFI Within User Main Beam

In this case the 15 dB gain factor of the 30-element AGIPA will enhance the RFI. In order to combat this extremely powerful RFI the AGIPA algorithm will again force a null to move onto the RFI direction of incidence. Because the RFI is in the main beam of the desired MA user, a null forming on the RFI will push the main beam peak away from the desired signal.

In order to estimate the loss of desired signal, we assume that the normalized array gain pattern (without RFI) as a function of incident angle θ is given by:

$$G(\theta) = \frac{\sin^2(\pi D\theta/\lambda)}{(\pi D\theta/\lambda)^2} \quad (5-69)$$

where D = diameter of the TDRS MA array.

The desired user is located at $\theta=0$ and the RFI is located at θ_I . The array pattern will shift the null from $\theta = \lambda/D$ to approximately θ_I . The resulting power pattern with strong RFI in the main beam is given by the approximation

$$G_{RFI}(\theta) = \frac{\sin^2 [(\theta - \theta_I + \frac{\lambda}{D}) (\pi D/\lambda)]}{(\theta - \theta_I + \frac{\lambda}{D})^2 (\pi/\lambda)^2} \quad (5-70)$$

Note that $G_{RFI}(\theta_I) = 0$.

The normalized array gain on the desired signal at $\theta=0$ is

$$G_{RFI}(0) = \frac{\sin^2 [\pi - (\pi D\theta_I/\lambda)]}{[\pi - (\pi D\theta_I/\lambda)]^2} \quad (5-71)$$

In order to numerically evaluate $G_{RFI}(0)$ we assume the following geometry for the TDRS MA array:

6x6 element square array

2.25 λ separation between closest elements

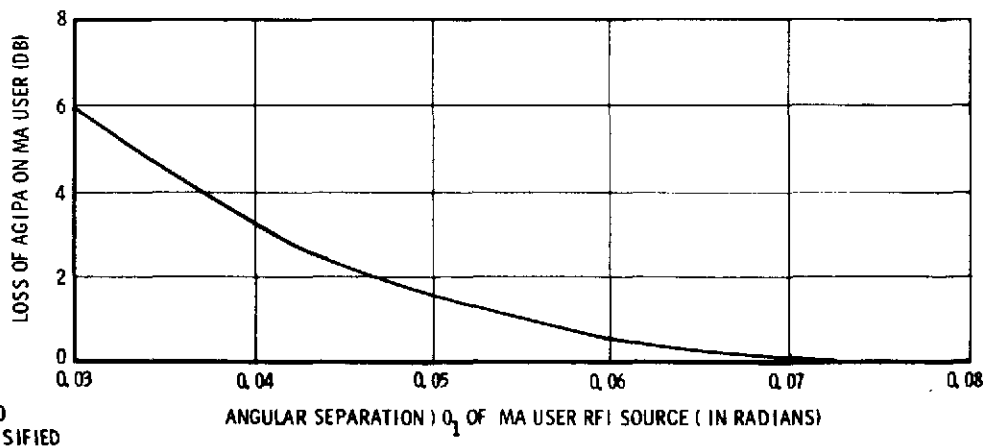
Hence $D = 6(2.25\lambda) = 13.5\lambda = 1.77$ m

We therefore obtain

$$G_{RFI}(0) = \frac{\sin^2 [\pi(1-13.5\theta_I)]}{[\pi(1-13.5\theta_I)]^2} \quad (5-72)$$

Figure 5-54 is a plot of $G_{RFI}(0)$ vs θ_I to demonstrate the loss of gain on desired signal as a function of angular separation between MA user and RFI source, on the assumption that the RFI is extremely strong.

Figure 5-54 gives a pessimistic view of the effects of pulsed RFI with a relatively low duty factor (.0467). Because of the low data rates (relative to RFI width) on the design signal, nonlinear processing (e.g., wideband limiting) will reduce the effect of the RFI pulses, and the AGIPA actually will tend to respond to $S/(N+I)$ during the pulse off times. Thus, the loss of gain on the desired signal will be much less than suggested by Figure 5-45, which applies for strong continuous RFI, rather than pulsed RFI.



974-2950
UNCLASSIFIED

Figure 5-54. Loss of MA Signal Due to AGIPA
Nulling Main Beam RFI

GROUND RECEIVER-TRANSMITTER DESIGN

This section briefly presents a ground receiver-transmitter design. Some of the unique aspects of the equipment implementation like the rate multiplier and incremental phase modulator are discussed in detail. A discussion on return link reacquisition for the M.A. S-band service is presented. A detailed description of a high-speed convolutional decoder and quadriphase demodulator for the SA Ku-band receiver is also discussed. Because of the similarity of the S-band MA and SA R-T's, as well as the Ku-band SA R-T, a generalized receiver-transmitter design is presented in this section.

5.5.1 RECEIVER TRANSMITTER FUNCTIONAL DESCRIPTION

Basic functions of a ground receiver-transmitter are shown in Figure 5-55. The receiver portion consists of a code tracking loop for demodulating the spread spectrum portion of the signal and a carrier tracking loop for demodulating the data from the signal. The transmitter portion consists of a frequency hop synthesizer for generating a FH preamble for initial acquisition in a horward link and a PN sequence generation for modulating the transmit carrier.

Note that all frequency synthesis is referenced to a station frequency reference (5MHz). Transmit carrier offsets are synthesized by a "digital VCO" which is a rate multiplier operating in conjunction with an incremental phase modulator. Receiver center frequency offsets (to compensate for the anticipated return link doppler) are generated from the same type of mechanism.

Range rate data are extracted from the digital filter of the carrier loop. Basically, this data are gathered by accumulating the carrier loop error signals (digital words at a fixed iteration rate) over a period of 1 or 10 seconds. The accumulated word is then scaled so that the digital-output word is in terms of meters/seconds. Range measurement is accomplished by counting the accumulated difference between receiver and transmitter code clock increment commands ($\pm 1/96$ chip steps). This accumulated difference is then scaled so that the digital word output is in terms of meters.

For users whose telemetry data is modulo-two added with a PN sequence, data is demodulated with a Costas demodulator after the pseudo-random sequence has been stripped from the signal. For users employing a clear mode for data along with a minimum power PN ranging signal, data is downconverted in a

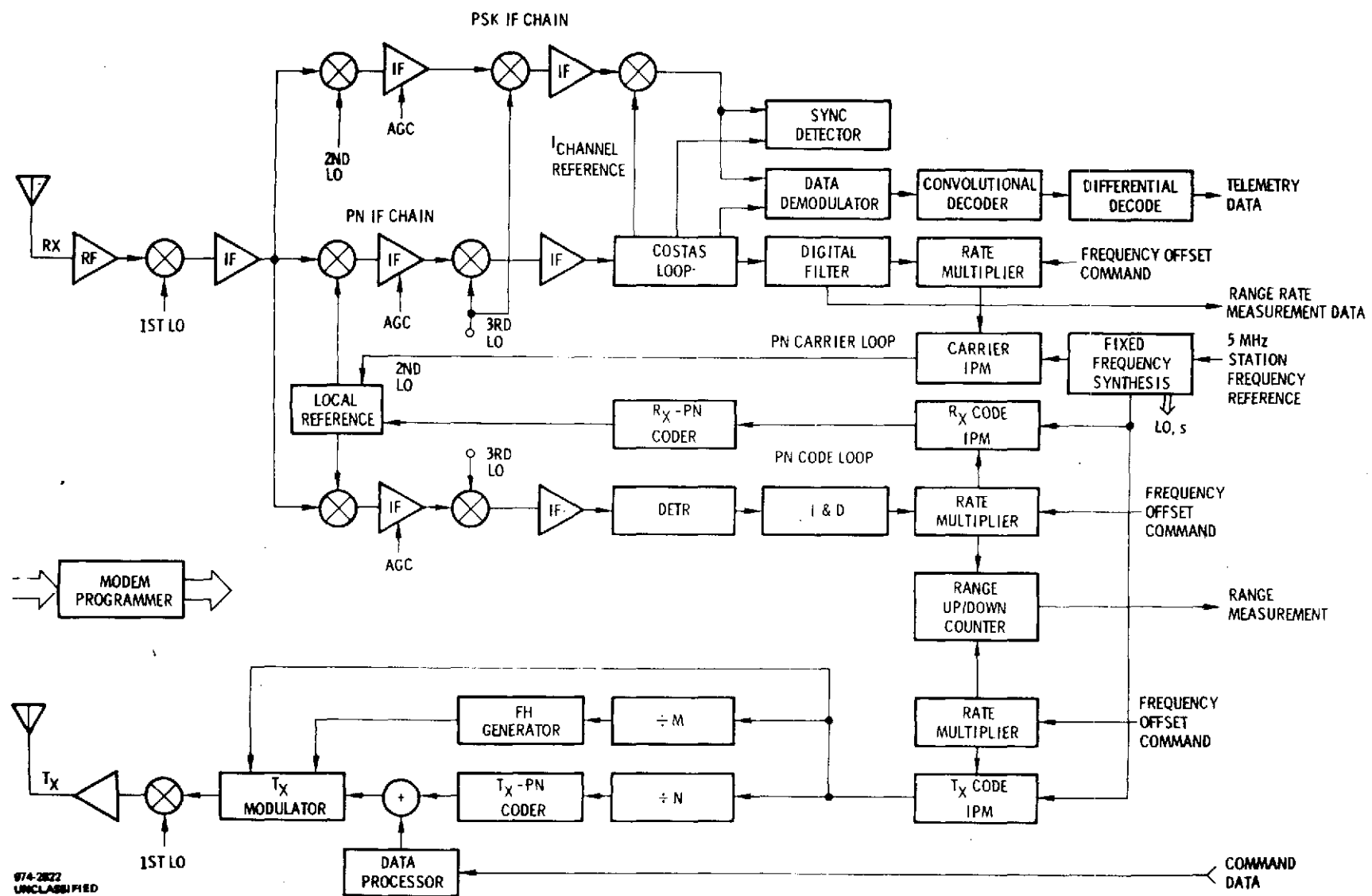


Figure 5-55. Ground Receiver-Transmitter Block Diagram

separate PSK IF chain and synchronously detected using a coherent I channel reference from the PN carrier tracking loop. For users employing a clear mode for data in the return link without a ranging signal, the PN local reference of the PN carrier loop is gated "off" and the data is extracted in the Costas demodulation. If quadriphase shift key modulation is employed in the return link, a separate QPSK demodulator described in section 5.5.4 must be used.

5.5.1.1 IPM and Rate Multiplier

This paragraph presents a description of an incremental phase modulator operating in conjunction with a rate multiplier circuit. This circuit combination is all digital and performs a function equivalent to an analog VCO. This digital VCO, operates from a fixed frequency reference and can be programmed to output a range of offset frequencies for the FH mode or to program doppler offsets in receiver L.O.'s during signal acquisition. These circuits are analyzed in the following section from a hardware standpoint with estimates of component counts.

5.5.1.1.1 Rate Multiplier

A rate multiplier may be considered as a circuit which, when supplied with an input frequency, provides an output frequency determined by a binary command word. The minimum output frequency is zero, and maximum is $(2^n - 1)/2^n$ times the input frequency where $n + 1$ is the number of bits in the command word and the resolution between the extremes is determined by the number of bits in the command word.

A basic representation of a rate multiplier is shown in Figure 5-56. The input frequency is designated frm and the command word is designated by A_0, A_1, \dots, A_n . The output frequency is shown in the figure as $M frm/2^n$. Thus if all the A 's are zero, the multiplier $M=0$, and the output frequency is zero. If all the A 's are 1, M equals $2^n - 1$ and the output frequency is $(2^n - 1)/2^n$ times the input frequency.

One important parameter of a rate multiplier is the cycle time. The cycle time is the time required to go through one complete frequency correction. One cycle is 2^n pulses of the frm input. Hence, the cycle time is

$$\text{Cycle Time} = \frac{2^n \text{ pulses}}{\text{frm pulses/sec}} = \frac{2^n}{\text{frm}} \text{ sec} \quad (5-73)$$

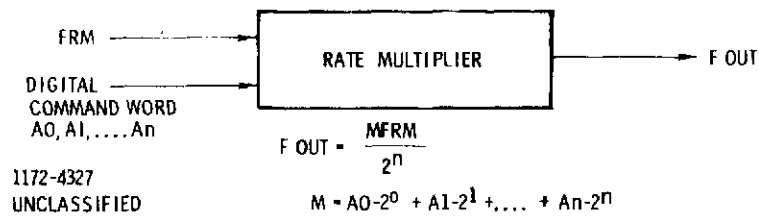


Figure 5-56. Basic Rate Multiplier

The number of pulses at the output per cycle is

$$\text{Pulses/Cycle} = \frac{Mfrm}{2^n} \text{ P/S} \times \frac{2^n}{frm} \text{ sec/cycle} \quad (5-74)$$

$$= M$$

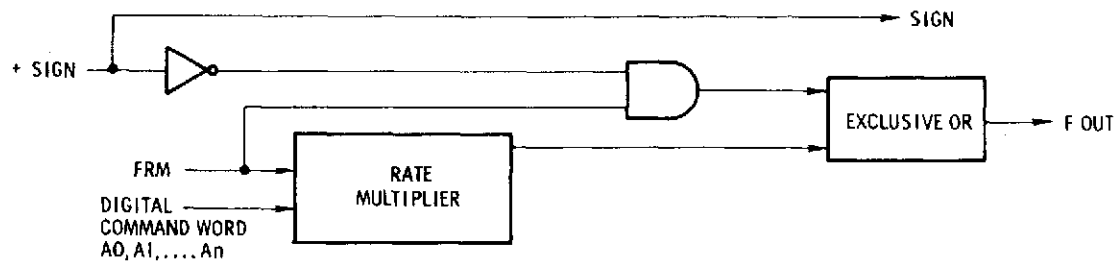
Thus for a particular M, there would be M pulses per cycle on the output. If M were increased by one for one cycle, there would be one additional pulse to the M pulses per cycle.

5.5.1.1.2 Basic Rate Multiplier with Sign

The basic rate multiplier discussed above only generates a rate. If sign information is to be included, then consideration should be given to the type of arithmetic used. Two's complement arithmetic is most common and is the easiest to use. If the digital command word for the rate multiplier, Ao through An and sign of Figure 5-57 is in two's complement form, the rate multiplier output is M for positive numbers and $2^n - M$ for negative numbers. However, we want M at the Fout for both positive and negative sign. The exclusive OR, which is a binary adder without the carry, converts the $2^n - M$ number back to M magnitude. The rate multiplier out for negative sign input is $-M frm/2^n$.

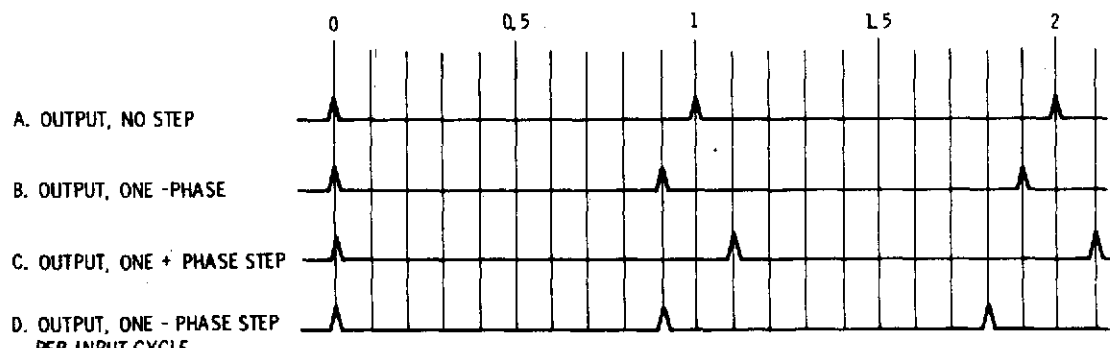
5.5.1.1.3 Incremental Phase Modulator (IPM)

The incremental phase modulator (IPM) function is diagrammed in Figure 5-58. The IPM functionally is a device which adds or subtracts a fixed number of electrical degrees to the nominally periodic output waveform per pulse on the step input. In part A of the figure, two cycles of the nominally periodic output are



1172-4328
UNCLASSIFIED

Figure 5-57. Basic Rate Multiplier With Sign



1172-4329
UNCLASSIFIED

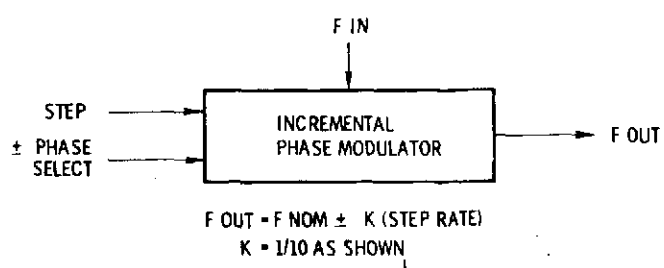


Figure 5-58. IPM Function

shown as 0 to 1 and 1 to 2. Each of 0 to 1 and 1 to 2 intervals correspond to 360 electrical degrees. In this example the magnitude of the phase step is 0.1 cycle or 36 degrees. In part B, a minus phase step is applied between 0 and 0.9 which subtracts 0.1 cycle from the output. In the absence of additional steps in part B, there will be 360 degrees in subsequent cycles of the output. Part C shows the effect of adding one phase step between 0 and 1. Part D shows the effect of subtracting one phase step at each cycle. If this were done continuously, the effect would be to increase the output frequency by 11.1 percent. The number of degrees per step is determined by particular design requirements.

5.5.1.1.4 Rate Multiplier and Incremental Phase Modulator Combination

A combination of an RM and IPM is shown in Figure 5-59. The RM step and sign control outputs are applied to the IPM step and sign inputs. Thus, the digital command word and sign determine the phase change on the IPM output frequency. As shown in the figure, the output frequency is:

$$F_{out} = F_{nom} \pm K \frac{M_{frm}}{2^n} \quad (5-75)$$

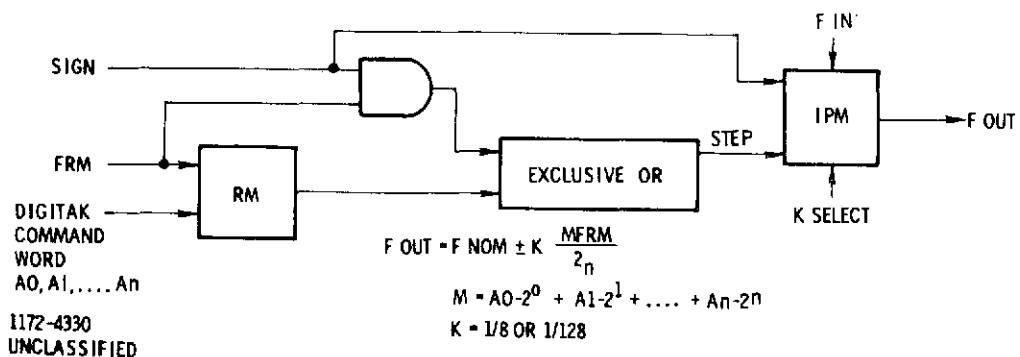


Figure 5-59. Rate Multiplier and IPM

5.5.1.1.5 Rate Multiplier - Frequency Hop Sequence Generator

The Rate Multiplier which is utilized on the frequency hop sequence generator provides an average frequency output to an 8-step IPM which provides the desired spectral line. The average frequency output of the rate multiplier is actually a series of step pulses with a corresponding direction (sign) output. These step and direction inputs to the IPM determine the phase change on the IPM output frequency. The Rate Multiplier block diagram is shown in Figure 5-60. The Rate Multiplier is driven with a reference clock and supplied with an 8-bit command word to select one of 256 frequencies.

The Rate Multiplier provides a symmetrical distribution of step pulses over the complete counting cycle of the binary counter. The hardware implementation of an 8-bit Rate Multiplier requires approximately 10 ICs. Magnavox has recently designed and developed a selectable 8-bit or 13-bit Rate Multiplier in a 0.9 inch by 1.65 inch hybrid microcircuit.

5.5.1.1.6 IPM - Code Tracking Loop

The IPM which is utilized on the code tracking loop of the single access S-band Receiver has a resolution of 1/128 cycle/step, and is implemented by using a digital synthesis of the single sideband modulator. The variable-modulo counter implementation to an IPM can provide the resolution requirements and, therefore, has been selected for use in the code tracking loop. The variable modulo counter approach to IPM design also provides coarse resolution from 1/8 to 1/4 cycle/step and is well suited for advancing and retarding the PN Code phase during a PN search mode.

The block diagram of the 128-step IPM is shown in Figure 5-61. As mentioned above, the 128-step IPM is implemented by using a digital synthesis of the single sideband modulator which can be represented by the trigonometric identity:

$$\cos(\omega_1 - \omega_2)t = \cos \omega_1 t \cos \omega_2 t + \sin \omega_1 t \sin \omega_2 t \quad (5-76)$$

The IPM uses a carrier or reference of 4 times the nominal output and the modulating signal is a pulse stream representing phase step commands. The modulating signal is converted to a digital word in an up/down counter. The results of the operations (2 multiplications, two 90° phase shifts, and the final summation) are stored in Read Only Memories (ROMs).

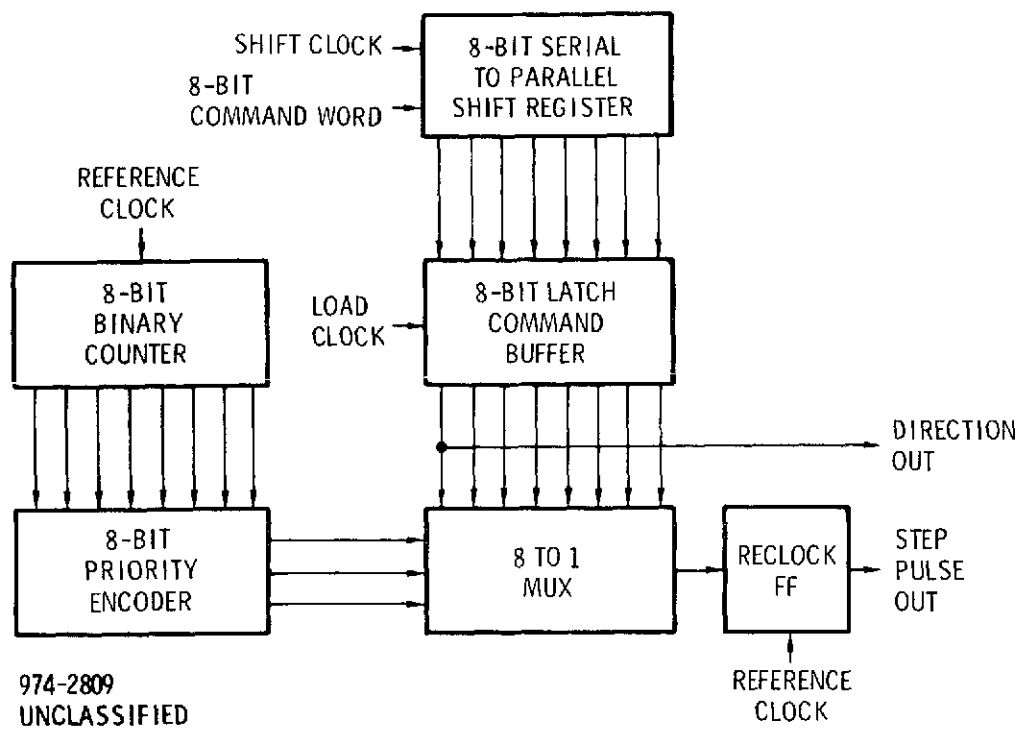


Figure 5-60. 8-Bit Rate Multiplier

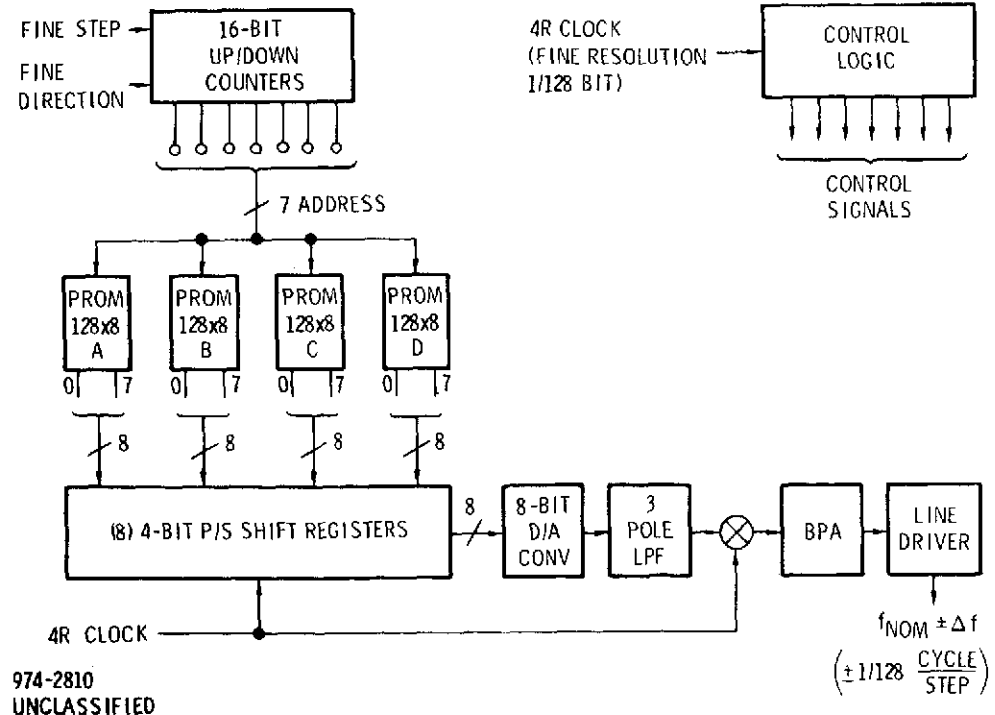


Figure 5-61. 128-Step IPM

The reference waveform is quantized into 4 states, each being 90° of the reference phase. The output waveform is reconstructed out of 4 discrete steps for each reference cycle in a digital-to-analog converter (DAC). Lowpass or bandpass filtering will select the fundamental or harmonics of the reference to complete the IPM operation. The 128-step IPM uses the PN clock from the frequency synthesizer as a 4R reference clock, and receives its step pulses from a summer output which represents an estimate of the range error.

The 128-step IPM provides the frequency and phase control capability for the coder clock phase lock loop of the Receiver-Transmitter. The code clock IPMs phase is controlled by the step and direction controls from the summer output. The 128-step IPM does not use coarse phase controls. The fine step (1/128 bit) control inputs a series of pulses which cause an 8-bit counter to count up or down as a function of the fine direction control. The lower order 7 bits of the counter define the phase of the IPM output with respect to the reference input which is the PN clock. The wiring of these lower order 7 bits will cause this clock IPM to have a sensitivity of 2^{-7} or 1/128 bit per fine step. The upper order 9 bits of the counter are used to store the phase accumulations of up to 2^9 or 512 Hz.

The low order 7 bits of the up/down counter are used to address 4 (128 x 8) Read-Only Memories (ROMs) which are programmed to contain the following:

$$\begin{aligned}
 A &\rightarrow \frac{1}{2} + \left(\frac{\sin \Theta + \cos \Theta}{2\sqrt{2}} \right) \\
 B &\rightarrow \frac{1}{2} + \left(\frac{\sin \Theta - \cos \Theta}{2\sqrt{2}} \right) \\
 C &\rightarrow \frac{1}{2} + \left(\frac{-\cos \Theta - \sin \Theta}{2\sqrt{2}} \right) \\
 D &\rightarrow \frac{1}{2} + \left(\frac{\cos \Theta - \sin \Theta}{2\sqrt{2}} \right)
 \end{aligned} \tag{5-77}$$

where Θ is the phase stored in the 7 low order bits of the counter, and can be represented by the expression

$$\Theta = \frac{M}{128} (2\pi) \quad M = 0, 1, 2, \dots, 127 \tag{5-78}$$

Each of the ROMs will store 128 8-bit words representing values for angles between 0° and 360° . Therefore, the smallest change in phase at the output of any ROM due to a single fine step will be $360^\circ/128$ or 2.81°

The modulating signal in equation 5-76 is ω_1 which represents our fine step and direction inputs. The reference clock in equation 5-56 is ω_2 which represents our PN clock to the IPM. If it is assumed that our reference is a square wave having a value of +1 over half the reference cycle ($0 \leq t \leq 2T$), and -1 over the second half of the reference cycle ($2T \leq t \leq 4T$), the right half of equation 5-56 can be broken down into the following four equations over the complete reference cycle $0 \leq t \leq 4T$.

$$\begin{aligned}
 1. \quad & \cos \omega_1 t (+1) + \sin \omega_1 t (+1) \quad 0 \leq t \leq T \\
 2. \quad & \cos \omega_1 t (-1) + \sin \omega_1 t (+1) \quad T \leq t \leq 2T \\
 3. \quad & \cos \omega_1 t (-1) + \sin \omega_1 t (-1) \quad 2T \leq t \leq 3T \\
 4. \quad & \cos \omega_1 t (+1) + \sin \omega_1 t (-1) \quad 3T \leq t \leq 4T
 \end{aligned} \tag{5-79}$$

The above four equations, plus some constants, represent the data stored in ROM's A, B, C, and D respectively. If the ROMs are sampled over their corresponding intervals and applied to a D/A converter, the synthesis of the trigonometric identity in equation 5-56 will be accomplished.

Since the $\sin \Theta$ or $\cos \Theta$ can take on negative values for Θ between 0° and 360° , scaling of the data stored in the ROMs is necessary to prevent the ROM outputs from being negative, and thus requiring 2's complement arithmetic. This scaling has been accomplished by dividing each of the equations 1 - 4 by " $2\sqrt{2}$ " and adding " $\frac{1}{2}$ " to the resulting term. Therefore, each of the ROM outputs can range in value between 0 and 1, but never negative, since the term in parenthesis can only vary between $\pm\frac{1}{2}$ for all values of Θ between 0° and 360° . Each ROM will exhibit its maximum value at the following values of Θ .

$$\begin{aligned}
 \text{ROM A at } \Theta &= 45^\circ \\
 \text{ROM B at } \Theta &= 135^\circ \\
 \text{ROM C at } \Theta &= 225^\circ \\
 \text{ROM D at } \Theta &= 315^\circ
 \end{aligned}$$

The maximum of each of the ROMs B, C, and D occur at integer multiples of 90° from that of ROM A. This should be no surprise, since each of the equations 1 - 4 is constrained to one-fourth of a carrier cycle. In fact, observation of equations 1 - 4 should indicate that the values stored in ROMs B, C, and D are 90° , 180° , and 270° displaced from the values stored in ROM A. Therefore, ROMs A, B, C, and D cover quadrants I, II, III, and IV, respectively of the reference cycle.

The four ROMs are sampled by 8, four-bit parallel to serial shift registers which are loaded synchronously from a divide-by-four counter which is clocked with the 4R reference clock. The 8-bit ROM data is shifted out of the register serially using the 4R reference clock; and the output of the shift register is fed back to its input so as to provide a continuous cycle at the output of the DAC when no phase-changes are being processed. Each of the 8 four-bit shift registers contains the $2^{n\text{th}}$ bit of the four ROMs, so, for example, the first shift register contains the LSB of each ROM. The ROMs are sampled in the following order: A, B, C, D, A, B, The 8-bit, shift register outputs are converted by the DAC to a sine wave approximation, which is quantized by 4 values, over the reference cycle, each value of which has an 8-bit resolution. Further smoothing of the sine wave approximation is done by a lowpass filter which removes any higher frequency harmonics of the reference. This nominal IPM output is bandpass amplified to obtain a very smooth sinusoidal output which is supplied to a line driver.

The hardware implementation of the 128-step IPM requires approximately 60 ICs. Magnavox has recently designed and developed an IPM having either coarse and/or fine stepping rates of about 2.5 MHz, a nominal frequency output of 78.6 MHz, and a fine resolution of 1/128 bit and/or a coarse resolution of $\frac{1}{4}$ bit. This IPM has been built using three 0.9 inch by 1.65 inch hybrid microcircuits and about 10 ICs.

5.5.1.1.7 IPM - Frequency Hop Sequence Generator

An 8-step IPM is used in the frequency hop sequence generator to provide the desired spectral line output. Actually, the 8-step IPM provides smoothing of the average frequency output of the Rate Multiplier which is represented by a series of step pulses which are symmetrically distributed over the counting cycle of the Rate Multiplier. The 8-step IPM is implemented by using a variable-modulo counter technique which provides a resolution of 1/8 cycle/step. The single sideband modulator implementation for an IPM has not been utilized because of the coarse resolution requirement.

The block diagram of the 8-step IPM is shown in Figure 5-62. The 8-step IPM is essentially a modulo 7, 8, 9 counter with various control circuitry to provide

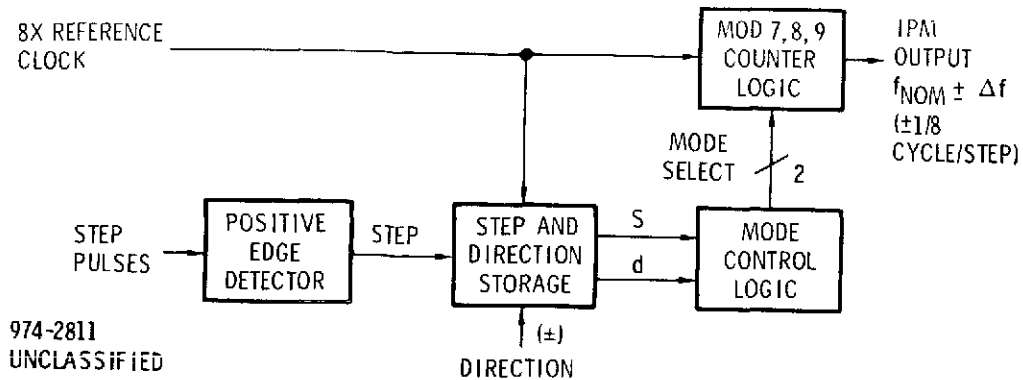


Figure 5-62. 8-Step IPM

synchronous stepping and mode control for the modulo counter. The modulo counter normally operates in a mod-8 mode when no step pulses are present at the IPM input, and a one times reference clock is provided at the output. When a step pulse and direction inputs are applied to the IPM, the modulo counter operates in the divide-by-9 mode for one counting cycle only, and then reverts back to the divide-by-8 mode thereby causing the output reference clock to be retarded (or decreased in frequency or phase) by 1/8 of a cycle since the IPM has a resolution of 1/8 cycle/step. When a step pulse and negative direction inputs are applied to the IPM, the modulo counter operates in the divide-by-7 mode for one counting cycle only, and then reverts back to the divide-by-8 mode thereby causing the output reference clock to be advanced (or increased in frequency or phase) by 1/8 of a cycle. Therefore, step pulse inputs to the IPM cause the output reference clock to be advanced or retarded in time.

The 8-step IPM requires a maximum frequency offset from the center frequency of $\pm 1\frac{1}{2}$ MHz. This frequency offset requires a maximum step pulse rate of 12 MHz since:

$$\pm \Delta f = (1/8 \frac{\text{cycle}}{\text{step}}) (12 \times 10^6 \frac{\text{steps}}{\text{sec}}) = 1.5 \times 10^6 \frac{\text{cycles}}{\text{sec}} \quad (5-80)$$

The hardware implementation of the 8-step IPM requires approximately 6 ECL-type ICs.

5.5.2 REACQUISITION OF MULTIPLE ACCESS SIGNAL

5.5.2.1 Introduction

Signal dropout during tracking necessitates signal reacquisition. The signal being reacquired is data modulated whereas during initial acquisition data modulation is absent for a sufficiently long time to allow initial acquisition.

This memorandum defines the worst case reacquisition condition and the subsequent methods which can be used to rapidly reacquire a signal. Consideration is limited to signal dropout times of 100 seconds or less.

To achieve synchronization of a PN signal, both time and frequency searches must be made. The time/frequency region to be searched represents an uncertainty region. For reacquisition, the size of the uncertainty region can increase with time. Factor contributing to the increasing uncertainty region are (1) transponder frequency instability and (2) inaccurate estimation of the rate of change of relative separation between the MA user and the TDRS. The problem of reacquiring a MA user signal is discussed in the following sections.

5.5.2.2 Signal Dynamics

To begin the analysis, we postulate a worst case condition. Consider that the MA user satellite has a retrograde orbit which is in the orbital plane of the TDRS. Considering a circular orbit, the largest signal dynamics is experienced at the TDRS suborbital point. At this point the doppler frequency (F_d) is zero but the doppler frequency rate of change (\dot{F}_d) is a maximum. Mathematically expressed, the rate of change of relative MA/TDRS separation is

$$\frac{dL^2(t)}{dt^2} = \frac{HR[L(t)\dot{\theta}^2(t) \cos \theta(t) - \dot{\theta}(t) \frac{dL(t)}{dt} \sin \theta(t)]}{L^2(t)} \quad (5-81)$$

where

$L(t)$ = Relative MA/TDRS separation

H = TDRS Synchronous Altitude (42,200 km earth center)

R = MA User Altitude (6,578 km earth center)

$\theta(t)$ = Angular Separation Between TDRS and MA User

$\dot{\theta}(t)$ = Rate of Change of $\theta(t)$.

This MA user altitude represents the minimum altitude of 200 km (sea level reference) which provides a minimum of 85 percent of signal relay coverage and a maximum $\theta(t)$. At the transponder transmission frequency of 2.287 GHz, $F_d = 93$ Hz/sec. Hence, if signal dropout occurs at the MA user's suborbital point, approximately 1 KHz of frequency uncertainty can accumulate after only a 10 second outage. The loop noise bandwidth of the Costas loop is 33 Hz, and hence, after only 1/3 second, the input frequency has drifted outside the loop noise bandwidth.

Through the use of aiding, the growth rate of the uncertainty region can be reduced. However, this requires a rather precise a priori knowledge of the TDRS/MA user orbit dynamics hence giving rise to the relative dynamics at any point in their orbits. This information would be available at a master control station but might not be available at a remote, mobile control station. Hence, it is presumed that the only a priori knowledge which is available is the value of the tracking frequency prior to loss of lock. Thus, as the signal dynamics change, there is a buildup in the size as the time/frequency uncertainty which must be searched for reacquisition. The time uncertainty is a direct result of holding the PN code generator at the driving frequency just prior to signal loss. As out of lock time increases, the frequency offset increases. Time uncertainty increases as the integral of frequency offset. For a 93 Hz/sec doppler rate, this corresponds to a rate of frequency change of approximately 40 parts in 10^9 per sec. After a signal outage of 100 seconds, there can be as much as a 1200 PN chip uncertainty.

5.5.2.3 Transponder Frequency Instability

The selected frequency synthesis approach for the MA transponder was shown in Section 2.2.5. After having established a two-way line with the MA transponder and having measured range and range rate, the forward link transmission is discontinued. At this point the carrier VCO input is clamped to a ground reference through the loop filter. Hence, the transmitted frequency is slewed lowly until the loop's error voltage reaches the new reference at ground potential. The slewing rate is slow enough so as not to stress the ground station's third order loop to the point of breaking lock. If signal dropout does occur during this procedure, the two-way link will be reestablished and the above procedure repeated. Hence, one-way signal reacquisition will be performed only after the MA transponder's carrier VCO has been clamped to a ground potential.

Because of MA transponder power limitations (20 watts maximum per transponder), the chosen carrier VCO is a TCVCXO. Typical, current, state-of-the-art oscillator characteristics are shown in Table 5-15. At the carrier frequency of 2.287 GHz, and for a VCO instability of one part in 10^7 , then after 100 seconds of signal outage, the time uncertainty due only to oscillator instability is ± 30 PN chips.

Table 5-15. TCVCXO Characteristics

Frequency Range	2-33 MHz
Frequency Stability	
1 second	$\pm 1 \text{ pp } 10^9$
1 hour	$\pm 1 \text{ pp } 10^7$
24 hours	$\pm 1 \text{ pp } 10^7$
1 year	$\pm 3 \text{ pp } 10^6$
Modulation Range	$\pm 10 \text{ pp } 10^6$
Modulation Rate	DC to 20 KHz
Modulation Sensitivity	-3 pp M/V
Modulation Linearity	$\pm 5\%$
Output Power	0 to +3 dBm
Temperature Range	-20°C to +70°C
Temp. Frequency Stability	$\pm 1 \text{ ppm}$
Stabilization Time	5 seconds
Input Voltage	+12 VDC $\pm 1\%$
Input Power	120 mW
Size	2" x 2" x .8"
Weight	4 oz.

5.5.2.4 Costas Loop Reacquisition

There are a number of methods which can be utilized to bring the Costas loop back into lock. There are loop types (including a second order loop) which will slowly drift toward the input frequency when the difference frequency between the input and VCO greatly exceeds the loop bandwidth. The maximum frequency difference Δf_p is called the pull-in frequency. However, the time associated with naturally allowing the loop to pull-in can take a long time and hence other methods are considered.

Provided that the noise level is sufficiently low, fast acquisition is possible if the loop bandwidth is widened. When the frequency difference between

input and VCO is less than the loop bandwidth, the loop will lock up very rapidly without slipping cycles. The maximum frequency difference for which this fast acquisition is possible is called the lock-in frequency Δf_L . If widening the loop bandwidth degrades the loop signal-to-noise ratio to an unacceptable level, a fixed loop bandwidth can be used and the VCO must be swept at a suitable rate in order to search for the input signal.

It is a difficult analytical problem to determine the acquisition performance for higher order phase lock loops having a constant input frequency offset. A straightforward method for solving the problem is by Monte Carlo Computer simulation^[26]. The phase lock loops which were simulated were second and third order loops which use a digital filter implementation.

Figures 5-63 through 5-65 show the cumulative probability of acquisition as a function of time for the second order loop for signal-to-noise ratios, $C/N_o B_L$, of 12, 6, and 3 dB respectively. The frequency offset is normalized by the loop noise bandwidth B_L and offsets greater than 1.5 are not shown since they require an inordinate amount of time for acquisition. In fact, the curve for $\Delta f/B_L = 1.5$ at $C/N_o B_L = 12$ dB shows that at this frequency offset, the acquisition time has already become extremely high. The time required to acquire with probability .9 at $\Delta f/B_L = 1.5$ is approximately 8 times the time required to acquire with probability .9 at $\Delta f/B_L = 0.5$. At a signal-to-noise ratio of 6 dB, as shown in Figure 5-65, it is seen that the loop starts to acquire poorly at offsets greater than .5. It is interesting to note that the acquisition time for a probability of .9 for zero offset frequency varies approximately as $(C/N_o B_L)^{-1}$. The simulation was run for $C/N_o B_L = 0$ dB but acquisition was not reliable enough to show meaningful results. The time required to acquire with probability .9 is shown plotted as a function of frequency offset in Figure 5-66. Figure 5-66 indicates that at low signal to noise ratios; i. e., 3 dB, the loop acquired reasonably well with offsets ($\Delta\omega$) as large as the corner frequency, ω_n . At moderate signal-to-noise ratios; i. e., 6 dB, frequency offsets as large as twice the corner frequency may be acquired and at large signal-to-noise ratios; i. e., 12 dB, offsets approaching three times the corner frequency may be acquired. Again, $C/N_o B_L$ is given as a parameter. It can be

26. Nilsen, P. W., "Acquisition Performance of Second and Third Order Phase Lock Loops", MRL Ref. No. MX-TM-3105-71, April 1971.

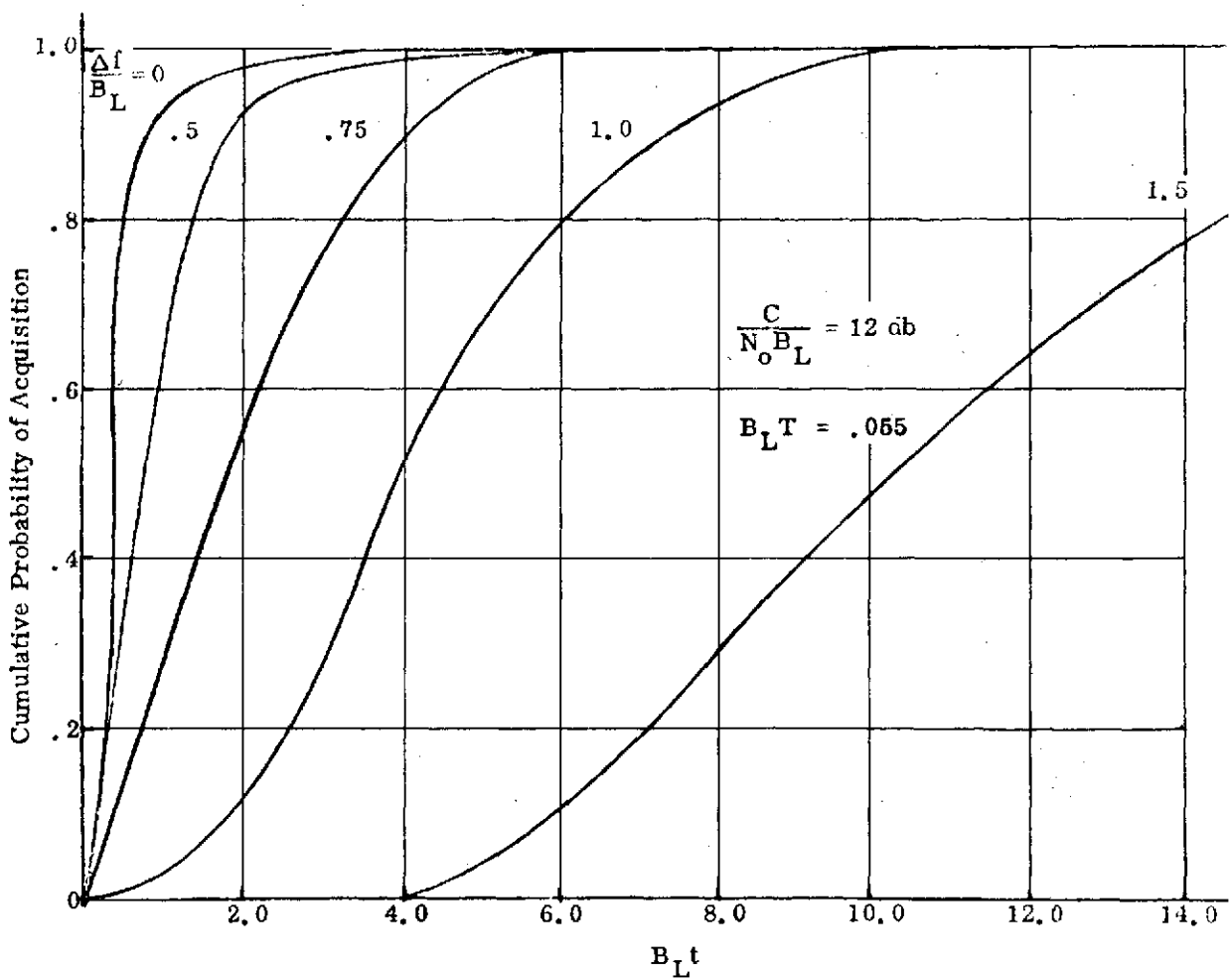


Figure 5-63. Cumulative Probability of Acquisition as a Function of Time (Normalized) for Second Order Phase Locked Loop,
 $C/N_0 B_L = 12 \text{ dB}$

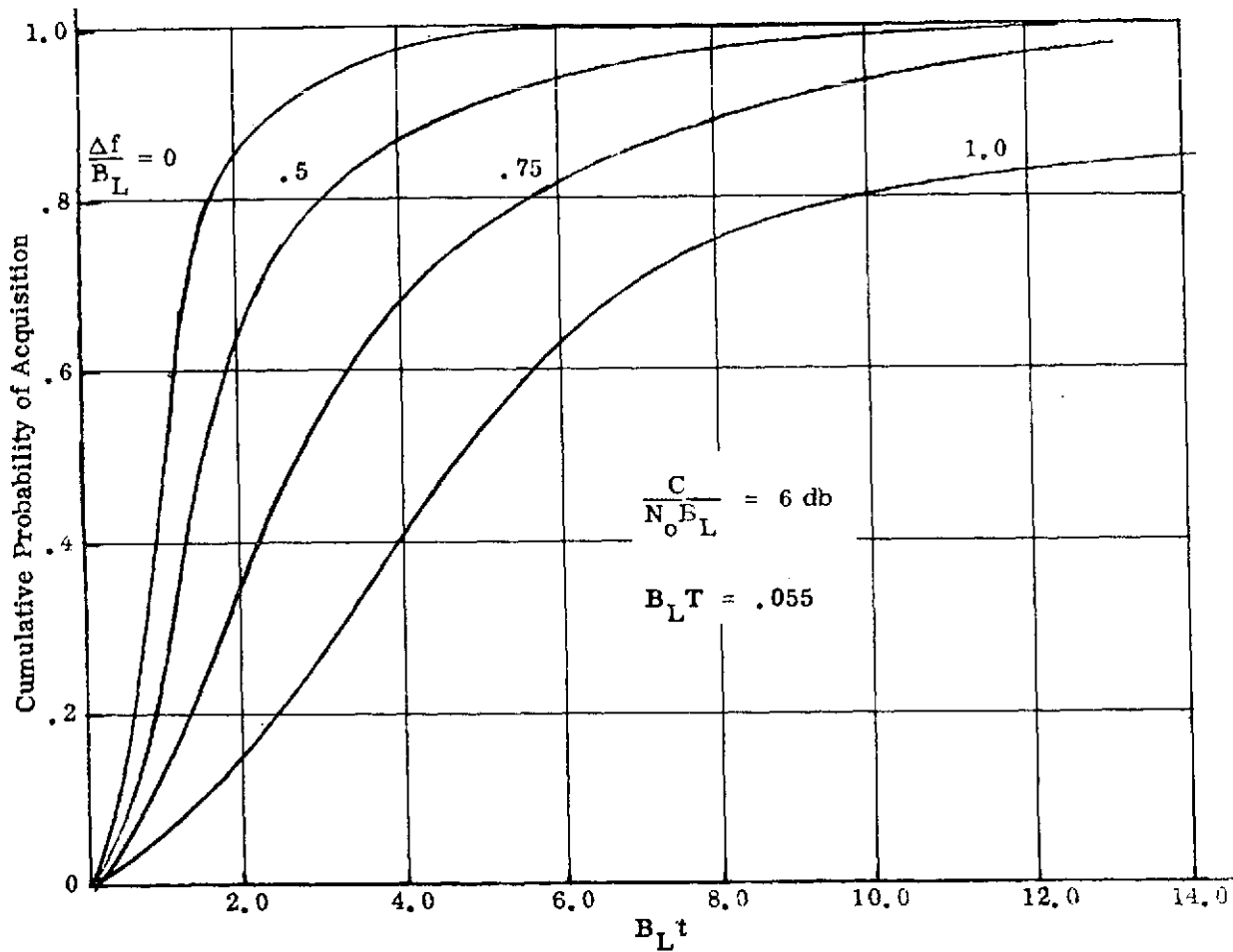


Figure 5-64. Cumulative Probability of Acquisition as a Function of Time (Normalized) for Second Order Phase Locked Loop,
 $C/N_0 B_L = 6 \text{ db}$

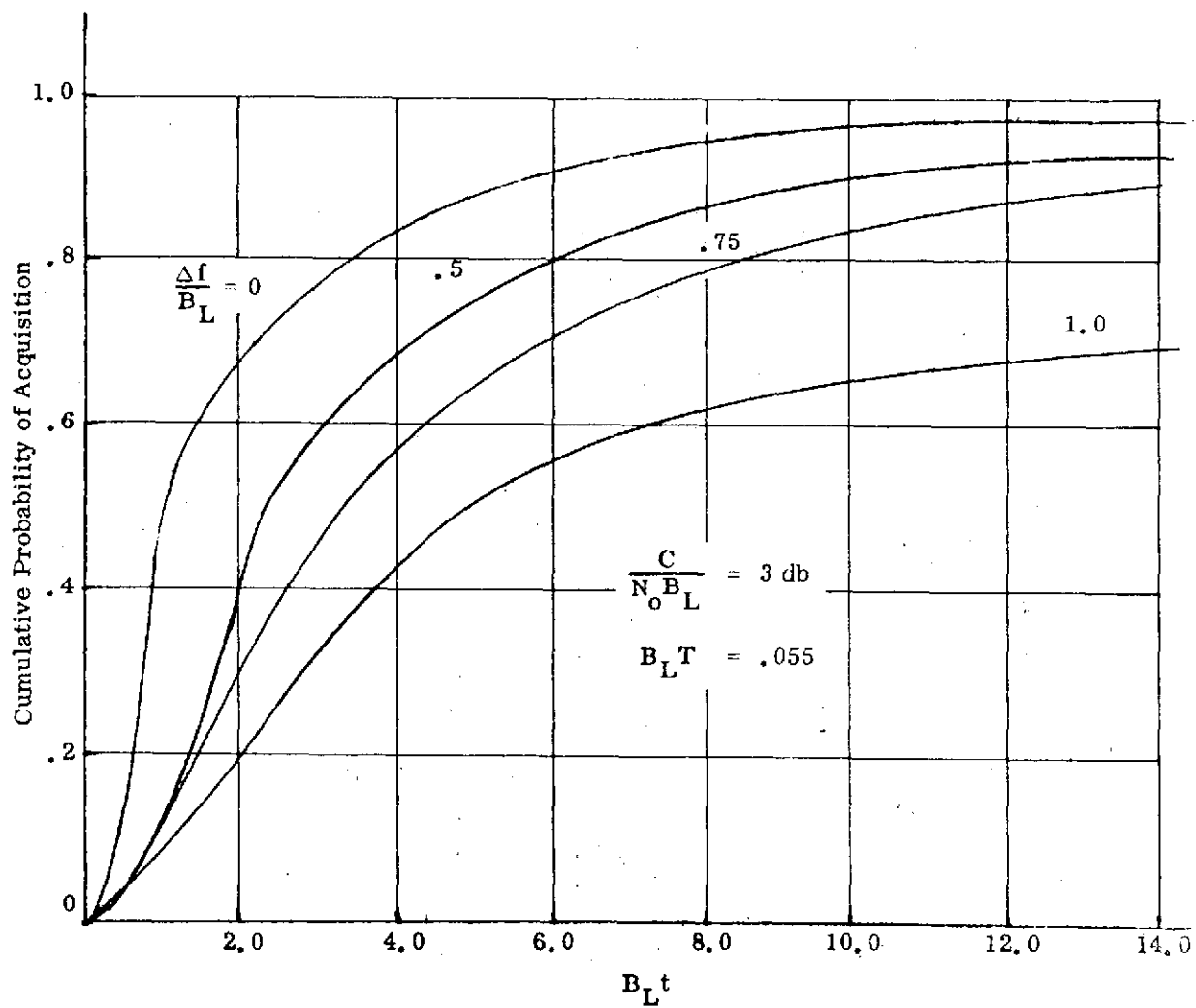


Figure 5-65. Cumulative Probability of Acquisition as a Function of Time (Normalized) for Second Order Phase Locked Loop,
 $C/N_0 B_L = 3 \text{ db}$

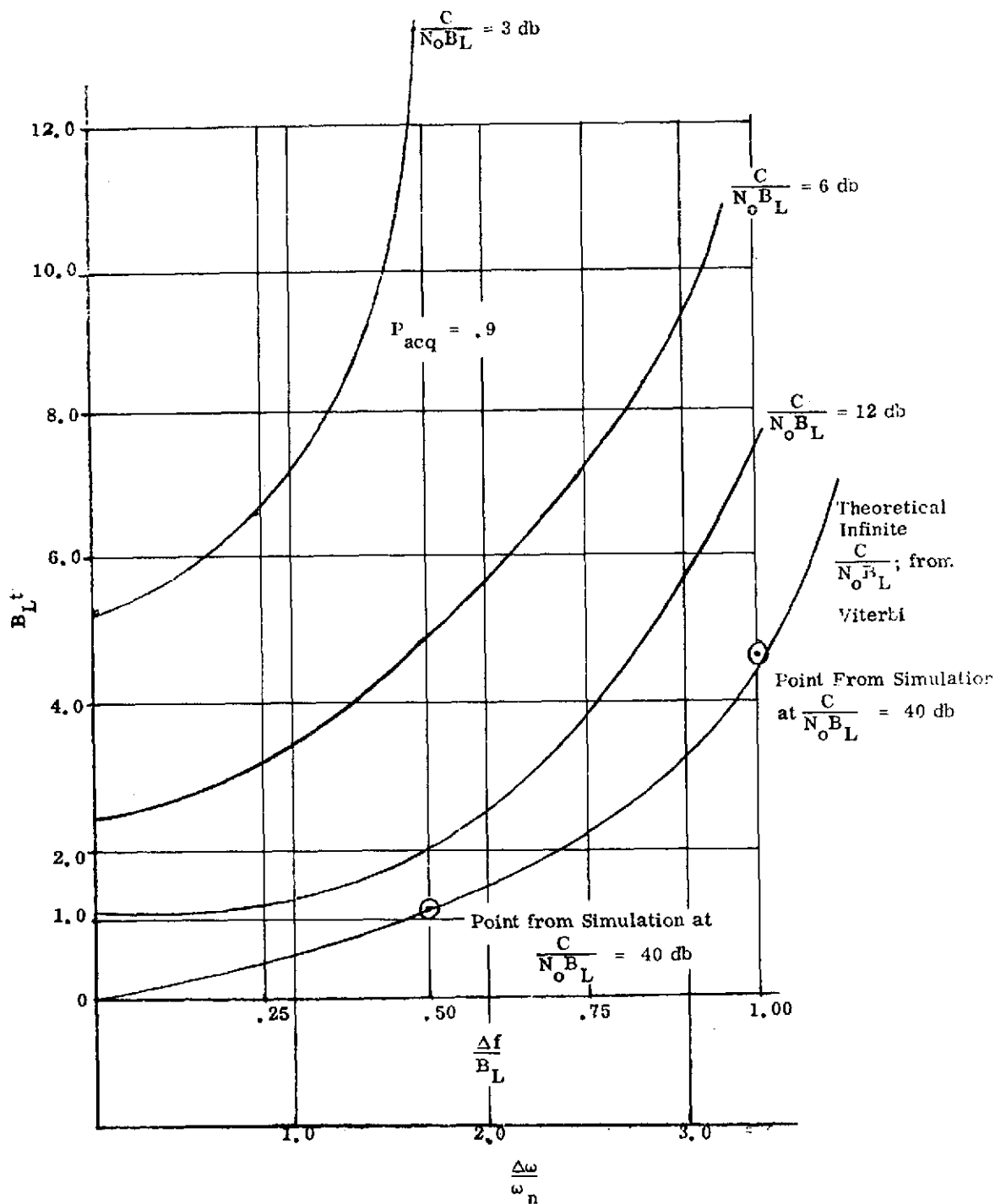


Figure 5-66. Second Order Phase Lock Loop Acquisition Time as a Function of Initial Frequency Offset

seen that for low signal-to-noise ratios; i.e., 3 dB, the loop will acquire with only very small frequency offsets. The validity of the simulation is demonstrated by the agreement between Viterbi's curve for acquisition time with no noise and the two points obtained from the simulation with $C/N_o B_L = 40$ dB^[27].

The cumulative probability of acquisition time for the third order loop for 12 dB and 6 dB is shown in Figures 5-67 and 5-68, respectively. Curves for 3 dB

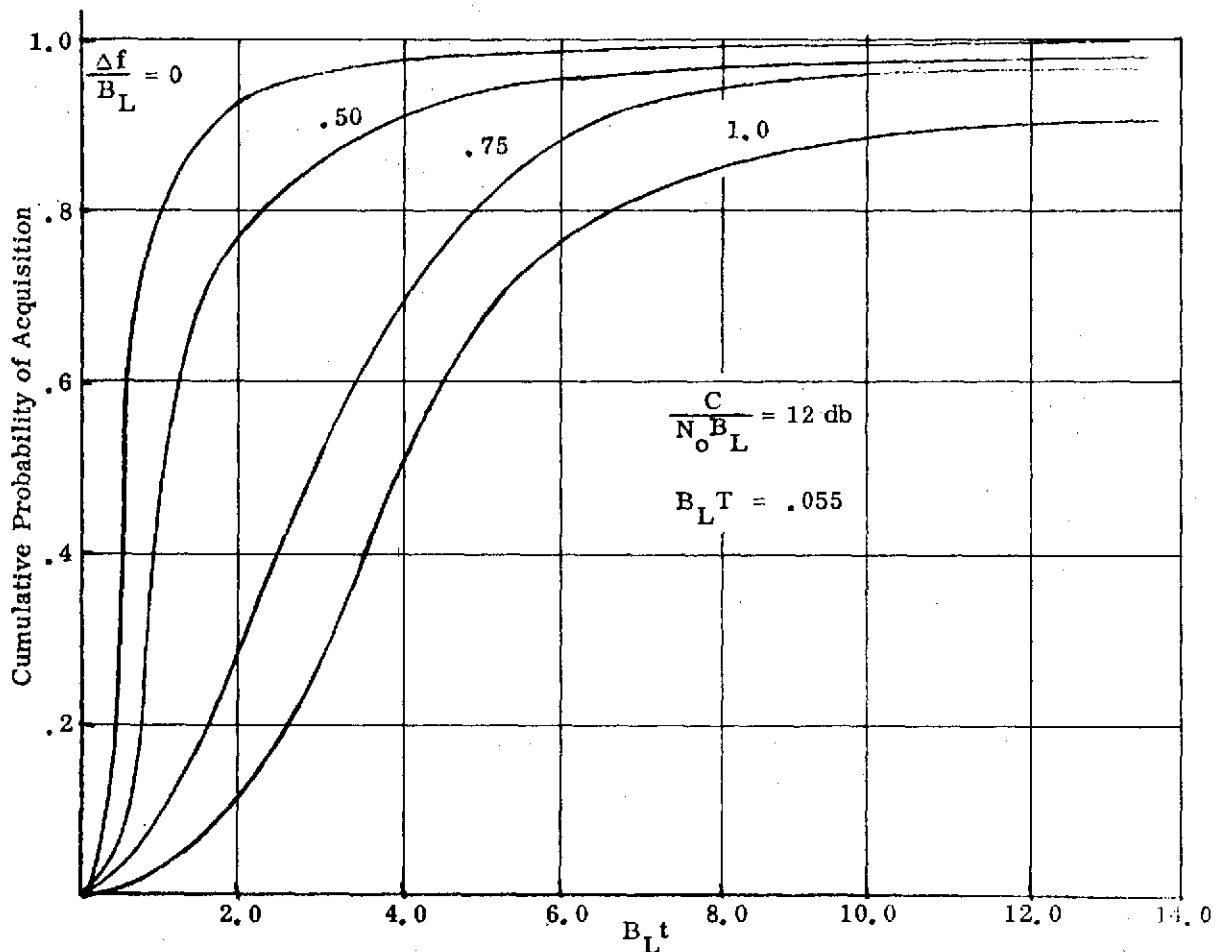


Figure 5-67. Cumulative Probability of Acquisition as a Function of Time (Normalized) for Third Order Phase Locked Loop,
 $C/N_o B_L = 12$ dB

27. Viterbi, Andrew J., "Principles of Coherent Communication", McGraw-Hill, 1966, p. 54.

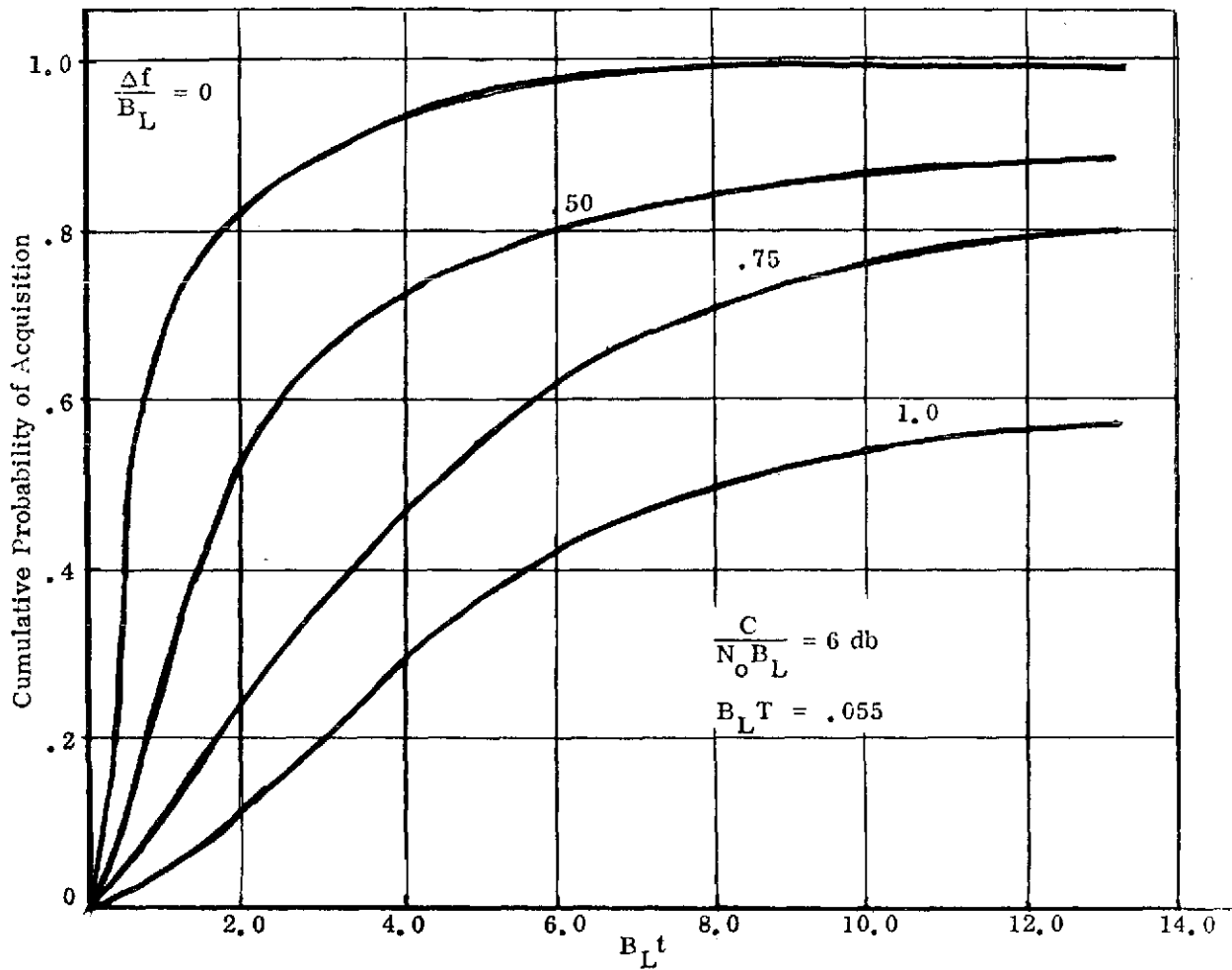


Figure 5-68. Cumulative Probability of Acquisition as a Function of Time (Normalized) for Third Order Phase Locked Loop,
 $C/N_0 B_L = \text{db}$

are now shown since the third order loop exhibited erratic acquisition behavior at this signal-to-noise ratio. Comparison of the third order loop acquisition probability curve for 12 dB, Figure 5-67, shows that the third order loop has inferior acquisition performance relative to the second order loop. In particular, the curve for $\Delta f / B_L = 1.0$ for the third order loop begins flattening out at a probability of approximately .9. The same curve for the second order loop reaches a probability of 1.0. At 6 dB, the third order loop acquires poorly at offsets of $\Delta f / B_L = .5$ and higher. The plot of acquisition time as a function of frequency offset for the third order loop, Figure 5-69 shows the

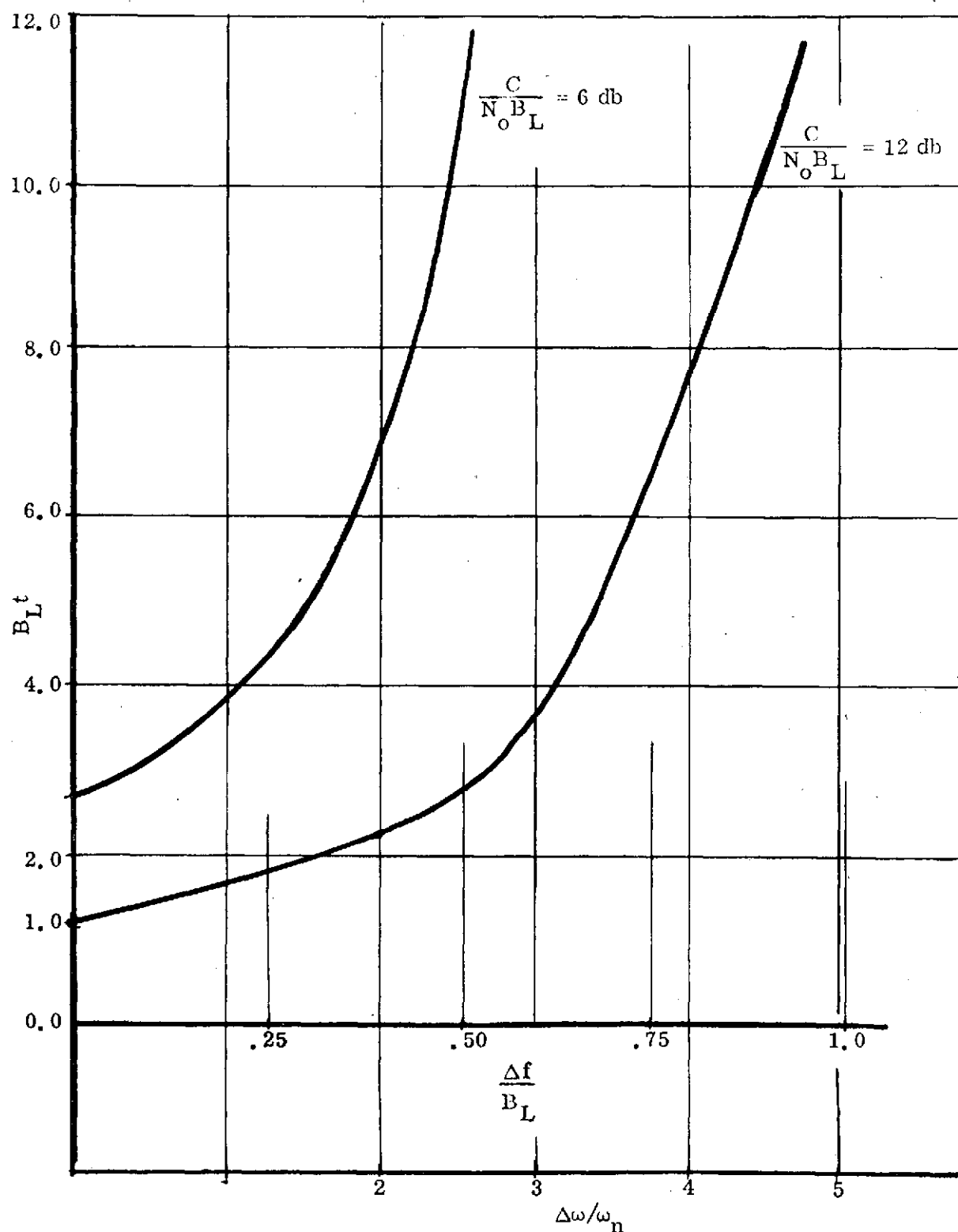


Figure 5-69. Acquisition Time as a Function of Frequency Offset for $P_{\text{acq}} = .9$ for Third Order Loops

existence of a frequency threshold, above which the acquisition time rapidly increases towards infinity. This threshold is approximately $\Delta f/B_L = .25$ for 6 dB and $\Delta f/B_L = .5$ for 12 dB. In the case of the second order loop, such a threshold is not quite as obvious. However, one seems to exist at approximately $\Delta f/B_L = .50$ for 6 dB and $\Delta f/B_L = .75$ for 12 dB. The acquisition time as a function of offset frequency is shown in Figure 5-69 where $P_{acq} = .9$ for the third order loop.

In general, the third order loop does not acquire as well as the second order loop. This is shown in Figure 5-70, where the acquisition probabilities for the two loops are compared.

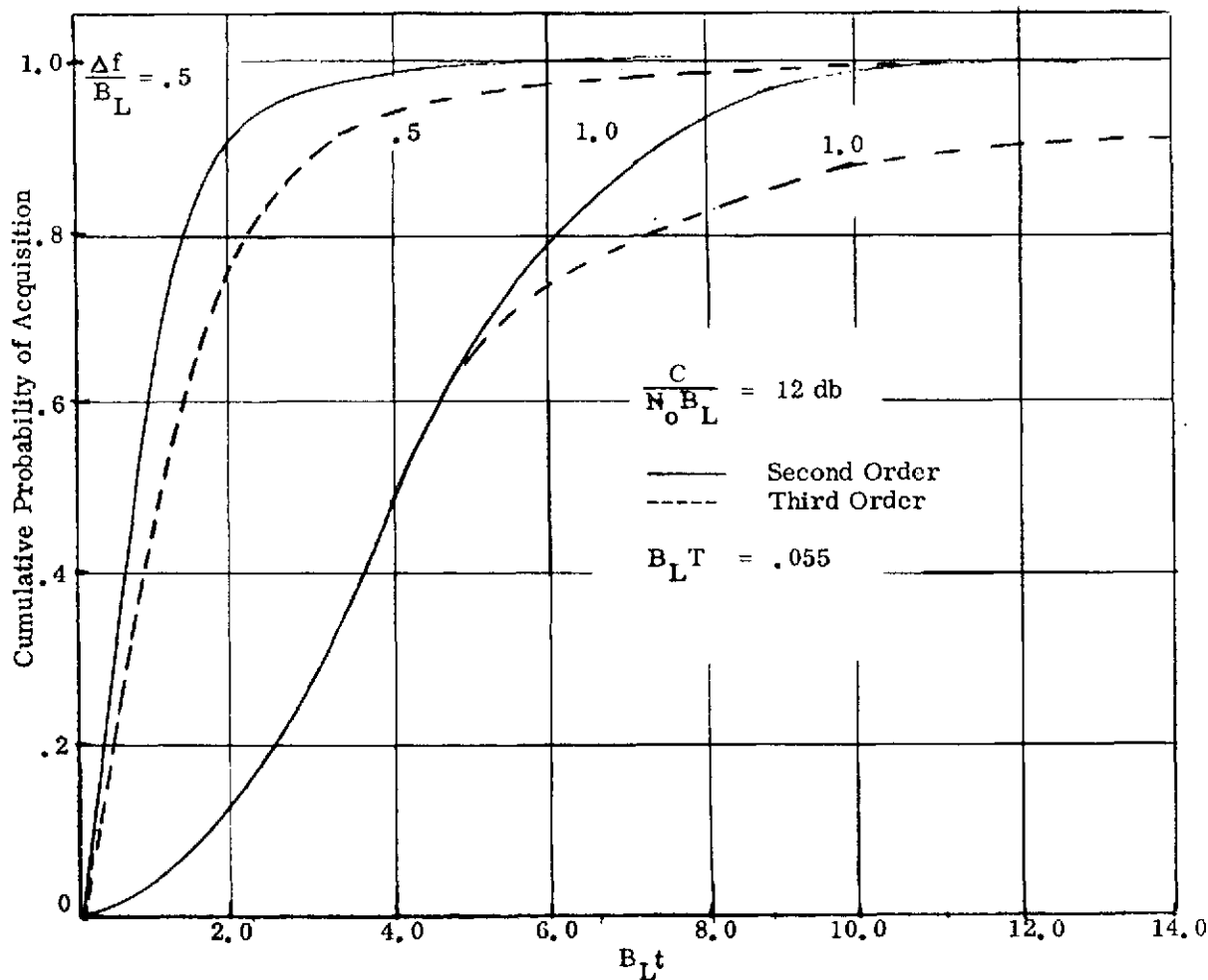


Figure 5-70. Comparison of Acquisition Performance of Second and Third Order Phase Locked Loops

It is of interest to determine whether an optimum bandwidth exists for acquisition for a given frequency offset and signal-to-noise density ratio. Intuitively, it would seem that optimization could be achieved, since to acquire a frequency offset in a minimum time, the loop noise bandwidth should be widened to include the offset within the loop bandwidth. However, as the loop is widened, the loop signal-to-noise ratio drops, thus degrading acquisition performance. Plots of acquisition probability as a function of loop noise bandwidth which are shown in Figures 5-71 and 5-72 show that an optimum bandwidth does exist. As might be expected, as the frequency offset is increased, the optimum bandwidth

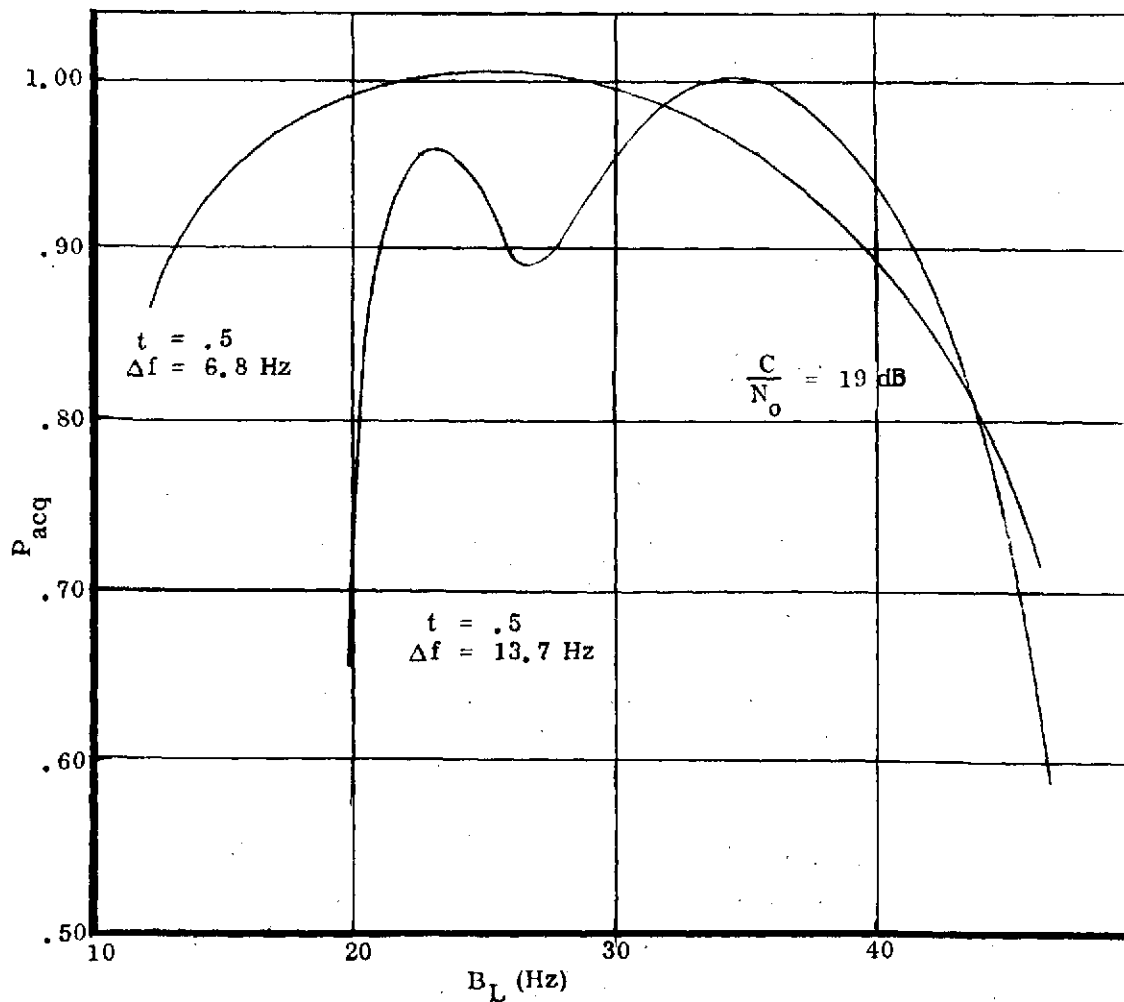


Figure 5-71. Probability of Acquisition Plotted Versus B_L to Illustrate Optimum Acquisition Bandwidth for Second Order Loop

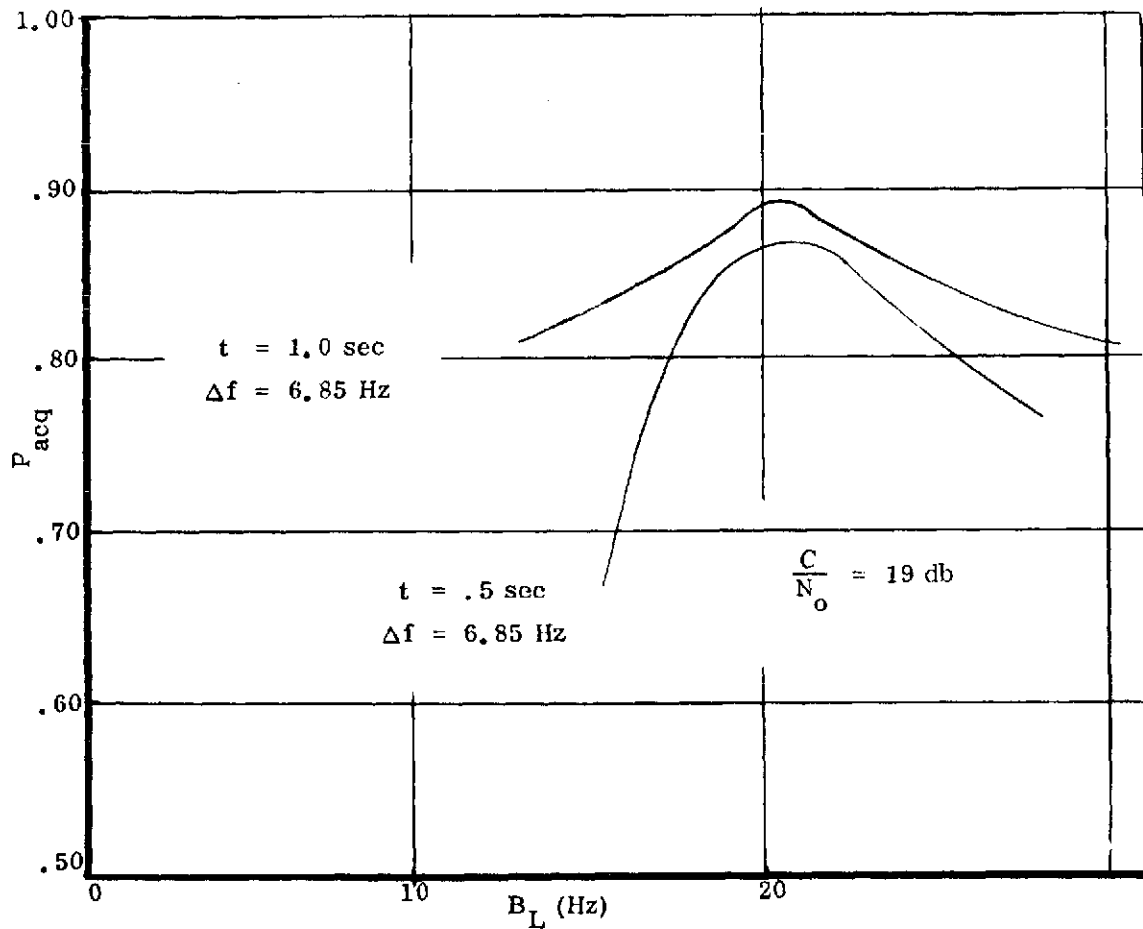


Figure 5-72. Probability of Acquisition Plotted Versus B_L to Illustrate Optimum Acquisition Bandwidth for Third Order Loop

Increases. This is shown in Figure 5-71. The dip in the curve for $\Delta f = 13.7 \text{ Hz}$ also occurred at $t = 1.0$ seconds and there seems to be no apparent explanation for it. It was thought that it might just be a statistical fluctuation but the random number generator was started at a different place on a repeat simulation and the phenomena repeated. When the simulations which resulted in the curves in Figure 5-72 for the third order loop were run for $\Delta f = 13.7 \text{ Hz}$, a curve having

several peaks and dips was obtained. Since no apparent meaningful information could be obtained from it, it is not shown. It should be noted that Figures 5-66 and 5-69 could be used to obtain an optimum bandwidth by varying $\Delta f/B_L$ and adjusting $C/N_o B_L$ accordingly and looking for a minimum acquisition time. However, due to the limited number of $C/N_o B_L$ cases, the optimization obtained in this manner would be somewhat more gross than that shown in Figures 5-71 and 5-72.

5.5.2.5 VCO Frequency Sweeping

Because of long pull-in time when the input frequency is outside the loop noise bandwidth, it is common to apply a sweep drive to the VCO to search for the input frequency. If designed properly, the loop will lock-up as the VCO frequency approaches the input frequency. The absolute maximum limit on the allowable sweep rate is $\Delta F < F_n^2$ [28]. Viterbi has investigated acquisition problems by means of phase-plane trajectories and discovered that acquisition is not certain, even if $\Delta F < F_n^2$ and the loop is noise free. When ΔF becomes larger than $F_n^2/2$, there is a possibility that the VCO can sweep past the input frequency without achieving lock.

Frazier and Page [29] have obtained an empirical equation which predicts the sweep rate that will provide 90% probability of acquisition. The results are

$$(\Delta F)_{\max} = \frac{[1 - (SNR)_L^{-1/2}] F_{no}^2}{1 + k} \quad (5-82)$$

where F_{no} is the loop natural frequency and k is a factor which depends upon loop damping ζ . Typically $\zeta = 0.707$ and therefore

$$k = \exp(-\zeta \pi / \sqrt{1 - \zeta^2}) \quad (5-83)$$

If $\zeta \geq 1$, then $k = 0$. In order to increase the probability of acquisition, one can either sweep at a lower than maximum rate or multiple sweeps can be made. Two overlapping sweeps increases the acquisition probability to 99%. The above

28. Gardner, Floyd M., "Phase Lock Techniques", John Wiley and Sons, Inc., April 1967.

29. J. P. Frazier and J. Page, "Phase Lock Loop Frequency Acquisition Study", Trans. IRE, SET-8, pp. 210-227, September 1962.

discussion applies to first and second order loops. Very little seems to be known about acquisition behavior of third order loops. There is a consensus of opinion that sweep acquisition with a closed loop for a third order loop is unstable. Various techniques to avoid such instability are (1) search for a signal with the loop open and then stop the sweep and close the loop when a signal is detected and (2) search for the signal using a second order loop and then switch the order of the loop filter when the signal is detected.

5.5.2.6 PN Code Resynchronization Time

During resynchronization, the PN code sequence is continuously data modulated by the MA satellite user. Data rates can vary anywhere from 1 kHz to 100 kHz. In order to maintain a constant data error probability at threshold for this wide range of data rates, increased power is transmitted for the higher data rates. At threshold for all data rates, there is an $E/N_o = 2$ dB per symbol. Rate 1/2 coding is assumed to be used. This means that for reacquisition, the duration of coherent integration ranges from 0.5×10^{-3} sec for a 1 kHz data rate to 0.5×10^{-5} sec for a 100 kHz data rate. Because E/N_o remains constant at 2 dB per symbol (increase in transmitted power at higher data rates), the search rate is fastest at the highest data rate. The worst case or slowest PN code search rate occurs at the 1 kHz data rate. Upon using the high bias sequential search acquisition strategy for post detection integration on one filter ($\Delta f = 0$), discussed in Appendix III, the search rate (SR) is

$SR = 0.053 \text{ chips/BIT}$ where BIT = duration of coherent integration. Coherent integration is limited to 0.5×10^{-3} sec, the symbol duration and hence, $SR = 106 \text{ chips/sec}$. Since $E_b/N_o = 2$ dB then $E/N_o = 14.8$ dB and therefore the probability of detection P_d in one pass is approximately 95%. For the chip uncertainty of 1300 chips, 1200 chips due to signal dynamics and 100 chips due to oscillator instability after 100 seconds, the search time per frequency bin (per search pass) is approximately 12.25 seconds. On a per pass basis the sequential detector only covers approximately 2 kHz of bandwidth. This is only approximately 20% of the total worst case frequency uncertainty of 9.3 kHz (assuming that the receiver can make an elementary decision as to the polarity of the doppler). Hence, at least 5 frequency bins must be searched which then require, in the worst case, 61.25 seconds for covering the entire time/frequency uncertainty. This is a very large percentage of the signal dropout time and realistically while the search is being conducted the size of the uncertainty is increasing at an ever increasing rate. Hence,

at most 10 frequency bins will be required to be searched resulting in approximately 122 seconds for a 95% probability of reacquisition after 100 seconds of signal dropout considering worst case signal dynamics at the lowest data rate at 1 kHz.

Upon considering the highest data rate at 100 kHz and worst case signal dynamics, the search time per frequency bin (1300 chip uncertainty) is only 0.125 seconds, a dramatic decrease in search time and a direct result of increased transmitted power. Only 5 passes are required to search the total frequency uncertainty resulting in a reacquisition time of less than 1 second for a 95% probability of success.

For a signal dropout time of only 50 seconds, there is approximately only 350 PN chips of uncertainty and 4.65 kHz of frequency uncertainty for worst case conditions. Therefore, for a 1 kHz data rate a frequency bin can be searched in only 3.3 seconds. Three frequency bins are required to search the entire frequency uncertainty hence requiring approximately 10 seconds for resynchronization at a 95% probability of success.

5.5.3 50 MBPS VITERBI DECODING

5.5.3.1 Introduction

The use of Viterbi decoding at Ku-band for the TDRSS, with rate 1/2 or rate 1/3 must consider the implementation complexity imposed by the high data rate requirement. The major impact upon complexity imposed by the data rate is on the decoder.

5.5.3.2 Decoder Implementation

The functional block diagram of the Viterbi decoder is given in Figure 5-73. Two critical areas for 50 Mbps operation exist. The first is the Metric Computations of which there are 128, 64 two-way comparisons and state decision selection which regenerates the 64-state metrics. This loop is shown in Figure 5-74 for a 3-bit soft-decision input and a 4-bit clamped metric which is adequate for the performance shown in Gaussian noise on Figure 5-75. The times in parentheses in Figure 5-74 indicate typical gate delays for the state of the art MECL3 implementation. The critical path timing is given by

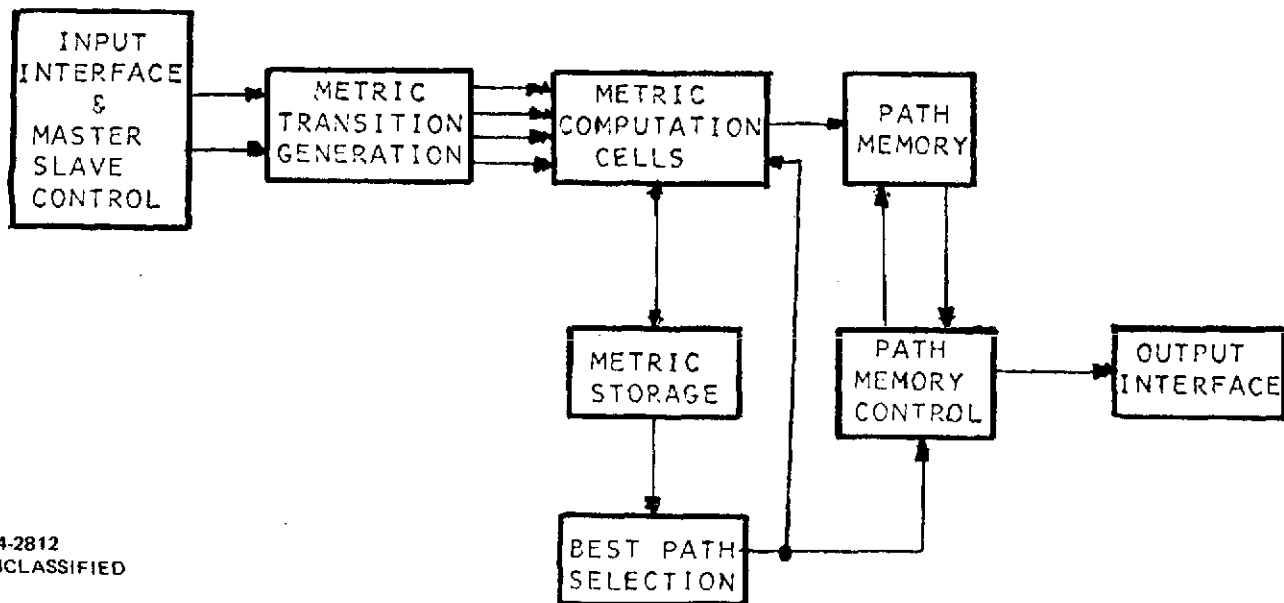


Figure 5-73. Functional Block Diagram of a Viterbi Decoder

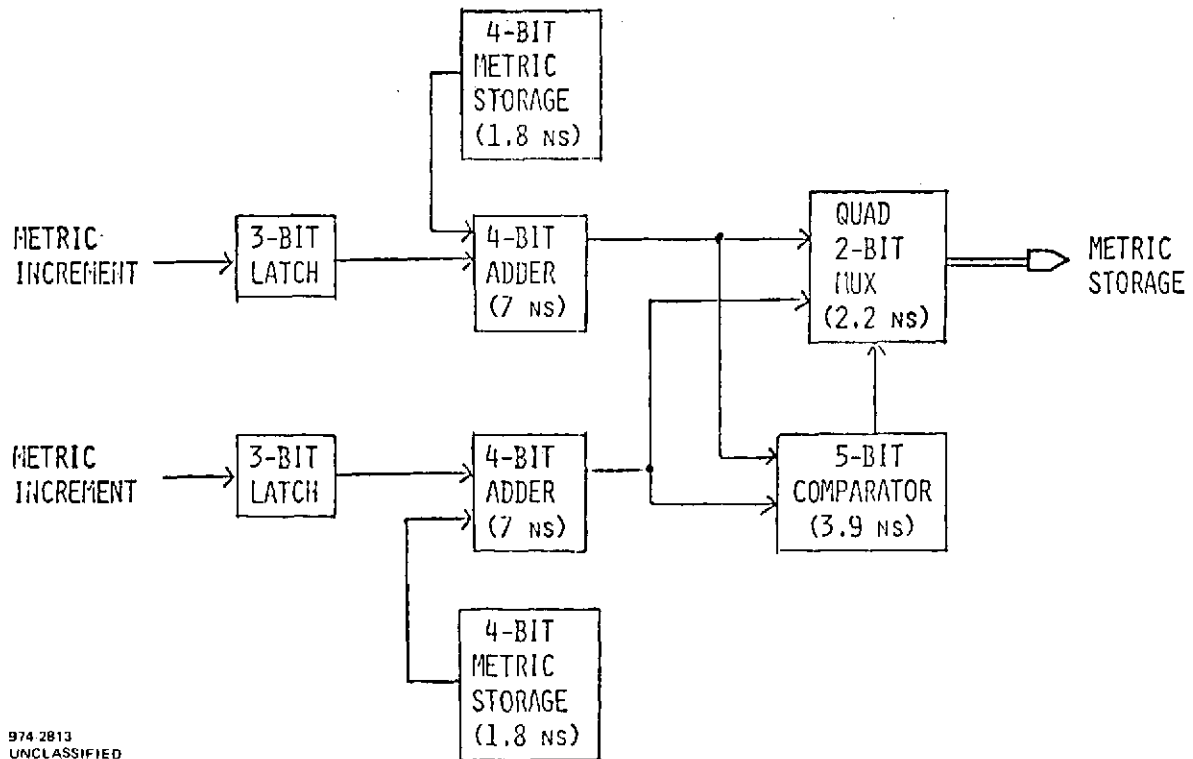


Figure 5-74. Critical Path (Typical) Viterbi Metric Computation

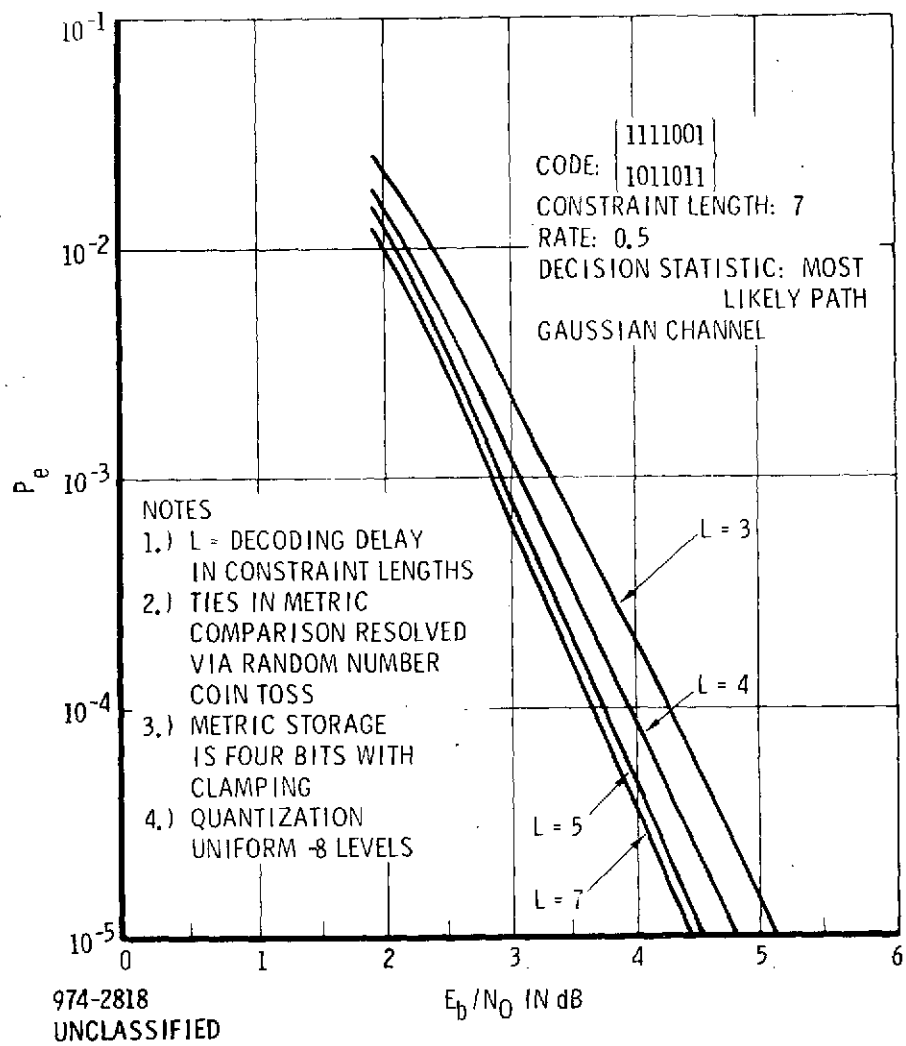


Figure 5-75. Soft Decision Maximum Likelihood Decoder Performance

4 Bit Adders	7.0 ns
5 Bit Comparators	3.9 ns
2 Bit MUX	2.2 ns
4 Bit Storage	1.8 ns
Cycle Time	14.9 ns

The worst-case cycle time is approximately 22 ns, which limits the data rate at 45 Mbps, assuming the various clock phases required to be generated precisely.

The complexity of the equipment cannot be reduced by taking advantage of identical computations performed on 64 state metrics at each information bit time because the initial loop timing does not allow time sharing of the equipment. An estimate of the ECL package count is 1200. The power dissipation can

be estimated at 600 watts not including power supply efficiency which may require a prime power of 1.2 kW.

In brief, direct implementation of the 50 Mbps system, while on the edge of the state of the art, is not recommended at this time. According to a private communication with Linkabit, Inc., development of custom ECL LSI logic would be required for this rate requirement.

An alternative approach exists which would provide the 50 Mbps rate. Rates of 10 Mbps are within today's state of the art and have been designed by Magnavox and Linkabit. The latter is under contract for delivery of 7 Mbps units to USASCA. These units can be connected very easily in a master/slave operation, as shown in Figure 5-76. This has the effect of decoding five independent, interleaved coded sequences. The only synchronization required is bit sync from the modem and the usual word sync of each of the decoders for bit pairs ($R = 1/2$) or triplets ($R = 1/3$). The state of the art for three-bit quantization is far superior to the requirements of the 150 Mbps ($R = 1/3$) A/D conversion.

The approximate size of a 10 Mbps Viterbi decoder is 8-3/4" x 19" rack mounted, including a power supply. If no LSI pieces are used, 400 dual in-line packages are required, comprising a mixture of MECL 10,000 and TTL technology. The dissipation is approximately 130 watts and, with power supply efficiency near 50%, approximately 250 watts are required.

5.5.3.3 The Encoder

The encoder can easily be implemented to encode the 50 Mbps source sequences. The inherent interleaving is accomplished as shown in Figure 5-77. The taps for an $R = 1/2$, $K = 7$ code are generated by

$$\begin{aligned}g_1(D) &= 1 + D + D^2 + D^3 + D^6 \\g_2(D) &= 1 + D^2 + D^3 + D^5 + D^6\end{aligned}\tag{5-84}$$

If we replace $g_i(D)$ by $g_i(D^5)$, the resulting encoder will perform interleaving of five code sequences. Operation of a shift register at 50 Mbps represents no difficulty. Delays through four gates (EOR's) do not generate timing difficulty.

5.5.3.4 Conclusion

If 50 Mbps coded data remain a requirement, we recommend implementation of a master/slave arrangement using five 10 Mbps decoders. The

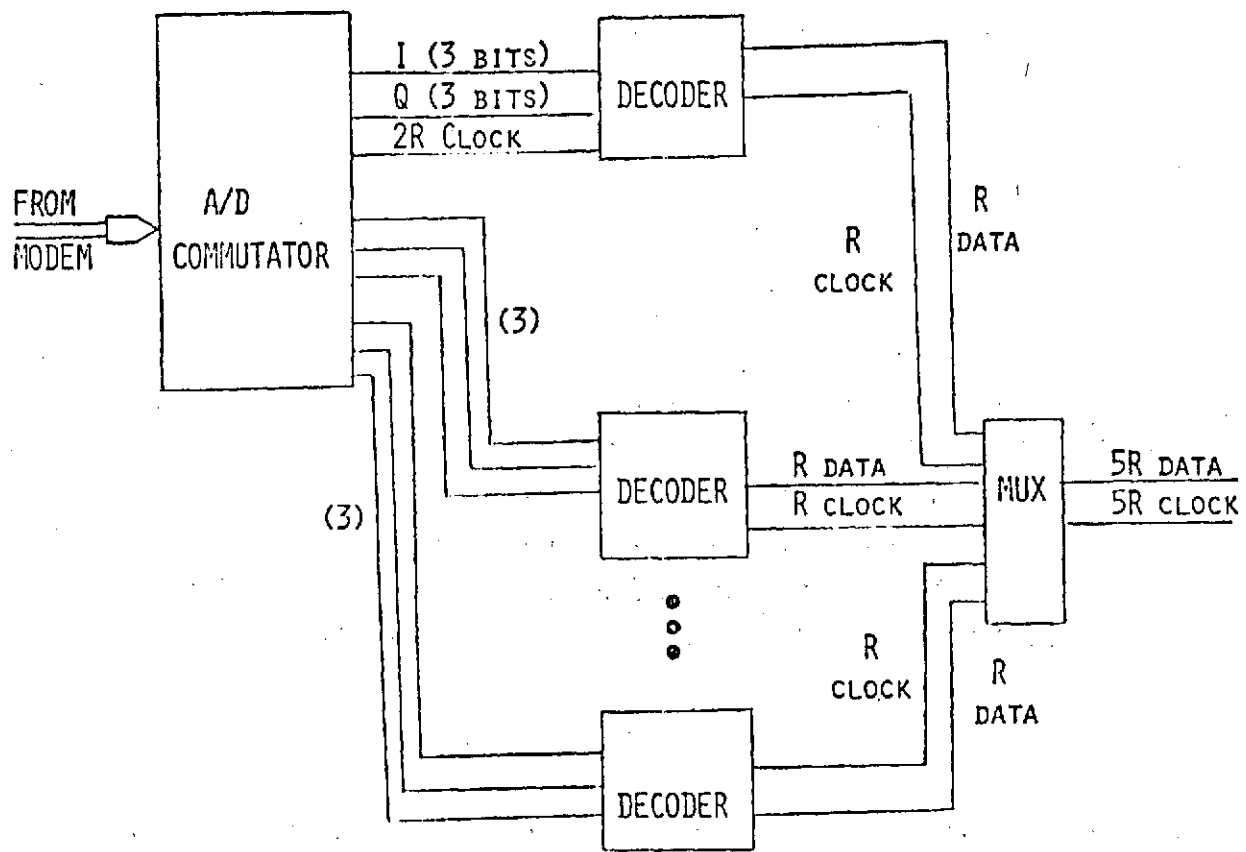


Figure 5-76. Parallel Decoder Operation

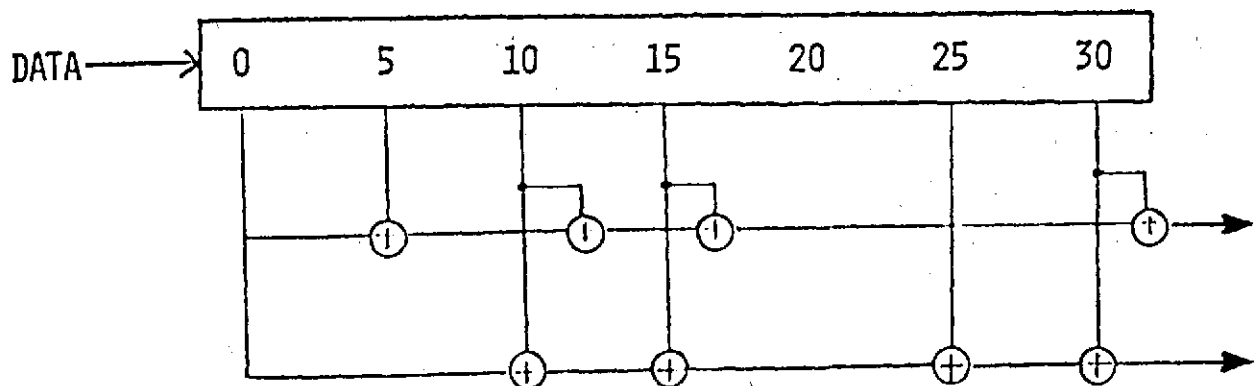


Figure 5-77. Encoder for Five Parallel Master/Slave Decoder –
 $R = 1/2$, $K = 7$

ground-based equipment (decoder) will consist of nearly a six-foot rack, including blowers, to accommodate the A/D, decommutator, decoders and multiplexer.

The major concern, however, remains the claim of the 5.2 or 5.7 dB gain ($R = 1/2$ and $R = 1/3$, respectively). These figures require independent errors in a basically white Gaussian additive noise environment. Section 4.1.2 discusses effects of hardlimiting in the TDRS channel.

5.5.4 QUADRIPHASE DEMODULATOR FOR 300 Mbps DATA RATE

This section indicates the feasibility of implementing the ground system demodulator for the Ku-band return link operating at 300 Mbps. QPSK or SQPSK modulation is utilized so that the symbol rate is 150 Mbps. The demodulator follows the conventional approach of obtaining a phase-locked reference carrier and using the reference to demodulate the in-phase and quadrature components, I and Q, of the incoming signal. The phase-locking technique is an extension of the Costas loop principle for BPSK, and derives a carrier tracking error ϵ by the function

$$\epsilon = I \operatorname{sign}(Q) - Q \operatorname{sign}(I) \quad (5-85)$$

where $\operatorname{sign}(x)$ denotes a hard limiter at baseband. This produces four stable tracking positions spaced by multiples of 90° , and the ambiguity must be resolved in the demodulator. (This ambiguity is inherent in all QPSK tracking schemes which are equivalent to frequency quadrupling, and a form of differential modulation can be employed as a solution.)

In one test configuration^[30] operating at 350 Mbps, use of a simple adaptive equalizer (transversal filter) is suggested to combat distortion due to multipath in the channel (which is in a line-of-sight microwave system). Figure 5-78 shows the block diagram of the system under test.

Test results are shown in Figure 5-79, showing the advantage realized from adaptive equalization and the relatively small degradation in E_b/N_o from

30. C. R. Ryan and J. H. Stilwell, "Performance of a 350 Mbps Adaptive Equalizer", IFT Journal, May/June 1974, Vol. 1, pp. 26-29.

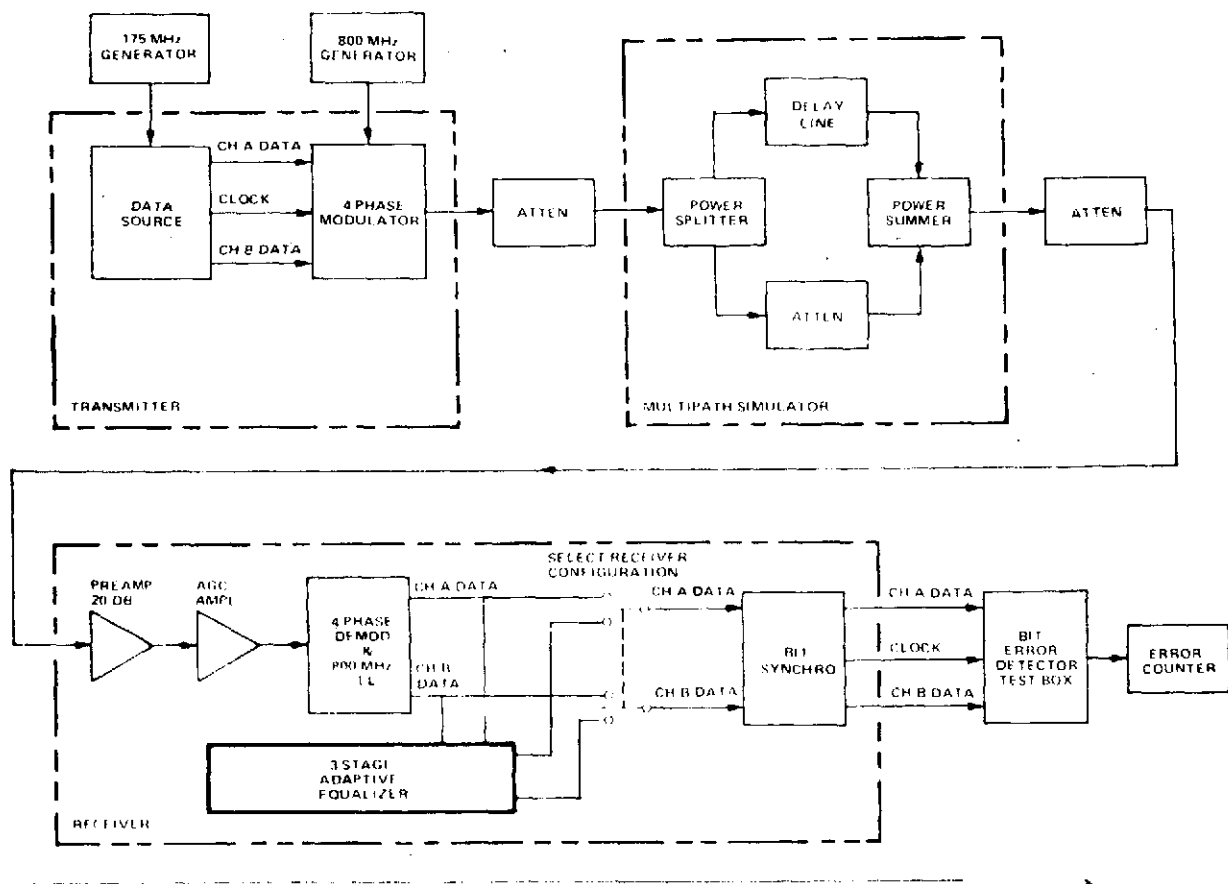


Figure 5-78. System Functional Diagram

REPRODUCIBILITY OF THE
ORIGINAL PAGE IS POOR

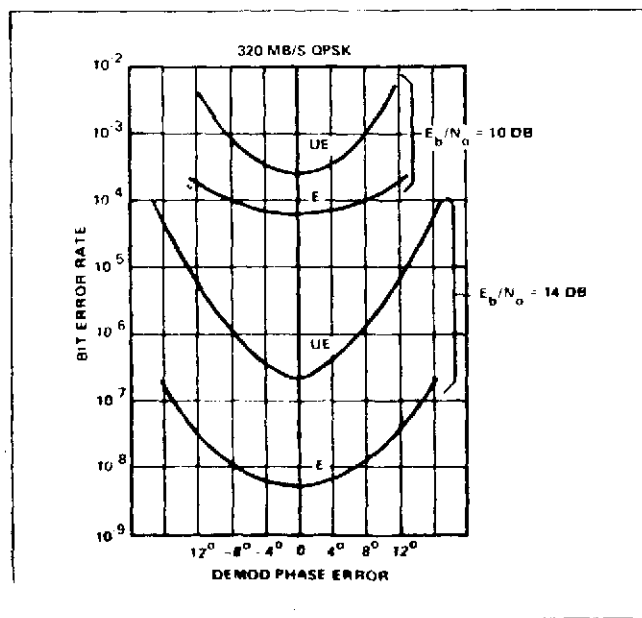


Figure 5-79. Effect of Demodulator Phase Error

theoretical (about 1 dB at $P_e = 10^{-5}$). The adaptive equalizer also appears to reduce the sensitivity to a phase error in reconstituting the phase reference for demodulation.

The implementation of the quadriphase modulator in the user spacecraft transmitter is straightforward, dependent mainly on availability of high speed circuits suitable for such an environment. Thus, the 300 Mbps data rate objective is considered to be within the state of the art.

APPENDIX I PN CORRELATION LOSS DUE TO CHANNEL DISPERSION

INTRODUCTION

Below, a computation is made of the effect of the dispersion of the channel transfer function on the correlation output and delay lock tracking position of a PN receiver. The PN signal is typically biphasic or quadriphase, with the latter being equivalent to the sum of two uncorrelated biphasic signals in phase quadrature. The bandpass channel is defined by either its frequency transfer function or its impulse response in the time domain. For simplicity, we simply use the notation, "bandpass filter".

COMPUTATION OF OUTPUT CORRELATION FUNCTION

The bandpass filter has a center frequency ω_c , which is the carrier frequency of the PN signal, and an equivalent low-pass transfer function $Y(j\omega)$ referred to this center frequency. For a general filter, we may write for possible convenience

$$Y(j\omega) = Y_1(j\omega) + jY_2(j\omega) \quad (1)$$

where the decomposition is used

$$Y_1(j\omega) = (Y(j\omega) + Y^*(-j\omega))/2 \quad (2)$$

$$Y_2(j\omega) = (Y(j\omega) - Y^*(-j\omega))/2j \quad (3)$$

Note that $Y_1(-j\omega) = Y_1^*(j\omega)$ and $Y_2(-j\omega) = -Y_2^*(j\omega)$. A filter which is (complex conjugate) symmetric about ω_c will have only the Y_1 portion.

The PN signal may be written

$$s(t) = \operatorname{Re} \left\{ a(t) e^{j\omega_c t} \right\} = \operatorname{Re} \left\{ e^{j\omega_c t} \frac{1}{2\pi} \int_{-\infty}^{\infty} A(j\omega) e^{j\omega t} d\omega \right\} \quad (4)$$

where $a(t)$ represents the PN modulation, and $A(j\omega)$ is the Fourier transform of the modulation. For a biphase signal, $a(t)$ is real, and we may write

$$s(t) \Big|_{2\omega} = \left\{ \frac{1}{2\pi} \int_{-\infty}^{\infty} A(j\omega) e^{j\omega t} d\omega \right\} \cos \omega_c t \quad (5)$$

After filtering by $Y(j\omega)$, we have

$$s_o(t) = \operatorname{Re} \left\{ e^{j\omega_c t} \frac{1}{2\pi} \int_{-\infty}^{\infty} A(j\omega) Y(j\omega) e^{j\omega t} d\omega \right\} \quad (6)$$

The reference function is $s(t)$ shifted in time and phase, or

$$\begin{aligned} s_r(t) &= \operatorname{Re} \left\{ a(t - \alpha) e^{j(\omega_c t - \alpha)} \right\} \\ &= \operatorname{Re} \left\{ e^{j(\omega_c t - \alpha)} \frac{1}{2\pi} \int_{-\infty}^{\infty} A(j\omega) e^{j\omega(t-\alpha)} d\omega \right\} \end{aligned} \quad (7)$$

Assume the received signal $s_o(t)$ is correlated with $s_r(t)$ in a product demodulator which yields product* of envelopes and difference of phases. Then, as a function of time error α and phase difference ω

$$R(\alpha, \omega) = \operatorname{Re} \int_{-\infty}^{\infty} dt \left[e^{j\omega} \frac{1}{2\pi} \left\{ \int_{-\infty}^{\infty} A(j\omega) Y(j\omega) e^{j\omega t} d\omega \right\} \left\{ \frac{1}{2\pi} \int_{-\infty}^{\infty} A^*(j\omega') e^{-j\omega'(t-\alpha)} d\omega' \right\} \right] \quad (8)$$

where (6) and (7) have been used. But, we have

*A physical product demodulator may not be linear in the reference amplitude, but this does not make any difference with a PN signal which has a constant envelope.

$$\frac{1}{2\pi} \int_{-\infty}^{\infty} e^{j(\omega' - \omega)t} dt = \delta(\omega' - \omega) \quad (9)$$

so that

$$R(\alpha, \omega) = \operatorname{Re} \left\{ \frac{1}{2\pi} \int_{-\infty}^{\infty} |A(j\omega)|^2 Y(j\omega) e^{j(\omega\alpha + \omega)} d\omega \right\} \quad (10)$$

is obtained as the general result. Computations can be carried out either in the frequency domain using the FFT or in the time domain using the impulse response corresponding to $Y(j\omega)$, which is the filter transfer function referred to the center frequency of the PN signal.

Since the power spectrum $|A(j\omega)|^2$ is the transform of the autocorrelation of the unfiltered signal, the correlation result can be interpreted as passing the autocorrelation through the filter $Y(j\omega)$, with the value obtained being a function of both phase ω and time shift α . These parameters are to be adjusted until the correlation result is maximized (or approximately maximized as with delay lock tracking). If $Y_2 = 0$, as in a symmetrical filter, the maximum occurs for $\omega = 0$.

If we wish to find the maximum correlation for any time error α as a function of phase ω , (10) shows that this maximum occurs when the real part is maximized. Hence, we may write

$$|R(\alpha)| = \left| \frac{1}{2\pi} \int_{-\infty}^{\infty} |A(j\omega)|^2 Y(j\omega) e^{j\omega\alpha} d\omega \right| \quad (11)$$

Alternatively, this may be written in terms of the real and imaginary parts of the integral, using Y_1 and Y_2 from time (2) and (3).

Equation (11) may also be interpreted in the time domain in terms of the filter's impulse response $h(t)$ and the unfiltered autocorrelation $R_o(\alpha)$. If, in addition, the carrier is offset by $\Delta\omega$ from the defined center frequency of the filter transfer function, we have

$$|R(\alpha)| = \left| \int_{-\infty}^{\infty} R_o(\beta) e^{j\Delta\omega(\alpha-\beta)} h(\alpha-\beta) d\beta \right| \quad (12)$$

Note that the impulse response is complex for an unsymmetrical filter transfer function. Equation (12) may be more convenient in some computations.

To interpret (11) and (12) in terms of the effect on AJ performance, $Y(j\omega)$ must be properly normalized. Four cases can be distinguished, depending on whether the received signal power is measured before or after the filter and whether the interference is introduced before or after the filter. Note that the power in the filtered signal is given by

$$P_{\text{Filtered}} = \frac{1}{2\pi} \int_{-\infty}^{\infty} |A(j\omega)|^2 |Y(j\omega)|^2 d\omega \quad (13)$$

If the interference is introduced before the filtering, it is appropriate to normalize gain so that

$$|Y(j\omega)|^2 |A(j\omega)|^2 \Big|_{\max \omega} = |A(0)|^2 \quad (14)$$

for AJ loss with worst case CW interference, and

$$\int_{-\infty}^{\infty} |Y(j\omega)|^2 |A(j\omega)|^2 d\omega = \int |A(j\omega)|^2 d\omega \quad (15)$$

for S/N loss with white noise interference.

If the signal is an ideal unfiltered PN waveform of unit power with chip duration T_c , the power spectrum (two-sided) is, for a nonrepetitive code,

$$|A(j\omega)|^2 = T_c \left| \frac{\sin(\omega T_c/2)}{\omega T_c/2} \right|^2 \quad (16)$$

SHARP CUTOFF, LINEAR PHASE FILTER

A simple example showing the effect of a restricted bandwidth has the signal centered in a sharp cutoff, linear phase filter of unity gain in the bandwidth W . The output correlation function is symmetrical in α , so that there is no delay lock tracking error. The correlation output amplitude is found from (11) to be

$$|R(0)| = \frac{T_c}{2\pi} \int_{-\pi W}^{\pi W} \left| \frac{\sin(\omega T_c/2)}{\omega T_c/2} \right|^2 d\omega$$

$$= \frac{2}{\pi} \text{Si}(\pi W T_c) - \frac{2}{\pi} \frac{\sin^2(\pi W T_c/2)}{\pi W T_c/2} \quad (17)$$

where $\text{Si}(x)$ is the sine integral function defined by

$$\text{Si}(x) = \int_0^x \frac{\sin x}{x} dx \quad (18)$$

Figure 1 plots the loss for this case, expressed in decibels for the normalization of (14) to give the AJ loss. Also plotted is the S/N loss for white noise, using the normalization (15).

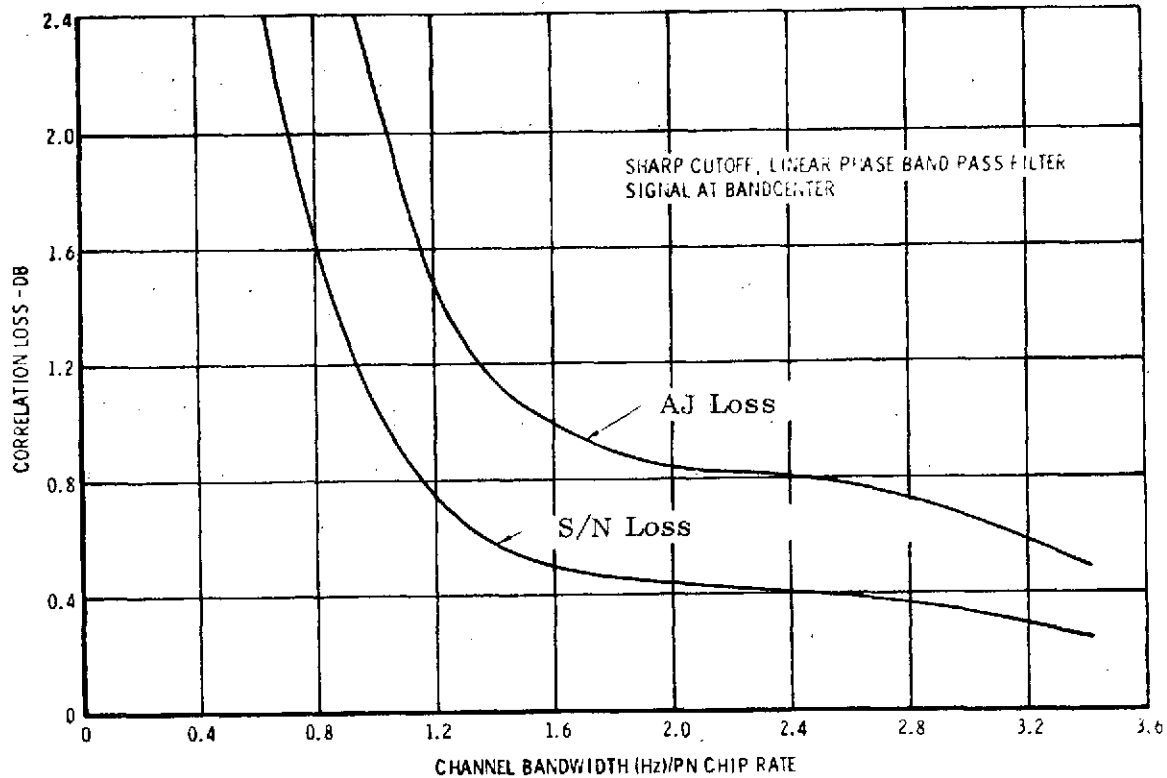


Figure 1. Correlation Loss Due to Filtering

A similar computation has been carried out for staggered quadriphase PN that has been filtered and hard limited in the transmitter. The results for a sharp cutoff receiver filter are plotted in Figure 2.

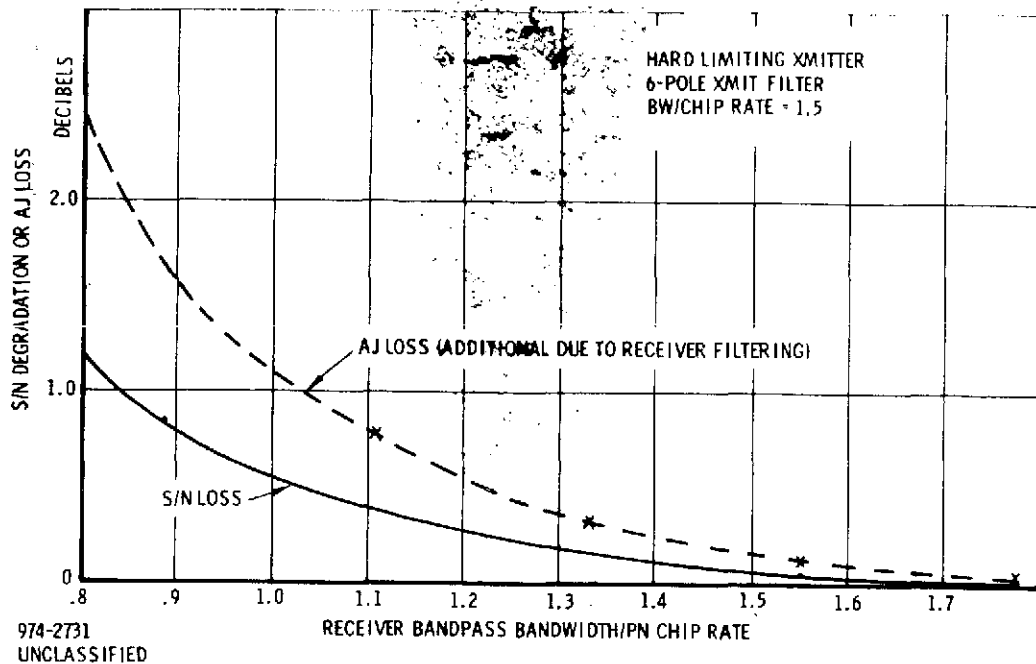


Figure 2. Correlation Loss for SQPN with Sharp Cutoff Receive Filter

PARABOLIC PHASE DISTORTION WITH SHARP BANDWIDTH CUTOFF

Suppose that the phase shift of the transmission filter is expressed in a power series referred to the center frequency of the PN spectrum:

$$\theta(\omega) = \theta(\omega_c) + \left. \frac{d\theta}{d\omega} \right|_{\omega_c} (\omega - \omega_c) + \frac{1}{2} \left. \frac{d^2\theta}{d\omega^2} \right|_{\omega_c} (\omega - \omega_c)^2 + \dots \quad (19)$$

The first term of the expansion is a fixed carrier phase shift which does not affect the correlation amplitude. The second term represents a fixed delay which the correlation receiver tracks. Hence, the parabolic term is the first actual distortion term; thus,

$$\theta_d(\omega) = D\omega^2 \quad (20)$$

where ω is now the offset from the center frequency ω_c .

W is

$$|R(0)| = \left| \frac{T_c}{2\pi} \int_{-\pi W}^{\pi W} \left[\frac{\sin(\omega T_c/2)}{\omega T_c/2} \right]^2 e^{jD\omega^2} d\omega \right| \quad (21)$$

where the peak correlation occurs at $\alpha = 0$. Equation (21) is numerically evaluated in Figure 3 for AJ loss. (Step size $\delta\omega = 2\pi/100T_c$.) (The dB separation between AJ loss and S/N loss is identical to that of Figure 1.) Note that the loss can increase as the bandwidth becomes wider due to phase cancellation when the distortion is present.

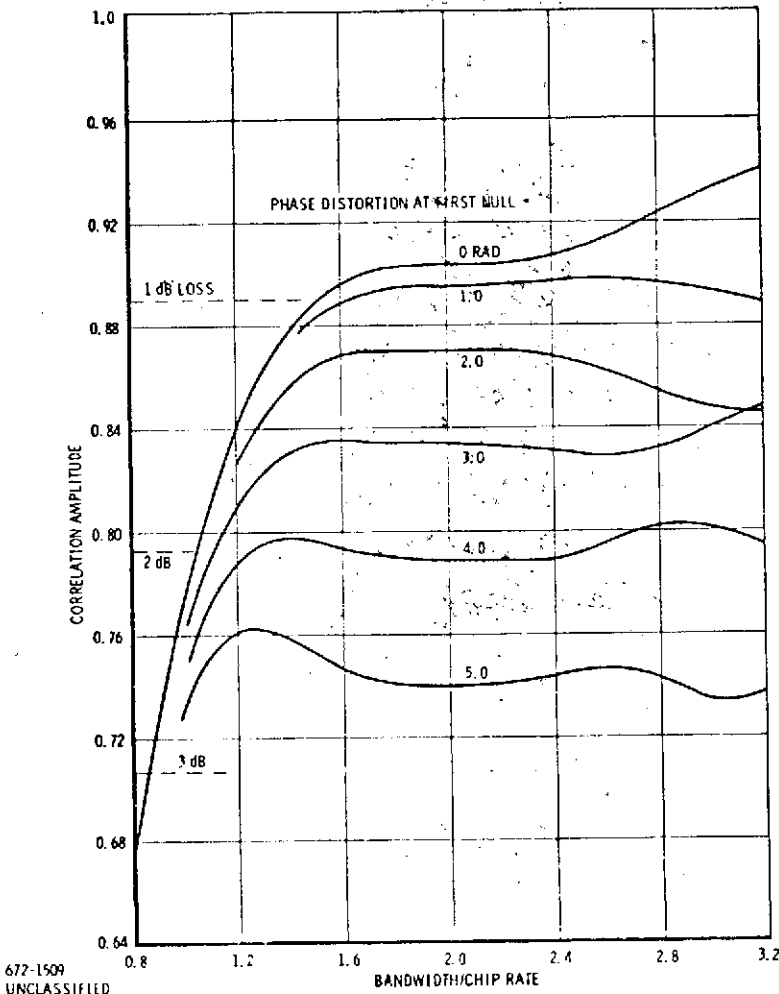


Figure 3. AJ Loss Due to Parabolic Phase Distortion and Finite Bandwidth

For normalization in Figure 3, the phase distortion at the first null is used to label the curves. That is

$$\theta_d(2\pi/T) = 4\pi^2 D/T_c^2 = \text{Phase Distortion at First Null in Radians.} \quad (22)$$

Note from Figure 3 that the degradation starts to become significant when this distortion parameter exceeds roughly one radian. An alternative measure is the time delay distortion $\Delta\tau$ over the null-to-null bandwidth. Now,

$$\begin{aligned} \Delta\tau &= 2D(2\pi\Delta f) \\ \Delta f &= 2/T_c \end{aligned} \quad (23)$$

hence

$$\Delta\tau/T_c = \frac{2}{\pi} (4\pi^2 D/T_c^2) \quad (24)$$

Thus, the degradation starts to become significant when the time delay distortion exceeds the code bit duration.

Let us now look at the shape of the correlation output as a function of α . We are interested in the magnitude as defined by (11), which becomes

$$|R(\alpha)| = \frac{T_c}{2\pi} \left| \int_{-\pi W}^{\pi W} \left[\frac{\sin(\omega T_c/2)}{\omega T_c/2} \right]^2 e^{j(D\omega^2 + \omega\alpha)} d\omega \right| \quad (25)$$

This is symmetrical in α so that there is no delay lock tracking error. We can evaluate $R(\alpha)$ approximately as a finite summation with the step size $\delta\omega$; thus,

$$R(\alpha) \approx \frac{T_c \delta\omega}{2\pi} \sum_{-KWT_c/2}^{KWT_c/2} \left[\frac{\sin k \delta\omega T_c/2}{k \delta\omega T_c/2} \right]^2 e^{j[D(k \delta\omega)^2 + k \delta\omega\alpha]} \quad (26)$$

where we define the number of points in a bandwidth equal to the code rate as

$$K = 2\pi/T_c \delta\omega \quad (27)$$

Since (26) is a Fourier series, we can compute the values at the discrete points $\alpha = m\delta t$ by using the Fast Fourier Transform algorithm. With an N -point algorithm,

we have the relation

$$\delta t \delta \omega = 2\pi/N \quad (28)$$

Suppose that M values of α are to be computed in the range $0 \leq \alpha \leq T_c$. Then, $\delta t = T_c/M$, and (27) and (28) yield

$$N = KM \quad (29)$$

as the required number of points in the FFT.

The FFT computation is performed by transforming the points

$$A_k = \frac{1}{K} \left[\frac{\sin k\pi/K}{k\pi/K} \right]^2 e^{jD(2\pi/KT_c)^2 k^2}; \quad 0 \leq k \leq KWT_c/2$$

$$A_k = 0; \quad KWT_c/2 \leq k \leq N - KWT_c/2$$

$$A_k = A_{N-k}; \quad N - KWT_c/2 \leq k \leq N \quad (30)$$

Figure 4 is an evaluation of the FFT of (30), with the magnitude $R(\alpha)$ being plotted for the parameters

$$M = 16$$

$$K = 256$$

$$WT_c = 2$$

The correlation function is observed to be considerably broadened by excessive phase distortion.

IONOSPHERIC PHASE DISPERSION

For propagation through a uniform ionosphere, the phase constant k may be written as^(1, 2)

$$\beta = (\omega^2 - \omega_p^2)^{0.5} / c \quad (31)$$

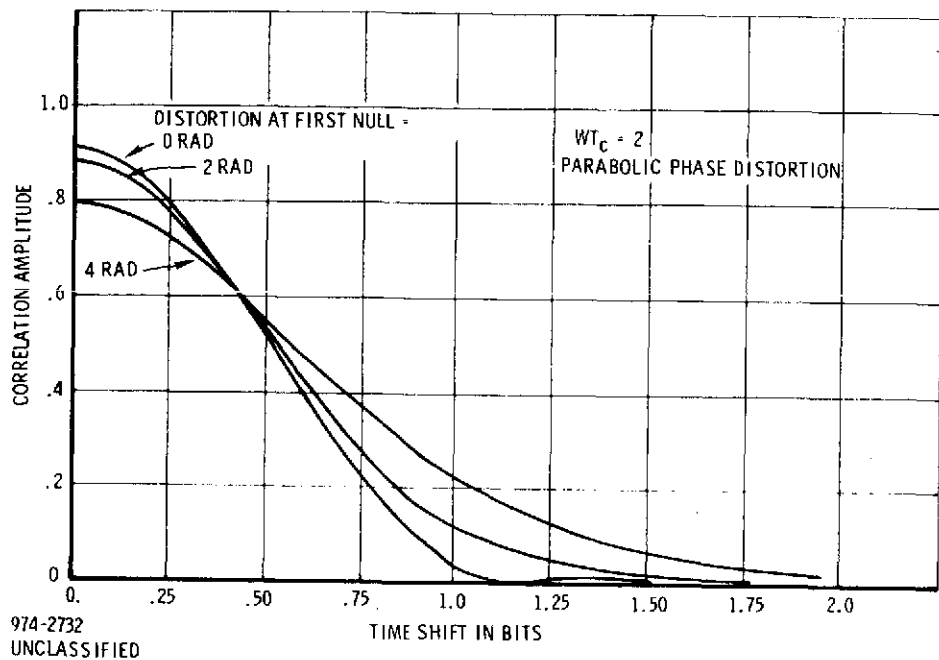


Figure 4. Magnitude of Correlation Output

where

$$\omega_p^2 = \frac{Nq^2}{\epsilon_0 m} = 324\pi^2 N \quad (32)$$

and

- c = velocity of light in free space, m/sec
- ω = $2\pi f$, radian frequency, rad/sec
- N = free electron density, number/m³
- q = electron charge, coulombs
- m = electron mass, kg
- ϵ_0 = dielectric constant of free space

Equation (31) can also be written as

$$\beta = \frac{2\pi f}{c} (1 - 81N/f)^{0.5} \approx \frac{2\pi f}{c} - \frac{81\pi N}{cf} \quad (33)$$

For propagation through a distance r , the total phase shift is $\theta = \beta r$.

Let us expand (31) in a power series about a center frequency ω_c according to (19). We have,

$$\begin{aligned} \beta(\omega_c) &= (\omega_c^2 - \omega_p^2)^{-0.5} / c \\ \left. \frac{d\beta}{d\omega} \right|_{\omega_c} &= \omega_c (\omega_c^2 - \omega_p^2)^{-1.5} / c \\ \left. \frac{d^2\beta}{d\omega^2} \right|_{\omega_c} &= -\omega_p^2 (\omega_c^2 - \omega_p^2)^{-2.5} / c \end{aligned} \quad (34)$$

Since a constant phase shift and a constant time delay (linear phase shift with frequency) do not produce distortion, we write the phase distortion as

$$\begin{aligned} \theta_d &= r[\beta - \beta(\omega_c) - \left. \frac{d\beta}{d\omega} \right|_{\omega_c} (\omega - \omega_c)] \\ &= \frac{r}{c} [(\omega^2 - \omega_p^2)^{0.5} - (\omega_c^2 - \omega_p^2)^{0.5} - \frac{\omega_c}{(\omega_c^2 - \omega_p^2)} (\omega - \omega_c)] \end{aligned} \quad (35)$$

As an approximation

$$\theta_d \approx -\frac{\frac{r\omega_p^2}{c} \frac{(\omega - \omega_c)^2}{1.5}}{2c(\omega_c^2 - \omega_p^2)} \approx -\frac{\frac{r\omega_p^2}{c}}{2c\omega_c^3} (\omega - \omega_c)^2 \quad (36)$$

where (36) retains the dominant parabolic distortion term. Figure 5 compares the parabolic approximation of (36) with the exact expression of (35) for the parameters

$$f_c = 2 \text{ GHz}$$

$$f_p = 120 \text{ MHz}$$

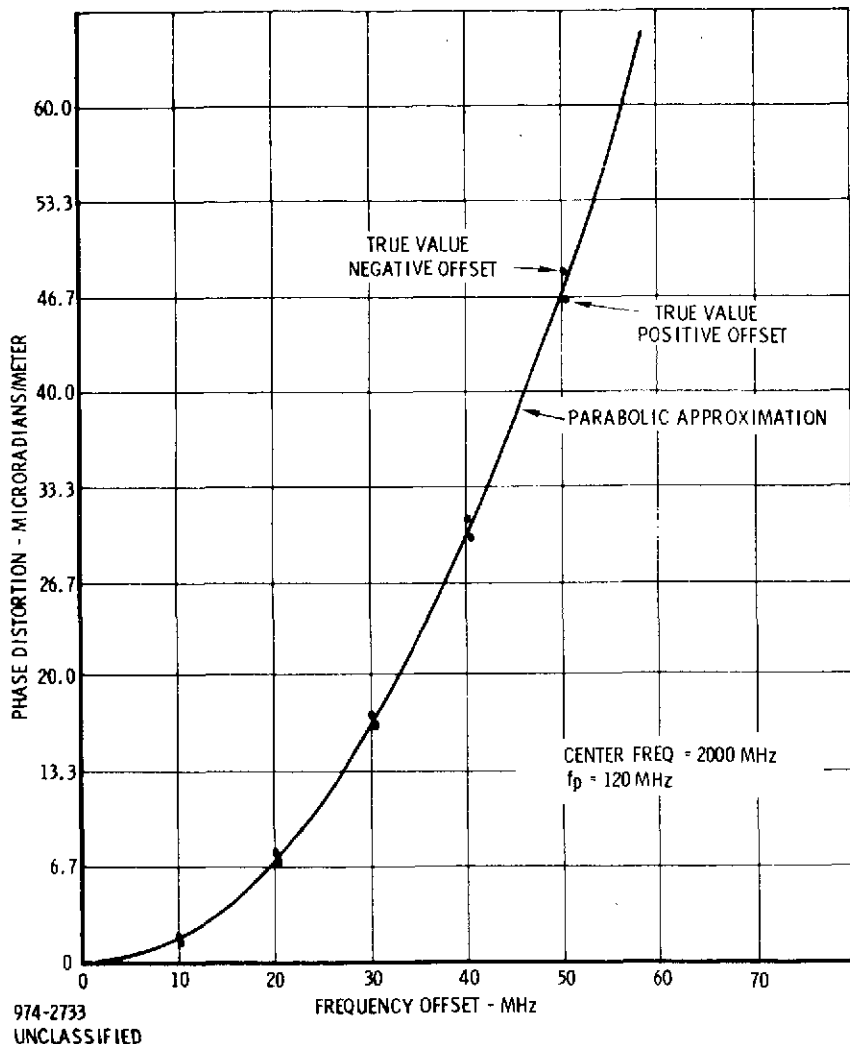


Figure 5. Comparison of Parabolic Approximation to True Ionospheric Phase Dispersion

It may be noted⁽³⁾ that a worst case value of N_r is roughly 2×10^{18} electrons/m²; hence, assuming $r = 10^5 \text{ m}$ yields $N = 2 \times 10^{13}$ electrons/m³ and $f_p = 40 \text{ MHz}$ for this worst case. From Figure (2), it was concluded that the maximum allowed phase distortion is approximately 2 radians at an offset equal to the PN chip rate T_c^{-1} . Hence, (36) yields the condition

$$T_c^{-1} < 13820 f_c^{1.5} / r^{0.5} f_p \quad (37)$$

For $f_c = 2000$ MHz and $r = 10^5$ m, we obtain Table I from Equation (31).

f_p	Max PN Rate
0 MHz	∞ Mbps
20	195
40	98
60	65
80	49
100	39
120	33

← Worst Case Ionosphere

Table I. Maximum PN Chip Rate for $r = 10^5$ meter and $f_c = 2000$ MHz.
Allowed Phase Distortion = 2 Radians at First Null

ANTISYMMETRICAL PHASE DISCONTINUITY

Let us now consider the case of phase distortion consisting of a discontinuity at the band center; i.e.,

$$\begin{aligned} \theta(\omega) &= +\theta; \quad \omega > 0 \\ &= -\theta; \quad \omega < 0 \end{aligned} \quad (38)$$

where ω is referenced to the center frequency. Then, (11) becomes (for T_c normalized to unity)

$$\begin{aligned} |R(\alpha)| &= \left| \frac{1}{\pi} \int_0^\infty |A(j\omega)|^2 \cos(\theta + \omega\alpha) d\omega \right| \\ &= \left| \frac{\cos \theta}{\pi} \int_0^\infty |A(j\omega)|^2 \cos \omega\alpha d\omega - \frac{\sin \theta}{\pi} \int_0^\infty |A(j\omega)|^2 \sin \omega\alpha d\omega \right| \\ &= \left| \cos \theta R_o(\alpha) + \sin \theta R_o^{(Q)}(\alpha) \right| \end{aligned} \quad (39)$$

where $R_o(\alpha)$ is the unfiltered autocorrelation and $R_o^{(Q)}(\alpha)$ is the quadrature or Hilbert transform, defined by

$$R_o^{(Q)}(\alpha) = -\frac{1}{\pi} \int_0^\infty |A(j\omega)|^2 \sin \omega \alpha d\omega \quad (40)$$

For a PN waveform with spectrum given by (16), the quadrature function may be evaluated, and is plotted in Figure 6. It should be remembered that the quadrature function is antisymmetric; hence, $R(\alpha)$ is no longer symmetrical in α .

For θ small, the peak of $R(\alpha)$ occurs at $\alpha = 0$, and the loss of correlation at the peak is given by $\cos \theta$. Thus, there is 1 dB loss at $\theta = .47$ radian for a PN receiver which tracks the correlation peak. However, a delay lock receiver will track to the null position α_o defined by

$$|R(\alpha_o + .5)| = |R(\alpha_o - .5)| \quad (41)$$

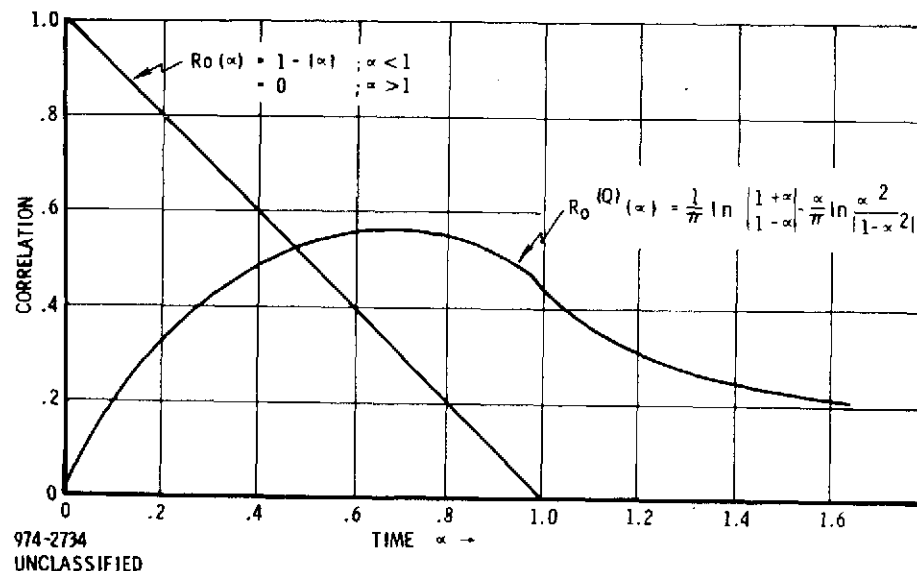


Figure 6. Quadrature Function for PN

and the correlation loss will be greater and due primarily to the displacement of the tracking null position. For θ small, the displacement is approximately

$$\alpha_o \approx -0.53\theta ; |\theta| \ll 1 \text{ rad.} \quad (42)$$

and the resulting correlation amplitude is approximately

$$|R(\alpha_o)| \approx 1 - 0.53|\theta| ; |\theta| \ll 1 \text{ rad.} \quad (43)$$

A loss of 1 dB results at $\theta = .2$ radian, by (43), and (42) shows the displacement of the tracking null due to the phase distortion to be about 0.1 chip.

SINUSOIDAL PHASE RIPPLE

To further study the effects of phase distortion, we consider the case of a sinusoidal phase ripple without amplitude distortion, so that

$$Y(j\omega) = e^{j\theta} \sin \omega \gamma \quad (44)$$

where θ is the peak phase distortion. It is seen that the transfer function is (complex) symmetric. It is easily shown [4] that (10) yields

$$R(\alpha, 0) = \sum_{k=-\infty}^{\infty} J_k(\theta) R_o(\alpha - \gamma k) \quad (45)$$

where $R_o(\alpha)$ is the unfiltered autocorrelation.

As one case, let there be one cycle of the sinusoidal phase distortion in the null-to-null bandwidth of the PN signal. Then

$$R_o(\alpha) = 1 - |\alpha|, |\alpha| < 1$$

$$\gamma = 0.5 \quad (46)$$

Note that the echoes are antisymmetric for k odd and symmetric for k even. They are small for larger k .

In the range $0 < \alpha < 1$, we have

$$\begin{aligned}
 R(\alpha, 0) = & +J_1(\theta) R_0(\alpha + 0.5) + J_0(\theta) R_0(\alpha) \\
 & - J_1(\theta) R_0(\alpha - 0.5) + J_2(\theta) R_0(\alpha - 1.0) \\
 & - J_3(\theta) R_0(\alpha - 1.5) \tag{47}
 \end{aligned}$$

where $R_0(\alpha)$ is given in (46). Equation (47) is plotted for both positive and negative values of time error α in Figure 7 for the three values of θ . It is seen that the loss for tracking at the correlation peak is about 1.0 dB for $\theta = 1.0$ radian, 0.5 dB for $\theta = 0.5$ radian and 0.1 dB for $\theta = 0.25$ radian.

With delay lock tracking, the null position is defined by (41), and a displacement of the null is evident from Figure 6, since $|R(\alpha)|$ is not symmetrical in α . For $\theta = .25$ radian, the displacement is about 0.1 chip, and the correlation amplitude is 0.9, causing 1 dB loss.

For a phase distortion consisting of several ripples, we can assume simply that γ is large, in which case the echoes move far away and no longer overlap the central peak. Then, the peak correlation occurs at $\alpha = 0$, and is

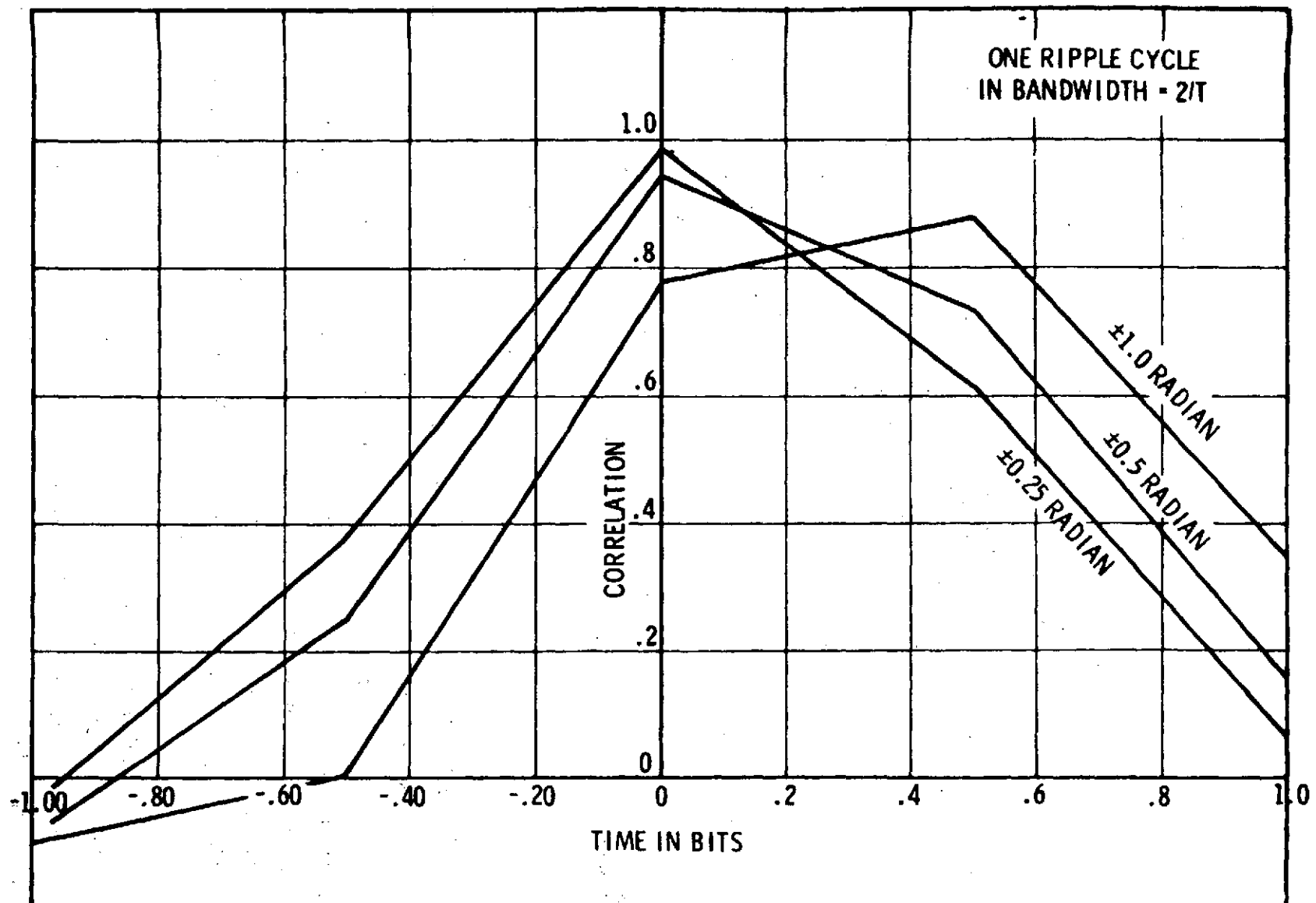
$$R(0, 0) = J_0(\theta) R_0(0) = J_0(\theta) \tag{48}$$

Furthermore, there is no displacement of the null tracking position for delay lock. Hence, the loss is 2.3 dB for $\theta = 1.0$ radian, 0.5 dB for $\theta = 0.5$, and 0.1 dB for $\theta = 0.25$. It is seen that with delay lock tracking, a fine phase distortion ripple produces less loss than a coarse ripple of the same peak excursion.

Figure 8 shows the correlation function in the vicinity of the peak for several values of θ when there are many cycles of the sinusoidal phase distortion over the null-to-null bandwidth of the PN signal.

The correlation loss due to a small displacement of the delay lock tracking null is less with filtered staggered quadriphase PN than with unfiltered PN. To see why, examine Figure 9, which plots the autocorrelation function of such a SQPN waveform*. There is less droop in the vicinity of the peak; for example, a tracking error of 0.1 chip now causes a loss of 0.2 dB, rather than 0.9 dB for the unfiltered PN.

*The autocorrelation is obtained by taking the Fourier transform (by an FFT algorithm) of the spectrum.



670-1349
UNCLASSIFIED

Figure 7. Correlation Function for Sinusoidal Phase Distortion

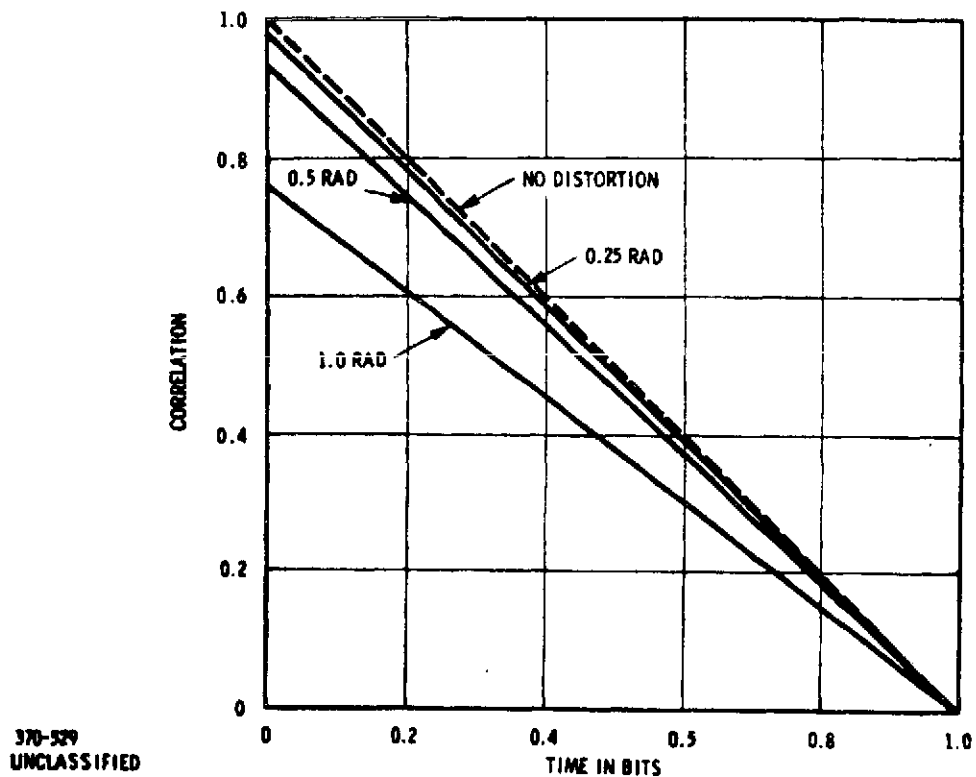


Figure 8. Sinusoidal Ripple (Several Cycles)

370-529
UNCLASSIFIED

CONCLUSIONS

The effects of channel distortion on correlation output from a PN receiver has been studied by a series of examples. As a general specification, the channel bandpass should be at least 1.5 times the PN chip rate, and the S/N loss is negligible for a staggered quadriphase PN waveform. The phase distortion (deviation from linearity) within this bandpass should not exceed ± 0.2 radian ($\pm 11^\circ$), at least for the coarse variation of distortion with frequency. Fine structure of phase distortion could have a peak variation up to ± 0.5 radian ($\pm 29^\circ$).

Considering the parabolic phase distortion caused by the ionosphere, it is found that the maximum integrated electron density still would allow a PN chip rate of 100 Mbps at S-band. The effect of the ionosphere in a 10 MHz bandwidth at S-band is negligible.

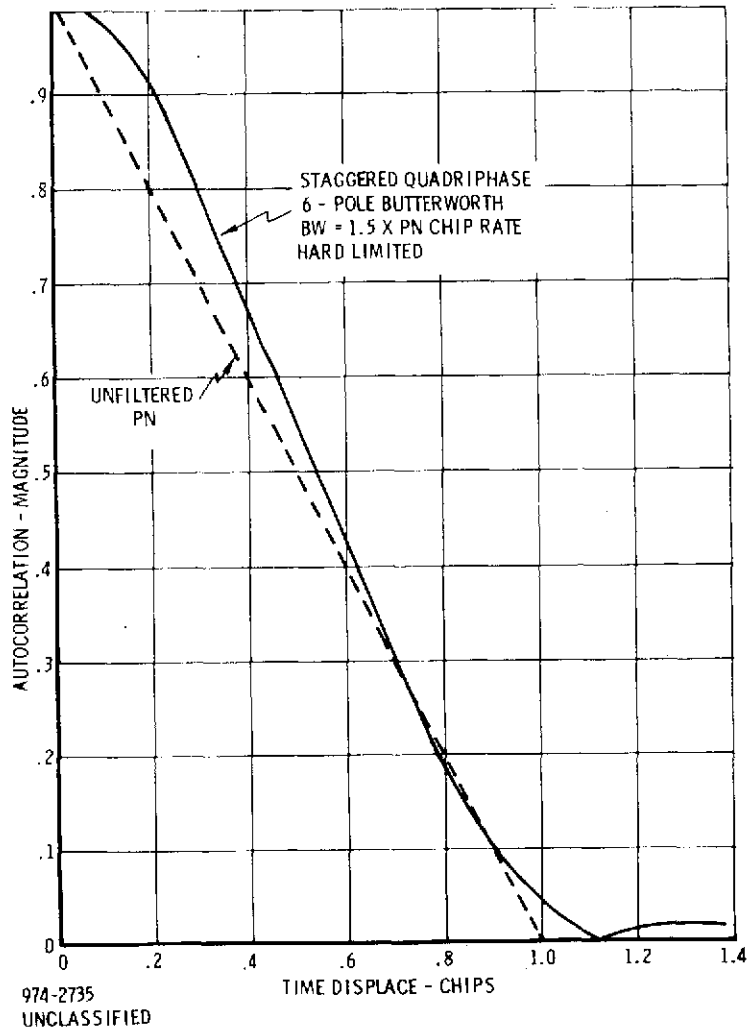


Figure 9. Autocorrelation of PN and SQPN

REFERENCES

1. Jordan, E. C., "Electromagnetic Waves and Radiating Systems", Prentice Hall, 1950, p. 664.
2. Staras, H., "The Propagation of Wideband Signals through the Ionosphere", IRE Proceedings, Volume 49, July 1961, p. 1211.
3. Hughes Aircraft Company, "System 621B - Satellite System for Precise Navigation (U)", Final Report (Part 2) SAMSO TR69-4, January 1969, Appendix III.
4. S. Goldman, Frequency Analysis, Modulation and Noise, McGraw-Hill, 1948, pp. 102-108.

APPENDIX II
CODE PHASE TRACKING WITH COHERENT FREQUENCY HOPPING

To study the behavior of the tracking loop controlling pseudorandom code phase in a coherent frequency hopping system, we assume a large number of channels and sufficient averaging that self noise is negligible. The general approach for tracking with any signal waveform is that of delay-lock, which implies the process of correlation with the derivative (or a finite-difference approximation) of the waveform.

For a uniform distribution of frequencies randomly selected over a bandwidth B (where zero frequency denotes the band center) the average correlation voltage is

$$a(\tau) = \frac{1}{2\pi B} \int_{-\pi B}^{\pi B} \langle \cos \omega(t + \tau) \cos \omega \rangle d\omega \quad (1)$$

where the brackets denote time averaging and τ is the tracking error. Performing the integration yields

$$a(\tau) = \frac{\sin(\pi B\tau)}{\pi B\tau} \quad (2)$$

The average error voltage produced by one implementation of delay-lock is

$$\begin{aligned} e(\tau) &= \left[\frac{1}{2\pi B} \int_{-\pi B}^{\pi B} \langle \cos \omega(t + \tau) \omega \sin \omega \rangle d\omega \right] a(\tau) \\ &= \frac{\sin(\pi B\tau) - (\pi B\tau) \cos(\pi B\tau)}{2\pi B\tau^2} \cdot \frac{\sin(\pi B\tau)}{\pi B\tau} \end{aligned} \quad (3)$$

where the correlation channel demodulates the delay-lock channel. This has an infinity of null points where the error goes through zero as a function of τ . Thus, delay-lock tracking can lead to possible ambiguities which could cause a false range measurement, and this is a problem in the TDRSS application.

The finite-difference implementation of delay-lock tracking subtracts early and late correlations after envelope detection, so that the error voltage is defined by

$$e(\tau) = a^2(\tau - \tau_d) - a^2(\tau + \tau_d) \quad (4)$$

Substituting (2) and setting $\tau_d = 1/2B$, the half clock, (4) becomes

$$e(\tau) = \cos^2(\pi B\tau) \frac{2B\tau}{\pi^2 [(B\tau)^2 - .25]^2} \quad (5)$$

Now, $e(\tau)$ goes through zero only at $\tau = 0$, and a tracking ambiguity does not exist.

Another possible implementation causes correlation to be performed with a 90° shifted version of the coherent frequency hopped waveform, rather than with the derivative. (The 90° phase shift is reversed for negative frequencies with respect to band center.) For this scheme, the error voltage is

$$e(\tau) = \left[\frac{1}{2\pi B} \int_{-\pi B}^{\pi B} \langle \cos \omega(t + \tau) \operatorname{sign}(\omega) \sin \omega \rangle d\omega \right] a(\tau) \quad (6)$$

where $\operatorname{sign}(\omega) = +1$ if $\omega > 0$ and -1 if $\omega < 0$. Performing the integration yields

$$e(\tau) = \frac{\sin^2(\pi B\tau/2)}{(\pi B\tau/2)} \cdot \frac{\sin(\pi B\tau)}{\pi B\tau} \quad (7)$$

Although there still is a possibility of ambiguous tracking, note that the correlation voltage, given by (2), is zero at the null points except for $\tau = 0$. Thus, the ambiguities can, in principle and in practice, be detected and avoided.

If the averaging performed in (2) and (6) is carried out presuming a finite number M of frequency channels distributed over a bandwidth B , the result is

$$a(\tau) = \frac{\sin(\pi B \tau)}{M \sin(\pi B \tau / M)} \quad (8)$$

$$\begin{aligned} a^2(\tau - 1/2B) - a^2(\tau + 1/2B) \\ = \frac{4 \sin(\pi/M) \cos^2(\pi B \tau)}{M^2} \cdot \frac{\sin(2\pi B \tau / M)}{[\cos(\pi/M) - \cos(2\pi B \tau / M)]^2} \end{aligned} \quad (9)$$

$$e(\tau) = \frac{2 \sin^2(\pi B \tau / 2)}{M \sin(\pi B \tau / M)} \cdot \frac{\sin(\pi B \tau)}{M \sin(\pi B \tau / M)} \quad (10)$$

For τ small, the behavior is the same as for the continuum of frequencies previously assumed. However, note that the functions are repetitive with the period $= M/B$. Therefore, if the hopping rate is less than B/M , which is the channel spacing, the secondary peak can occur for τ shifts still within the same hop.* For this reason, we set the hopping rate equal to the channel spacing.

*The averaging leading to (8) and (10) has not taken into account amplitude reduction due to partial overlap of the hop dwells.

APPENDIX III

DETAILED SYNCHRONIZATION STUDY

INTRODUCTION

Estimates of acquisition time have been based in previous memos on use of a post-detection integration with a fixed sample duration. We now wish to introduce the concept of sequential detection in conjunction with post-detection integration on the output of the Doppler processor. Figure 1 shows the conceptual implementation.

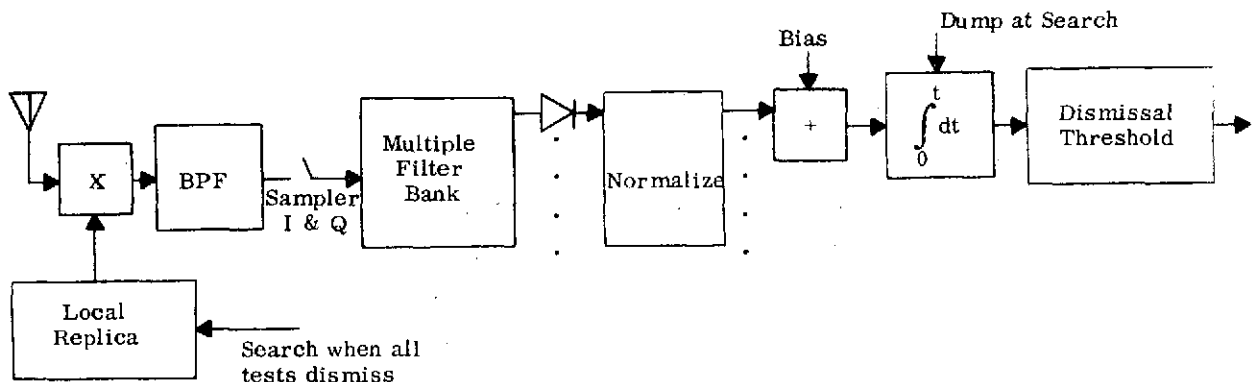


Figure 1. Essentials of Sequential Detection Search Strategy

The correlator output for a given search position will contain only noise until the matching time position is reached. For a PN system (unfiltered signal), the correlated amplitude will rise in accordance with a triangular function, as shown in Figure 2. The amplitude drops to zero for an error of one chip T_c . The amplitude actually appears as the envelope of a carrier offset from the nominal center frequency by the Doppler offset on the received signal.

The purpose of the multiple filter bank is to perform a Fourier resolution over the total Doppler uncertainty. Let T_b denote the duration of a signal sample to be coherently processed by the multiple filter bank. The

in-phase and quadrature components (with respect to center frequency) are sampled, and the Fourier coefficients are computed for the spacing T_b^{-1} (or possibly a smaller spacing). The magnitudes (combining in-phase and quadrature) are output in parallel for each harmonic for subsequent noncoherent processing by post-detection integration.

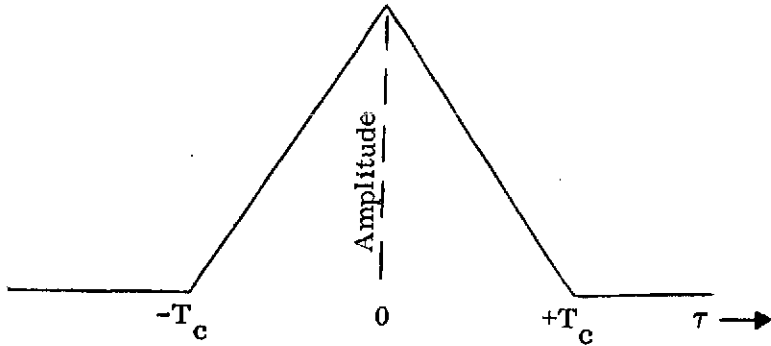


Figure 2. Correlation Amplitude as Function of Time Error τ

The post-detection integration over successive samples of duration T_b is performed in parallel for each harmonic output C_k . For the k th harmonic, compute after processing each sample of duration T_b

$$\text{sum}(k) = \text{sum}(k) + C_k - \text{BIAS} \quad (1)$$

Then, as soon as all sums fall below a dismissal threshold, absence of a correlated amplitude is declared, and all sums are reset to zero. Then, the next search position is tested. Synchronization is declared at any search position by failure to dismiss after a specified number of integrations (the truncation of the sequential test). By making the truncation sufficiently long, false alarms can be made negligible.

It is necessary to empirically optimize the bias and threshold settings. The measure of performance can be defined by E/N_0 , where E denotes the received signal energy over the average time to search one chip. Minimizing E/N_0 for a given probability of detection is equivalent to minimizing the acquisition time. The bias and threshold settings will be proportional to the rms noise level; hence, a normalization process can be applied so as to estimate the noise level and proportionately scale the filter bank outputs, either on the basis of one T_b sample or by averaging over many such samples.

Another design parameter is the step size while searching. Previous studies have indicated that this parameter is not critical, and throughout this discussion, we assume searching in half chip steps. An example of a previous simulation result is shown in Figure 3. Here, there is only a single filter, rather than a multiple filter bank, the output of which is envelope detected for a sequential test. Note that a fairly high probability of detection (0.7) is realized for a Doppler offset of 3 times the search rate in chips/sec at $E/N_0 = 12$ dB.

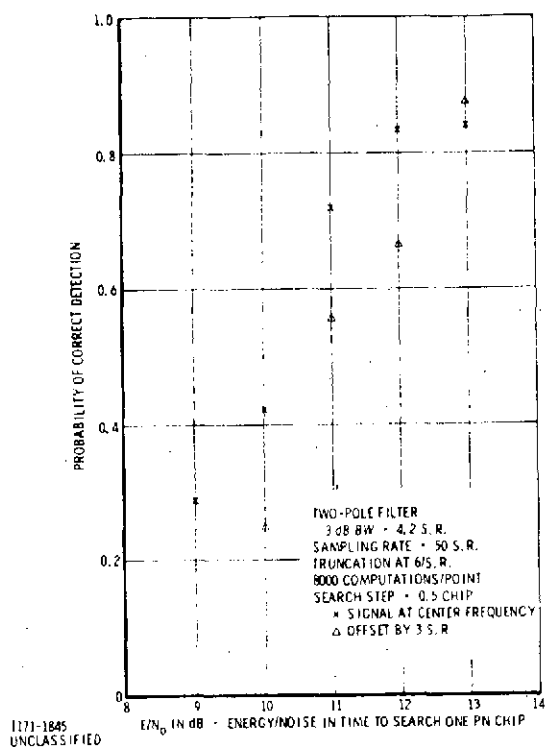


Figure 3. Search Performance With Two-Pole Filter

The TDRS application requires consideration of much higher Doppler offsets relative to the search rate; hence, we go to a multiple filter bank. We also require a low E_b/N_0 for the signal energy over the sample of duration T_b which is coherently processed by the multiple filter bank. The study will utilize computer simulations. The probability of detection is measured by averaging over repeated trials, which search through the triangular correlation function of Figure 2 in half-chip steps. The starting value of τ is randomized over the half-chip interval.

ONE FILTER DESIGN

To begin the study, we consider a single filter design consisting of integrate-and-dump at T_b intervals. This design is applicable when the a priori Doppler uncertainty is small. The normalization (see Figure 1) is presumed done by a separate averaging process. Thus, we have the basic sequential detection scheme summing envelope samples from the integrate-and-dump filter. In this case, the effect of a frequency offset is given by the amplitude response of the integrate-and-dump filter; thus,

$$\text{Loss due to offset } \Delta f = 20 \log_{10} \frac{\sin(\pi \Delta f T_b)}{\pi \Delta f T_b} \quad (2)$$

For example, an offset of $\pm .25 T_b^{-1}$ causes a loss of 0.9 dB.

The effect of varying the bias, and the threshold correspondingly, while holding, roughly, a constant average search rate (measured by the average number of bits per dismissal) is seen in Figure 4. Note that increasing the bias tends to pull the integrated voltage down more rapidly, and this shows up as a reduced probability of getting a large number of bits before dismissal occurs.

The probability of detection when signal is present is shown in Figure 5, as a function of E/N_0 . Note that the higher bias, which reduces false alarms more effectively, displays only a slightly poorer detection performance. The Doppler coverage is in excess of ± 5 times the search rate, which is better than shown in Figure 3.

FIVE FILTER BANK DESIGN

As a next study, we postulate a multiple filter bank containing 5 filters spaced by $0.75 T_b^{-1}$. The signal sample over the duration T_b is time-quantized into 12 instantaneous values, and normalization of the filter bank output is performed for each T_b sample by scaling with the sum of the absolute value of in-phase and quadrature components of these 12 values in time. With a view of achieving processing simplicity, the sines and cosines were approximated by integer values as shown in Table I, with an overall scaling by $\sqrt{2}$. Similarly, the magnitude of the in-phase and quadrature outputs, which ideally is $(I^2 + Q^2)^{.5}$, was approximated by

$$\text{Magnitude} = .75(|I| + |Q|) + .25 |(|I| - |Q|)| \quad (3)$$

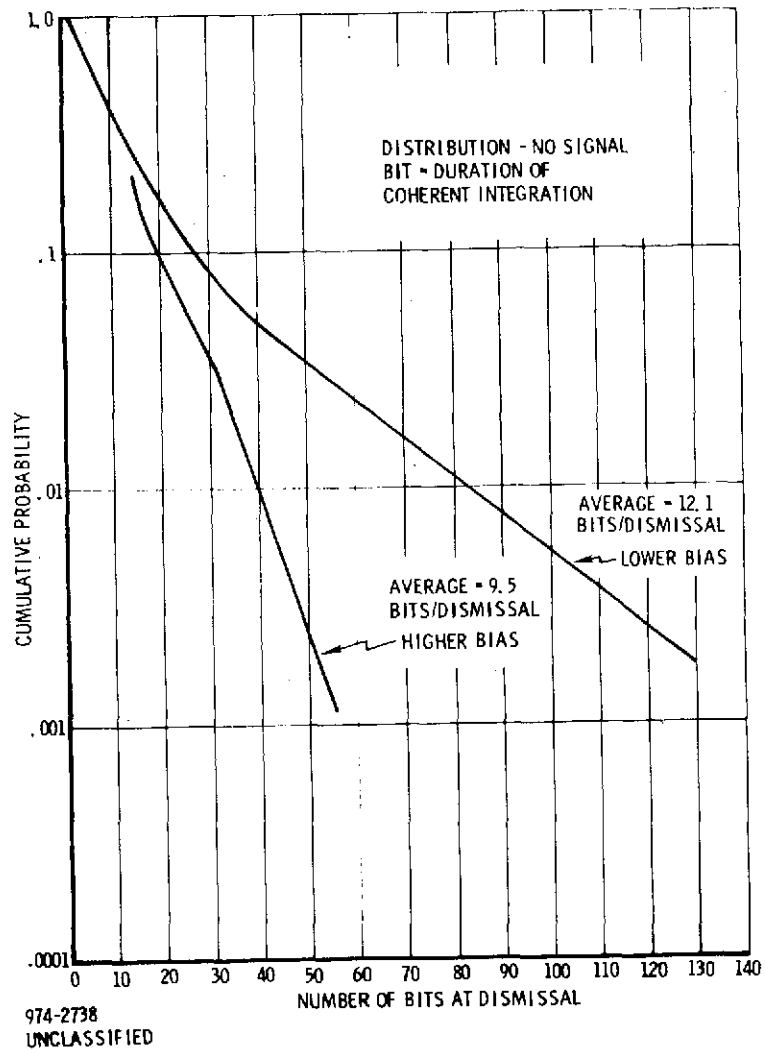


Figure 4. Post-Detection Integration on One Filter

which has a maximum variation of ± 6 percent as a function of the phase.

Table I. Integer Approximation to Sine and Cosine

θ (degrees)	11.25	33.75	56.25	78.75	101.25	123.75	146.25	168.75	191.25	213.75	236.25	258.75
	22.5	45.	67.5	90.	112.5	135.	157.5	180.	202.5	225.	247.5	270.
$\sin(\theta)$	1	2	2	1	-1	-2	-2	-1	1	2	2	1
$\cos(\theta)$	2	1	-1	-2	-2	-1	1	2	2	1	-1	-2

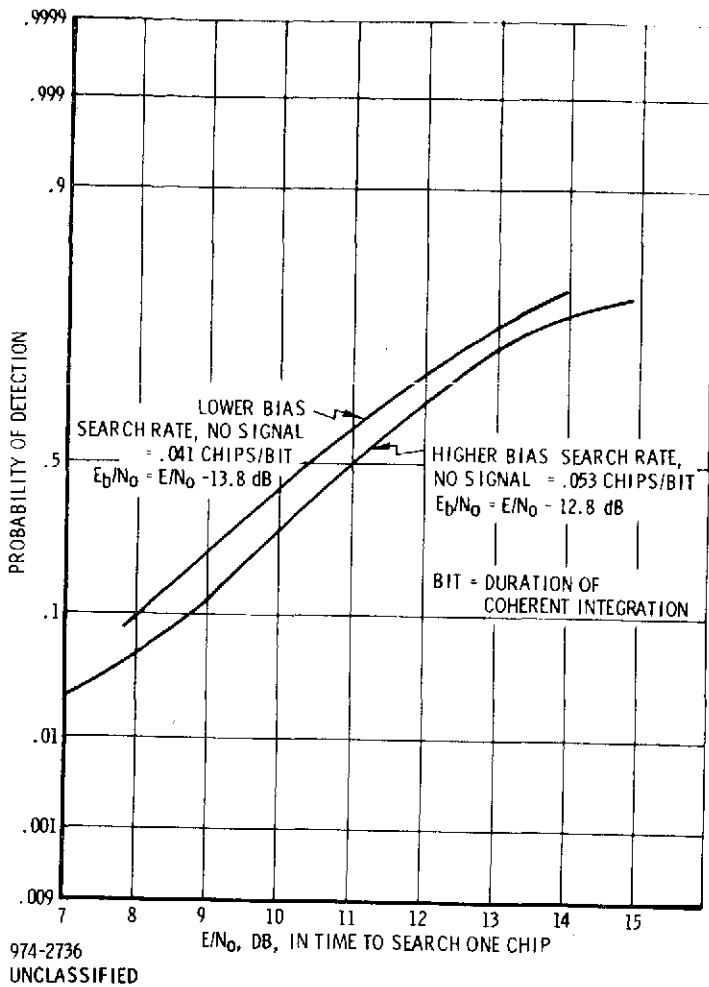


Figure 5. Post-Detection Integration on One Filter ($\Delta f = 0$)

Results are shown in Figures 6-8. Figures 7 and 8 show the probability of detection as a function of E/N_0 , for two choices of bias and threshold, while Figure 6 displays the distribution of the number of T_b samples integrated prior to dismissal in the absence of signal. Because of the sequential test, this number is a statistical variable, and Figure 6 enables selection of the truncation so as to insure a low false alarm probability. As with Figure 4, the tail of the distribution appears to decrease exponentially with the number.

We observe from Figure 8 that a probability of detection of 0.7 is achieved at $E/N_0 = 14.5$ dB with a Doppler coverage exceeding ± 12 times the search rate. This is a definite improvement in Doppler coverage compared with the single filter design of Figure 3 or Figure 5. Note that $E_b/N_0 = 5.5$ dB at this design point.

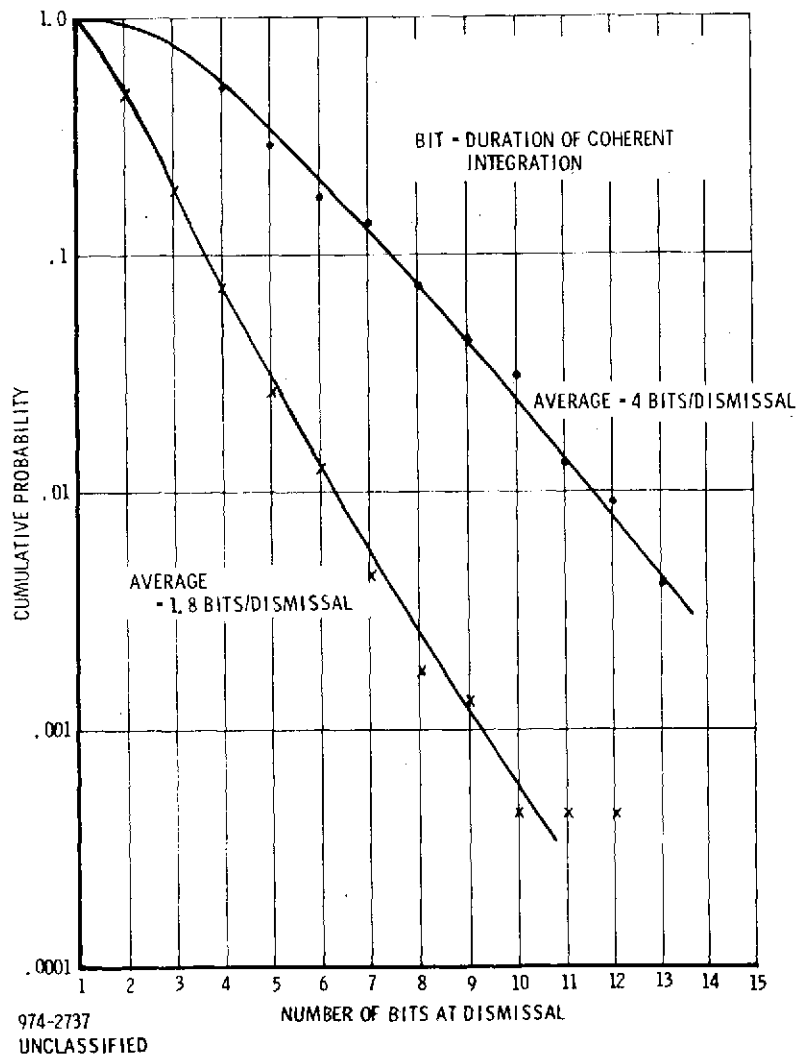


Figure 6. Post-Detection Integration on 5 Filters at 0, $\pm .75$, $\pm 1.5 \times$ Bit Rate

32 FILTER BANK DESIGN

We now study a system based on the parameters of the steered transmit beam multiple access forward link. This calls for post-detection integration on the outputs of 32 filters (spaced by 4 KHz to cover the total Doppler). Figure 9 gives the distribution of the number of bits to dismiss, corresponding to setting the bias and threshold to yield an average of 23.4 bits/dismissal. Thus, the search rate, taking half-chip steps, is 46.8 bits/chip.

Figure 10 shows the probability of detection as a function of E/N_0 . Two values of frequency are indicated, one corresponding to falling on the peak of a filter response, the other falling midway between two adjacent peaks, where the filter response is 3.9 dB below the peak. Figure 10 shows only about 3 dB

degradation at the midpoint, which is due to the signal having response from two adjacent filters. The loss due to frequency offset can be reduced by spacing filters more closely. For example, spacing by half the bit rate, thereby doubling the number of filters, should reduce the separation of the curves to roughly 1 dB.

We may now compare the performance results of Figure 10 with previous estimates such as in Section 2. With 32 filters, it was previously estimated that the probability of detection would be 0.9 at a search rate of .0093 chips/bit ($n_I = 54$ searching in half-chip steps) with $E_b/N_o = 0$ dB. Figure 9 yields probability of detection of 0.6 (for $\Delta f = 0$) at the same E_b/N_o but searching more than twice as fast. It is concluded that previous estimates of acquisition time with fixed sample post-detection integration are conservative.

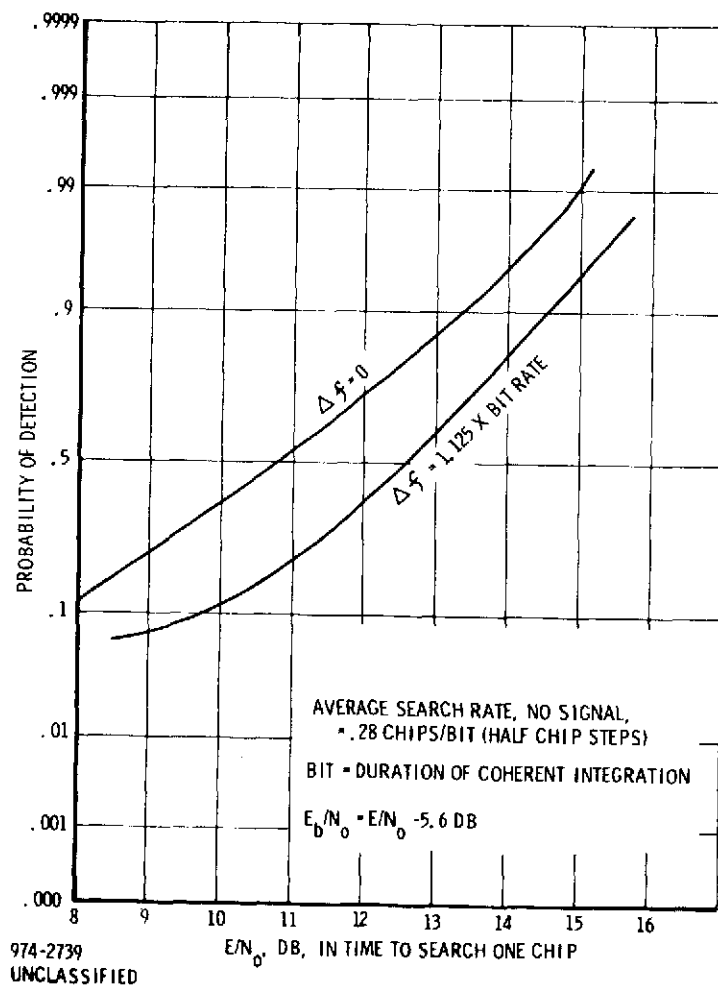


Figure 7. Post-Detection Integration on 5 Filters at 0, $\pm .75$, $\pm 1.5 \times$ Bit Rate

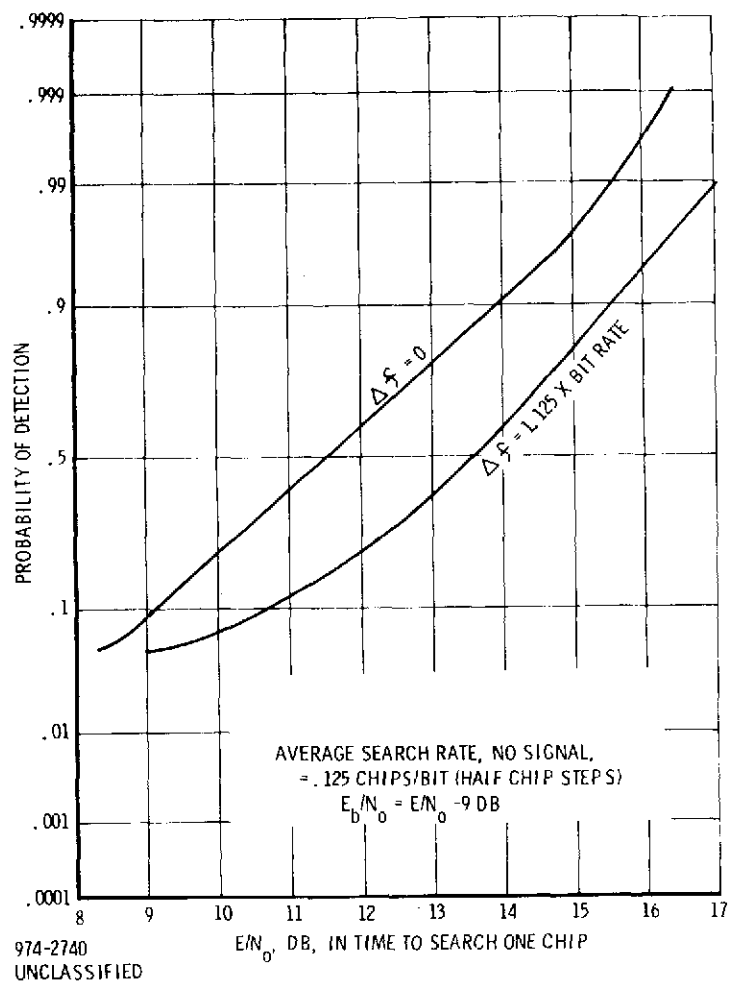


Figure 8. Post-Detection Integration on 5 Filters at 0, $\pm .75$, $\pm 1.5 \times \text{Bit Rate}$

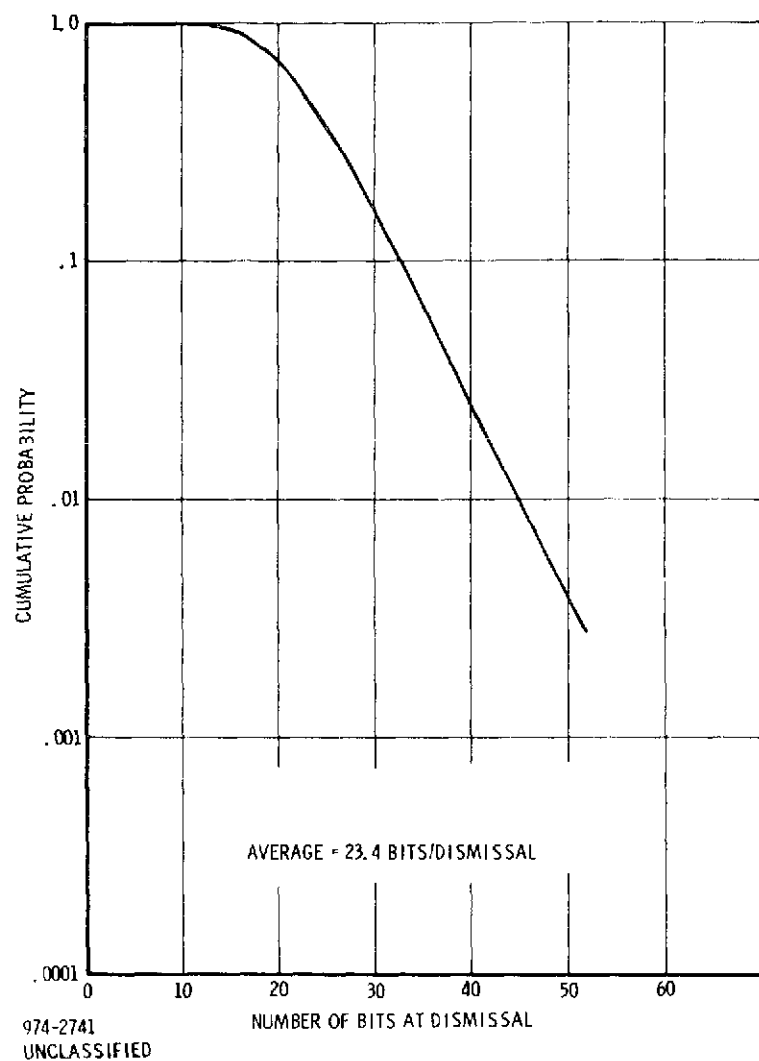


Figure 9. Post-Detection Integration on 32 Filters Spaced by Bit Rate

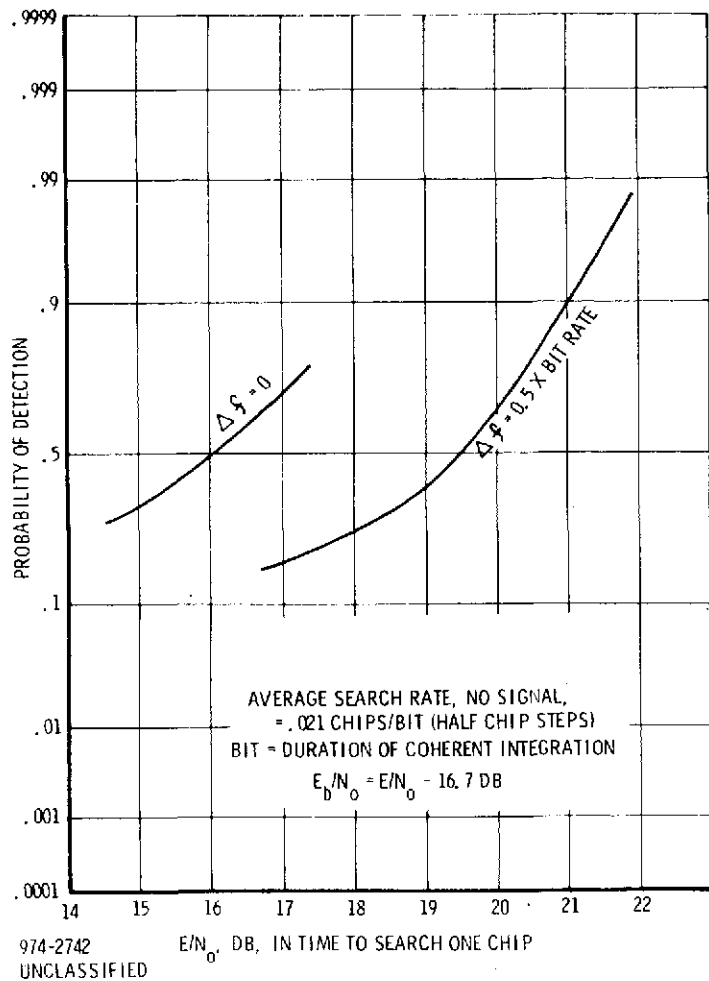


Figure 10. Post-Detection Integration on 32 Filters Spaced By Bit Rate

CONCLUSIONS

Computer simulations are given to enable more accurate estimates of acquisition time. They indicate that a sequential detection process enables a faster search than derived from previous estimates based on fixed sample integration.

APPENDIX IV

DOPPLER PROCESSOR FOR TDRSS TELECOMMUNICATIONS SYSTEM

INTRODUCTION

The following paper presents an analysis of various Doppler processor configurations which are possible candidates for use in the TDRSS Telecommunication System. A summary of performance characteristics and implementation problems will be presented for each configuration. A suitable Doppler processor configuration will be selected for use in the TDRSS Telecommunication System. The operation of the selected TDRSS Doppler processor configuration will be discussed at a block diagram level. In addition, performance tradeoffs will be presented for the selected configuration. Finally, the selected TDRSS Doppler processor configuration will be analyzed from a hardware implementation standpoint. The approximate quantity of ICs necessary to implement the TDRSS Doppler processor will be presented and compared with the present multimode transponder hardware configuration.

ANALYSIS OF DOPPLER PROCESSOR CONFIGURATIONS

There are essentially three Doppler processor configurations which are possible candidates for use in the TDRSS Telecommunication System. The first configuration to be analyzed is the serial search/MOS memory type implementation which is similar to the present Doppler processor configuration in the multimode transponder (MMT). This configuration involves searching the complete Doppler frequency range (± 64 KHz) in a serial fashion such that the full Doppler range is searched in one, two, or even four frequency sweeps. The second configuration to be analyzed is the parallel search/MOS memory configuration which involves parallel searching the full Doppler uncertainty range in two or four segments by arranging MMT-type Doppler processors in a parallel configuration. The third and last configuration to be analyzed is the parallel search/RAM memory-type implementation which involves parallel searching the full Doppler uncertainty range in four segments by utilizing a completely new parallel processing technique which incorporates random access memories (RAMs) and read-only memories (ROMs).

The operational specifications for a Doppler processor are developed from various communication system characteristics such as satellite dynamics, data rates, detection threshold (C/N_0), and acquisition time. Given the Doppler uncertainty range of ± 64 KHz, tradeoffs between the Doppler resolution and the search time are made for each of the three Doppler processor configurations mentioned above. The search time (which is the time required to search the complete Doppler uncertainty range) is determined by calculating the process time and sample time for a certain Doppler resolution and selecting the larger of the two quantities. In other words, the search time is equal to the larger of either the process time or sample time. In order to consider all of the possible tradeoffs between search time and Doppler resolution, it is necessary to have a thorough understanding of the process time and sample time equations which are as follows:

$$\text{Sample Time} = \frac{\text{No. of Samples}}{\text{Sampling Clock}} \quad (1)$$

$$\text{Process Time} = \frac{\text{No. of Windows} \times \text{Memory Length}}{\text{Memory Clock}} \quad (2)$$

Although it is very advantageous to have the sample time equal to the process time since it reduces the hardware implementation, there are many cases to be considered in which the two quantities are not equal. The sample time, which is shown in Equation (1), is the time necessary to load "X" samples of the input signal into a memory using a "Y" KHz sampling clock; both "X" and "Y" must satisfy Nyquist's sampling theorem. For example, the sampling clock must be greater than or equal to two times the highest Doppler frequency that is being resolved. In addition, there must be a minimum of two samples per KHz of Doppler, and the sample time must be greater than or equal to the inverse of the Doppler frequency resolution.

The process time, which is shown in equation (2) is the time necessary to recirculate "X" bits of data in memory "W" times using a memory clock of "M" MHz. The "X" bits of data, which is really the "memory length" in the process time equation, should be equal to the "number of samples" in the sample time equation. The "W" times memory recirculation factor is the "number of windows" shown in the process time equation. The number of windows (W) should be equal to two times the absolute Doppler frequency range divided by the Doppler frequency resolution or

$$W = \frac{2 \text{ (absolute Doppler range)}}{\text{Doppler Resolution}} = \frac{2(\pm f)}{\text{resolution}}$$

The memory clock of "M" MHz shown in the process time equation is the inhibiting factor in attempting to reduce the process time. With a MOS memory implementation which is utilized in the first and second Doppler processor configurations to be analyzed, the maximum memory clock speed is about 2.5 MHz. However, with a RAM memory implementation such as used in the third Doppler processor configuration to be analyzed, the memory clock speed can be as high as 20 MHz.

The ratio between the Memory Clock (M) and the sampling clock (Y) is known as the speed-up factor for the Doppler processor. In order to obtain a better understanding of the speed-up factor, consider the following example in which the Doppler range is ± 64 KHz and the Doppler frequency resolution is 1 KHz. The process time, sample time, and speed-up factor are as follows:

$$\text{Sample Time} = \frac{\text{No. of Samples}}{\text{Sampling Clock}} = \frac{128 \text{ Samples}}{128 \text{ KHz}} = 1 \text{ ms}$$

$$\text{Process Time} = \frac{\text{No. of Windows} \times \text{Memory Length}}{\text{Memory Clock}}$$

$$= \frac{(128) (128)}{2.048 \text{ MHz}} = 8 \text{ ms}$$

$$\text{Speed-Up Factor} = \frac{\text{Memory Clock}}{\text{Sampling Clock}} = \frac{2048 \text{ KHz}}{128 \text{ KHz}} = 16$$

The speed-up factor is a measure of how fast the samples of the input signal can be processed using a recirculating memory processing technique as compared to a real time processing technique. In the above example, the ± 64 KHz Doppler range is searched in 1 KHz steps and requires 128 windows or frequency cells. Using a real time processing technique in this example, each frequency cell requires 1 ms process time and therefore the total Doppler range requires a 128 ms process time. Utilization of a recirculated memory processing technique can reduce the process time for each frequency cell to 1/16 ms and therefore the total Doppler range can be processed in 8 ms. In conclusion, the speed-up factor of 16 in the above example means that the samples of the input signal can be processed 16 times faster using the circulating memory processing technique than by using a real time processing technique. The use of a recirculating memory processing technique can speed-up the resolution of frequency uncertainties by a factor of 100 compared to real time frequency search techniques.

The analysis of the three Doppler processor configurations in the following sections will essentially involve tradeoff considerations of hardware implementation and performance requirements. Improvements in process time can be achieved by a reduction in the number of windows or frequency cells or an increase in the speed of the memory clock. The memory length is essentially a fixed quantity and should be equal to the number of samples in the sample time equation. Given the Doppler uncertainty range and the desired frequency resolution, the sample time is fixed in value and cannot be decreased since Nyquist's sampling theory cannot be violated. Each of the Doppler processor configurations will include the option of processing the positive and negative Doppler ranges simultaneously to reduce the required quantity of windows by 50%, and thereby reduce the process time by 50% (assuming the memory length and memory clock remain fixed). This simultaneous processing of the positive and negative Doppler can cause a significant reduction in search time.

SERIAL SEARCH/MOS MEMORY CONFIGURATION

The first Doppler processor configuration to be analyzed is the serial search/MOS memory implementation. This configuration involves searching the ± 64 KHz Doppler uncertainty range in a serial fashion such that the full Doppler range is searched in one, two, or four frequency sweeps. Each frequency sweep requires the stepping of a voltage-controlled oscillator (VCO) within the carrier tracking loop until the Doppler frequency is located. For example, the ± 64 KHz Doppler range may be divided up into four frequency sweeps of ± 16 KHz each, and therefore will require stepping of the VCO after each ± 16 KHz sweep until the Doppler frequency is located. This Doppler processor configuration also incorporates a recirculating MOS memory which operates at a maximum (safe) clock speed of 2.048 MHz.

The serial search/MOS memory configuration is fairly similar to the Multi-mode Transponder (MMT) Doppler processor configuration except for the addition of various output circuitry to provide stepping of the carrier VCO. This configuration also includes the option of processing the positive and negative Doppler ranges simultaneously to yield better performance specifications. (A listing of various performance specifications) for serial search/MOS memory type configurations is shown in Table IV-1. These performance specifications have been generated by considering the various trade-offs between Doppler resolution, number of frequency sweeps, and by considering the hardware option of processing both the positive and negative Doppler ranges simultaneously. The best performance characteristics of the 13 serial search/MOS memory type configurations listed in Table IV-1 is the last configuration in which the ± 64 KHz

Doppler range is divided up into four frequency sweeps of ± 16 kHz each. This configuration offers the best tradeoff between frequency resolution and search time which are 1 kHz and 1 ms respectively. The performance specifications for this configuration are listed in Table IV-4, and will be compared from a hardware implementation standpoint with the best performance characteristics obtainable from alternate type Doppler processor configurations.

Table IV-1. Serial Search/MOS Memory Doppler Processor Configurations

Doppler Range	Resolution	Search Time	Process Time	Sample Time	No. of Freq. Sweeps	Process Positive and Negative Doppler Range Simultaneously
± 64 KHz	1 KHz	8 ms	8 ms	1 ms	One	No
± 64 KHz	2 KHz	2 ms	2 ms	1/2 ms	One	No
± 64 KHz	4 KHz	1/2 ms	1/2 ms	1/4 ms	One	No
± 32 KHz	1 KHz	4 ms	4 ms	1 ms	Two	No
± 32 KHz	2 KHz	1 ms	1 ms	1/2 ms	Two	No
± 16 KHz	1 KHz	2 ms	2 ms	1 ms	Four	No
± 16 KHz	4 KHz	1/4 ms	1/8 ms	1/4 ms	Four	No
± 64 KHz	1 KHz	4 ms	4 ms	1 ms	One	Yes
± 64 KHz	2 KHz	1 ms	1 ms	1/2 ms	One	Yes
± 64 KHz	4 KHz	1/4 ms	1/4 ms	1/4 ms	One	Yes
± 32 KHz	1 KHz	2 ms	2 ms	1 ms	Two	Yes
± 32 KHz	2 KHz	1/2 ms	1/2 ms	1/2 ms	Two	Yes
± 16 KHz	1 KHz	1 ms	1 ms	1 ms	Four	Yes

The serial search/MOS memory type configuration has a number of disadvantages which stem from the requirement of multiple stepping of the VCO after each frequency sweep. The multiple stepping of the VCO requires approximately 50% more Doppler processor output circuitry than the MMT configuration, and in addition, results in a much longer search time. The utilization of a MOS memory in this configuration results in an increased process time due to its clock speed limitation.

Therefore, in order to attain a reasonable frequency resolution (1 KHz) and search time (1 ms), the hardware option of processing the positive (0 to +16 KHz) and negative (0 to -16 KHz) Doppler ranges simultaneously must be incorporated to reduce the process time from 2 ms to 1 ms as shown in Table IV-1, (by observing the cases of ± 16 KHz Doppler range at 1 KHz resolution using four frequency sweeps). However, this hardware option requires approximately two-thirds more arithmetic logic than the existing Multimode Transponder Doppler processor. In conclusion, the serial search/MOS memory configuration offers reasonable performance specifications at an overall total cost of approximately 35% more hardware than the MMT Doppler processor. Finally, this configuration does not result in a complete redesign of the MMT Doppler processor since the input and control logic are essentially unchanged.

PARALLEL SEARCH/MOS MEMORY CONFIGURATION

The second Doppler processor configuration to be analyzed is the parallel search/MOS memory implementation. This configuration involves parallel searching the ± 64 KHz Doppler range in two or four segments by utilizing MMT type Doppler processors in a parallel configuration. For example, the ± 64 KHz Doppler range may be divided into two ± 32 KHz Doppler segments which are searched in a parallel fashion simultaneously.

A listing of various performance specifications for parallel search/MOS memory type configurations is shown in Table IV-2. These performance specifications have been generated by considering the various tradeoffs between Doppler resolution, number of Doppler processors in parallel, and by considering the hardware option of processing both the positive and negative Doppler ranges simultaneously. The best performance characteristics of the 7 parallel search/MOS memory type configurations listed in Table IV-2 is the fourth case in which the ± 64 KHz Doppler range is divided up into two Doppler ranges of ± 32 KHz which are parallel searched using two Doppler processors in parallel. This configuration offers the best performance/hardware tradeoff and provides a frequency resolution of 1 KHz and a search time of 1 ms. The performance specifications for this configuration are listed in Table IV-4, and will be compared from a hardware implementation standpoint with the best performance characteristics obtainable from alternate type Doppler processor configurations.

The parallel search/MOS memory type configuration has a number of disadvantages which stem from the requirement of having multiple (2 or 4) Doppler processors in parallel to cover the complete Doppler range. This parallel search/parallel

hardware requirement means that for two Doppler processors in parallel, for example, all circuitry of the MMT Doppler processor must be duplicated except for the control logic circuitry which can be time shared. Therefore, for the best performance case of ± 32 kHz Doppler range at 1 kHz resolution and 1 ms search time using two Doppler processors in parallel, there will be two input interface modules, two arithmetic logic modules, and two output circuitry modules. This hardware addition results in approximately 70% more hardware than the MMT Doppler processor. Another distinct disadvantage of the parallel search/MOS memory type configuration is that it requires as many in-phase and quadriphase (I and Q) channels as there are Doppler processors in parallel.

In order to attain a reasonable frequency resolution (1 kHz) and search time (1 ms), the hardware option of processing the positive (0 to $+32$ kHz) and negative (0 to -32 kHz) Doppler ranges simultaneously must again be incorporated for both parallel Doppler processors to reduce the process time from 2 ms to 1 ms as shown in Table IV-2. However, this hardware option requires approximately two-thirds more arithmetic logic per Doppler processor than the existing MMT Doppler processor. In conclusion, the parallel search/MOS memory type configuration offers reasonable performance characteristics at an overall total cost of approximately 95% more hardware than the MMT Doppler processor. Finally, this configuration also does not result in a complete redesign of the MMT Doppler processor since the redesign is essentially just a parallel add-on to the existing configuration with a time sharing of the control logic circuitry.

Table IV-2. Parallel Search/MOS Memory Doppler Processor Configurations

Doppler Range	Resolution	Search Time	Process Time	Sample Time	No. of Doppler Processors In Parallel	Process Positive and Negative Doppler Range Simultaneously
± 32 kHz	1 kHz	2 ms	2 ms	1 ms	Two	No
± 32 kHz	2 kHz	1/2 ms	1/2 ms	1/2 ms	Two	No
± 16 kHz	1 kHz	1 ms	1/2 ms	1 ms	Four	No
± 32 kHz	1 kHz	1 ms	1 ms	1 ms	Two	Yes
± 32 kHz	2 kHz	1/2 ms	1/4 ms	1/2 ms	Two	Yes
± 16 kHz	1 kHz	1 ms	1/4 ms	1 ms	Four	Yes
± 16 kHz	2 kHz	1/2 ms	1/16 ms	1/2 ms	Four	Yes

PARALLEL SEARCH/RAM MEMORY CONFIGURATION

The last Doppler processor configuration to be analyzed is the parallel search/RAM memory type implementation. This configuration involves parallel searching the ± 64 KHz Doppler uncertainty range in four segments by utilizing a completely different parallel processing technique which does not use a time sharing of accumulators concept such as the MMT Doppler processor. The utilization of a recirculating random access memory (RAM) in this configuration results in decreased process time due to its high clock speed capability which is about 20 MHz (almost ten times faster than the MOS memory of the previous two Doppler processor configurations). In addition, the parallel search/RAM memory configuration utilizes the processing technique of searching the positive (0 to $+64$ KHz) and negative (0 to -64 KHz) Doppler ranges simultaneously to further reduce the process time.

Since the objective of the Doppler Processor is to track the Doppler frequency of the satellite, a Fourier analysis of the input is required to find the frequency having the highest spectral density. The Fourier integral theorem is as follows:

$$X(f) = \int_{-\infty}^{\infty} x(t)e^{-j\omega t} dt, \quad (3)$$

where $x(t)$ is the input to the Doppler processor from the in-phase and quadrature (I and Q) channels and is defined as

$$x(t) = I(t) \pm jQ(t). \quad (4)$$

Since the input signal is sampled over a finite time (NT), the limits on the integral on equation (3) becomes

$$X(f) = \int_1^{NT} x(t)e^{-j\omega t} dt. \quad (5)$$

Replacing the integral in equation (5) by a summation sign yields

$$X(f) = T \sum_{n=1}^N X(nT)e^{-j\omega T}; \quad (6)$$

where

$$X(nT) = I(nT) \pm jQ(nT) = I_n \pm jQ_n, \quad (7)$$

and n takes on values of $n = 1, 2, 3, \dots, N$; and

$$e^{-j\omega T} = \cos n\omega T - j \sin n\omega T. \quad (8)$$

Multiplying $X(nT)$ by $e^{-j\omega T}$ gives

$$X(nT)e^{-j\omega T} = I_n \cos n\omega T \pm Q_n \sin n\omega T \pm j Q_n \cos n\omega T - j I_n \sin n\omega T. \quad (9)$$

Separating the real part (R_n) and imaginary part (J_n) yields

$$R_n = I_n \cos n\omega T \pm Q_n \sin n\omega T \quad (10)$$

$$J_n = -I_n \sin n\omega T \pm Q_n \cos n\omega T \quad (11)$$

$$\therefore X(nT)e^{-j\omega T} = R_n + j J_n. \quad (12)$$

Substituting equation (12) into equation (6) yields

$$X(f) = T \left(\sum_{n=1}^N R_n + \sum_{n=1}^N J_n \right). \quad (13)$$

The energy spectral density, $S(f)$, for nonperiodic signals is

$$S(f) = |X(f)|^2. \quad (14)$$

Consider now the interpretation of $|X(f)|^2$. If $x(t)$ is a voltage waveform, then $X(f)$ has dimensions of voltage per unit frequency and describes the distribution, or density, of the signal voltage in frequency. By like reasoning, $|X(f)|^2$ is the density of energy in the frequency domain. This conceptual viewpoint is both physically meaningful and useful; its importance is the basic concept of the Doppler processor. Therefore, the spectral density, $S(f)$, of $X(f)$ becomes

$$|X(f)|^2 = T^2 \left[\left(\sum_{n=1}^N R_n \right)^2 + \left(\sum_{n=1}^N J_n \right)^2 \right]. \quad (15)$$

Since we are only interested in the relative energy spectral density, the Doppler processor actually performs an approximation of the following equation:

$$\frac{|X(f)|^2}{T^2} = \left(\sum_{n=1}^N R_n \right)^2 + \left(\sum_{n=1}^N J_n \right)^2. \quad (16)$$

The parallel search/RAM memory Doppler processor configuration parallel searches the Doppler frequency range by calculating the value of equation (16) for both positive (0 to +64 KHz) and negative (0 to -64 KHz) frequency simultaneously. In other words, equation (10) and (11) can be divided into four equations for both positive and negative frequency which are as follows:

$$R_n(+f) = I_n \cos n\omega T + Q_n \sin n\omega T \quad (17)$$

$$R_n(-f) = I_n \cos n\omega T - Q_n \sin n\omega T \quad (18)$$

$$J_n(+f) = -I_n \sin n\omega T + Q_n \cos n\omega T \quad (19)$$

$$J_n(-f) = -I_n \sin n\omega T - Q_n \cos n\omega T. \quad (20)$$

The parallel search/RAM memory type configuration essentially performs the following four calculations simultaneously:

$$\left(\sum_{n=1}^N R_n(+f) \right)^2 = \left(\sum_{n=1}^N I_n \cos n\omega T + \sum_{n=1}^N Q_n \sin n\omega T \right)^2 \quad (21)$$

$$\left(\sum_{n=1}^N R_n(-f) \right)^2 = \left(\sum_{n=1}^N I_n \cos n\omega T - \sum_{n=1}^N Q_n \sin n\omega T \right)^2 \quad (22)$$

$$\left(\sum_{n=1}^N J_n(+f) \right)^2 = \left(\sum_{n=1}^N (-I_n) \sin n\omega T + \sum_{n=1}^N Q_n \cos n\omega T \right)^2 \quad (23)$$

$$\left(\sum_{n=1}^N J_n(-f) \right)^2 = \left(\sum_{n=1}^N (-I_n) \sin n\omega T - \sum_{n=1}^N Q_n \cos n\omega T \right)^2. \quad (24)$$

The final outputs of the parallel search/RAM memory configuration therefore provide the relative energy spectral density over the +64 KHz Doppler range which is

$$\frac{|X(+f)|^2}{T^2} = \left[\sum_{n=1}^N R_n(+f) \right]^2 + \left[\sum_{n=1}^N J_n(+f) \right]^2 \quad (25)$$

$$\frac{|X(-f)|^2}{T^2} = \left[\sum_{n=1}^N R_n(-f) \right]^2 + \left[\sum_{n=1}^N J_n(-f) \right]^2 \quad (26)$$

where equation (25) represents a summation of equations (21) and (23), and equation (26) represents a summation of equations (22) and (25).

A listing of various performance specifications for parallel search/RAM memory type configurations is shown in Table IV-3. These performance specifications have been generated by considering the various tradeoffs between Doppler resolution, and the RAM memory clock speed. The best performance characteristic of the 4 parallel search/RAM memory type configurations listed in Table IV-3 is the second configuration in which the ± 64 KHz Doppler range is search in 1 ms at a Doppler resolution of 1 KHz. The performance specifications for this configuration are listed in Table IV-4, and will be compared from a hardware implementation standpoint with the best performance characteristics obtainable from alternate type Doppler processor configurations.

The parallel search/RAM memory configuration has the disadvantage of requiring a complete redesign of the MMT Doppler processor. This basic requirement results from the utilization of the parallel processing technique discussed above, and from the use of RAM memories instead of MOS type memories. In conclusion, the parallel search/RAM memory configuration offers very reasonable performance specifications at an overall total cost of approximately 26% more hardware than the MMT Doppler processor.

Table IV-3. Parallel Search/RAM Memory Doppler Processor Configurations

Doppler Range	Resolution	Search Time	Process Time	Sample Time	Memory Clock Frequency	Process Positive and Negative Doppler Range Simultaneously
± 64 KHz	.5 KHz	2 ms	2 ms	2 ms	16.384 MHz	Yes
± 64 KHz	1 KHz	1 ms	1 ms	1 ms	8.192 MHz	Yes
± 64 KHz	2 KHz	1/2 ms	1/2 ms	1/2 ms	4.096 MHz	Yes
± 64 KHz	4 KHz	1/4 ms	1/4 ms	1/4 ms	2.048 MHz	Yes

RECOMMENDED DOPPLER CONFIGURATION

The recommended Doppler processor configuration for use in the TDRSS Telecommunication System is the parallel search/RAM memory implementation. Table IV-4 is a comparison of the characteristics for each of the three Doppler processor configuration types analyzed. The most reasonable performance specification of 1 ms search time and 1 KHz Doppler resolution is listed in Table IV-4 for each configuration type. As can be seen by observing Table IV-4, the parallel search/RAM memory configuration requires less hardware than the other two types of configurations.

The serial search/MOS memory configuration has not been recommended for use in the Telecommunication System because of the additional hardware needed, and the potential interface problems that could be created in the carrier and clock tracking loops as a result of doing four frequency sweeps to cover the full Doppler range of ± 64 KHz. In addition, the use of the MOS memory in both the serial search and parallel search configurations has the effect of limiting the various overall performance specifications attainable with each configuration. The parallel search/MOS memory configuration has not been recommended for use in the Telecommunication System because of the excessive amount of additional hardware required for both the Doppler processor and the I and Q channels.

The parallel search/RAM memory configuration uses the least amount of hardware and offers the best overall performance characteristics. In addition, there are no potential problems associated with interfacing this configuration with the carrier or clock tracking loops since the Doppler can be located in one frequency sweep. Finally, since this configuration utilizes a RAM memory which can operate at clock speeds up to 20 MHz, a broader selection of reasonable performance specifications can be attained.

The sample time and process time equations for the case of 1 ms search time and 1 KHz resolution are as follows:

$$\text{Sample Time} = \frac{\text{No. of Samples}}{\text{Sampling Clock}} = \frac{128 \text{ samples}}{128 \text{ KHz}} = 1 \text{ ms} \quad (27)$$

$$\text{Process Time} = \frac{\text{No. of Windows} \times \text{Memory Length}}{\text{Memory Clock}} = \frac{(64)(128)}{8.129 \text{ MHz}} = 1 \text{ ms} \quad (28)$$

Table IV-4. Doppler Processor Configurations having Best Performance Characteristics and Candidates for Analysis

Serial Search/MOS Memory Doppler Processor Configuration	Parallel Search/MOS Memory Doppler Processor Configuration	Parallel Search/RAM Memory Doppler Processor Configuration
Doppler Range: <u>±16</u> KHz	Doppler Range: <u>±32</u> KHz	Doppler Range: <u>±64</u> KHz
Resolution: 1 KHz Search Time: 1 ms	Resolution: 1 KHz Search Time: 1 ms	Resolution: 1 KHz Search Time: 1 ms
Process Positive and Negative Doppler Range Simultaneously	Process Positive and Negative Doppler Range Simultaneously	Process Positive and Negative Doppler Range Simultaneously
No. of Frequency Sweeps: Four	No. Doppler Processors in Parallel: Two	Memory Clock Frequency: 8.192 MHz
Process Time: 1 ms Sample Time: 1 ms	Process Time: 1 ms Sample Time: 1 ms	Process Time: 1 ms Sample Time: 1 ms
Amount of Hardware: 35% more than the MMT Doppler Processor	Amount of Hardware: 95% more than the MMT Doppler Processor	Amount of Hardware: 26% more than the MMT Doppler Processor

The parallel search/RAM memory implementation offers another distinct advantage of utilizing a commonality of hardware. The configuration incorporates 12 RAMs, 4 ROMs, 4 multipliers, 6 accumulators and 6 digital summers. Table IV-5 presents a hardware implementation comparison for the TDRSS MMT Doppler processor and the TDRSS Telecommunication System Doppler processor. The proposed Doppler processor will require approximately 195 ICs to implement which represents only about 26% more hardware than the MMT Doppler processor. The additional 26% more hardware for the new Doppler processor will result in four times better performance specifications since the Telecommunication System Doppler processor covers 4 times the Doppler range than the MMT Doppler processor (as shown in Table IV-5).

Table IV-5. Hardware Implementation Comparison For Doppler Processors

Module Description	Present Doppler Processor for TDRSS Multimode Transponder Program	Proposed Doppler Processor for TDRSS Telecommunication System
	Performance Spec. +16 KHz at 1 KHz in 1 ms	Performance Spec. +64 KHz at 1 KHz in 1 ms
Doppler Processor Input Interface (DPII)	25 ICs (plus approximately 100 passive components)	30 ICs
Doppler Processor Arithmetic Logic (DPAL)	36 ICs	70 ICs
Doppler Processor Control Logic (DPCL)	55 ICs	50 ICs
Doppler Processor Output Interface (DPOI)	40 ICs	45 ICs
Total Quantity of ICs	155 ICs	195 ICs

APPENDIX V

FFT DOPPLER PROCESSOR IMPLEMENTATION

INTRODUCTION

It is well known that the optimum detector for a sinusoid pulse of known frequency accompanied by additive Gaussian noise is a matched filter. When the pulse duration is T seconds and the frequency uncertainty is less than T^{-1} Hz, the matched filter will detect the sinusoid pulse with a small loss in efficiency. However, when the frequency uncertainty is greater than T^{-1} Hz, it becomes necessary to use multiple filters spaced T^{-1} Hz apart. This filter bank is referred to as a Doppler processor in this report.

Consider the sinusoid pulse

$$S(t) = \begin{cases} \sqrt{2C} \cos[(\omega_c + \omega_d)t + \theta], & 0 \leq t \leq T \\ 0 & \text{elsewhere} \end{cases}$$

where ω_c is the nominal center frequency and ω_d is the unknown frequency offset constrained to the interval $|\omega_d| \leq 2\pi W$. The pulse is accompanied by additive white Gaussian noise with one-sided spectral density N_o . The pulse is detected with a bank of $N = 2WT \gg 1$ matched filters spaced T^{-1} Hz apart across the $2W$ uncertainty band. The k th matched filter may be mathematically described by

$$Z_k = \left| \int_0^T r(t) e^{-j\omega_c t} e^{-j(kN\Omega/T)t} dt \right|^2, \quad k = -N/2 + 1, \dots, N/2$$

where $\Omega = 2\pi/N$ and $r(t)$ is the received pulse plus noise.

Suppose a sinusoid matched to the k th filter and with amplitude $\sqrt{2C}$ is applied to the processor input. The output is given by

$$Z_k \Big|_{\text{signal } k} = CT^2/2.$$

If noise with spectral density N_o is applied to the input, the expected output is

$$\overline{Z_k} \Big|_{\text{noise only}} = N_o T/2.$$

The output signal-to-noise ratio is taken to be the ratio of Z_k to $\overline{Z_k}$, i.e.,

$$\text{SNR}_o \equiv \frac{Z_k \Big|_{\text{signal } k}}{Z_k \Big|_{\text{noise}}} = N \frac{C}{2N_o W} = N \cdot \text{SNR};$$

which shows that the detection efficiency increases with N . The ratio of output to input signal-to-noise ratios is called the processing gain and is theoretically equal to N .

When N is large, a digital implementation of the matched filter becomes more economical. This is done by sampling the received signal every $T_s = T/N$ seconds and computing

$$Z_k = \left| \sum_{i=0}^{N-1} r(iT_s) e^{-j(i\omega_c T_s)} e^{-j(ki\Omega)} \right|^2, \quad k = -N/2 + 1, \dots, N/2.$$

In order to satisfy the Nyquist rate requirement, the received signal must be filtered to be within a band $2W$ Hz wide. It may be necessary to overspecify W in order to practically meet this requirement. In addition, it will be shown that it is advantageous to choose N to be a power of two. Such a digital implementation has been built for the TDRSS multimode transponder.

The processor was mechanized as is shown in Figure 1. The received signal is converted to baseband and N samples of $I(i)$ and $Q(i)$ are stored, where

$$I(i) = \text{Re} \left[r(iT_s) e^{-j i \omega_c T_s} \right] = r(iT_s) \cos(i\omega_c T_s)$$

and

$$Q(i) = \text{Im} \left[r(iT_s) e^{-j i \omega_c T_s} \right] = r(iT_s) \sin(i\omega_c T_s).$$

The power in each component, Z_k , is then computed using a sine/cosine lookup table by

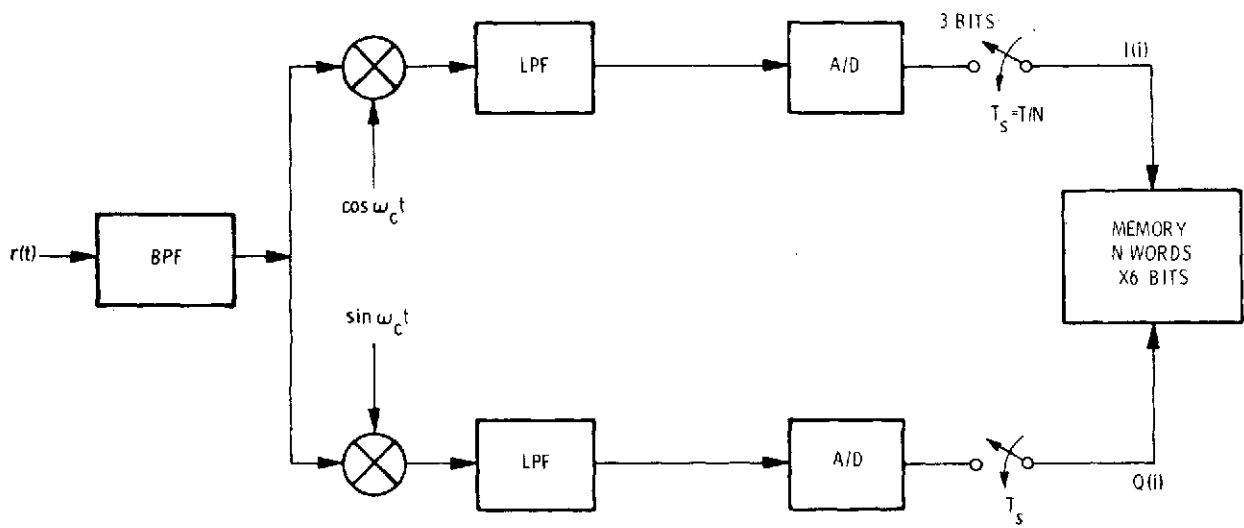
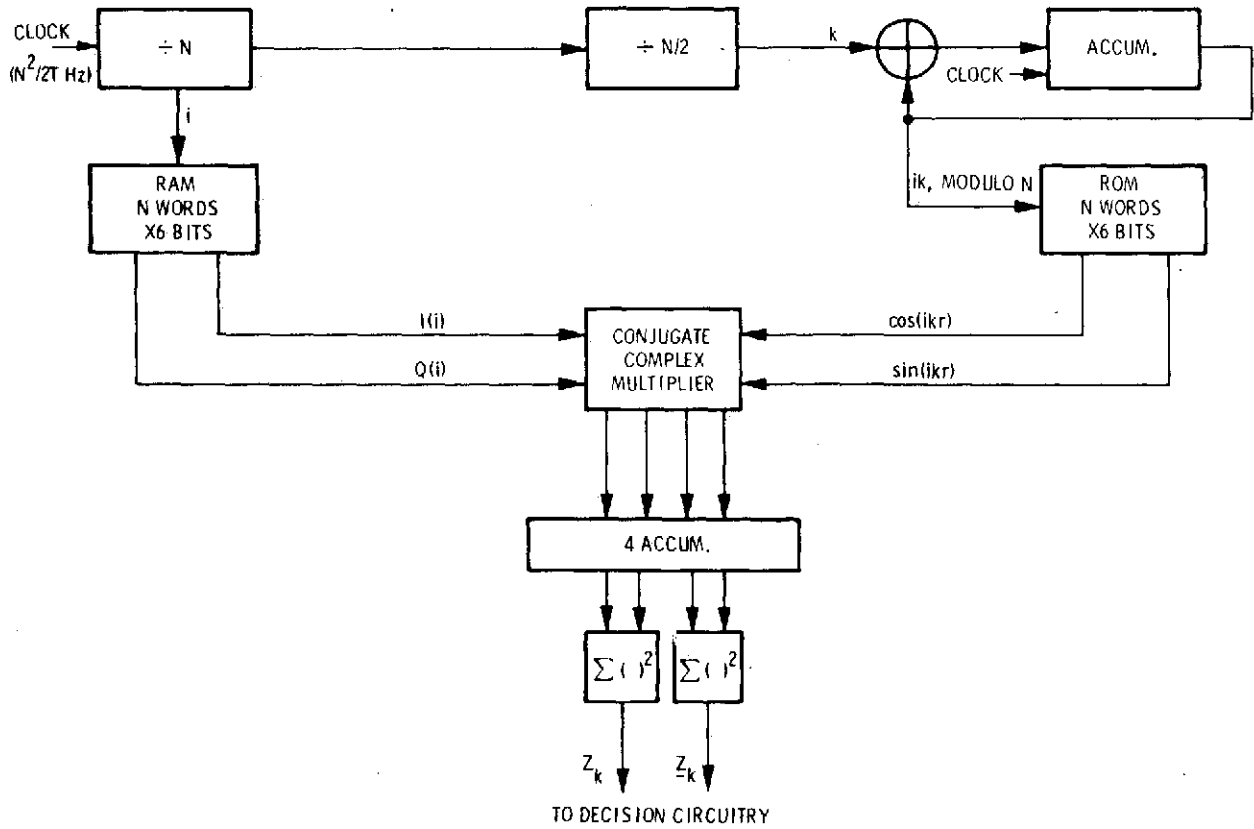


Figure 1a. Block Diagram - Loading Section



674-2135
UNCLASSIFIED

Figure 1b. Block Diagram - DFT Processor Section

$$Z_k = \left[\sum_{i=0}^{N-1} I(i) \cos(ik\Omega) + Q(i) \sin(ik\Omega) \right]^2$$

$$+ \left[\sum_{i=0}^{N-1} Q(i) \cos(ik\Omega) - I(i) \sin(ik\Omega) \right]^2.$$

The processing is completed by comparing the largest component to a decision threshold to determine signal presence. Since N complex multiplications must be performed to compute each of the N coefficients, there are N^2 complex multiplications required to process an entire set of samples. This can be reduced to $N^2/2$ by computing positive and negative frequency coefficients simultaneously by noting that

$$Z_{\pm k} = \left[\sum_{i=0}^{N-1} I(i) \cos(ik\Omega) \pm Q(i) \sin(ik\Omega) \right]^2$$

$$+ \left[\sum_{i=0}^{N-1} Q(i) \cos(ik\Omega) \mp I(i) \sin(ik\Omega) \right]^2.$$

In general, $N^2/2$ complex multiplications must be done before N new samples arrive, thus requiring each complex multiplication to be performed in $2T/N^2$ seconds.

When T is small and N is large, it becomes necessary to examine the feasibility of using fast Fourier transform (FFT) algorithms.

FFT ALGORITHM

The fast Fourier transform (FFT) is a method for efficiently computing the discrete Fourier transform (DFT) of a sequence of samples. The DFT of a sequence of N samples, $f(i)$, $0 \leq i \leq N - 1$ is defined to be

$$F_k = \sum_{i=0}^{N-1} f(i) W^{ik}, \quad k = 0, 1, \dots, N - 1$$

where

$$W = e^{-j2\pi/N}.$$

It is easy to show that F_k is periodic so that $F_{-k} = F_{N-k}$.

If N is divisible by 2, the time sequence may be separated into two subsequences: g_i , composed of the even indexed samples, and h_i , composed of the odd indexed samples (thus, the name decimation in time). The two subsequences

$$g_i = f(2i)$$

$$h_i = (2i+1) \quad i = 0, 1, \dots, N-1$$

have DFTs which may be written

$$G_k = \sum_{i=0}^{N/2-1} g_i W^{2ik}$$

$$H_k = \sum_{i=0}^{N/2-1} h_i W^{2ik}.$$

The DFT of the entire sequence may not be written in terms of g_i and h_i as

$$\begin{aligned} F_k &= \sum_{i=0}^{N/2-1} \left(g_i W^{2ik} + h_i W^{(2i+1)k} \right) \\ &= G_k + W^k H_k \end{aligned}$$

Since G_k and H_k have a period $N/2$, F_k may be expressed equivalently as

$$F_k = G_k + W^k H_k \quad 0 \leq k \leq N/2 - 1$$

$$= G_{k+N/2} - W^{k+N/2} H_{k+N/2} \quad -N/2 \leq k < 0.$$

Notice that only $N/2$ complex multiplications are required. If $N/2$ is also divisible by 2, g_i and h_i may also be decimated in time and a similar reduced form for G_k and H_k may be found. Finally, if N is a power of two, the entire DFT may be performed in only $\log_2 N$ steps each requiring $N/2$ complex multiplications. Consequently the FFT is $N/\log_2 N$ times faster than a conventional DFT algorithm.

Figure 2 flowcharts the FFT algorithm and Figure 3 shows the signal flow for $N = 8$ points. Each mode represents the addition of two previous samples where one has been rotated as indicated. Arithmetic operations are performed on the samples two at a time with the results replaced in the same memory locations so that additional memory is not required. The input sequence is required to be shuffled by reversing the bits of the time indexing. Conversely, if the input sequence is not shuffled, the output sequence index will be bit reversed.

TDRSS DOPPLER PROCESSOR

The TDRSS Doppler processor is required (TSA-FVD-09) to search a frequency uncertainty of 128 KHz with 1 KHz resolution. This results in the parameters $W = 64$ KHz, $T = 10^{-3}$ sec, and $N = 128$.

An FFT implementation of the Doppler processor is block diagrammed in Figure 4. The sampler/memory-loader is the same as the DFT except the address of each sample is bit reversed. Although 3 bits quantization of the input is sufficient, 9 bits of memory is required to accommodate the iterated arithmetic results. Although both sine/cosine look-up tables were the same size, 16 words x 6 bits, the same values were not used in the FFT table as in the DFT table. It was found by computer simulation that the values tabulated in Figure 5 worked best for their respective processor.

The algorithm is controlled by the countdown chain and the memory-indexing logic. Four clock times are required for each recursion of I, J, and L (see Figure 2). For each recursion, the four operations to be performed are:

- a. load $I(LJ)$ and $Q(LJ)$ into temporary storage $X1$,
- b. load $I(IJL)$ and $Q(IJL)$ into temporary storage $X2$,
- c. store the addition result in $I(LJ)$ and $Q(LJ)$, and
- d. store the subtraction result in $I(IJL)$ and $Q(IJL)$.

The required clock rate must therefore be greater than $4(N \log_2 N/2T) = 650$ KHz.

After completion of the FFT, the power in each component must be computed and the largest one selected. This is not shown since it is independent of the FFT algorithm and is essentially the same as is used with the DFT processor.

RESULTS

Although the FFT is much faster than the conventional DFT, its sensitivity to quantization effects is not as predictable. In order to determine the extent of loss of detectability, the DFT and FFT processors were computer simulated as they are shown in Figures 1 and 4 respectively.

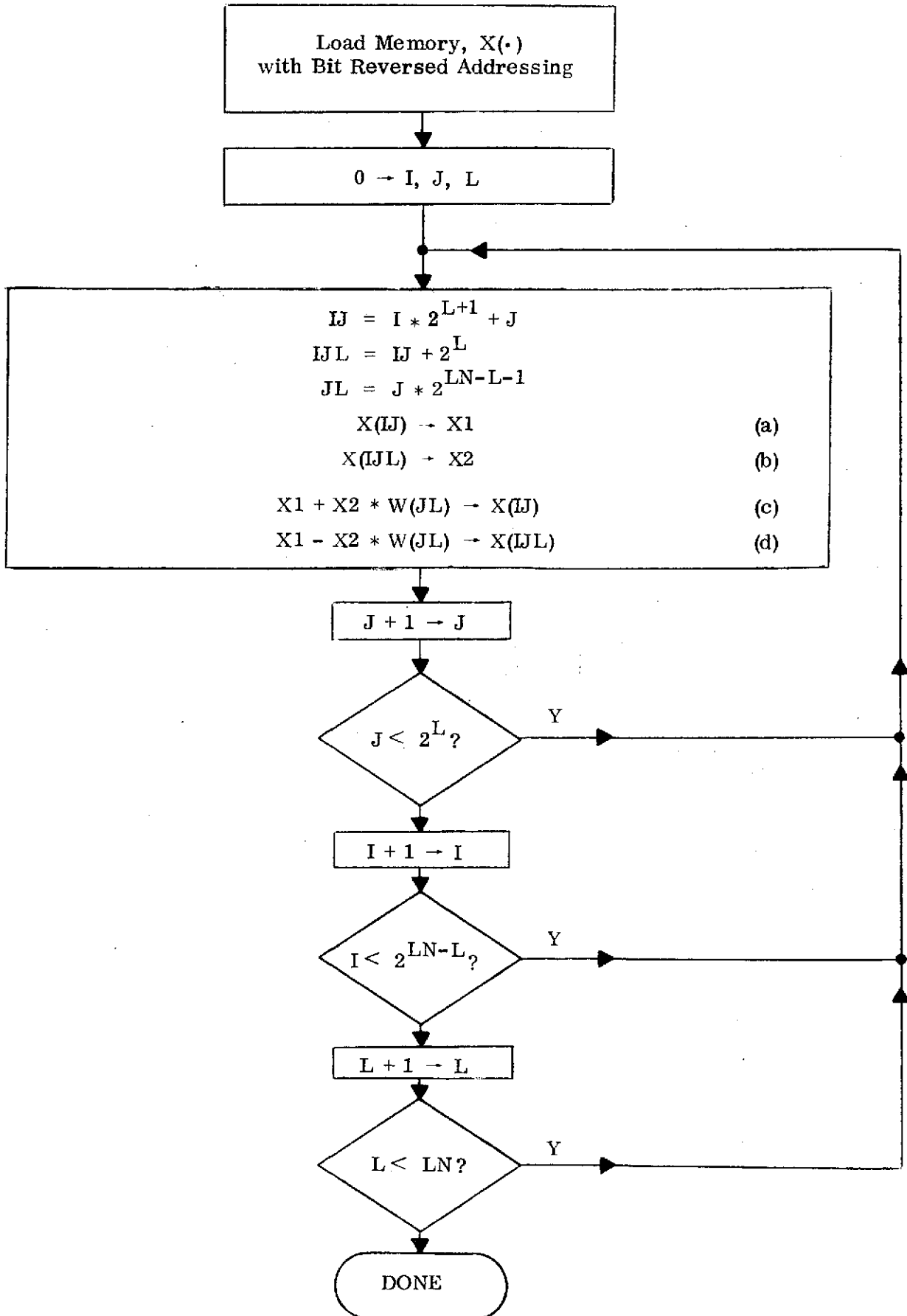


Figure 2. FFT Program Flow Diagram (Decimation in time, bit reversed input). X is the complex memory array and W is the complex rotation coefficients. $LN = \log_2 N$.

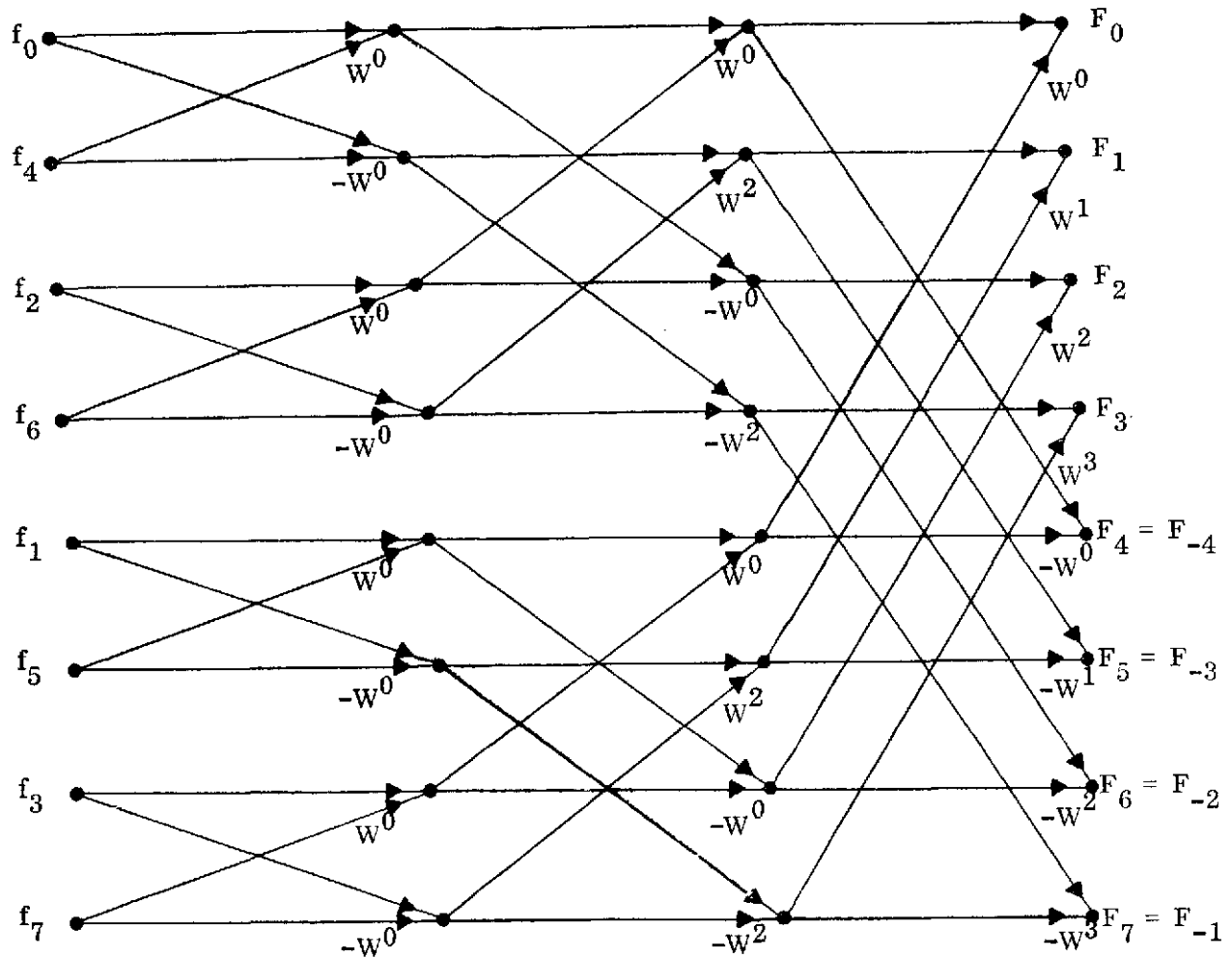
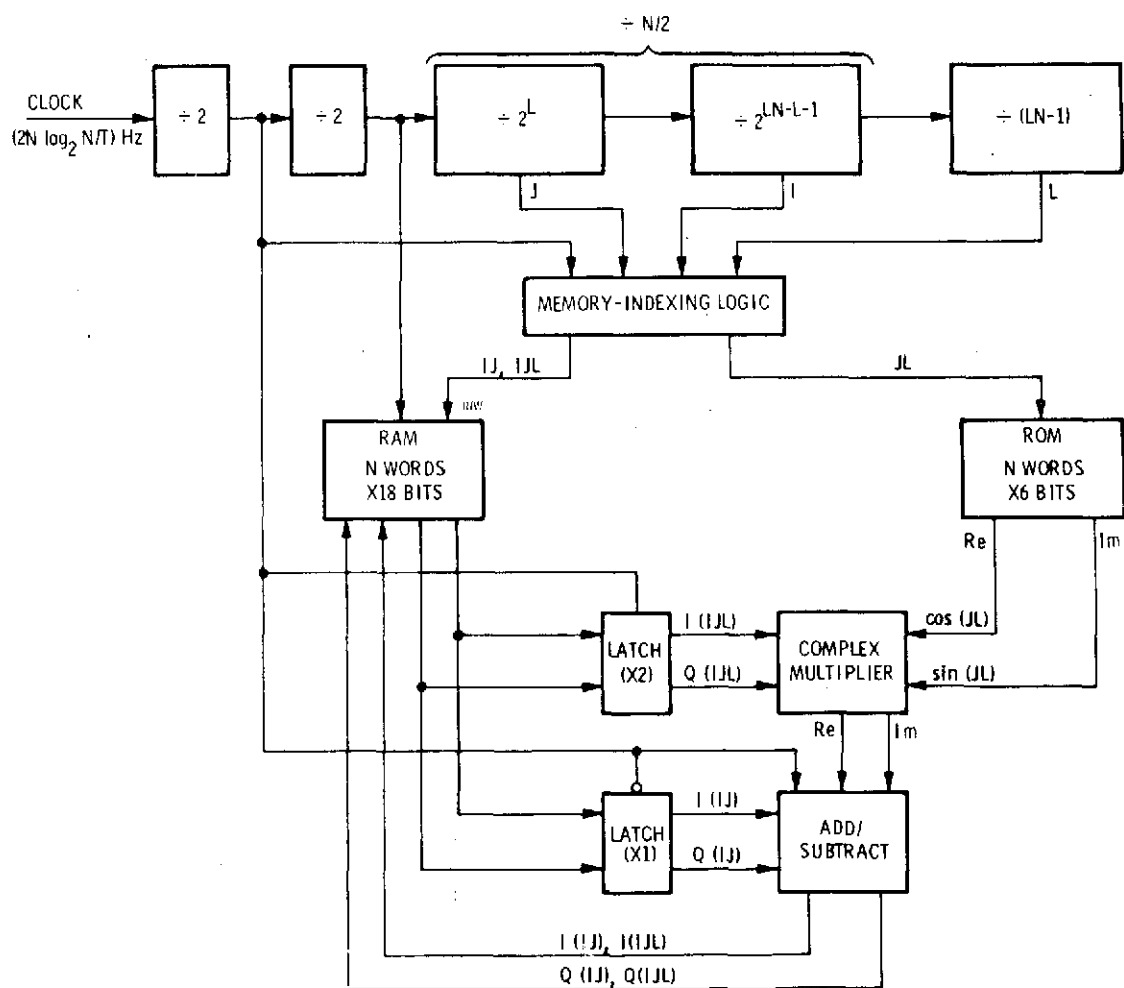


Figure 3. Eight-Point FFT Signal Flow Diagram (Decimation in Time). The inputs are required to be in bit reversed order.



674-2136
UNCLASSIFIED

Figure 4. Block Diagram - FFT Processor

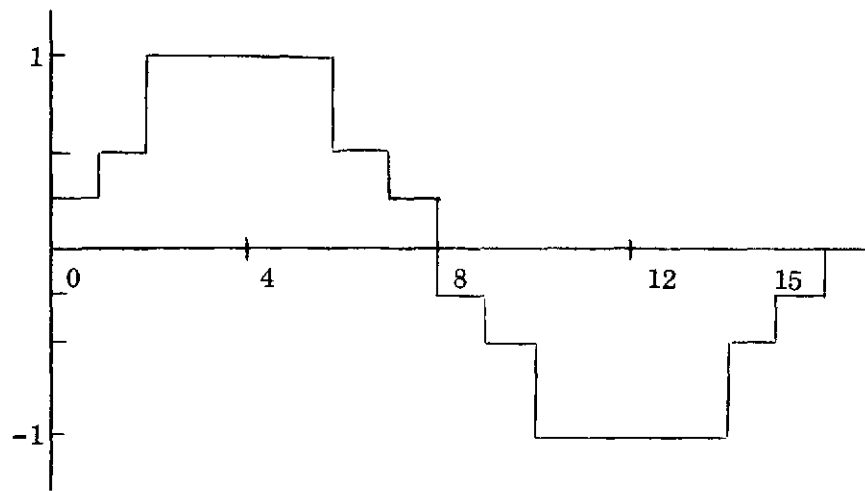


Figure 5a. Sine Table Used in DFT Processor.

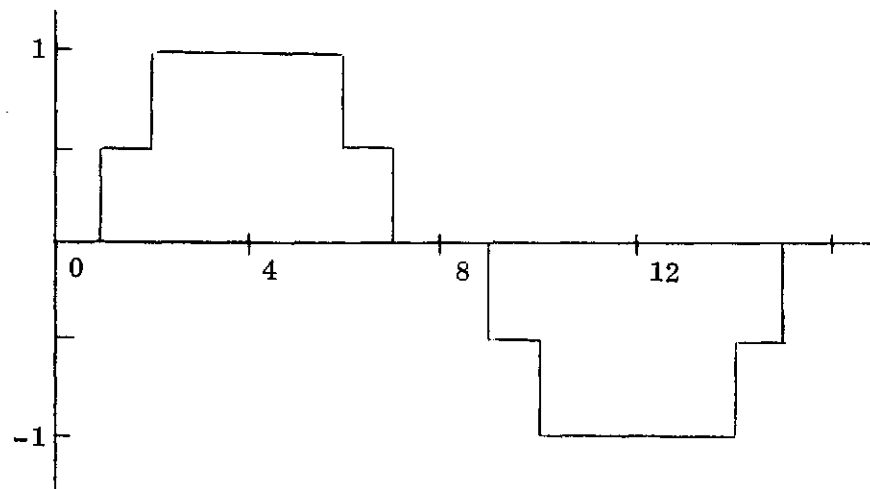


Figure 5b. Sine Table Used in FFT Processor.

The noise at the input of the sampler was assumed to have constant expected power. The A/D quantizer spacing was chosen to equal $\sqrt{N_0} W$ volts. The signal power, C , was varied from 0 to $20 N_0 W$. The effective processing gain was computed using the formula

$$\text{Effective Proc. Gain} = \frac{P_{S+N} - P_N}{P_N}$$

where P_N is the average power measured to be in the k th component by the processor when noise only is present, and P_{S+N} is the average power measured to be in the k th component by the processor when noise and the k th signal are present.

Based upon an average of 100 simulation runs, the computed processing gains are plotted in Figure 6. As can be seen, there is little difference in the performance of the DFT and FFT algorithms. Note that for both algorithms, the processing gain is reduced for large signal levels since the A/D quantizer is saturating. Furthermore, the output can be expected to have harmonic responses when the quantizer saturates.

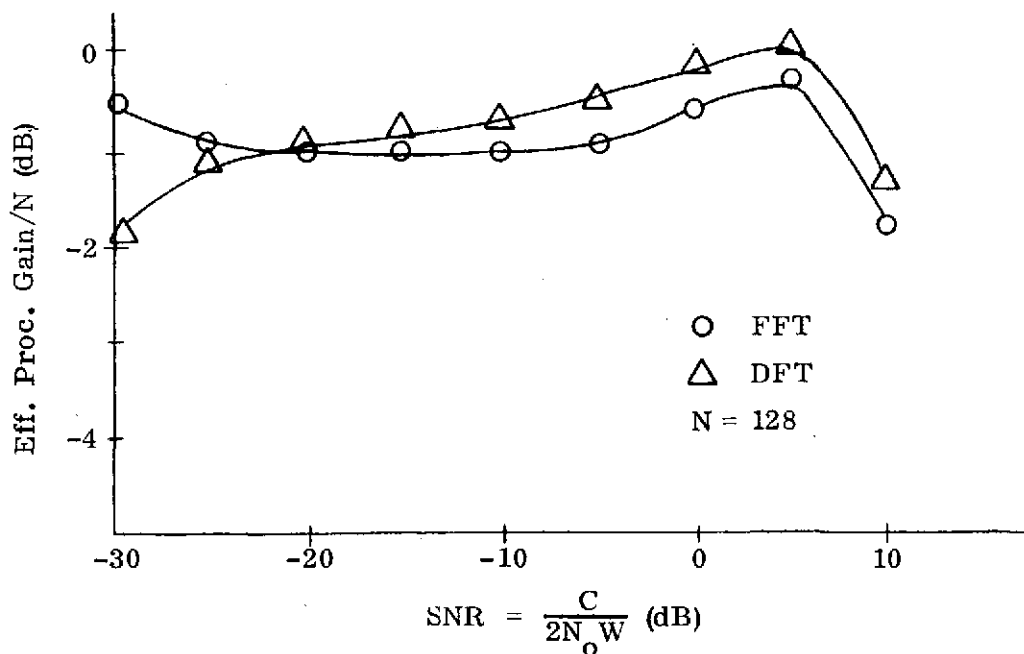


Figure 6. Degradation in Processing Gain for 3 Bit Quantization of Input and Look-Up Table Coefficients. Averaged of 100 Monte Carlo Simulations.

CONCLUSIONS

An FFT implementation of a Doppler processor was described. The FFT was shown to be $N/\log_2 N$ faster than a DFT implementation. Moreover quantization effects were shown to be essentially equivalent.

APPENDIX VI

EIRP MONITORING FOR MULTIPLE ACCESS S-BAND USERS

INTRODUCTION

Let us consider the high data rate users for the MA S-band system. The multiplicity of co-channel users, in conjunction with the near-far disadvantage a user may have, can contribute to the jamming of a high rate user. In an attempt to alleviate the problem, we propose a method whereby the EIRP can be monitored via the behavior of the Viterbi decoder. If the indication shows that a user cannot sustain a given BER (say 10^{-5}), he can be directed to increase his EIRP by 3 dB. If, on the other hand, the indication shows that a user can sustain a 3 dB reduction in his EIRP and retain a 10^{-5} (say) BER, he can be directed to reduce his power and alleviate the interference to other users.

DECISION METRIC

The Viterbi decoder measures for each state a metric which is indicative of the number of errors which must be hypothesized in order to reconcile the sequence of bits assumed to lead the decoder to that state and the received sequence. The decoder attempts to decide on the sequence of states (and therefore on information bits) which minimize that metric. Typically, the metric increments have nonnegative values. For the sake of implementation the metrics must, therefore, be reset to keep their value within the number of bits in the registers allocated to them. A practical metric storage element in a Viterbi decoder is a four-bit register. Since the relative values of the metrics are important, the following scheme is used. The metrics are clamped at 15, as if it were an absorbing barrier. If all metrics reach the value of 4 or above, they are all reset by the value 4. The monitoring of the channel can most conveniently be performed by monitoring the rate of these resets.

Figure 1 shows the probability of a reset at each step of the decoder; i.e., per decoded bit.

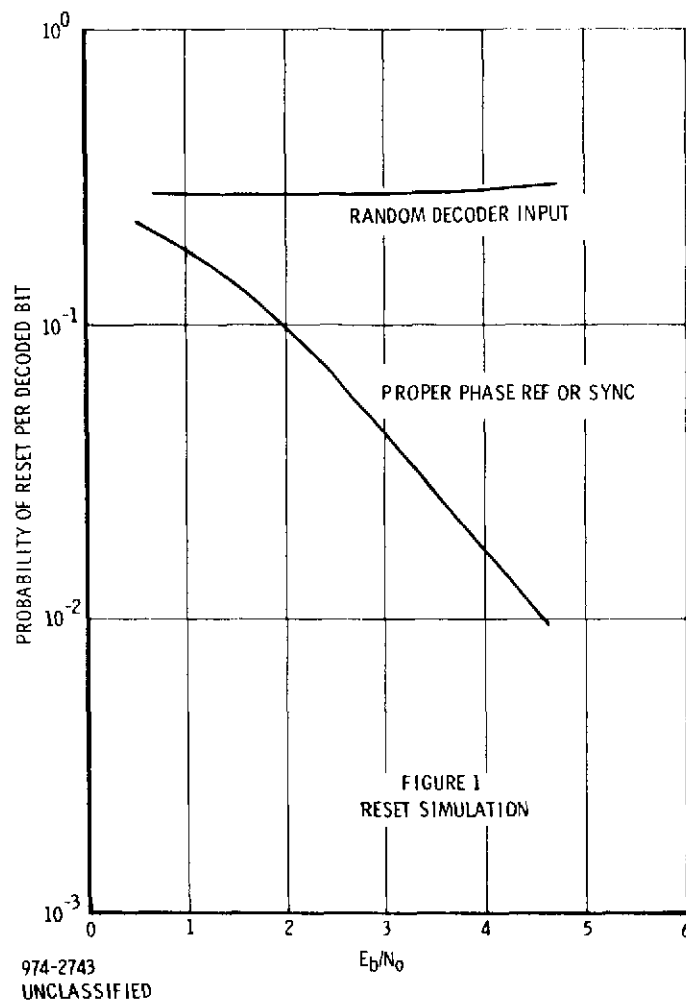


Figure 1. Reset Simulation

Let us assume that the required SNR for proper communication is $E_b/N_o = 5$ dB ($< 10^{-5}$ BER). If steps can be taken to change the EIRP by 3 dB, then we must establish the following measurements.

- Is estimated $E_b/N_o > 8$ dB (command a -3 dB step)?
- Is estimated $2 \text{ dB} < E_b/N_o < 5 \text{ dB}$ (command a +3 dB step)?
- Is estimated $E_b/N_o < 2 \text{ dB}$ (user may command a +3 dB step but this is an indication that it will not be enough and he may wish to repeat the process, or other problems exist)?

Table 1 shows the reset rate.

Table 1.

<u>E_b/N_o</u>	<u>Reset Rate per Bit</u>
2 dB	0.1
5 dB	0.008
8 dB	0.0004

Let us consider two counters: one to count the resets, the other to count the number of bits. Let the reset counter be 6 bits (maximum: 63) and the bit counter be a 16-bit counter (64K).

At 8 dB, the bit counter will reach overflow, at which time the test stops and the reset counter will have count C , such that

$$E[C] = 26$$

$$\sigma_C \approx 5$$

Thus, if we set a threshold T_1 three sigma points below mean; i.e., $T_1 = 11$, then with probability 2×10^{-3} , there will be an erroneous declaration that the EIRP can be reduced by 3 dB.

At 5 dB, $E[C] = 524$, which far exceeds the reset counter. In this case we can therefore look at the bit counter at the time the reset counter reaches overflow ($C = 64$). Let n = bit count on which this occurs, and let us determine the mean and variance of the bit count on which the reset count will reach overflow at 64.

Let $z_i = 1$ if a reset occurs and 0 if it does not at time i . We define

$$g(\xi) \triangleq E[e^{\xi}]$$

where ξ is a random variable with the same probability density function as any of the z_i . Let

$$D_n = \sum_{i=1}^n z_i$$

where n is the smallest integer such that D_n exceeds the reset counter size (63 in our case).

Consider now the fundamental identity^[1]

$$E\left\{e^{D_n \xi} [g(\xi)]^{-n}\right\} = 1$$

Differentiating with respect to ξ at $\xi = 0$

$$E\left[D_n e^{D_n \xi} [g(\xi)]^{-n} - n[g(\xi)]^{-n-1} g'(\xi) e^{D_n \xi}\right]_{\xi=0} = 0$$

and since $g(0) = 1$ and $g'(0) = p$

$$E[D_n] = \frac{D_n}{p} = \frac{64}{p}$$

Similarly, we compute the variance by differentiating the fundamental identity twice at $\xi = 0$.

$$\begin{aligned} & E\left\{D_n^2 e^{D_n \xi} [g(\xi)]^{-n} - nD_n e^{D_n \xi} [g(\xi)]^{-n-1} g'(\xi) - n(n-1) [g(\xi)]^{-n-2} g'(\xi) e^{D_n \xi} \right. \\ & \quad \left. - n[g(\xi)]^{-n-1} g''(\xi) e^{D_n \xi} - n[g(\xi)]^{-n-1} g'(\xi) D_n e^{D_n \xi}\right\}_{\xi=0} \\ &= E\left\{[D_n - n \frac{g'(\xi)}{g(\xi)}]^2 - \frac{ng''(\xi)g(\xi) - n[g'(\xi)]^2}{[g(\xi)]^2}\right\}_{\xi=0} \end{aligned}$$

But

$$g(0) = 1$$

$$g'(0) = p$$

$$g''(0) = pq + p^2 = p$$

$$E(D_n) = 64$$

Hence

$$\sigma_n^2 = \overline{n^2} - \overline{n}^2 = \frac{64(1-p)}{p^2}$$

For 5 dB,

$$E[n] = \frac{64}{7 \times 10^{-3}} = 9143$$

and

$$\sigma_n = 1139$$

This, if we set a threshold T_2 on the bit count to reset count to 5000, the probability is less than 2×10^{-3} that T_2 will not be exceeded if the signal-to-noise ratio is less than 5 dB.

At 2 dB, the expected value of the length of the test is

$$\bar{n} = \frac{64}{0.1} = 640$$

with standard deviation

$$\sigma_n = \left[\frac{64(0.9)}{0.012} \right]^{1/2} \simeq 76$$

Thus, if T_3 is set at 863, the probability is 2×10^{-3} that the threshold will be exceeded when the SNR is greater than 2 dB.

Figure 2 illustrates these results.

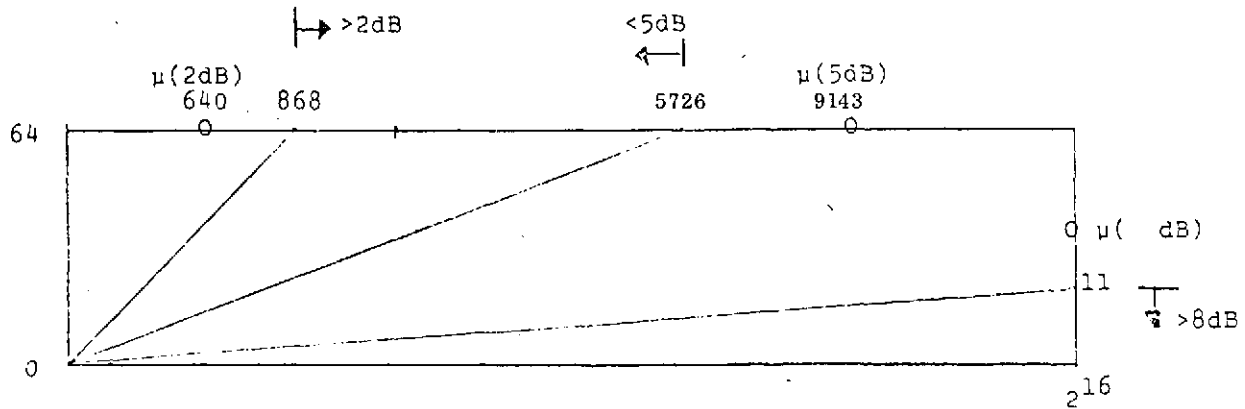


Figure 2. EIRP Monitor Example

The standard deviation in dB is measured as the increment or decrement in the SNR to obtain a mean count one σ away from the nominal mean. For instance, the SNR required for $\bar{n} = 640 + 76 = 716$ is obtained by computing p ; i.e., 0.089 and from Figure 1, $\sigma_{dB} = 0.5$ dB. If the counter size is increased to 256, the standard deviation is reduced to 0.15 dB.

REFERENCE

1. Fisz, M., "Probability Theory and Mathematical Statistics", John Wiley and Sons, New York, 1963, Chapter 17.

APPENDIX VII
SIMULATION OF MULTIPLE ACCESS WITH COHERENT FH

INTRODUCTION

Coherent frequency hopping (FH) is theoretically advantageous, compared with PN, for enabling a high rate, high EIRP user to coexist with a low rate user in a multiple access channel. We present here computer simulation results of the postulated system model, in which a single high rate, high EIRP user interferes with a low EIRP user. Gaussian receiver noise is included in the simulation, which measures signal-to-noise ratio at the demodulation output.

SYSTEM MODEL

It is assumed that perfect synchronization exists in the receiver for the desired signal; thus, the hopping has been correctly stripped off the desired signal. The interfering signal is assumed to be hopping randomly over the total spread bandwidth with ideal rectangular pulses. Figure 1 shows the system model to be simulated. Use of complex quantities creates a bandpass representation about an arbitrary center frequency, and the receiver noise is represented by two-dimensional independent Gaussian samples generated at the sampling rate of the simulation. The desired signal is at zero phase, centered in the band, while the interfering signal is randomly hopped in frequency with a uniform distribution.

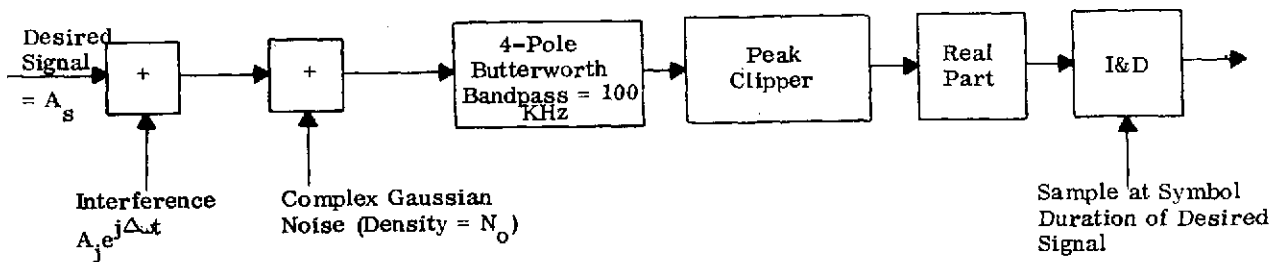


Figure 1. Simulation Model

The sum of desired signal, interfering signal, and Gaussian noise is passed through a bandpass filter, chosen to approximate a 4-pole Butterworth symmetrical transfer function. The 3- dB half bandwidth is 50 KHz, yielding a bandpass of 100 KHz. The output of the filter is peak clipped without any phase distortion, according to the envelope transfer function of Figure 2. The output of the peak clipper is coherently demodulated by taking the real part, which is summed over the symbol duration of the desired signal by an integrate-and-dump process. This is done repetitively for many symbols. A short time for transient decay is allowed prior to the start of each symbol.

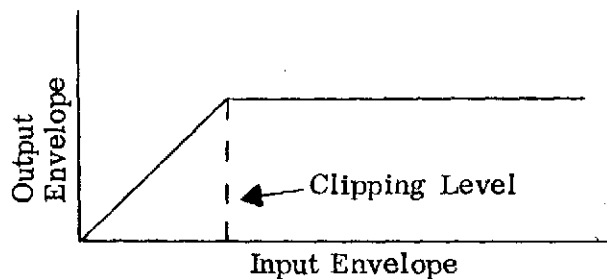


Figure 2. Envelope Transfer Function Of Peak Clipper

The sample mean and variance are computed for the output of the integrate-and-dump, and an output signal-to-noise ratio (mean squared/variance) is also computed.

Since Doppler causes the interference to have an arbitrary frequency offset, the averaging was done for a continuous distribution of frequency offset rather than a discrete. Also, the clock of the hopping on the interference is randomized relative to the start of each symbol.

SIMULATION RESULTS

The high rate interfering user has an EIRP of 35 dBw as previously discussed. This signal has the characteristics

$$[\text{S}/\text{N}]_{\text{interference}} = 20 \text{ dB in } 100 \text{ KHz}$$

$$\text{Interference hopping rate} = 100 \text{ Khops/sec}$$

$$\text{Hopping bandwidth} = 3 \text{ MHz}$$

The desired user has a much lower EIRP and symbol rate. In the interests of conserving computer time, the symbol duration of the desired signal was set equal to 100 microseconds, or 10 hops by the interfering signal.

For an ideal linear system without interference, the output signal-to-noise ratio after coherent demodulation is $2E_s/N_o$, and the validity of the simulation may be tested thereby. When the peak clipper is introduced, the output signal-to-noise ratio displays an apparent increase, depending on the signal-to-noise ratio at the clipping point; however, this does not imply a true performance improvement. This apparent increase has been computed for coherent demodulation after hard-limiting^[1]; nevertheless, probability of a decision error for biphase demodulation is degraded. Since the quadrature noise is not similarly suppressed by the clipping, an alternate measurement is based on the in-phase mean and the quadrature variance.

Typical simulation results are presented in Table I. Agreement with theory for the no clipping case is excellent in the absence of interference, although the quadrature noise is somewhat below theoretical. Note that the clipping reduces the mean desired amplitude, as is to be expected. Over the indicated range, of more than 3 dB, setting the clipping level does not appear to be critical, and the loss due to clipping is small. The degradation due to the interference may be estimated by comparing output signal-to-noise ratios when the interference is, respectively, absent and present; of course, this does not bring in effects due to a change in the output probability distribution. With the high EIRP interference present, note that the total degradation is roughly 3 dB, in agreement with the degradation predicted in Section 2.1.5.3.

S/N In 100 KHz		Clipping Level	Mean Desired Amplitude	Estimate of $2E_s/N_o$	
Interference	Desired			Symbol Duration = 100 μ sec	In-Phase
None	-3 dB	No Clipping	.994 (1.0 theory)	9.9 dB (10 dB theory)	11.5 dB
None	-3 dB	1.5	.733	10.6 dB	11.3 dB
20 dB	-3 dB	1.5	.606	7.2 dB	8.5 dB
20 dB	-3 dB	1.0	.531	10.7 dB	---
20 dB	-3 dB	1.0	.419	6.9 dB	---

Table I. Simulation Results, Average Over 100 Symbols

CONCLUSIONS

The computer simulation supports the analysis in Section 2.1.5.3 to evaluate the multiple access interference effects with coherent FH modulation. The simulation measures an output signal-to-noise ratio; however, there still may be further performance degradation associated with soft-decision error correction decoding, since the effects of the interference and the peak clipping tend to produce a non-Gaussian noise.

REFERENCE

1. W. C. Lindsey, *Synchronization Systems in Communication and Control*, Prentice-Hall, 1972, p. 195.

APPENDIX VIII
POSSIBILITY OF UNDESIRED MINOR CORRELATION PEAK WITH SQPN

INTRODUCTION

Staggered quadriphase PN (SQPN) is generated by biphasic modulating a pair of carriers in phase quadrature with two binary codes displaced by a half chip; i.e., if $a(t)$ and $b(t)$ denote the two codes (each chip is ± 1) with chip duration T_c , the SQPN waveform is

$$s(t) = a(t) \cos \omega_0 t + b(t - T_c/2) \sin \omega_0 t \quad (1)$$

The half chip displacement of the two binary codes is overtly shown in (1). The pair of codes can be distinct, such as two different members of a Gold family or two different maximal PN codes. Alternatively, $a(t)$ and $b(t)$ can be the same maximal PN code of period T (odd), with exactly a half period shift such that

$$b(t - T_c/2) = a(t - T/2) \quad (2)$$

Since T is odd, the requisite half chip displacement is necessarily introduced. It is easy to show that $s(t)$ given by (1) then has exactly the same autocorrelation function, and therefore spectrum, as the biphasic signal produced by $a(t)$ alone.

In a hardware sense, the relation (2) is automatically produced when the binary code generator (of odd period) is run at twice the desired chip rate and successive chips are alternately routed to $a(t)$ and $b(t)$. This generation scheme was employed in the computer program to obtain the spectra of paragraph 2.1, with $a(t)$ being generated as a maximal period binary PN code. However, when a computation was made for Appendix I of the autocorrelation of the SQPN signal after filtering and hard limiting, a minor correlation peak of amplitude about equal to 0.1 was observed at a location which depended on the particular maximal. A physical explanation has now been found for this unexpected phenomenon.

AM CAUSED BY FILTERING AND HARD LIMITING

The filter causes the abrupt code transitions of the ideal binary code to occur smoothly. With a symmetrical filter about the center frequency, there is no crosstalk between the $a(t)$ and $b(t)$ codes. Figure 1 shows the effects of filtering and then hard limiting, at a point in time where $b(t)$ has a transition. The significant effect is the amplitude modulation placed on $a(t)$ whenever $b(t)$ has a transition. (Similarly, transitions of $a(t)$ put AM on $b(t)$.) This AM is due to the hard limiter increasing gain as the filtered $b(t)$ becomes small in the middle of a transition, so as to hold a constant output envelope.

Thus, we observe that the AM on $a(t)$ occurs in accordance with the binary code corresponding to transitions in $b(t)$. Then, we can write.

$$a_f(t) \cong a(t) [1 + m b(t) b(t - T_c)] = a(t) + m a(t) b(t) b(t - T_c) \quad (3)$$

where a_f is the filtered and limited chip, and m denotes the AM index.

MINOR CORRELATION PEAK WHEN THE QUADRATURE CODES ARE DISPLACEMENTS OF THE SAME MAXIMAL

If $b(t)$ is a half period displacement of $a(t)$, as defined by (2), and $a(t)$ is a maximal PN code, we find from (3)

$$\begin{aligned} a_f(t) &\cong a(t) [1 + m a(t - [T + T_c]/2) a(t - [T - T_c]/2)] \\ &= a(t) [1 + m a(t - \alpha_1)] \\ &= a(t) + m a(t) a(t - \alpha_1) \\ &= a(t) + m a(t - \alpha_2) \end{aligned} \quad (4)$$

We have made use of the "shift and add" property of a maximal PN code*. The resulting shift α_2 depends on the particular maximal, and can be computed in a straightforward (but brute force) manner. Equation (4) leads to the conclusion that a minor correlation peak of magnitude proportional to m exists at the time shift α_2 .

*Note, multiplication of ± 1 codes is equivalent, mathematically to modulo-2 addition of 1, 0 codes.

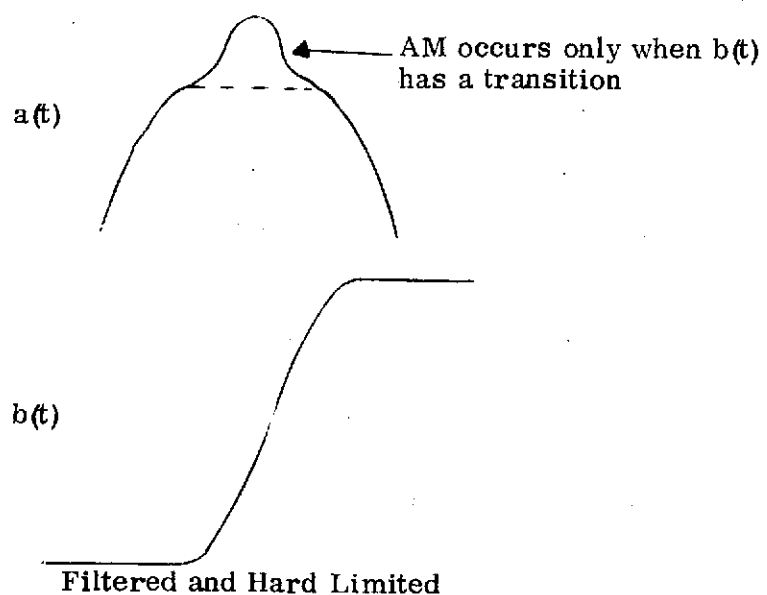
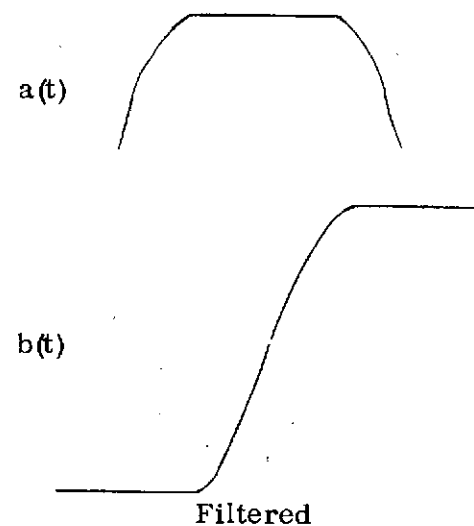
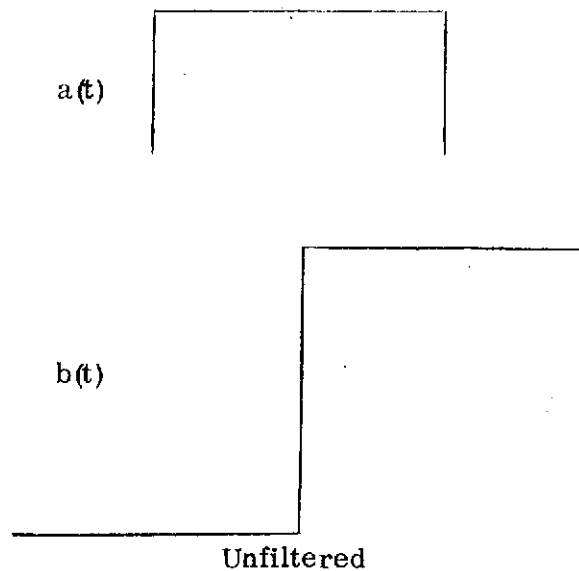


Figure 1. Effects of Filtering and Hard Limiting

Computations for codes of period 31 and 63 yielded minor correlation peaks at the predicted location specified by (4). The minor peaks were of the same amplitude for all 63 period codes but at different locations, and the minor peak for the code of period 31 was only slightly higher. Note that the theory of (4) predicts a minor correlation peak with a relative amplitude independent of code length. The peak is observed to be of 0.095 amplitude for a code period of 63 and a 6-pole Butterworth filter of bandpass bandwidth equal to 1.5 times the PN chip rate.

To illustrate by one numerical example, a 63 period maximal code is generated by the polynomial $x^6 + x + 1$. For this code, α_1 in (4) is $31 + 6 = 37$, and $\alpha_2 = 44$ (found by generating the sequence manually). Thus, a minor auto-correlation peak is expected at a displacement of 44 chips and at the symmetrical displacement $63 - 44 = 19$ chips. The computer result showed the minor peaks for this code at displacements of 43.8 and 19.2 chips.

USE OF A PAIR OF MAXIMALS

Let $a(t)$ and $b(t)$ be selected as different maximals with low cross-correlation (which is to be expected of long period codes). Using (3) gives

$$a(t) b(t) b(t - T_c) = a(t) b(t - \beta_1) \quad (5)$$

which never matches with $a(t)$ alone. Thus, there is no minor correlation peak except that inherent in the pair $a(t)$ and $b(t)$ itself.

USE OF GOLD FAMILY

If $a(t)$ and $b(t)$ are selected as a pair of codes from a Gold family formed by the maximal pair $x(t)$ and $y(t)$, we have

$$\begin{aligned} a(t) &= x(t) y(t - t_a) \\ b(t) &= x(t - t_o) y(t - t_o - t_b) \end{aligned} \quad (6)$$

where an arbitrary shift t_o has been put into $b(t)$. Code pair selection for a given user is by the pair of displacements t_a and t_b . Using (3), we find

$$\begin{aligned}
 a(t) b(t) b(t - T_c) &= x(t) x(t - t_o) x(t - t_o - T_c) \\
 &\cdot y(t - t_a) y(t - t_o - t_b) y(t - t_o - t_b - T_c) \\
 &= x(t - \alpha) y(t - \alpha - \beta)
 \end{aligned} \tag{7}$$

where the shift and add property of maximals has again been invoked. Note that α and β depend on the choice of t_o .

There will be a minor correlation peak if $\beta = t_a$, and this could possibly happen for some selection of t_a and t_b , with t_o fixed arbitrarily. However, by changing t_o for that user, the minor peak can be eliminated. Note that we must also reverse the roles of $a(t)$ and $b(t)$ in (3) and (7) in checking for the possible existence of a minor correlation peak.

There is the further problem for multiple access that β in (7) for one user might correspond to t_a or t_b selected for another user. In general, the likelihood of such excessive interference between different users is negligible because it can occur only for a particular time displacement somewhere within the relatively long code period.

CONCLUSIONS

SQPN when filtered and hard limited can display a minor correlation peak. Such a peak was observed of amplitude 0.1, in a short period code, and the physical explanation indicates no reduction in amplitude as the code period is increased. The best way of eliminating the effect is to generate the SQPN by a pair of maximal codes having a low crosscorrelation (which is normally the case anyway for long period maximal codes). Then, different users are addressed by assigning a distinct pair of maximals to each user.

Alternatively, a Gold family can be employed. A pair of codes from the family is assigned to each user; however, now there is the possibility of finding minor autocorrelation or crosscorrelation peaks.

APPENDIX IX

SOFT-DECISION DECODING FOR BIPHASE MODULATION FOR THE Ku-BAND RETURN LINK

INTRODUCTION

The Ku-band downlink channel in the TDRS contains hard limiting. The noise limited portion of the tandem, user-TDRS and TDRS-ground, link is the former. Thus at high data rate, above approximately one bit per hertz of the 88 or 225 MHz bandwidth, soft decisions at the input of the ground-based decoder may not provide the "soft decision" gain of Viterbi decoding usually claimed at 5.2 dB for the $R = 1/2$, $K = 7$ and 5.7 dB for the $R = 1/3$, $K = 7$ codes. These figures have been derived for the white Gaussian additive noise channel.

THE CHANNEL

Figure 1 illustrates a first order model of the channel under consideration. We assume for the purpose of this derivation that the noise and data bandwidths are comparable. We have simplified the model by assuming that the noise is introduced in the user to TDRS path. The stronger link to the ground is modelled as a noise-free channel. This restriction will be removed later when the Viterbi decoder performance is simulated to establish the exact coding gain in various contingencies.

For purposes of simplification, let us assume that the data signal corresponding to a period of the receiver's integrate-and-dump (I&D) is given by

$$s(t) = \sqrt{S} \cos(\omega_0 t + \omega)$$

where ω_0 is the carrier frequency and ω , the data modulation. Without loss of generality we can take $\omega = 0$ since our span of observation is one baud.

Similarly, the noise can be written in terms of its baseband components

$$n(t) = n_C(t) \cos \omega_0 t + n_S(t) \sin \omega_0 t$$

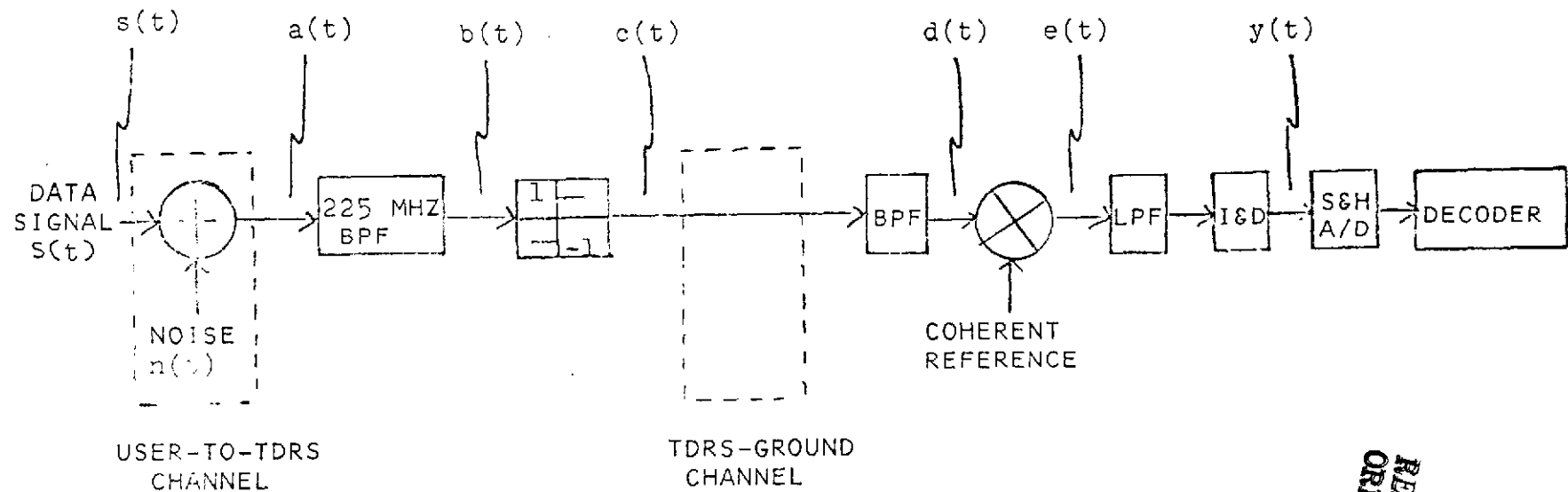


Figure 1. Hard Limiting Channel

REPRODUCIBILITY OF THE
ORIGINAL PAGE IS POOR

where $n_C(t)$ and $n_S(t)$ are independent Gaussian processes with an equivalent nominal baseband spectral occupancy of 112.5 MHz (W/2) for the 225 MHz passband application. Thus,

$$\begin{aligned}\overline{n(t)} &= \overline{n_C(t)} = \overline{n_S(t)} = 0 \\ \overline{n(t)^2} &= \overline{n_C^2(t)} = \overline{n_S^2(t)} = \sigma_n^2 = N_0 W\end{aligned}$$

We define the signal-to-noise ratio γ to be

$$\gamma = \frac{E[S^2(t)]}{E[n^2(t)]} = \frac{S}{2\sigma_n^2}$$

The signal $b(t)$ in Figure 1 can be written

$$b(t) = [\sqrt{S} + n_C(t)] \cos \omega_0 t + n_S(t) \sin \omega_0 t$$

or in polar form,

$$b(t) = [(\sqrt{S} + n_C(t))^2 + n_S^2(t)]^{1/2} \cos(\omega_0 t + \theta(t))$$

where

$$\theta(t) = \arctan \frac{n_S(t)}{\sqrt{S} + n_C(t)}$$

The output of the hard limiter can be written^[1]

$$c(t) = \frac{4}{\pi} \cos[\omega_0 t + \theta(t)] + \frac{4}{\pi} \left\{ \sum_{k=1}^{\infty} \frac{1}{2k+1} \cos[(2k+1)(\omega_0 t + \theta(t))] \right\}$$

The effect of the bandpass filter at the ground station (ref: Figure 1) eliminates the second term in the expression for $c(t)$; i.e.,

$$d(t) = \frac{4}{\pi} \cos[\omega_0 t + \theta(t)]$$

Demodulation and integrate-and-dump of the biphase data yield

$$\begin{aligned} y(t) &= \frac{4}{\pi} \int_0^T \cos[\omega_0 t + \theta(t)] \cos(\omega_0 t + \xi) dt \\ &= \frac{2T}{\pi} \{ \cos \xi \cos \theta(t) + \sin \xi \sin \theta(t) \} \end{aligned}$$

where ξ is the coherent reference phase error term.

We now take the particular simplification of $\xi = 0$; i.e., no error in the Costas loop, for instance. Thus,

$$y(t) \sim \tilde{y}(t) = \cos \theta(t)$$

Two important factors come into play. The first is the effect on the probability of error for a given signal-to-noise ratio. The second is the soft-decision measurement which led to the decision which the Viterbi decoder must use.

BIT ERROR RATE

Consider the signal space of Figure 2. Let r be the received test statistic if the hard limiter did not exist. Then,

$$d(t) = A(t) \cos[\omega_0 t + \theta(t)]$$

where $A(t)$ is the envelope of the process given by

$$A(t) = [(\sqrt{S} + n_C(t))^2 + n_S(t)^2]^{1/2}$$

Thus, after demodulation, filtering of the baseband signal and integration-and-dump, the nonlimited test statistic would be given by $z(t)$ where

$$\begin{aligned} z(t) &= A(t) \cos \theta(t) \\ &= A(t) \tilde{y}(t) \end{aligned}$$

Since $A(t)$ has no phase information, the decisions based on $z(t)$ and $\tilde{y}(t)$ must be identical. Therefore, the BERs remain unchanged when the hard limiter is introduced, at least within the first order analysis of the previous section.

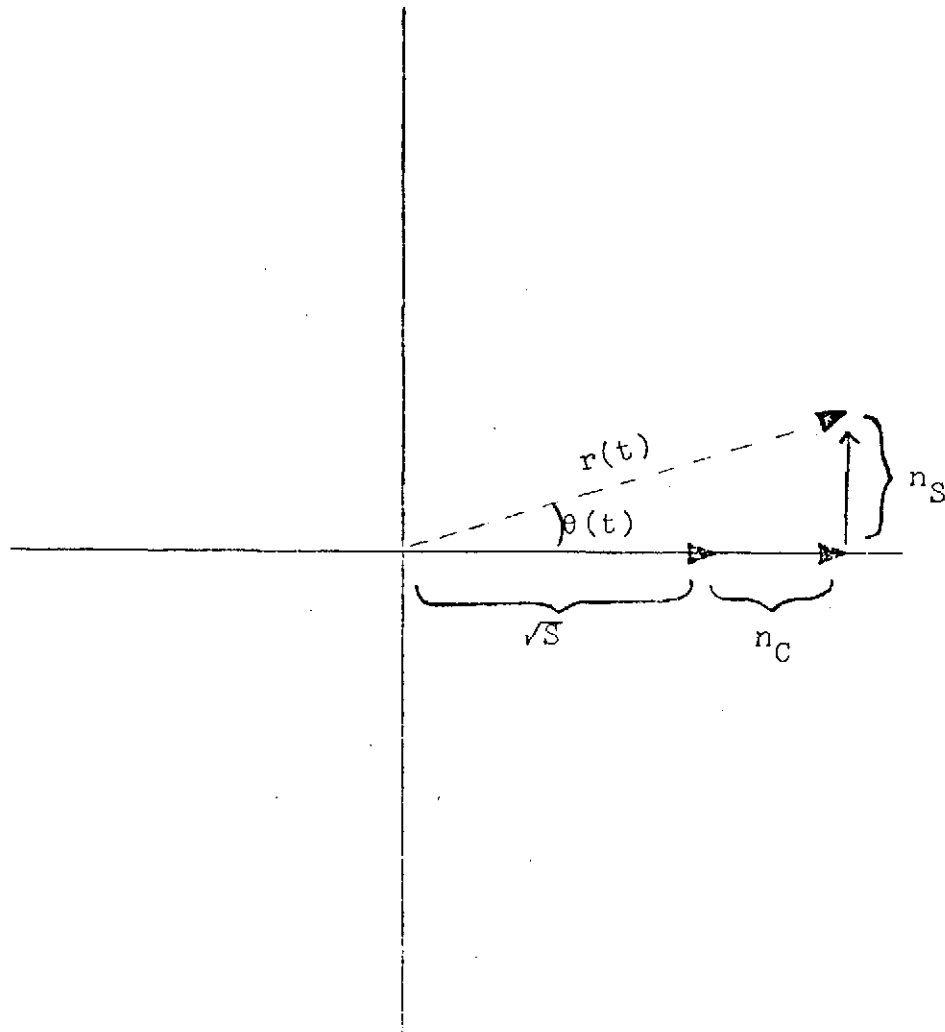


Figure 2. Signal Space

SOFT-DECISION STATISTICS

A preview of the quantitative effect on the soft decision due to the hard limiter can be provided by some qualitative evaluation of the test statistic $\tilde{y}(t)$.

For coherent demodulation, and from Figure 2, it is obvious that

$$z(t) = A(t) \cos \theta(t) = \sqrt{S} + n_C(t)$$

and thus the soft decision has a Gaussian distribution with mean \sqrt{S} and variance σ_n^2 .

On the other hand, with the hard limiter

$$\tilde{y}(t) = \cos \theta(t)$$

$$= \frac{\sqrt{S} + n_C(t)}{\{[\sqrt{S} + n_C(t)]^2 + n_S^2(t)\}^{1/2}}$$

In other words, the decision statistic is merely a normalized version of the linear system statistic. In particular,

a. $-1 \leq \tilde{y}(t) \leq 1$

b. Assume that $\sqrt{S} + n_C(t) = -\epsilon$; i.e., a small value which led to an error because of $n_C(t)$ being slightly larger and of opposite sign to the signal. Since $n_S(t)$ is independent, it is probable that it is not of large magnitude and therefore the normalizing factor of $\tilde{y}(t)$ will cause the soft decision to be near -1 instead of near 0. The effect is necessarily detrimental to the soft-decision decoder.

A quantitative evaluation is now presented. Let

$$u = A \cos \theta$$

$$v = A \sin \theta$$

where we have dropped the dependence on time for simplicity. A and θ retain their earlier definition. The processes u and v are Gaussian and

$$\bar{u} = \sqrt{S}$$

$$\bar{v} = 0$$

$$\bar{u}^2 = \bar{v}^2 = \sigma_n^2$$

The joint distribution for u and v is given by

$$f_{u, v}(u, v) = \frac{1}{2\pi\sigma_n^2} e^{-[(u - \sqrt{S})^2 + v^2] / 2\sigma_n^2}$$

Thus, by linear transformation

$$f_{A,\theta}(a, \theta) = f_{u,v}(u(A, \theta), v(A, \theta)) |J|$$

where $|J|$ is the Jacobian. Hence,

$$f_{A,\theta}(a, \theta) = \frac{a}{2\pi\sigma_n^2} e^{-(a^2 + S - 2\sqrt{S}a \cos \theta)/2\sigma_n^2}$$

Since we are interested in the distribution of $\cos \theta$, let us find $f_\theta(\theta)$ first; i.e.,

$$\begin{aligned} f_\theta(\theta) &= \int_0^\infty \frac{a}{2\pi\sigma_n^2} e^{-(a^2 + S - 2\sqrt{S}a \cos \theta)/2\sigma_n^2} da \\ &= \frac{1}{2\pi\sigma_n^2} e^{-(S - S \cos^2 \theta)/2\sigma_n^2} \int_0^\infty a e^{-(a - \sqrt{S} \cos \theta)^2/2\sigma_n^2} da \end{aligned}$$

By transformation of variables, the above expression is evaluated to be

$$\begin{aligned} f_\theta(\theta) &= \frac{1}{2\pi} e^{-S/2\sigma_n^2} \left\{ 1 + e^{S \cos^2 \theta / 2\sigma_n^2} \left[\left(\frac{\pi S}{2} \right)^{1/2} \frac{\cos \theta}{\sigma_n} \right] \right. \\ &\quad \left. \cdot \left[1 + \operatorname{erf} \left(\frac{\sqrt{S} \cos \theta}{\sqrt{2}\sigma_n} \right) \right] \right\} \end{aligned}$$

where we understand $\operatorname{erf}(-x) = -\operatorname{erf}(x)$. Since the test statistic is $\cos \theta$, the distribution is given, again with a change of variable $t = \cos \theta$, by

$$f_T(t) = \frac{e^{-\gamma}}{\pi(1-t^2)^{1/2}} \left\{ 1 + e^{\gamma t^2} (\pi\gamma)^{1/2} t \left[1 + \operatorname{erf}(\gamma^{1/2} t) \right] \right\} \quad -1 < t < 1$$

Figures 3 and 4 illustrate the probability density functions of the received statistic for a transmitted unit signal at +1.0 for the hard limiter (solid line) and the linear additive noise system (dotted line). Figures 3 and 4 illustrate the cases for 2 and 5 dB, respectively.

Similarly, Figures 5 and 6 show the density functions for the test statistic, given that an error was made; i.e., given that the test statistic is negative (we assume +1 was transmitted), for the cases of 5 and 14 dB, respectively. We see, in

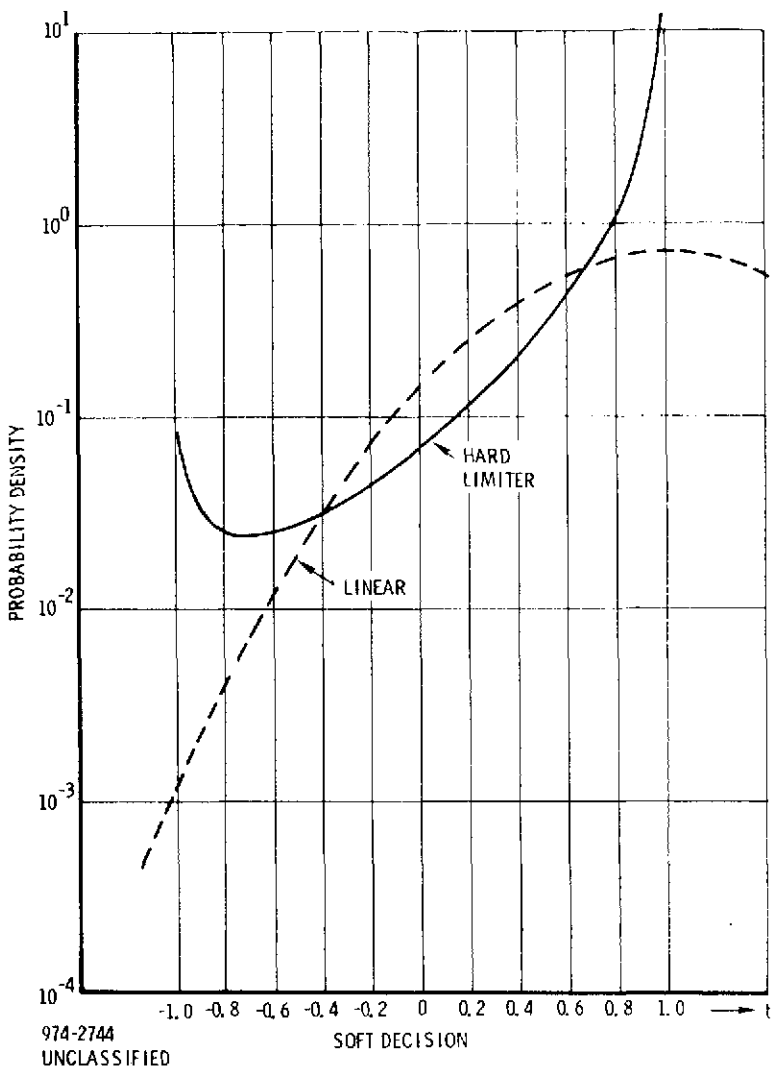


Figure 3. Received Test Statistic Density Function for SNR = 2 dB

particular, that the density for the hard limiter forces a wide density which will generate large "soft decisions" when errors are made. In contradistinction, the case of linear channel (dotted line in Figure 6) guarantees a low value for the soft incorrect decision. This characteristic will cause a degeneration of the usual claims of soft-decision decoding, as compared to the linear white additive Gaussian noise.

DECODER METRIC

In order to establish the functional relationship between the received sequence \hat{x}_i , given x_i was transmitted, the magnitude α_i of the decision statistic t_i and a decoder metric, we consider the likelihood ratio.

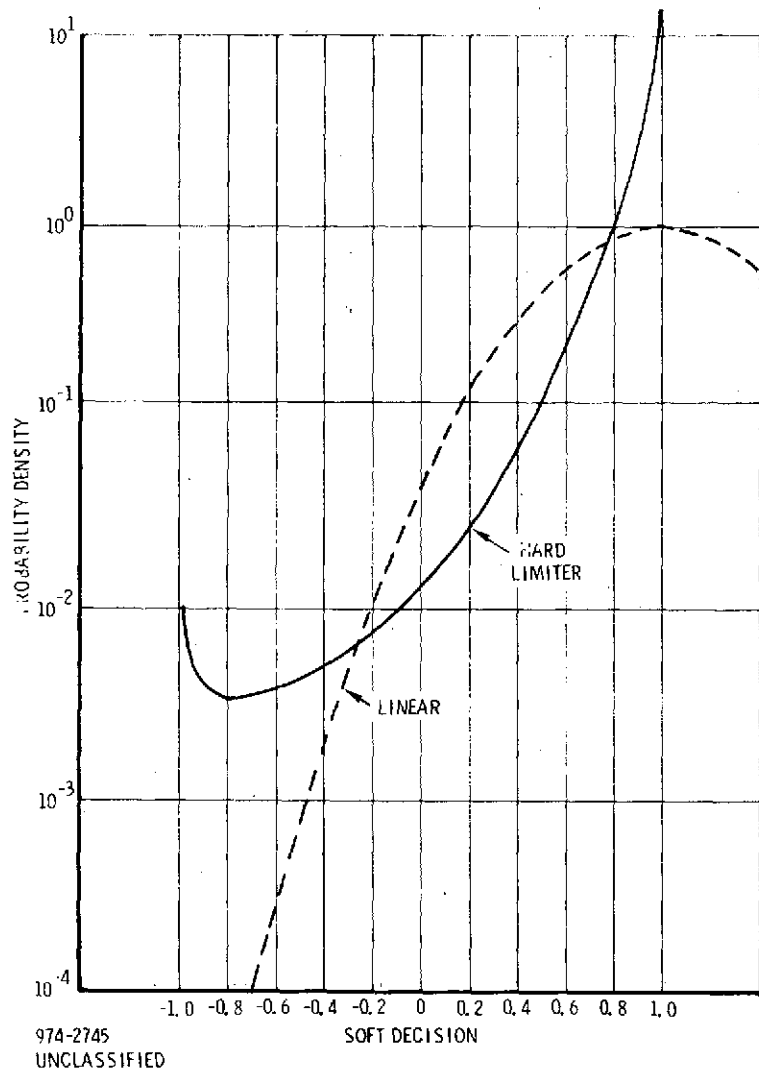


Figure 4. Received Test Statistic Density Function for SNR = 5 dB

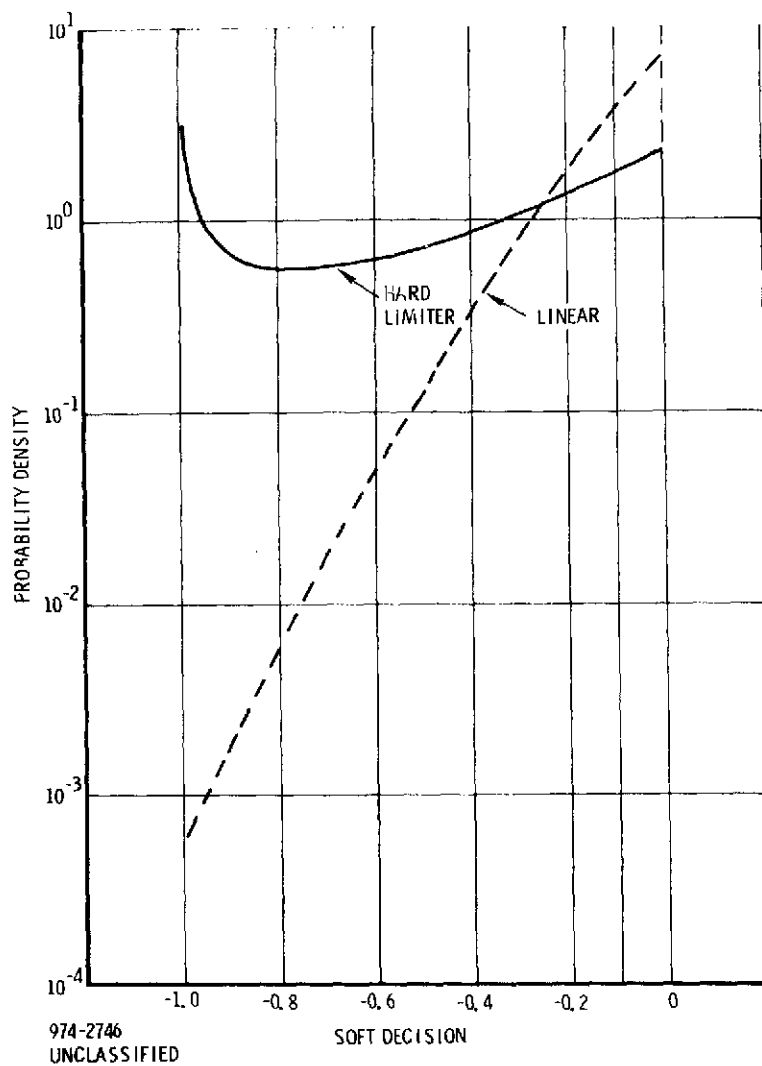


Figure 5. Conditional Density Function Given an Error for SNR = 5 dB

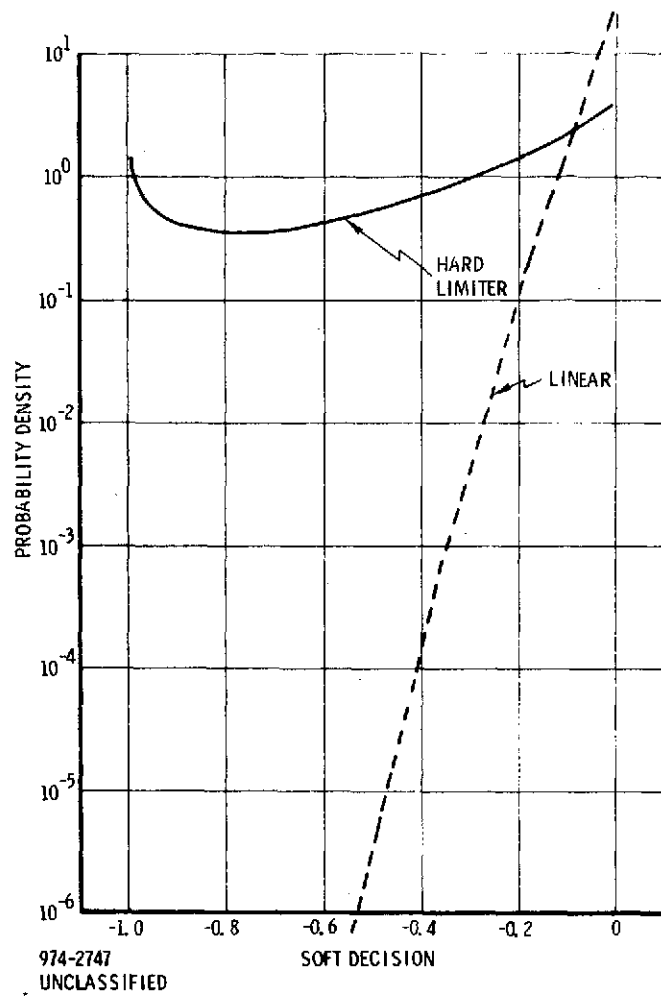


Figure 6. Conditional Density Function Given an Error for SNR = 14 dB

Consider the received sequence \hat{x}_i . The optimal joint n-sequence decision \tilde{x} is chosen such that

$$f(\underline{\alpha}, \hat{\underline{x}} | \tilde{\underline{x}}) = \underset{\underline{x}}{\text{Max}} f(\underline{\alpha}, \hat{\underline{x}} | \underline{x})$$

Hence, we maximize

$$\prod_{i=1}^n \frac{e^{-\gamma}}{\pi(1-\alpha_i^2)^{1/2}} \cdot 1 + e^{\gamma t^2} (\pi\gamma)^{1/2} \alpha_i \text{erf}(\gamma^{1/2} \alpha_i) + \beta(\hat{x}_i, \tilde{x}_i) e^{\gamma \alpha_i^2} (\pi\gamma)^{1/2} \alpha_i$$

where

$$\beta(\hat{x}_i, \tilde{x}_i) = \begin{cases} 1 & \text{if } \hat{x}_i = \tilde{x}_i \\ -1 & \text{if } \hat{x}_i \neq \tilde{x}_i \end{cases}$$

Dividing by terms which do not involve \tilde{x}_i , namely

$$f(\underline{\alpha}, \hat{\underline{x}} | \hat{\underline{x}})$$

and taking negative logarithms, we wish to minimize

$$\sum_{i=1}^n \log \frac{\left\{ 1 + \frac{e^{\gamma \alpha_i^2} (\pi\gamma)^{1/2} \alpha_i}{1 + e^{\gamma \alpha_i^2} (\pi\gamma)^{1/2} \alpha_i \text{erf}(\gamma^{1/2} \alpha_i)} \right\}}{\left\{ 1 + \beta(\hat{x}_i, \tilde{x}_i) \frac{e^{\gamma \alpha_i^2} (\pi\gamma)^{1/2} \alpha_i}{1 + e^{\gamma \alpha_i^2} (\pi\gamma)^{1/2} \alpha_i \text{erf}(\gamma^{1/2} \alpha_i)} \right\}}$$

The metric contribution to an hypothesis which agrees with the sign of the decision statistic contributes zero. We now estimate the preferred contribution due to an hypothesis which differs from the assumed transmitted bit; i.e., when $\beta(\hat{x}_i, \tilde{x}_i) = -1$.

Figure 7 illustrates the metric as a function of α_i ($0 \leq \alpha_i \leq 1$) for various values of γ when normalized to unity for $\alpha_i = 1$. From Figure 7, it is evident that no degradation is suffered if the metric is chosen to be linear; i.e., α_i itself, when an error is hypothesized and zero when an agreement is hypothesized.

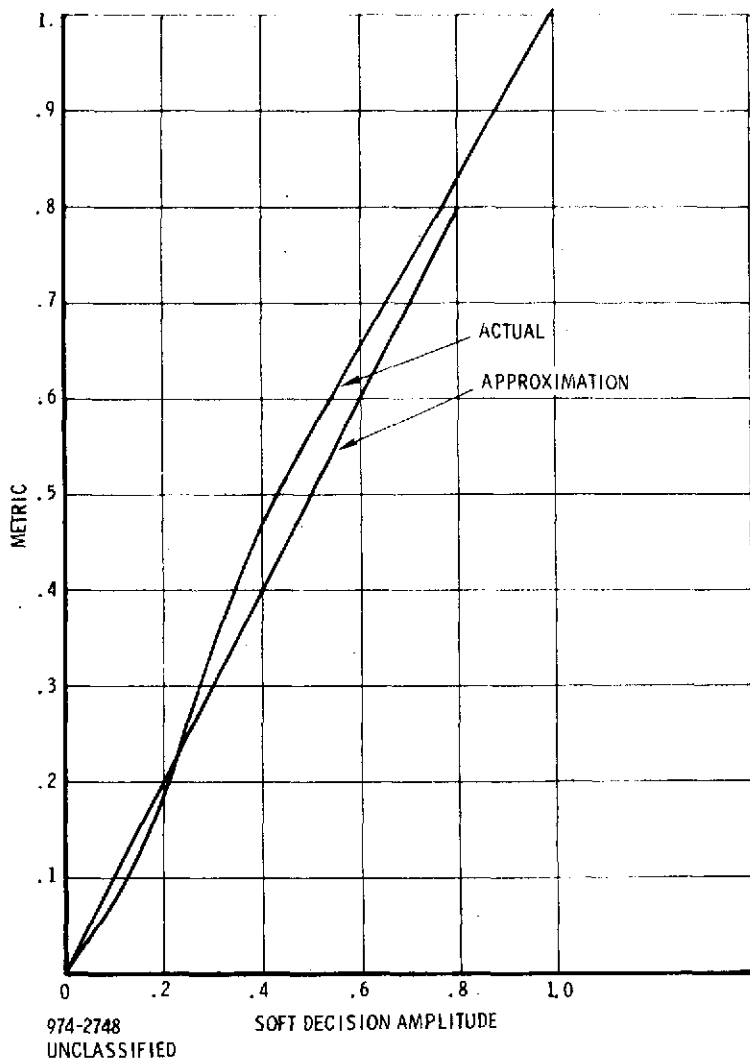


Figure 7. Optimal Metric for Soft-Decision Decoding

PERFORMANCE OF K = 5 VITERBI DECODER

A soft-decision Viterbi decoder under the above channel conditions was simulated to determine the degradation in performance. For the simulation, the optimum $K = 5 \begin{pmatrix} 10011 \\ 11101 \end{pmatrix}$ nontransparent convolutional code was used. The simulation was performed for $K = 5$ to minimize the processing time required to obtain statistically significant data at the higher signal-to-noise ratios. The results are general and will reflect the overall degradation in system performance for higher constraint lengths.

The comparison of the probability of error after decoding versus E_b/N_o for the $K = 5$ soft-decision decoder operating on the Gaussian channel and the band-

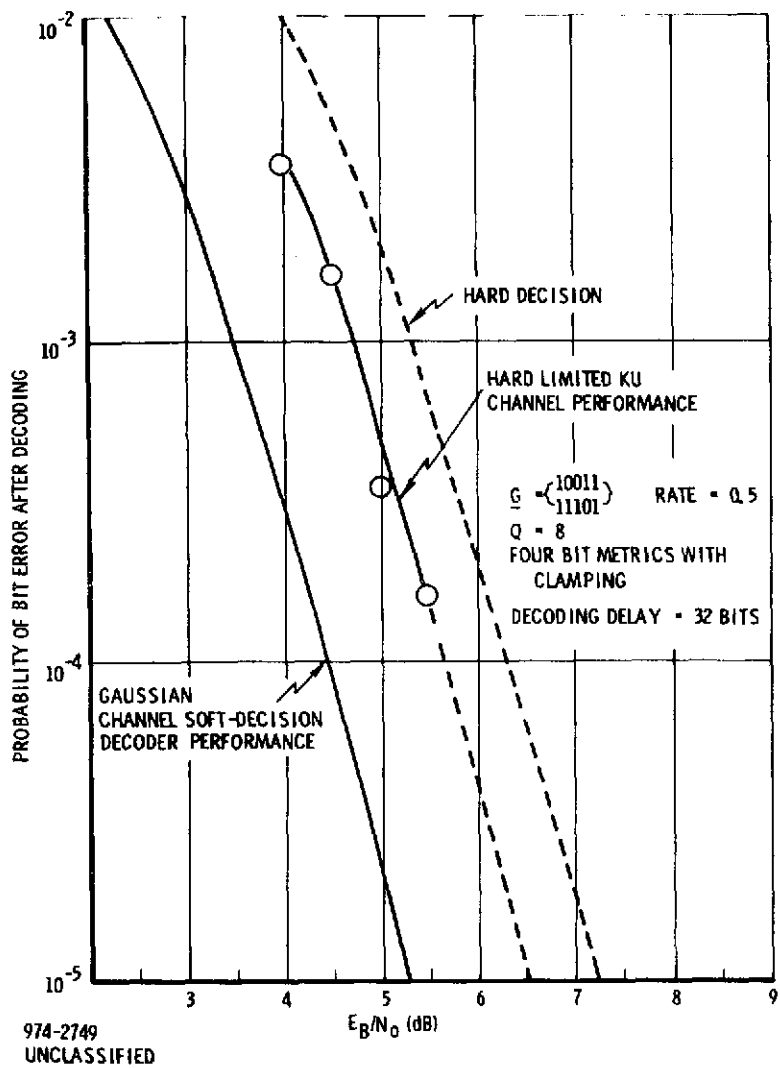


Figure 8. Performance of $K = 5$ Soft-Decision Viterbi Decoder on Hard Limited Ku-Channel

limited Ku channel are shown in Figure 8. Also on the figure, the hard-decision performance is shown. The overall loss in performance of the soft-decision $K = 5$ Viterbi decoder on the bandlimited Ku channel is 1.3 dB when compared to the Viterbi performance on the Gaussian channel at a decoded error rate of 10^{-5} . The results show that the soft-decision decoder is still better than a hard-decision decoder on the Ku channel. The improvement in performance, however, is less than 1 dB.

REFERENCE

1. J. C. Springett and M. K. Simon, "An Analysis of the Phase Coherent-Incoherent Output of the Bandpass Limiter", IEEE Trans. on Comm., Vol. 19-1, February 1971, p. 42.

APPENDIX X
SOFT-DECISION DECODING FOR QUADRIPHASE MODULATION
FOR THE Ku-BAND RETURN LINK

INTRODUCTION

This appendix is an extension to Appendix IX which treats the biphase modulation when the repeater contains a hardlimiter and the data bandwidth is nearly equal to the spectral bandwidth allocated to the return Ku-link.

THE CHANNEL

With reference to Appendix IX, we can still assume that the signal is

$$s(t) = \sqrt{S} \cos(\omega_0 t + \phi)$$

where ω_0 is the carrier frequency and ϕ is the data modulation. Without loss of generality, we can take the dabit to be 0,0 and the related angle $\phi = 45^\circ$. Figure 1 illustrates the signal space.

Similarly, the noise can be written in terms of its baseband components.

$$n(t) = n_C(t) \cos \omega_0 t + n_S(t) \sin \omega_0 t$$

where

$$\overline{n(t)} = \overline{n_C(t)} = \overline{n_S(t)} = 0$$

$$n^2(t) = n_C^2(t) = n_S^2(t) = \sigma^2 = N_0 W$$

The signal-to-noise ratio is defined as

$$\gamma = \frac{S}{2\sigma^2}$$

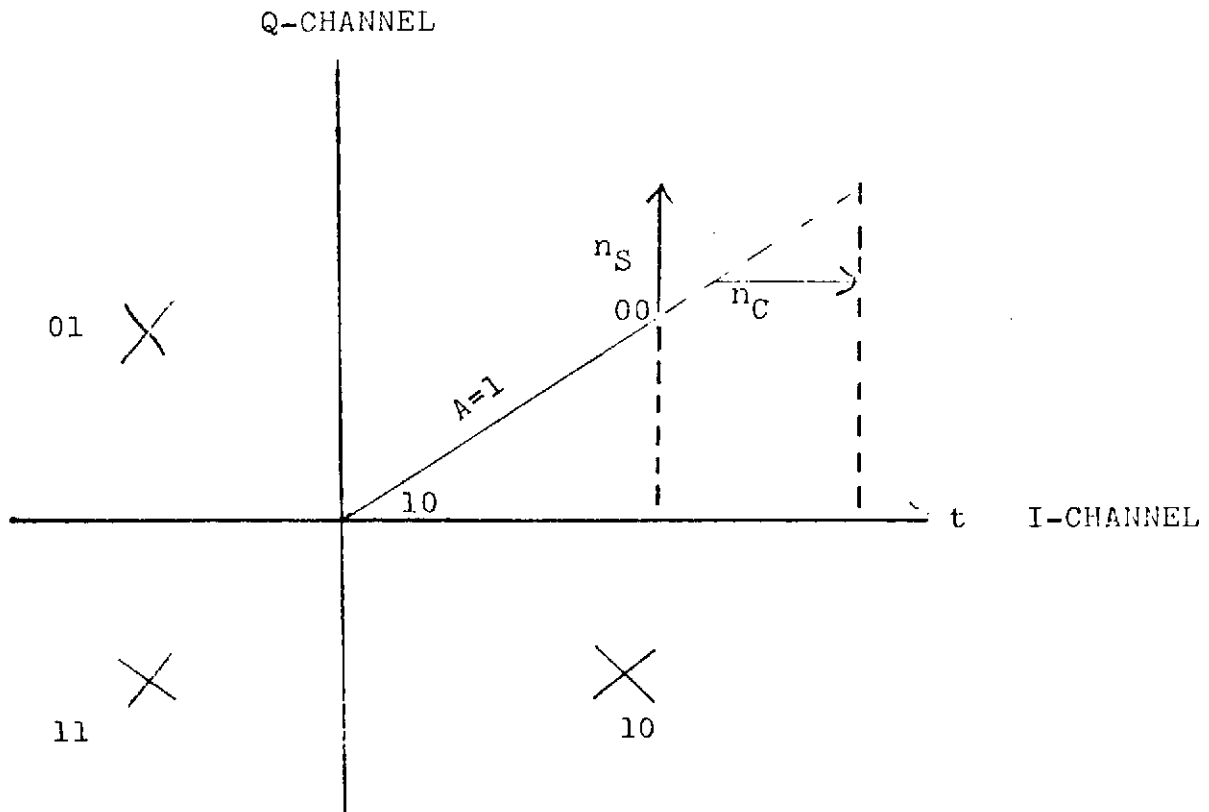


Figure 1. Signal Space (Dibit 00 Illustrated)

Let Figure 1 of Appendix IX define the signals at various points in the channel. Hence,

$$b(t) = [\sqrt{S/2} + n_C(t)] \cos \omega_0 t + [\sqrt{S/2} + n_S(t)] \sin \omega_0 t$$

or in polar form,

$$b(t) = [(\sqrt{S/2} + n_C)^2 + (\sqrt{S/2} + n_S)^2]^{1/2} \cos(\omega_0 t + \theta)$$

where

$$\theta = \arctan \left[\frac{\sqrt{S/2} + n_S(t)}{\sqrt{S/2} + n_C(t)} \right]$$

As previously derived for the biphasic case, the output of the hardlimiter can be written [1]

$$c(t) = \frac{4}{\pi} \cos[\omega_0 t + \theta(t)] + \frac{4}{\pi} \left\{ \sum_{k=1}^{\infty} \left(\frac{1}{2k+1} \right) \cos[(2k+1)(\omega_0 t + \theta(t))] \right\}$$

The effect of the bandpass filter at the ground station (ref: Fig. 1 of Appendix IX) eliminates the second term in the expression for $c(t)$, i.e.,

$$d(t) = \frac{4}{\pi} \cos[\omega_0 t + \theta(t)]$$

Demodulation and integrate-and-dump of the I channel yield

$$\begin{aligned} y(t) &= \frac{4}{\pi} \int_0^T \cos[\omega_0 t + \theta(t)] \cos(\omega_0 t + \xi) dt \\ &= \frac{2T}{\pi} \{ \cos \xi \cos \theta(t) + \sin \xi \sin \theta(t) \} \end{aligned}$$

where ξ is the coherent reference phase error term.

We now take the particular simplification of $\xi = 0$, i.e., no error in the Costas loop, for instance. Thus,

$$y(t) \sim \tilde{y}(t) = \cos \theta(t)$$

Two important factors come into play. The first is the effect on the probability of error for a given signal-to-noise ratio. The second is the soft-decision measurement which led to the decision which the Viterbi decoder must use.

BIT ERROR RATE

Consider the signal space of Figure 1. Let r be the received test statistic if the hardlimiter did not exist. Then,

$$d(t) = A(t) \cos[\omega_0 t + \theta(t)]$$

where $A(t)$ is the envelope of the process given by

[1] J. C. Springett and M. K. Simon, "An Analysis of the Phase Coherent-Incoherent Output of the Bandpass Limiter," IEE Trans on Communications, vol. 19-1, February 1971, p. 42.

$$A(t) = [(\sqrt{S/2} + n_C(t))^2 + (\sqrt{S/2} + n_S(t))^2]$$

Thus, after demodulation, filtering of the baseband signal and Integration-and-Dump, the nonlimited test statistic would be given in the I-channel by $z(t)$ where

$$\begin{aligned} z(t) &= A(t) \cos\theta(t) \\ &= A(t) \tilde{y}(t) \end{aligned}$$

Similarly, the test statistic in the Q-channel would be given by

$$q(t) = A(t) \sin\theta(t)$$

Since $A(t)$ has no phase information, the decisions based on $z(t)$ and $y(t)$ must be identical. Therefore, the BER's remain unchanged when the hardlimiter is introduced, at least within the first order analysis of the previous section.

SOFT-DECISION STATISTICS

The soft-decision statistics are provided by the derivation of the probability density function for

$$\tilde{y} = \frac{\sqrt{S/2} + n_C}{[(\sqrt{S/2} + n_C)^2 + (\sqrt{S/2} + n_S)^2]^{1/2}}$$

Let

$$u = A \cos\theta$$

$$v = A \sin\theta$$

where we have dropped the dependence on time for simplicity. The processes u and v are Gaussian and

$$\bar{u} = \bar{v} = \sqrt{S/2}$$

$$u^2 = v^2 = \sigma^2$$

The joint distribution for u and v is given by

$$f_{U,V}(u,v) = \frac{1}{2\pi\sigma^2} e^{-[(u-\sqrt{S/2})^2 + (v-\sqrt{S/2})^2]/2\sigma^2}$$

and, by linear transformation to the polar coordinates,

$$f_{A,\theta}(a,\theta) = f_{U,V}[u(a,\theta),v(a,\theta)]|J|$$

where $|J|$ is the Jacobian. Hence

$$f_{A,\theta}(a,\theta) = \frac{a}{2\pi\sigma^2} e^{-[a^2 + S - 2\sqrt{S/2} a(\cos\theta + \sin\theta)]/2\sigma^2}$$

Let us derive the test statistic for the I-channel, and later call upon a symmetry argument to establish the same result for the Q-channel.

Let us derive the marginal density for θ .

$$\begin{aligned} f_\theta(\theta) &= \int_0^\infty f_{A,\theta}(a,\theta) da \\ &= \frac{1}{2\pi\sigma^2} e^{-(S/2\sigma^2)(\frac{1}{2} - \sin\theta\cos\theta)} \\ &\cdot \int_0^\infty a e^{-[a - \sqrt{S/2}(\cos\theta + \sin\theta)]^2/2\sigma^2} da \end{aligned}$$

By transformation of variables, $f(\cdot)$ is evaluated to be

$$\begin{aligned} f_\theta(\theta) &= \frac{1}{2\pi} e^{-\frac{S}{2\sigma^2}} \left\{ 1 + e^{\frac{S}{2\sigma^2} \left[\frac{\cos\theta + \sin\theta}{\sqrt{2}} \right]^2} \right. \\ &\quad \left. \cdot \left[1 + \operatorname{erf}\left(\frac{\sqrt{S/2\sigma^2} \frac{\cos\theta + \sin\theta}{\sqrt{2}}}{\sqrt{2}}\right) \right] \right\} \end{aligned}$$

At this point we must make the dichotomy between two situations. One is the case where a Viterbi decoding process is used on the I- and the Q-channels independently, the other is when the dibits corresponding to the dual outputs of the rate 1/2

encoder modulate the I- and Q-channel. This latter case is treated first, as it is likely to be the usual mode of operation.

For simplicity of notation, let us call the projections on the quadrature channels of the normalized received vector

$$T = \cos\theta$$

$$Q = \sin\theta$$

with the obvious restriction that $T^2 + Q^2 = 1$. Thus,

$$f_{T,Q}(T,Q) = \frac{1}{2\pi} e^{-\frac{S}{2\sigma^2} \left\{ 1 + e^{\frac{S}{2\sigma^2} \frac{T+Q}{\sqrt{2}}} \right\}^2} \cdot \left[1 + \operatorname{erf} \left(\frac{\frac{T+Q}{\sqrt{2}}}{\sqrt{S/2^2}} \right) \right]$$

The reason that the density of T and Q cannot be treated in terms of the marginal densities for T and Q is their dependence. The metric must reflect this fact. In contra-distinction, the independent I- and Q-channels' performance can be derived by considering the marginal density function.

The test statistic T for the I-channel is given by

$$T = \cos\theta$$

Thus

$$f_T = \{ f_\theta(\theta(T)) + f_\theta(-\theta(T)) \} \left| \frac{d\theta}{dT} \right|$$

Since $\cos\theta = \cos(-\theta) = T$,

$$f_T(t) = \frac{e^{-\gamma}}{2\pi\sqrt{1-t^2}} \left\{ 2 + e^{\frac{\gamma(\frac{T+\sqrt{1-t^2}}{\sqrt{2}})^2}{2}} \left[1 + \operatorname{erf} \left(\frac{\frac{T+\sqrt{1-t^2}}{\sqrt{2}}}{\sqrt{\gamma}} \right) \right] + e^{\frac{\gamma(\frac{T-\sqrt{1-t^2}}{\sqrt{2}})^2}{2}} \left[1 + \operatorname{erf} \left(\frac{\frac{T-\sqrt{1-t^2}}{\sqrt{2}}}{\sqrt{\gamma}} \right) \right] \right\}$$

The characteristics of this probability density function (conditional on a +1 transmission bit) are shown in Figure 2 for 5 and 8 dB

It now becomes apparent that as the signal-to-noise ratio increases, the density function exhibits a node at $1/\sqrt{2}$ which is the projection on the I- and the Q-channel outputs of a noise-free signal located in the middle of the first quadrant at unity energy. (The joint density considered earlier had the same behavior.)

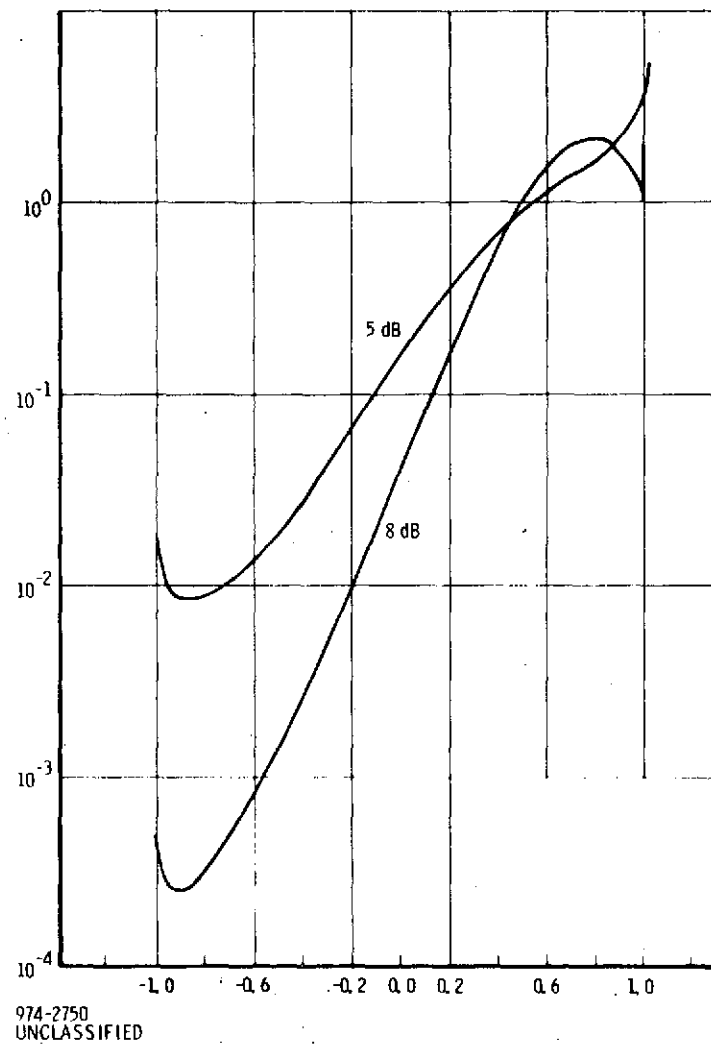


Figure 2. Received Test Statistic Marginal Density Function for the I- or Q-Channel

974-2750
UNCLASSIFIED

DECODER METRIC - CASE 1

The metric must now be determined for the Viterbi decoder, in terms of the density functions derived in the last section. In the case of the single decoder with the coded dubits on the quadrature channels, let r_i be the sequence of received complex samples, x_i , the transmitted dubits and \hat{x}_i , the pair of bit decisions based on the sign of the I and Q components in the I- and Q-channels. The likelihood is

$$\Lambda = \prod_i f_{T,Q}(r_i | x_i)$$

By considering logarithms and dividing by a constant terms, i.e., $\prod_i f_{T,Q}(r_i | \hat{x}_i)$, we obtain a metric Δ_i given by

$$\Delta_i = 0 \text{ if no errors are assumed in the dubit}$$

$$\Delta_i = \log \frac{\frac{S}{2\sigma^2} \left[\frac{T+Q}{\sqrt{2}} \right]^2}{1 + e^{2\sigma^2} \left[\frac{T+Q}{\sqrt{2}} \right]^2} \frac{(\pi S/2\sigma^2) \left(\frac{T+Q}{\sqrt{2}} \right) [1 + \operatorname{erf}(\sqrt{S/2\sigma^2} \frac{T+Q}{\sqrt{2}})]}{\frac{S}{2\sigma^2} \left[\frac{-T+Q}{\sqrt{2}} \right]^2} \frac{(\pi S/2\sigma^2) \left(\frac{-T+Q}{\sqrt{2}} \right) [1 + \operatorname{erf}(\sqrt{S/2\sigma^2} \frac{-T+Q}{\sqrt{2}})]}{1 + e^{2\sigma^2} \left[\frac{-T+Q}{\sqrt{2}} \right]^2}$$

when a single error is assumed in the dubit and its soft-decision magnitude is assigned to T.

$$\Delta_i = \log \frac{\frac{S}{2\sigma^2} \left[\frac{T+Q}{\sqrt{2}} \right]^2}{1 + e^{2\sigma^2} \left[\frac{T+Q}{\sqrt{2}} \right]^2} \frac{(\pi S/2\sigma^2) \left(\frac{T+Q}{\sqrt{2}} \right) [1 + \operatorname{erf}(\sqrt{S/2\sigma^2} \frac{T+Q}{\sqrt{2}})]}{\frac{S}{2\sigma^2} \left[\frac{T+Q}{\sqrt{2}} \right]^2} \frac{(\pi S/2\sigma^2) \left(\frac{T+Q}{\sqrt{2}} \right) [1 - \operatorname{erf}(\sqrt{S/2\sigma^2} \frac{T+Q}{\sqrt{2}})]}{1 - e^{2\sigma^2} \left[\frac{T+Q}{\sqrt{2}} \right]^2}$$

When two errors are assumed in the dubit,

Figure 3 illustrates these metrics for a $E_N/N_0 = 2$ dB (energy per channel bit to noise density). We see that the metric, if only one bit is assumed in error, is nearly linear (not as linear as in the biphase case). The two-error case, however, is highly non-linear and special care may have to be taken in implementing the metric.

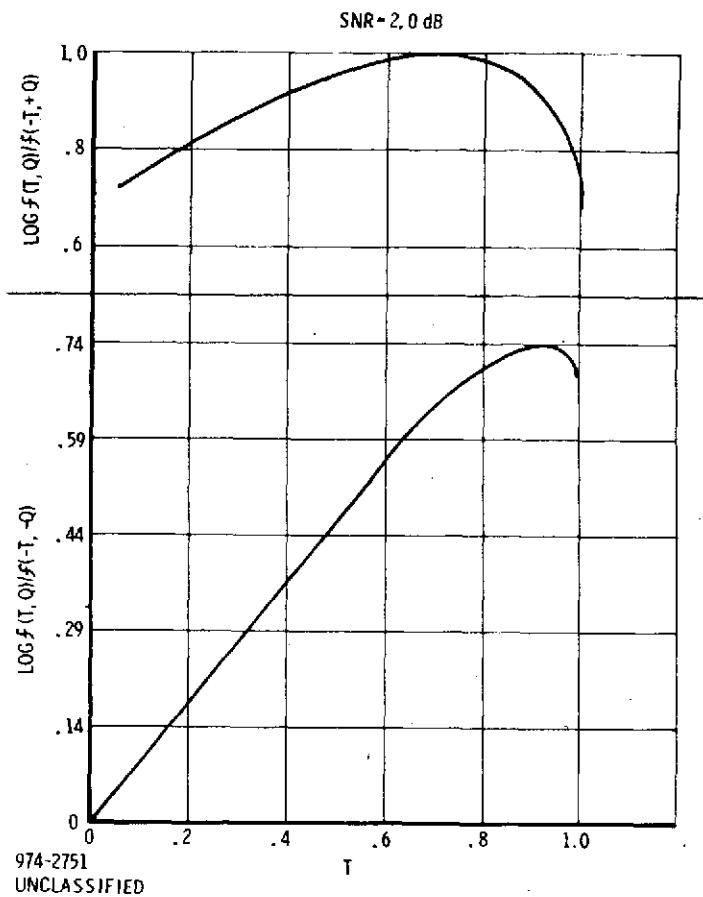


Figure 3. QPSK Viterbi Metric

DECODER METRIC - CASE 2

When each bit in the dibits is independent, a similar derivation, based on the bits rather than the dibits leads to the metric Δ_i (defined for each bit now) as given by the expression on the following page.

Figure 4 illustrates the normalized values of the metric. In view of its shape, we have chosen to consider a linear metric as nearly optimum for the Viterbi decoder.

$$2 + e^{\frac{\gamma(\frac{T+\sqrt{1-T^2}}{\sqrt{2}})^2}{(\pi\gamma)^{1/2}(\frac{T+\sqrt{1-T^2}}{\sqrt{2}})}} + e^{\frac{\gamma(\frac{T+\sqrt{1-T^2}}{\sqrt{2}})^2}{(\pi\gamma)^{1/2}(\frac{T+\sqrt{1-T^2}}{\sqrt{2}})} \operatorname{erf}(T+\sqrt{1-T^2})}$$

$$+ e^{\frac{\gamma(T-\sqrt{1-T^2})^2}{(\pi\gamma)^{1/2}(\frac{T-\sqrt{1-T^2}}{\sqrt{2}})}} + e^{\frac{\gamma(\frac{T-\sqrt{1-T^2}}{\sqrt{2}})^2}{(\pi\gamma)^{1/2}(\frac{T-\sqrt{1-T^2}}{\sqrt{2}})} \operatorname{erf}(T+\sqrt{1-T^2})}$$

$$\Delta_i = \log \frac{2 + e^{\frac{\gamma(\frac{-T-\sqrt{1-T^2}}{\sqrt{2}})^2}{(\pi\gamma)^{1/2}(\frac{-T-\sqrt{1-T^2}}{\sqrt{2}})}} + e^{\frac{\gamma(\frac{-T-\sqrt{1-T^2}}{\sqrt{2}})^2}{(\pi\gamma)^{1/2}(\frac{-T-\sqrt{1-T^2}}{\sqrt{2}})} \operatorname{erf}(-T-\sqrt{1-T^2})}}{2 + e^{\frac{\gamma(\frac{-T+\sqrt{1-T^2}}{\sqrt{2}})^2}{(\pi\gamma)^{1/2}(\frac{-T+\sqrt{1-T^2}}{\sqrt{2}})}} + e^{\frac{\gamma(\frac{-T+\sqrt{1-T^2}}{\sqrt{2}})^2}{(\pi\gamma)^{1/2}(-T+\sqrt{1-T^2})} \operatorname{erf}(T-\sqrt{1-T^2})}}$$

when an error is assumed

= 0, otherwise

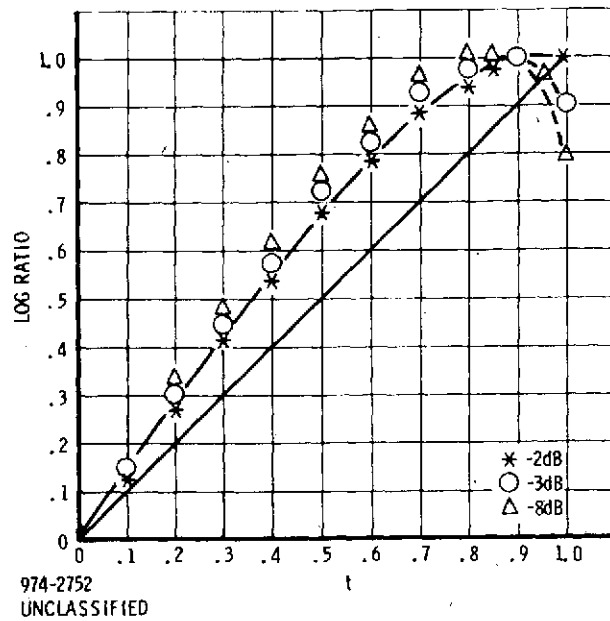


Figure 4. Independent Channel QPSK Viterbi Metric

Figure 5 shows the behavior of the Viterbi decoder in Case 1 of the last section when the dabit is transmitted as a quadriphase signal. Using the nonlinear metric, the loss relative to the nonlimited case is approximately 0.5 dB, somewhat less than the 1.25 dB loss of the biphase case.

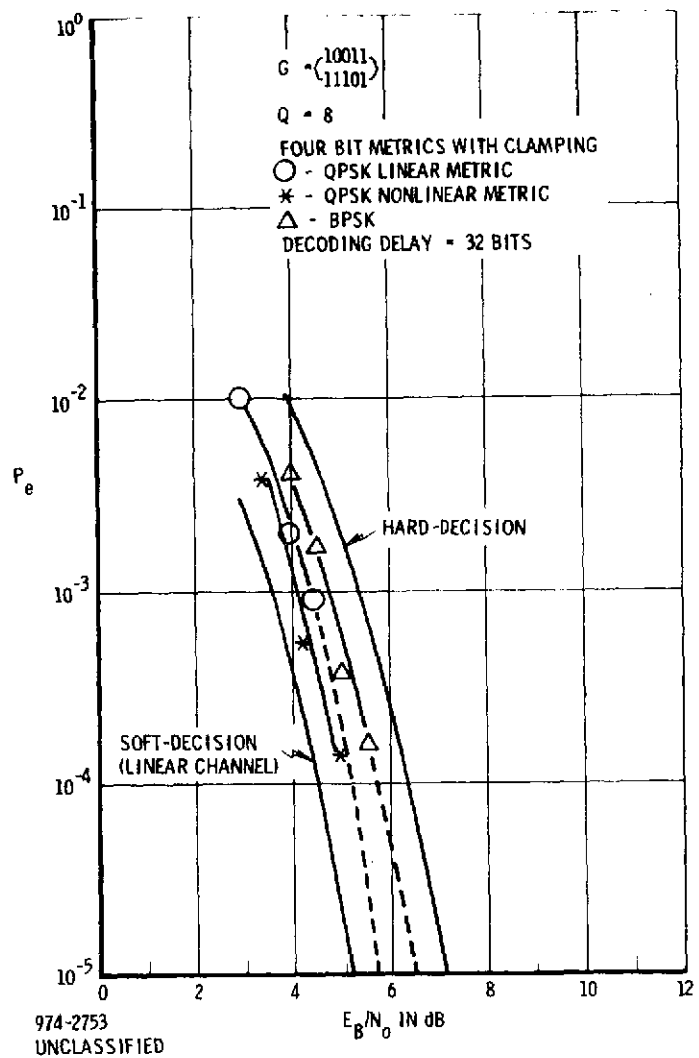


Figure 5. Simulated Performance K = 5 R = 1/2

APPENDIX XI
DYNAMIC SERVO LAG IN THE TDRS AUTOTRACK ANTENNA

TDRS/USER AUTOTRACK GEOMETRY

The response time required in the TDRS autotrack control system is determined by user space vehicle dynamics. The angular velocity required of the TDRS autotrack antenna is maximized when the trajectory of the low altitude user to be tracked bisects the earth as viewed by the TDRS. Assuming this condition, the geometry is diagrammed in Figure 1.

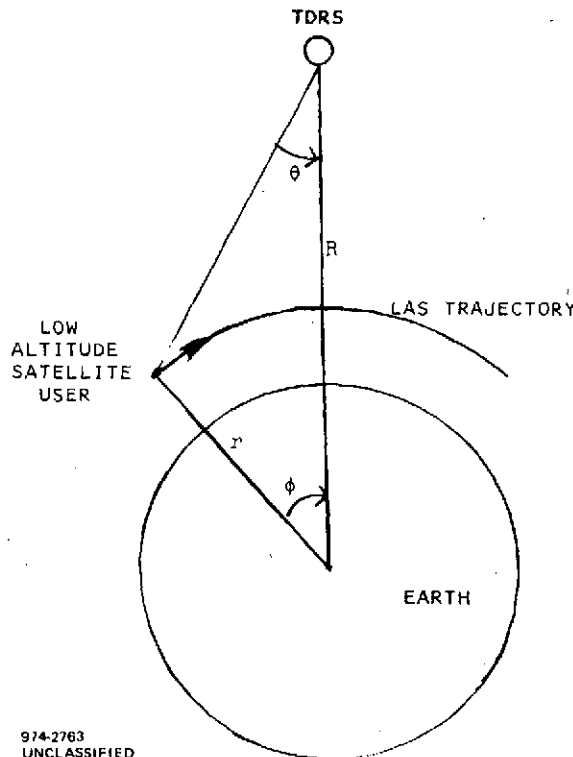


Figure 1. Geometry for Computation of Maximum Autotrack Angular Velocity Requirements

Applying the law of sines to Figure 1 gives

$$\frac{r}{\sin \theta} = \frac{R}{\sin(\theta + \phi)} \quad (1)$$

whence

$$r(\sin \theta \cos \omega + \sin \omega \cos \theta) = R \sin \theta \quad (2)$$

and

$$\tan \theta = \frac{r \sin \omega}{R - r \cos \omega} \quad (3)$$

Taking the time derivative of both sides with r and R constant gives

$$\dot{\theta} \frac{d \tan \theta}{d \theta} = \frac{d}{dt} \left[\frac{r \sin \omega}{R - r \cos \omega} \right] \quad (4)$$

or

$$\dot{\theta} = \frac{\frac{d}{dt} \left[\frac{r \sin \omega}{R - r \cos \omega} \right]}{1 + \tan^2 \theta} = \frac{\frac{d}{dt} \left[\frac{r \sin \omega}{R - r \cos \omega} \right]}{1 + \left(\frac{r \sin \omega}{R - r \cos \omega} \right)^2} \quad (5)$$

Thus,

$$\dot{\theta} = \frac{\dot{\omega} [R r \cos \omega - r^2]}{R^2 - 2 r R \cos \omega + r^2} \quad (6)$$

Assuming user angular velocity $\dot{\omega}$ to be constant, the above expression (6) is maximized when $\omega = 0$, so that the worst case is obtained:

$$\dot{\theta}_{\max} = \frac{\dot{\omega} (r/R)}{1 - (r/R)} \quad (7)$$

Using the above result (7), $\dot{\theta}_{\max}$ has been tabulated for various LAS users in [1]. It is found that for users tabulated,

$$\dot{\theta}_{\max} = 0.0127 \text{ deg/sec} = 2.22 \times 10^{-4} \text{ rad/sec} \quad (8)$$

AUTOTRACK CONTROL SYSTEM ANALYSIS

The control system requirements will be analyzed using a linear curve of θ versus time over the 30° FOV, as shown in Figure 2. A sketch of what the actual relationship might look like is shown for comparison. The control system input is thus modelled as

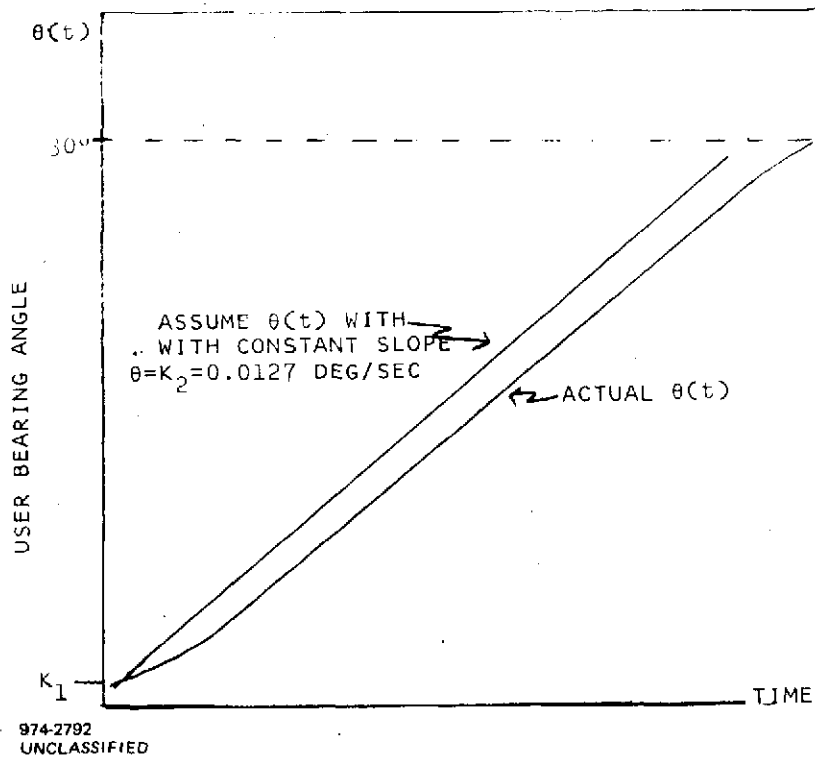


Figure 2. Dynamic Model for Control Loop Tracking Analysis

$$\theta(t) = (K_1 + K_2 t) u(t)$$

where $u(t)$ is the unit step function.

In Laplace transform notation we have

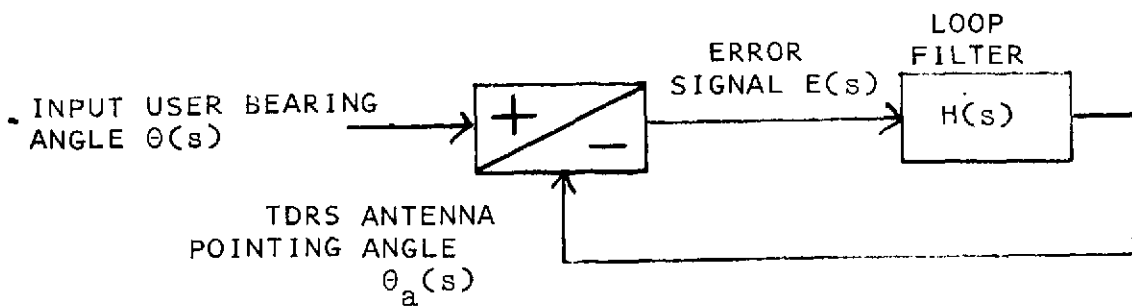
$$\theta(s) = \frac{K_1}{s} + \frac{K_2}{s^2} \quad (9)$$

This input is applied to a feedback control system configured as in Figure 3. The error signal is given by

$$E(s) = \frac{\theta(s)}{1 + H(s)} \quad (10)$$

We first consider a type "0" system in which

$$H(s) = \frac{G\omega_0}{s + \omega_0} \quad (11)$$



974-2791
UNCLASSIFIED

Figure 3. General Autotrack Control System Model

where G is the loop gain and ω_0 is the filter cutoff frequency (in rad/sec). From (9), (10) and (11) we find

$$E(s) = \left[\frac{K_1}{s} + \frac{K_2}{s^2} \right] \left[\frac{s + \omega_0}{s + (G + 1)\omega_0} \right] \quad (12)$$

With the output of the loop filter initially zero, Equation (12) transforms to the time domain as:

$$e(t) = \left[K_1 \frac{1}{G+1} + \frac{G}{G+1} e^{-\frac{(G+1)\omega_0 t}{\omega_0}} \right] u(t) + K_2 \left\{ \frac{G}{\omega_0 (G+1)^2} \left[1 - e^{-\frac{(G+1)\omega_0 t}{\omega_0}} \right] + \frac{t}{G+1} \right\} u(t) \quad (13)$$

As time increases, (13) becomes

$$e(t) \approx \frac{K_1}{G+1} + \frac{K_2}{G+1} \left[\frac{G}{\omega_0 (G+1)} + t \right] \quad \text{for } (G+1)\omega_0 t \gg 1 \quad (14)$$

As the user leaves the view of the TDRS, we assume that $\omega_0 t \gg 1$ so that the angular tracking error becomes:

$$e(t) \approx \frac{K_1 + K_2 t}{G+1} \approx \frac{30}{G+1} \text{ degrees} \quad (15)$$

Thus, in order to keep the final tracking error below 0.3 degrees, a minimum loop gain of 100 is required. It is felt that with

$$\omega_0 \approx 0.1 \text{ rads/sec}$$

and structural resonance near 1 Hz, a loop gain this large would invite loop instability. Thus, a type "1" tracking system will be considered instead of the type "0".

For the type "1" system we use

$$H(s) = \frac{G\omega_0/T_i}{s(s + \omega_0)} \quad (16)$$

where $1/T_i$ is a normalizing factor associated with the integrator. From (9), (10) and (16) we find

$$E(s) = \left[K_1 + \frac{K_2}{s} \right] \cdot \frac{s + \omega_0}{s^2 + \omega_0 s + G\omega_0/T_i} \quad (17)$$

$$= \left[K_1 + \frac{K_2}{s} \right] \cdot \frac{s + \omega_0}{(s + \alpha)(s + \beta)} \quad (18)$$

where

$$\begin{aligned} \alpha &= \frac{1}{2} \omega_0 + \sqrt{\omega_0^2 - 4G\omega_0/T_i} \\ \beta &= \frac{1}{2} \omega_0 - \sqrt{\omega_0^2 - 4G\omega_0/T_i} \end{aligned} \quad (19)$$

Transforming to the time domain gives

$$e(t) = \left[K_1 \frac{\alpha - \omega_0}{\alpha - \beta} e^{-\alpha t} - \frac{\beta - \omega_0}{\alpha - \beta} e^{-\beta t} \right] + K_2 \left[\frac{\omega_0}{\alpha \beta} + \frac{\omega_0 - \alpha}{\alpha(\alpha - \beta)} e^{-\alpha t} + \frac{\omega_0 - \beta}{\beta(\beta - \alpha)} e^{-\beta t} \right] \quad (20)$$

In the limit of large t , (20) becomes

$$e(t) \approx \frac{K_2 \omega_0}{\alpha \beta} \approx K_2 T_i/G \quad \text{for } \text{Re}\{\alpha t\}, \text{Re}\{\beta t\} \gg 1 \quad (21)$$

If the system is critically damped,

$$\omega_0 = 4G/T_i \quad (22)$$

whence $\alpha = \beta = \omega_0/2$. Therefore:

$$e(t) \simeq 4K_2/\omega_0 \quad \text{for } \omega_0 t/2 \gg 1 \quad (23)$$

For $\omega_0 = 0.2$ rad/sec and $K_2 = 0.0127$ deg/sec, the final value of the tracking error is

$$e(t)_{\text{final}} = 0.25 \text{ degrees} \quad (24)$$

The noise bandwidth of this critically damped system is defined to be

$$b_n \triangleq \frac{1}{2\pi} \int_0^{\infty} \left| \frac{H_{CL}(j\omega)}{H_{CL}(0)} \right|^2 d\omega \text{ in Hertz} \quad (25)$$

where

$$H_{CL}(s) = \frac{H(s)}{1 + H(s)} \quad (26)$$

After carrying out the integration, one obtains the result:

$$b_n = \frac{\omega_0}{16} \text{ Hz} \quad (27)$$

The noise bandwidth will be an important parameter in calculating the noise-induced random tracking errors in the autotrack system.

REFERENCE

1. Pullara, J. C., et al, "Dual S- and Ku-Band Tracking Feed for a TDRS Reflector Antenna", Final Report (Phase I) submitted by Martin-Marietta Aerospace Corp. to GSFC, July 1974, Table 4.4-2-1.

APPENDIX XII

NOISE ANALYSIS OF AN AUTOTRACK ANTENNA SYSTEM

NOISE ON THE AUTOTRACK CONTROL SIGNAL

A block diagram of the autotrack antenna system to be analyzed is given in Figure 1, applicable to either of two orthogonal autotrack systems (horizontal and vertical steering). The signal received at two separate antenna feeds are processed in a sum and difference hybrid to form a sum beam signal Σ and a difference beam signal Δ . These two signals are amplified and filtered in identical receivers, each having bandwidth W , and then correlated in a multiplier-integrator combination to form the antenna steering control signal. We will examine the mean and variance of the control signal as a function of receiver noise $n_R(t)$ and received interference noise $n_I(t)$. Both are modelled as white Gaussian noise processes. The received signal $s(t)$ is considered to be deterministic and constant power.

The signal and noise components at the two multiplier inputs are $s_1(t)+n_1(t)$ and $s_2(t)+n_2(t)$. Complex envelope notation is used throughout this analysis. The control signal is given by

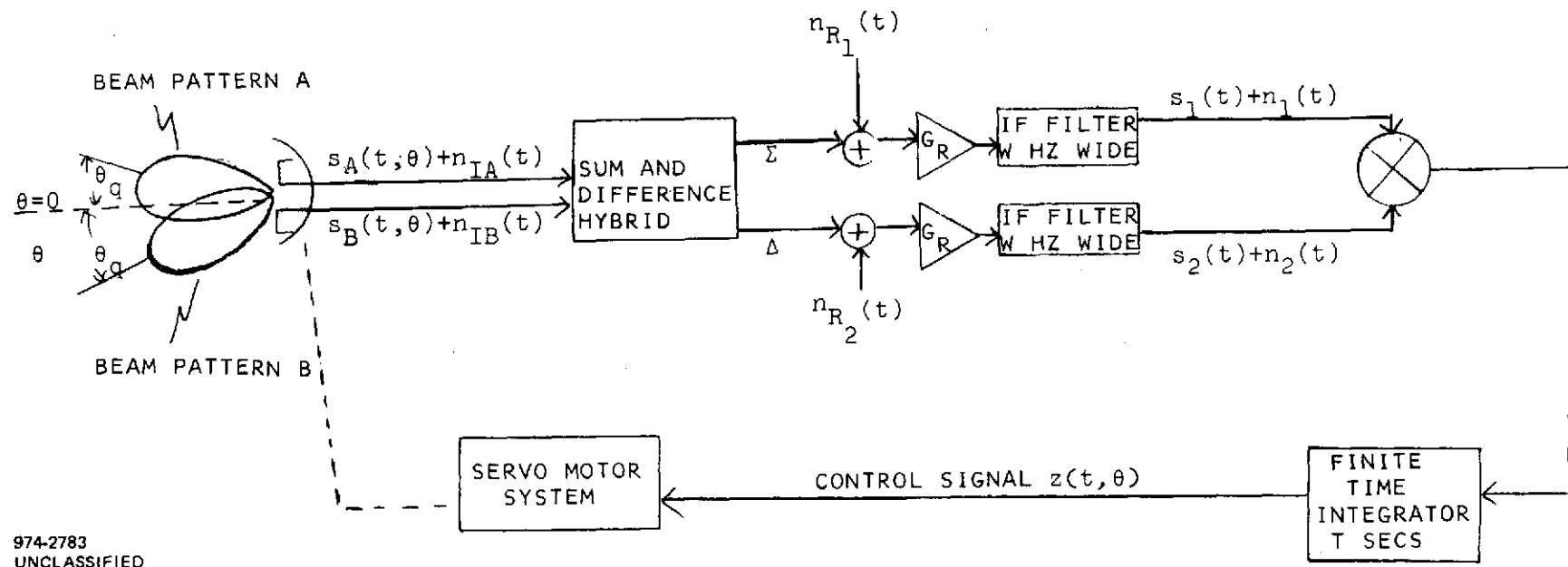
$$z(t) = \frac{1}{T} \int_{t-T}^t [s_1(\tau) + n_1(\tau)][s_2^*(\tau) + n_2^*(\tau)] d\tau. \quad (1)$$

This integral may be approximated by a sum of TW statistically independent samples [1], namely

$$z(t) = \frac{1}{TW} \sum_{i=1}^{TW} (s_{1i} + n_{1i})(s_{2i}^* + n_{2i}^*) \quad (2)$$

Using an overbar to represent the statistical expectation operator $E\{\cdot\}$, the mean is

[1] E. Baghdady, *Lectures on Communication Theory*, McGraw-Hill, 1961, pp. 282-286.



974-2783
UNCLASSIFIED

Figure 1. Block Diagram of Autotrack Antenna System

$$\begin{aligned}
\bar{z} &= \frac{1}{TW} \sum_{i=1}^{TW} (s_{1i} s_{2i}^* + \overline{n_{1i} n_{2i}^*}) \\
&= s_1 s_2^* + \overline{n_1 n_2^*}
\end{aligned} \tag{3}$$

where the time dependence has been dropped under the assumption of stationary noise processes.

The second moment of z is

$$\begin{aligned}
\overline{zz^*} &= \frac{1}{(TW)^2} \sum_{i=1}^{TW} \sum_{j=1}^{TW} E\{(s_{1i} s_{2i}^* + s_{1j} n_{2i}^* + n_{1i} s_{2j}^* + n_{1j} n_{2i}^*) \cdot \\
&\quad (s_{1j} s_{2j}^* + s_{1j} n_{2j}^* + n_{1j} s_{2j}^* + n_{1j} n_{2j}^*)\} \\
&= \frac{1}{(TW)^2} \sum_{i=1}^{TW} \sum_{j=1}^{TW} (s_{1i} s_{2i}^* s_{1j} s_{2j}^* + s_{1i} s_{2i}^* \overline{s_{1j} n_{2j}^*} + s_{1i} s_{2i}^* \overline{n_{1j} s_{2j}^*} s_{2j} + \\
&\quad + s_{1i} s_{2i}^* \overline{n_{1j} n_{2j}^*} + s_{1i} \overline{n_{2i}^*} s_{1j} s_{2j}^* + s_{1i} s_{2i}^* \overline{n_{1j} n_{2j}^*} + s_{1i} \overline{n_{2i}^*} n_{1j} s_{2j}^* + \\
&\quad + s_{1i} \overline{n_{2i}^*} \overline{n_{1j} n_{2j}^*} + \overline{n_{1i} s_{2i}^*} s_{1j} s_{2j}^* + \overline{n_{1i} n_{2i}^*} s_{1j} s_{2j}^* + \overline{n_{1i} n_{2i}^*} s_{2i}^* s_{2j} + \\
&\quad + \overline{n_{1i} n_{2i}^*} n_{2j} s_{2i}^* + \overline{n_{1i} n_{2i}^*} s_{1j} s_{2j}^* + \overline{n_{1i} n_{2i}^*} n_{2i} s_{1j} s_{2j}^* + \overline{n_{1i} n_{2i}^*} n_{1j} s_{2j}^* + \\
&\quad + \overline{n_{1i} n_{2i}^*} n_{1j} n_{2j}^*) \tag{4}
\end{aligned}$$

Application of Reed's Theorem [2] to (4) gives

$$\begin{aligned}
\overline{zz^*} &= \frac{1}{(TW)^2} \sum_{i=1}^{TW} \sum_{j=1}^{TW} (s_{1i} s_{2i}^* s_{1j} s_{2j}^* + s_{1i} s_{2i}^* \overline{n_{1j} n_{2j}^*} + s_{1i} s_{2i}^* \overline{n_{2i}^* n_{1j} n_{2j}^*} \\
&\quad + \overline{n_{1i} n_{1j}^*} s_{2i}^* s_{2j}^* + \overline{n_{1i} n_{2i}^*} s_{1j} s_{2j}^* + \overline{n_{1i} n_{2i}^*} \overline{n_{1j} n_{2j}^*} + \overline{n_{1j} n_{1j}^*} \overline{n_{2i}^* n_{2j}^*}) \\
&= s_1 s_2^* s_1 s_2 + s_1 s_2^* \overline{n_1 n_2^*} + s_1 s_2^* \overline{n_1 n_2^*} / TW + \overline{n_1 n_2^*} s_2 / TW \\
&\quad + \overline{n_1 n_2^*} s_1 s_2 + \overline{n_1 n_2^*} \overline{n_1 n_2^*} + \overline{n_1 n_2^*} \overline{n_1 n_2^*} / TW \tag{5}
\end{aligned}$$

The variance of z is then obtained from (3) and (5) as

$$\begin{aligned}
\text{Var}(z) &= \overline{zz^*} - z z^* \\
&= s_1 s_2^* \overline{n_1 n_2^*} / TW + \overline{n_1 n_2^*} s_2 s_2^* / TW + \overline{n_1 n_2^*} \overline{n_1 n_2^*} / TW
\end{aligned} \tag{6}$$

[2] I. S. Reed, "On a Moment Theorem for Complex Gaussian Processes," IRE Trans on Information Theory, April 1962, pp. 194-195.

The following relationships apply from Figure 1.

$$\begin{aligned} n_1/G_R &= n'_{R1} + \frac{n'_{IA} + \alpha n'_{IB}}{\sqrt{2}} \\ n_2/G_R &= n'_{R2} + \frac{n'_{IA} - \alpha n'_{IB}}{\sqrt{2}} \end{aligned} \quad (7)$$

where the prime indicates the IF filtered version of the noise processes. The symbol α , which is presumed to be near one, is used to indicate a slight gain imbalance between the A and B beams. We assume that neither n_{R1} nor n_{R2} is correlated with n_{IA} or n_{IB} , so that

$$\begin{aligned} \overline{n_1 n_1^*} &= G_R^2 \{ \overline{n'_{R1} n'_{R1}^*} + \frac{1}{2} [\overline{n'_{IA} n'_{IA}^*} + \alpha^2 \overline{n'_{IB} n'_{IB}^*} + 2\alpha \text{Re}(\overline{n'_{IA} n'_{IB}^*})] \} \\ \overline{n_2 n_2^*} &= G_R^2 \{ \overline{n'_{R2} n'_{R2}^*} + \frac{1}{2} [\overline{n'_{IA} n'_{IA}^*} + \alpha^2 \overline{n'_{IB} n'_{IB}^*} - 2\alpha \text{Re}(\overline{n'_{IA} n'_{IB}^*})] \} \\ \overline{n_1 n_2^*} &= G_R^2 \{ \overline{n'_{R1} n'_{R2}^*} + \frac{1}{2} [\overline{n'_{IA} n'_{IA}^*} - \alpha^2 \overline{n'_{IB} n'_{IB}^*} + 2\alpha \text{Im}(\overline{n'_{IA} n'_{IB}^*})] \} \end{aligned} \quad (8)$$

We also assume that the IF filter is symmetric about its center frequency so $\overline{n'_{IA} n'_{IB}^*}$ is real. We now define

$$\begin{aligned} N_{R1} &\triangleq \text{noise power of } n_{R1} \text{ in IF bandwidth} = \frac{1}{2} \overline{n'_{R1} n'_{R1}^*} \\ N_{R2} &\triangleq \text{noise power of } n_{R2} \text{ in IF bandwidth} = \frac{1}{2} \overline{n'_{R2} n'_{R2}^*} \\ N_{IA} &\triangleq \text{noise power of } n_{IA} \text{ in IF bandwidth} = \frac{1}{2} \overline{n'_{IA} n'_{IA}^*} \\ N_{IB} &\triangleq \text{noise power of } n_{IB} \text{ in IF bandwidth} = \frac{1}{2} \overline{n'_{IB} n'_{IB}^*} \\ \lambda &= \text{correlation coefficient of } n_{R1} \text{ and } n_{R2} \\ \rho &= \text{correlation coefficient of } n_{IA} \text{ and } n_{IB}, \end{aligned}$$

where the factor 1/2 in the noise power definitions arises from the complex envelope notation. Thus, (8) becomes

REPRODUCIBILITY OF THE
ORIGINAL PAGE IS POOR

$$\begin{aligned}
 \overline{n_1 n_1^*} &= 2G_R^2 [N_{R_1} + \frac{1}{2}(N_{IA} + \alpha^2 N_{IB} + 2\alpha\rho\sqrt{N_{IA} N_{IB}})] \\
 \overline{n_2 n_2^*} &= 2G_R^2 [N_{R_2} + \frac{1}{2}(N_{IA} + \alpha^2 N_{IB} - 2\alpha\rho\sqrt{N_{IA} N_{IB}})] \\
 \overline{n_1 n_2^*} &= 2G_R^2 [\lambda\sqrt{N_{R_1} N_{R_2}} + \frac{1}{2}(N_{IA} - \alpha^2 N_{IB})]
 \end{aligned} \tag{9}$$

Using (9) in (3) and (6) gives

$$\begin{aligned}
 \bar{z} &= s_1 s_2^* + G_R^2 (2\lambda\sqrt{N_{R_1} N_{R_2}} + N_{IA} - \alpha^2 N_{IB}) \\
 \text{Var}(z) &= \frac{s_1 s_2^*}{TW} G_R^2 (2N_{R_1} + N_{IA} + \alpha^2 N_{IB} - 2\rho\alpha\sqrt{N_{IA} N_{IB}}) \\
 &\quad + \frac{s_2 s_2^*}{TW} G_R^2 (2N_{R_1} + N_{IA} + \alpha^2 N_{IB} + 2\rho\alpha\sqrt{N_{IA} N_{IB}}) \\
 &\quad + \frac{G_R^4}{TW} (2N_{R_1} + N_{IA} + \alpha^2 N_{IB} + 2\rho\alpha\sqrt{N_{IA} N_{IB}}) (2N_{R_2} + N_{IA} + \alpha^2 N_{IB} \\
 &\quad \quad \quad - 2\rho\alpha\sqrt{N_{IA} N_{IB}})
 \end{aligned} \tag{10}$$

CLOSED LOOP BEAM POINTING ERROR DUE TO NOISE

Let us assume for analysis purposes a Gaussian antenna power pattern

$$G(\theta) = G_0 e^{-a^2 \theta^2} \tag{11}$$

where the two-sided beamwidth, as measured between the half-power points, is θ_B , so that

$$a^2 = \frac{2.776}{\theta_B^2} \tag{12}$$

This representation has been verified to hold for all pencil beams near their peak within 5% accuracy from the beam peak to the -6 dB points [3]. If the feed is split to form the A and B beams, each squinted from $\theta = 0$ by θ_q , then the power patterns are

$$\begin{aligned}
 G_A(\theta) &= \frac{G_0}{2} e^{-a^2 (\theta + \theta_q)^2} \\
 G_B(\theta) &= \frac{G_0}{2} e^{-a^2 (\theta - \theta_q)^2}
 \end{aligned} \tag{13}$$

[3] J. W. Duncan, "Maximum Off-Axis Gain of Pencil Beams," Proc IEEE (Letters), October 1969, p. 1791.

A signal $s(t)$ arriving from direction θ produces antenna voltage outputs

$$s_A(t, \theta) = s(t) \sqrt{G_0/2} e^{-a^2(\theta+\theta_q)^2/2} \quad (14)$$

$$s_B(t, \theta) = s(t) \sqrt{G_0/2} e^{-a^2(\theta-\theta_q)^2/2}$$

The sum and difference beams at the IF outputs are then

$$s_1(t, \theta) = \frac{[s_A(t, \theta) + \alpha s_B(t, \theta)]}{\sqrt{2}} \quad (15)$$

$$= \frac{s(t)}{2} \sqrt{G_0} G_R [e^{-a^2(\theta+\theta_q)^2/2} + \alpha e^{-a^2(\theta-\theta_q)^2/2}]$$

$$s_2(t, \theta) = \frac{[s_A(t, \theta) - \alpha s_B(t, \theta)]}{\sqrt{2}} \quad (15)$$

$$= \frac{s(t)}{2} \sqrt{G_0} G_R [e^{-a^2(\theta+\theta_q)^2/2} - \alpha e^{-a^2(\theta-\theta_q)^2/2}]$$

The control signal with no noise is then

$$z(t, \theta) = s_1(t, \theta) s_2^*(t, \theta) \quad (16)$$

$$= \frac{s(t) s^*(t)}{4} G_0 G_R^2 [e^{-a^2(\theta+\theta_q)^2} - \alpha^2 e^{-a^2(\theta-\theta_q)^2}]$$

Let us define P_S as the power received in the sum beam at the peak of its pattern, i.e.,

$$P_S = \left. \frac{s_1(t, \theta) s_1^*(t, \theta)}{2 G_R^2} \right|_{\theta=0} = \frac{s(t) s^*(t)}{8} G_0 (1+\alpha)^2 e^{-a^2 \theta_q^2} \quad (17)$$

Then, from (16) and (17)

$$z(t, \theta) = \frac{2 P_S G_R^2}{(1+\alpha)^2} e^{a^2 \theta_q^2} [e^{-a^2(\theta+\theta_q)^2} - \alpha^2 e^{-a^2(\theta-\theta_q)^2}] \quad (18)$$

In the region of interest ($\theta \approx 0$), the slope of $z(t, \theta)$ with respect to θ is

$$m = \left. \frac{\partial z(t, \theta)}{\partial \theta} \right|_{\theta=0} = -4a^2 \theta_q \frac{(1+\alpha^2)}{(1+\alpha)^2} P_S G_R^2 \quad (19)$$

The reason that the slope m is of interest is that for $\theta=0$ the autotrack system may be viewed as a linear feedback control system, as shown in Figure 2. The additive noise shown on the diagram causes a shift in the mean of z and a variance on z , as analyzed in the preceding section. If the loop gain is much greater than unity, then the effect of this noise on θ is simply its effect on z reduced by the factor m . That is,

$$\bar{\theta} = \bar{z}/m$$

and

$$\text{Var}(\theta) = \text{Var}(z)/m^2 \quad (20)$$

It should be noted that the dependence of m on signal power P_S means that the loop gain is dependent on signal power. This effect may be removed by AGC in the sum and difference beam receivers, making $P_S G_R^2$ constant.

To use the results in (10) near $\theta=0$, we have from (15), (16), (17) and (18)

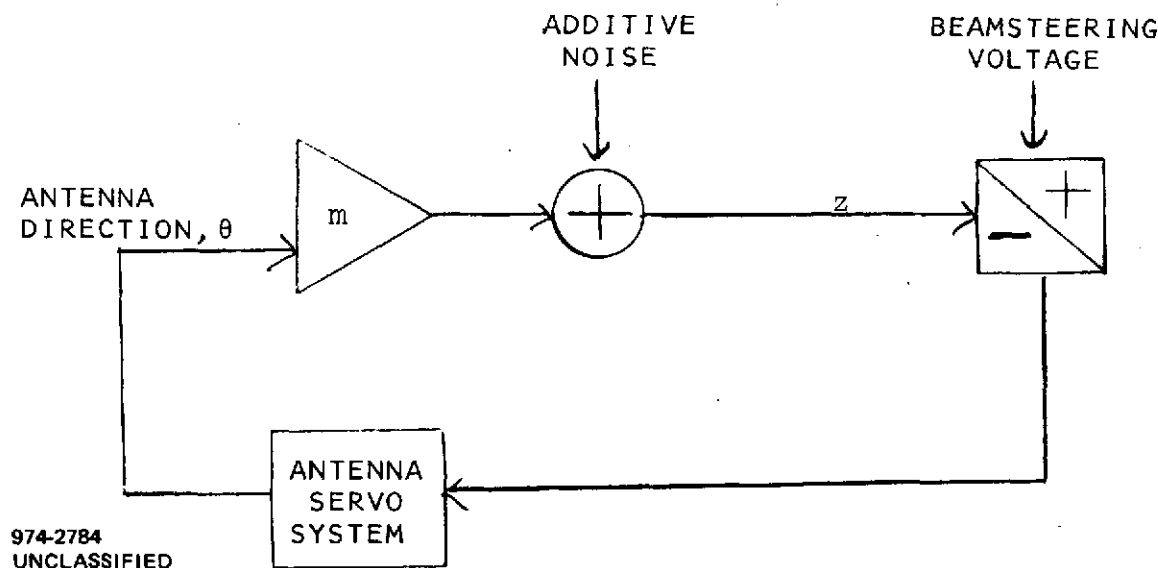


Figure 2. Linearized Autotrack Control System

$$\begin{aligned}
s_1 s_1^* &= 2P_S G_R^2 \\
s_2 s_2^* &\approx 0 \\
s_1 s_2^* &= z \Big|_{\theta=0} = \frac{2P_S G_R^2 (1-\alpha^2)}{(1+\alpha)^2}
\end{aligned} \tag{21}$$

Thus, from (10), (12), (19), (20) and (21), the effect of noise and gain imbalance on the beam pointing angle θ is to contribute a mean offset of

$$\bar{\theta} = \frac{\bar{z}}{m} = - \frac{(1-\alpha^2)\theta_B^2}{5.55(1+\alpha^2)\theta_q^2} - \frac{(1+\alpha)^2\theta_B^2}{11.1P_S(1+\alpha^2)\theta_q^2} (2\lambda\sqrt{N_{R1}N_{R2}} + N_{IA} - \alpha^2 N_{IB}) \tag{22}$$

with a variance of

$$\begin{aligned}
\sigma^2 &= \text{Var}(\theta) = \text{Var}(z)/m^2 \\
&= \frac{(1+\alpha)^4 \theta_B^4}{61.6TWP_S(1+\alpha^2)^2 \theta_q^2} (2N_{R2} + N_{IA} + \alpha^2 N_{IB} - 2\rho\alpha\sqrt{N_{IA}N_{IB}}) \\
&\quad + \frac{(1+\alpha)^4 \theta_B^4}{123.2TWP_S^2(1+\alpha^2)^2 \theta_q^2} (2N_{R1} + N_{IA} + \alpha^2 N_{IB} + 2\rho\alpha\sqrt{N_{IA}N_{IB}}) \\
&\quad \cdot (2N_{R2} + N_{IA} + \alpha^2 N_{IB} - 2\rho\alpha\sqrt{N_{IA}N_{IB}})
\end{aligned} \tag{23}$$

Assuming that the receiver noises are uncorrelated ($\lambda=0$), and the received interference noises are uncorrelated as well ($\rho=0$), results in

$$\frac{\bar{\theta}}{\theta_B} = - \frac{(1-\alpha^2)}{5.55(1+\alpha^2)} (\theta_B/\theta_q) - \frac{(1+\alpha)^2 (N_{IA} - \alpha^2 N_{IB})}{11.1(1+\alpha^2)P_S} (\theta_B/\theta_q) \tag{24}$$

and

$$\begin{aligned}
\frac{\sigma_\theta^2}{\theta_B^2} &= \frac{(1+\alpha)^4 (2N_{R2} + N_{IA} + \alpha^2 N_{IB})}{61.6TWP_S(1+\alpha^2)^2} (\theta_B/\theta_q)^2 \\
&\quad + \frac{(1+\alpha)^4 (2N_{R1} + N_{IA} + \alpha^2 N_{IB}) (2N_{R2} + N_{IA} + \alpha^2 N_{IB}) (\theta_B/\theta_q)^2}{123.2TWP_S^2(1+\alpha^2)^2 P_S^2}
\end{aligned} \tag{25}$$

Under idealized conditions of no gain imbalance ($\alpha=1$) and interference noises equal in strength in the two squinted beams ($N_{IA}=N_{IB}$), the bias error in (24) is zero. More realistically, if a 0.5 dB gain imbalance ($\alpha^2 \approx 0.9$) were present, with interference noises differing so that

$$\frac{N_{IA} - \alpha^2 N_{IB}}{P_S} = 0.1 \quad (26)$$

then there would be a bias error of

$$\bar{\theta}/\theta_B = (0.027)(\theta_B/\theta_q)$$

which, for $\theta_B \approx 2\theta_q$, will produce negligible loss of main beam gain. However, a strong directional interference, for which $(N_{IA} - \alpha^2 N_{IB})/P_S$ is greater than 1, can cause a significant bias error.

The usual case, however, will be one for which the bias error may be neglected and attention focused on the variance. For this case, we assume that

$$\alpha = 1$$

$$N_{R_1} = N_{R_2} \quad (27)$$

$$\theta_B = 2\theta_q$$

resulting in

$$\sigma_\theta^2/\theta_B^2 = 4 \left[\frac{0.13}{TW(CNR_\Sigma)} + \frac{0.13}{(TW(CNR_\Sigma))^2} \right] \quad (28)$$

where $CNR_\Sigma \stackrel{\Delta}{=} \text{carrier-to-noise ratio in the } \Sigma \text{ channel}$

$$= \frac{P_S}{N_{R_1} + (N_{IA} + \alpha^2 N_{IB})/2} \quad (29)$$

The noise integration time T may be replaced by the reciprocal of the servo system noise bandwidth, so that

$$(\sigma_\theta/\theta_B)^2 = \frac{0.52}{CNR_\Sigma} \left(\frac{b_n}{W} \right) \left(1 + \frac{1}{CNR_\Sigma} \right) \quad (30)$$

where $b_n \stackrel{\Delta}{=} \text{servo system noise bandwidth in Hz.}$

APPENDIX XIII

AN APC LOOP FOR PARAMP PHASE CORRECTION IN TDRSS AUTOTRACK SYSTEMS

INTRODUCTION

Analyses of the S-band user and the TDRSS autotrack systems have assumed a maximum phase offset between Σ - and Δ -receivers of 20° . This assumption was taken from the work by Martin-Marietta on TDRS autotrack design [1]. Subsequent communication from L. Deerkoski and P. Dalle-Mura of NASA-GSFC has indicated that NASA's experience does not support this assumption when a paramp receiver is used. In fact, no data exist to support any assumption of phase offset.

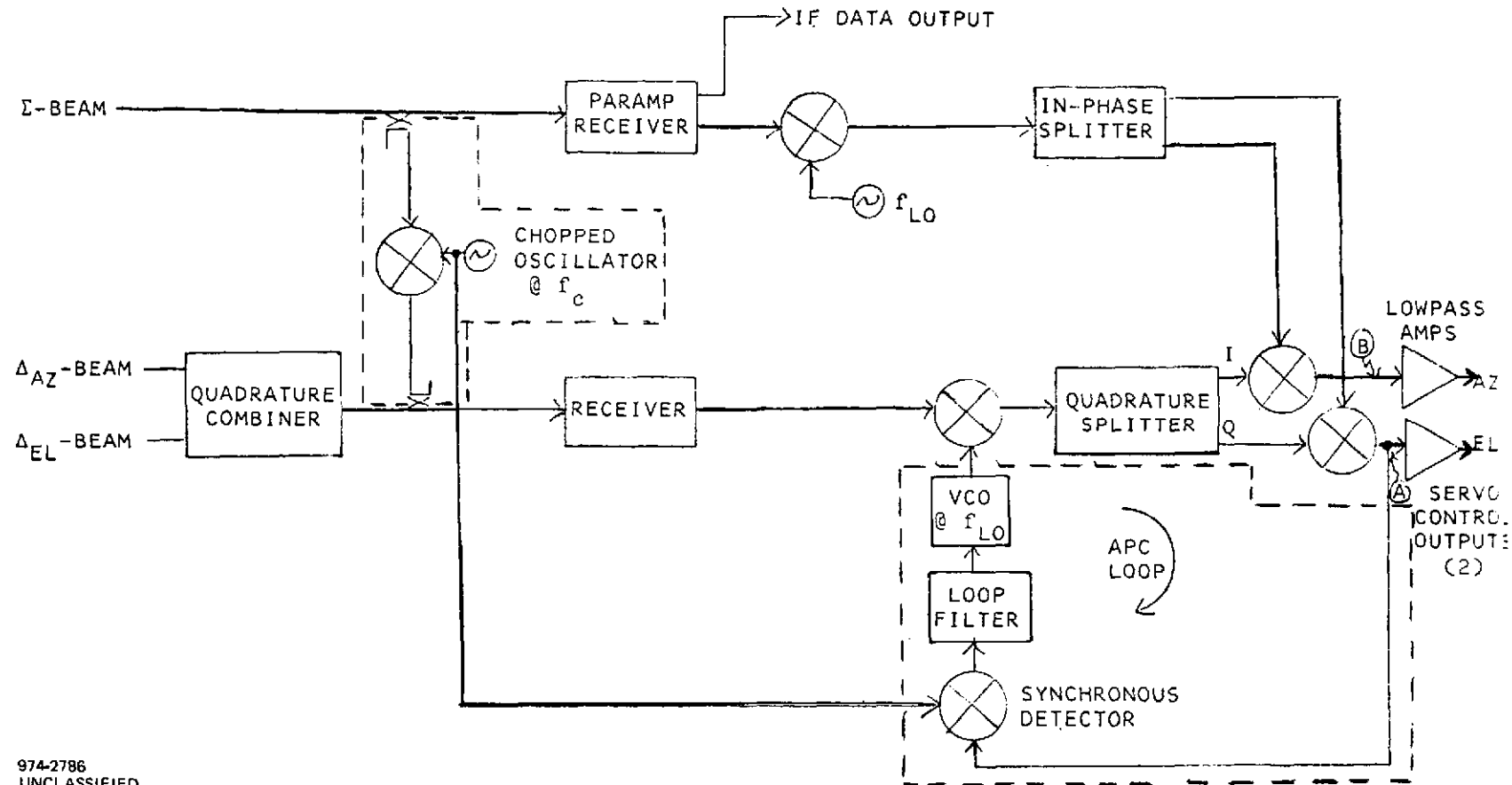
If the phase offset between the Σ - and Δ -receivers reaches 90° , the autotrack loop gain goes to zero. If it wanders between 90° and 270° , the loop gain changes sign and the system becomes unstable.

An automatic phase control (APC) loop is described and analyzed in this appendix so that the phase shift in the Δ -channel tracks that in the Σ -channel, keeping the phase offset near 0° .

DESCRIPTION OF THE APC LOOP

A functional block diagram of a two-channel monopulse system using quadrature multiplexing of the Δ -beams and incorporating the APC loop is given in Figure 1. The dotted-line boxes are used to indicate those items added to implement the APC. Some of the Σ -beam signal is coupled into the Δ -channel receiver after biphasic chopping at frequency f_c . After passing through the Δ -channel receiver and phase detectors, it causes an f_c component to appear at point A whose amplitude is proportional to the sine of the phase offset between the Σ - and Δ -receivers. This signal is then synchronously detected and used to control the phase of a VCO operating at f_{LO} to establish the desired phase correction.

One may note that the insertion of the chopped Σ -beam signal into the Δ -channel receiver is similar to a monoscan technique in which time-multiplexed Δ -beam signals are chopped and coherently combined with the Σ -beam to use a common



974-2786
UNCLASSIFIED

Figure 1. Functional Block Diagram of Two-Channel Monopulse with APC Stabilization

receiver. A significant difference in the hardware, however, is that the monoscan converter generally uses low loss diode switches for multiplexing and chopping because the autotrack system cannot tolerate excessive Δ -channel losses. In this APC approach, however, the chopped signal is used only for phase control, and not directly for autotrack control. As will be seen in the analysis to follow, it is fairly tolerant to chopper losses, so that a diode mixer may be used instead of an RF switch. An RF switch and its driver may be expected to require 1 watt of DC power [2], whereas the mixer with its oscillator can be operated with about 50 milliwatts of DC power.

NOISE EFFECTS ON THE APC LOOP

Figure 2 has been drawn to aid in the noise analysis of the APC loop. All noises shown are assumed to be zero mean, complex Gaussian random processes. From that figure it may be seen that the open loop phase error signal in complex envelope notation is given by

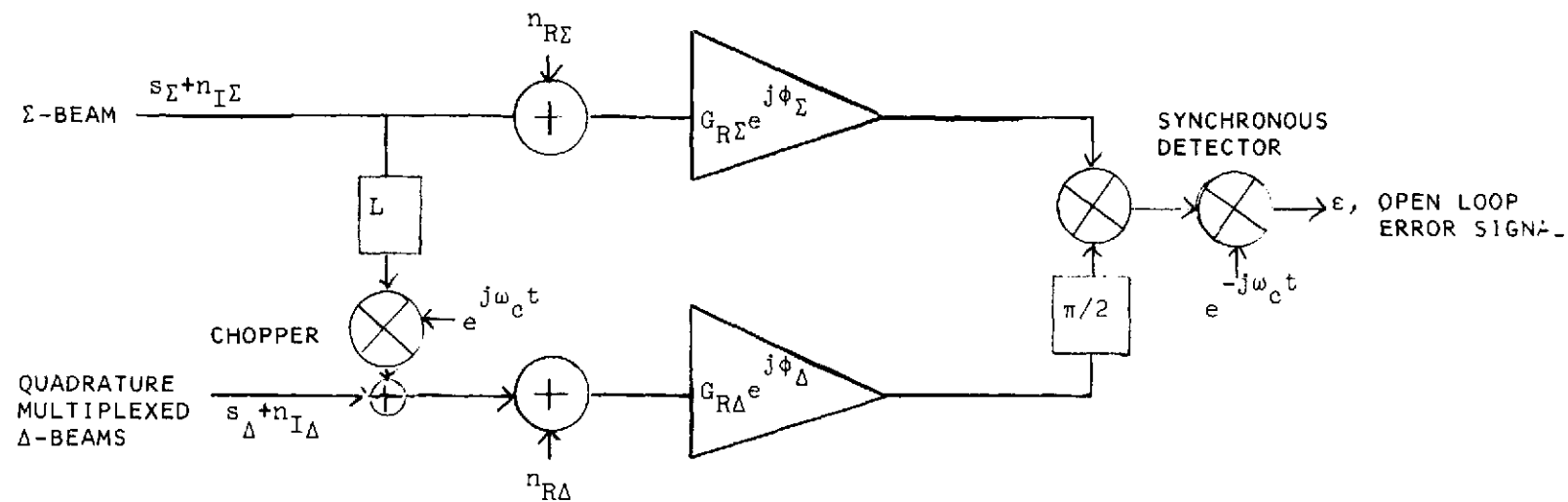
$$\begin{aligned}
 \epsilon &= [L(s_{\Sigma}^{+n_{I\Sigma}})e^{j\omega_c t} + s_{\Delta}^{+n_{I\Delta}} + n_{R\Delta}]G_{R\Delta}e^{j(\phi_{\Delta} + \pi/2)} \\
 &\quad \cdot (s_{\Sigma}^{*+n_{I\Sigma}^*} + n_{R\Sigma}^*)G_{R\Sigma}e^{-j\phi_{\Sigma}} \cdot e^{-j\omega_c t} \\
 &= G_{R\Delta}G_{R\Sigma}e^{j(\phi_{\Delta} - \phi_{\Sigma} + \pi/2)} [L(s_{\Sigma}^{+n_{I\Sigma}}) + (s_{\Delta}^{+n_{I\Delta}} + n_{R\Delta})e^{-j\omega_c t}] \\
 &\quad \cdot (s_{\Sigma}^{*+n_{I\Sigma}^*} + n_{R\Sigma}^*)
 \end{aligned} \tag{1}$$

The actual error signal appearing at this point is $\text{Re}\{\epsilon\}$.

The mean value of ϵ has a DC component given by

$$\bar{\epsilon}_{DC} = G_{R\Delta}G_{R\Sigma}L e^{j(\phi_{\Delta} - \phi_{\Sigma} + \pi/2)} [|s_{\Sigma}|^2 + \overline{|n_{I\Sigma}|^2}], \tag{2}$$

indicating that the Σ -beam antenna noise aids the Σ -beam signal in controlling the APC loop. The squared magnitude $\bar{\epsilon}_{DC}^2$ is a measure of the signal power in the APC loop. The APC input signal-to-noise ratio will be defined as the ratio of $|\bar{\epsilon}_{DC}|^2$ to the variance of ϵ at DC.



DEFINITION OF SYMBOLS (COMPLEX ENVELOPE NOTATION)

- s_{Σ} = Σ -BEAM SIGNAL INTO Σ -RECEIVER
- $n_{I\Sigma}$ = Σ -BEAM ANTENNA NOISE (INTERFERENCE)
- s_{Δ} = MULTIPLEXED Δ -BEAM SIGNALS INTO Δ -RECEIVER
- $n_{I\Delta}$ = MULTIPLEXED Δ -BEAM ANTENNA NOISE (INTERFERENCE)
- L = COUPLER AND CHOPPER LOSS FACTOR FOR INSERTION OF Σ -SIGNAL INTO Δ -RECEIVER (VOLTAGE RATIO)
- ω_c = CHOPPER FREQUENCY (RAD/SEC)
- $n_{R\Sigma}$ = Σ -RECEIVER FRONT END NOISE
- $n_{R\Delta}$ = Δ -RECEIVER FRONT END NOISE
- $G_{R\Sigma}$ = VOLTAGE GAIN OF Σ -RECEIVER
- ϕ_{Σ} = PHASE SHIFT OF Σ -RECEIVER
- $G_{R\Delta}$ = VOLTAGE GAIN OF Δ -RECEIVER
- ϕ_{Δ} = PHASE SHIFT OF Δ -RECEIVER
- ϵ = APC LOOP ERROR SIGNAL (OPEN LOOP CONDITION)

974-2787

UNCLASSIFIED

Figure 2. Block Diagram for Noise Analysis of APC Loop

In determining the variance of ϵ at DC, several assumptions are necessary. First, it will be assumed that the doppler frequency f_c is high enough compared to the loop bandwidth so that $n_{I\Delta}e^{j\omega_c t}$ is uncorrelated with $n_{I\Sigma}$, even though $n_{I\Delta}$ and $n_{I\Sigma}$ may be highly correlated. The four noise processes, $n_{I\Sigma}$, $n_{R\Sigma}$, $n_{I\Delta}e^{-j\omega_c t}$, and $n_{R\Delta}e^{-j\omega_c t}$, are assumed to all be uncorrelated. However, their bandwidth (the IF receiver bandwidth) is assumed to be much greater than f_c , so that all have significant spectral content at DC. It should be noted that one of the signal terms, $s_{\Delta}e^{-j\omega_c t}s^*_\Sigma$ has all its power at f_c and none at DC. This is tantamount to the assumption of perfect balance in the synchronous detector.

The second moment of ϵ has the form

$$\overline{|\epsilon|^2} = \overline{\epsilon\epsilon^*} = G_{R\Delta}^2 G_{R\Sigma}^2 \overline{(s_1 + n_1)(s_1^* + n_1^*)(s_2 + n_2)(s_2^* + n_2^*)} \quad (3)$$

where

$$\begin{aligned} s_1 &= Ls_\Sigma + s_\Delta e^{-j\omega_c t} \\ s_2 &= s_\Sigma \\ n_1 &= Ln_{I\Sigma} + (n_{I\Delta} + n_{R\Delta})e^{-j\omega_c t} \\ n_2 &= n_{I\Sigma} + n_{R\Sigma} \end{aligned}$$

Applying Reed's Theorem 3 to (3) gives

$$\begin{aligned} \overline{|\epsilon|^2} &= G_{R\Delta}^2 G_{R\Sigma}^2 [|s_1 s_2^*|^2 + |s_1|^2 \overline{|n_2|^2} + s_1 s_2^* \overline{n_1^* n_2} \\ &\quad + s_1^* s_2 \overline{n_1 n_2^*} + |s_2|^2 \overline{|n_1|^2} + \overline{|n_1|^2} \overline{|n_2|^2} + \overline{|n_1^* n_2|^2}] \end{aligned} \quad (4)$$

Using the assumptions listed above with (3) and (4) gives

$$\begin{aligned} \overline{|\epsilon|^2}_{DC} &= G_{R\Delta}^2 G_{R\Sigma}^2 [L^2 |s_\Sigma|^4 + (L^2 |s_\Sigma|^2 + |s_\Delta|^2) (\overline{|n_{I\Sigma}|^2} + \overline{|n_{R\Sigma}|^2}) \\ &\quad + 3L^2 |s_\Sigma|^2 \overline{|n_{I\Sigma}|^2} + |s_\Sigma|^2 (\overline{|n_{I\Delta}|^2} + \overline{|n_{R\Delta}|^2}) \\ &\quad + (L^2 \overline{|n_{I\Sigma}|^2} + \overline{|n_{I\Delta}|^2} + \overline{|n_{R\Delta}|^2}) (\overline{|n_{I\Sigma}|^2} + \overline{|n_{R\Sigma}|^2}) + L^2 (\overline{|n_{I\Sigma}|^2})^2] \end{aligned} \quad (5)$$

Note that we have used $L^2|s_\Sigma|^4$ as the DC component of $|s_1 s_2^*|^2$, since $s_\Delta e^{-j\omega_c t} s_\Sigma^*$ has all its power at f_c . The DC variance of ϵ then is given by

$$\begin{aligned}
 \text{Var}(\epsilon)_{\text{DC}} &= \overline{|\epsilon|_{\text{DC}}^2} - |\overline{\epsilon}_{\text{DC}}|^2 \\
 &= G_{R\Delta}^2 G_{R\Sigma}^2 [(L^2|s_\Sigma|^2 + |s_\Delta|^2)(\overline{|n_{I\Sigma}|^2} + \overline{|n_{R\Sigma}|^2}) \\
 &\quad + L^2|s_\Sigma|^2 \overline{|n_{I\Sigma}|^2} + |s_\Sigma|^2 (\overline{|n_{I\Delta}|^2} + \overline{|n_{R\Delta}|^2}) \\
 &\quad + (L^2 \overline{|n_{I\Sigma}|^2} + \overline{|n_{I\Delta}|^2} + \overline{|n_{R\Delta}|^2})(\overline{|n_{I\Sigma}|^2} + \overline{|n_{R\Sigma}|^2})] \quad (6)
 \end{aligned}$$

Equation (6) may be simplified by introducing several additional assumptions. First, we assume that the Σ -channel preamp is a low noise type while the Δ -channel preamp has a higher noise level, so that we will assume

$$\overline{|n_{R\Sigma}|^2} + \overline{|n_{I\Sigma}|^2} \leq \overline{|n_{R\Delta}|^2} + \overline{|n_{I\Delta}|^2} \quad (7)$$

Secondly, we assume high enough Σ -beam signal power so that

$$|s_\Sigma|^2 > \overline{|n_{I\Sigma}|^2} \quad (8)$$

Finally, we assume the coupling and chopper loss factor L be such that

$$L^2 \ll 1 \quad (9)$$

Then (6) gives

$$\begin{aligned}
 \text{Var}(\epsilon)_{\text{DC}} &\approx G_{R\Delta}^2 G_{R\Sigma}^2 [|s_\Delta|^2 (\overline{|n_{I\Sigma}|^2} + \overline{|n_{R\Sigma}|^2}) \\
 &\quad + |s_\Sigma|^2 (\overline{|n_{I\Delta}|^2} + \overline{|n_{R\Delta}|^2}) \\
 &\quad + (\overline{|n_{I\Delta}|^2} + \overline{|n_{R\Delta}|^2})(\overline{|n_{I\Sigma}|^2} + \overline{|n_{R\Sigma}|^2})] \quad (10)
 \end{aligned}$$

Introducing the following notational changes:

$S_{\Sigma} = |s_{\Sigma}|^2$, the Σ -channel signal power
 $S_{\Delta} = |s_{\Delta}|^2$, the Δ -channel signal power
 $N_{\Sigma} = |n_{I\Sigma}|^2 + |n_{R\Sigma}|^2$, the total Σ -channel noise power
 $N_{\Delta} = |n_{I\Delta}|^2 + |n_{R\Delta}|^2$, the total Δ -channel noise power
 gives

$$\text{Var}(\epsilon)_{\text{DC}} \approx G_{R\Delta}^2 G_{R\Sigma}^2 [S_{\Delta} N_{\Sigma} + S_{\Sigma} N_{\Delta} + N_{\Delta} N_{\Sigma}] \quad (11)$$

Although S_{Δ} is small compared to S_{Σ} during tracking, that may not be the case during acquisition, so the $S_{\Delta} N_{\Sigma}$ term in (11) is not discarded.

Defining the APC loop input signal-to-noise ratio as

$$\text{SNR}_i \triangleq \frac{|\bar{\epsilon}_{\text{DC}}|^2}{\text{Var}(\epsilon)_{\text{DC}}} \quad (12)$$

we have from (2) and (11)

$$\begin{aligned}
 \text{SNR}_i &= \frac{L^2 (S_{\Sigma} + N_{I\Sigma})^2}{S_{\Delta} N_{\Sigma} + S_{\Sigma} N_{\Delta} + N_{\Delta} N_{\Sigma}} \\
 &= \frac{L^2 (1 + N_{I\Sigma}/S_{\Sigma})^2 (S_{\Sigma}/N_{\Delta})}{[1 + (\frac{N_{\Sigma}}{S_{\Sigma}})(1 + \frac{N_{\Delta}}{N_{\Sigma}})]} \quad (13)
 \end{aligned}$$

where $N_{I\Sigma} = |n_{I\Sigma}|^2$, the Σ -beam antenna noise (interference) power.

When the APC loop is closed and allowed to perform the phase correction, the signal-to-noise ratio is improved [4] by the ratio of the two-sided IF noise bandwidth (B_{IF}) to twice the closed loop APC lowpass noise bandwidth (B_L). That is,

$$\text{SNR}_L \approx \text{SNR}_i (B_{\text{IF}}/2B_L), \quad \text{for } \text{SNR}_L \gg 1 \quad (14)$$

The resulting rms phase jitter is [4]

$$\sigma_\phi = \frac{1}{\sqrt{2\text{SNR}_L}} \text{ radians, for } \text{SNR}_L \gg 1 \quad (15)$$

Thus, even if SNR_i is not large, low jitter APC operation can be provided by making B_L small compared to B_{IF} .

APPLICATION TO THE Ku-BAND TDRS AUTOTRACK SYSTEM

An analysis of the recommended Ku-band TDRS autotrack system was performed in Section 4.2. Table I of this report gives the signal and noise power levels required in (13), derived from the levels used in Section 4.2.

TABLE I

SIGNAL AND NOISE POWER LEVELS FOR TDRS AUTOTRACK SYSTEM

<u>Symbol</u>	<u>Value from [1, Table I]</u>
$N_{I\Sigma}$	-141.4 dBW
N_Δ	-136.6 dBW
N_Σ	-140.3 dBW
S_Σ	-130.9 dBW
S_Δ^*	-133.9 dBW

REPRODUCIBILITY OF THE
ORIGINAL PAGE IS POOR

*We assume at a maximum $S_\Delta = \frac{1}{2}S_\Sigma$, the factor 1/2 arising from a 3 dB loss in the quadrature hybrid.

Using these power levels in (13) results in

$$\text{SNR}_i = 3.31L^2 \quad (14)$$

Assuming 30 dB of loss in the couplers and chopper, we have

$$L^2 = 10^{-3} \quad (15)$$

and

$$\text{SNR}_i = 3.31 \times 10^{-3} \quad (16)$$

If an rms phase jitter of

$$\begin{aligned}\sigma_\phi &= 0.1 \text{ radian} \\ &= 5.7 \text{ degrees}\end{aligned} \quad (17)$$

is desired, then from (15) we have

$$\text{SNR}_L = 50 \quad (18)$$

Using (16) and (18) in (14) relates the APC loop noise bandwidth to the autotrack IF bandwidth by

$$B_L = 3.31 \times 10^{-5} B_{IF} \quad (19)$$

The IF bandwidth used is 1.5 MHz, giving a loop noise bandwidth requirement of

$$B_L = 49.7 \text{ Hz} \quad (20)$$

EFFECT OF INCIDENTAL AM

If there is incidental AM on the received signal with modulation frequency f_c , then the chopper will demodulate the AM component from the Σ -signal and place it in the Δ -channel. This will cause a bias on the autotrack control signal whose effect will now be determined under the assumption of small APC phase error.

We first consider the autotrack system with no incidental AM. With no noise the autotrack error signal (at either point A or point B in Figure 1) is

$$z(t) = G_{R\Sigma} G_{R\Delta} s_\Sigma^*(t) [s_\Delta(t) + L s_\Sigma(t) \cos \omega_c t] \quad (21)$$

which has a DC component of

$$z(t)_{DC} = G_{R\Sigma} G_{R\Delta} s_{\Sigma}^*(t) s_{\Delta}(t) \quad (22)$$

If the received signal is assumed to have incidental AM at f_c of modulation index m that is in phase with the chopper oscillator, then the autotrack error signal is

$$\begin{aligned} z(t) &= \frac{G_{R\Sigma} G_{R\Delta} s_{\Sigma}^*(t)(1+m\cos\omega_c t)}{(1+m^2/2)} [s_{\Delta}(t)(1+m\cos\omega_c t) \\ &\quad + Ls_{\Sigma}(t)\cos\omega_c t(1+m\cos\omega_c t)] \\ &= \frac{G_{R\Sigma} G_{R\Delta} s_{\Sigma}^*(t)(1+m\cos\omega_c t)^2 [s_{\Delta}(t) + Ls_{\Sigma}(t)\cos\omega_c t]}{(1+m^2/2)} \end{aligned} \quad (23)$$

The DC component of (23) is

$$z(t)_{DC} = G_{R\Sigma} G_{R\Delta} s_{\Sigma}^*(t) [s_{\Delta}(t) + \frac{mL}{1+m^2/2} s_{\Sigma}(t)] \quad (24)$$

For small modulation index, the second term of (24) contributes a control signal error

$$z_e(t)_{DC} = mL G_{R\Sigma} G_{R\Delta} s_{\Sigma}^*(t) s_{\Sigma}(t) \quad (25)$$

Following a development as in Appendix XII, it may be shown that the slope of the control signal voltage with respect to pointing error θ is

$$\mu = \frac{\partial z}{\partial \theta} = \frac{2.773}{2\theta_B} G_{R\Sigma} G_{R\Delta} s_{\Sigma}^*(t) s_{\Sigma}(t) \quad (26)$$

where θ_B is the full 3 dB beamwidth of the Σ -beam. Thus, the control signal error in (25) corresponds to a pointing error of

$$\theta_e = \frac{z_e(t)_{DC}}{\mu} = \frac{2mL}{2.773} \theta_B \quad (27)$$

The pointing loss (assuming a Gaussian beam shape) is then

$$\begin{aligned} L_P &= -10 \log_{10} [e^{-2.773(\theta_e/\theta_B)^2}] \\ &= -10 \log_{10} [e^{-(2mL)^2/2.773}] \end{aligned} \quad (28)$$

If $mL < 0.09$, then the pointing loss from this contribution alone is less than 0.05 dB. Typically, APC designs will have $L < 0.1$ (20 dB loss), so that the effect of moderate index incidental AM will be negligible.

AN IMPROVED AUTOTRACK AGC

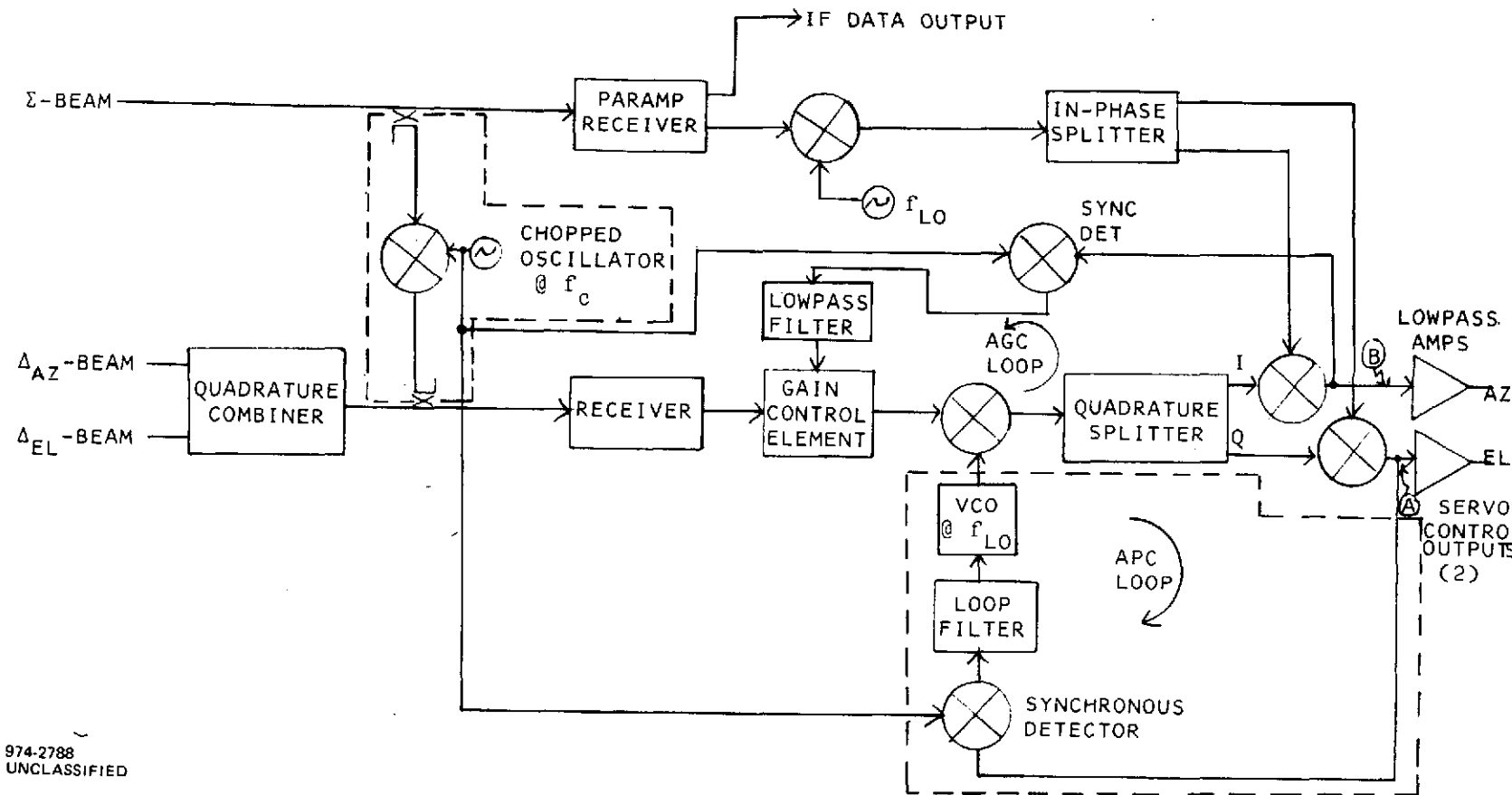
Generally, automatic gain control (AGC) in an autotrack system is implemented using noncoherent (square law) detection of the sum channel signal. The detector output in such systems has a DC component whose voltage is proportional to $G_R^2 (S_\Sigma + N_\Sigma)$ [5], and other frequency-distributed noise components which may be rejected by lowpass filtering. If N_Σ is unknown, it introduces a fundamental limitation on the accuracy of AGC control at low signal-to-noise ratio.

In a two-channel monopulse system with APC correction, as diagrammed in Figure 1, a signal exists at point B which may be used for gain control in a manner analogous to the use of the signal at point A for phase control. A block diagram incorporating this type of AGC is given in Figure 3.

As may be seen from Figure 3, the AGC implementation is no more complicated than noncoherent detection of the Σ -channel signal driving a gain control element. It has two important advantages over the Σ -channel AGC: Δ -channel gain variations are detected and partially corrected, and the DC noise component is smaller relative to the DC signal component.

Both of these claims are evident from the fact that the AGC control voltage is equal to the imaginary part of Equation (2). Once the APC loop acquires lock, the AGC control voltage after lowpass filtering is given by

$$V_{AGC} = G_R \Delta G_R \Sigma I_\epsilon (S_\Sigma + N_{I\Sigma}) \quad (29)$$



974-2788
UNCLASSIFIED

Figure 3. Functional Block Diagram of Two-Channel Monopulse with APC Stabilization and Improved AGC

APPENDIX XIV

USER EIRP REQUIREMENTS FOR TDRS AUTOTRACK ALTERNATIVES

INTRODUCTION

Three alternative autotrack configurations for the TDRS antenna are considered in this memo. They are S-band autotrack, Ku-band autotrack with a spoiled beam, and Ku-band autotrack with an unspoiled beam. For each of these configurations, both tunnel diode amplifier (TDA) and parametric amplifier (paramp) front ends are considered.

The initial pointing uncertainty of the TDRS antenna, upon command from the ground station is $\pm 0.45^\circ$. This uncertainty is within the tracking range of the S-band and spoiled beam Ku-band systems, but not within the tracking range of the unspoiled beam Ku-band system. Thus, the unspoiled beam Ku-band system would need an acquisition mode different from the normal tracking mode, while the other two systems would not. This report is concerned with the user EIRP requirements for the tracking mode.

AUTOTRACK BEAMPOINTING ERRORS

The most severe pointing requirements are for steering the narrow Ku-band beam at a single access user. The unspoiled Ku-band beam may be modelled as having a Gaussian shape near its peak,

$$G(\theta) = G_0 \exp(-2.773\theta^2/\theta_b^2) \quad (1)$$

where $\theta_b = 0.35^\circ$ is the 3 dB beamwidth. If $\theta = \theta_e$ represents the allowable pointing error for a 1/2 dB loss in $G(\theta)$, it may be determined from (1) that

$$\theta_e = 0.2038\theta_b \approx 0.0713 \text{ degrees} \quad (2)$$

There are a number of sources of pointing error in an autotrack system. There are offset errors due to slight misalignment of the autotrack feed system from

the data beam feed system, and due to precomparator and post-comparator amplitude and phase imbalance. These errors can be significant but are not discussed at this time. The pointing errors of concern in this memo are tracking errors arising from dynamic servo lag and noise effects. The relative contributions of these error components are interrelated through their dependence on the servo loop noise bandwidth b_n and the sum beam carrier-to-noise ratio CNR_Σ .

TRACKING ERROR ANALYSIS

In Appendix XI, the worst-case dynamic servo lag is found from Equations (23) and (27) to be

$$\theta_L = K_{2\max} / 4b_n \quad (3)$$

where $K_{2\max} = 0.0127 \text{ deg/sec}$ is the maximum angular velocity to be tracked, and b_n is the servo loop noise bandwidth in Hz.

In Appendix XII, noise was found to have two effects. First, noise (interference) received on the antenna can contribute a bias error, particularly if there is a precomparator amplitude imbalance. In Equation (24) of that memo, the noise bias error $\bar{\theta}$ was determined to be

$$\frac{\bar{\theta}}{\theta_B} = \frac{(1+\alpha)^2 (N_{IA} - \alpha^2 N_{IB})}{11.1(1+\alpha^2)P_S} (\theta_B/\theta_q)$$

where

- θ_B is the 3 dB beamwidth of each of the squinted beams (beam A and beam B)
- θ_q is the squint angle
- α is the amplitude imbalance factor
- P_S is the signal power in the sum beam
- $N_{IA(B)}$ is the received noise power in the A(B) beam.

We will use as a worst case a 0.4 dB amplitude imbalance factor, * so that

$$\alpha = (0.1)^{0.02} = 0.955 \quad (5)$$

Assuming that $\theta_B = 2\theta_q$ and $N_{IA} = N_{IB}$, we obtain

$$\bar{\theta} = 3.17 \times 10^{-2} \theta_B N_{IA} / P_S \quad (6)$$

The second effect of noise is to cause a variance in the pointing angle σ_θ , found in Equation (30) of Appendix XII to be

$$\sigma_\theta = \theta_B \sqrt{\frac{0.52}{CNR_\Sigma} \left(\frac{b_n}{W} \right) \left(1 + \frac{1}{CNR_\Sigma} \right)} \quad (7)$$

where W is the IF bandwidth of the autotrack receivers, and CNR_Σ is the sum beam channel carrier-to-noise ratio in the band W .

The total tracking error is determined by combining the three components in (3), (6) and (7) and requiring that they be equal to the allowable pointing error given by (2). The combination will use $3\sigma_\theta$, so that with Gaussian jitter the required pointing accuracy is maintained at least 99.6% of the time. Thus, we have

$$\theta_L + \bar{\theta} + 3\sigma_\theta = \theta_e$$

or

$$\frac{0.0127}{4b_n} + 3.17 \times 10^{-2} \theta_B \frac{N_{IA}}{P_S} + 3\theta_B \sqrt{\frac{0.52}{CNR_\Sigma} \left(\frac{b_n}{W} \right) \left(1 + \frac{1}{CNR_\Sigma} \right)} = 0.713 \quad (8)$$

Now

$$N_{IA} = kW T_A \quad (9)$$

*J. C. Pullara, et al, "Dual S- and Ku-Band Tracking Feed for a TDRS Reflector Antenna," Final Report (Phase 1) to NASA GSFC, June 1974, p. 4-51.

and

$$CNR = P_S / kWT_R \quad (10)$$

where

T_A is the antenna noise temperature

T_R is the total receiver noise temperature

$k = 1.38 \times 10^{-23}$ watts/Hz/° K (Boltzmann's constant)

Combining (8), (9) and (10) results in

$$\frac{0.0127}{4b_n} + 3.17 \times 10^{-2} \theta_B \frac{kWT_A}{P_S} + 3\theta_B \sqrt{\frac{0.52kT_R b_n}{P_S}} \left(1 + \frac{kWT_R}{P_S}\right) = 0.0713 \quad (11)$$

Now θ_L varies as b_n^{-1} and $3\sigma_\theta$ varies as $\sqrt{b_n}$. Minimizing the sum of these two terms with respect to b_n results in

$$2\theta_L = 3\sigma_\theta \quad (12)$$

whence

$$3\theta_L + \bar{\theta}_B = \theta_e = 0.0713 \quad (13)$$

or

$$\frac{3(0.0127)}{4b_n} + 3.17 \times 10^{-2} \theta_B \frac{kWT_A}{P_S} = 0.0713 \quad (14)$$

Thus,

$$b_n^{-1} = 7.49 \left(1 - 0.444 \theta_B \frac{kWT_A}{P_S}\right) \quad (15)$$

Combining (15) and (12) results in

$$\frac{P_S}{k} = \frac{278\theta_B^2 T_R (1+kWT_R/P_S)}{(1-0.444\theta_B kWT_A/P_S)^3} \quad (16)$$

For each of the three autotrack systems, known values of θ_B , T_A and T_R will be used in (16), along with the known relationship between user EIRP and P_S , to determine the required user EIRP vs W for the autotrack system to provide the desired pointing accuracy. The P_S vs EIRP relationship and the pertinent noise temperatures are calculated in Table I. Equation (15) will then be used to determine the required value of b_n vs W for this performance to be achieved.

S-BAND AUTOTRACK

The following parameters will be applied to the S-band autotrack analysis:

$$\theta_B = 2.33^\circ$$

$$T_A = 270^\circ\text{K}$$

$$T_R = \begin{cases} 1270^\circ\text{K (TDA)} \\ 520^\circ\text{K (paramp)} \end{cases} \quad (17)$$

Equations (15) and (16) then give

$$b_n^{-1} = 7.47(1-279\text{kW}/P_S) \quad (18)$$

$$P_S/k = \begin{cases} 1.92 \times 10^6 (1-279\text{kW}/P_S)^{-3} (1+1270\text{kW}/P_S) & \text{TDA} \\ 7.85 \times 10^5 (1-279\text{kW}/P_S)^{-3} (1+520\text{kW}/P_S) & \text{paramp} \end{cases} \quad (19)$$

UNSPOILED KU-BAND AUTOTRACK

The following parameters will be applied to the unspoiled Ku-band autotrack analysis:

$$\theta_B = 0.35^\circ$$

$$T_A = 300^\circ\text{K}$$

$$T_R = \begin{cases} 1800^\circ\text{K (TDA)} \\ 450^\circ\text{K (paramp)} \end{cases} \quad (20)$$

Table I. Signal and Noise Power Calculations

Relationship Between EIRP and P_S/k	S	Ku	Ku Spoiled
Signal Power at antenna output* (dBw)	-157.2+EIRP	-157.6+EIRP	-157.6+EIRP
Line Losses* (dB)	-2	-2	-2
Beam-Spoiling Loss	--	--	-15
Signal Power at Sum Receiver Input* (dBw)			
= $10 \log_{10} P_S$	-159.2+EIRP	-159.6+EIRP	-174.6+EIRP
$10 \log_{10} (P_S/k)$ where $k = 1.38 \times 10^{-23}$	EIRP+69.4	EIRP+69.0	EIRP+54.0

Noise Temperature Calculations

Paramp Receiver Noise Temperature at			
Preamp Front End ($^{\circ}$ K), T_R	520	450	450
Paramp Preamp Noise Temperature ($^{\circ}$ K)	250	150	150
Antenna Output Noise Temperature at			
Preamp Front End ($^{\circ}$ K), T_A	270	300	300
TDA Preamp Noise Temperature ($^{\circ}$ K)	1000	1500	1500
TDA Receiver Noise Temperature at			
Preamp Front End ($^{\circ}$ K), T_R	1270	1800	1800

*Refer to GSFC Definition Phase Study Report of the TDRSS, Table 3-2.

ORIGINAL COPY OF THE
PAGE IS POORLY
REPRODUCIBLE

Equations (15) and (16) then give

$$b_n^{-1} = 7.47(1-46.6 \text{ kW}/P_S) \quad (21)$$

$$P_S/k = \begin{cases} 6.13 \times 10^4 (1-46.6 \text{ kW}/P_S)^{-3} (1+1800 \text{ kW}/P_S) & \text{TDA} \\ 1.53 \times 10^4 (1-46.6 \text{ kW}/P_S)^{-3} (1+450 \text{ kW}/P_S) & \text{paramp} \end{cases} \quad (22)$$

SPOILED BEAM KU-BAND AUTOTRACK

Beamspoiling of the TDRS Ku-band antenna has been analyzed at NASA-GSFC. It has been found that the separation of the difference beam peaks could be increased from $\pm 0.2^\circ$ in the unspoiled case to $\pm 0.5^\circ$ in the spoiled case. A similar increase of approximately 2.5:1 is present in the 3 dB beamwidth θ_B as well. A loss of 15 dB in the sum channel antenna gain has been found to accompany the beamspoiling, as indicated in Table I.

The following parameters will be applied to the spoiled beam Ku-band autotrack analysis:

$$\theta_B = 0.875^\circ$$

$$T_A = 300^\circ\text{K}$$

$$T_R = \begin{cases} 1800^\circ\text{K} & \text{(TDA)} \\ 450^\circ\text{K} & \text{(paramp)} \end{cases} \quad (23)$$

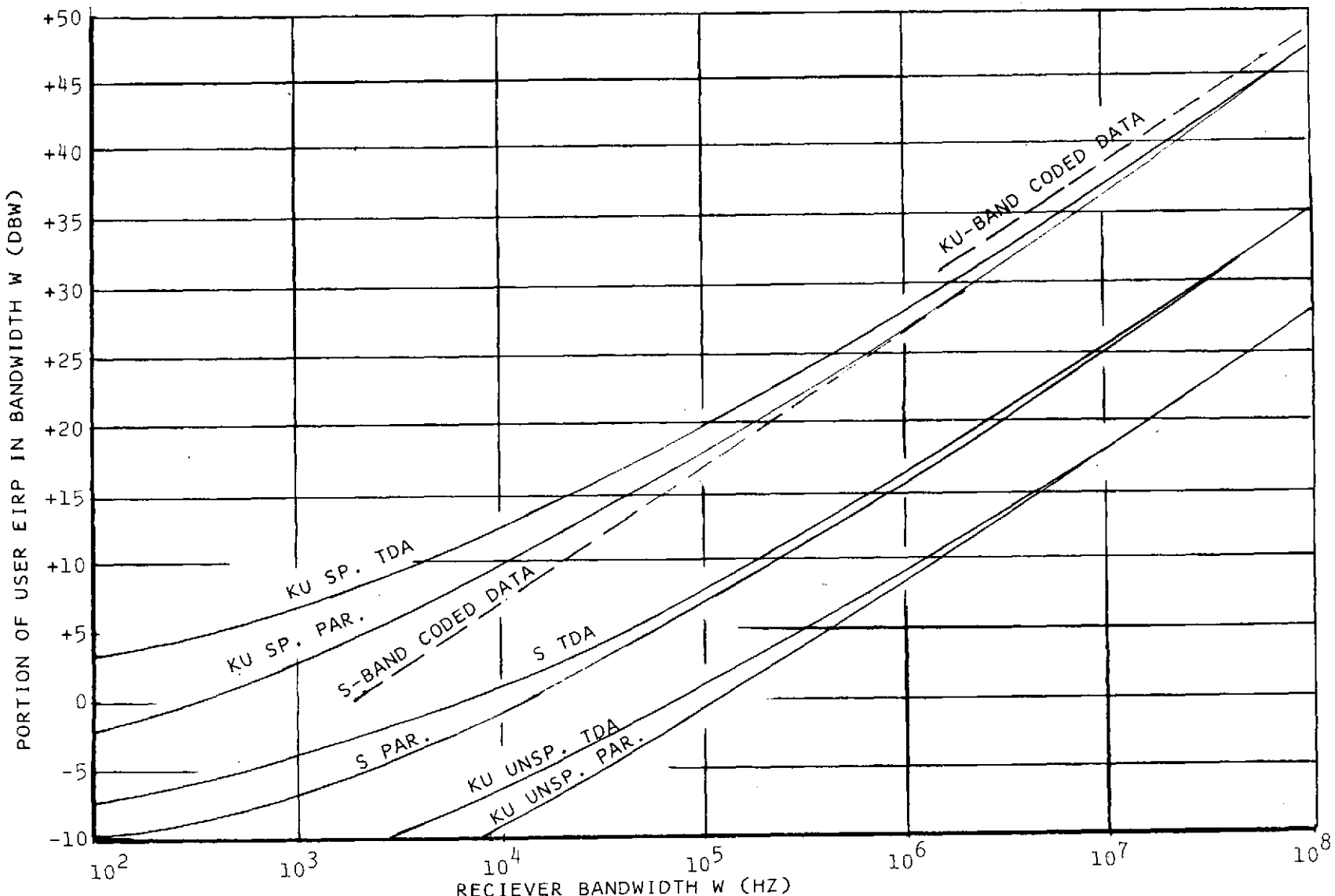
Equations (15) and (16) then give

$$b_n^{-1} = 7.47(1-116.6 \text{ kW}/P_S) \quad (24)$$

$$P_S/k = \begin{cases} 3.83 \times 10^5 (1-116.6 \text{ kW}/P_S)^{-3} (1+1800 \text{ kW}/P_S) & \text{TDA} \\ 9.58 \times 10^4 (1-116.6 \text{ kW}/P_S)^{-3} (1+450 \text{ kW}/P_S) & \text{paramp} \end{cases} \quad (25)$$

COMPARISON OF RESULTS

Using Equations (19), (22) and (25) along with the relationship between user EIRP and P_S/k given in Table I results in the curves of Figure 1. Equations (18), (21) and (24) are then used to derive the required servo loop noise bandwidth, plotted in Figure 2, for the curves of Figure 1 to apply.



974-2789
UNCLASSIFIED

Figure 1. User EIRP Requirements Vs Autotrack Receiver Bandwidth For Steering Ku-Band Beam to Within 0.5 dB Points (Solid Curves)

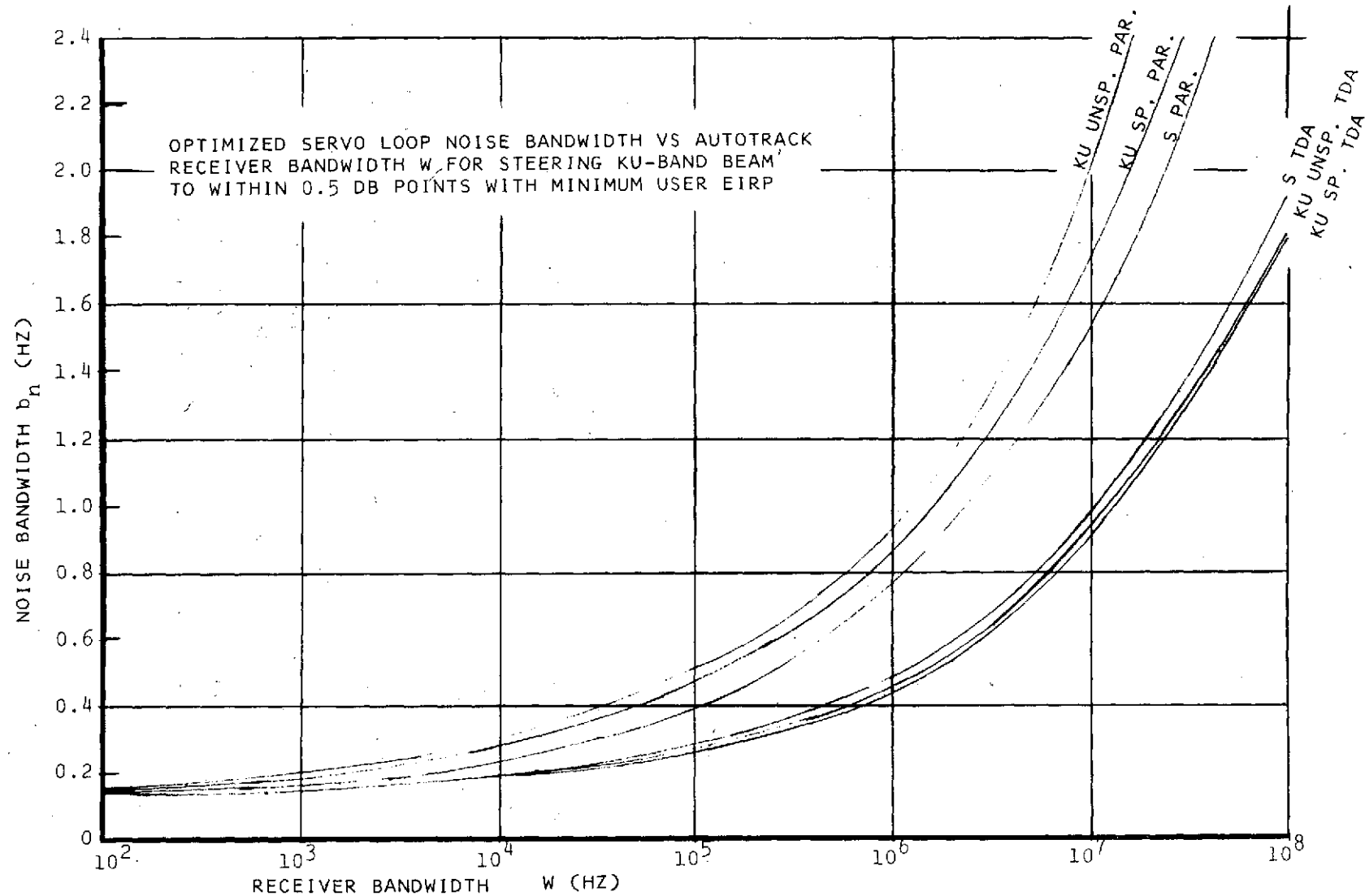


Figure 2. Optimized Servo Loop Noise Bandwidth Vs Autotrack Receiver Bandwidth W
For Steering Ku-Band Beam to Within 0.5 dB Points With Minimum User EIRP

It should be emphasized that the user EIRP in Figure 1 is only that portion that falls within the autotrack receiver band W . For example, if the user transmission is 100 MHz wide and W is 1 MHz, then the number on the ordinate of Figure 1 is approximately 1% of the required user EIRP. If the user transmits a narrowband pilot of bandwidth W or less to aid the TDRS autotrack system, then the ordinate of Figure 1 represents the required pilot EIRP.

To determine whether the normal user data transmissions are of sufficient power for autotrack use, the user EIRP for data vs W is also plotted in Figure 1 as dotted lines. These curves were obtained from Figures 3-4 and 3-6 of the GSFC Definition Phase Study Report of the TDRSS, assuming coded data and $W = 1.5 \times$ data rate in bits per second. It is seen that in all cases the autotrack EIRP requirements are exceeded by the data requirements. As a specific example, let us consider Ku-band autotrack on user data transmission, for which the minimum data rate is 10^6 bps. The required power spectral density is +33 dBW/MHz, and its bandwidth always exceeds 1 MHz. An autotrack receiver bandwidth of 1 MHz then will always see an effective user EIRP of +33 dBW, which exceeds the autotrack EIRP requirements. Thus, no autotrack pilot is required when data are transmitted.

In many cases, continual autotracking may be required when no data are transmitted. During those times, the user will have to transmit an autotrack pilot. The EIRP required for this pilot decreases with the receiver bandwidth W , as shown in Figure 1.

SUMMARY AND CONCLUSIONS

An analysis of the tracking errors in three potential TDRS autotrack systems has been performed to determine the user EIRP requirements for each to keep the tracking error within the 0.5 dB points of the Ku-band beam. Figure 1 shows that the user EIRP requirements of all three TDRS autotrack systems are below the levels required for user transmission of coded data. Figure 2 gives the optimum servo loop noise bandwidth required to obtain the performance in Figure 1. These results give important information on which to base the choice and design of autotrack implementation.

APPENDIX XV

TDRS AUTOTRACK INITIAL ACQUISITION PROBABILITY

The acquisition probability for the performance measurement system of Figure 4-8 of Section 4.2.2 is determined in this appendix. If ρ_1 is the system output when the beam center is closest to the user direction and ρ_2 is the system output when the beam is at any position out of the autotrack range, the probability of false acquisition at that position is

$$P_{fa} = \Pr\{\rho_2 < \rho_1\} \quad (1)$$

The test statistic ρ is determined from

$$\rho \approx \frac{1}{T} \int_{t-T}^t [y^2(t)/A^2] dt \quad (2)$$

With $y(t)$ a low pass Gaussian random process of bandwidth B , the integral can be approximated by a sampled sum

$$\rho \approx \frac{1}{BT} \sum_{i=1}^{BT} y_i^2 / A^2 \quad (3)$$

where the samples are all mutually uncorrelated.

The mean of ρ is given by

$$\mu = \bar{\rho} \approx \frac{1}{BT} \sum_{i=1}^{BT} \bar{y}_i^2 / A^2 \quad (4)$$

$$= \sigma_y^2 / A^2 \quad (5)$$

Since the signal-to-noise ratio in the TDRS receiver is given by

$$SNR = A^2 / (2\sigma_y^2) \quad (6)$$

we have

$$\mu = 1/(2 \text{SNR}) \quad (7)$$

The variance of ρ is given by

$$\begin{aligned} \sigma^2 &= \overline{\rho^2} - \mu^2 \\ &= \frac{1}{A^4 (BT)^2} \sum_{i=1}^{BT} \sum_{j=1}^{BT} \overline{y_i^2 y_j^2} - \sigma_y^4 / A^4 \\ &= \frac{1}{A^4 (BT)^2} \sum_{i=1}^{BT} \sum_{j=1}^{BT} \left[\overline{y_i^2 y_j^2} + 2 \overline{(y_i y_j)^2} \right] - \sigma_y^4 / A^4 \\ &= 2\sigma_y^4 / BT A^4 \end{aligned} \quad (8)$$

Using (6) in (8) gives

$$\sigma^2 = \frac{1}{2BT(\text{SNR})^2} \quad (9)$$

We will assume that the number of samples in the summation, BT, is sufficiently large to approximate ρ as a Gaussian random variable. If ρ_1 has mean μ_1 and variance σ_1^2 , and ρ_2 has mean μ_2 and variance σ_2^2 , then $\rho_0 = \rho_1 - \rho_2$ is also Gaussian with mean

$$\begin{aligned} \mu_0 &= \mu_1 - \mu_2 \\ &= \frac{1}{2(\text{SNR}_1)} - \frac{1}{2(\text{SNR}_2)} \end{aligned} \quad (10)$$

and variance

$$\begin{aligned} \sigma_0^2 &= \sigma_1^2 + \sigma_2^2 \\ &= \frac{1}{2BT(\text{SNR}_1)^2} + \frac{1}{2BT(\text{SNR}_2)^2} \end{aligned} \quad (11)$$

The probability of a false acquisition on position 2 is then

$$\begin{aligned}
 P_{fa} &= \Pr\{\rho_2 < \rho_1\} \\
 &= \Pr\{\rho_0 > 0\} \\
 &= \frac{1}{\sqrt{2\pi}\sigma_0} \int_0^\infty e^{-(\rho_0 - \mu_0)/2\sigma_0^2} d\rho_0 \\
 &= 1/2 [1 - \operatorname{erf}(-\mu_0/\sigma_0)] \tag{12}
 \end{aligned}$$

where

$$\operatorname{erf} x \triangleq \frac{1}{\sqrt{\pi}} \int_x^\infty e^{-z^2} dz \tag{13}$$

is the tabulated error function.

A worst-case situation occurs when the user is located at the edge of the uncertainty region of Figure 4-9 of Section 4.2.2, so that the closest it comes to beam center during the search is on the -2.2 dB gain contour. The most likely false alarm position is when the beam sees the user just beyond the edge of its autotrack range, which is on the 5 dB gain contour. Assuming $\text{SNR} = 5 \text{ dB}$ at beam center, then

$$\text{SNR}_1 = 5 \text{ dB} - 2.2 \text{ dB} = 1.90 \tag{14}$$

and

$$\text{SNR}_2 = 5 \text{ dB} - 5.0 \text{ dB} = 1.00 \tag{15}$$

Using (14) and (15) in (10) and (11) gives

$$\begin{aligned}
 \mu_0 &= -0.237 \\
 \sigma_0^2 &= \frac{0.638}{BT} \tag{16}
 \end{aligned}$$

Using $BT = 10^3$ in (16), so that the integration time is

$$T = \frac{10^3}{750 \times 10^3} = 1.33 \text{ ms} \quad (17)$$

(12) gives

$$P_{fa} = 1/2 [1 - \text{erf}(9.38)] \ll 10^{-9} \quad (18)$$

From equation (18), the total search time is

$$T_S = 2 \text{ seconds} \quad (19)$$

so that there are at most

$$T_S/T = 1500$$

independent test positions at which a false alarm could occur. Using the union bound, the total probability of a missed acquisition is bounded by

$$\Pr \text{ missed acquisition} < 1 - (1 - P_{fa})^{T_S/T} \ll 1.5 \times 10^{-6} \quad (20)$$

APPENDIX XVI

TWO DATA STREAMS ON THE SQPN SIGNAL

A user transmitting staggered quadriphase PN may require the capability of transmitting two data streams simultaneously at different data rates. (Say, the second stream is a data dump.) This is a multiplexing problem, and the objective is to minimize performance degradation (as measured by E_b/N_o to support the total data rate).

One basic approach for efficient multiplexing is time division (TDM), which places the burden entirely on the user and leaves the modulation unchanged except for total data rate. The advantage of this approach is negligible E_b/N_o degradation, provided that the overhead bits associated with framing are a small fraction of the total. A disadvantage is the need to synchronize the clocks of the two data streams, so as to eliminate bit stuffing. Presumably this restriction is not a problem for a typical user as long as the data can be asynchronous to the PN. From the TDRSS system viewpoint, TDM is the preferred approach, since the system then handles a serial data stream already multiplexed by the user before mod-2 addition to the SQPN.

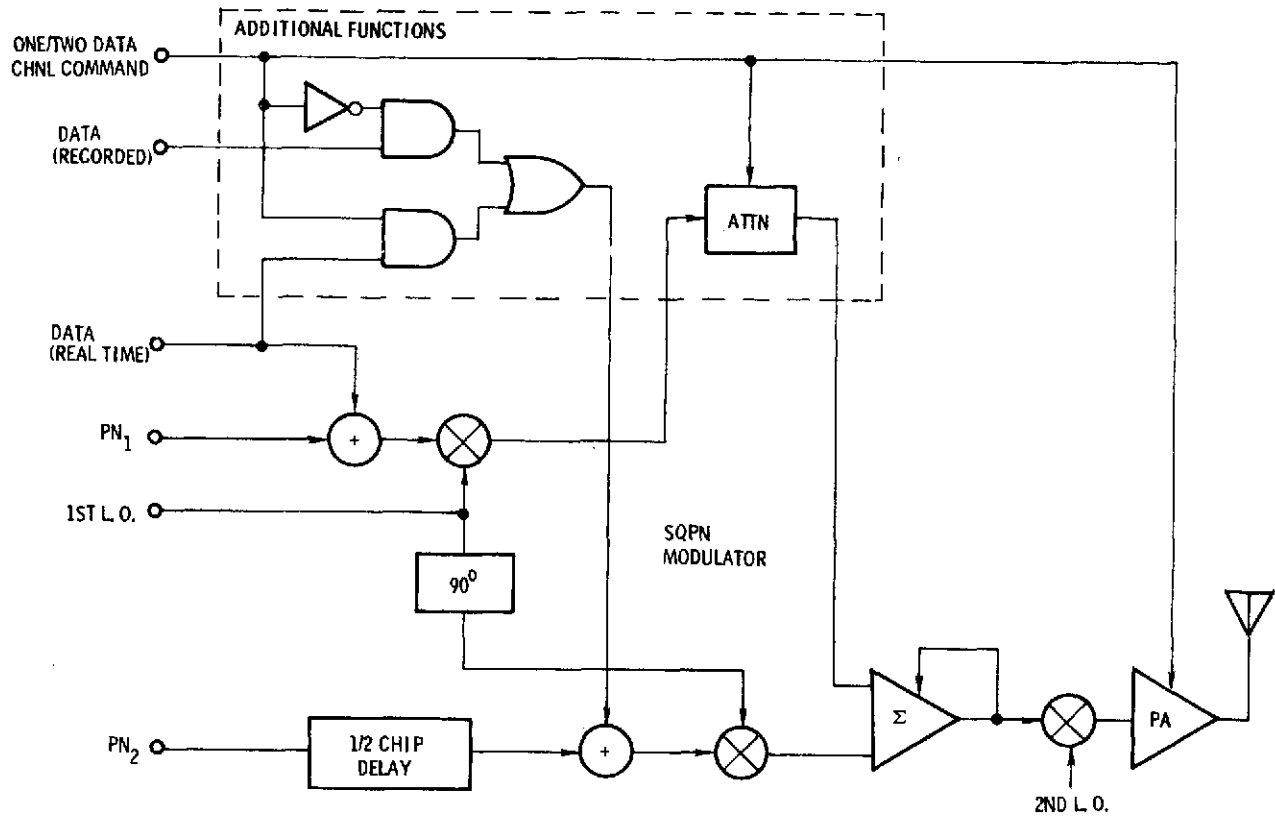
If the user cannot conveniently TDM the two data streams, or if the data clocks are asynchronous to each other as well as to the PN, an alternate approach is suggested. Referring to Figure 2-26 of Section 2.1.7.1.2 and Also Figure 2-41 of Section 2.3.2.6.2, it is observed that SQPN is generated with a pair of biphase PN codes modulating quadrature carriers, and these are two different codes for the reason discussed in Appendix VIII. Normally, the same data streams is mod-2 added to both codes; this is equivalent to biphase data modulation impressed on the SQPN carrier. It is suggested as the second approach for multiplexing that the two separate data streams be individually mod-2 added to the separate PN codes. The resulting waveform is still SQPN.

The ground receiver is implemented as two separate PN receivers, each using the biphase PN code corresponding to its designated data stream. Then, in each receiver, the other PN signal tends to act as an interference to the desired PN signal. Since this interference is in phase quadrature, it does not affect data decisions

(orthogonality) but only tends to cause a random phase error in Costas loop tracking. The Costas loop S/N should exceed approximately 20 dB to produce an rms error of 0.1 radian or less. By this criterion, the interference from the other PN signal is negligible provided that the Costas loop bandwidth is less than one percent of the PN chip rate. For multiple access, the chip rate is 3 Mbps; hence, the Costas loop bandwidth needs to be less than 30 KHz. According to Section 2.1.2.4.1, the Costas loop bandwidth can be narrowbanded to 5 Hz (third-order loop) which is much narrower than necessary for success of this multiplexing technique.

If the two data streams have unequal data rates, assignment of equal powers to the two biphase PN signals, as described above to generate SPQN, is somewhat inefficient. To approach ideal multiplexing efficiency, the powers should be assigned to the two biphase signals proportional to data rate. This is done by attenuating the amplitude of the biphase PN conveying the lower data rate. Note that the resultant signal is still constant envelope; however, the phases are distorted from quadriphase. Practically, the maximum attenuation can be of the order of 5 to 10 dB. As an example, with a data rate ratio of 100 but using only 10 dB of attenuation on the lower data rate signal, the E_b/N_o degradation to the higher data rate signal is only 0.37 dB.

The user transponder hardware impact in providing a one or two data channel capability is negligible. Figure 1 shows the additional functions required. The SQPN modulator located in the transmitter modulator module of the MA user transponder must be modified to include (1) gating circuits for the two data streams and (2) an RF attenuator to ratio the signal levels of the two biphase PN signals in proportion to their data rates. Also, a provision must be made to increase the Power Amplifier output level to support the combined data rate over the return link.



974-2903
UNCLASSIFIED

Figure 1. Transmitter Modulator Modified for One or Two Data Streams

The AGC will act to hold V_{AGC} essentially constant. Thus, variations in $G_{R\Delta}$ are removed. Furthermore, the DC noise component is now $N_{I\Sigma}$, the Σ -beam antenna noise power, instead of the total Σ -channel noise power $N_{\Sigma} = N_{I\Sigma} + N_{R\Sigma}$. For the recommended TDRS autotrack system, the power levels in Table I indicate an increase of 1.1 dB in AGC signal-to-noise ratio margin by the reduction of the DC noise component. In an S-band system where $N_{R\Sigma}$ is a larger proportion of N_{Σ} , the improvement will be correspondingly greater.

SUMMARY AND CONCLUSIONS

An APC loop has been described which compensates for paramp phase instability in a two-channel autotrack system. Noise effects on the phase accuracy of the APC loop have been analyzed. It was shown that incidental AM on the received signal can cause a pointing error, but its magnitude is insignificant. An AGC loop, similar to the APC loop, has also been described which offers improved performance over the conventional noncoherent Σ -channel AGC detector in the areas of increased SNR margin and compensation for Δ -channel gain variations.

REFERENCES

- [1] Pullara, J. C., et al, "Dual S- and Ku- Band Tracking Feed for a TDRS Reflector Antenna," Final Report Phase I , submitted by Martin-Marietta Aerospace Corp. to GSFC, July 1974.
- [2] Eggart, D. , "A High Gain Autotrack Antenna System for a Low Altitude Satellite Utilizing a Data Relay Satellite System," Phase III Final Report, Volume 2, submitted by Hughes Aircraft Co. to GSFC, November 1970, Table 2-1.
- [3] Reed, I. S. , "On a Moment Theorem for Complex Gaussian Processes," IRE Trans on Information Theory, April 1962, pp. 194-195.
- [4] Gardner, F. M. , Phaselock Techniques, John Wiley and Sons, New York, 1966, p. 21.
- [5] Davenport, W. B. and W. L. Root, An Introduction to the Theory of Random Signals and Noise, McGraw-Hill Book Co., New York, 1958, Ch. 12.